UNIVERSITY OF MINNESOTA
ST. ANTHONY FALLS HYDRAULIC LABORATORY

Project Report No. 361

Hydraulic Transient Study of Mainstream Tunnel System and Control System

by

Jianming He, Charles C.S. Song

Ying Liu, and Cuiling Gong

Prepared for

U.S. ARMY CORPS OF ENGINEERS
CHICAGO DISTRICT
111 North Canal Street
Chicago, Illinois 60606

October 1994

TABLE OF CONTENTS

LIST OF FIGURES

I. INTRODUCTION

Numerical studies of hydraulic transients for the TARP Phase I system were conducted in 1988 [1]* and 1992 [2]. These studies revealed that due to storage and/or conveyance limitations of the TARP Phase I Mainstream system using the Keifer/Song maximum hydrograph, inflow must be substantially reduced to avoid geysering problems induced by hydraulic transients. In order to improve the hydraulic transient condition, TARP Phase II has been proposed to add additional water storage and increase the conveyance ability. A hydraulic transient study for the TARP Phase II system was also conducted recently [3]. However, before the TARP Phase II is completed, a reasonable tunnel operation method for the current TARP Phase I system must be sought to minimize the potential of the hydraulic transient problems. This study is to investigate the extent and nature of hydraulic transients in the current TARP Phase I Mainstream tunnel under the existing flow control structures for different hydrographs. The tasks of the study include:

1. Determine the hydraulic loading on the main gate close to the downstream end during gate opening and closure under various hydrographs;

2. Assess the effect of main gate opening speed on hydraulic transient characteristics;

3. Evaluate the occurrence of surge/overflow due to a small inflow hydrograph after the downstream reservoir is full;

4. Evaluate the proposed operating plans of the dropshaft gates to avoid backflow from the dropshafts;

5. Appraise the outcome due to early opening of the main gate at high reservoir levels.

The fully dynamic transient mixed flow mathematical model (MXTRANS) [4] developed at the University of Minnesota was used for this study. Based on a number of initial test runs, the final study cases listed in Table 1 were selected by the Corps of Engineers [5] to evaluate the above study tasks.

---

* Numbers in brackets indicate references on page 20.

Table 1. Final Study Cases

Case	Main Gate	Reservoir Level	Dropshaft Gates	Storm Events
1	Closed	Empty (initial)	Open	PMF, 500, 100, 20, 5yr, and MAX Storms
2	Opening in 10 and 30 min.	Empty and –198 (initial)	Open	100yr Storm
3	Closed	–70 (initial)	Open	Total inflow 5,000 and 10,000 cfs
4	Opening in 30 min.	–198 (initial)	Plans 1, 2, 3, 4	5yr, 100yr and MAX Storms
5	Opening in 30 min.	–150 (initial)	Open	500 and PMF Storms
6	Opening in 10 and 30 min.	–150 (initial)	Open	PMF Storm
7	Closure in 30 min.	–70	Open	Total inflow 5,000 and 10,000 cfs, and PMF event

This report includes all the simulation results of the total of above 27 cases listed under Table 1.

II. THE MIXED TRANSIENT FLOW MODEL

2.1 Modeling Equations

The flow to be simulated is very unsteady and contains highly dynamic phenomena such as pressurization surge. The model used, then, must be able to simultaneously calculate unsteady open channel flows and unsteady pressurized flows, including the abrupt change that occurs at the shock or the surge front.

The well–known St. Venant equations:

$$\frac{\partial y}{\partial t} + v \frac{\partial y}{\partial x} + \frac{c^2}{g} \frac{\partial v}{\partial x} = 0 \tag{1}$$

$$g \frac{\partial y}{\partial x} + \frac{\partial v}{\partial t} + v \frac{\partial v}{\partial x} + g(S_f - S_o) = 0 \tag{2}$$

are used to represent the unsteady open channel flow. In the above equations, y is the flow depth, v is the flow velocity, c is the gravity wave speed, S_o is the channel slope, S_f is the energy slope, and g is the acceleration due to gravity, x is the distance along a tunnel, and t is time.

The corresponding equations for unsteady pressurized flow are:

$$\frac{\partial y}{\partial t} + V \frac{\partial y}{\partial x} + \frac{a^2}{g} \frac{\partial v}{\partial x} = 0 \tag{3}$$

$$g \frac{\partial y}{\partial x} + \frac{\partial v}{\partial t} + v \frac{\partial v}{\partial x} + g(S_f - S_o) = 0 \tag{4}$$

in which a is the pressure wave speed, while y takes the meaning of piezometric head measured from the tunnel invert. The systems of equations (1) ~ (4) are solved by the methods of characteristics [4].

Because the transition from the open channel flow condition to the pressurized flow condition must be abrupt, as in the case of a hydraulic jump, the special shock boundary conditions must be applied. It was shown by Cardle and Song [4], for a pressurization surge or a positive surge, that three characteristic equations plus two shock boundary conditions can be used to calculate five unknowns at the interface. These five unknowns are v and y on both sides of the interface and the speed of the interface movement. The

model can also simulate the negative surge which occurs during the depressurization process.

A number of other boundary conditions representing junctions, dropshafts, upstream end, downstream end, reservoirs, and other accessories are also provided in the model. Inflow hydrographs, outflow conditions, and other active or passive flow control methods can also be included in the input data file. Velocity, depth, discharge, and other variables at any location and any time may be specified as outputs.

2.2 Configuration of the Mainstream System

2.2.1 Tunnel Configuration

As suggested by The Corps of Engineers, the modeling configuration of the Mainstream tunnel system in this study includes the main tunnel and three branches (North Branch, Chicago River Branch and South Fork Branch), as shown in Fig. 2.1. There are a total of 442 computation stations with this modeling configuration. The distance between two neighboring stations is 500 ft. The stationing schematic of the main tunnel, excluding the branches, is shown in Fig. 2.2. All the dropshafts and junctions are set to have the same outlet elevation of 4 feet CCD by The Corps of Engineers.

2.2.2 Downstream Gate and Reservoir

As shown in Fig. 2.1, the tunnel system includes a reservoir at the downstream end and a main gate close to the reservoir. The maximum water level elevation of the reservoir at the current stage is –70 ft. The total storage of the reservoir at different water levels is listed as follows,

Elevation(ft)	Area($ft^2 x 10^6$)	Volume ($ft^3 x 10^6$)
–298	0.172	0.0
–244	0.779	8.65
–221	2.530	26.99
–199	7.690	88.22
–182	10.560	175.53
–70	10.926	1,390.05

2.2.3 Hydrographs

The hydrographs at each dropshaft, except for the Keifer/Song maximum hydrograph, used in the modeling are provided by The Corps of Engineers. They include 5–year, 20–year, 100–year, 500–year, SPF and PMF. The Keifer/Song maximum storm event is based on the peak inflow rate data at each dropshaft and junction. The peak inflow data are also provided by The Corps of Engineers. Their distribution pattern is chosen based on the storm event of Oct. 18, 1985, in the same area. The Keifer inflow hydrograph for all

the dropshafts has been stored. If the design peak inflow of a dropshaft coincides with the peak value of the Keifer hydrograph, then the Keifer's hydrograph is used. If the two peak values don't agree, then the Keifer hydrograph is considered as a unit hydrograph, and it is scaled up or down according to the ratio of the two peak values.

Fig. 2.3 shows the total inflow rate of all the hydrographs. The hydrograph called MAX Storm in Fig. 2.3 is the total inflow hydrograph in all the dropshaft and junctions based on Keifer's hydrograph shapes and The Corps of Engineers' peak values (based on the July 12–13, 1957, storm). Note that the MAX storm hydrograph has a short duration but the strongest inflow peak.

3.1.2 20–year storm event (Case 1–2)

The modeling results for the 20–year storm event are shown in Figs. 3.2(a) to 3.2(i), which are similar to the figures described for Case 1–1 above. In this case, general hydraulic transient characteristics are the same as the above case, except the tunnel system is pressurized about 1.5 hours earlier since the inflow increases. As shown in Fig. 3.2(a), the tunnel is fully filled at t=9.0 hours. The overflow and backflow in Fig. 3.2(h) are also larger than those in Case 1–1. However, the maximum loading on the main gate is the same since the final water depth at the gate does not change.

3.1.3 100–year storm event (Case 1–3)

The modeling results for the 100–year storm event are shown in Figs. 3.3(a) to 3.3(i). Again, general hydraulic transient characteristics are not different than the above two cases. Quantitatively, the tunnel is pressurized earlier, as shown in Fig. 3.3(a), and there is more overflow and backflow, which also starts earlier (t=7 hours), as shown in Fig. 3.3(h), due to the increased inflow hydrograph. The maximum loading on the main gate is still the same, as shown in Fig. 3.3(i).

3.1.4 500–year storm event (Case 1–4)

The modeling results for the 500–year storm event are shown in Figs. 3.4(a) to 3.4(i). In this case, the time to fill the tunnel system is further reduced due to the larger inflow storm. The maximum loading on the main gate still does not change, as shown in Fig. 3.4(i).

3.1.5 PMF storm event (Case 1–5)

The modeling results for the PMF storm event are shown in Figs. 3.5(a) to 3.5(i). As indicated in Fig. 2.3, the PMF hydrograph has the largest inflow volume. During the first one and a half hours, the inflow rate is also larger than the MAX storm hydrograph. As a result of the strong inflow, it takes less than two hours to fill the entire tunnel, and the overflow and backflow appear after the first hour, as shown in Fig. 3.5(h). The maximum loading is still the same, although it takes only two hours to reach the maximum value.

The other significant feature in the results is that at two upstream ends (Stations 1 and 84) the water level increases extremely fast due to backward surge, as shown in Fig. 3.5(b). At station 1, the water depth rapidly rises from 5.2 ft. to 200.0 ft. in less than 3 minutes. Such a strong backward surge may have some effects on the dropshaft structure.

3.1.6 MAX storm event (Case 1–6)

The modeling results for the MAX storm event are shown in Figs. 3.6(a) to 3.6(i). As indicated in Fig. 2.3, the MAX hydrograph has a short duration, but has the largest peak inflow. As mentioned above, during the first one and a half hours, the inflow of MAX hydrograph is still smaller than that of the PMF hydrograph. Consequently, it takes longer to fill the tunnel system than the PMF event. As shown in Figs. 3.6(h) and 3.6(i), it is about 2:10 when the entire tunnel is pressurized. Since the MAX inflow hydrograph is stronger than the PMF event, the backward surge is much more severe. At Station 1, the water depth rises from 2.8 ft. to 203.1 ft. in less than one minutes, as shown in Fig. 3.6(b). The other hydraulic transient characteristics are almost the same as before.

In summary, in the case when the main gate is closed, general hydraulic transient features are similar for the simulated hydrographs. The differences between the storm events involve the time of the tunnel being fully pressurized, the strength of the surge, and the amount of overflow and backflow. For the PMF and MAX storm events, the water level at two upstream ends (Stations 1 and 84) increases very fast due to the strong backward surge. It may have some effects on the dropshaft structures depending on the detailed structural design of the dropshafts. The maximum loading on the main gate is the same for each storm event. The dynamic portion of the loading can be ignored since the velocity at the gate does not change.

3.2 100–Year Storm without Inflow Control

The tunnel design is mainly based on the 100–year storm event. It is important to study both the hydraulic transient with different downstream reservoir levels and the effects of the main gate opening time (speed) on the surge movement. In this case, two reservoir levels, empty and –198, are simulated with two gate opening schedules, 10 and 30 minutes.

3.2.1 Empty reservoir and gate opening in 10 min.(Case 2–1)

Figs. 3.7(a) to 3.7(h) show the modeling results with an empty reservoir at the downstream end and the main gate opening in 10 minutes. In this case, the gate starts to open when the modeling starts. Each figure in this case represents the same quantity as described above. Comparing the results with those in Case 1–3 (with the same hydrograph), it can be found that the existence of the downstream reservoir strongly affects the transient movement and overflow, as well as backflow. As shown in Fig. 3.7(h), the tunnel starts to have overflow after t=10.5 hours, which ends at t=18 hours. The maximum overflow and backflow are also much smaller when compared with the case without the reservoir (Case 1–3). At the final stage of the hydrograph, the velocity in the tunnel system approaches zero, and the water surface elevations are almost at the same level in the entire tunnel system, as shown in Figs. 3.7(a), 3.7(c), and 3.7(e).

3.2.2 Empty reservoir and gate opening in 30 min.(Case 2–2)

Figs. 3.8(a) to 3.8(h) show the modeling results with an empty reservoir at the downstream end and the main gate opening in 30 minutes. Compared with the above case, it is difficult to notice a difference between the two cases. In fact, the tunnel is not pressurized until t=3 hours. During the first 30 minutes, the water depth at the gate is only about 5 ft. Therefore, the gate opening time at initial stage apparently does not affect the transient flow in the tunnel.

3.2.3 Reservoir water level at –198 and gate opening in 10 min.(Case 2–3)

Figs. 3.9(a) to 3.9(h) show the modeling results with the initial reservoir water level at –198 and the main gate opening in 10 minutes. As indicated in Fig. 3.9(e), it takes about 5 hours for the water elevation at the gate to rise to the initial reservoir water level (–198). At that time, the backward surge has already arrived at the upstream end (Sta. 001), as shown in Fig. 3.9(b). Therefore, the first backward surge is not affected by the reservoir. In fact, during the first 5 hours, the results in this case is the same as those in Case 1–3. However, when the main gate starts to open, the water elevation is strongly affected by the downstream reservoir, especially the stations close to the reservoir. Due to the initial storage, the final water level of the tunnel system is slightly higher than the last case.

3.2.4 Reservoir water level at –198 and gate opening in 30 min.(Case 2–4)

Figs. 3.10(a) to 3.10(h) show the modeling results with the initial reservoir water level at –198 and the main gate opening in 30 minutes. The results appear to be similar to those in Case 2–3, except for a slightly different fluctuation at the gate area during the gate opening period, as shown in Fig. 3.9(e) and Fig. 3.10(e). Overall the gate opening speed has almost no effect on the transient phenomena for the 100–year hydrograph.

In summary, for the 100–year hydrograph, the gate opening time length (speed) has almost no effect on the hydraulic transient flow, or overflow and backflow, in the empty reservoir and –198 high water level reservoir cases. Overflow and backflow for the two reservoir conditions are also the same.

3.3 Small Inflow with Gate Closed (Fully Filled Reservoir)

The purpose of this part of the study is to evaluate the hydraulic transient feature when a small flood occurs after the downstream reservoir is already at the full capacity level (–70). Two small inflow events (5,000 and 10,000 cfs in total) are used in the modeling study. The total amount is equally distributed to each dropshaft. Since the main gate is always closed in this case, the modeling condition is very similar to the cases in Section 3.1, with a dead–end.

3.3.1 5,000 cfs inflow event (Case 3–1)

Figs. 3.11(a) to 3.11(h) show the modeling results for 5,000 cfs total inflow with a full reservoir. Each figure here represents the same quantity as the case described above. Since the modeling condition is the same as in Case 1, except for the hydrograph, the hydraulic transient characteristics are similar to those in the cases described in Section 3.1. For this inflow rate it takes about seven hours to fill the tunnel system; then, all the inflow becomes overflow. In some lower locations the overflow is larger than the inflow; hence, backflow also occurs.

3.3.2 10,000 cfs inflow event (Case 3–2)

Figs. 3.12(a) to 3.12(h) show the modeling results for 10,000 cfs total inflow with a full reservoir. As the inflow is doubled in this case, the pressurization time of the tunnel is shorter, and the overflow is also doubled after the tunnel is fully pressurized.

In summary, when the downstream reservoir is initially full (–70), the modeling condition is the same as the dead–end (closed gate) case. Since the inflow is small in this case, there is no serious transient problem. After the tunnel system is filled to its capacity, all the inflow becomes a steady overflow.

3.4 Inflow Control Plans

The purpose of this part of the study is to seek a reasonable inflow control operation plan at the dropshafts for different storm events to avoid potential backflow due to the hydraulic transients. A total of three storm events, 5–year, 100–year, and MAX, are investigated here. The main gate opening time is fixed within 30 minutes for all the events, and the initial water elevation at the downstream reservoir is set at –198. The inflow control schedule designed by the Corps of Engineers includes four plans based on the priority of the drainage area, listed as follows:

Plan 1: All system gates left open.
Plan 2: 13A and DS 53 closed when tunnel is 40% full, then DS 27, 28, and 29 closed at tunnel 50% full.
Plan 3: Plan 2 plus operation of selected gates (total of 43 dropshafts) to be closed at the time the tunnel is 50% full.
Plan 4: Plan 2 plus operation of more selected gates (total of 70 dropshafts) to be closed at the time the tunnel is 50% full.

3.4.1 5–year storm event with operation of Plan 1 (Case 4–1)

Figs. 3.13(a) to 3.13(h) show the modeling results with the initial reservoir water level at –198 and Plan 1 operation for the 5–year storm event. As mentioned above, Plan 1 has no inflow control. This case is similar to Case 1–1 except the reservoir becomes effective after the water elevation

reaches –198 at the downstream end. Compared with Case 1–1, there is no overflow and backflow in this case, as shown in Fig. 3.13(h). The results show that the downstream reservoir is essential for eliminating the overflow and backflow problem. Therefore, inflow control plan is not necessary for the 5–year storm event.

3.4.2 100–year storm event with operation of Plan 2 (Case 4–2)

The modeling condition of Plan 1 for the 100–year storm event is exactly the same as Case 2–4. The results have been described before. As shown in Fig. 3.10(h), there is a large amount of overflow and backflow associated with Plan 1.

Figs. 3.14(a) to 3.14(h) show the modeling results with Plan 2 inflow control operation for the 100–year storm event. As shown in Fig. 3.14(h), the overflow and backflow are still quite large, but the maximum overflow and backflow decrease from 17,887 and 6,948 cfs in Plan 1 to 13,390 and 5,883 cfs, respectively. Hence, Plan 3 must be implemented to avoid the backflow problem.

3.4.3 100–year storm event with operation of Plan 3 (Case 4–3)

Figs. 3.15(a) to 3.15(h) show the modeling results of the Plan 3 inflow control operation for the 100–year storm event. As shown in Fig. 3.15(h), the overflow and backflow is significantly reduced with this plan, but the maximum overflow and backflow are still as large as 1,002 and 569 cfs. Their duration lasts less than 1.5 hours. Fig. 3.15(h) also shows that the total inflow is dramatically cut with this plan. The scaled–up overflow and backflow are displayed in Fig. 3.15(i).

3.4.4 100–year storm event with operation of Plan 4 (Case 4–4)

Figs. 3.16(a) to 3.16(h) show the modeling results of the Plan 4 inflow control operation for the 100–year storm event. As shown in Fig. 3.16(h), the overflow and backflow is finally eliminated with this plan. But most of the inflow is not allowed to enter the tunnel under this inflow control plan.

3.4.5 MAX storm event with operation of Plan 1 (Case 4–5)

Figs. 3.17(a) to 3.17(h) show the modeling results of the Plan 1 inflow control operation for the MAX storm event. As shown in Fig. 3.17(c), the main gate starts to open about 1:45, and ends at 2:15. During the first 10 minutes of the opening, the water elevation continues to rise due to the strong inflow hydrograph; after that, it decreases as the gate opening increases. As shown in Figs. 3.17(a), 3.17(e), and 3.17(h), at the end of the storm period (t=4.5 hours), the downstream reservoir water elevation is only –172, but the upstream area still has a large amount of overflow and backflow. Therefore, as

concluded in the previous studies [2,3], the conveyance limitation exists in the TARP Phase I Mainstream system for the MAX storm event. Inflow control is necessary to avoid the large amount of overflow and backflow.

Similar to Case 1–6, the strong backward surge due to the too large an inflow hydrograph leads to a rapid water depth rise at two upstream ends (Stations 001 and 084).

3.4.6 MAX storm event with operation of Plan 2 (Case 4–6)

Figs. 3.18(a) to 3.18(h) show the modeling results of the Plan 2 inflow control operation for the MAX storm event. As shown in Fig. 3.18(h), the overflow and backflow is reduced with this plan, compared to the results in Plan 1, but the maximum overflow is still very large (up to 35,260 cfs).

3.4.7 MAX storm event with operation of Plan 3 (Case 4–7)

Figs. 3.19(a) to 3.19(h) show the modeling results of the Plan 3 inflow control operation for the MAX storm event. As shown in Fig. 3.19(h), the overflow and backflow is significantly reduced with this plan, and the duration of the overflow and backflow is much shorter, compared to the results of the first two plans. The maximum overflow is about 8,066 cfs in this case. The backward surge is still very strong.

3.4.8 MAX storm event with operation of Plan 4 (Case 4–8)

Figs. 3.20(a) to 3.20(h) show the modeling results of the Plan 4 inflow control operation for the MAX storm event. As shown in Fig. 3.20(h), there are no more overflows and backflows. Compared with Fig. 3.17(h) in Case 4–5 (without inflow control), however, the total inflow allowed to enter the tunnel under this plan is very small.

In summary, for the 5–year storm event, there is no overflow and backflow. For the 100–year and MAX storm events, however, Plan 4 is necessary to avoid the overflow and backflow. For the MAX storm event, due to the steep inflow peak, the strong backward surge in the upstream area still exists like the deadend case (Case 1–6), and may have some effects on the dropshaft structures.

3.5 500–Year and PMF Events and Gate Opening in 30 Minutes

The purpose in this part of the study is to investigate the hydraulic transient phenomena at a higher initial reservoir water level (–150 feet CCD) during two large storm events, 500–year storm and PMF event.

3.5.1 500–year storm and gate opening in 30 min.(Case 5–1)

Figs. 3.21(a) to 3.21(h) show the modeling results of the initial reservoir water level at –150 and the main gate opening within 30 minutes. Since the gate remains closed before the water elevation at the gate is larger than the initial reservoir elevation, the transient characteristics are the same as those in Case 1–4 before the gate starts to open. As indicated in Fig. 3.21 (e), as the gate opening increases, the water elevation at the gate, already rising before the gate starts to open, begins to decrease. As a result, a small peak in water elevation can be identified. The magnitude of this peak grows somewhat as it travels upstream, as shown in Fig. 3.21(c).

3.5.2 PMF event and gate opening in 30 min.(Cases 5–2)

Figs. 3.22(a) to 3.22(h) show the modeling results with the initial reservoir water level at –150 and the main gate opening within 30 minutes. The downstream reservoir appears to have little effect on the hydraulic surge in the upstream area. Like the deadend case (Case 1–5) for the same storm, the backward surge in the upstream area is still very strong.

In summary, for the large storm events (500–year and PMF) the downstream reservoir has little effect on the hydraulic surge in the upstream area because the tunnel system has an insufficient capacity to convey such a high concentration of water to the downstream reservoir during the storm event.

3.6 Early Opening of The Main Gate

The Corps of Engineers expressed an interest in studying the feasibility of pre–filling the tunnel before a major storm to prevent the possibility of a severe surge. It may also happen that the main gate is opened before the water elevation is larger than the reservoir level due to mis–operation or accident. When this happens, the water in the reservoir will pour into the tunnel system, which may cause a more serious problem. In this study, the initial reservoir level is assumed to be at –150, and the PMF event is used.

3.6.1 Gate Opening in 10 min. when Y_{gate}> half tunnel diameter (Cases 6–1)

Figs. 3.23(a) to 3.23(h) show the modeling results of the initial reservoir water level at –150 and gate opening within 10 minutes when the water depth at the gate is larger than half the tunnel diameter. As the results indicate, the backward flow from the reservoir after the gate is opened encounters the strong forward inflow into the middle area, such as at Sta. 260 and Sta. 316, which results in a large surge in that area. Apparently, the magnitude of the surge depends on both the inflow hydrograph and the initial downstream reservoir water level. The location of the surge is closely related to the schedule of the gate opening, including speed and timing.

3.6.2 Gate Opening in 30 min. when Y_{gate}> half tunnel diameter (Cases 6–2)

Figs. 3.24(a) to 3.24(h) show the modeling results of the initial reservoir water level at –150 and the gate opening within 30 minutes after the water depth at the gate becomes larger than half the tunnel diameter. As indicated in Fig. 24(a), at t=1.0 hour, which is the time when the first surge occurred at Sta. 260 and Sta. 316 under Case 6–1, the gate is still being opened. Because of the slower development of backward flow, the first surge takes place later and a little closer to the downstream area. Compared with Case 6–1 above, the surge peak at Sta. 260 is smaller, as shown in Fig. 3.23(b), but the total overflow and backflow in the two cases are the same, although they may happen at different locations. In addition, like the other PMF storm cases, the strong surge in the upstream area still exists.

In summary, the early opening, when the reservoir is loaded, may cause a serious surge problem even with a small storm event. The surge movement is affected by a number of factors such as storm event, gate opening schedule, and the reservoir water level.

3.7 Gate Closure Cases

Most of the cases discussed before are associated with the gate opening process. During a gate closure process, the dynamic loading on the main gate is also of concern. The following three gate closure cases were studied here. The first two cases have a steady inflow (5,000 and 10,000 cfs), like Case 3–1 and Case 3–2, but the gate is closed in 30 minutes after the downstream reservoir water level reaches –70 feet CCD. The third case is for a PMF storm, and the gate starts to close after the total inflow approaches its peak value (about 8 hours from the storm start, shown in Fig. 2.3).

3.7.1 Steady 5,000 cfs inflow (Case 7–1)

Similar to Case 3–1, the 5,000 cfs total inflow is equally distributed to each dropshaft and junction. Since the main concern in this case is the gate loading during the gate closure process, the initial water surface elevation in the entire tunnel system is assumed to be at –88 ft CCD.

Figs. 3.25(a) to 3.25(i) show the modeling results under the above condition. As indicated in the results, during the first two hours, there are some fluctuations in water depth in the upstream area because the storm suddenly starts to move against initially hydro static conditions. After that, the water depth steadily increases as the steady inflow enters the tunnel system. At t=9.4 hours, the downstream reservoir water level reaches –70 ft CCD, and the gate starts to close. As a result, the water level in the tunnel system increases rapidly to dropshaft outlet level (–4 ft CCD). At t=10.0 hours, all the inflow becomes overflow. The gate net loading shown in Fig. 3.25(i) is the loading difference between the two sides of the gate. The small loading peak during the closure period is due to the dynamic loading. Apparently, the net loading is dominated by the hydro static loading since the

flow rate is relatively small. The maximum net loading on the gate is 32.7 psi, which is much smaller than the deadend cases (Case 3–1) because the pressure on the gate outside balances some loading on gate inside.

3.7.2 Steady 10,000 cfs inflow (Case 7–2)

Figs. 3.26(a) to 3.26(i) show the modeling results under a similar condition as above but the total flow rate is increased to 10,000 cfs. Comparing with the above case, the main hydraulic features are similar, but the increased inflow rate apparently makes it faster for the downstream reservoir water level to reach –70 feet CCD. The gate starts to close at t=4.9 hours. As indicated in Fig. 3.26(i), the dynamic loading on the gate during the gate closure increases due to the larger velocity when the gate starts to close. But the static loading in two cases are almost the same. The maximum net loading on the gate is 33.3 psi, which is slightly larger than the above case.

3.7.3 PMF event and gate closure in 30 minutes

Figs. 3.27(a) to 3.27(i) show the modeling results for PMF hydrograph and gate closure in 30 minutes after the total inflow reaches its peak value. As shown in Fig. 3.27(e), the gate starts to close at t=8.0 hours. At that time, the downstream reservoir water level is at –142 feet CCD. Therefore, the static net loading on the gate is larger than that in the above two cases. Because a PMF storm is much stronger than the above two cases, the dynamic loading on the gate is also much larger, as shown in Fig. 3.27(i). The maximum net loading on the gate is 81.3 psi, which occurs when the gate starts to close.

In summary, when the reservoir is not empty, the static loading on the gate is smaller due to the static pressure of the reservoir water. The dynamic loading on the gate during gate closure is dependent on the storm hydrograph. A stronger hydrograph will generate a stronger dynamic loading peak. In the simulated three cases, the maximum net loading is smaller than that in the deadend cases (Cases 1–1 to 1–6 and 3–1 to 3–2) with an empty reservoir.

IV CONCLUSIONS AND RECOMMENDATIONS

Following is a list of the important conclusions drawn from the results of the computer simulations:

1. For the cases when the main gates are closed, the general hydraulic transient features, including surge production and movement as well as overflow and backflow, are similar for different storm events. The differences are in the timing and the magnitude of the events. The critical event affecting the safety of the tunnel system is the BACKFLOW. Even for a very small amount of backflow, the impact force generated by the water surging up the dropshaft can cause structural damage and geysering.

2. The computed maximum loading on the main gate is 112 psi for all the closed gate cases with an empty reservoir. The dynamic portion of the loading in the cases is very small. A suitable factor of safety should be applied when using this figure for gate design. In addition to the maximum loading, the oscillatory loading, including its amplitude and frequency, may need to be considered when evaluating possible vibration and fatigue of the gates.

3. For the 100–year, 500–year, and PMF hydrographs, the gate opening time interval (speed) has little effect on the hydraulic transients, or overflow and backflow, in the case where initial reservoir elevation is lower than –150 ft. For a given hydrograph, the overflow and backflow are not affected by any change of initial reservoir water level in the range tested (empty to –150).

4. When the reservoir is initially full (–70), the modeling condition becomes the same as the gate closed case. There is no serious transient problem if the total inflow rate is 5,000 cfs or 10,000 cfs. If the inflow is allowed to continue everywhere long after the tunnel is filled, steady amounts of overflow as well as backflow may occur.

5. For the 5–year storm event, there are no overflow and backflow. This means that for the 5–year storm event inflow control is not necessary as far as hydraulic transient and tunnel capacity are concerned. But for the 100–year and MAX storm events, inflow control plan up to Plan 4 is necessary to avoid backflow.

6. For all cases tested, except the deadend cases, backflow takes place at shafts located near the upstream end of the system. This is because the outlet elevation of all the dropshaft is set at 4 feet CCD by The Corps of Engineers. The water surface elevations in the downstream area cannot reach their outlet elevation because of the large capacity reservoir. The actual locations of the backflow will depend on the actual dropshaft design.

7. Under the following conditions:

100–year storm hydrograph;
Initial reservoir level at –150 feet CCD;
Gate opening in 30 minutes after the water level at the gate is larger than the initial reservoir level,

the overflow amounts are as follows:

Case	Control Plan	Overflow Amount (ft^3)
Case 2–4	Plan 1	2.87×10^8
Case 4–2	Plan 2	2.01×10^8
Case 4–3	Plan 3	4.73×10^6
Case 4–4	Plan 4	0.0

8. Early opening of the main gate when the reservoir is loaded may cause serious surge problems even with a small storm event. The surge movement is affected by three main factors: storm size, gate opening time and speed, and the initial reservoir water level.

9. If the storm is large and the gate is opened when the water level in front of the gate is at half the tunnel diameter, a strong surge occurs in the middle area of the tunnel system. For the same storm, if the gate is opened when water in front of the gate is equal to the tunnel diameter, the flow from the reservoir has little effect and the surge is dominated by the storm inflow.

10. When the reservoir is not empty, the static loading on the gate is smaller due to the static pressure of the reservoir water. The dynamic loading on the gate during gate closure is dependent on the storm hydrograph. A stronger hydrograph will generate a stronger dynamic loading peak. In the simulated gate closure cases, the PFM storm case has the largest peak net loading of 81.3 psi, which is still smaller than that in the deadend cases (112 psi) with a empty reservoir.

11. The computed results indicate that, for the simulated hydrographs under normal operating conditions, most of overflow and backflow are not induced by the transient surge, but instead by the limited conveyance capacity of the tunnel system for the specific storm events. Therefore, the existence of surge shafts at the upstream area is not effective to avoid the large amount of overflow and backflow volumes, unless their capacity is large enough to contain all the overflow water.

However, all the simulated cases with the PMF and MAX storm events have identified a strong surge in the upstream area. The worst locations are two upstream ends, the main tunnel upstream end (Station 001), and the North branch upstream end (Station 084). The surge causes water level at the dropshafts to rise rapidly, which may lead to a geysering problem. The quantitative determination of the effects needs a dropshaft transient model based on the detailed design of the dropshaft. To prevent the geysering problem, large–size surge shafts are very effective. Therefore, for the PMF and

MAX storm events, the surge shafts at the upstream area are necessary to prevent the potential geysering problem. The shaft size and locations need to be studied in detail.

12. More detailed modeling results for the 100–year storm event cases can be found in separate disks.

Some comments on the current work and recommendations for further works are listed below.

1. All three control plans considered here appear to favor inflow limitations in the downstream area of the system. However, the flow analyses indicate that most of the backflows occur in the upstream region. A more efficient control plan may require inflow limitations in the upstream region as well. Therefore, it is recommended that alternative control plans, including control in the upstream region, be studied.

2. All the simulated cases are based on the same outlet elevation (4 feet CCD set by The Corps of Engineers) for all the dropshafts. But in reality, where the overflow and backflow occur strongly depends on the dropshaft outlet elevation. This is also why most overflow and backflow predicted by this model under the assumed condition occur in the upstream area from a large number of dropshafts. It is believed that the actual outlet elevations of the dropshafts are not the same. Dropshafts with lower elevations will have more overflow and backflow. Therefore, the computed overflow and backflow results at a specific dropshaft may not be realistic if the dropshaft outlet elevations are not used.

3. As stated in the conclusions, surge shafts at the upstream area may be needed under the PMF and MAX storm event to prevent the geysering problem. The size and locations can be optimized by numerical modeling. A further study in this aspect is recommended.

4. Different storm events require different control plans. This indicates that a means must be available to determine the storm size on a real time bases. A way to do this is to use the information from the tunnel filling condition, including the current storage and the rate of filling. Accurate calculations of the filling process on a real time basis can be made using water depth data at three locations in the tunnel. A study of control methods based on the real time tunnel data is recommended.

5. Early opening of the main gate or pre–filling when the reservoir is filled may results in serious surge problems. However, its effectiveness is very sensitive to four factors: the reservoir water level, the current inflow hydrograph, the current water level in the tunnel, and the gate opening schedule (timing and speed). It is recommended that appropriate processes under different conditions be studied.

REFERENCES

1. Song, C.C.S., Guo, Q., and Zheng, Y., "Hydraulic Transient Modeling of TARP Systems," University of Minnesota, St. Anthony Falls Hydraulic Laboratory, Project Report No. 270, March 1988.

2. Song, C.C.S., Lin, W., and Gong, C., "Hydraulic Transient Modeling of TARP Systems," University of Minnesota, St. Anthony Falls Hydraulic Laboratory, Project Report No. 332, March 1992.

3. Song, C.C.S., He, J., Liu, Y., and Gong, C., ""Hydraulic Transient Study of Mainstream & Des Plaines TARP Phase II Systems," University of Minnesota, St. Anthony Falls Hydraulic Laboratory, Project Report No. 353, March 1994.

4. Cardle, J. A. and Song, C.C.S., "Mathematical Modeling of Unsteady Flow in Storm Sewers." *International Journal of Engineering Fluid Mechanics*, Vol. 1, No. 4, 1988.

5. Facsimile Transmittal from Mr. Rao Manam to Prof. Charles C. S. Song, Sept. 27, 1994.

Figures 2.1 through 3.27

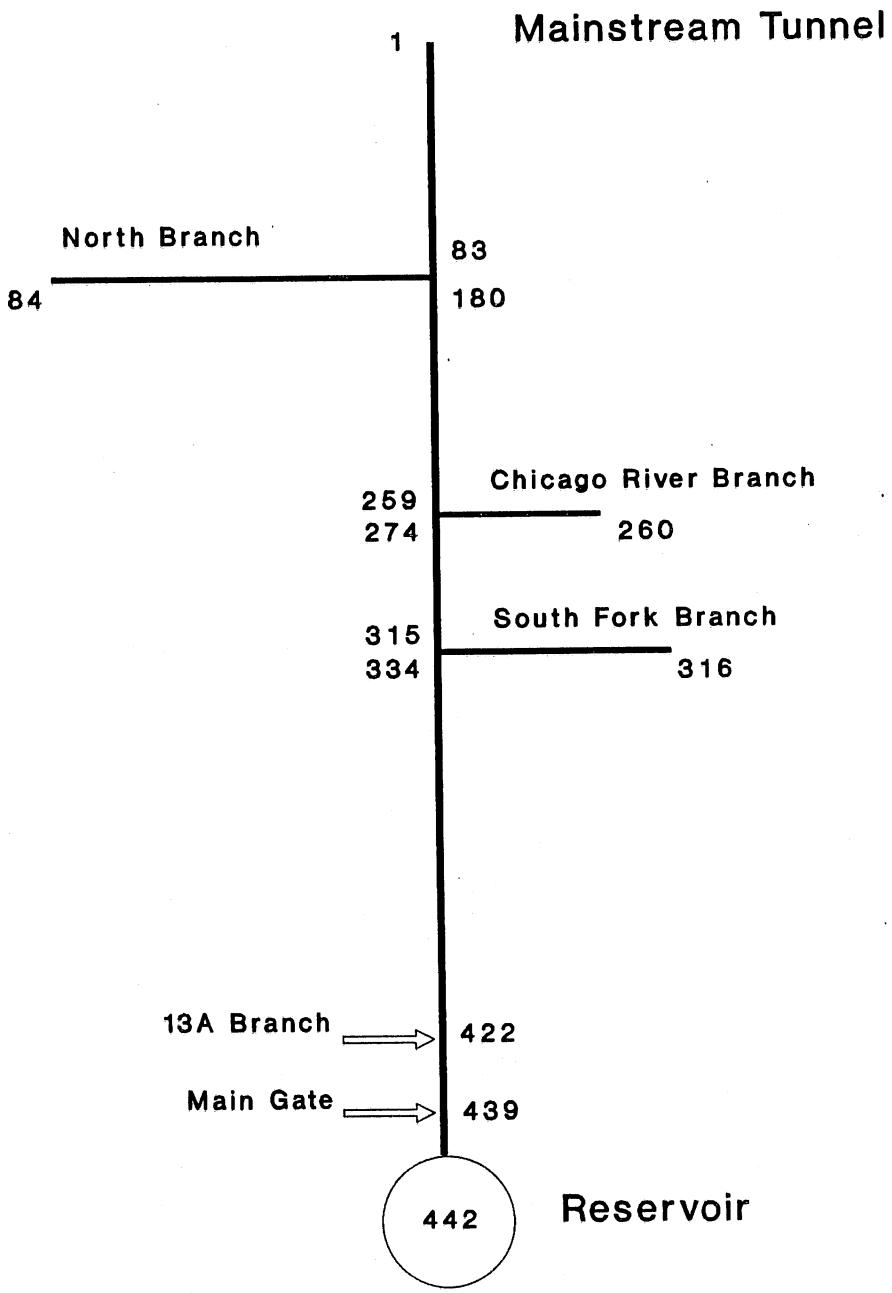

Fig. 2.1 Schematic of the Mainstream tunnel system for modeling purpose

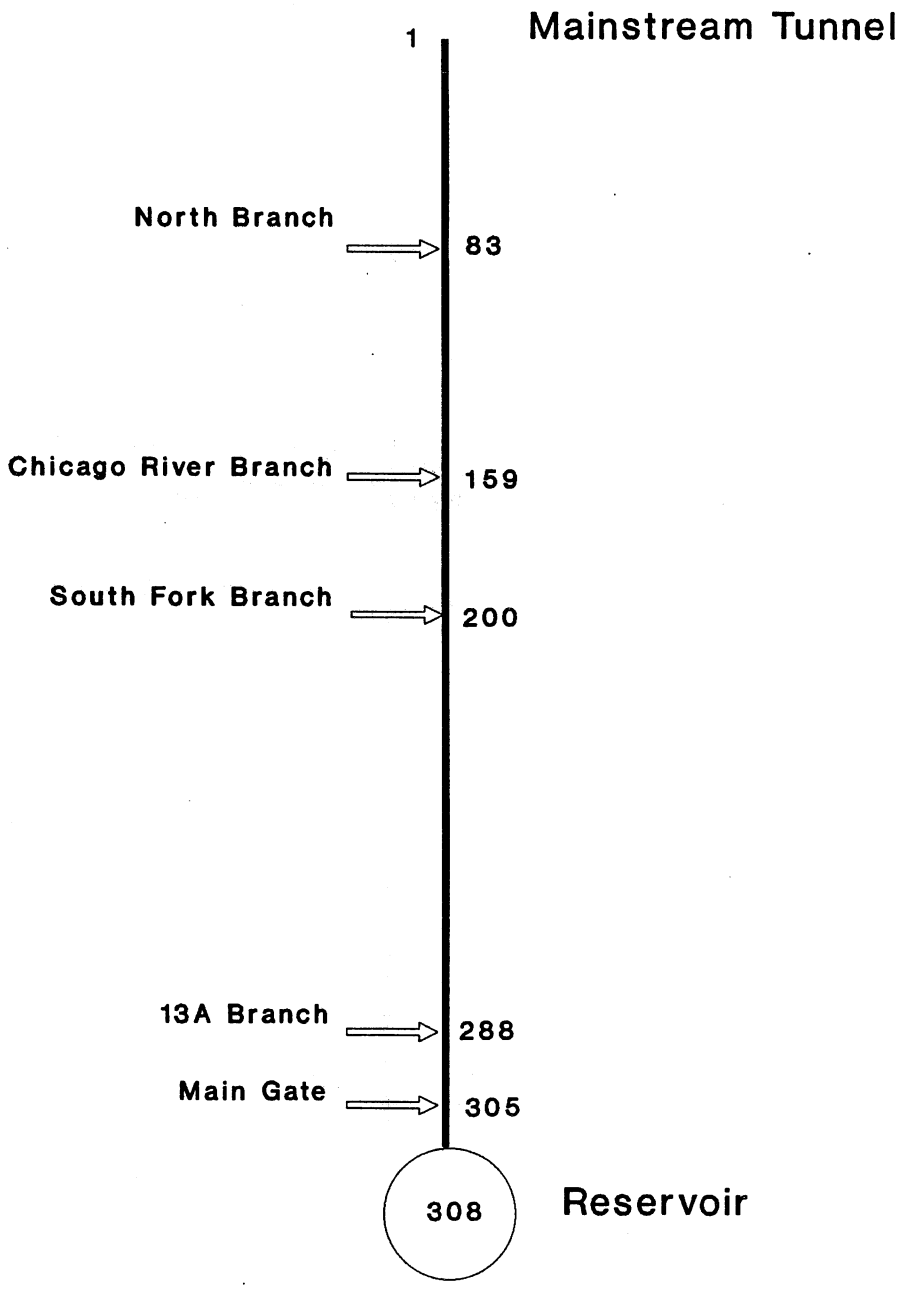

Fig. 2.2 Stationing of the main tunnel (excluding all branch tunnels) of the Mainstream tunnel system

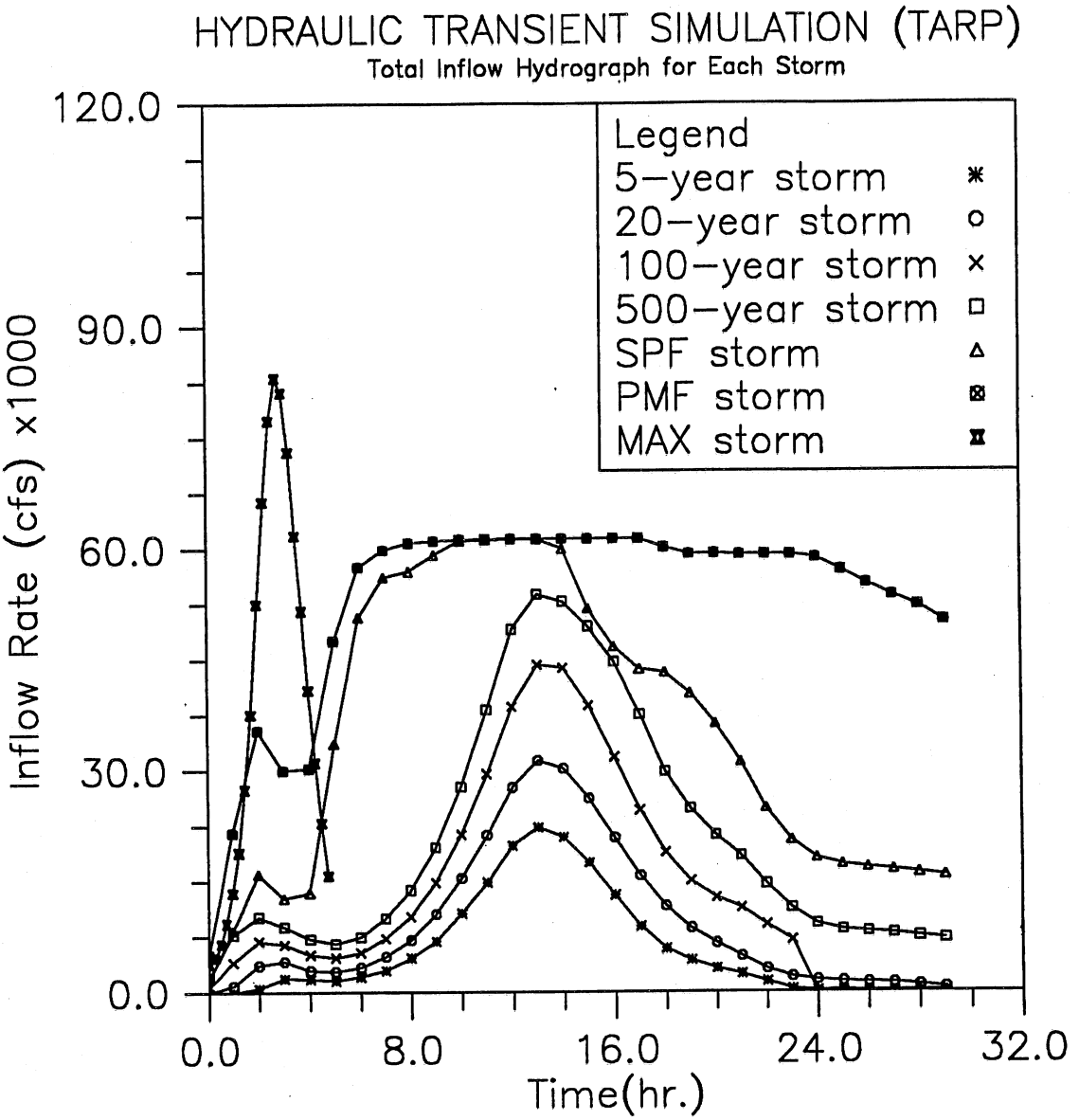

Fig. 2.3 Total inflow rate of the hydrographs (5-year, 20-year, 100-year, 500-year, SPF, PMF, and MAX) used in the modeling study

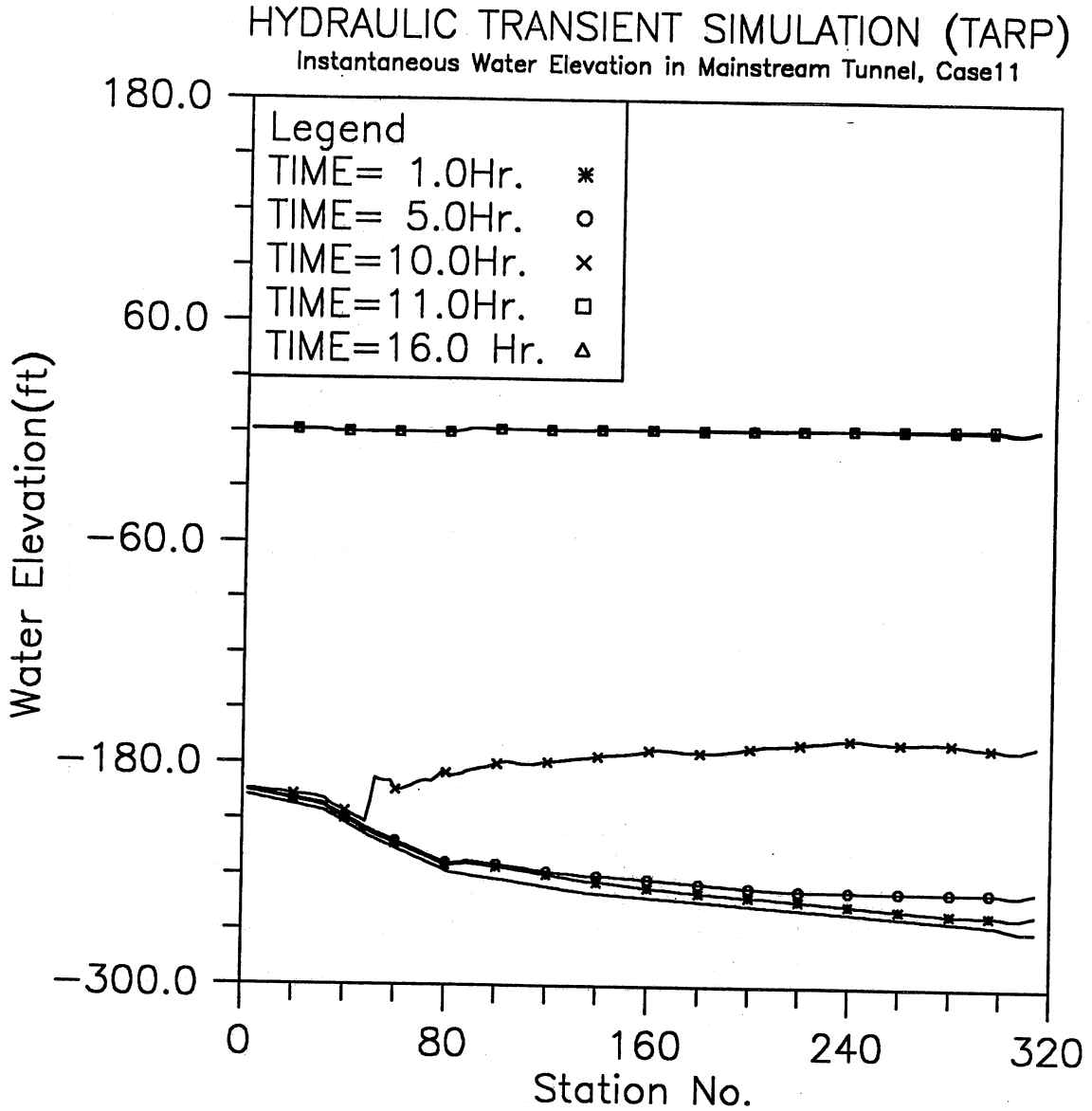

Fig. 3.1(a) Instantaneous hydraulic gradelines along the main tunnel; Modeling case: closed main gate and 5-year storm event (Case 1-1)

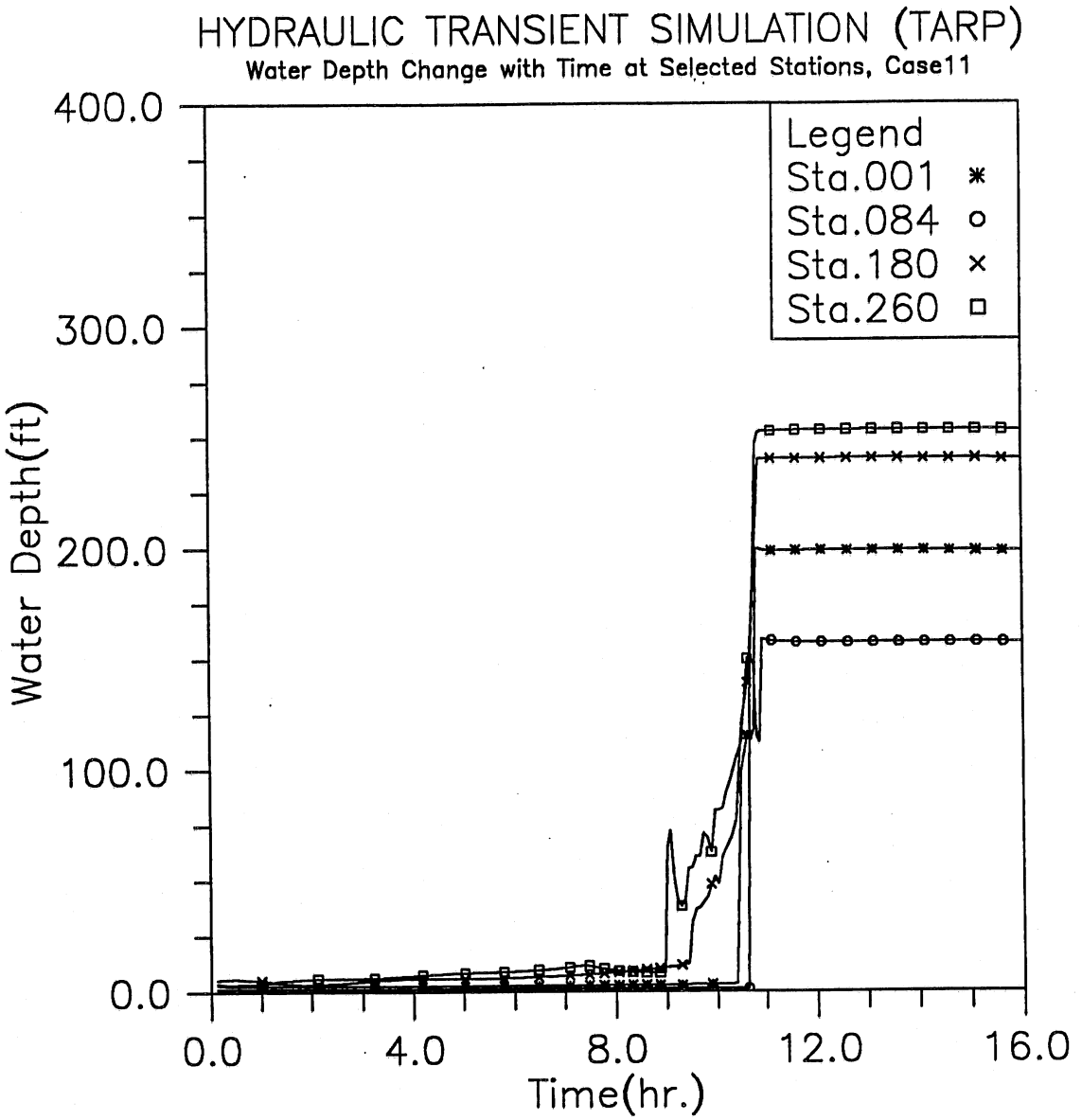

Fig. 3.1(b) Time variation of water depth at four upstream locations; Modeling case: closed main gate and 5–year storm event (Case 1–1)

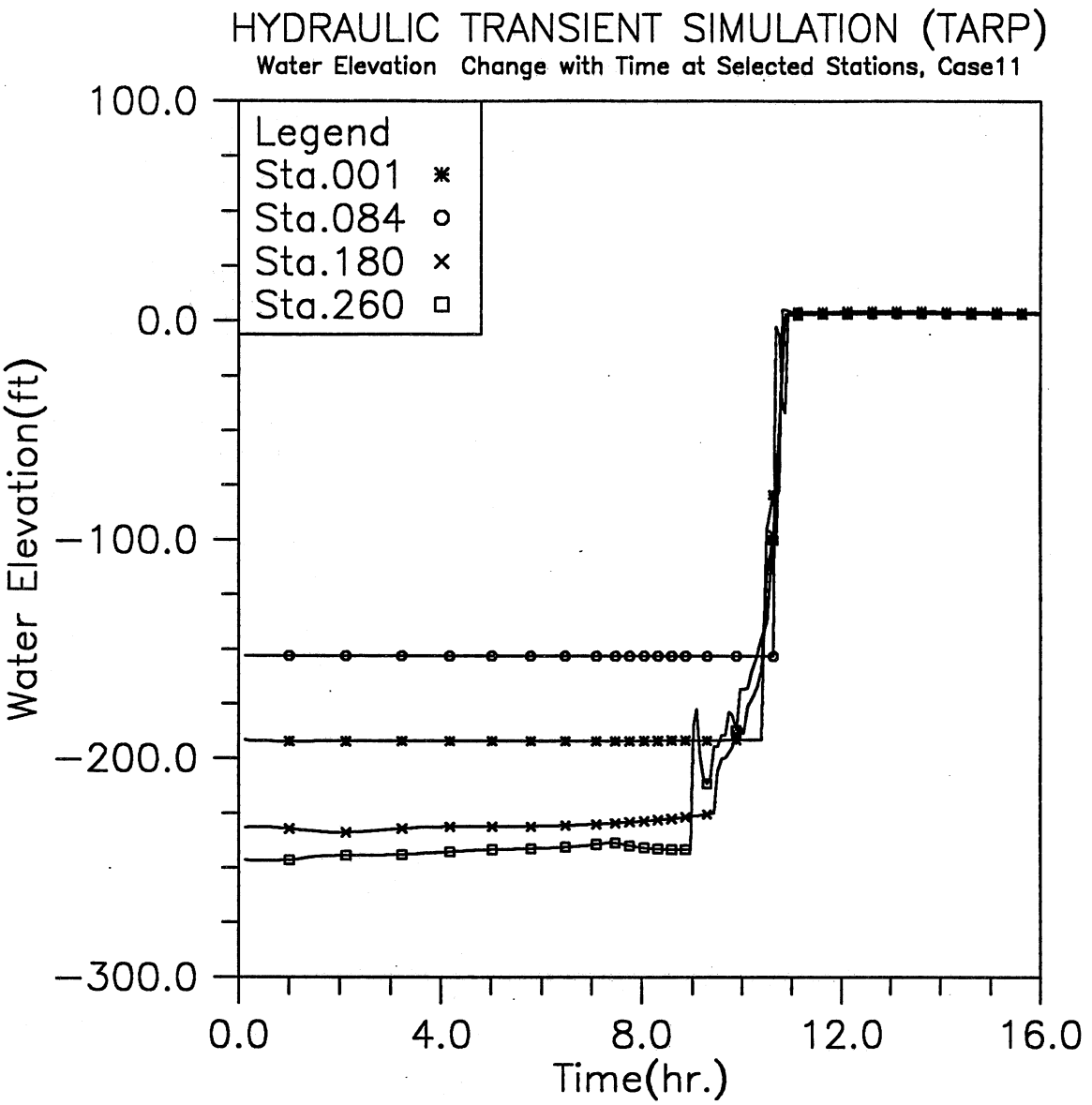

Fig. 3.1(c) Time variation of water elevation at four upstream locations; Modeling case: closed main gate and 5–year storm event (Case 1–1)

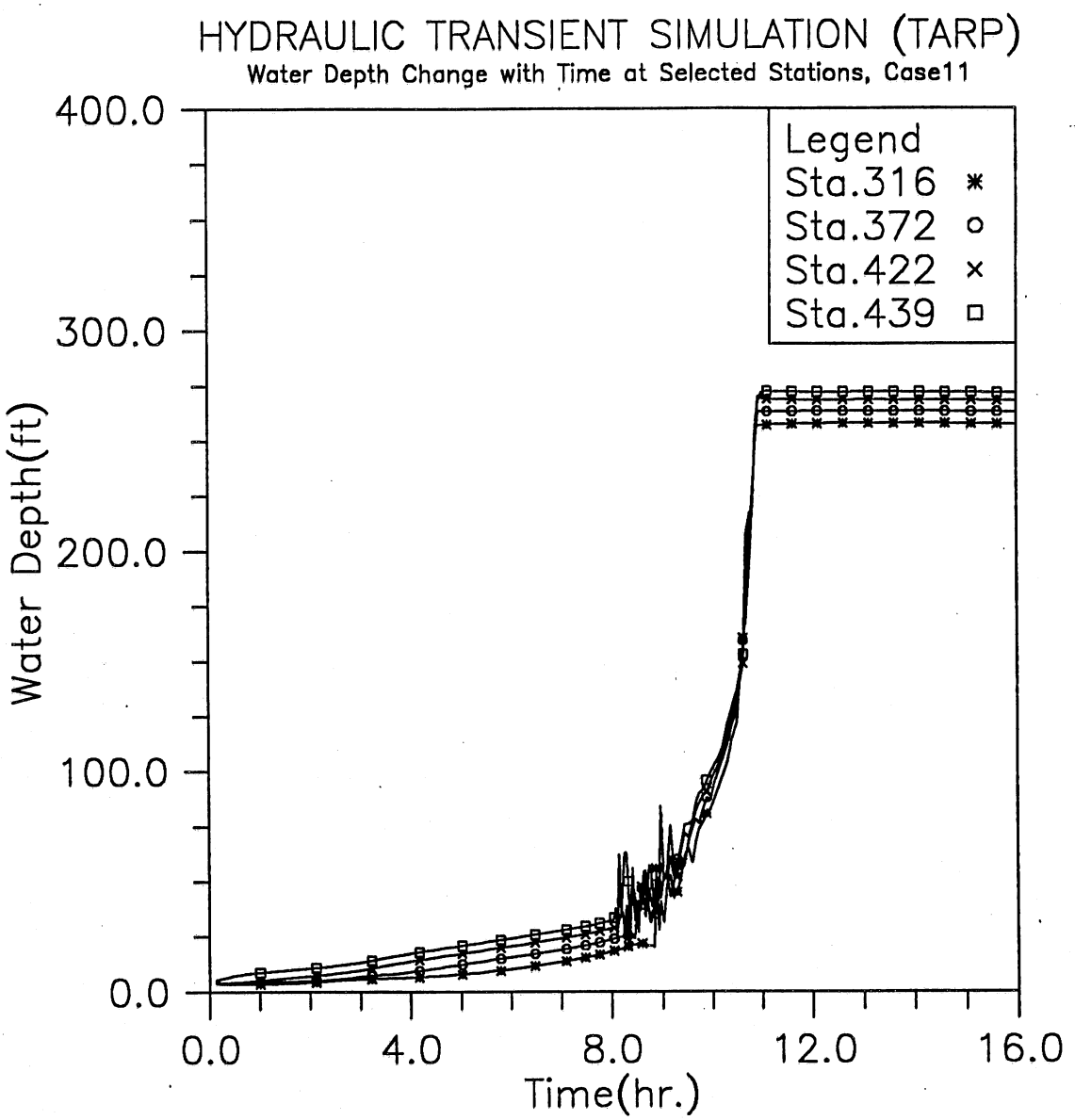

Fig. 3.1(d) Time variation of water depth at four downstream locations; Modeling case: closed main gate and 5–year storm event (Case 1–1)

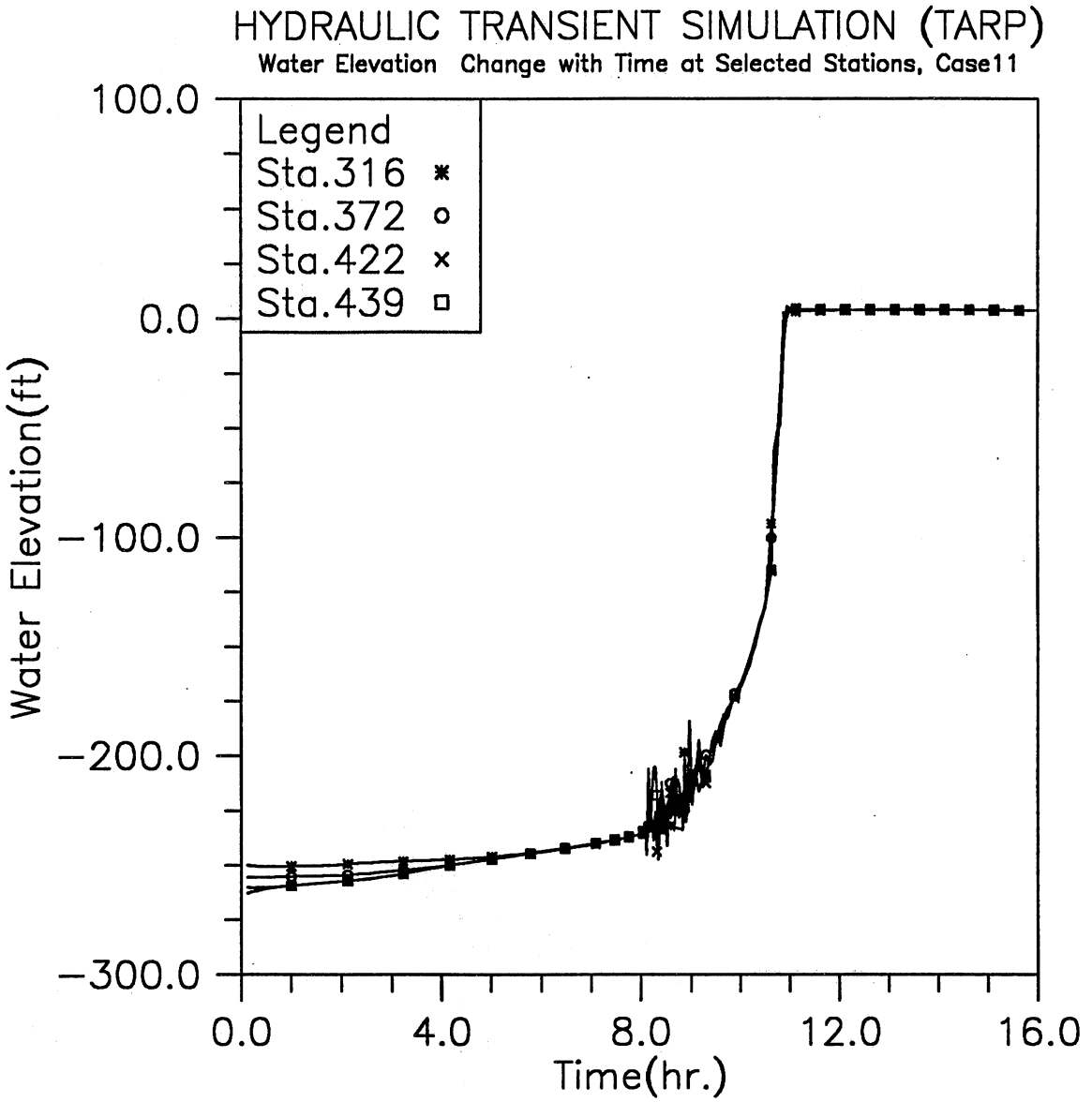

Fig. 3.1(e) Time variation of water elevation at four downstream locations; Modeling case: closed main gate and 5–year storm event (Case 1–1)

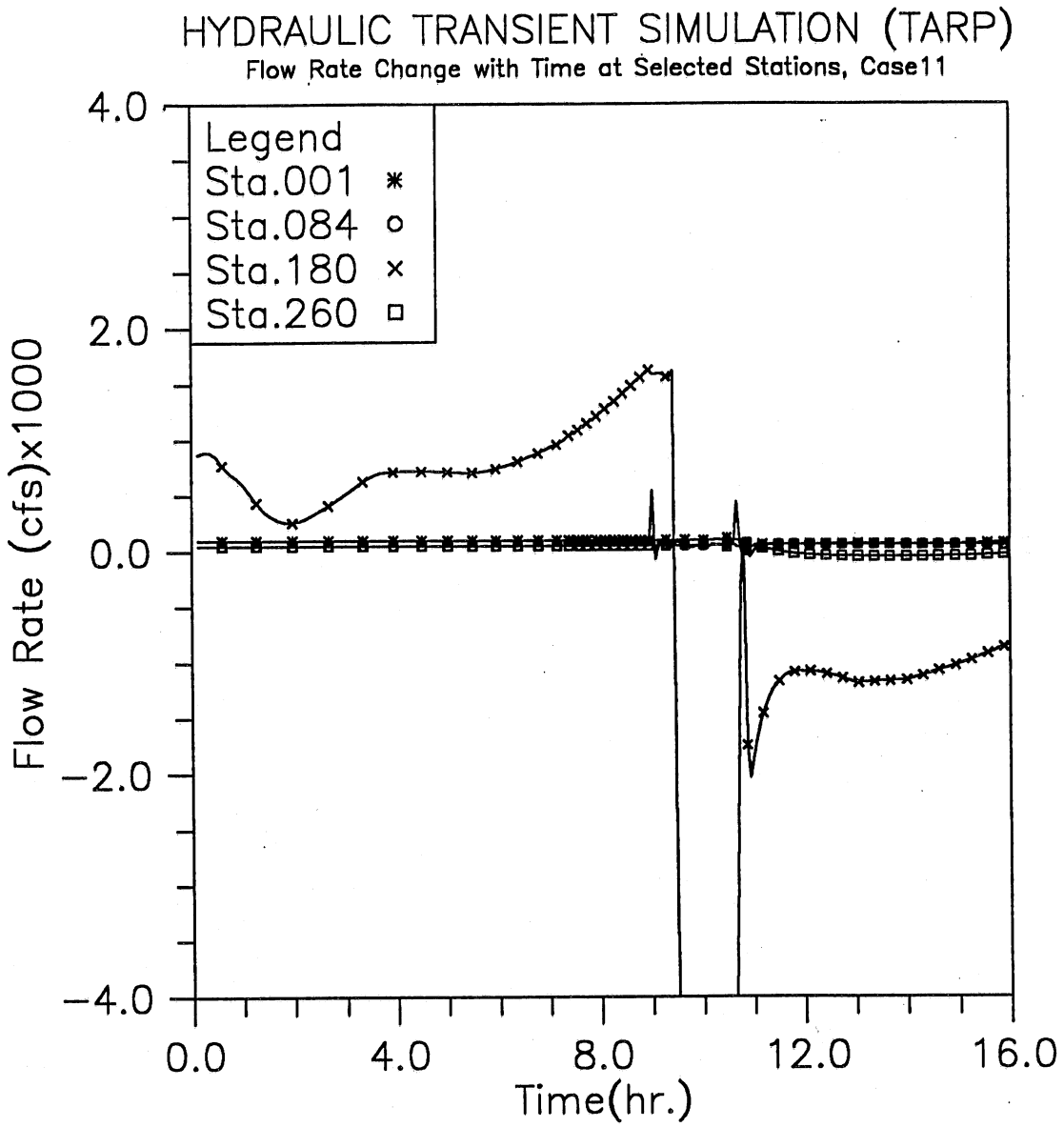

Fig. 3.1(f) Time variation of flow rate at four upstream locations; Modeling case: closed main gate and 5–year storm event (Case 1–1)

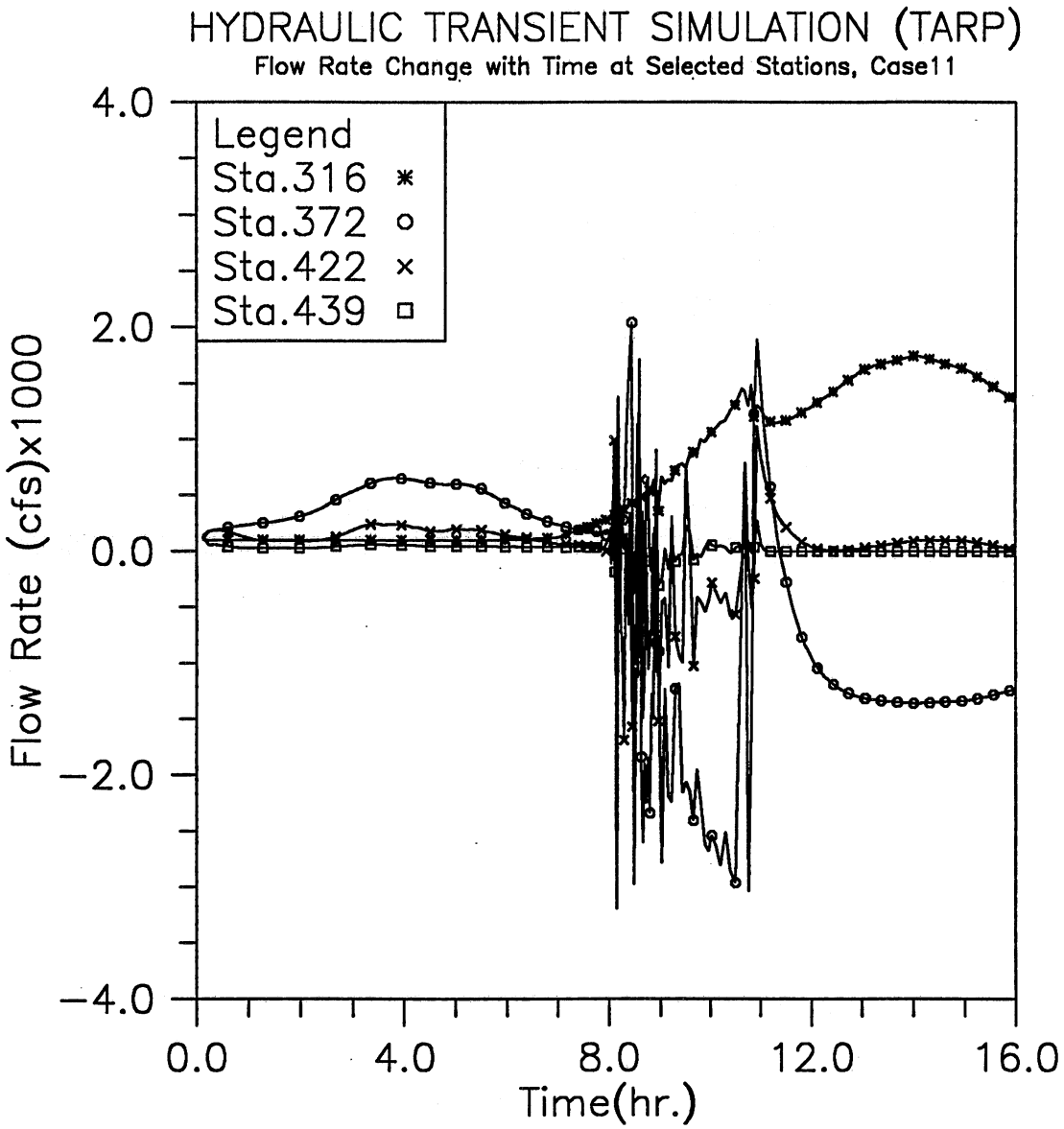

Fig. 3.1(g) Time variation of flow rate at four downstream locations; Modeling case: closed main gate and 5–year storm event (Case 1–1)

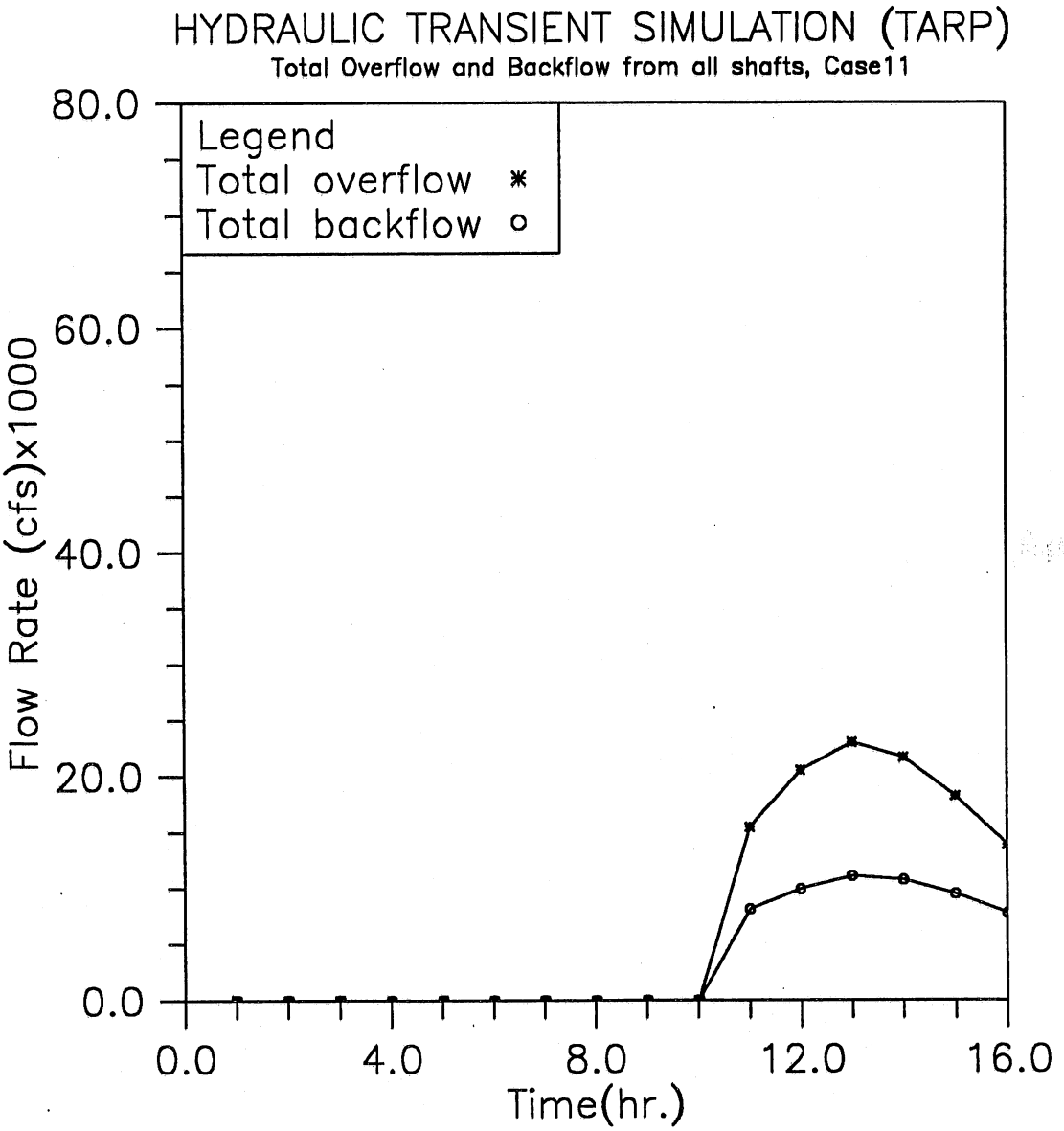

Fig. 3.1(h) Time variation of total overflow and backflow; Modeling case: closed main gate and 5–year storm event (Case 1–1)

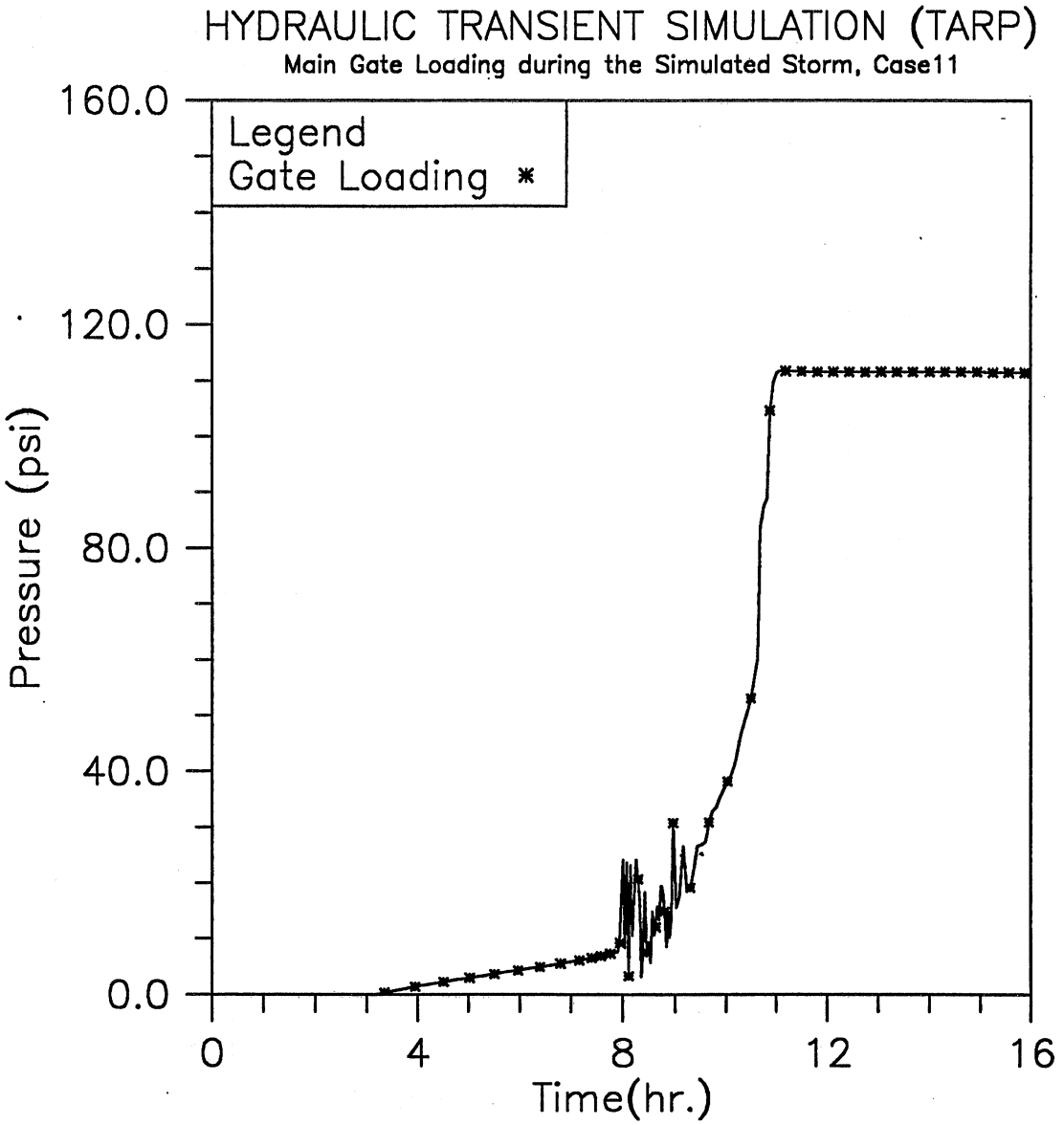

Fig. 3.1(i) Time variation of the averaged loading on the main gate; Modeling case: closed main gate and 5–year storm event (Case 1–1)

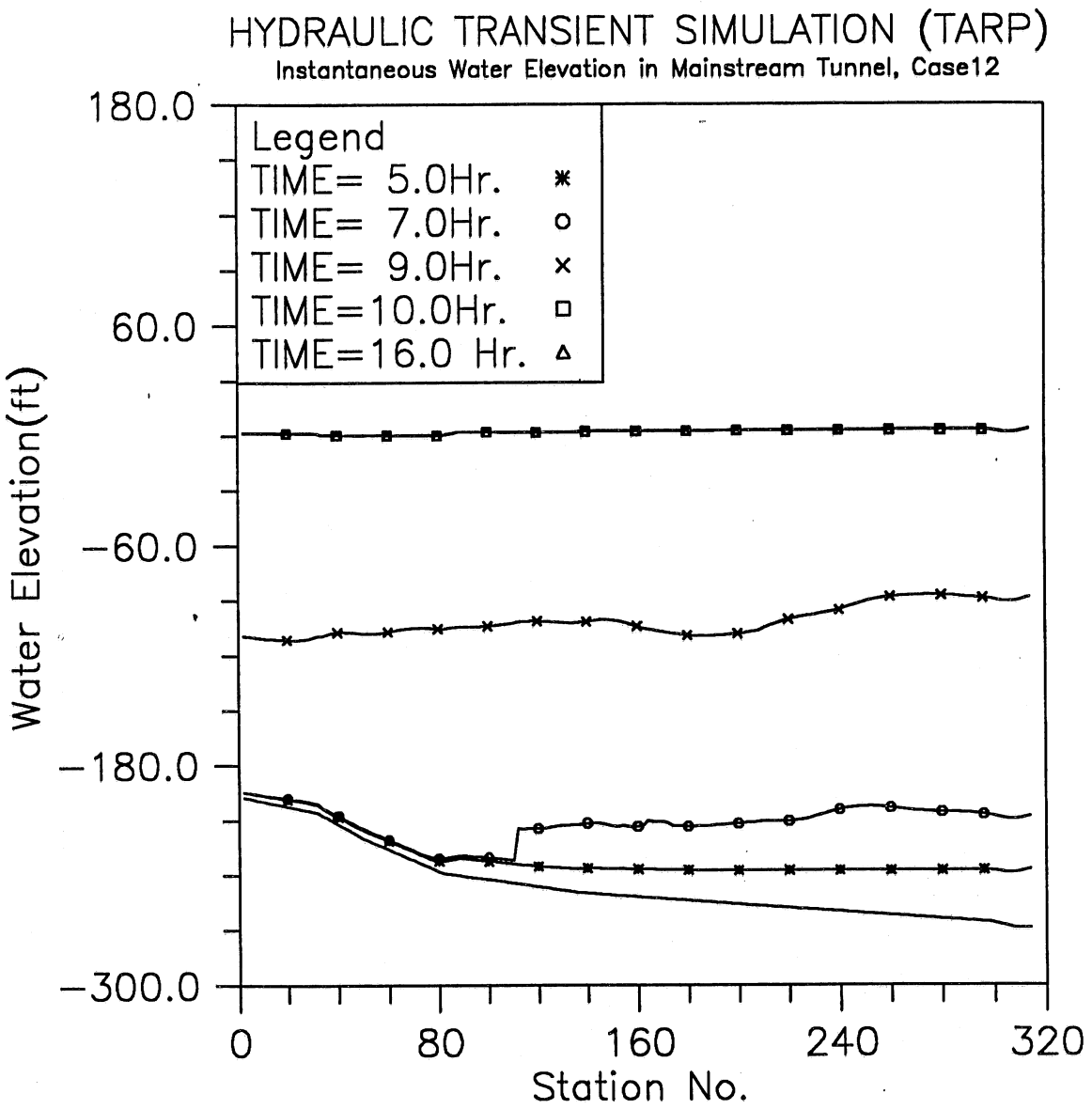

Fig. 3.2(a) Instantaneous hydraulic gradelines along the main tunnel; Modeling case: closed main gate and 10-year storm event (Case 1-2)

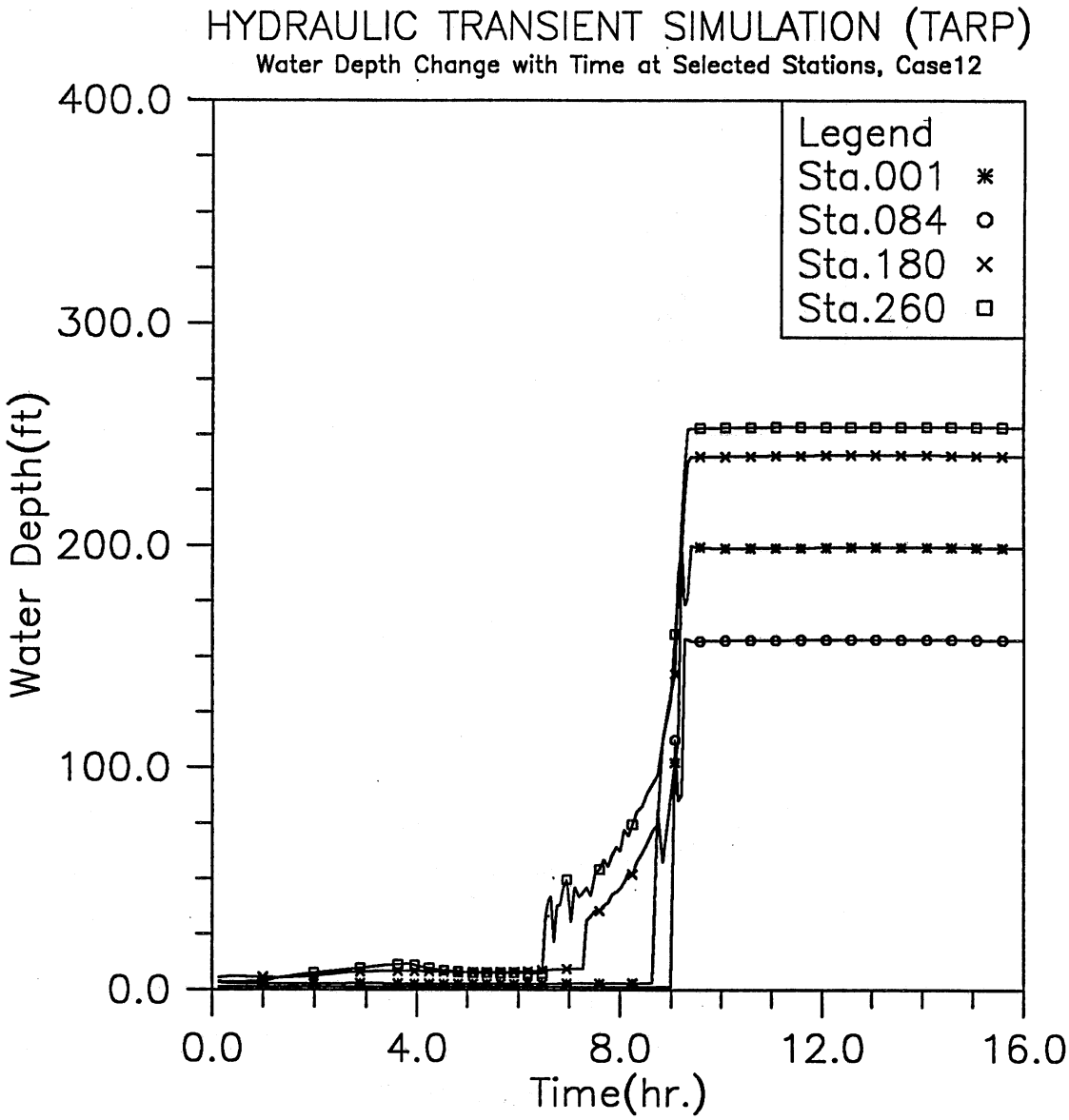

Fig. 3.2(b) Time variation of water depth at four upstream locations; Modeling case: closed main gate and 20–year storm event (Case 1–2)

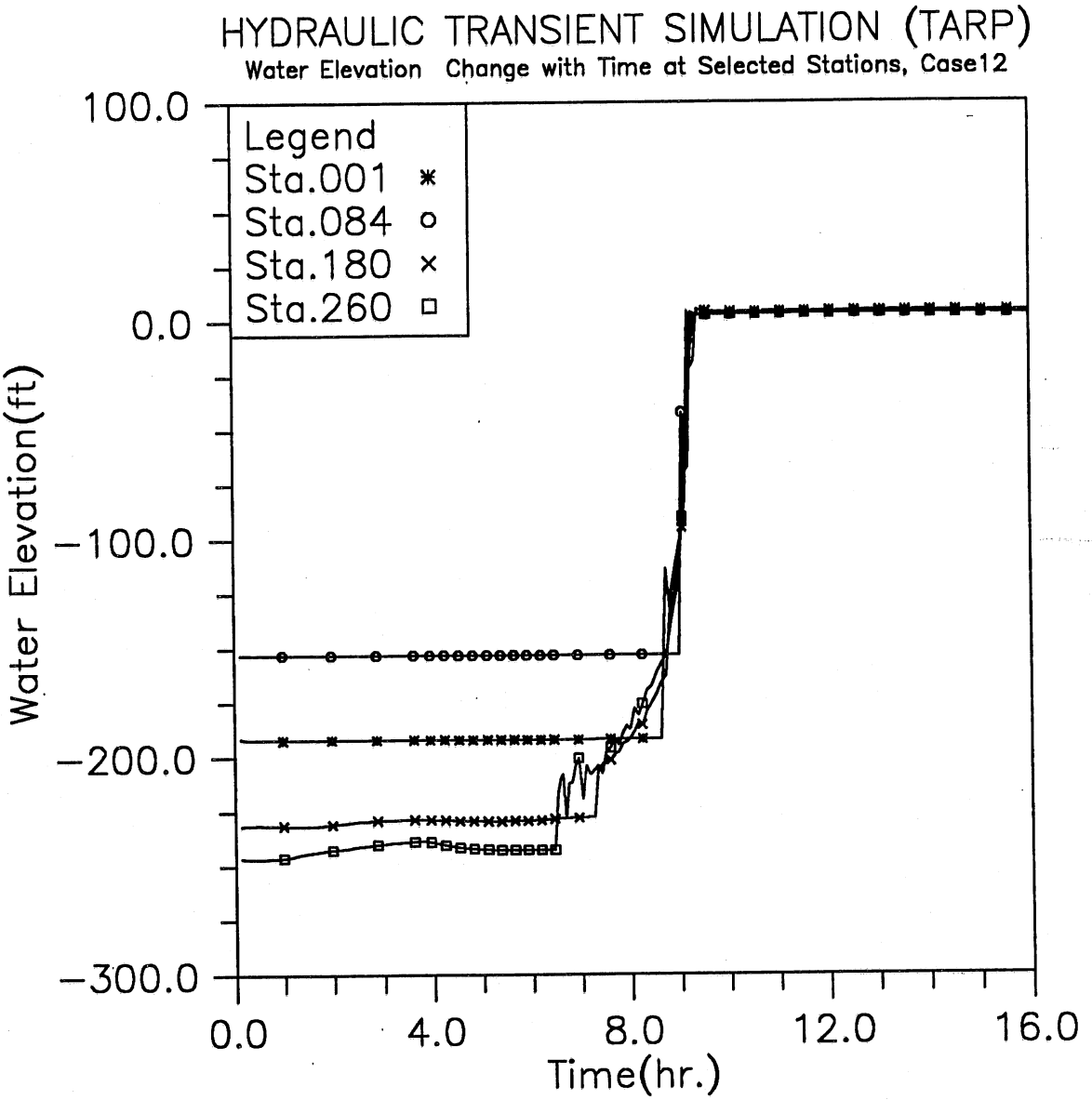

Fig. 3.2(c) Time variation of water elevation at four upstream locations; Modeling case: closed main gate and 20–year storm event (Case 1–2)

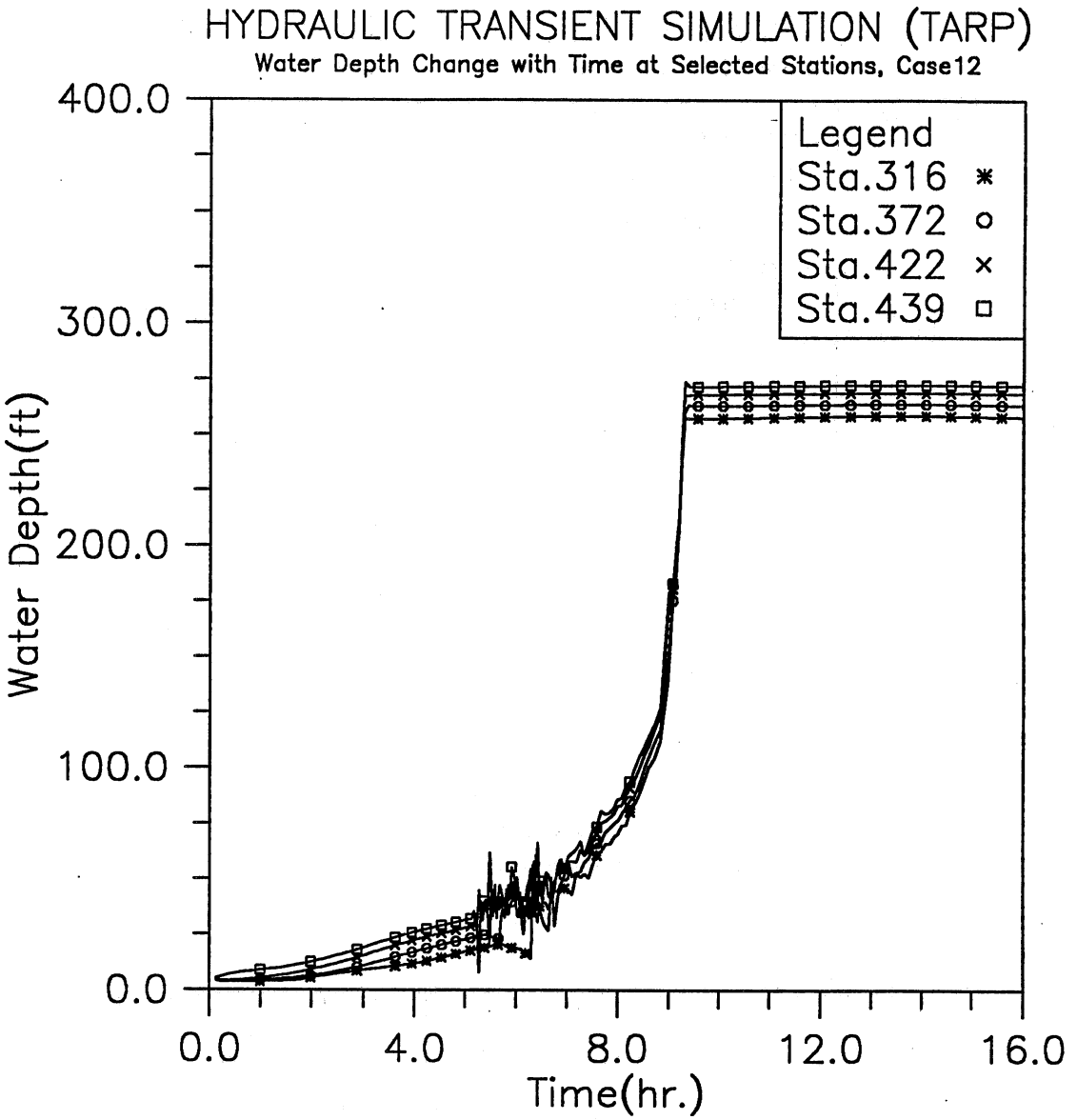

Fig. 3.2(d) Time variation of water depth at four downstream locations; Modeling case: closed main gate and 20-year storm event (Case 1-2)

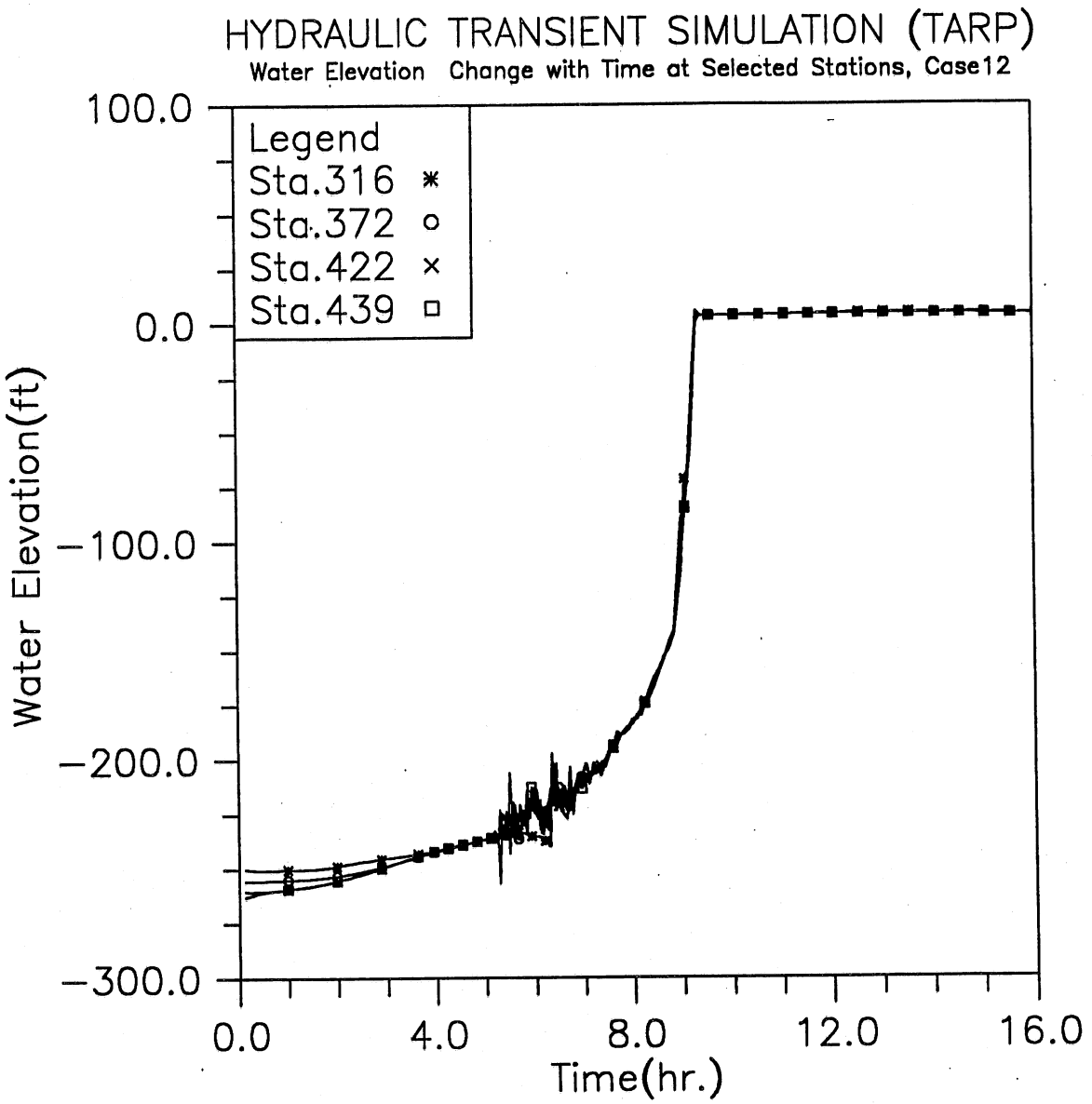

Fig. 3.2(e) Time variation of water elevation at four downstream locations; Modeling case: closed main gate and 20–year storm event (Case 1–2)

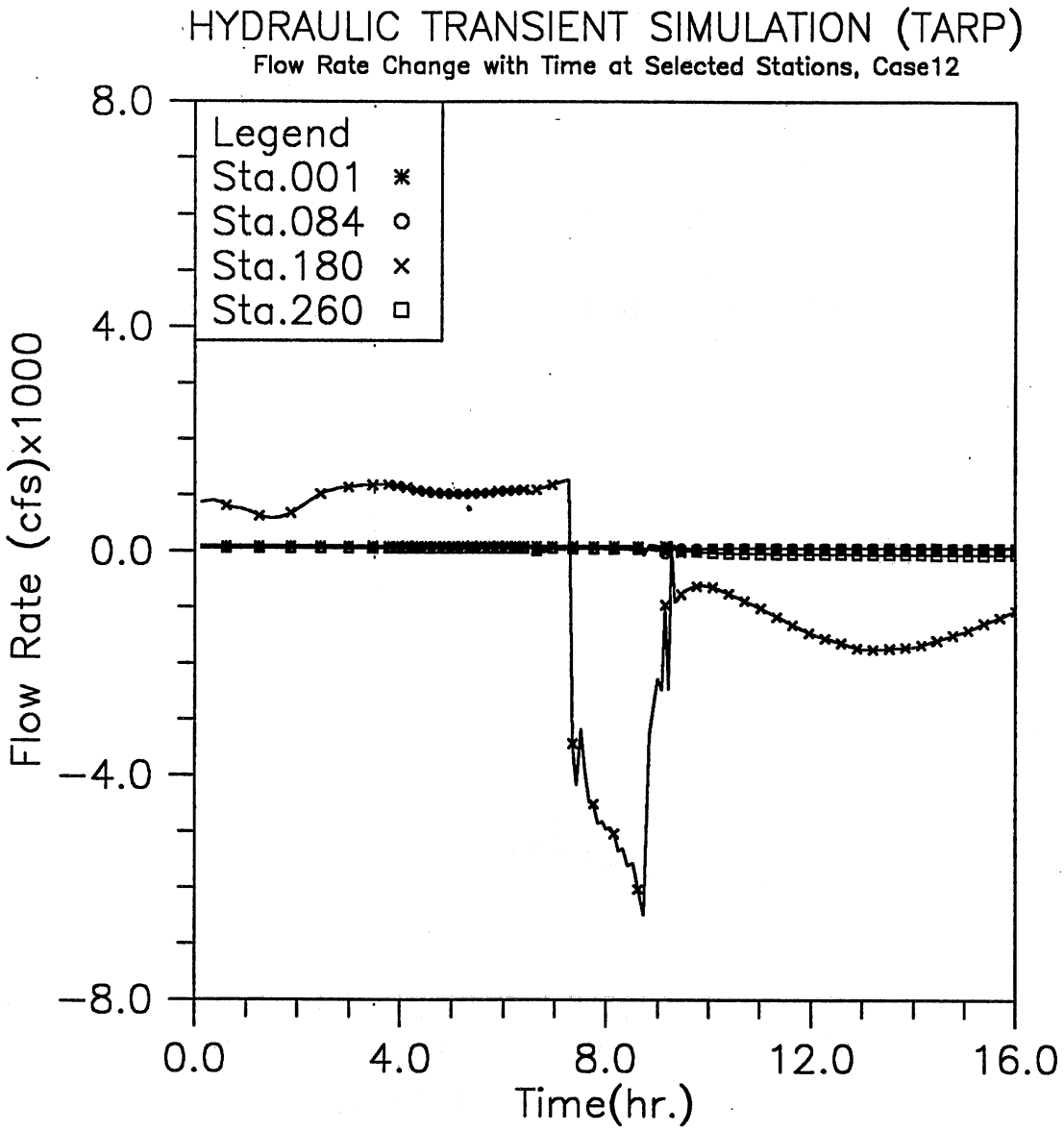

Fig. 3.2(f) Time variation of flow rate at four upstream locations; Modeling case: closed main gate and 20–year storm event (Case 1–2)

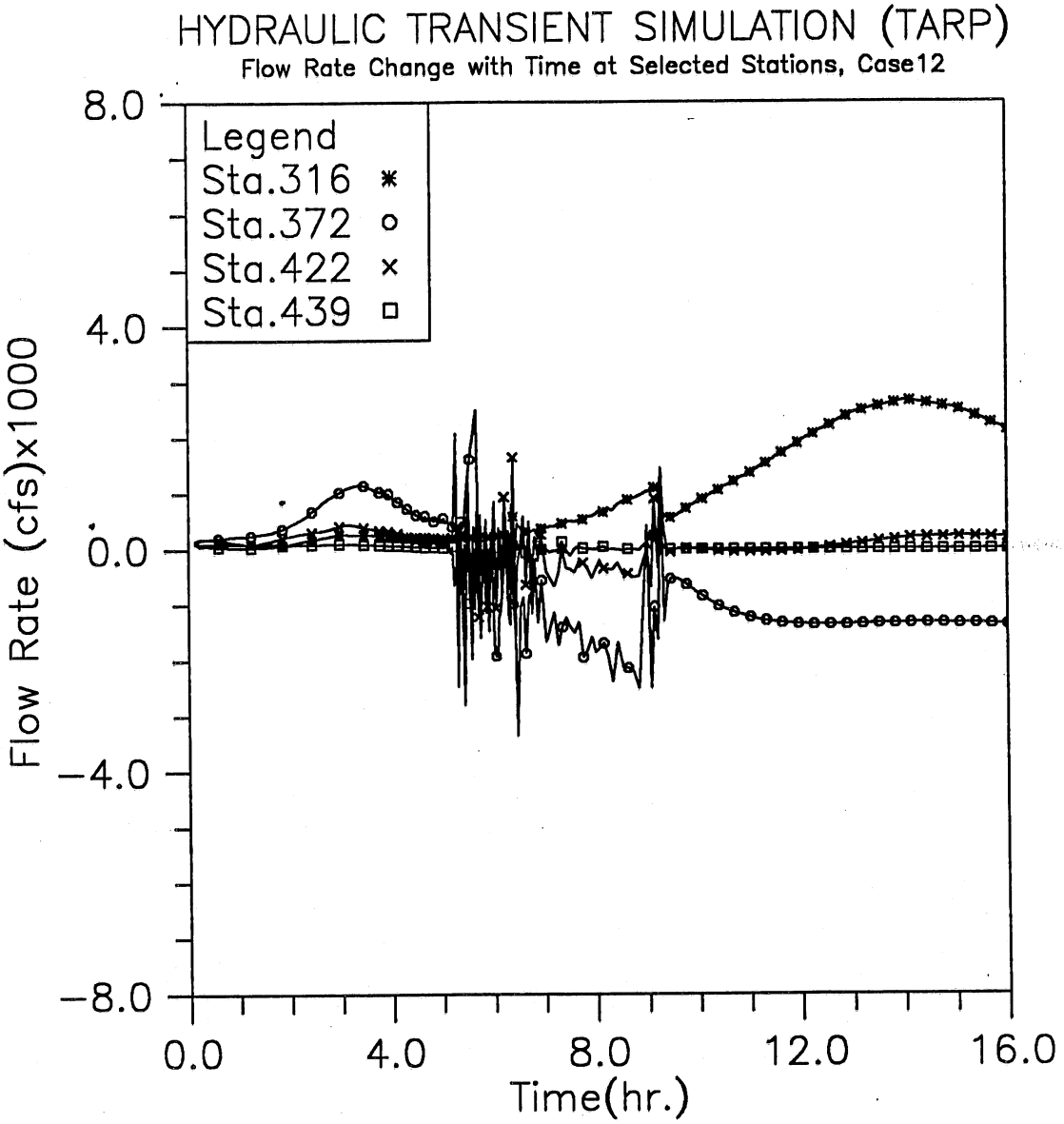

Fig. 3.2(g) Time variation of flow rate at four downstream locations; Modeling case: closed main gate and 20–year storm event (Case 1–2)

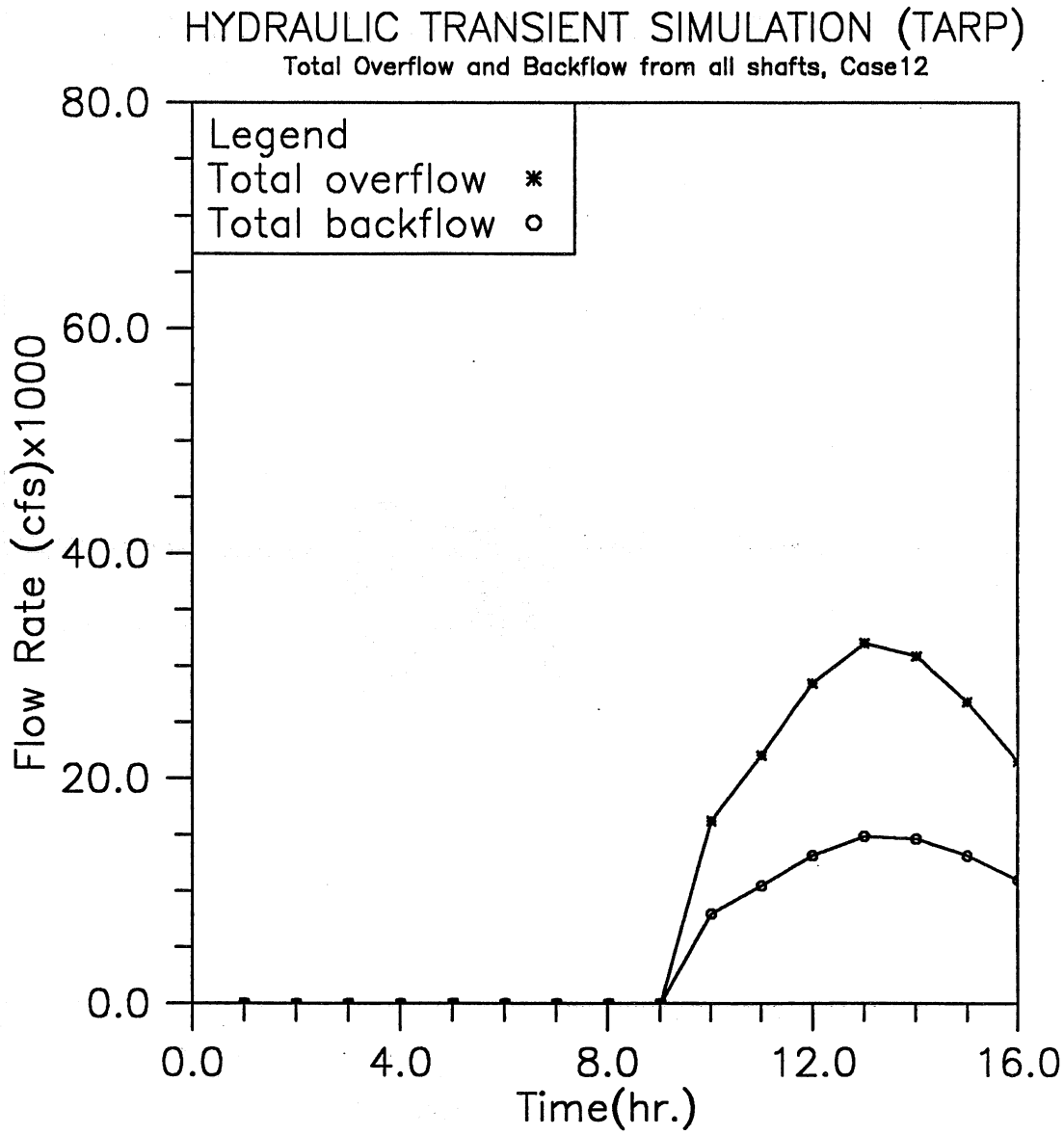

Fig. 3.2(h) Time variation of total overflow and backflow; Modeling case: closed main gate and 20–year storm event (Case 1–2)

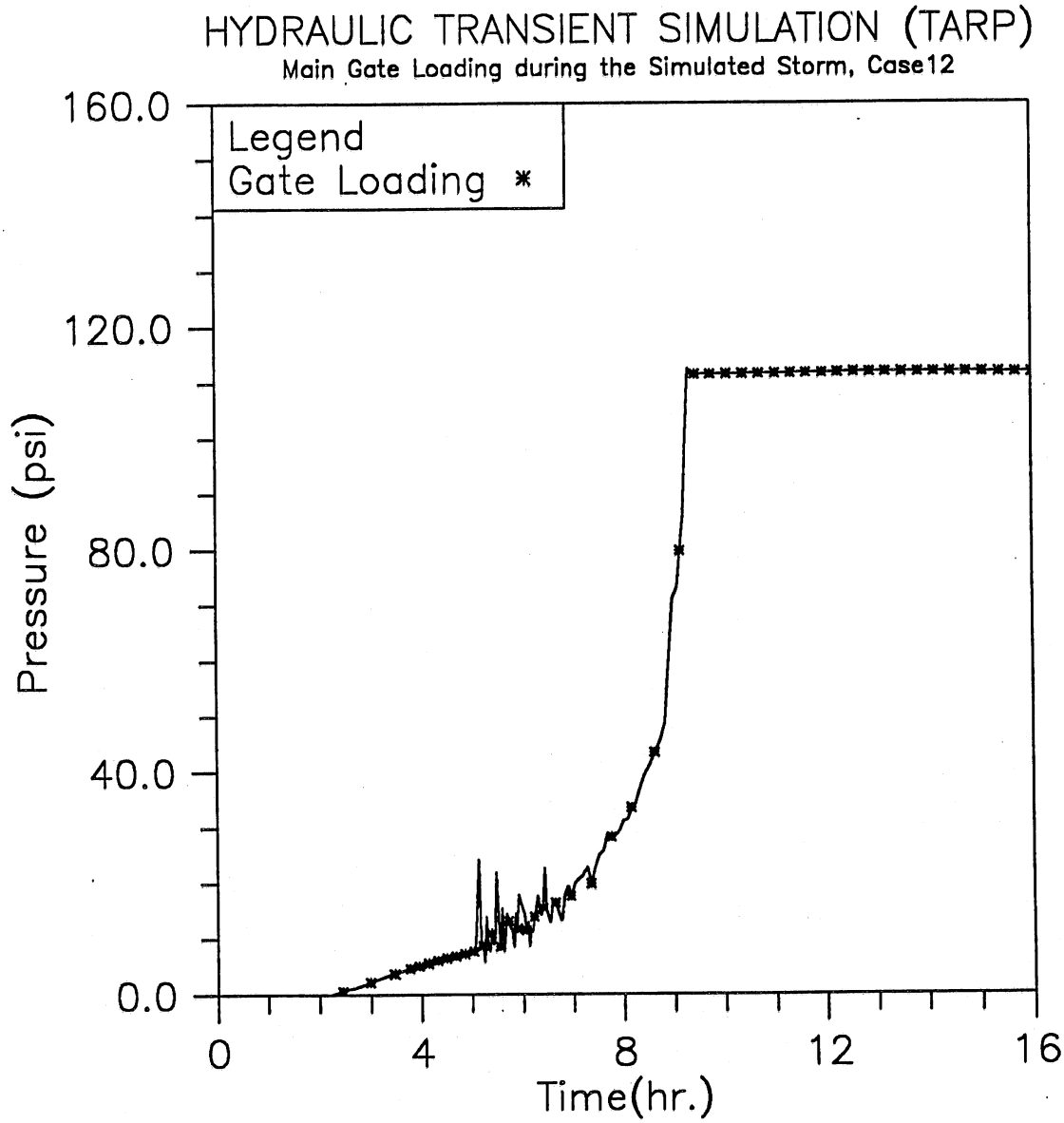

Fig. 3.2(i) Time variation of the averaged loading on the main gate; Modeling case: closed main gate and 20–year storm event (Case 1–2)

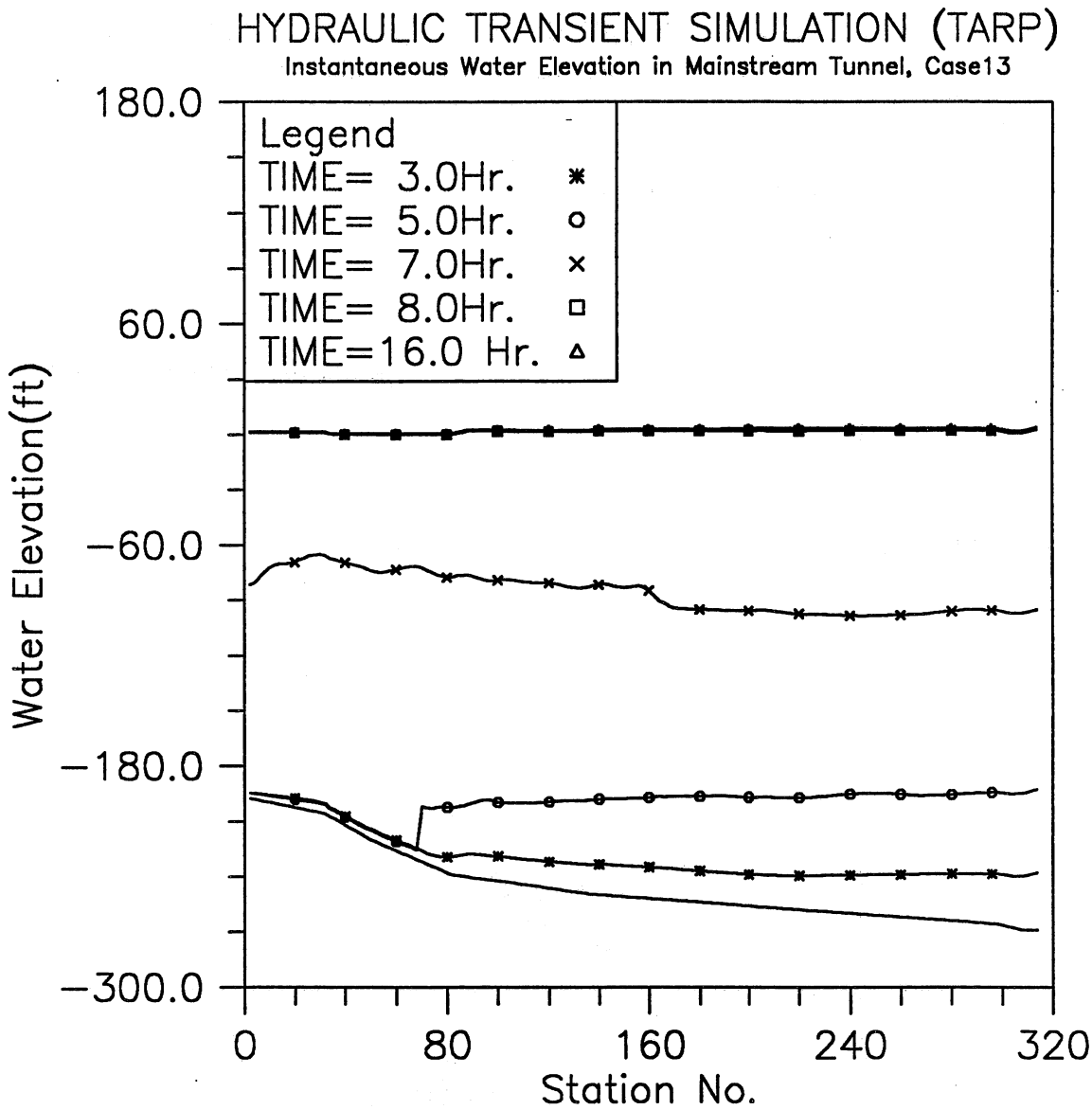

Fig. 3.3(a) Instantaneous hydraulic gradelines along the main tunnel; Modeling case: closed main gate and 100–year storm event (Case 1–3)

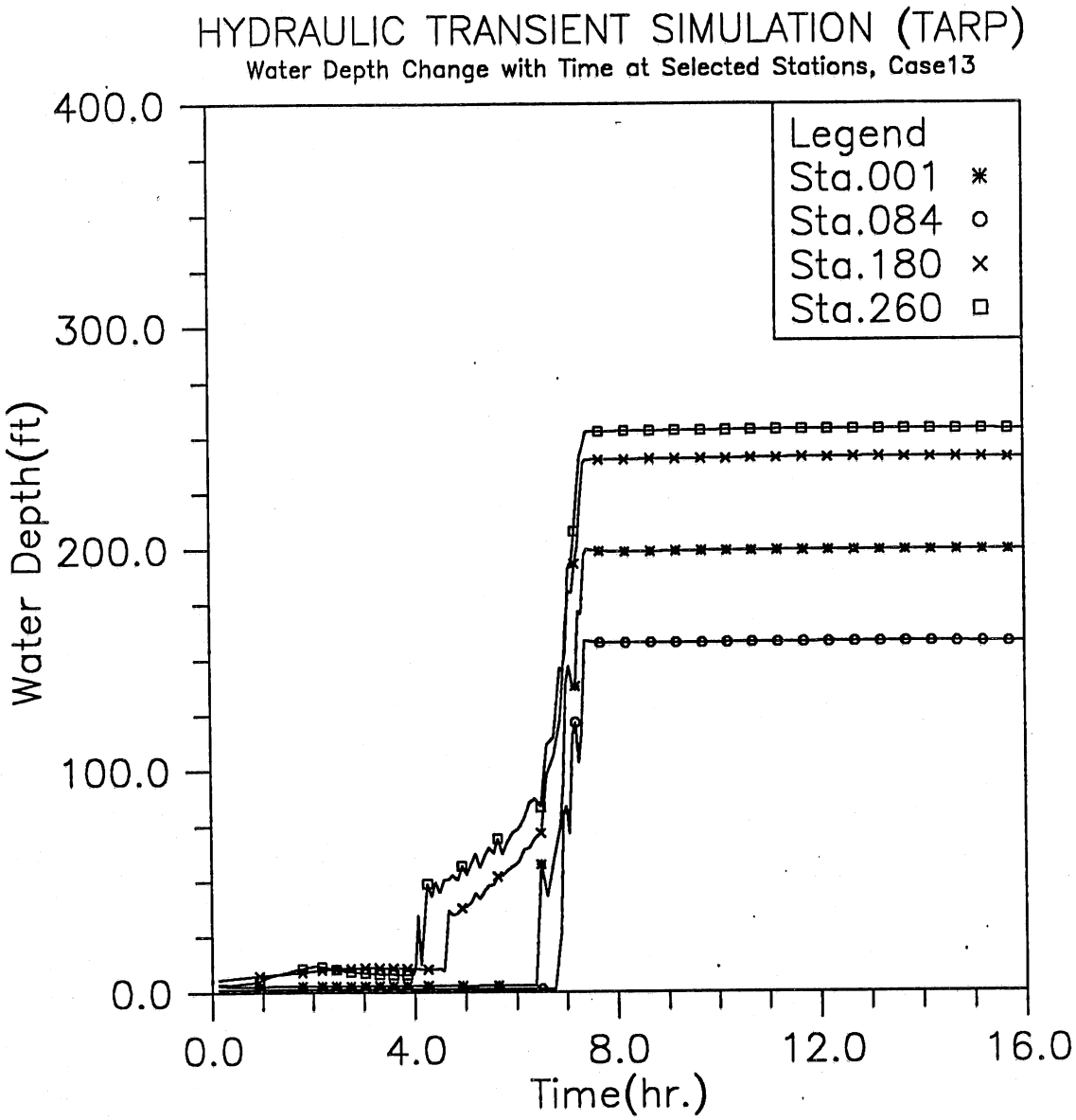

Fig. 3.3(b) Time variation of water depth at four upstream locations; Modeling case: closed main gate and 100–year storm event (Case 1–3)

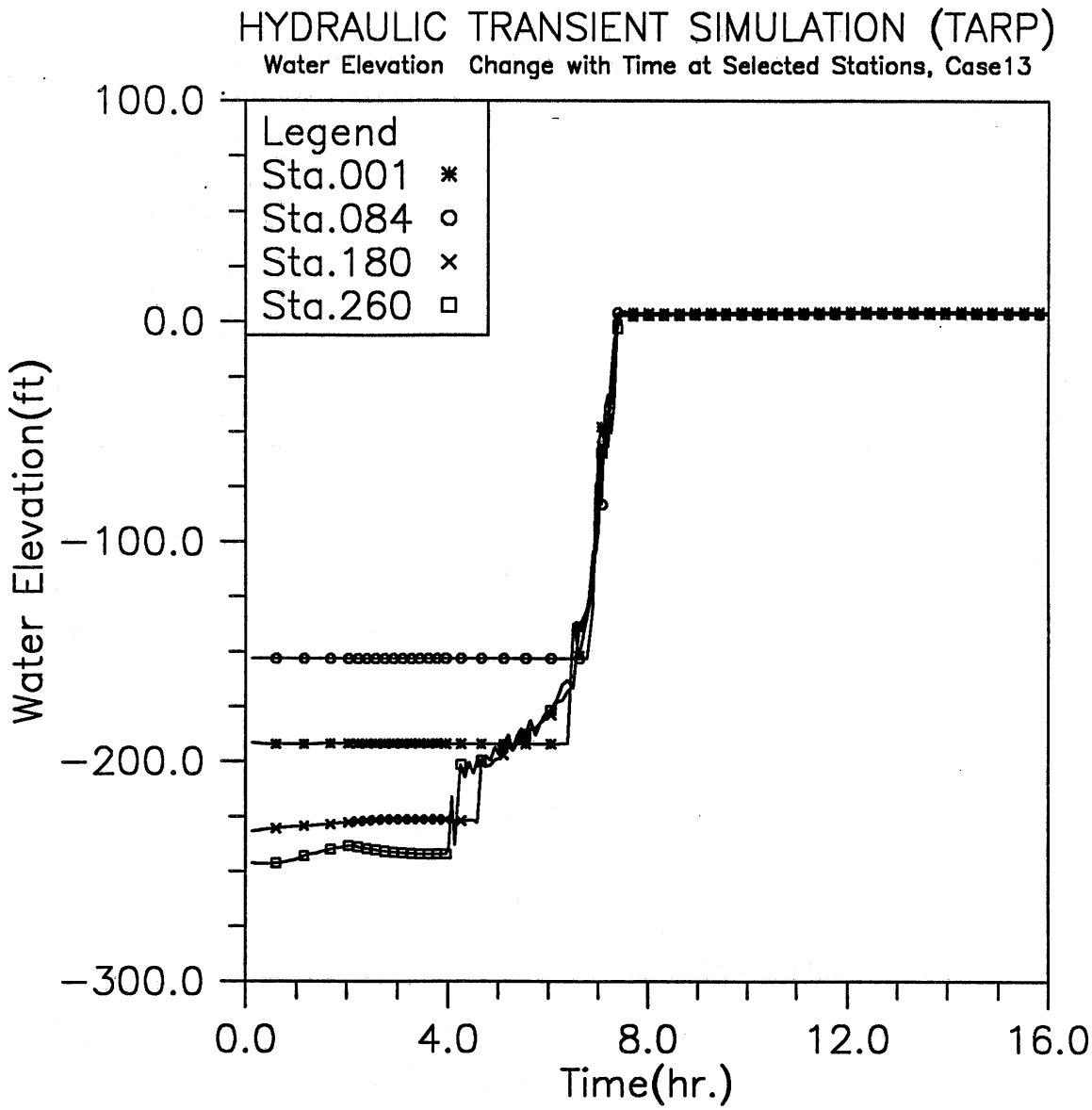

Fig. 3.3(c) Time variation of water elevation at four upstream locations; Modeling case: closed main gate and 100–year storm event (Case 1–3)

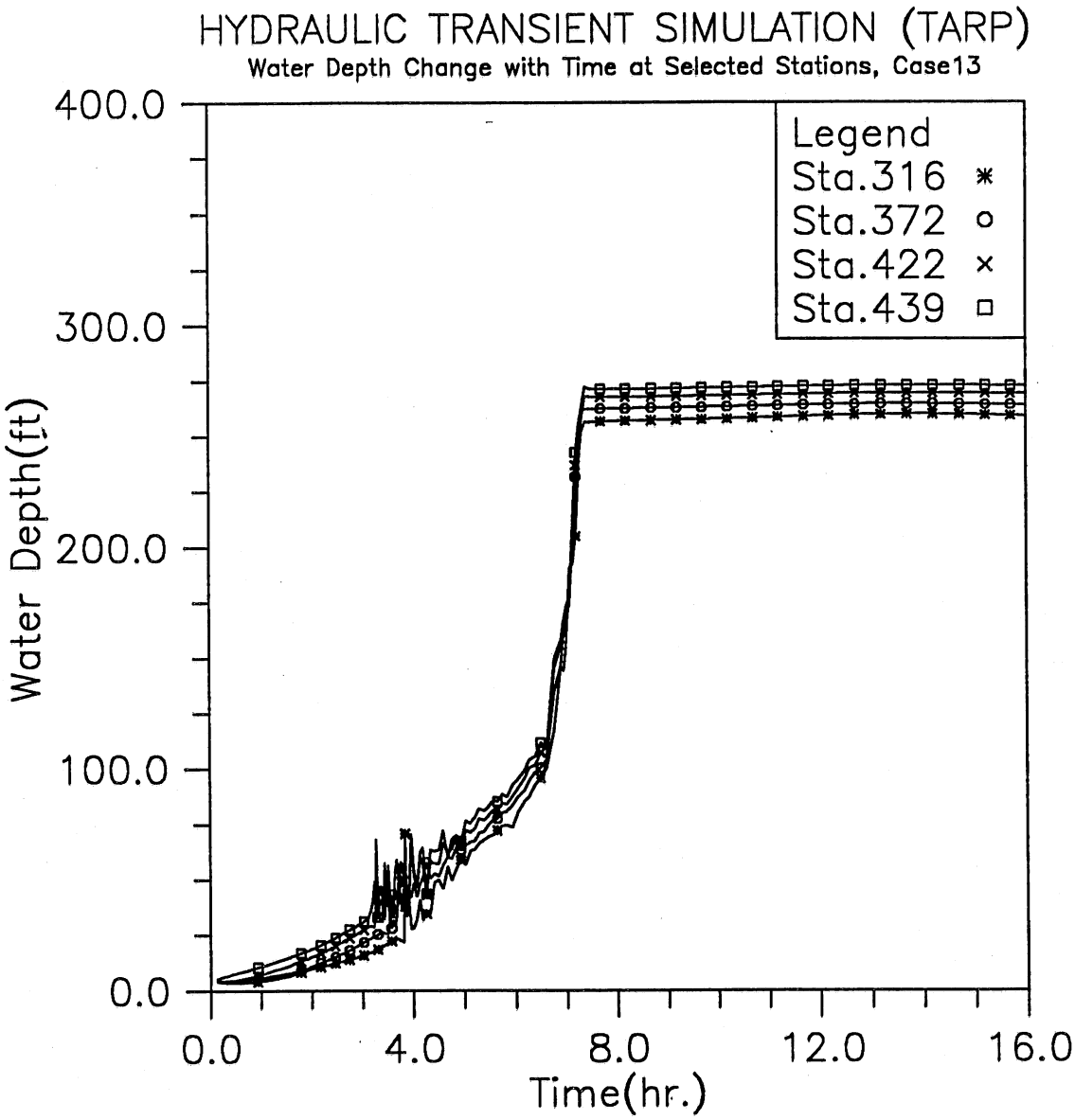

Fig. 3.3(d) Time variation of water depth at four downstream locations; Modeling case: closed main gate and 100–year storm event (Case 1–3)

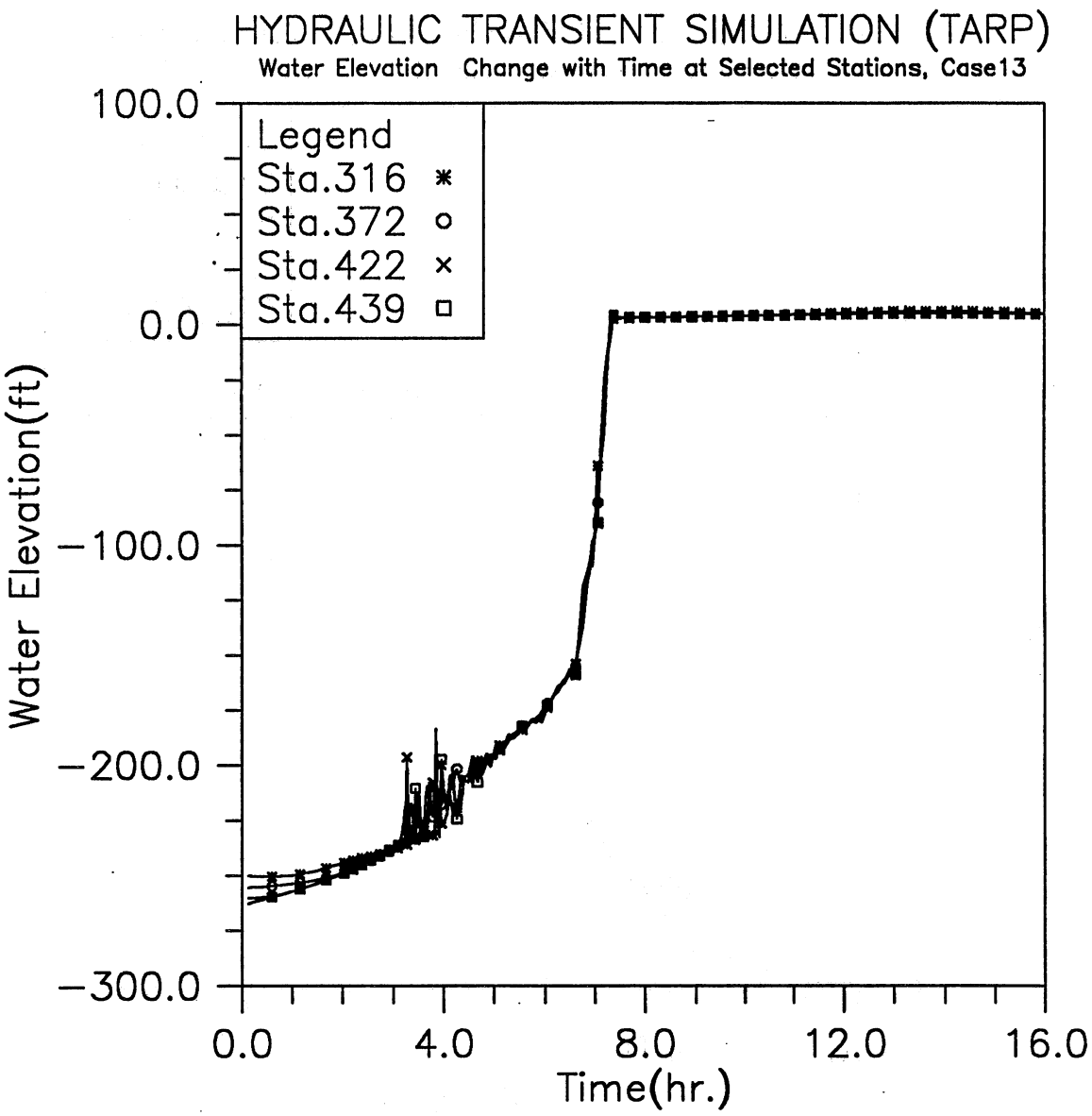

Fig. 3.3(e) Time variation of water elevation at four downstream locations; Modeling case: closed main gate and 100–year storm event (Case 1–3)

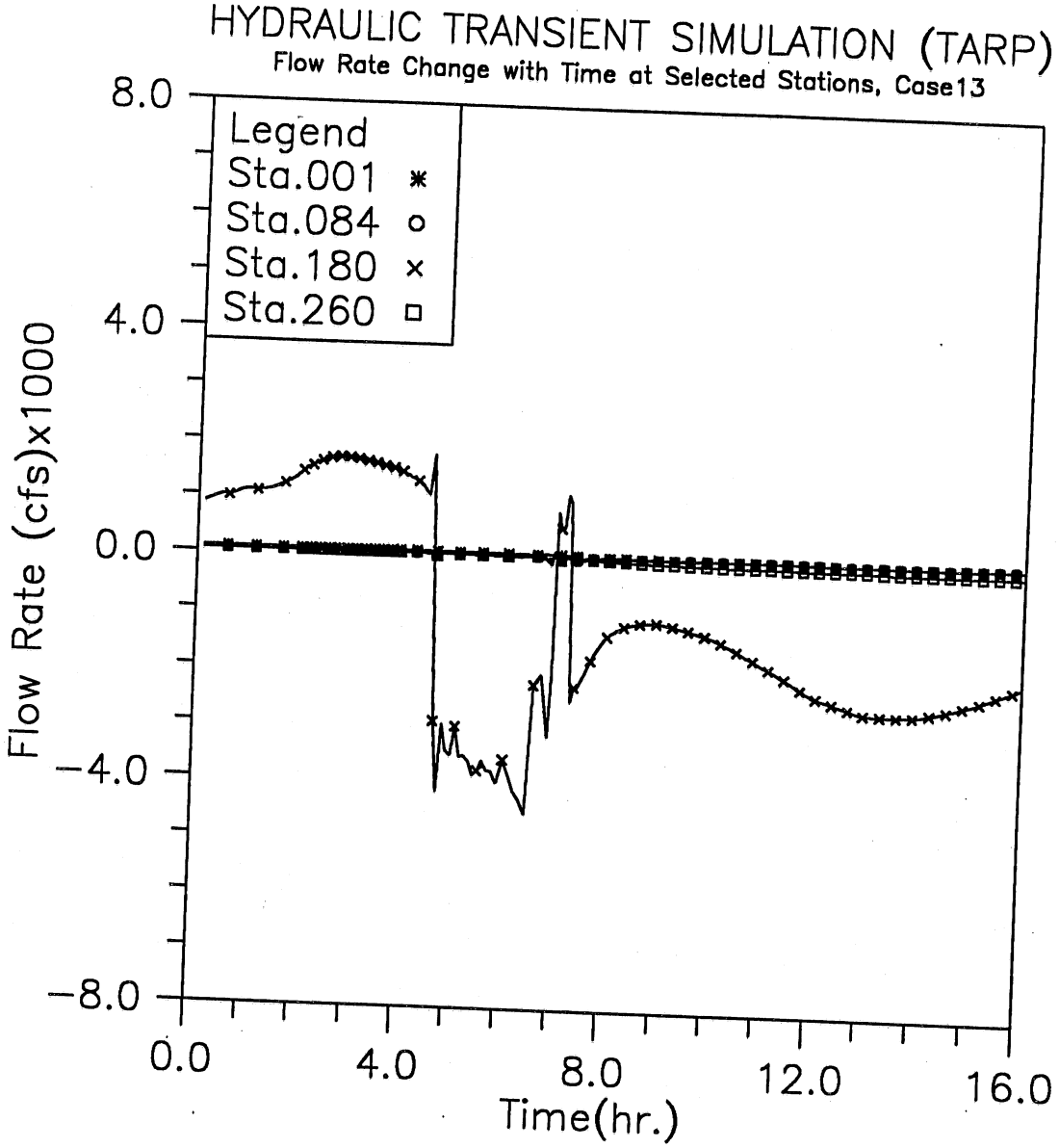

Fig. 3.3(f) Time variation of flow rate at four upstream locations; Modeling case: closed main gate and 100–year storm event (Case 1–3)

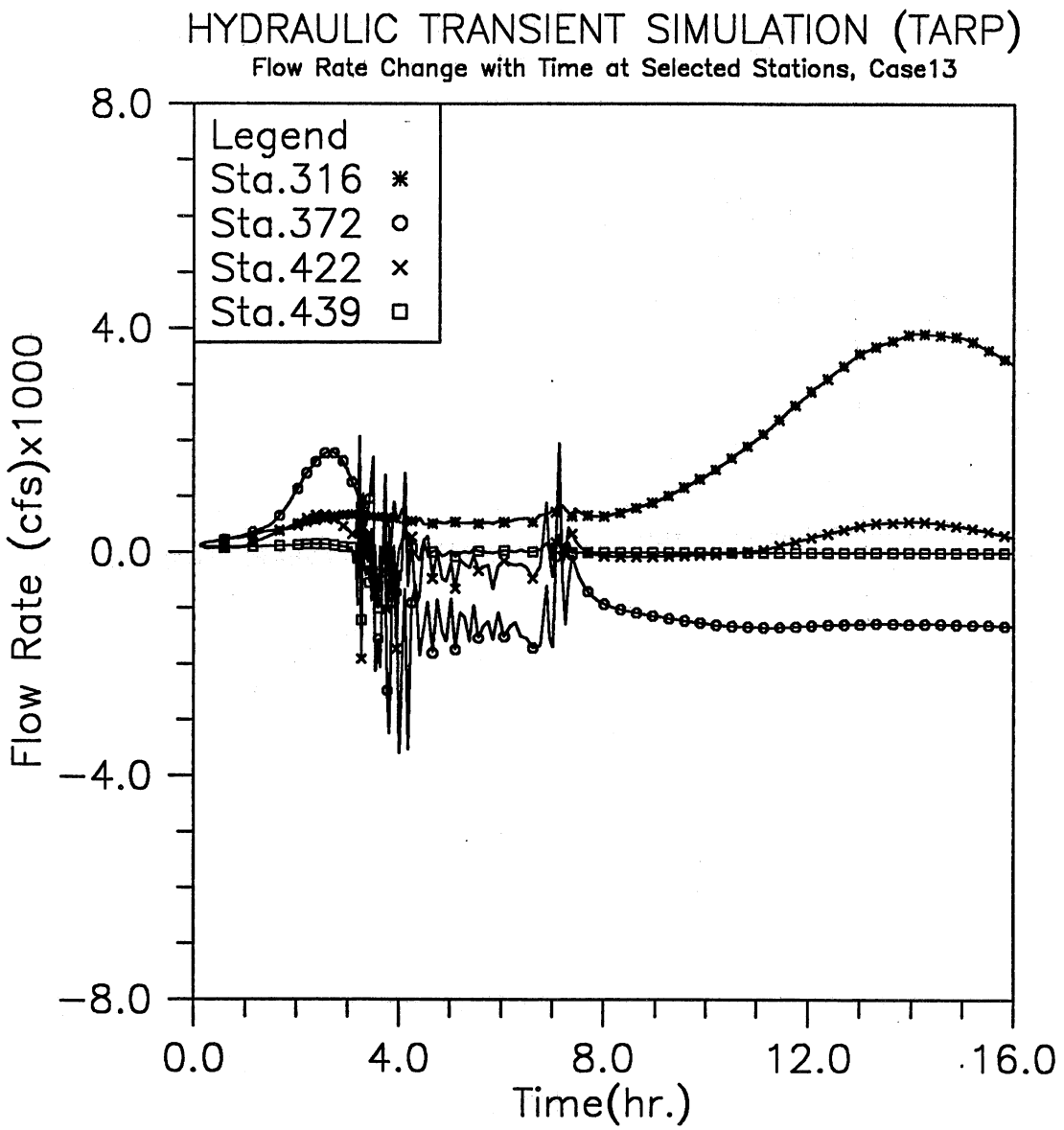

Fig. 3.3(g) Time variation of flow rate at four downstream locations; Modeling case: closed main gate and 100–year storm event (Case 1–3)

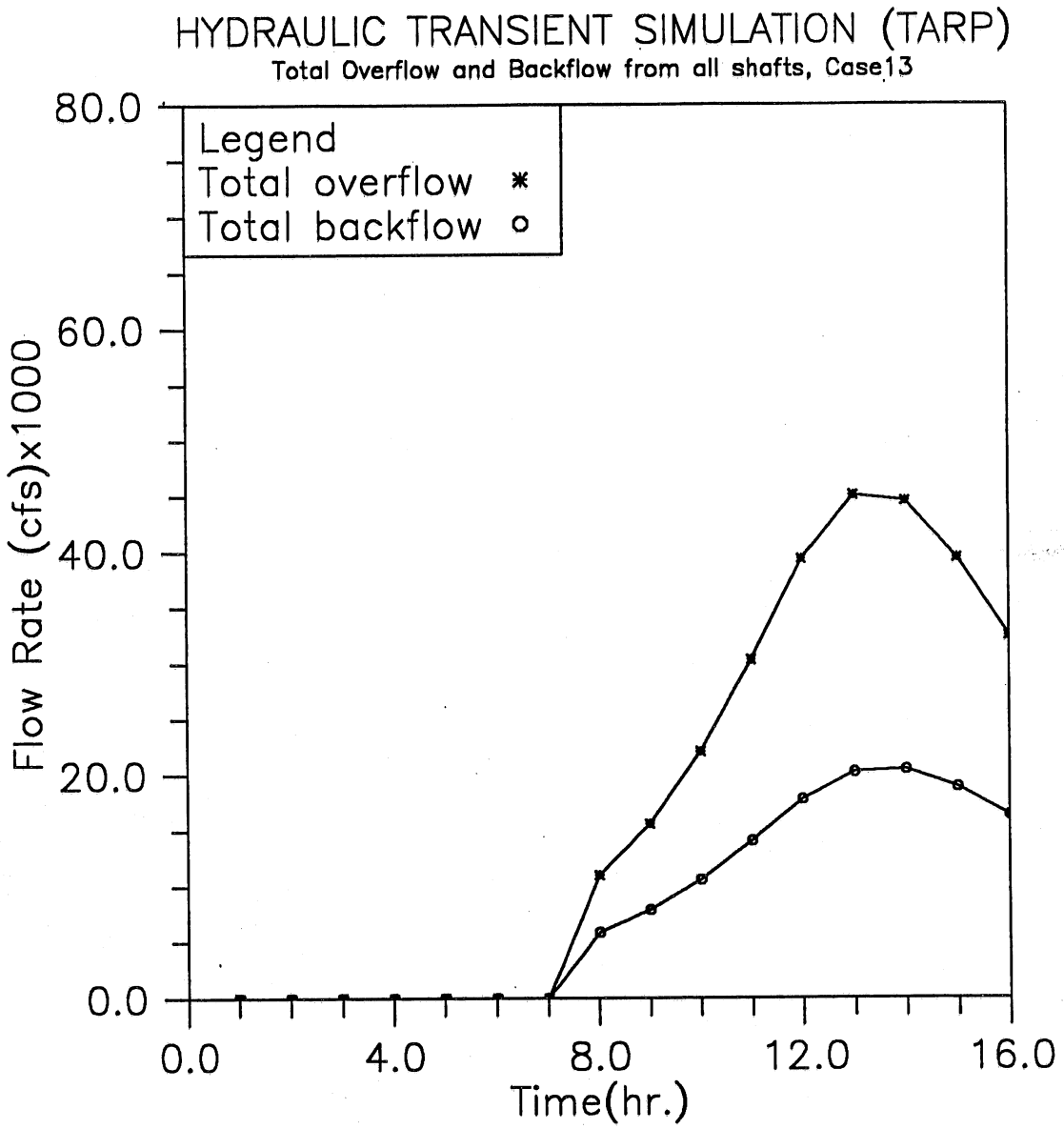

Fig. 3.3(h) Time variation of total overflow and backflow; Modeling case: closed main gate and 100–year storm event (Case 1–3)

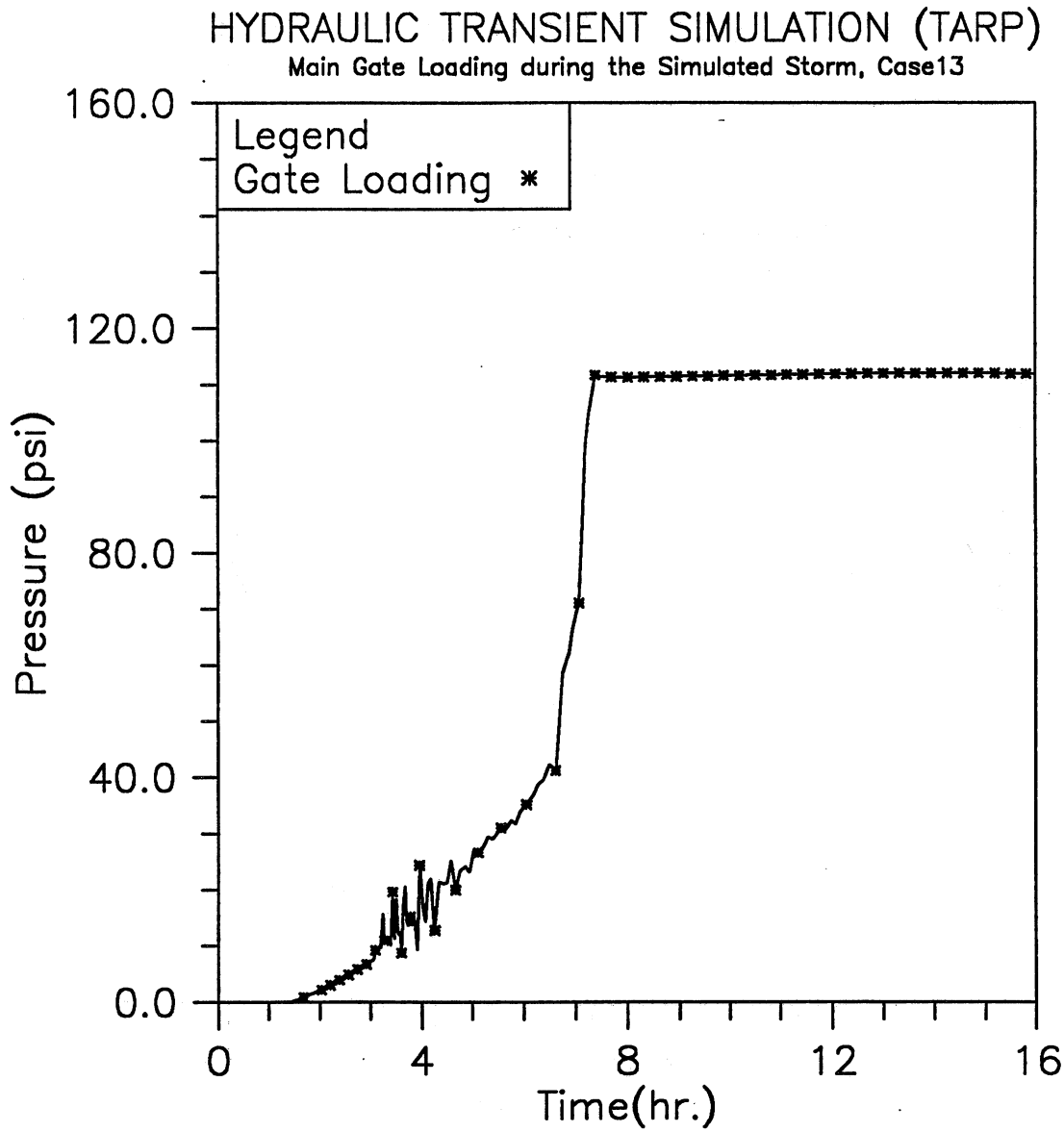

Fig. 3.3(i) Time variation of the averaged loading on the main gate; Modeling case: closed main gate and 100–year storm event (Case 1–3)

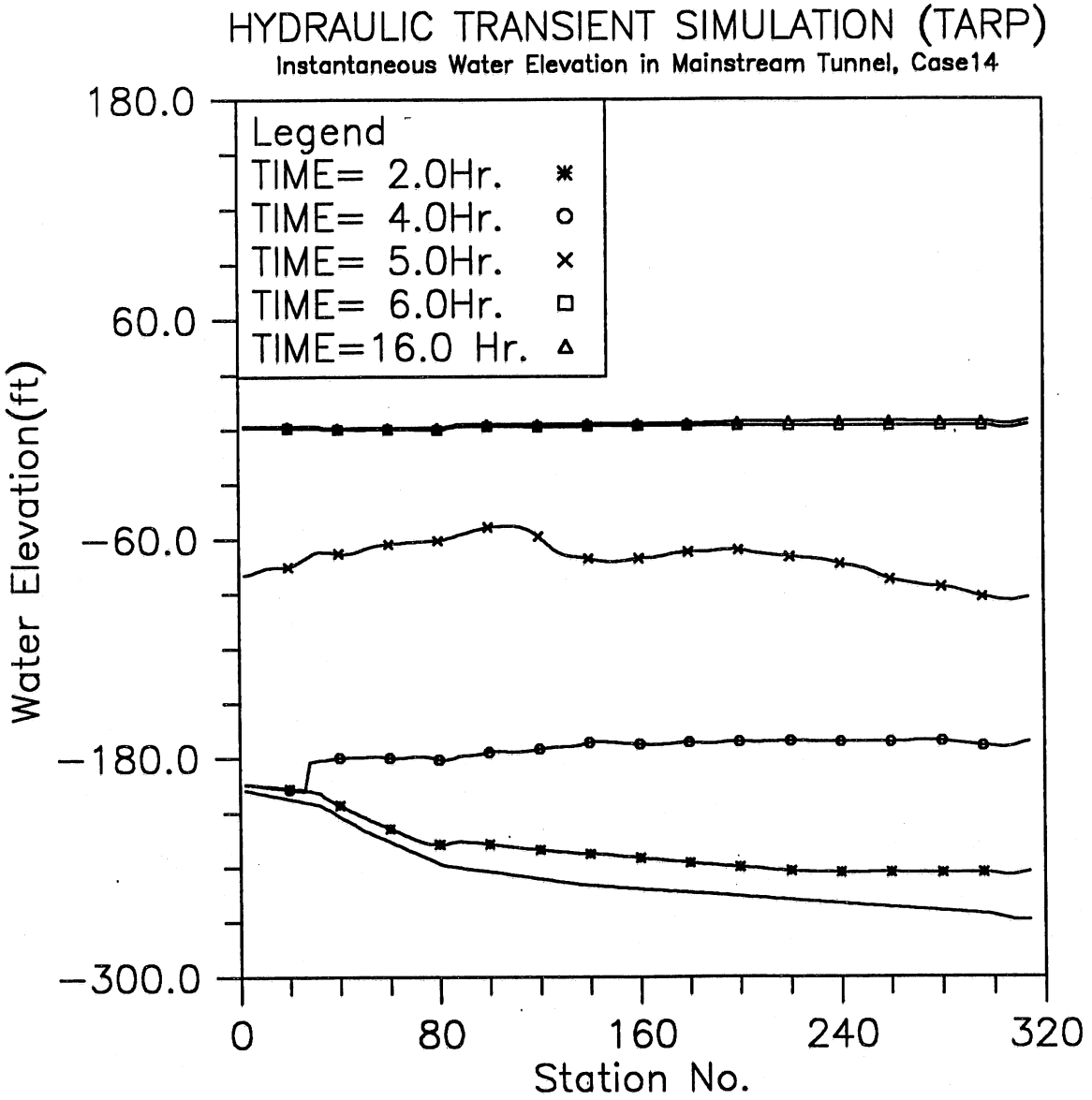

Fig. 3.4(a) Instantaneous hydraulic gradelines along the main tunnel; Modeling case: closed main gate and 500–year storm event (Case 1–4)

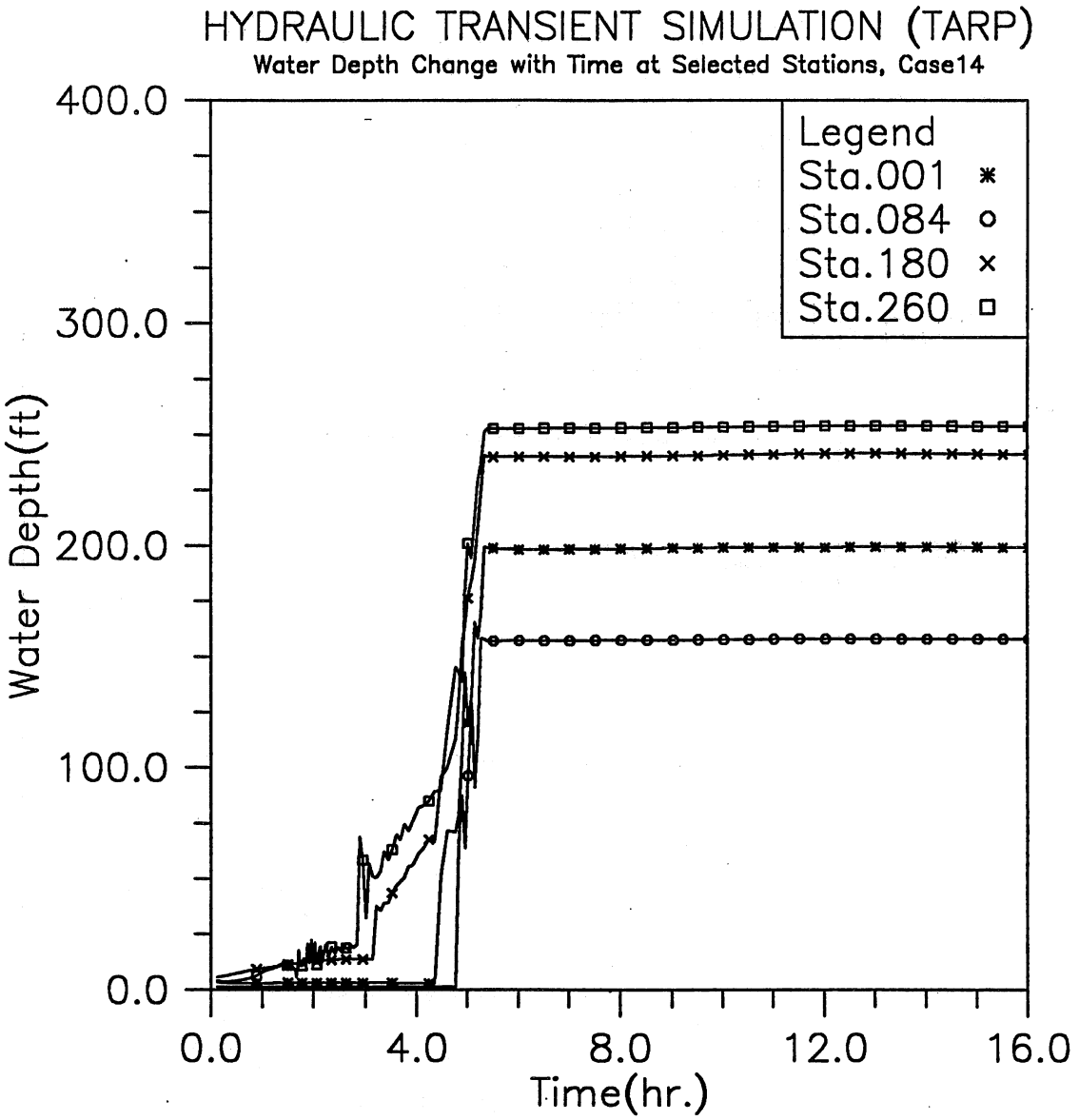

Fig. 3.4(b) Time variation of water depth at four upstream locations; Modeling case: closed main gate and 500–year storm event (Case 1–4)

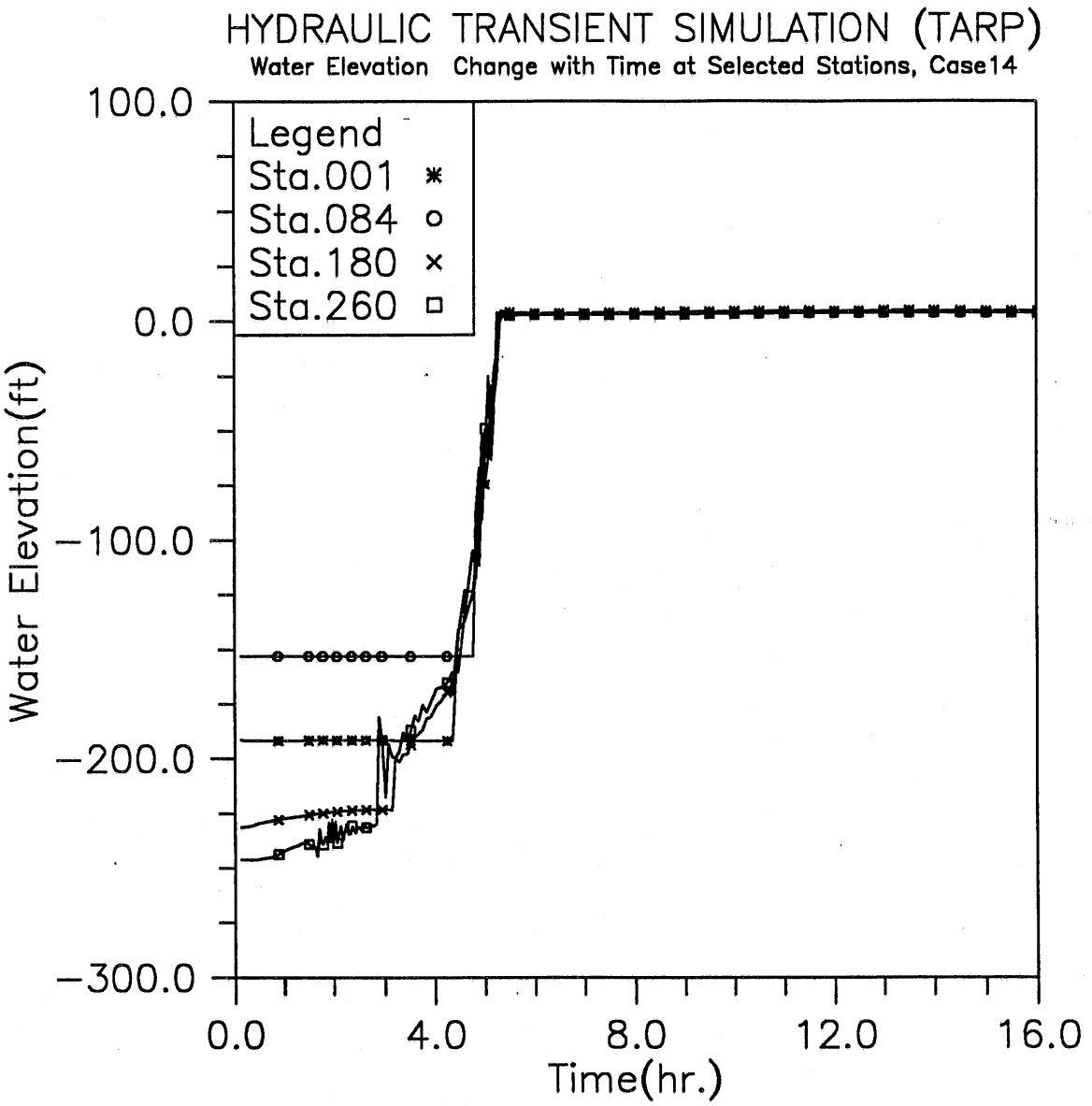

Fig. 3.4(c) Time variation of water elevation at four upstream locations; Modeling case: closed main gate and 500–year storm event (Case 1–4)

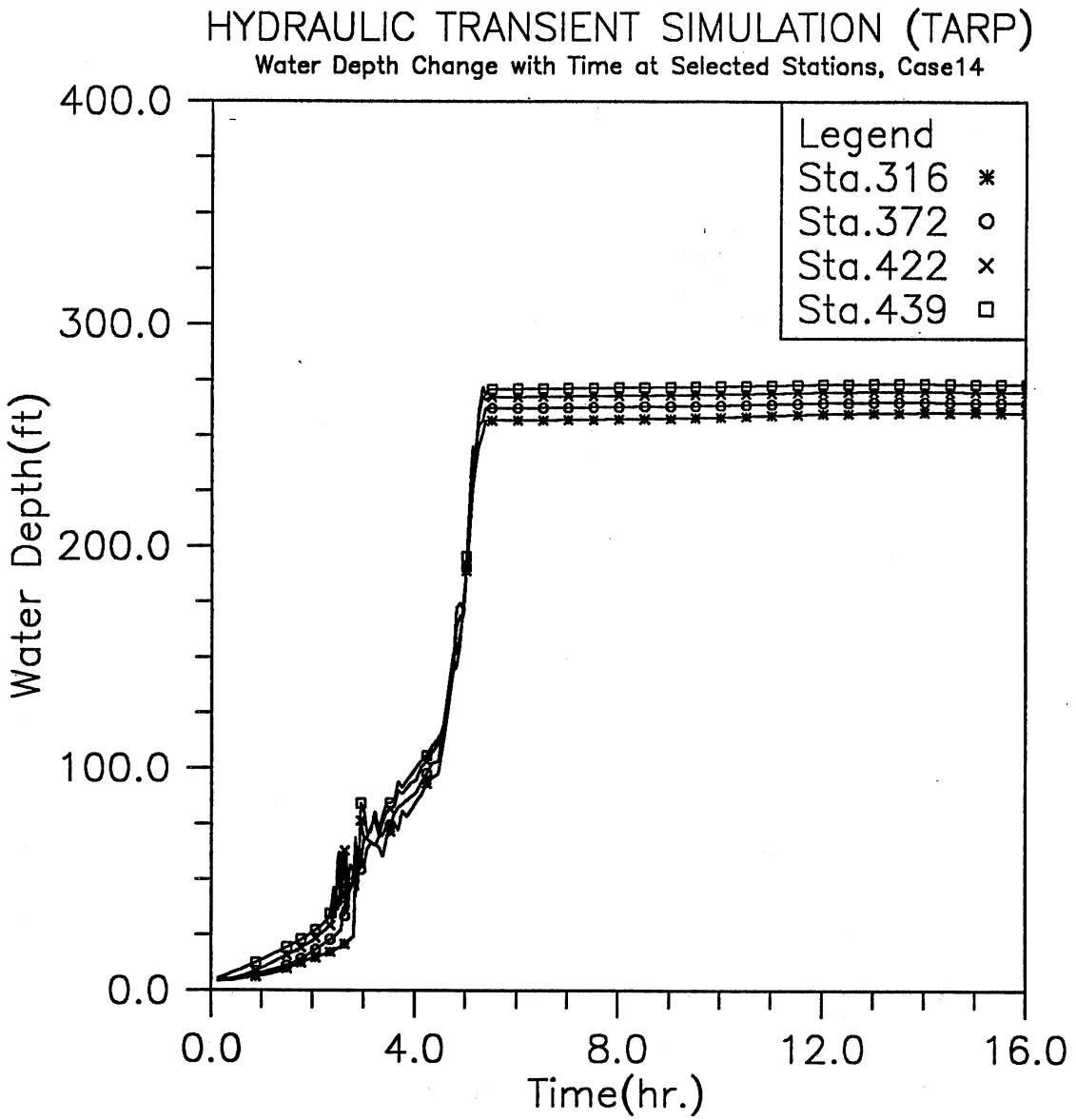

Fig. 3.4(d) Time variation of water depth at four downstream locations; Modeling case: closed main gate and 500–year storm event (Case 1–4)

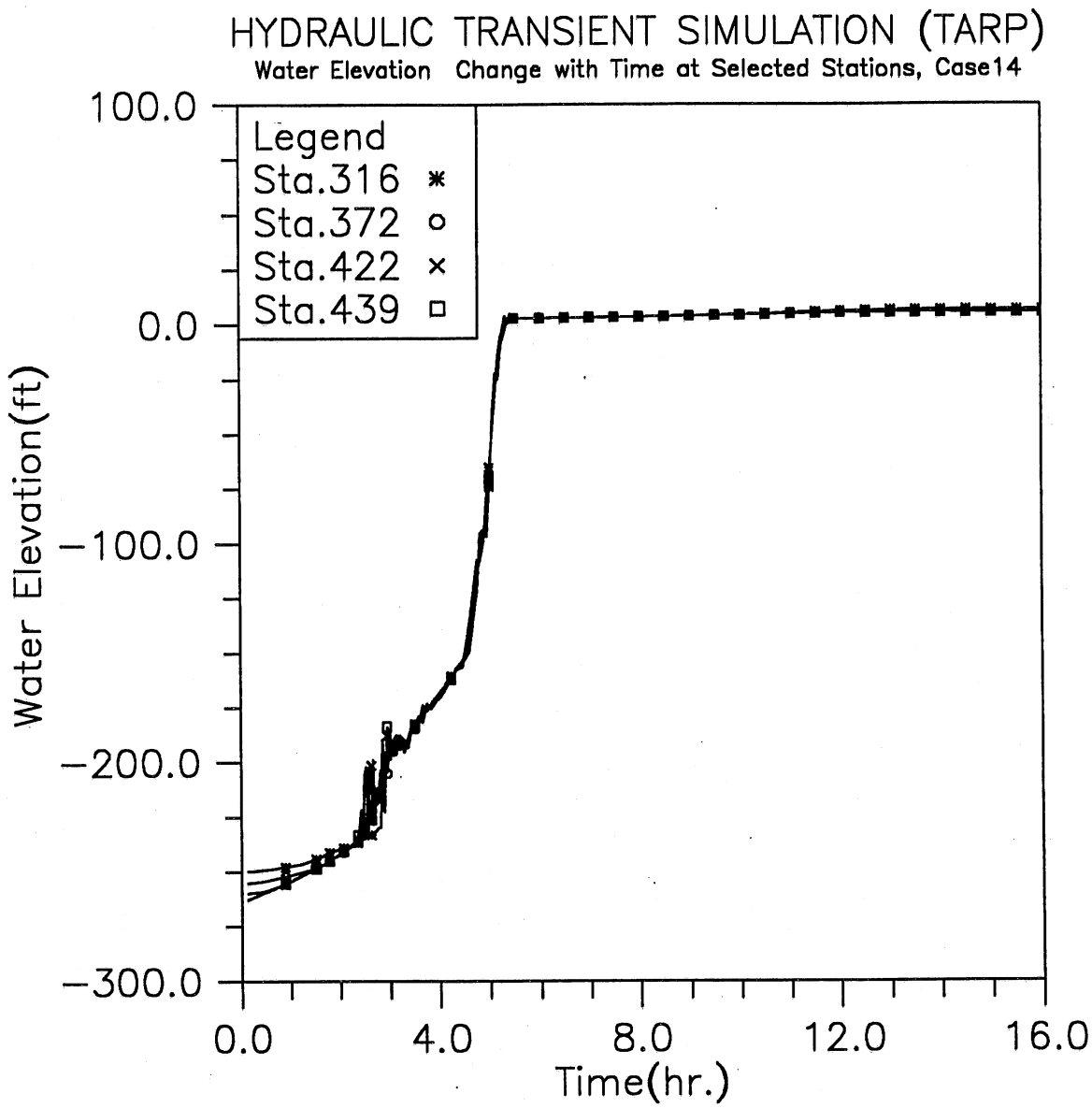

Fig. 3.4(e) Time variation of water elevation at four downstream locations; Modeling case: closed main gate and 500–year storm event (Case 1–4)

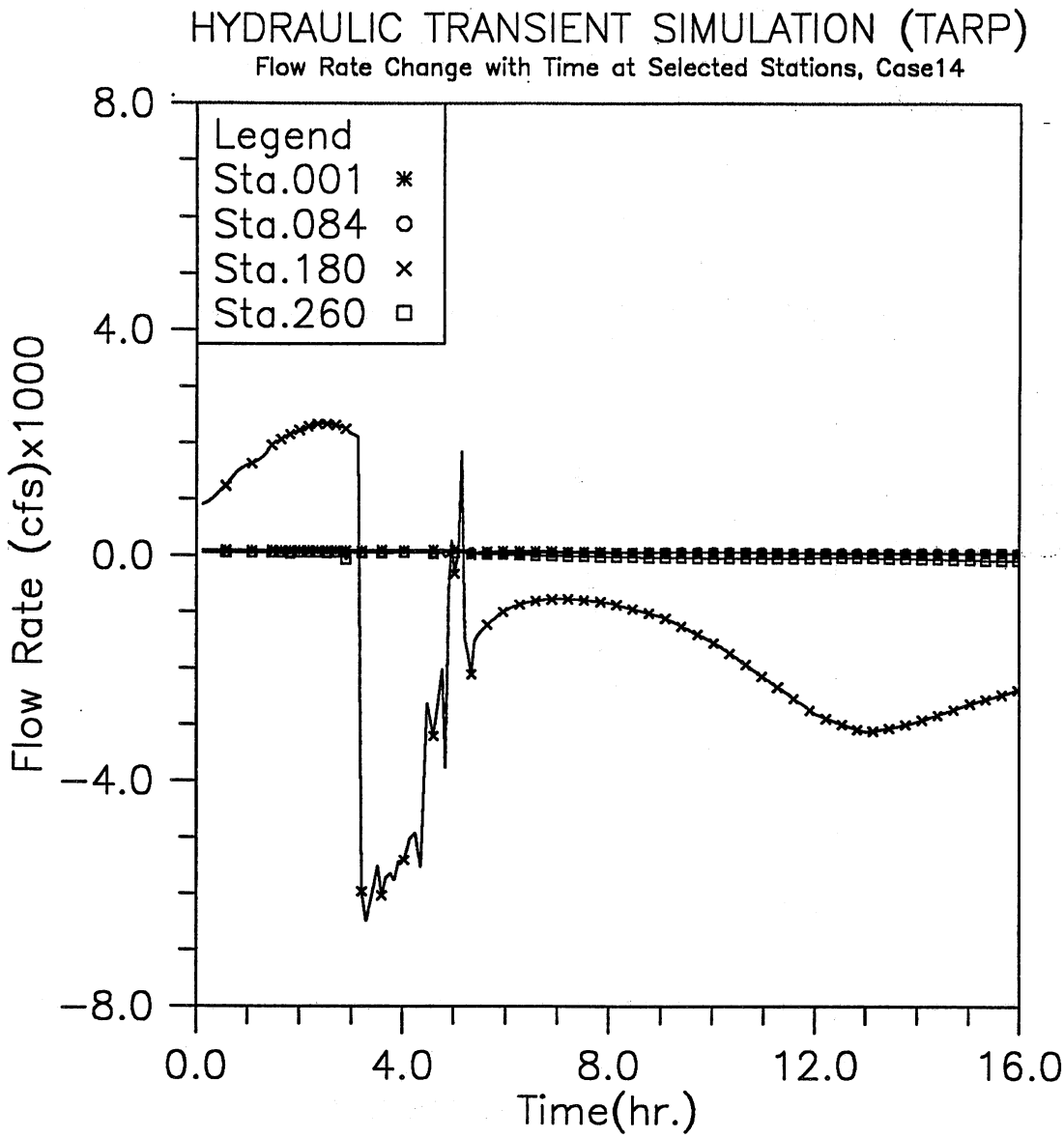

Fig. 3.4(f) Time variation of flow rate at four upstream locations; Modeling case: closed main gate and 500–year storm event (Case 1–4)

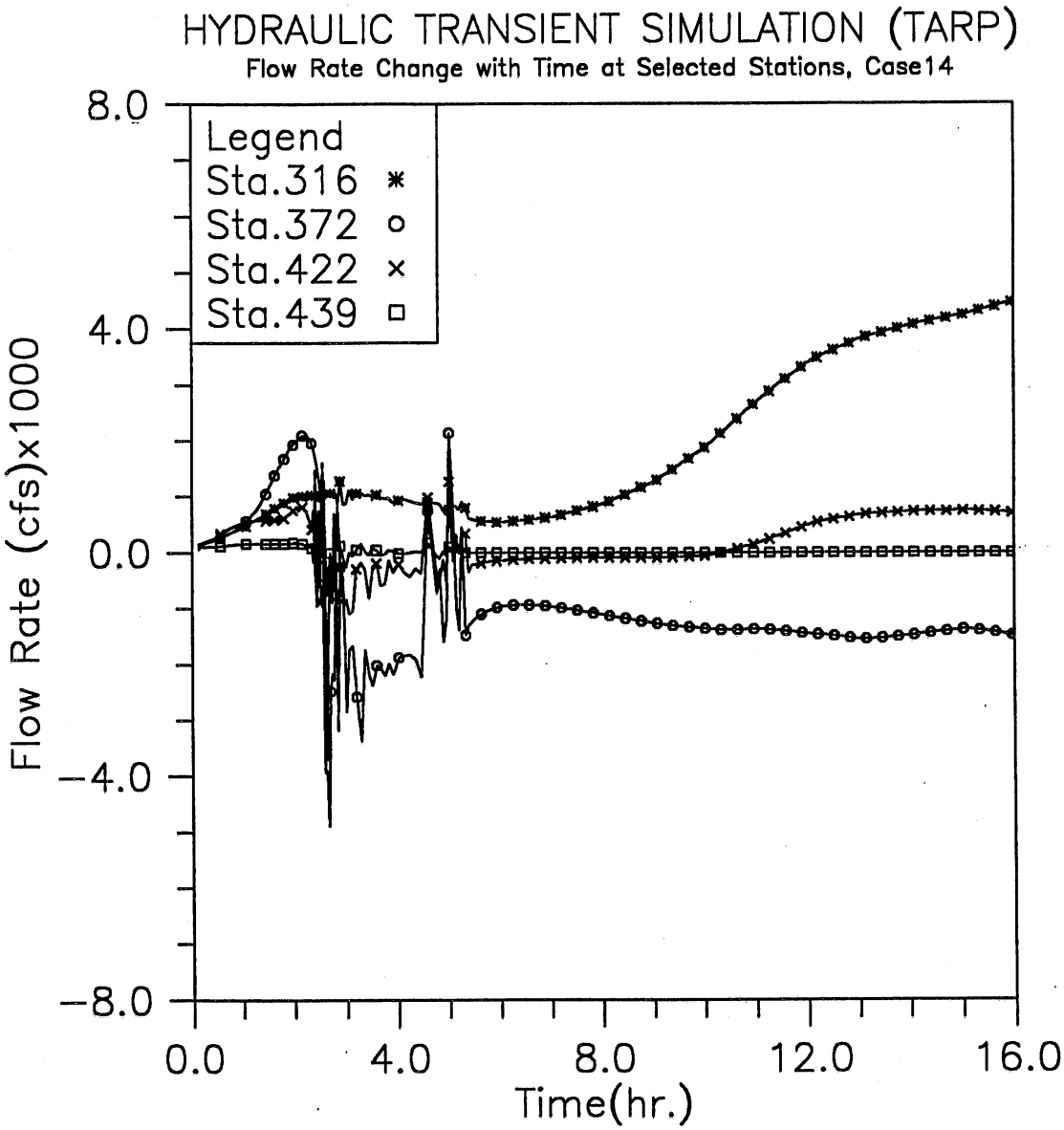

Fig. 3.4(g) Time variation of flow rate at four downstream locations; Modeling case: closed main gate and 500–year storm event (Case 1–4)

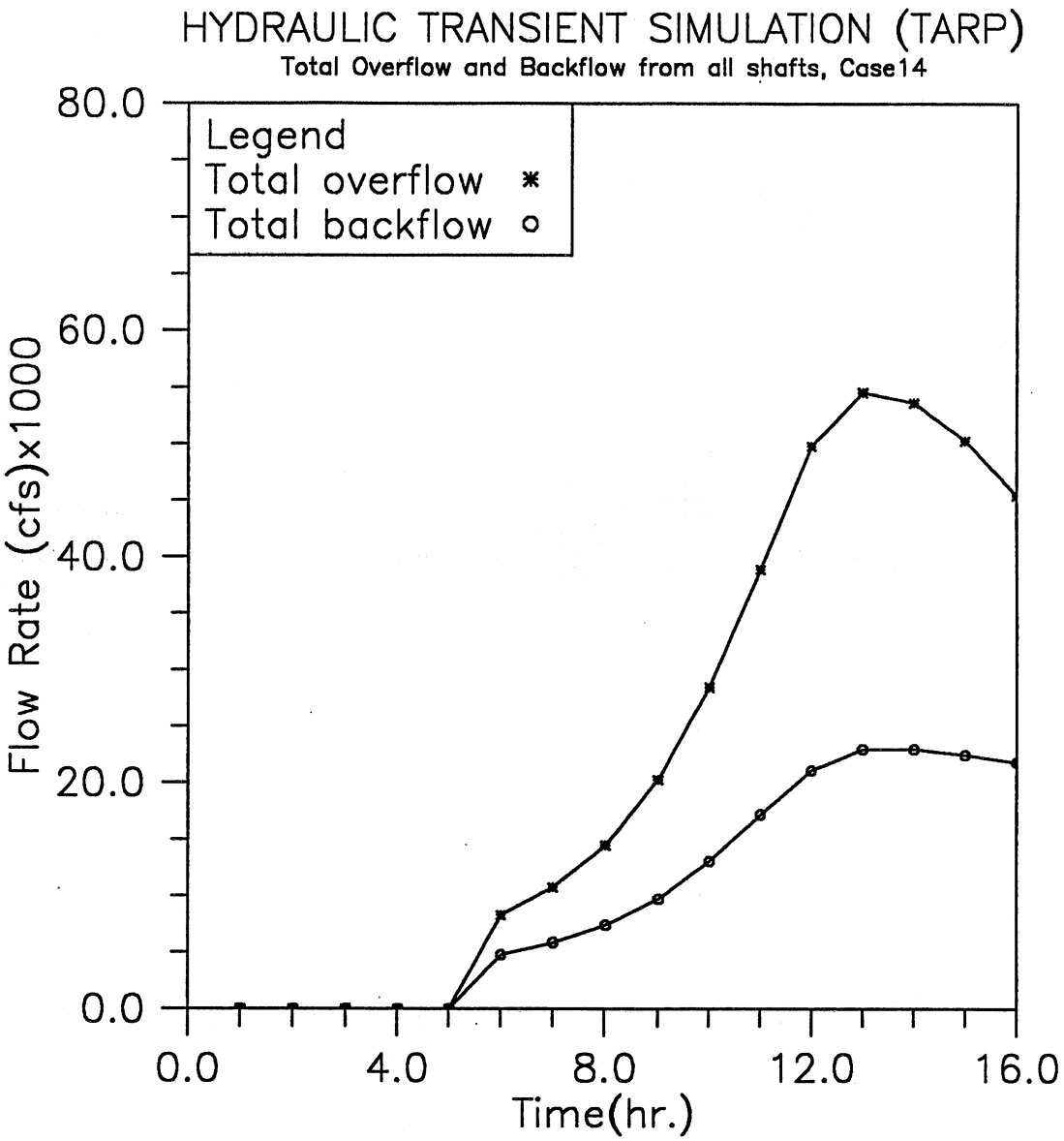

Fig. 3.4(h) Time variation of total overflow and backflow; Modeling case: closed main gate and 500–year storm event (Case 1–4)

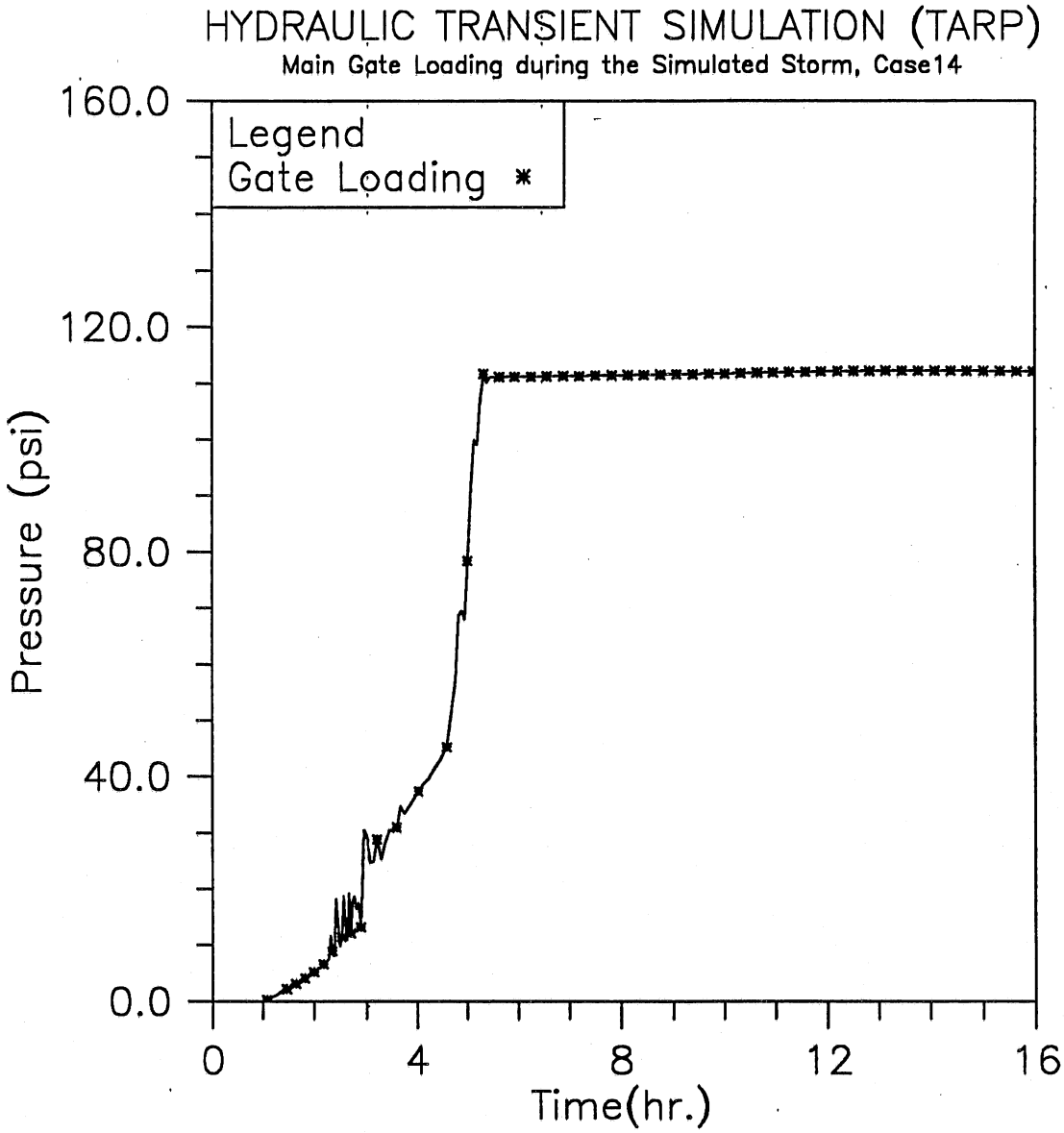

Fig. 3.4(i) Time variation of the averaged loading on the main gate; Modeling case: closed main gate and 500–year storm event (Case 1–4)

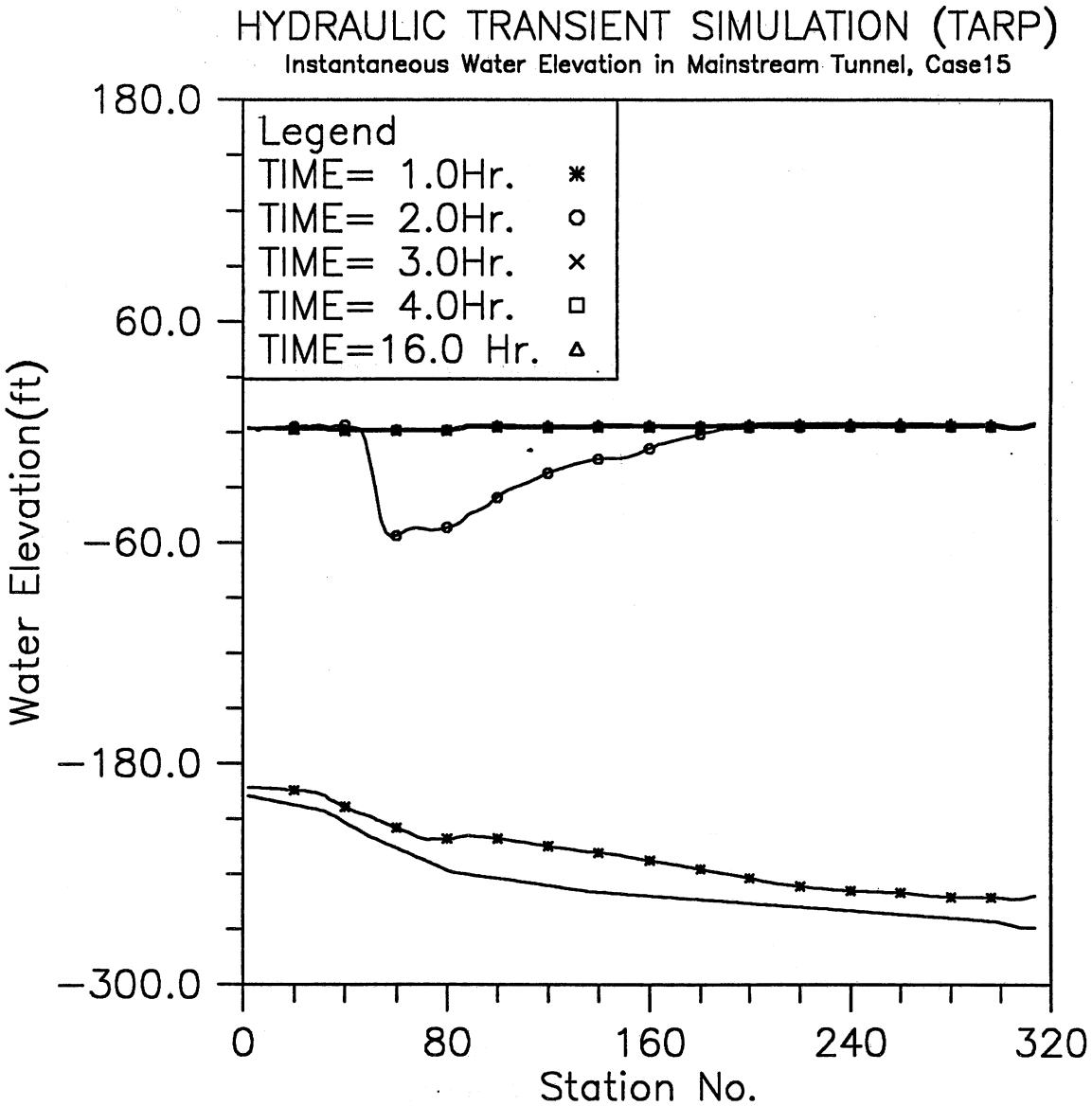

Fig. 3.5(a) Instantaneous hydraulic gradelines along the main tunnel; Modeling case: closed main gate and PMF event (Case 1–5)

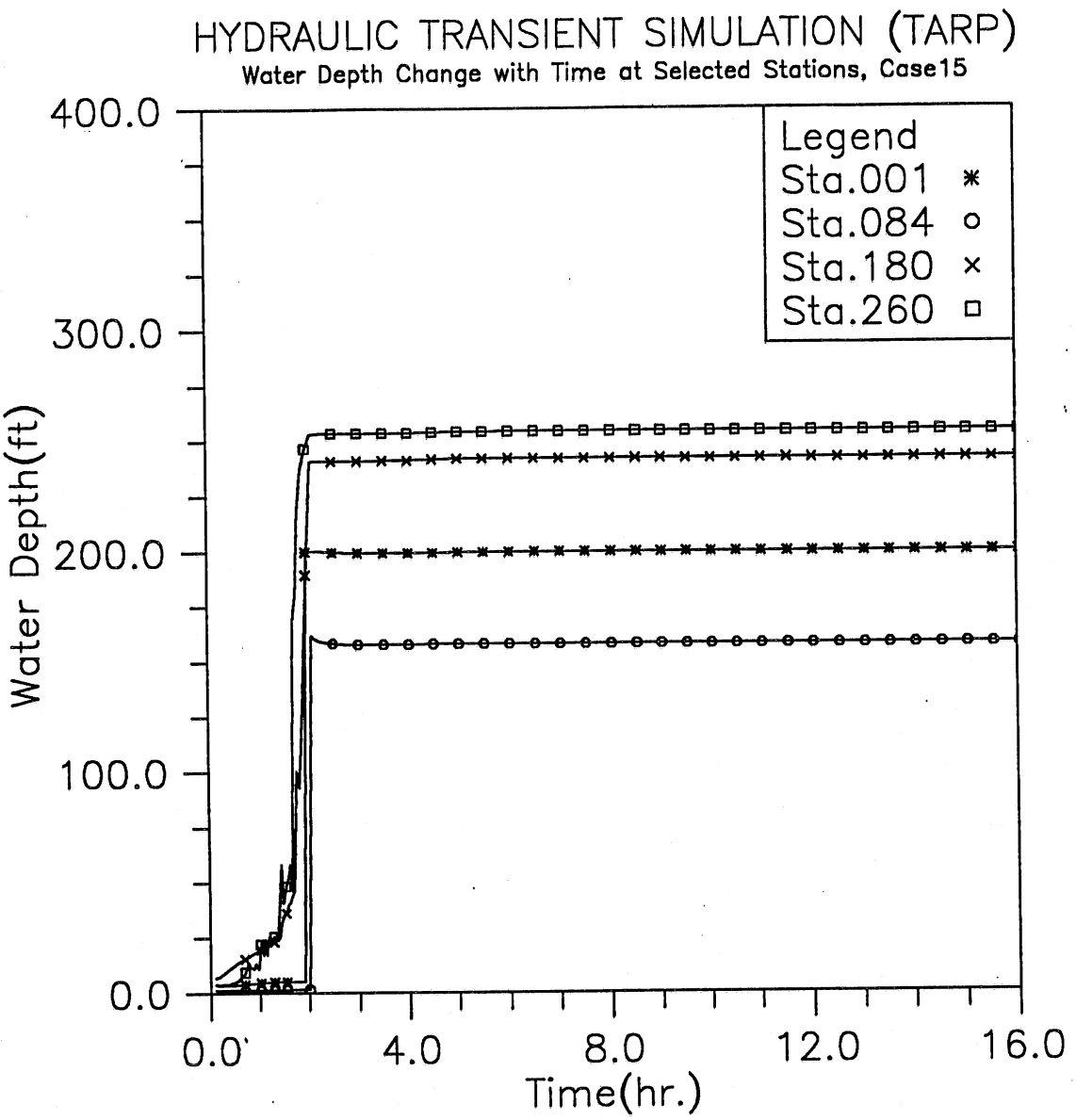

Fig. 3.5(b) Time variation of water depth at four upstream locations; Modeling case: closed main gate and PMF event (Case 1–5)

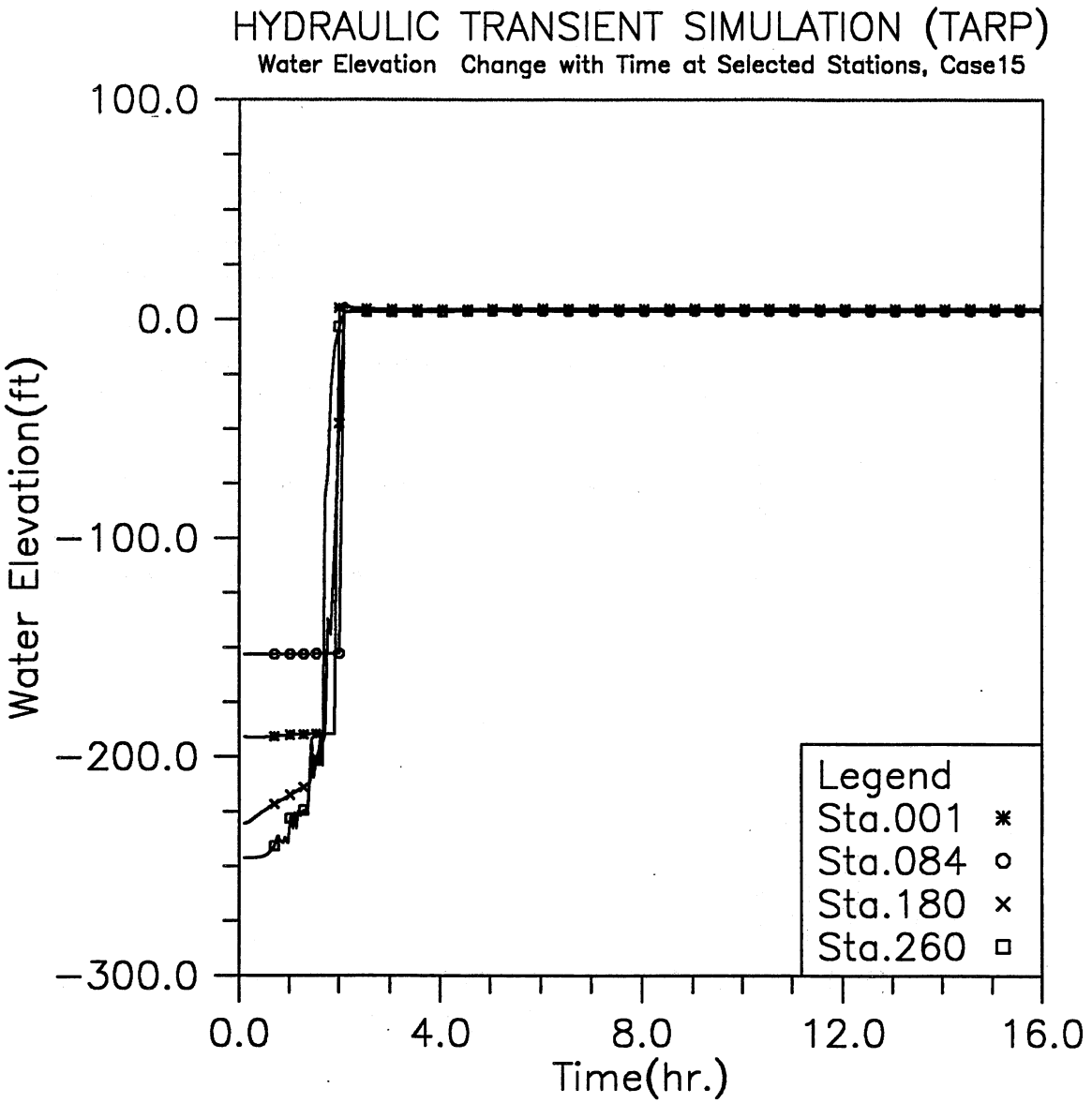

Fig. 3.5(c) Time variation of water elevation at four upstream locations; Modeling case: closed main gate and PMF event (Case 1–5)

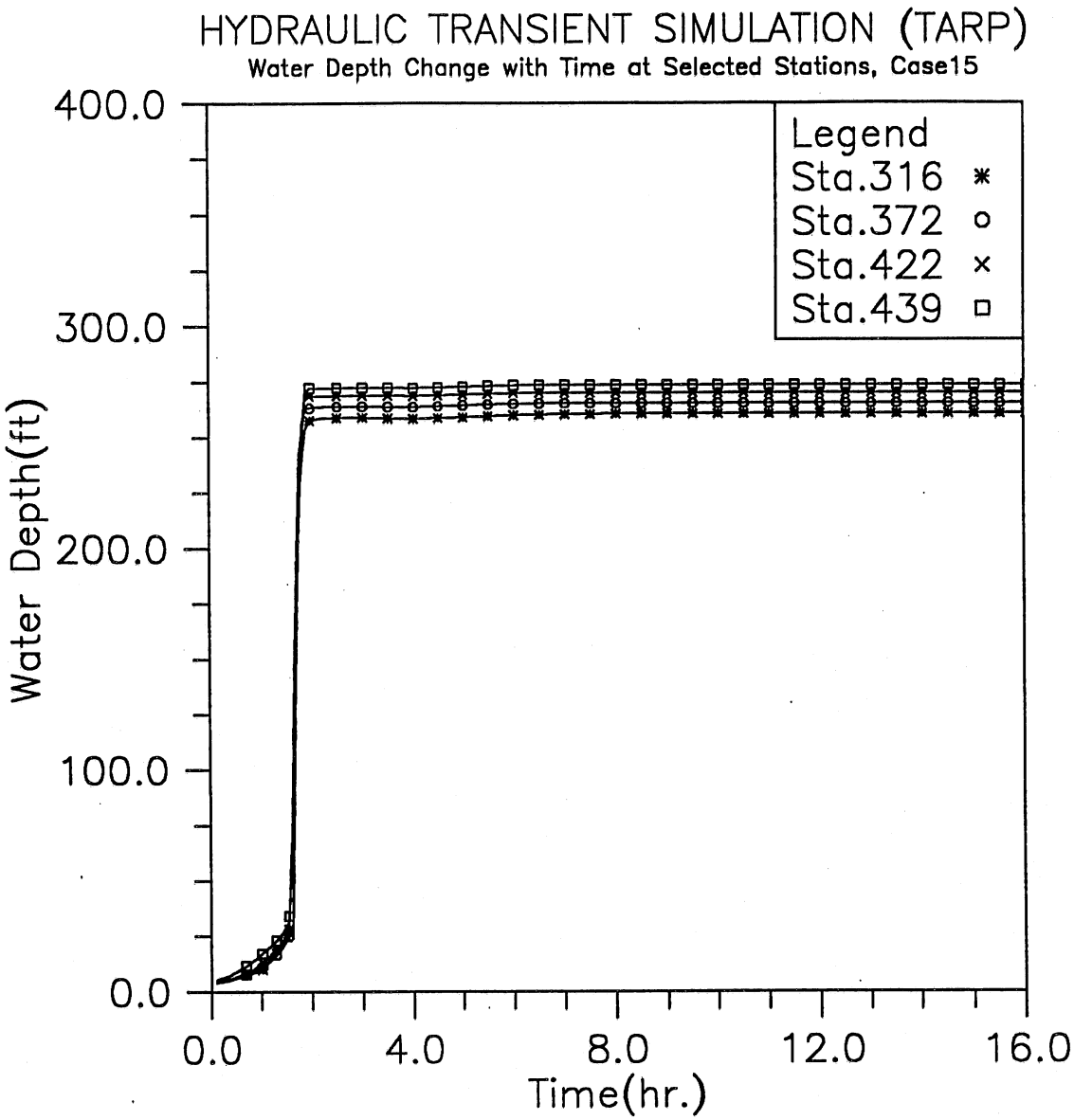

Fig. 3.5(d) Time variation of water depth at four downstream locations; Modeling case: closed main gate and PMF event (Case 1–5)

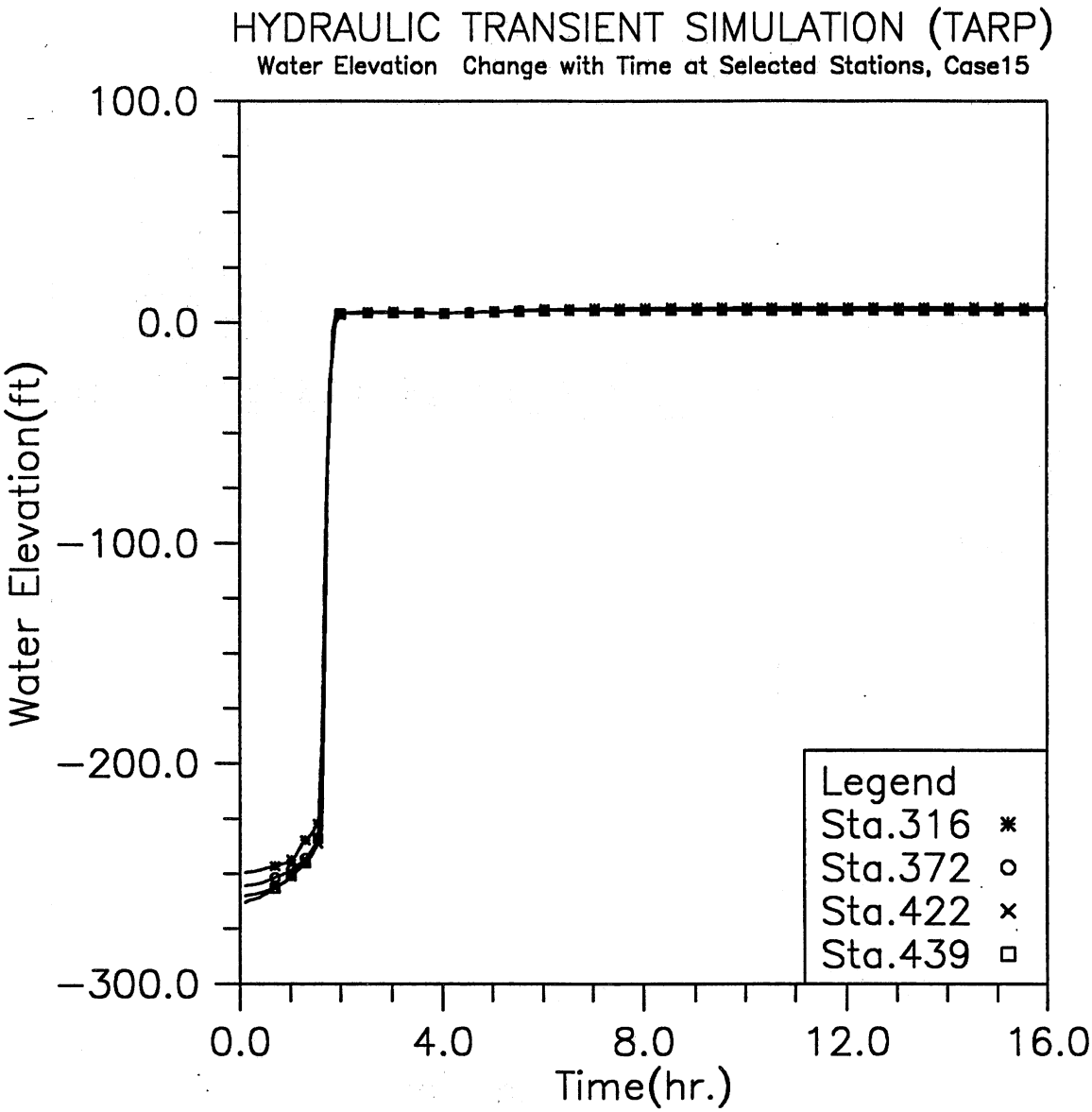

Fig. 3.5(e) Time variation of water elevation at four downstream locations; Modeling case: closed main gate and PMF event (Case 1–5)

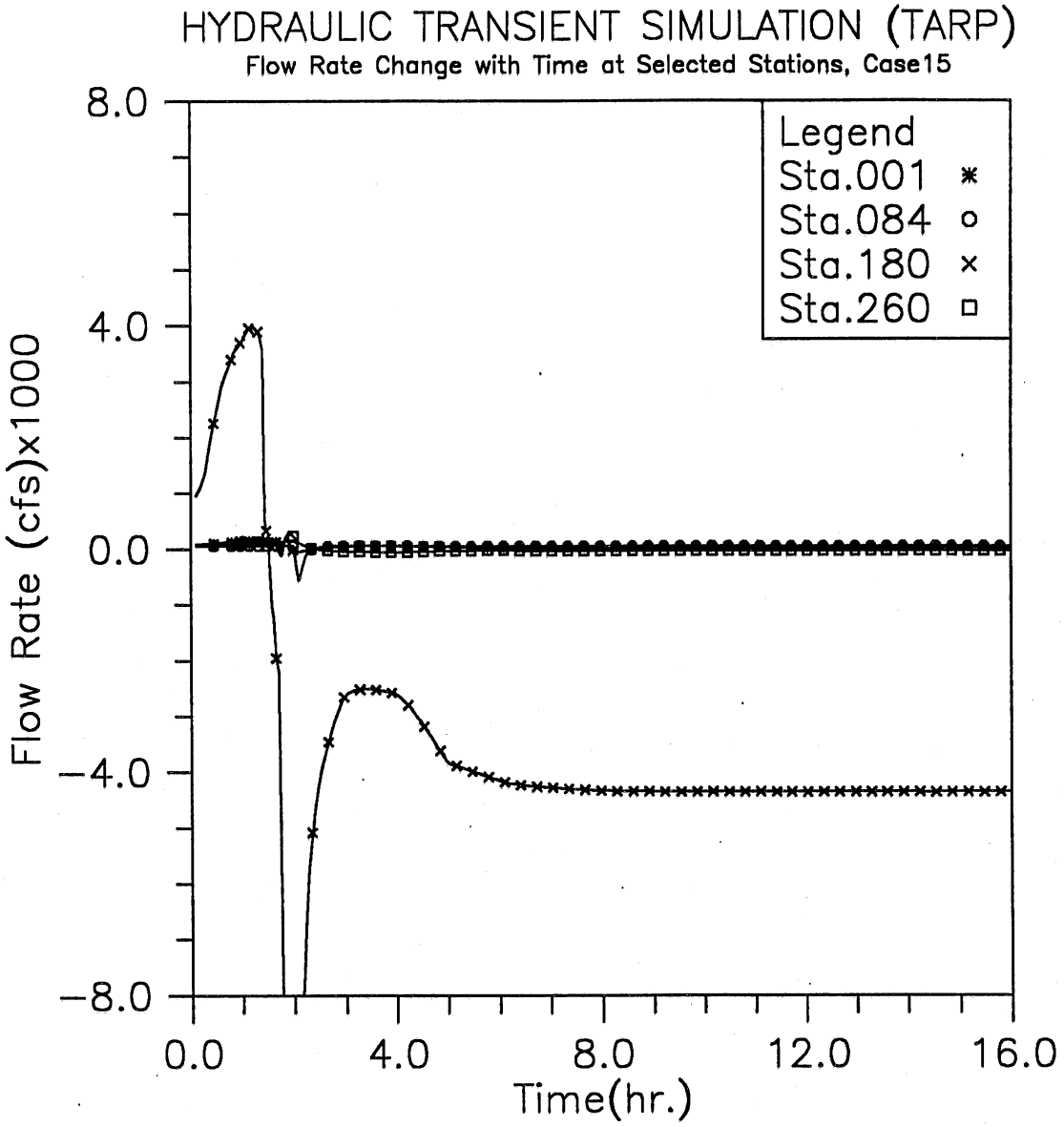

Fig. 3.5(f) Time variation of flow rate at four upstream locations; Modeling case: closed main gate and PMF event (Case 1–5)

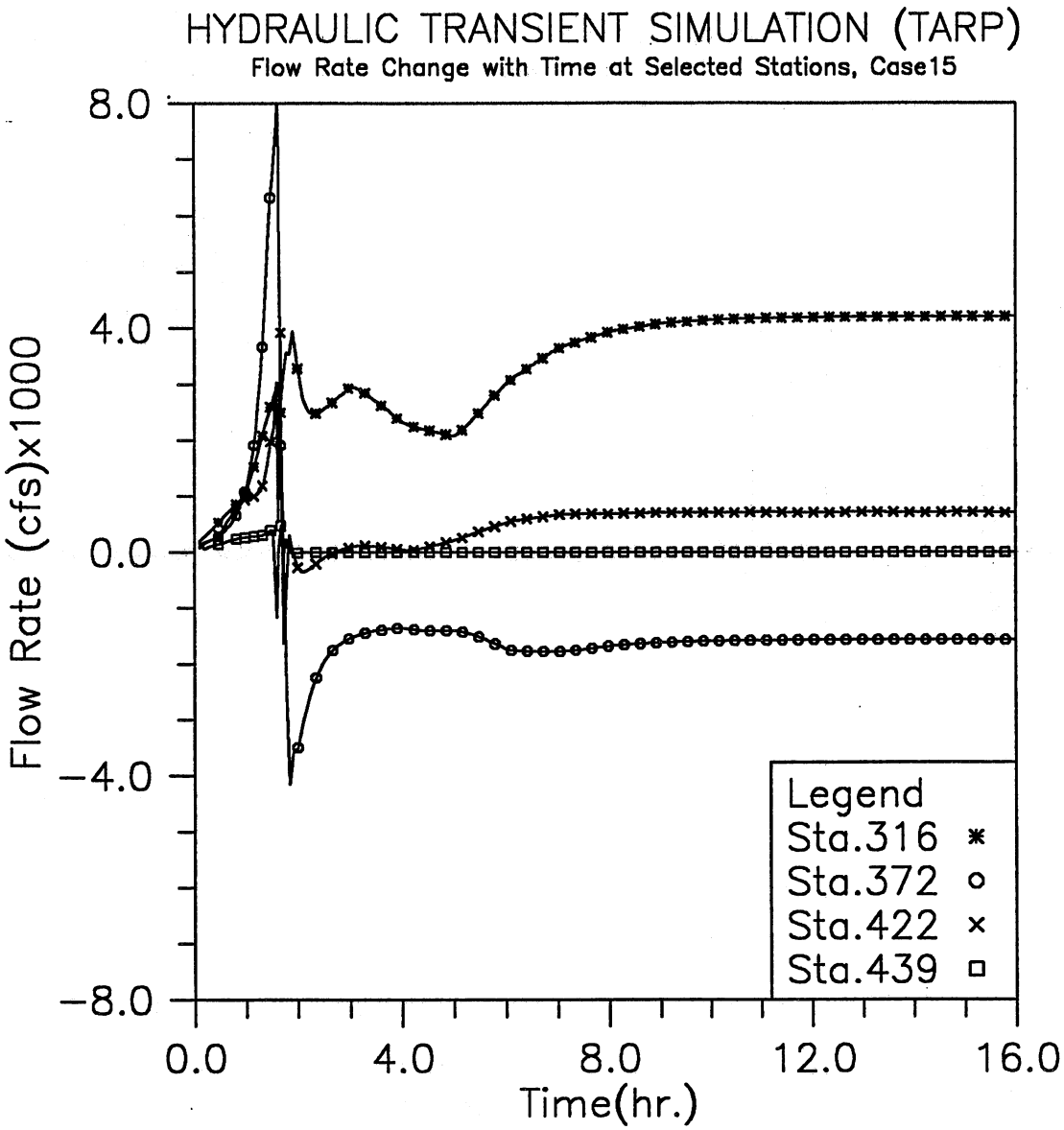

Fig. 3.5(g) Time variation of flow rate at four downstream locations; Modeling case: closed main gate and PMF event (Case 1–5)

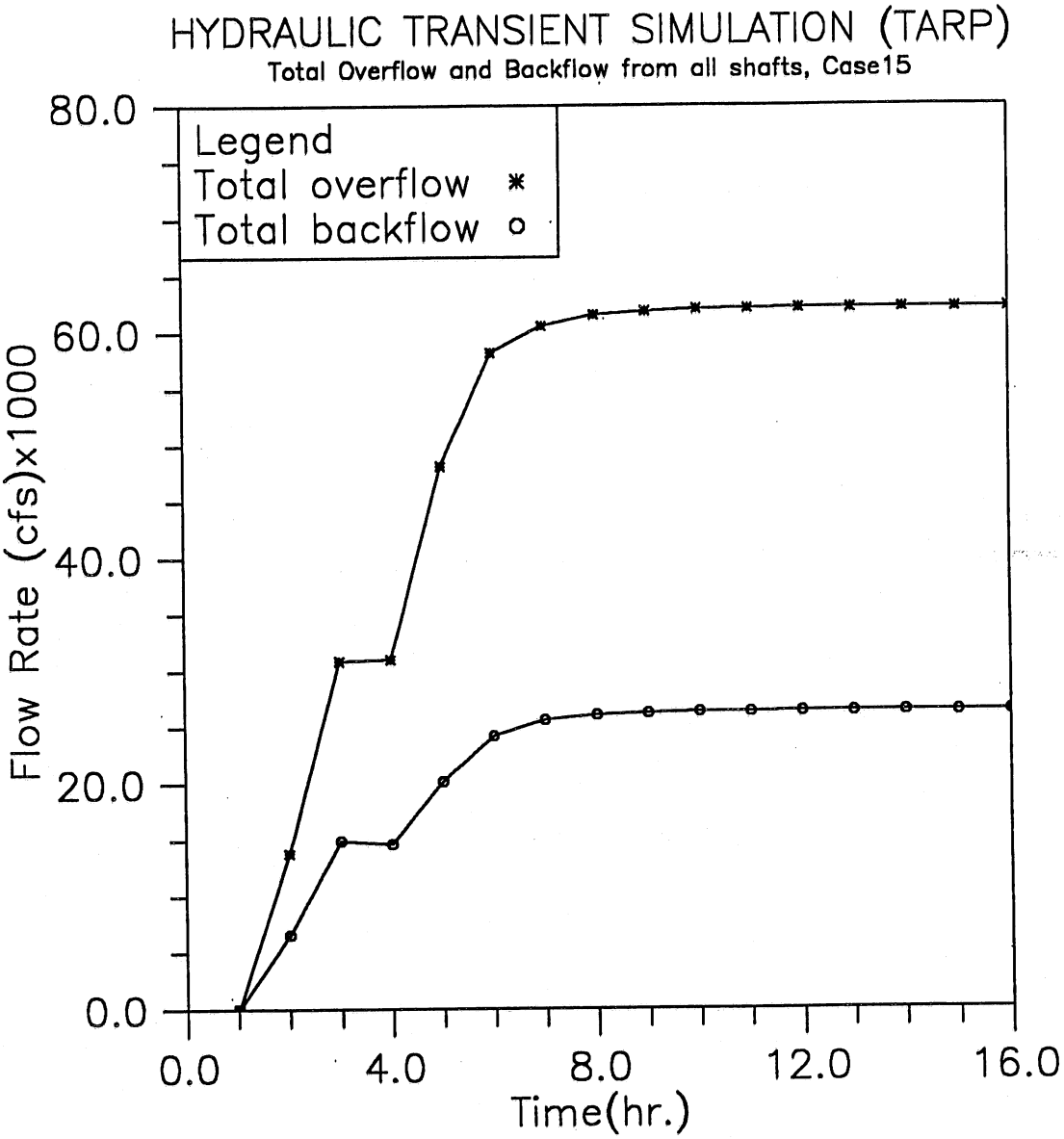

Fig. 3.5(h) Time variation of total overflow and backflow; Modeling case: closed main gate and PMF event (Case 1–5)

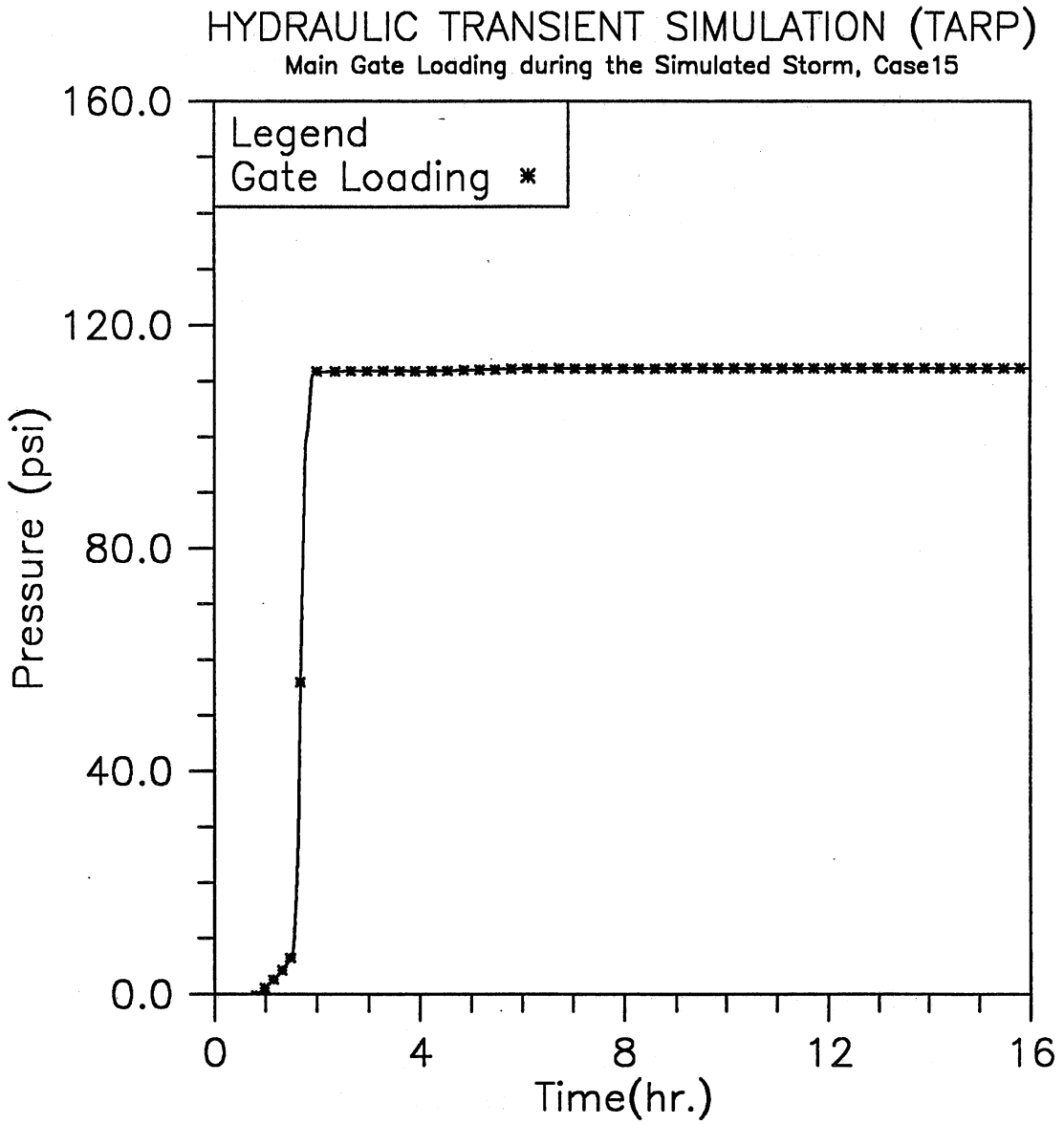

Fig. 3.5(i) Time variation of the averaged loading on the main gate; Modeling case: closed main gate and PMF event (Case 1–5)

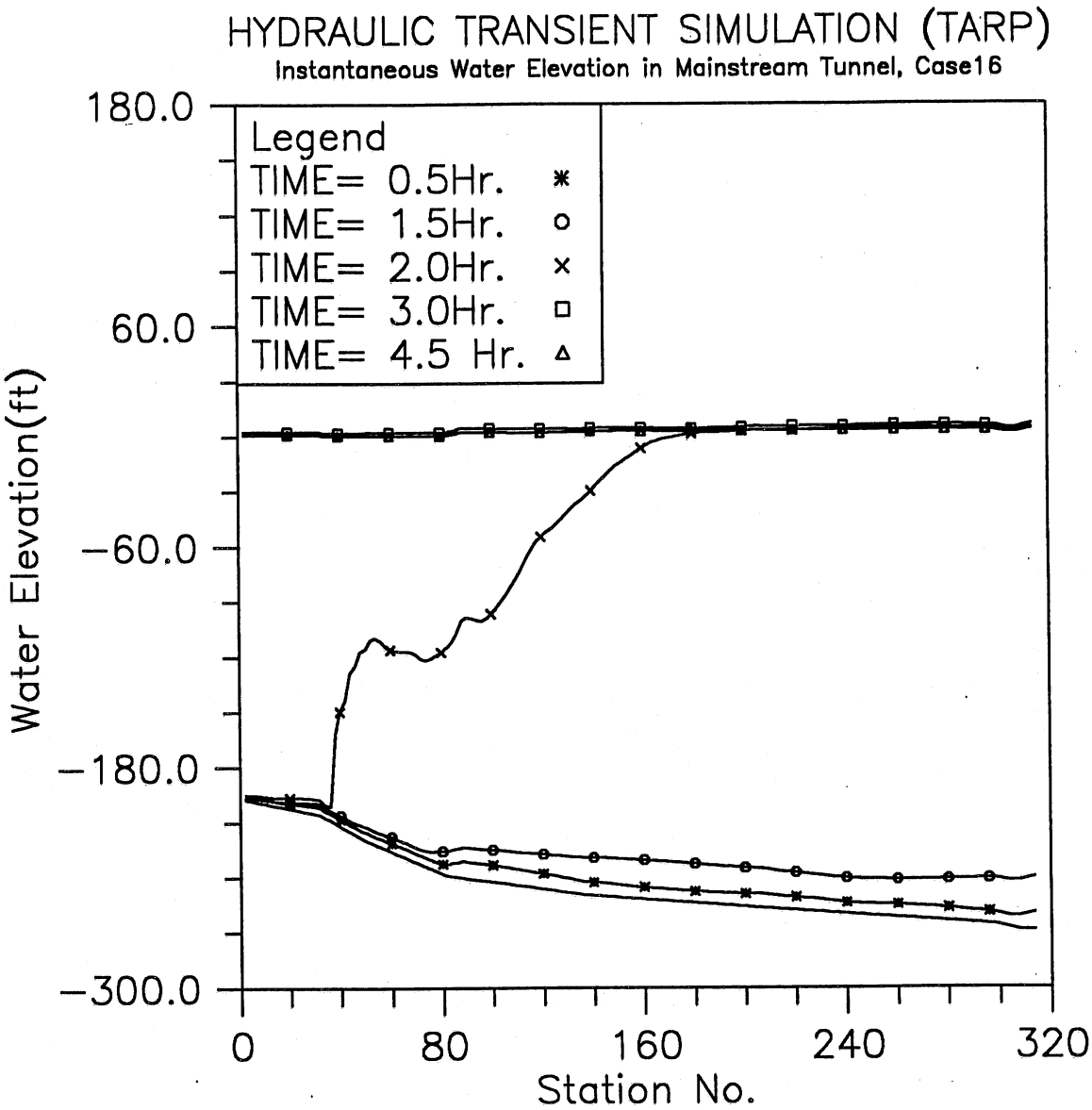

Fig. 3.6(a) Instantaneous hydraulic gradelines along the main tunnel; Modeling case: closed main gate and MAX event (Case 1–6)

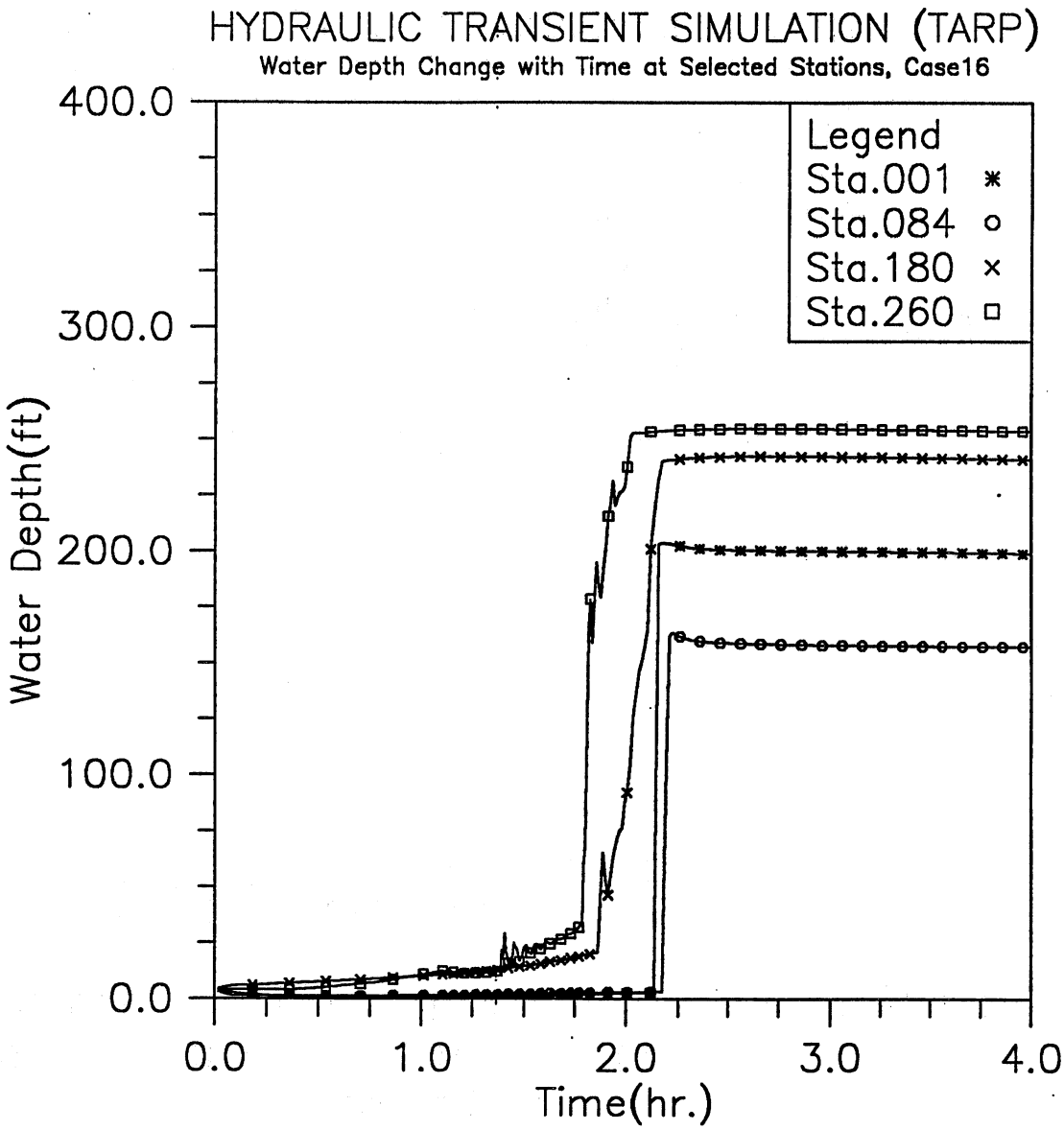

Fig. 3.6(b) Time variation of water depth at four upstream locations; Modeling case: closed main gate and MAX event (Case 1–6)

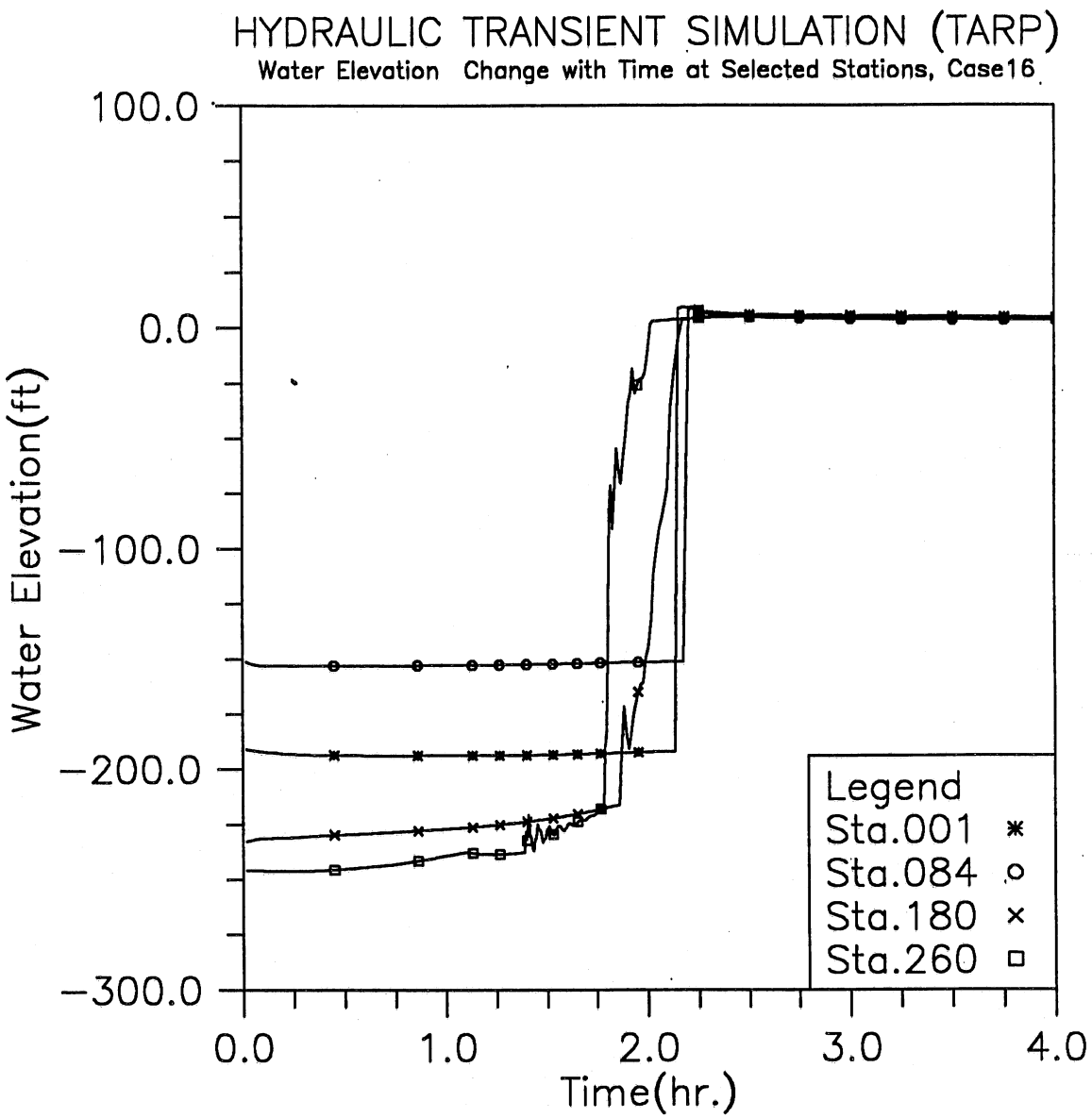

Fig. 3.6(c) Time variation of water elevation at four upstream locations; Modeling case: closed main gate and MAX event (Case 1–6)

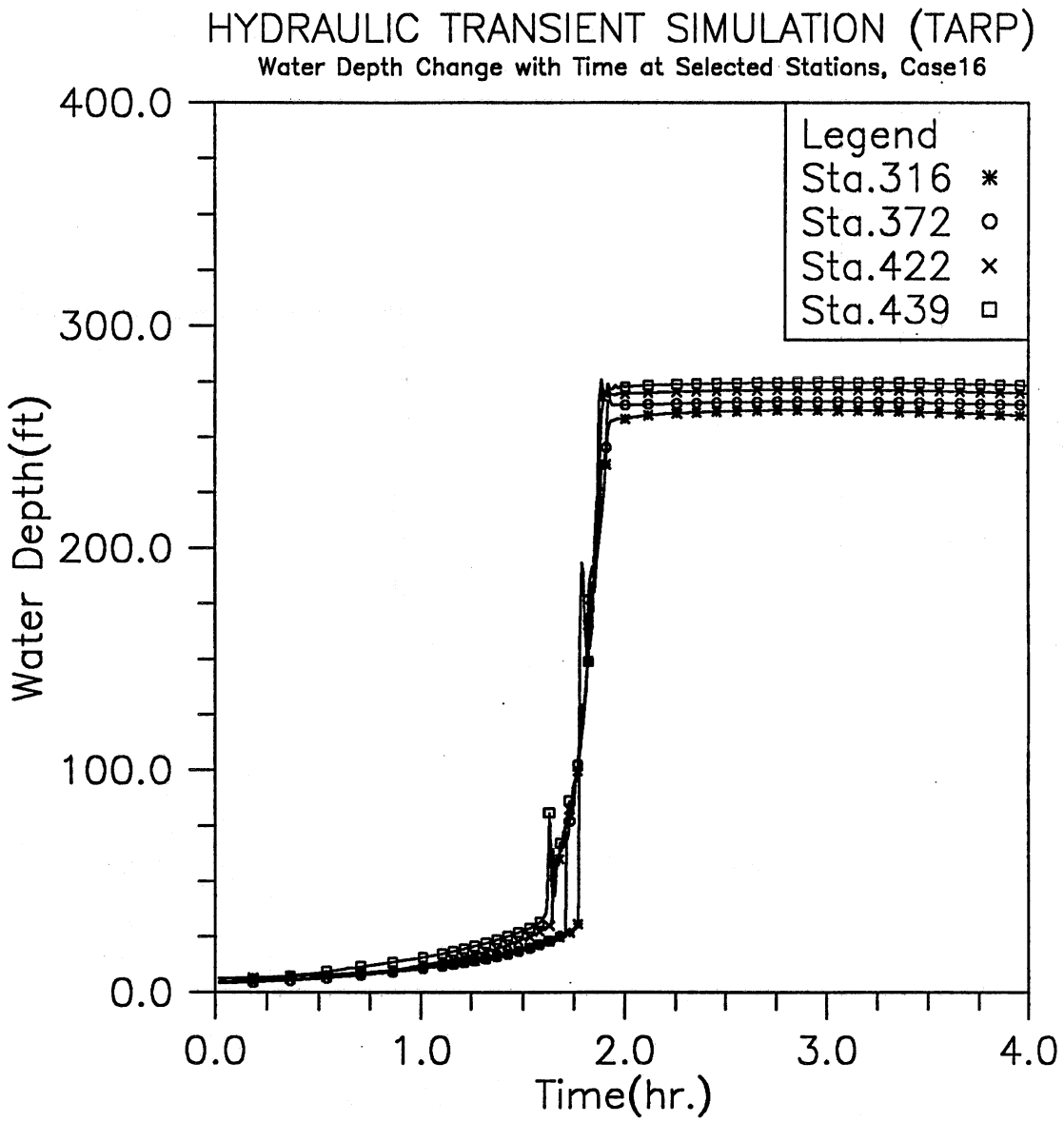

Fig. 3.6(d) Time variation of water depth at four downstream locations; Modeling case: closed main gate and MAX event (Case 1–6)

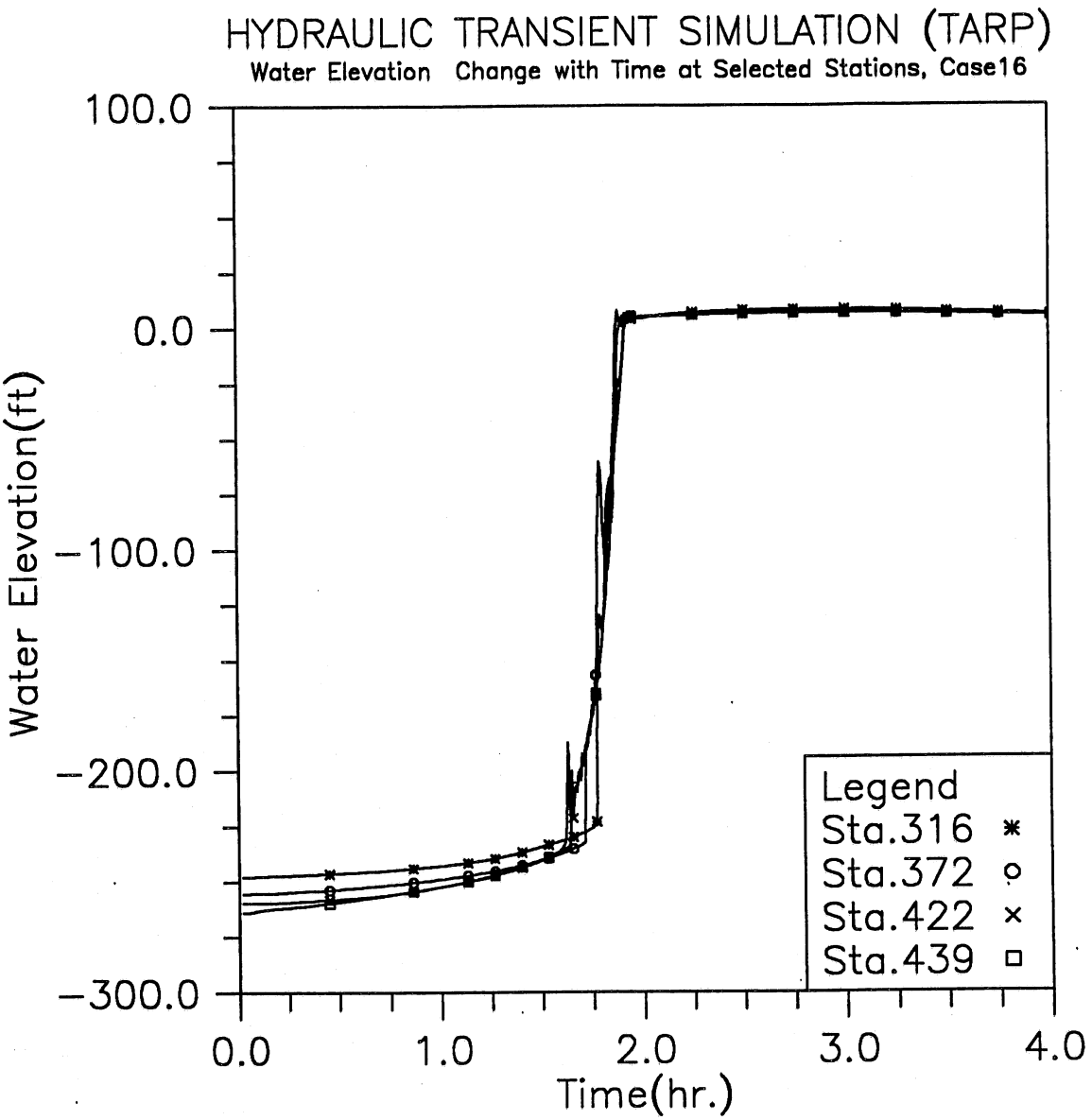

Fig. 3.6(e) Time variation of water elevation at four downstream locations; Modeling case: closed main gate and MAX event (Case 1–6)

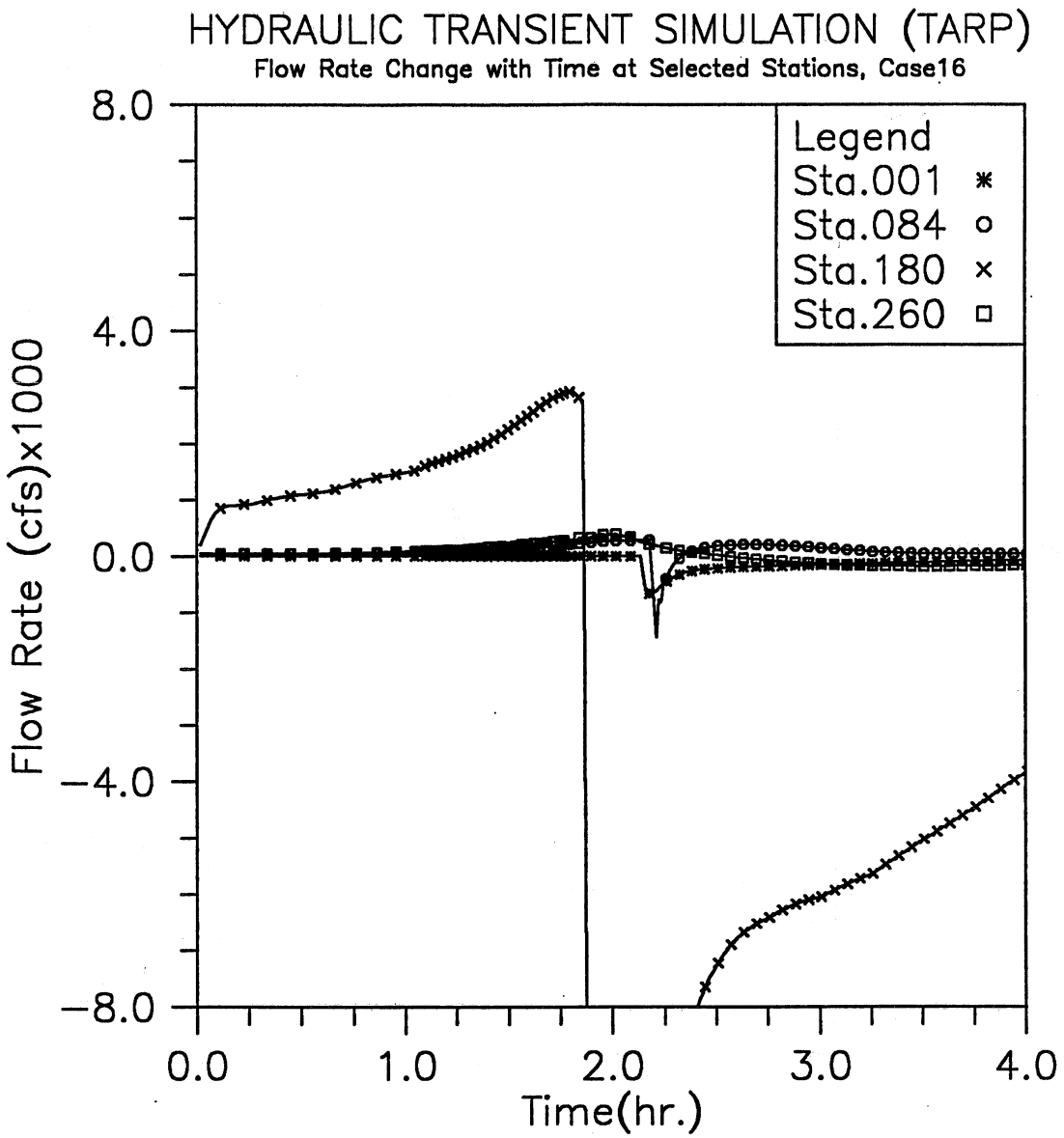

Fig. 3.6(f) Time variation of flow rate at four upstream locations; Modeling case: closed main gate and MAX event (Case 1–6)

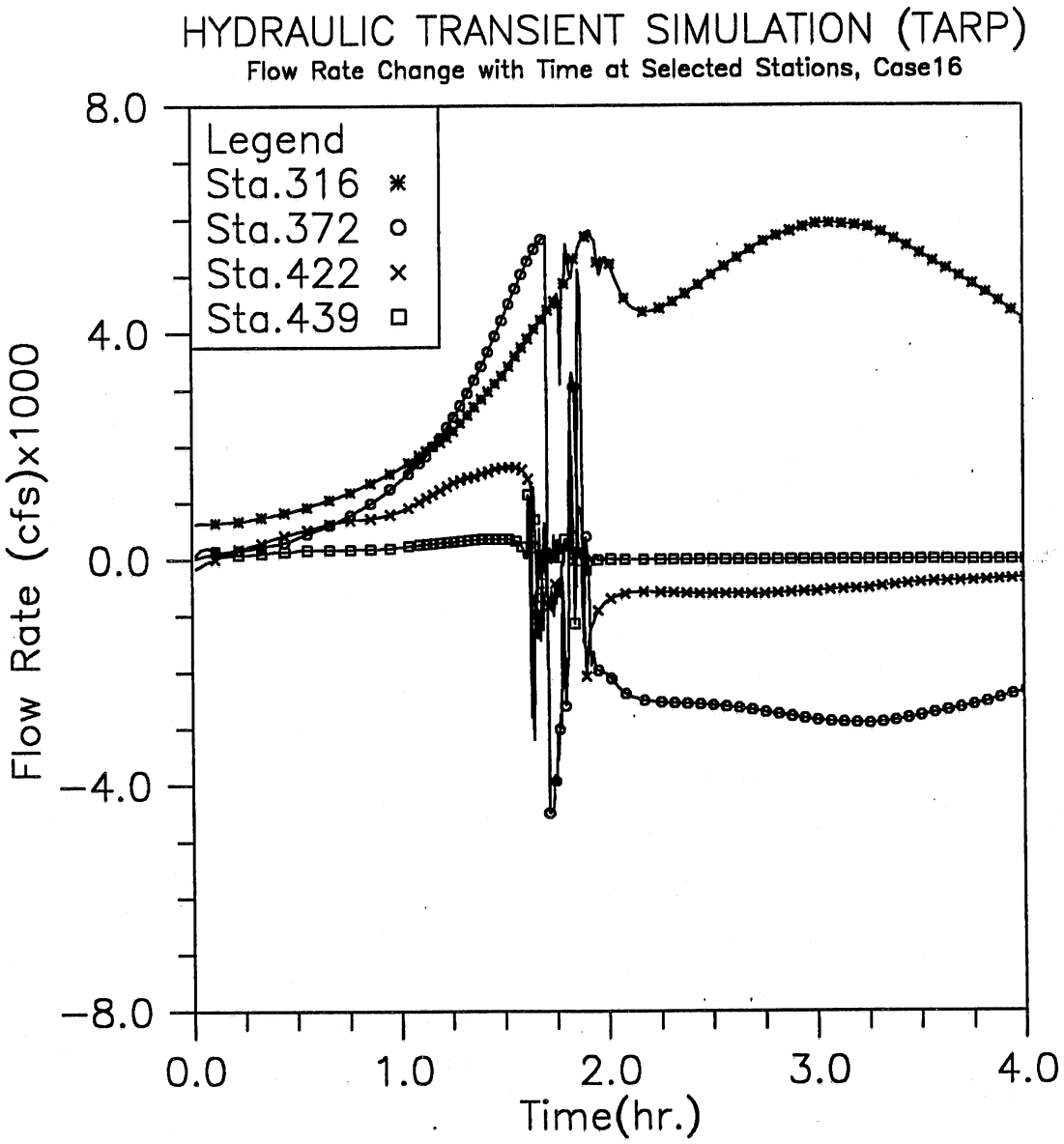

Fig. 3.6(g) Time variation of flow rate at four downstream locations; Modeling case: closed main gate and MAX event (Case 1–6)

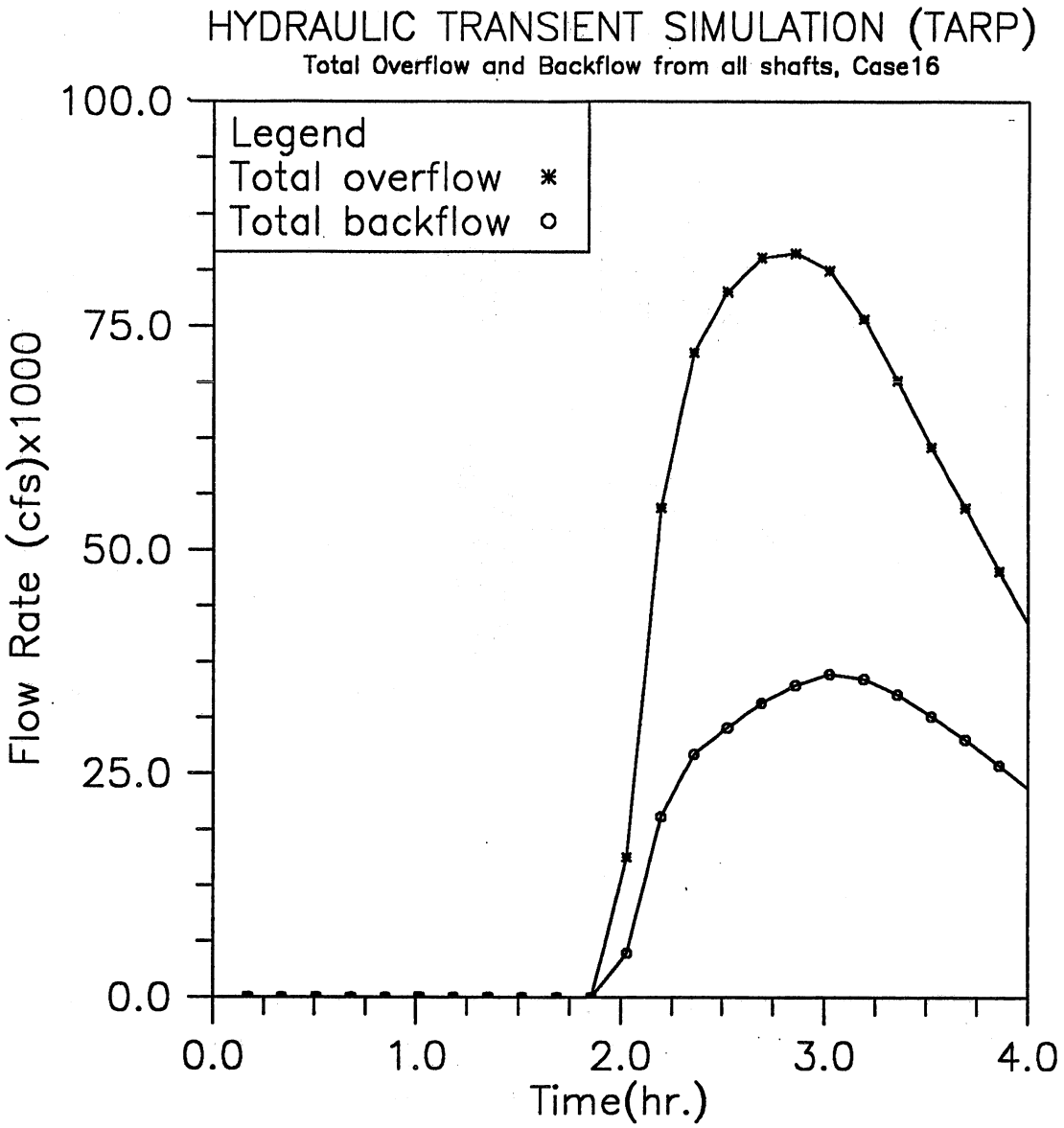

Fig. 3.6(h) Time variation of total overflow and backflow; Modeling case: closed main gate and MAX event (Case 1–6)

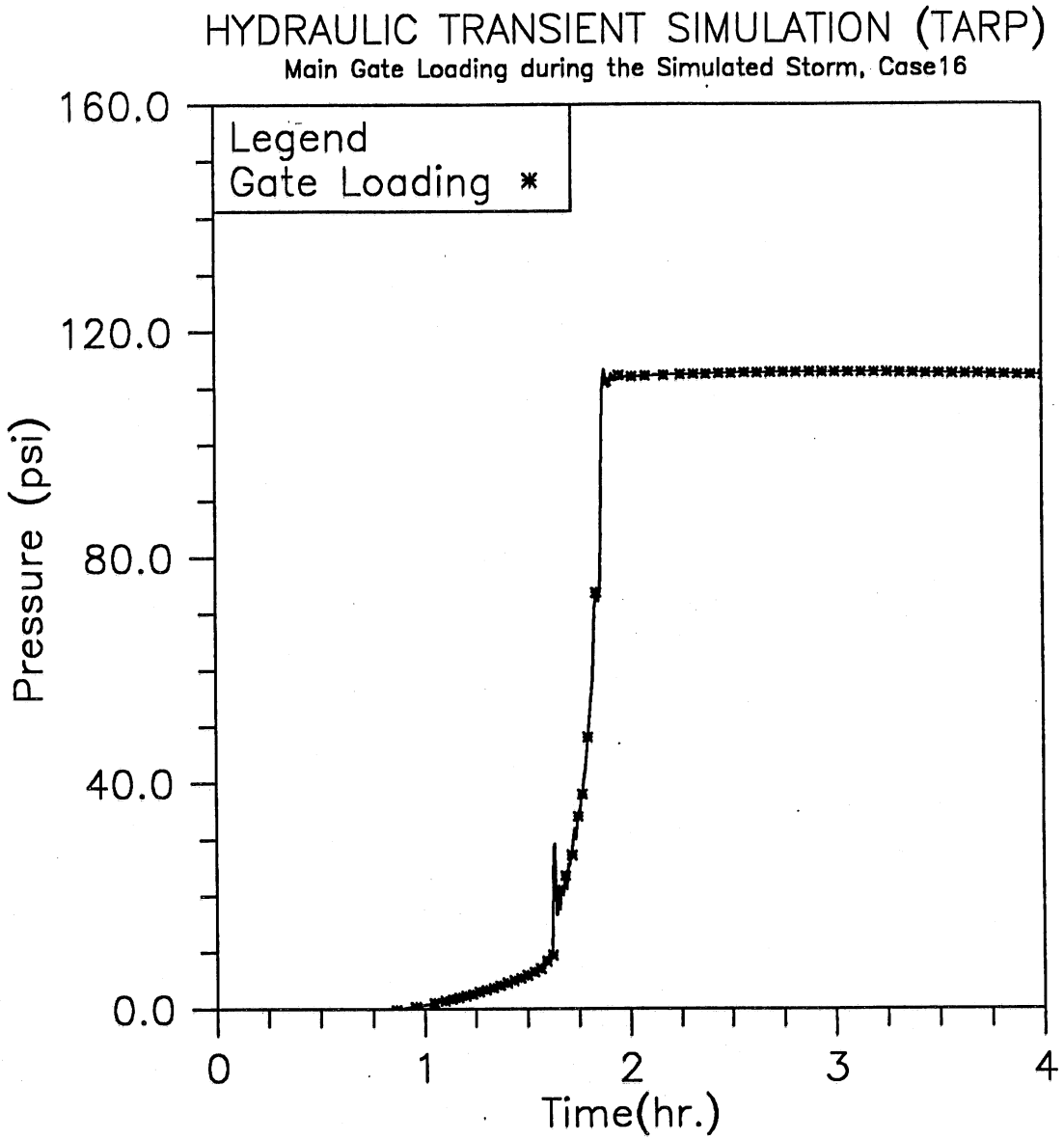

Fig. 3.6(i) Time variation of the averaged loading on the main gate; Modeling case: closed main gate and MAX event (Case 1–6)

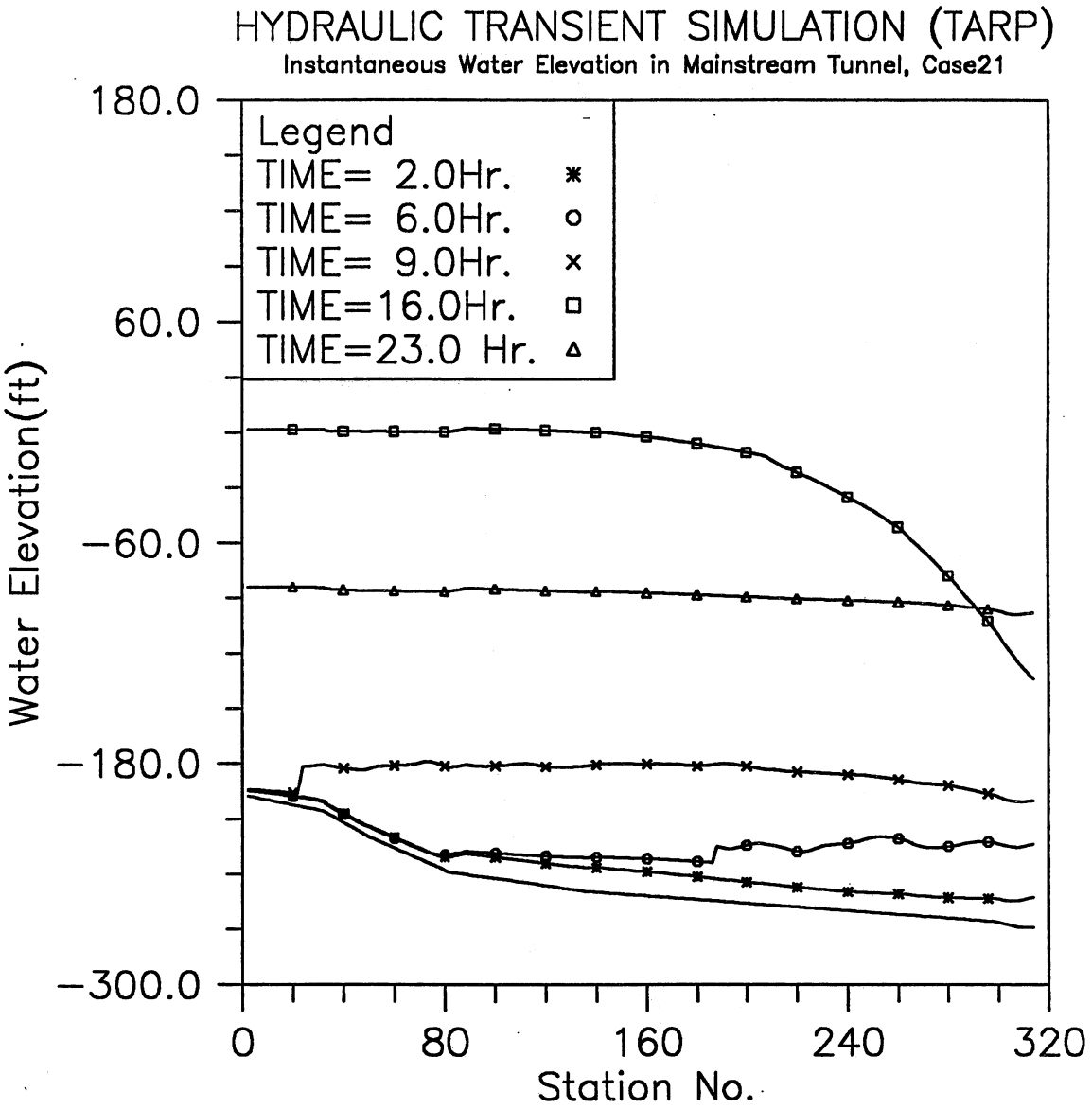

Fig. 3.7(a) Instantaneous hydraulic gradelines along the main tunnel; Modeling case: gate opening in 10 min., empty reservoir, and 100-year storm event (Case 2-1)

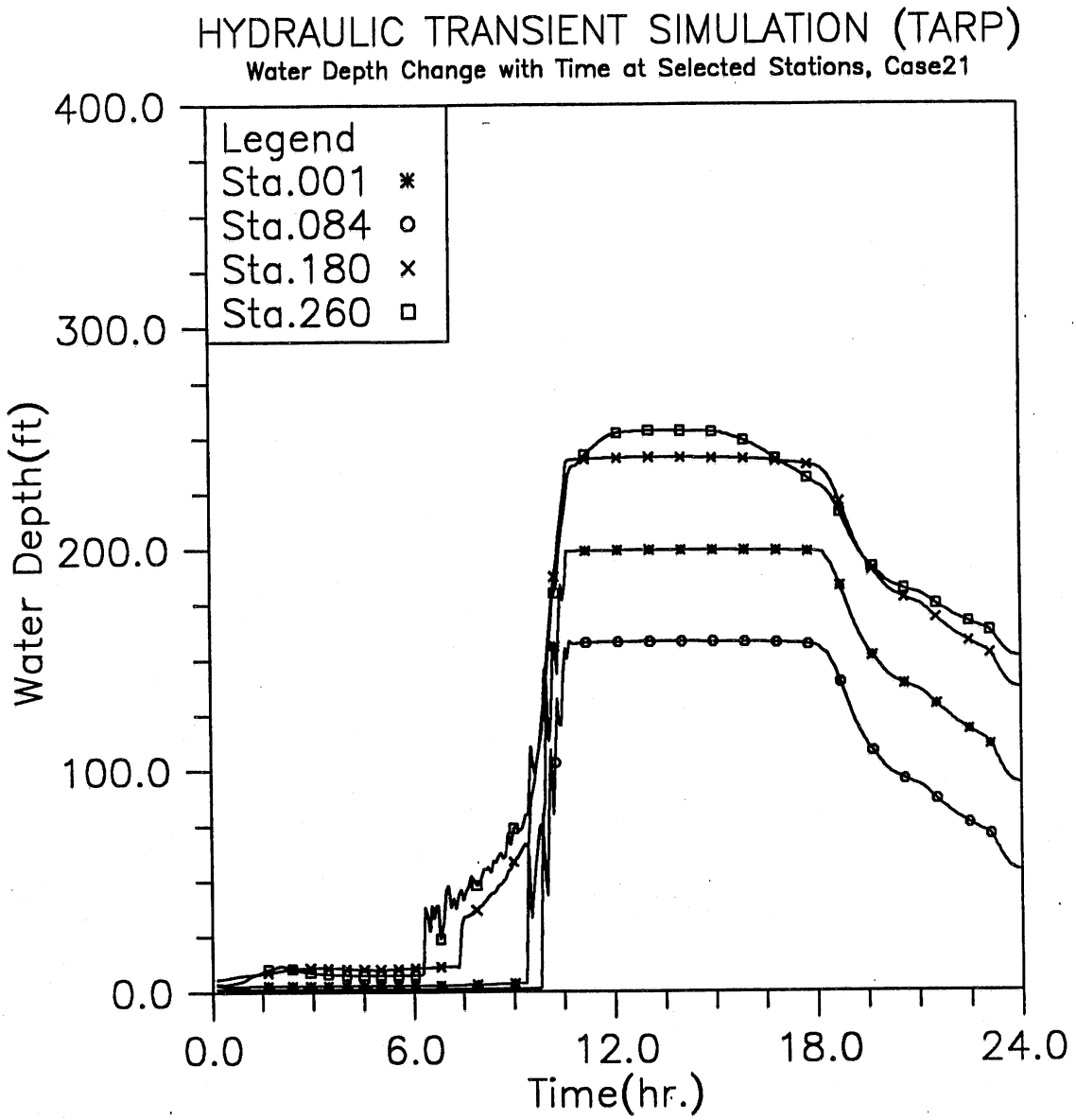

Fig. 3.7(b) Time variation of water depth at four upstream locations; Modeling case: gate opening in 10 min., empty reservoir, and 100–year storm event (Case 2–1)

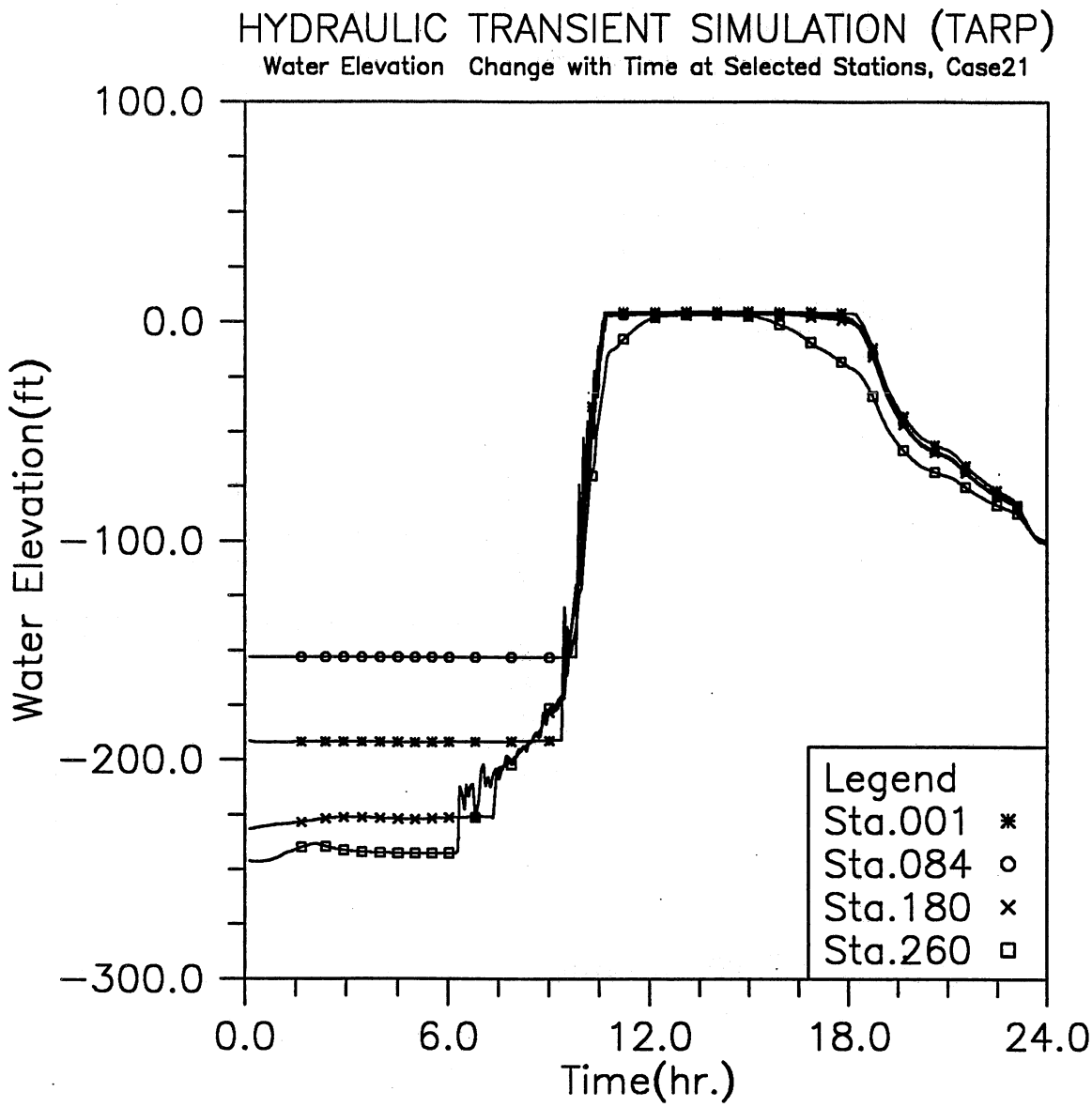

Fig. 3.7(c) Time variation of water elevation at four upstream locations; Modeling case: gate opening in 10 min., empty reservoir, and 100–year storm event (Case 2–1)

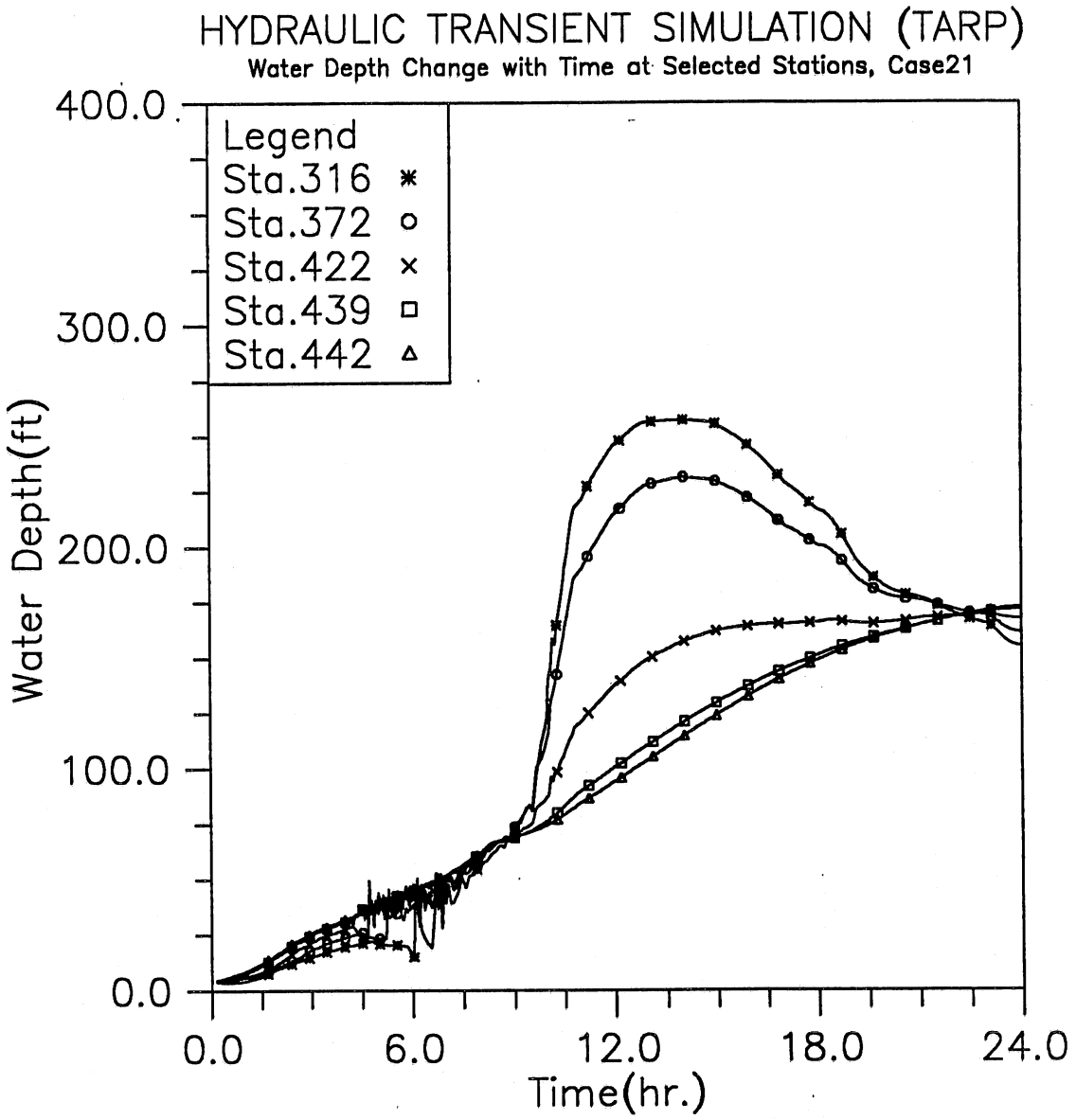

Fig. 3.7(d) Time variation of water depth at five downstream locations; Modeling case: gate opening in 10 min., empty reservoir, and 100–year storm event (Case 2–1)

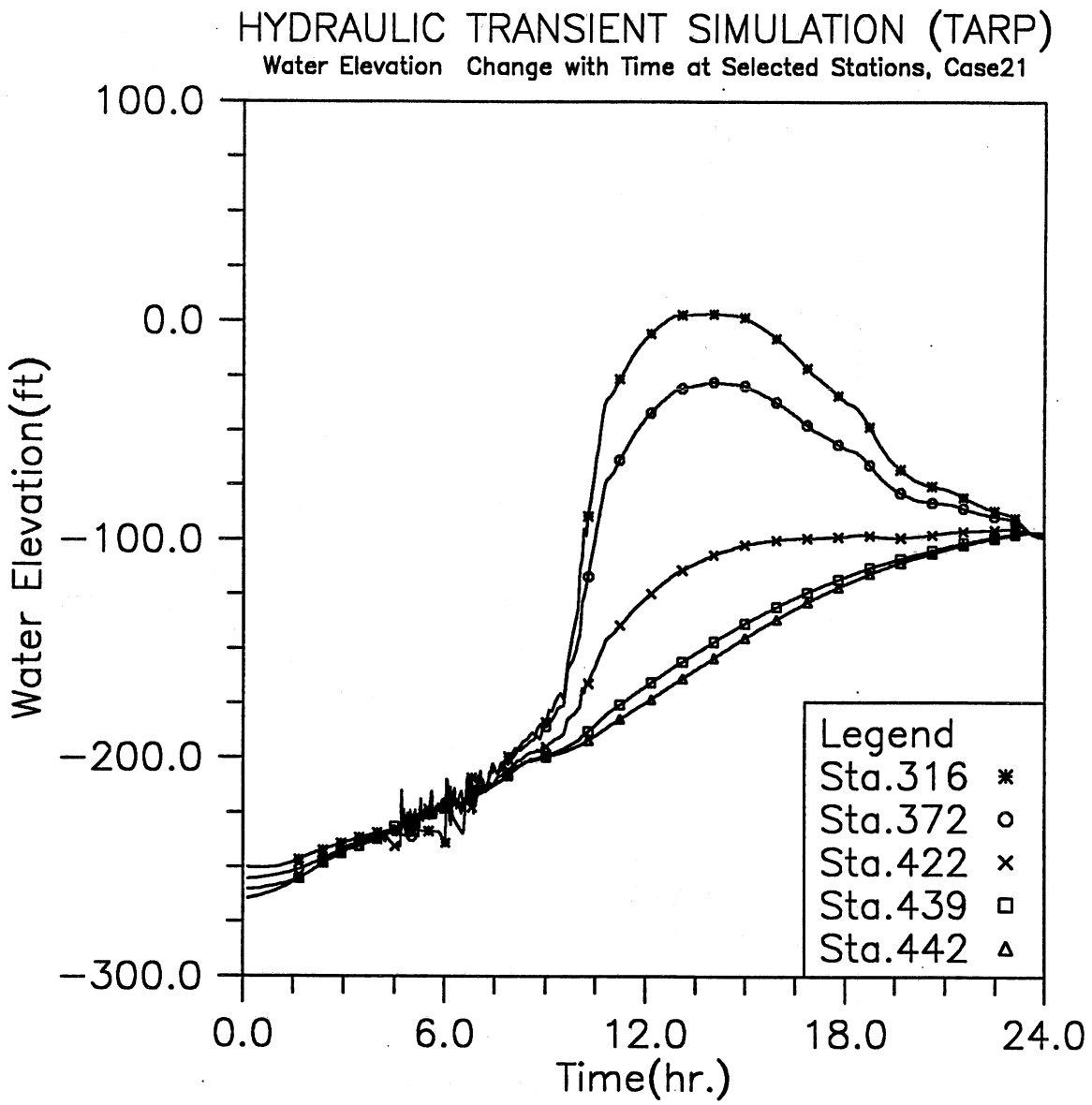

Fig. 3.7(e) Time variation of water elevation at five downstream locations; Modeling case: gate opening in 10 min., empty reservoir, and 100–year storm event (Case 2–1)

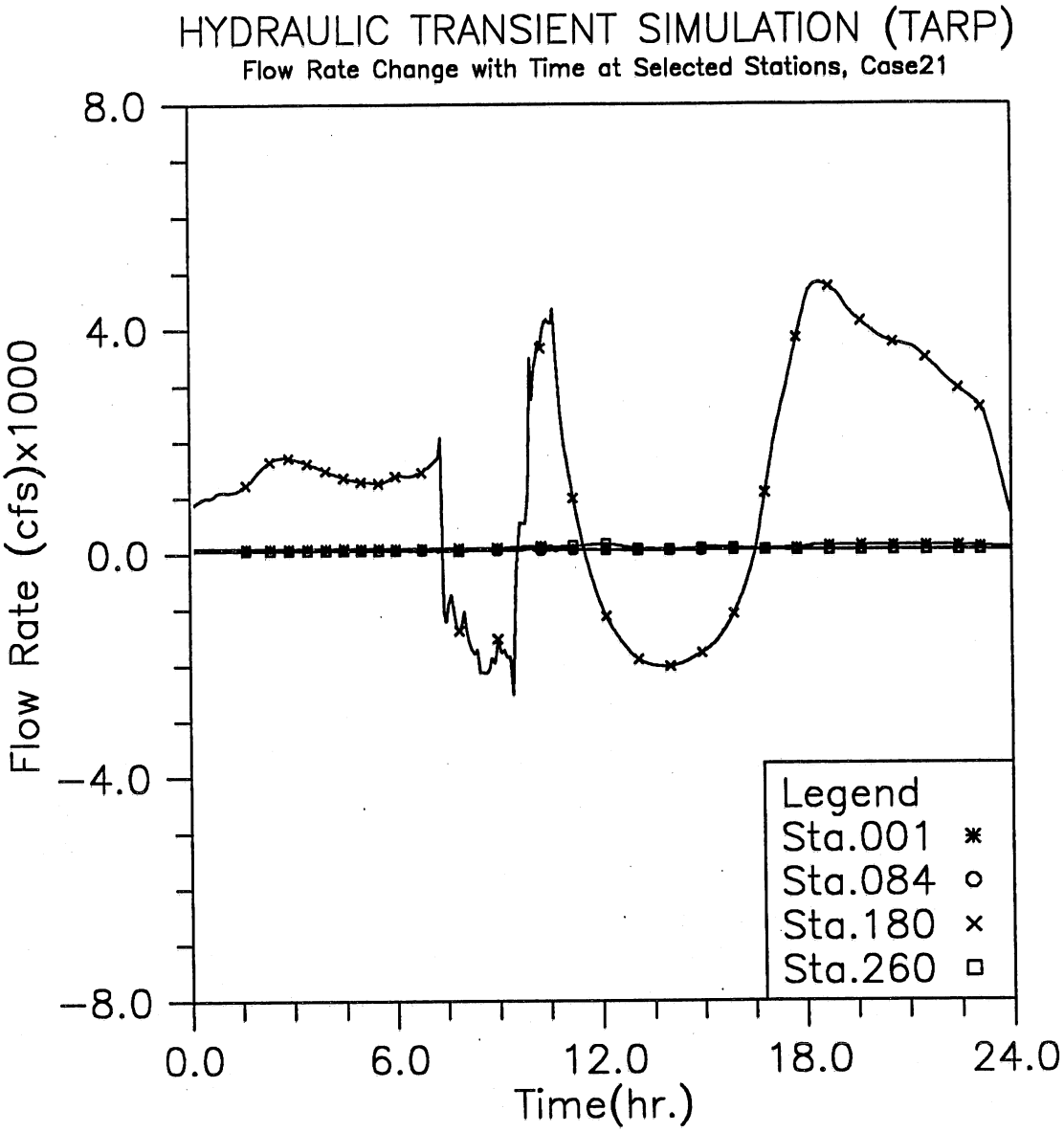

Fig. 3.7(f) Time variation of flow rate at four upstream locations; Modeling case: gate opening in 10 min., empty reservoir, and 100–year storm event (Case 2–1)

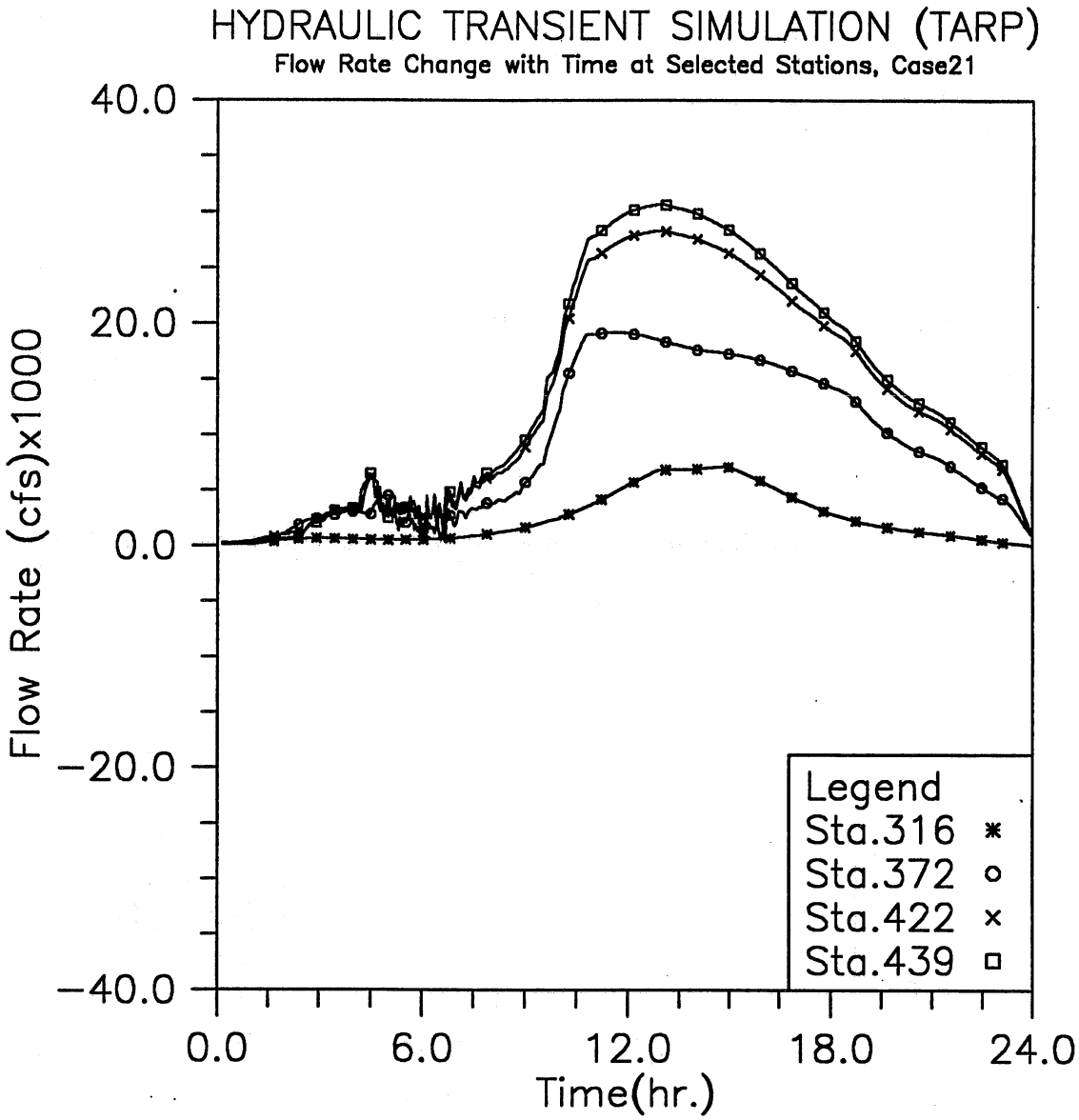

Fig. 3.7(g) Time variation of flow rate at four downstream locations; Modeling case: gate opening in 10 min., empty reservoir, and 100–year storm event (Case 2–1)

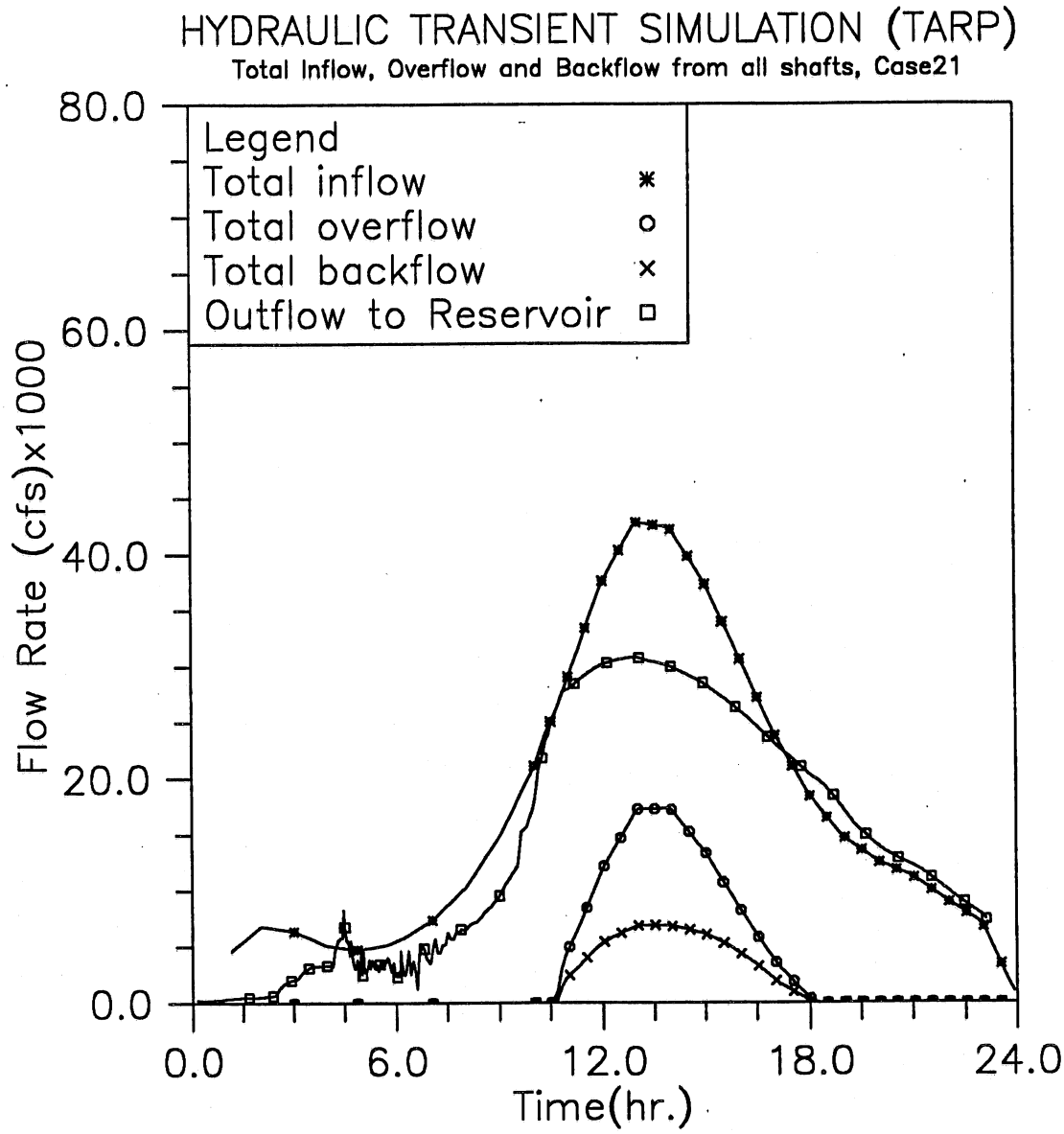

Fig. 3.7(h) Time variation of total inflow, overflow, backflow, and outflow to the reservoir; Modeling case: gate opening in 10 min., empty reservoir, and 100–year storm event (Case 2–1)

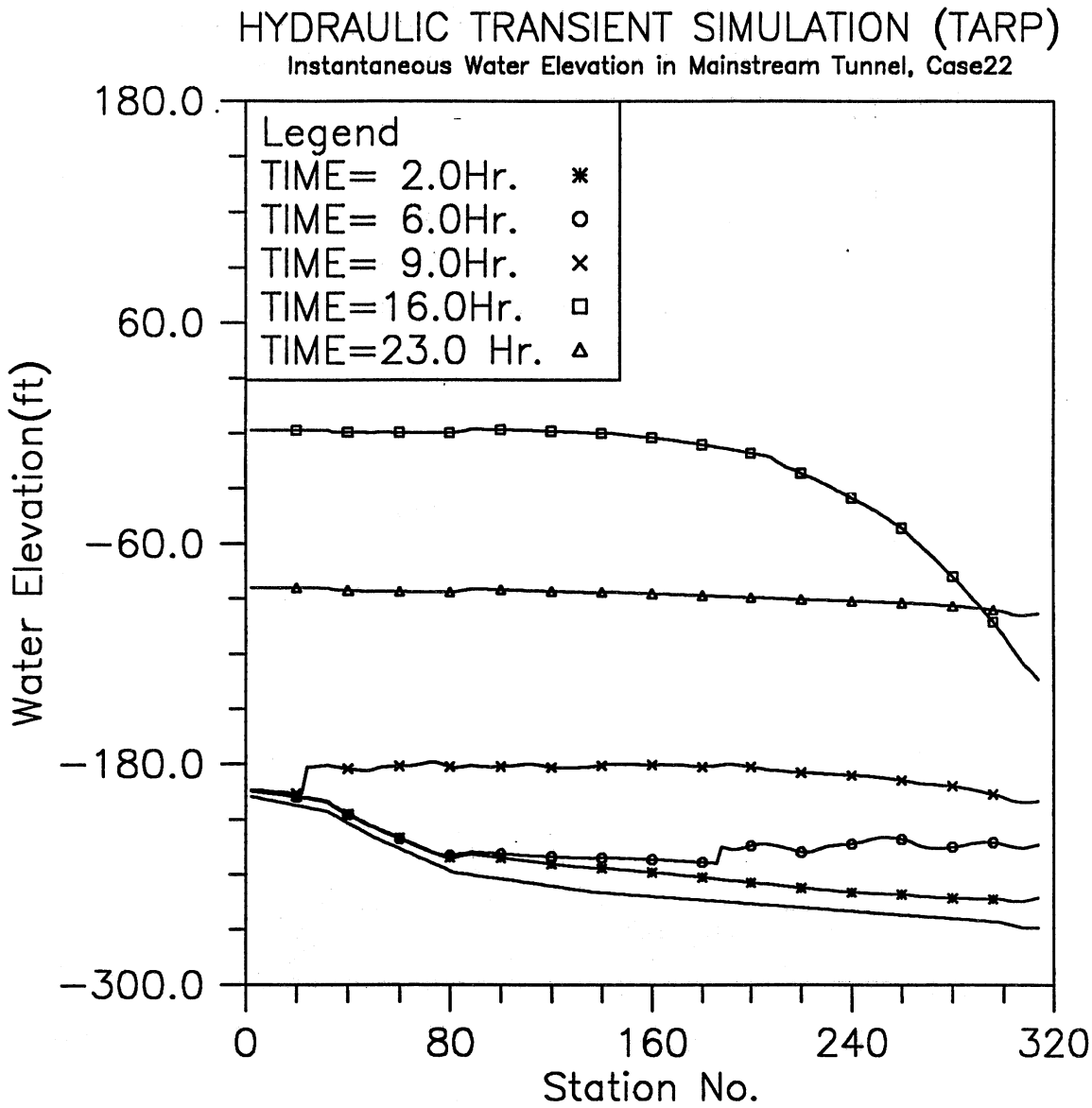

Fig. 3.8(a) Instantaneous hydraulic gradelines along the main tunnel; Modeling case: gate opening in 30 min., empty reservoir, and 100-year storm event (Case 2-2)

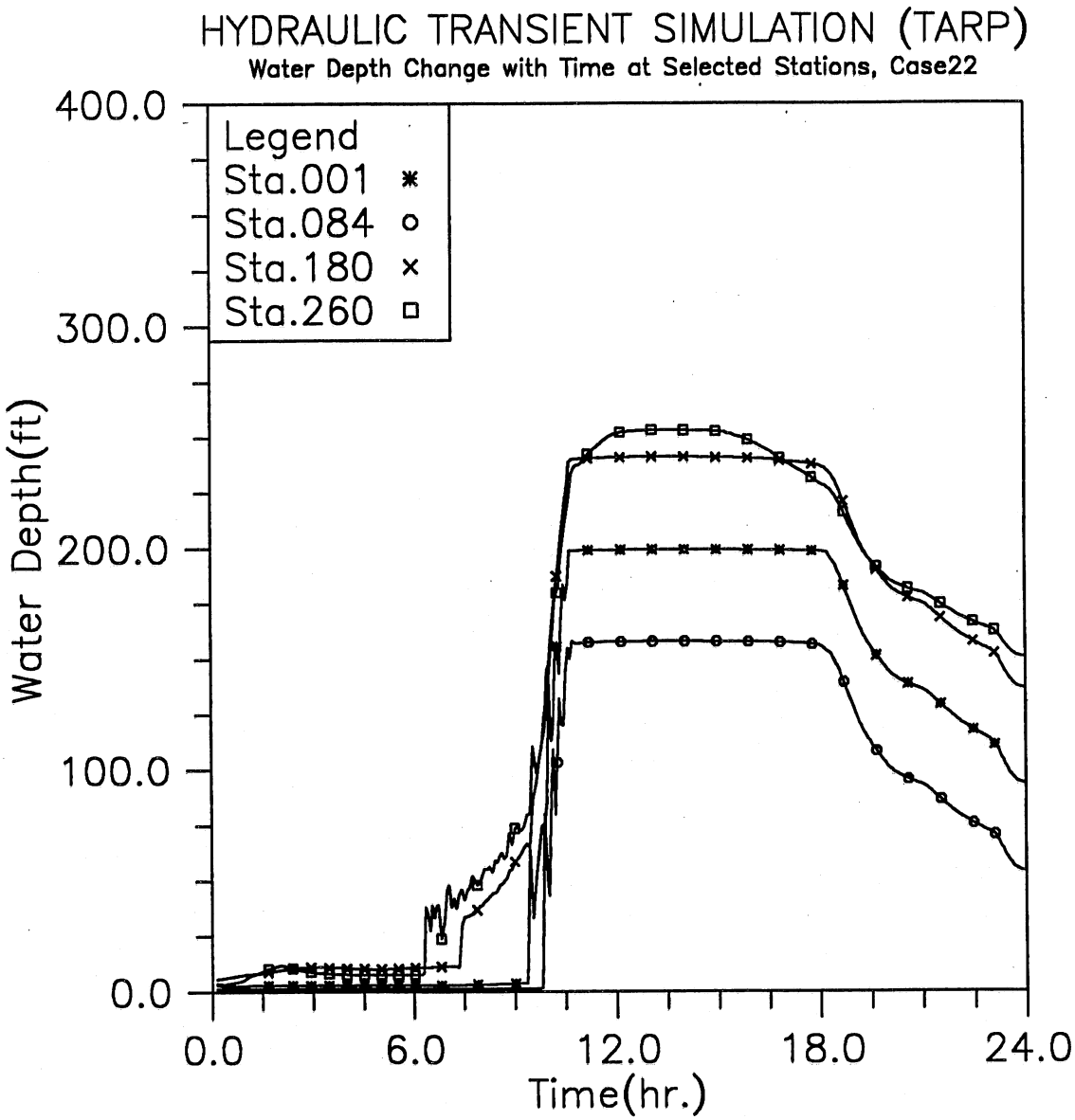

Fig. 3.8(b) Time variation of water depth at four upstream locations; Modeling case: gate opening in 30 min., empty reservoir, and 100–year storm event (Case 2–2)

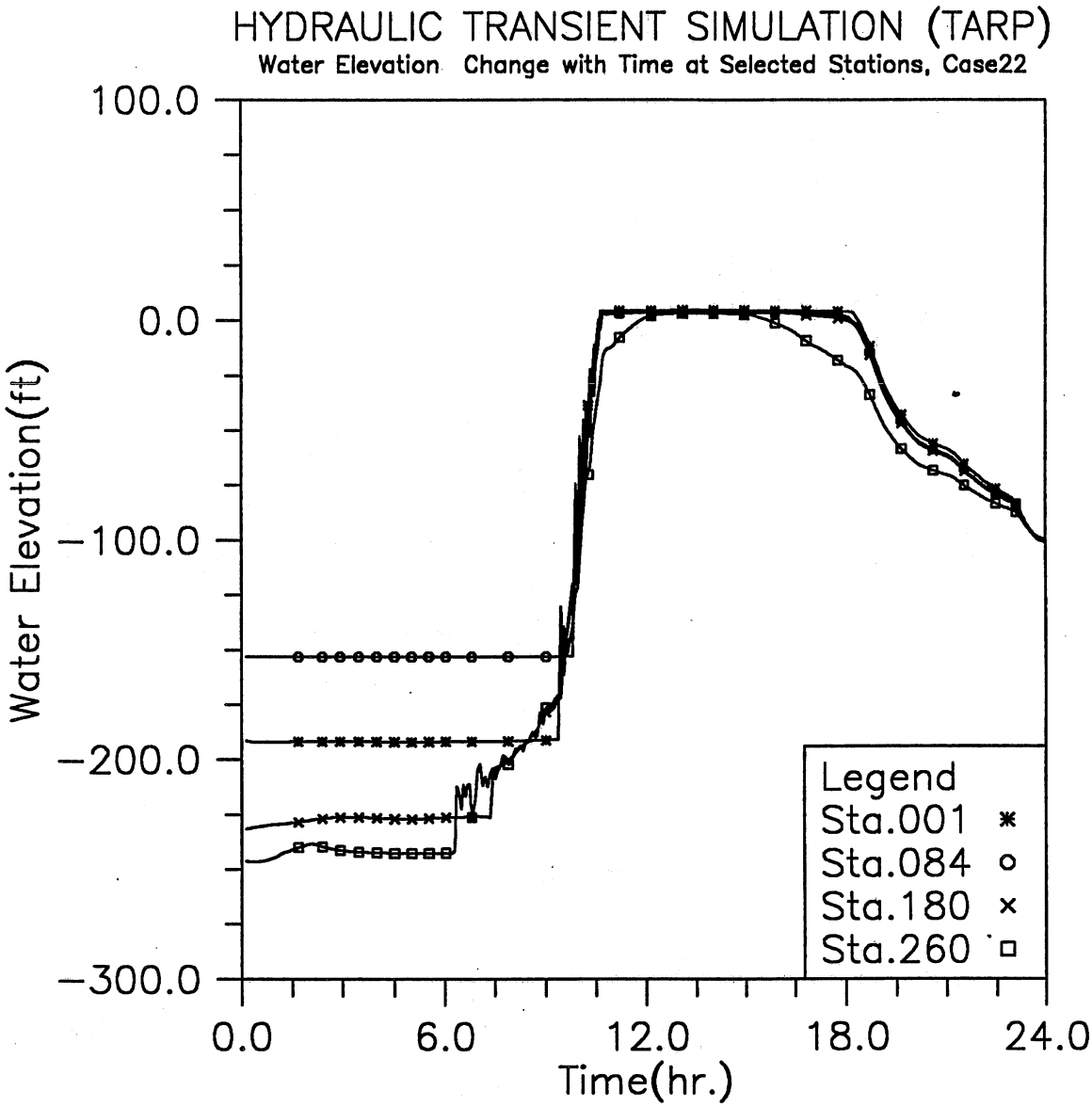

Fig. 3.8(c) Time variation of water elevation at four upstream locations; Modeling case: gate opening in 30 min., empty reservoir, and 100–year storm event (Case 2–2)

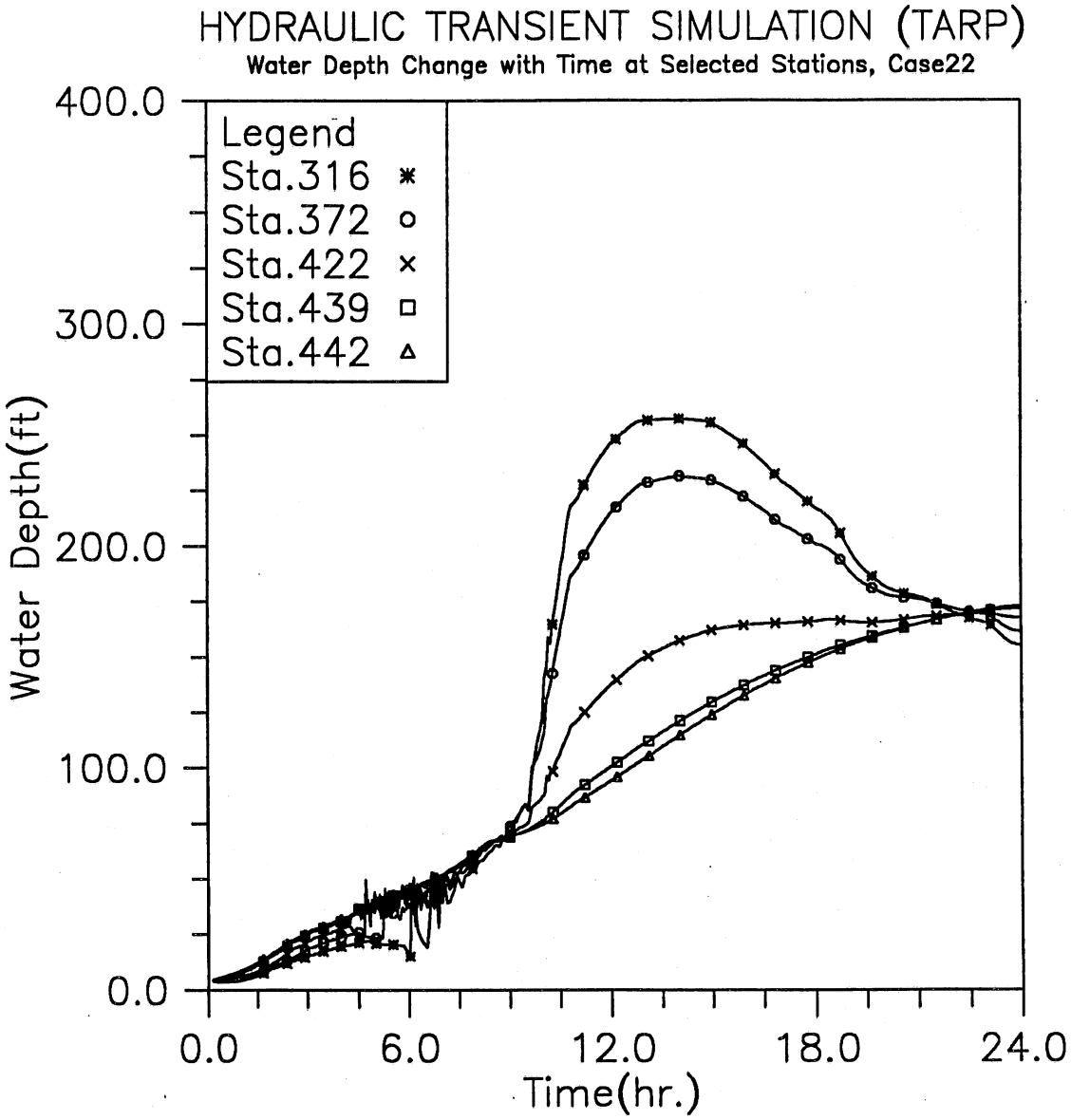

Fig. 3.8(d) Time variation of water depth at five downstream locations; Modeling case: gate opening in 30 min., empty reservoir, and 100–year storm event (Case 2–2)

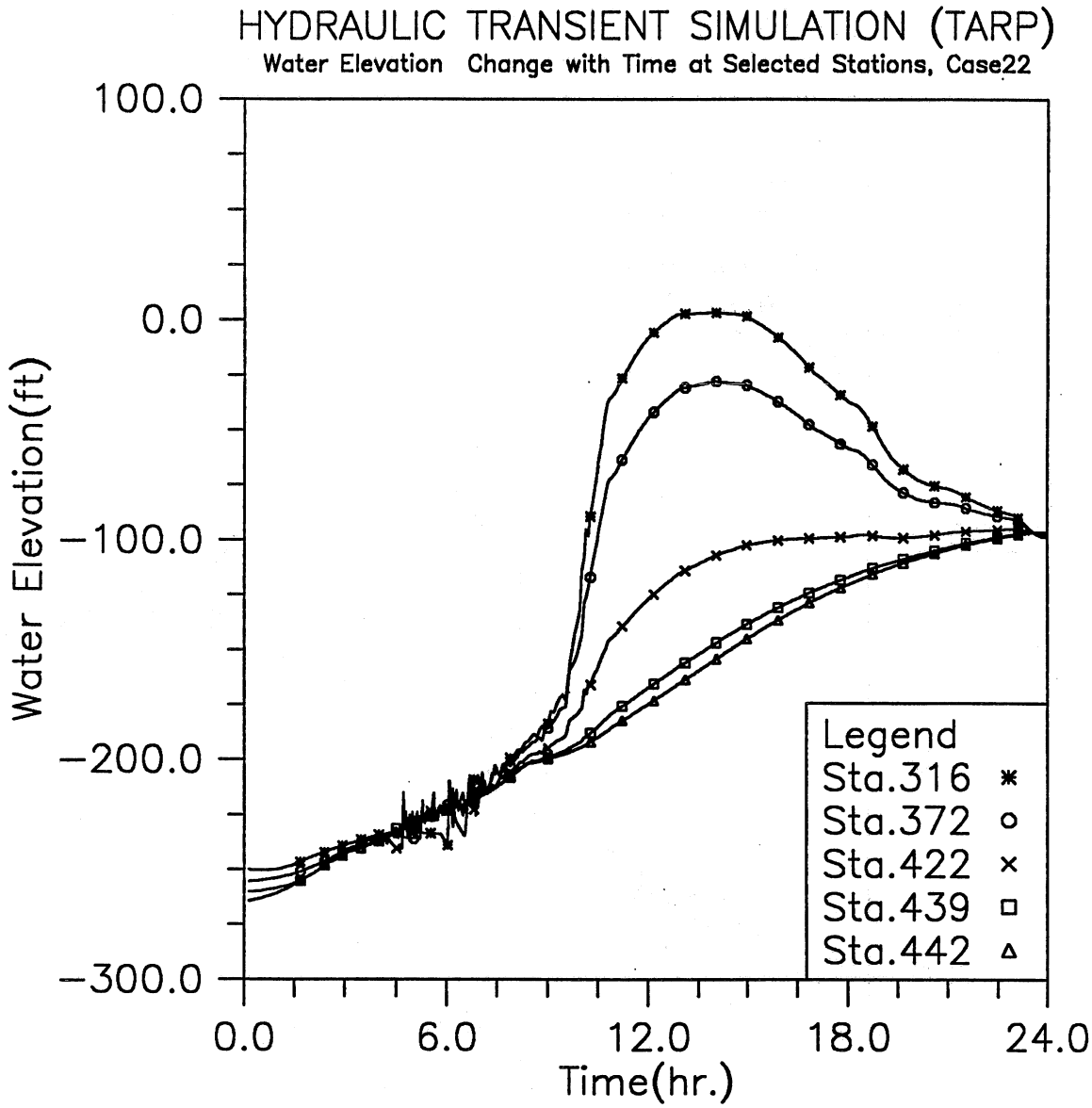

Fig. 3.8(e) Time variation of water elevation at five downstream locations; Modeling case: gate opening in 30 min., empty reservoir, and 100–year storm event (Case 2–2)

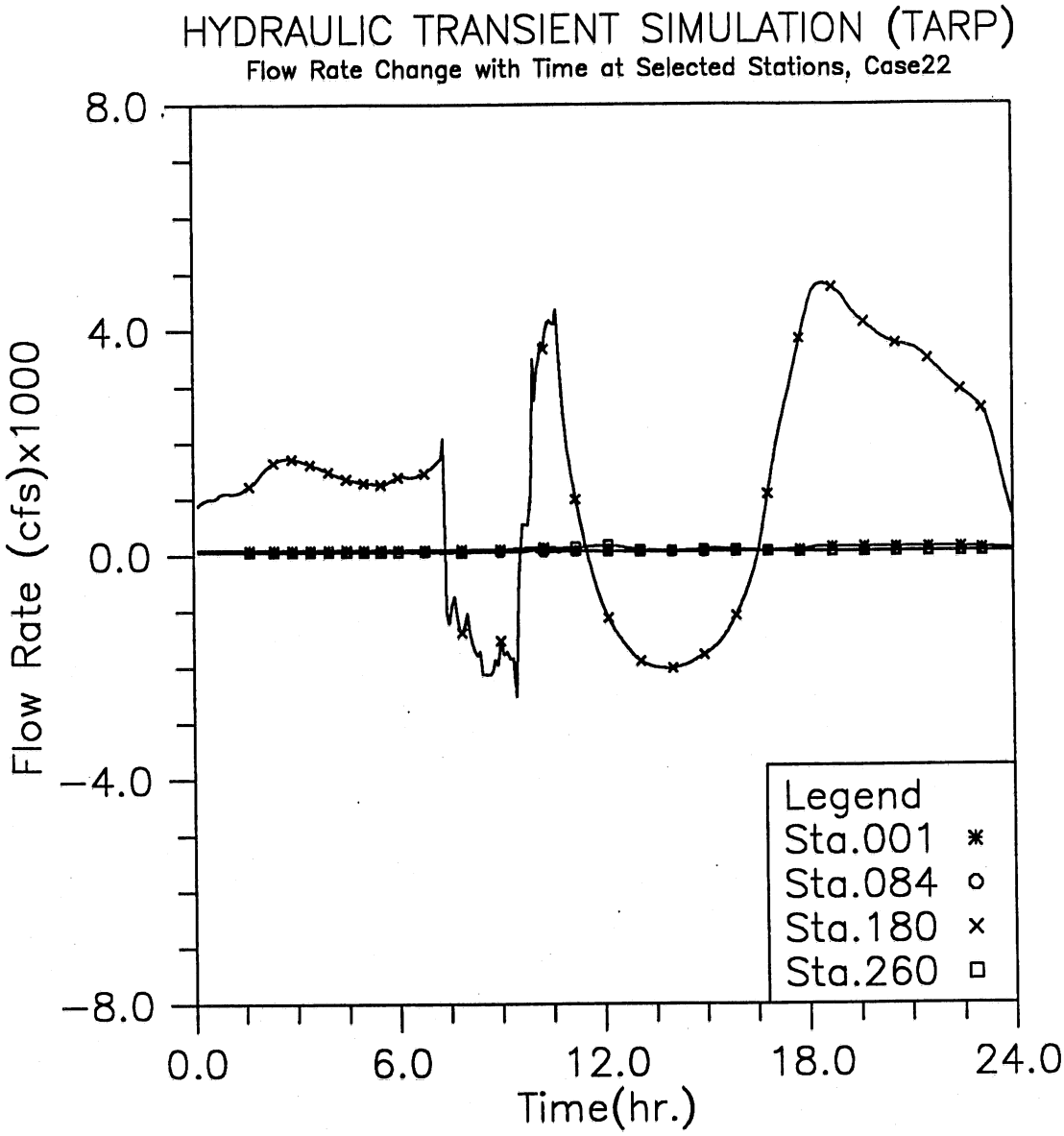

Fig. 3.8(f) Time variation of flow rate at four upstream locations; Modeling case: gate opening in 30 min., empty reservoir, and 100-year storm event (Case 2-2)

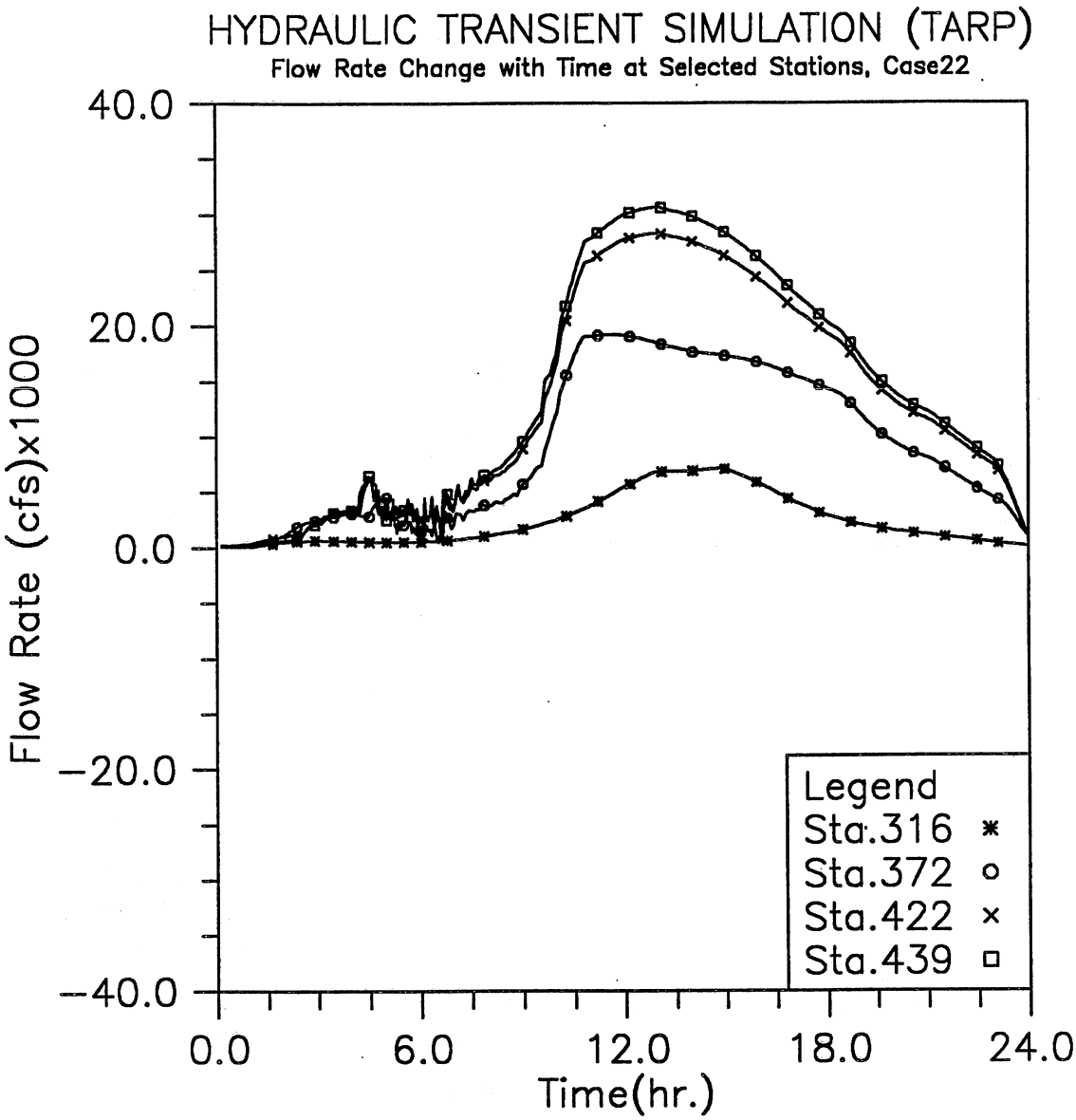

Fig. 3.8(g) Time variation of flow rate at four downstream locations; Modeling case: gate opening in 30 min., empty reservoir, and 100–year storm event (Case 2–2)

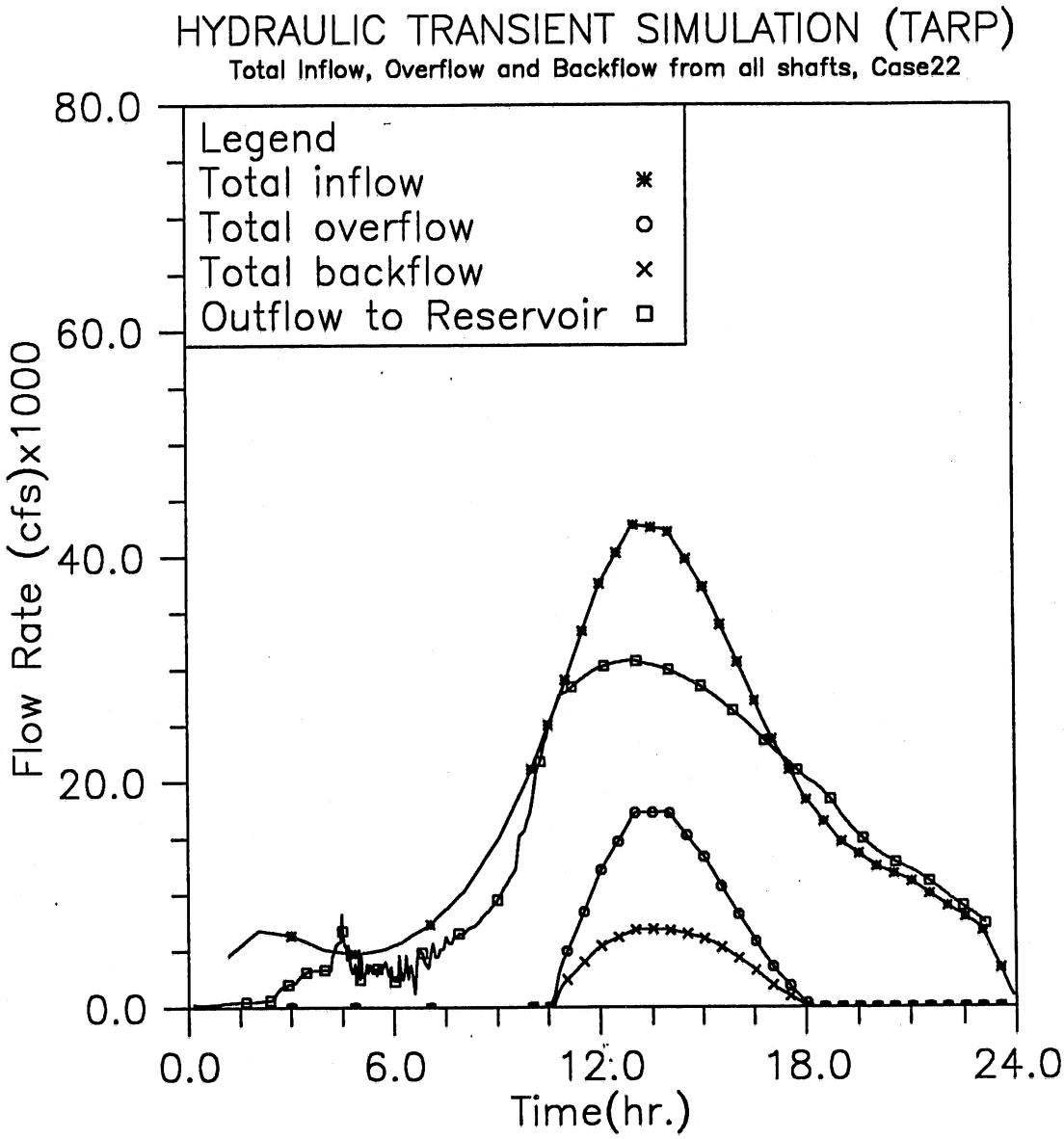

Fig. 3.8(h) Time variation of total inflow, overflow, backflow, and outflow to the reservoir; Modeling case: gate opening in 30 min., empty reservoir, and 100–year storm event (Case 2–2)

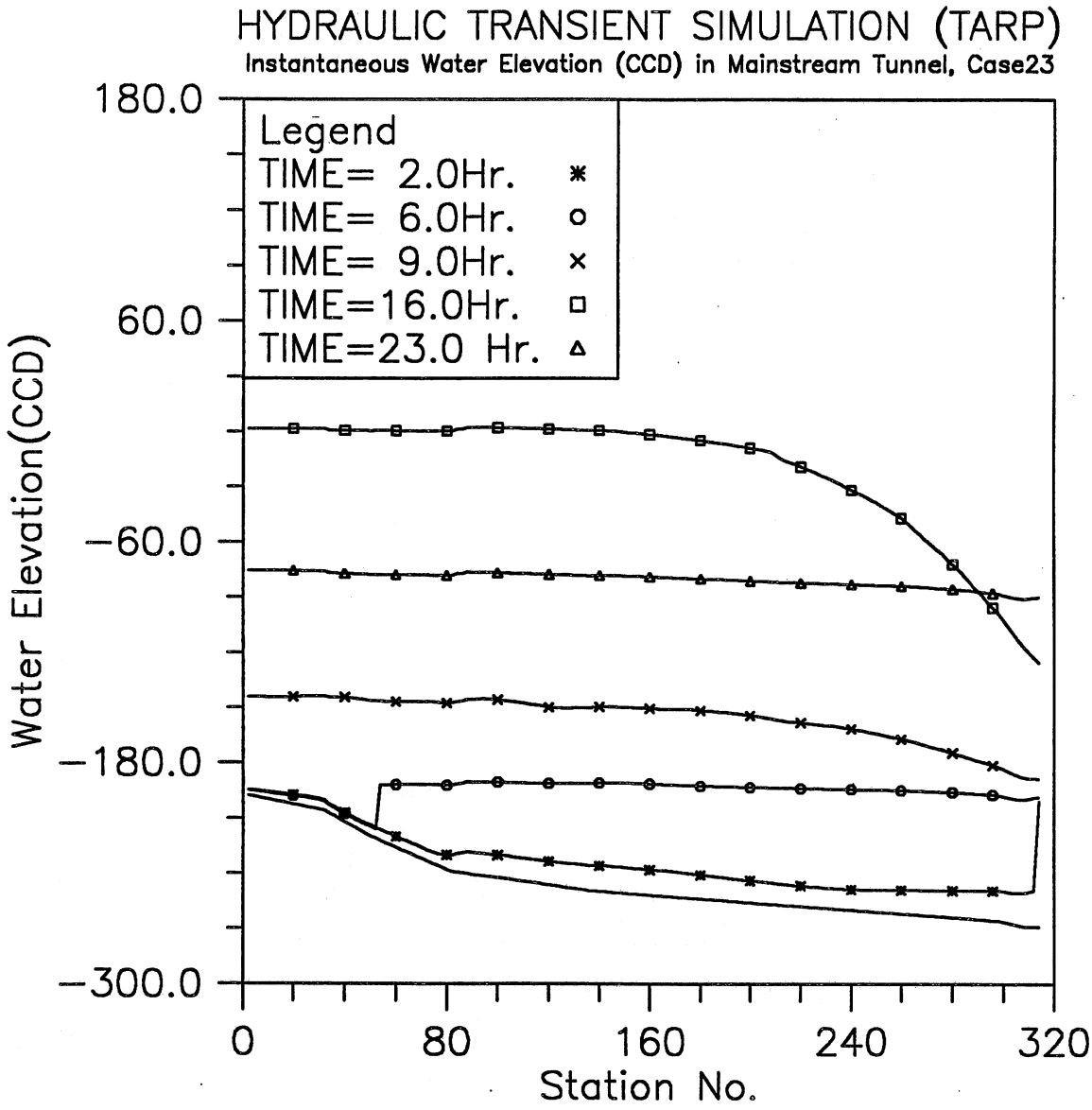

Fig. 3.9(a) Instantaneous hydraulic gradelines along the main tunnel; Modeling case: gate opening in 10 min., initial reservoir level at –198, and 100–year storm event (Case 2–3)

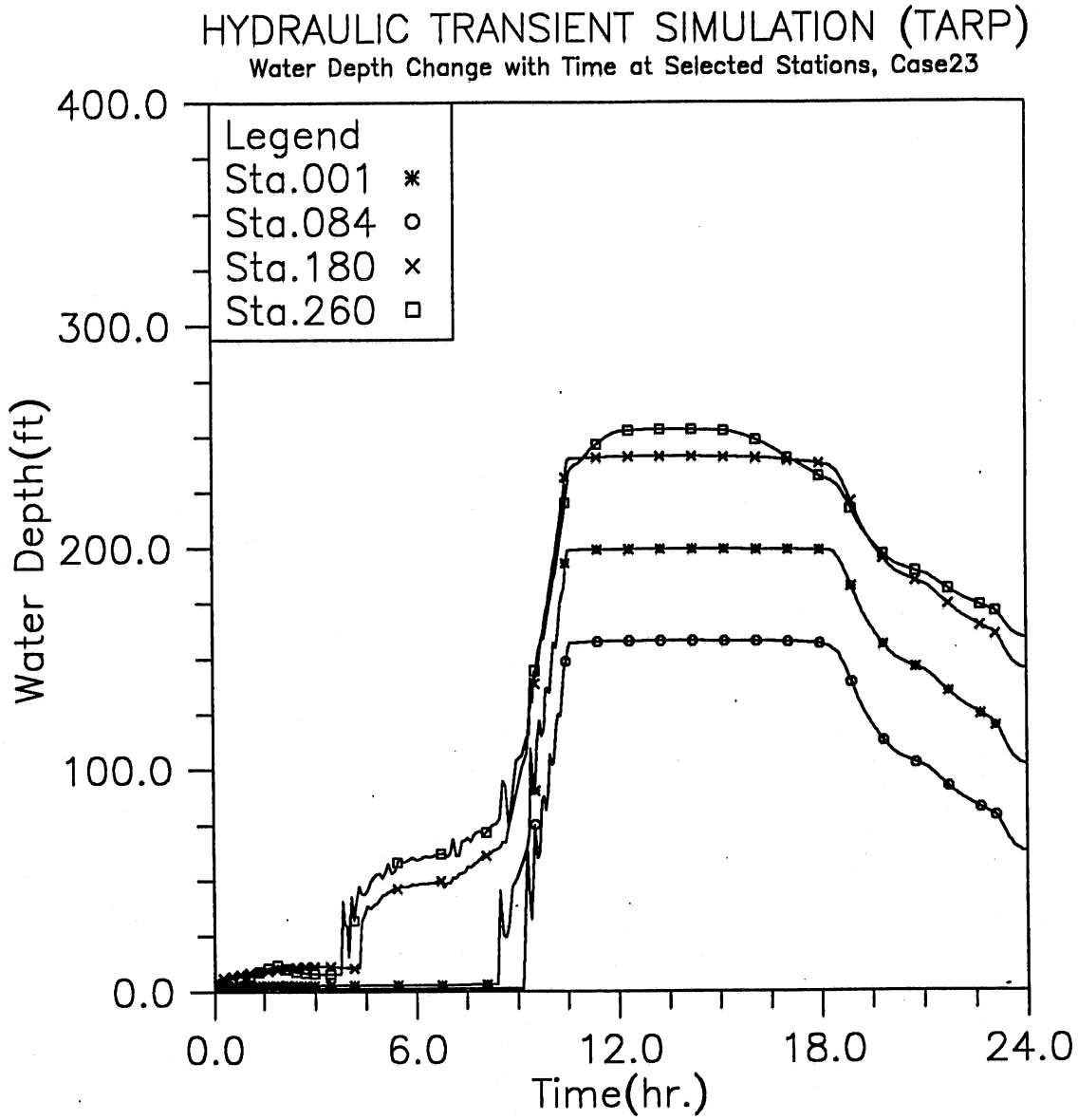

Fig. 3.9(b) Time variation of water depth at four upstream locations; Modeling case: gate opening in 10 min., initial reservoir level at –198, and 100–year storm event (Case 2–3)

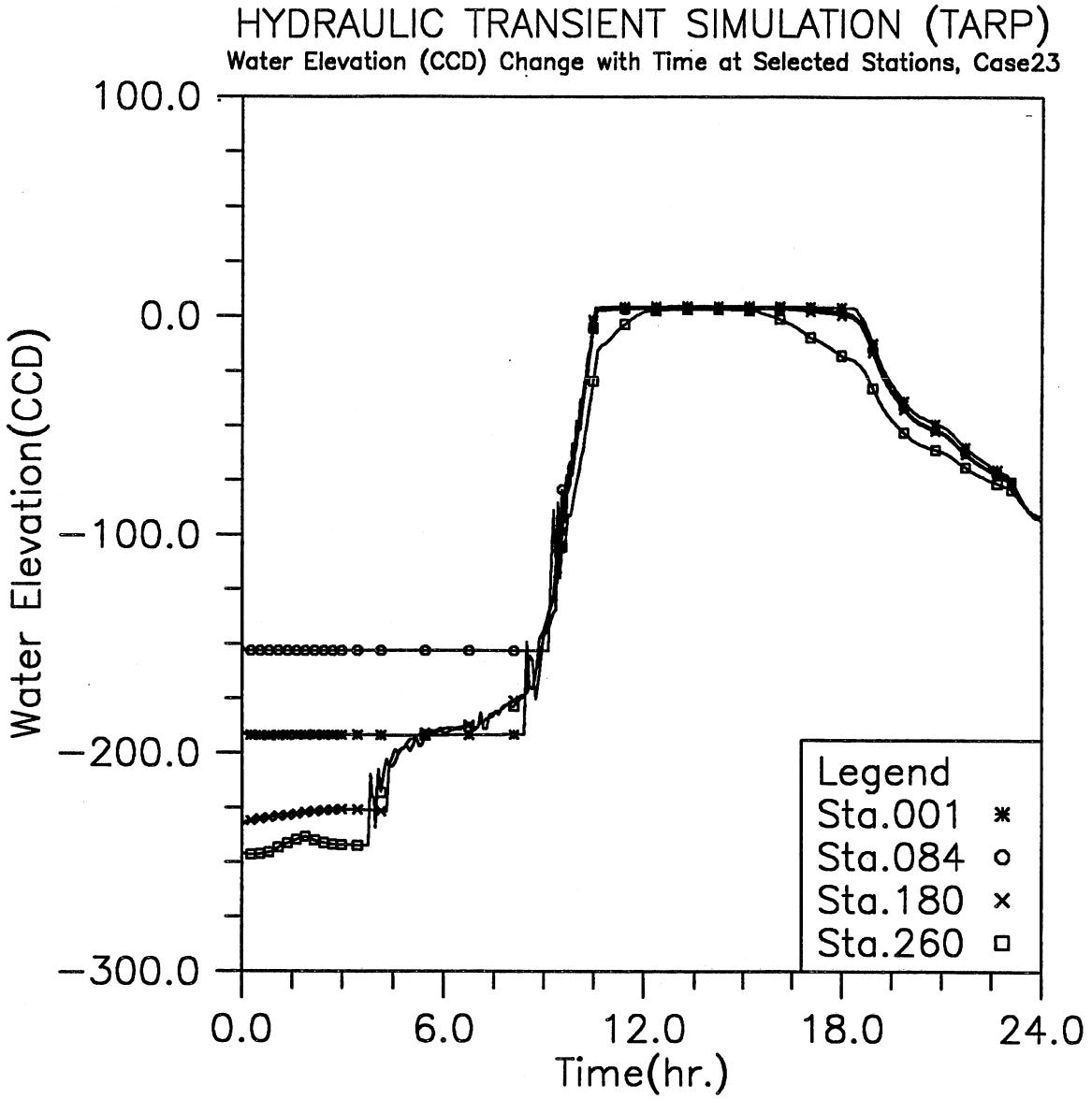

Fig. 3.9(c) Time variation of water elevation at four upstream locations; Modeling case: gate opening in 10 min., initial reservoir level at –198, and 100–year storm event (Case 2–3)

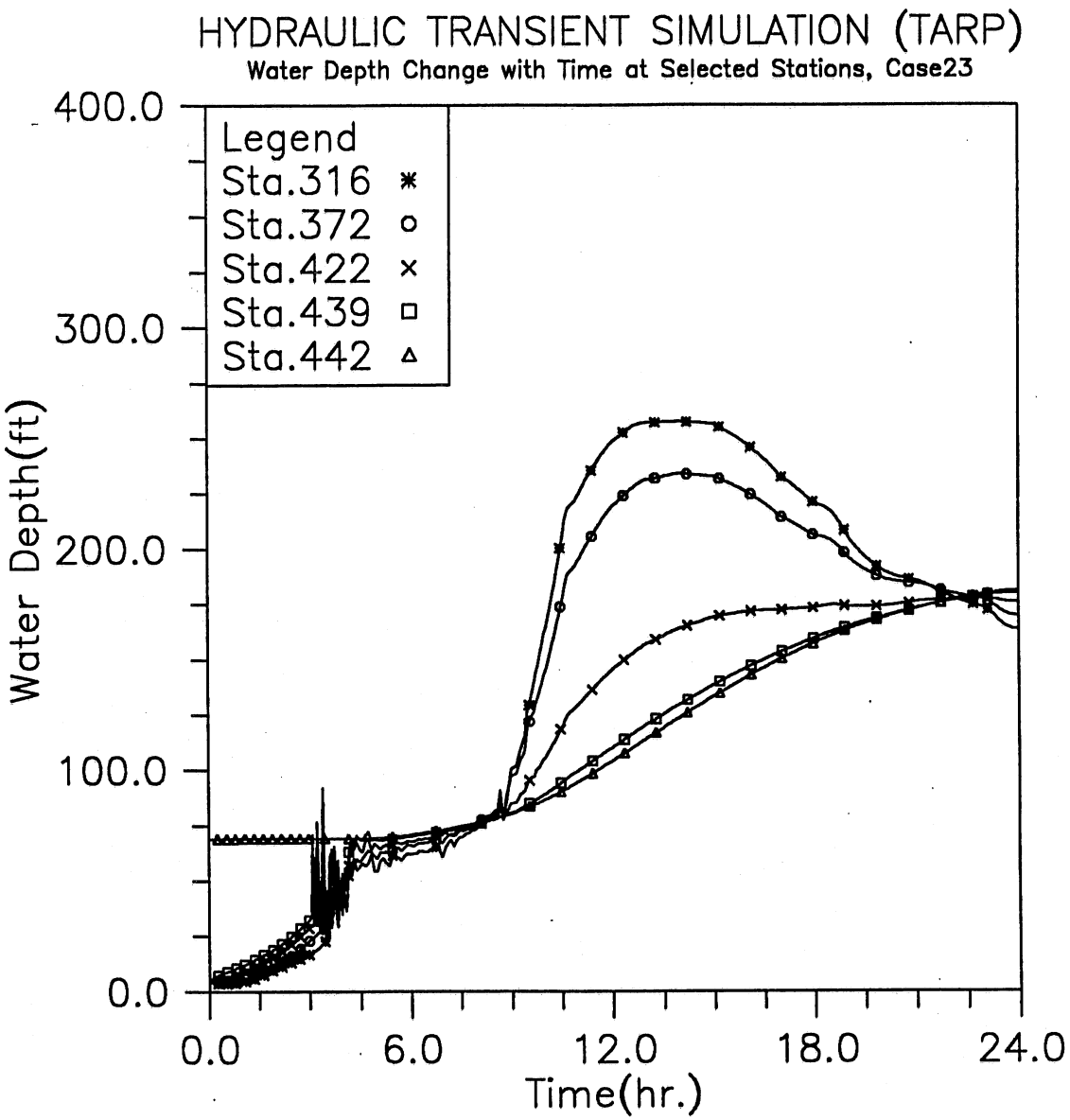

Fig. 3.9(d) Time variation of water depth at five downstream locations; Modeling case: gate opening in 10 min., initial reservoir level at –198, and 100–year storm event (Case 2–3)

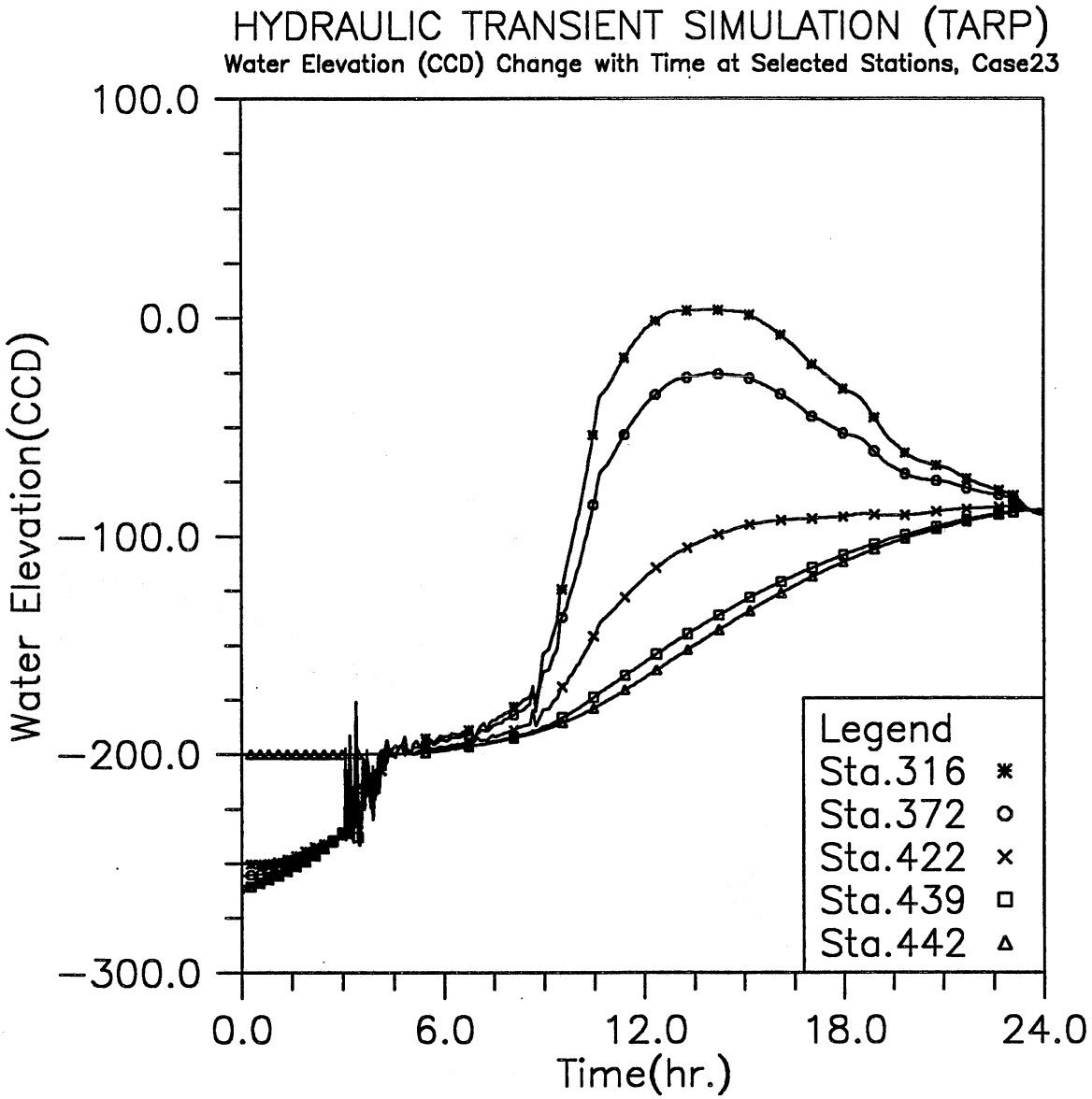

Fig. 3.9(e) Time variation of water elevation at five downstream locations; Modeling case: gate opening in 10 min., initial reservoir level at –198, and 100–year storm event (Case 2–3)

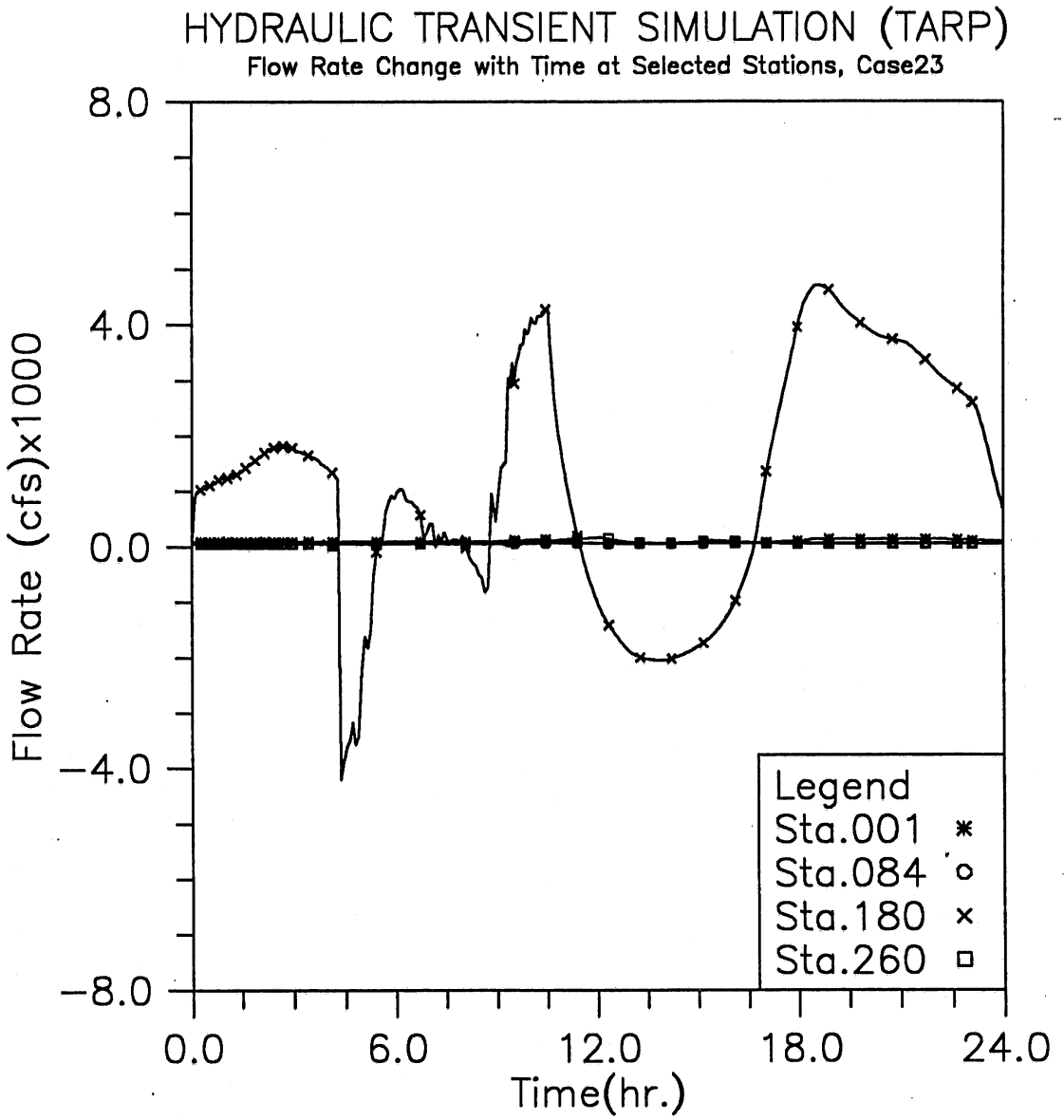

Fig. 3.9(f) Time variation of flow rate at four upstream locations; Modeling case: gate opening in 10 min., initial reservoir level at –198, and 100–year storm event (Case 2–3)

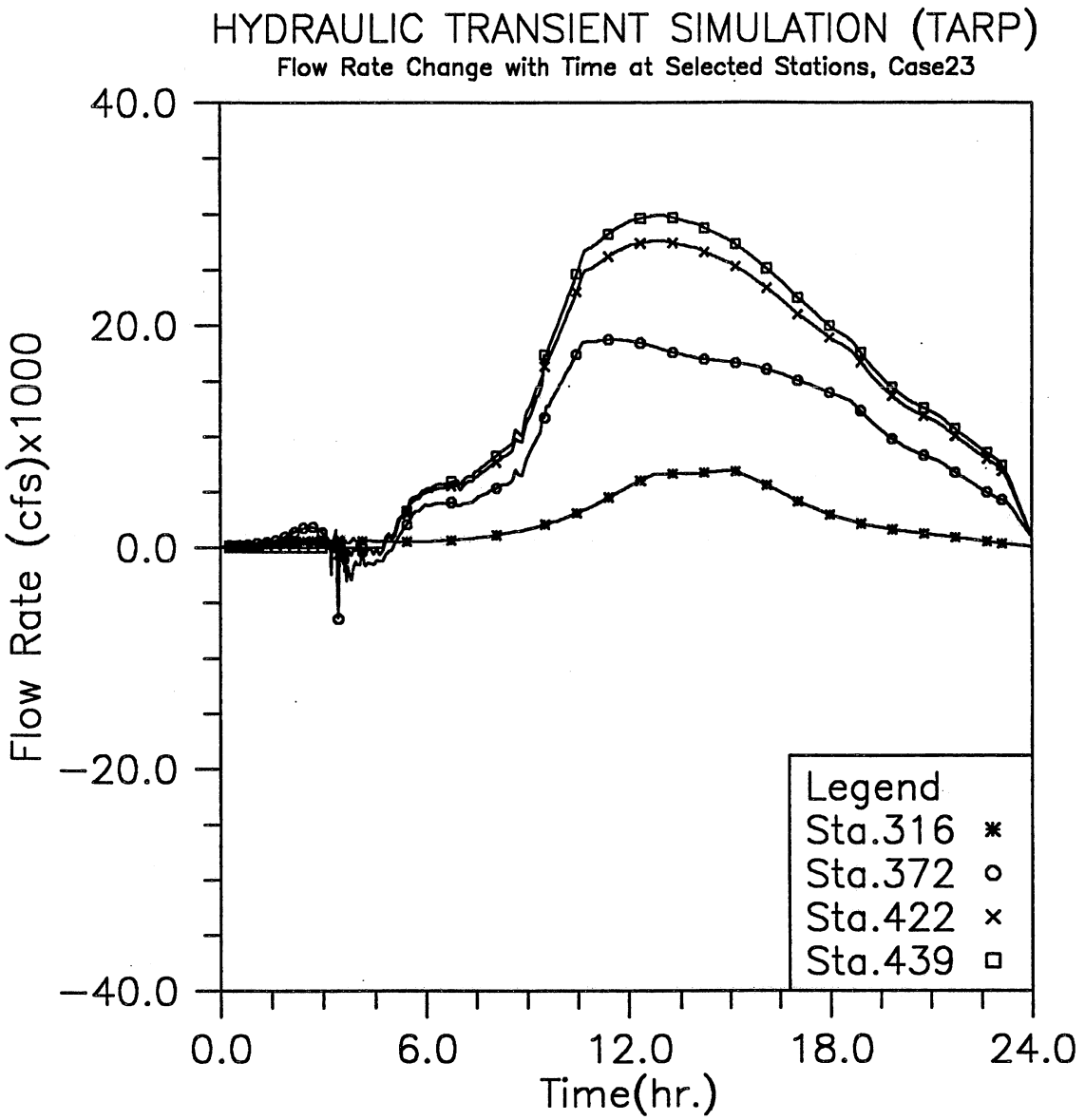

Fig. 3.9(g) Time variation of flow rate at four downstream locations; Modeling case: gate opening in 10 min., initial reservoir level at −198, and 100-year storm event (Case 2-3)

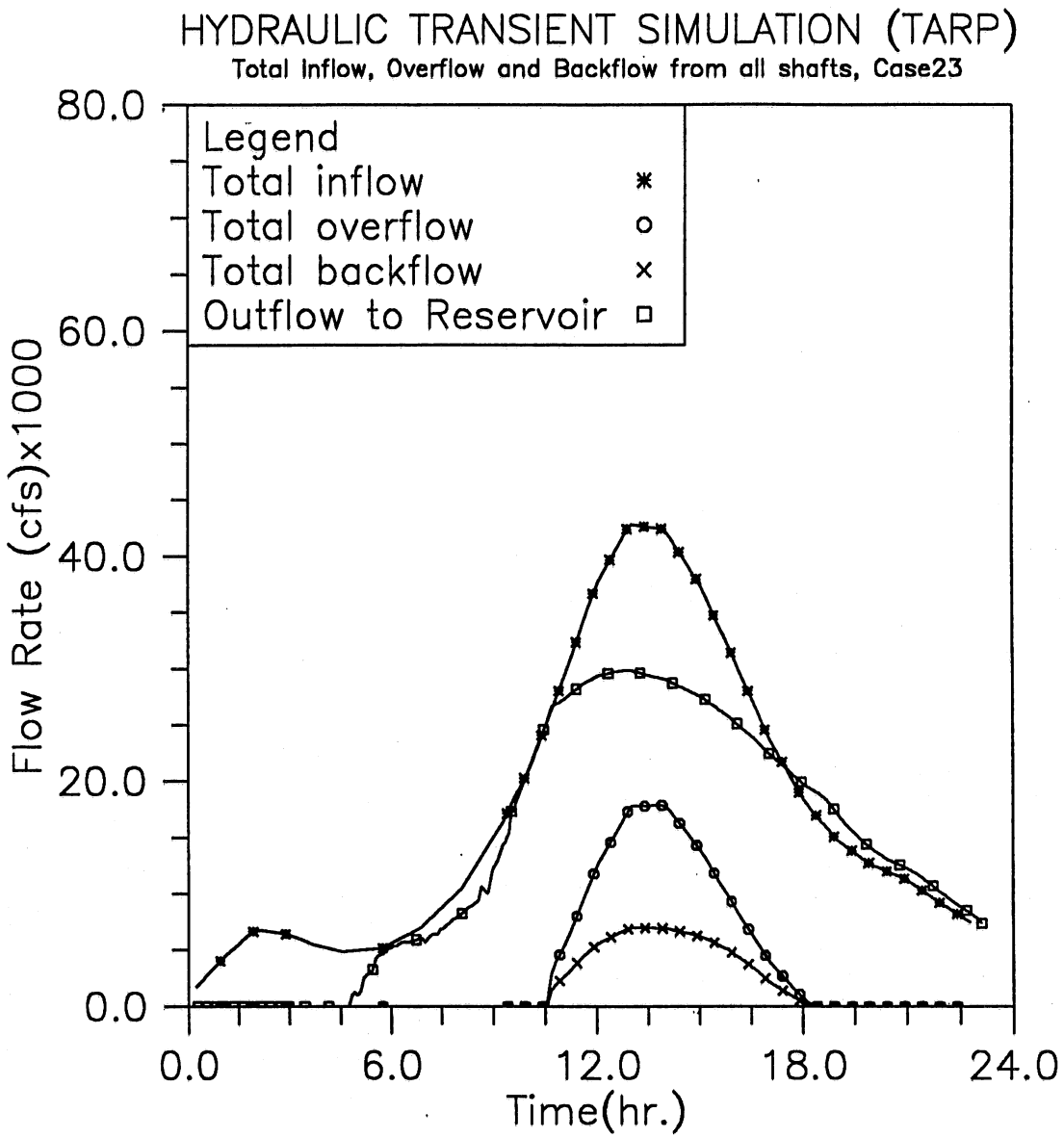

Fig. 3.9(h) Time variation of total inflow, overflow, backflow and outflow to the reservoir; Modeling case: gate opening in 10 min., initial reservoir level at –198, and 100–year storm event (Case 2–3)

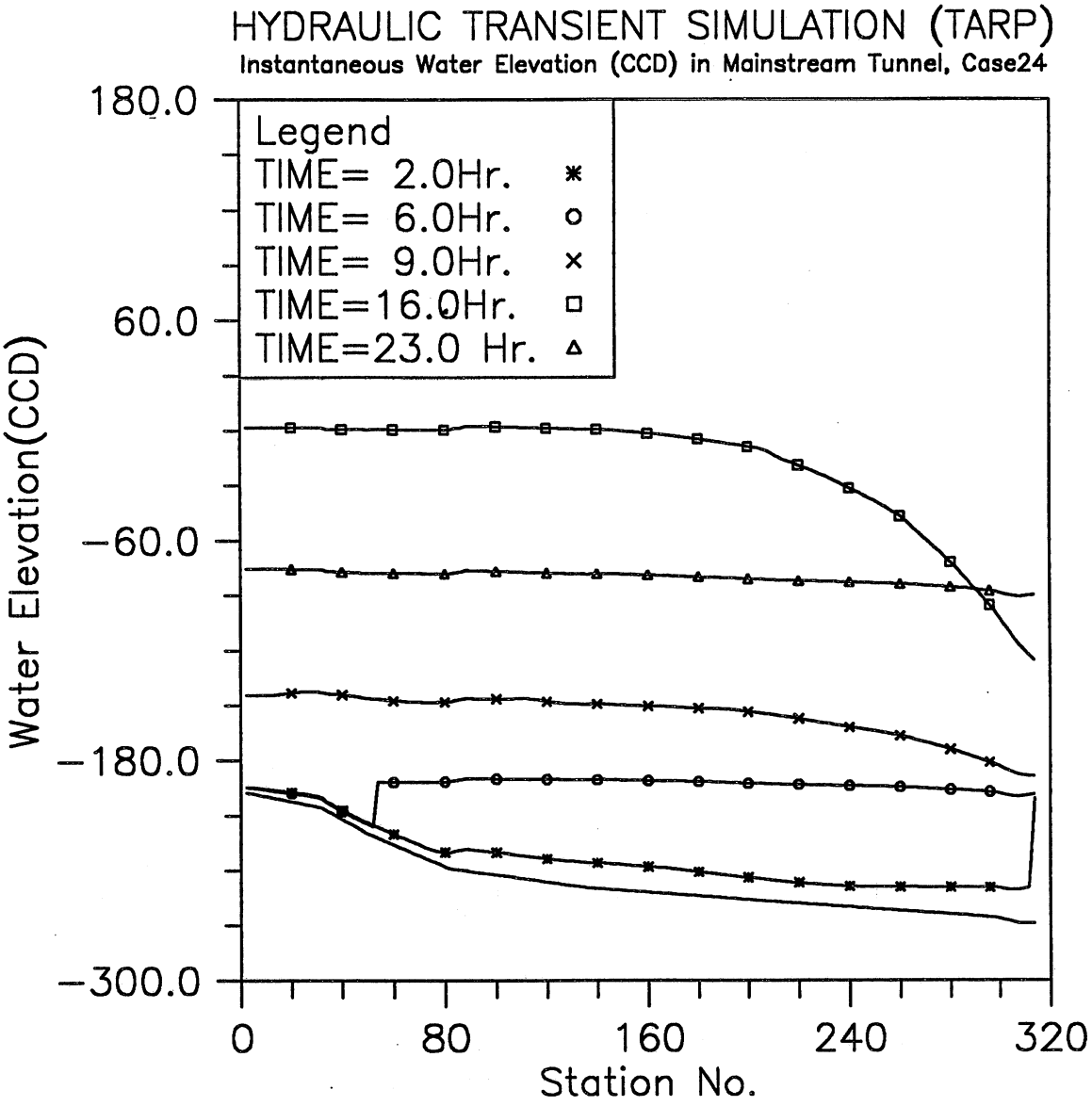

Fig. 3.10(a) Instantaneous hydraulic gradelines along the main tunnel; Modeling case: gate opening in 30 min., initial reservoir level at –198, and 100–year storm event (Case 2–4)

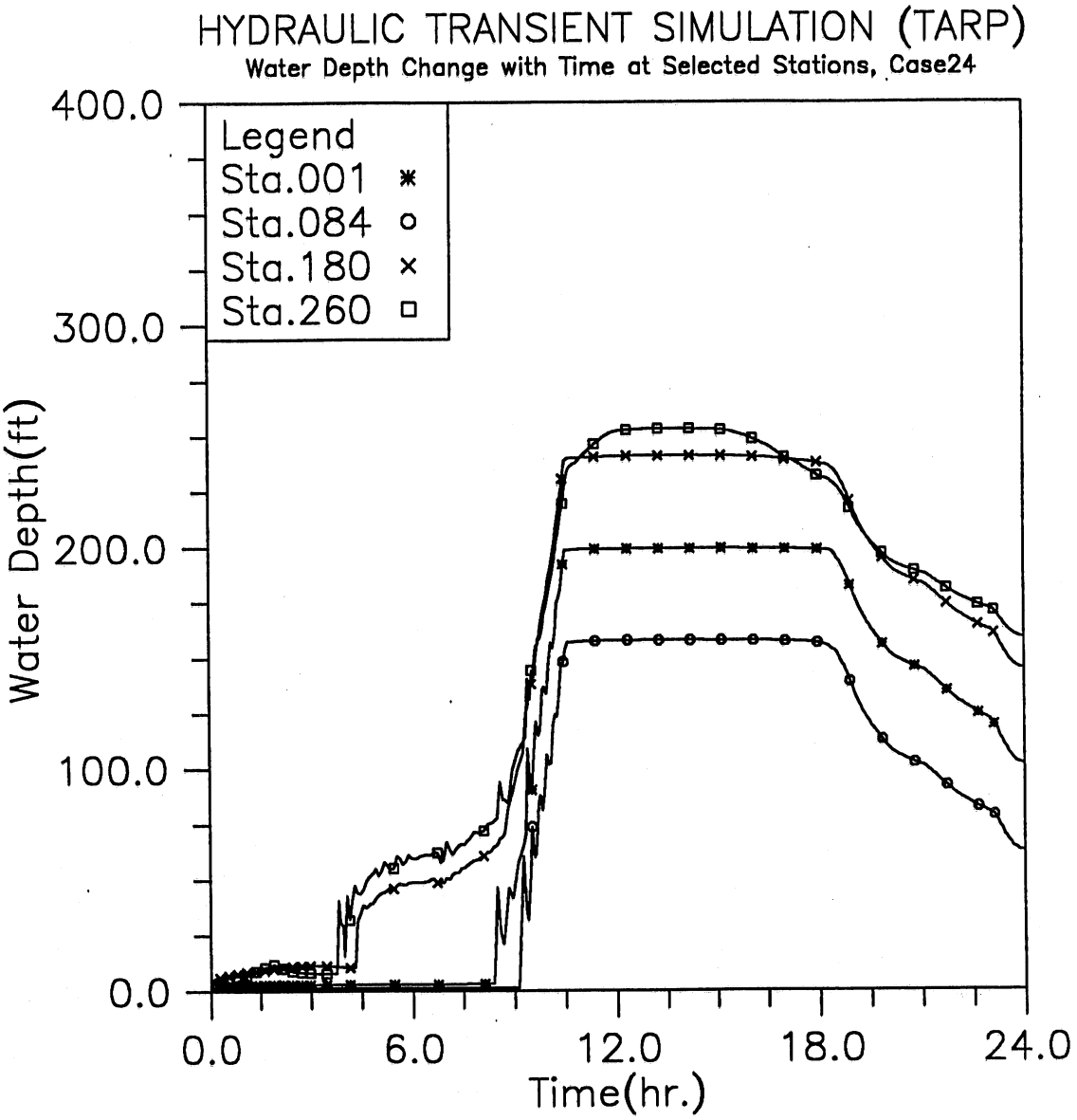

Fig. 3.10(b) Time variation of water depth at four upstream locations; Modeling case: gate opening in 30 min., initial reservoir level at –198, and 100–year storm event (Case 2–4)

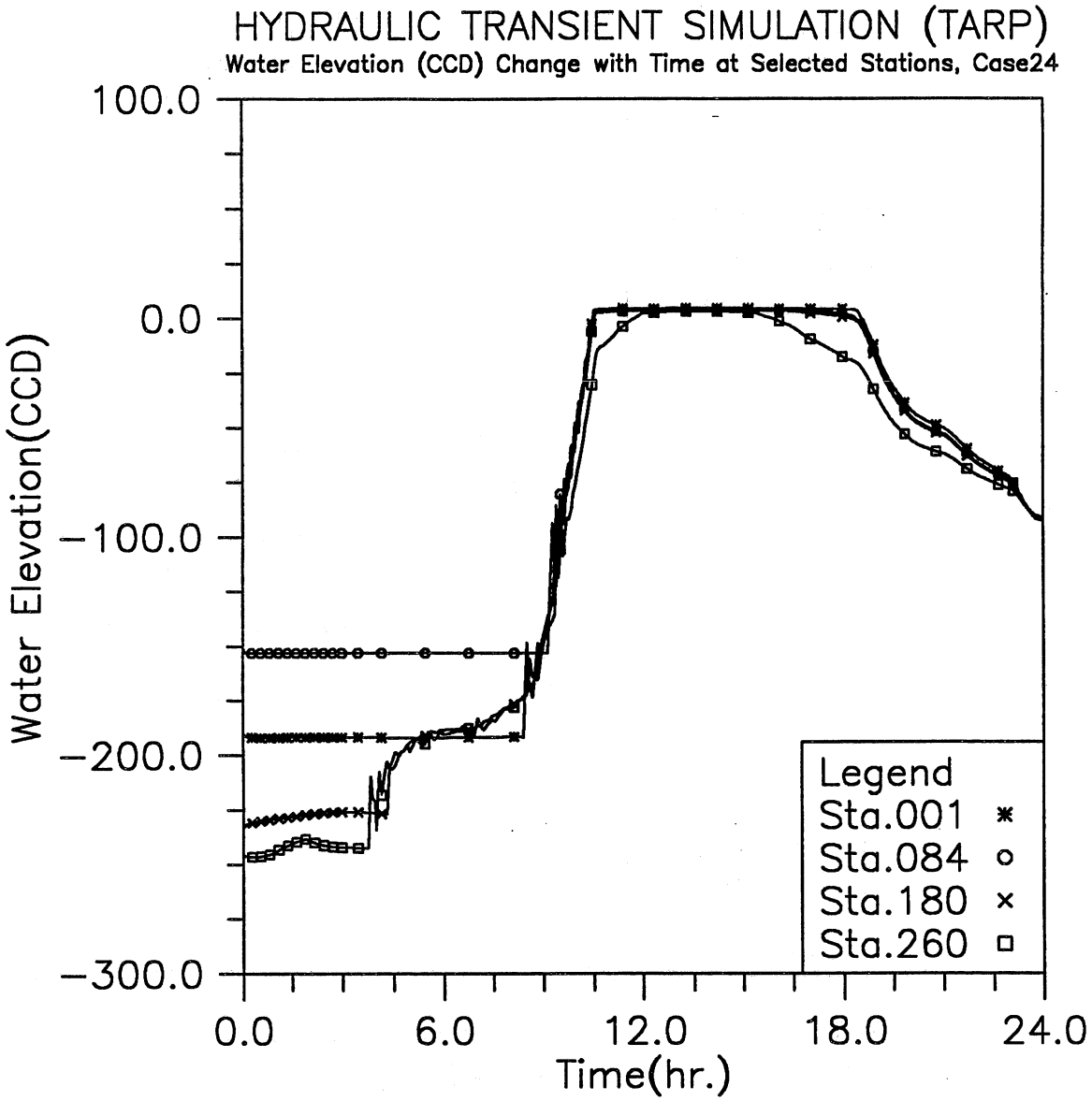

Fig. 3.10(c) Time variation of water elevation at four upstream locations; Modeling case: gate opening in 30 min., initial reservoir level at –198, and 100–year storm event (Case 2–4)

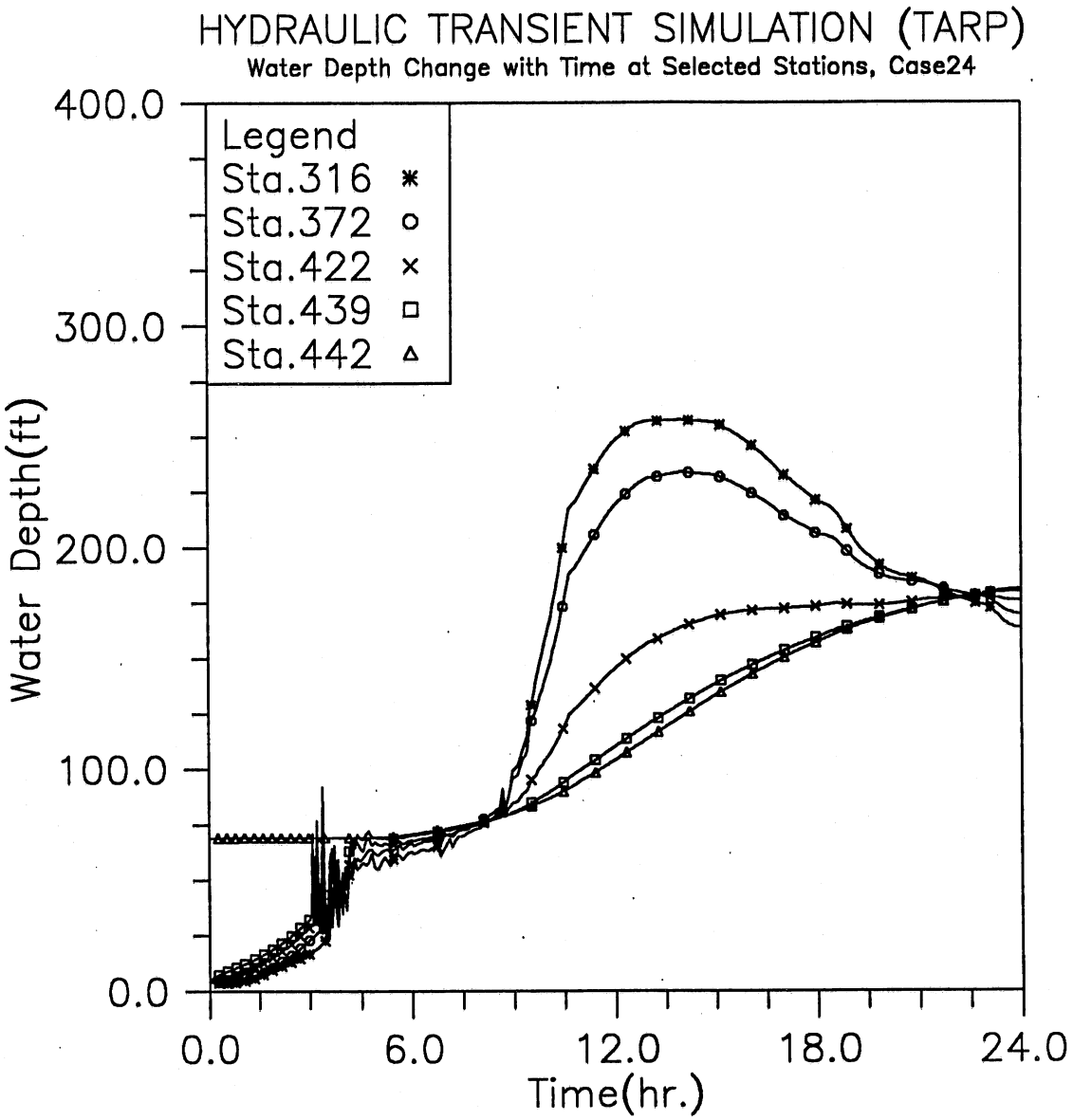

Fig. 3.10(d) Time variation of water depth at five downstream locations; Modeling case: gate opening in 30 min., initial reservoir level at –198, and 100–year storm event (Case 2–4)

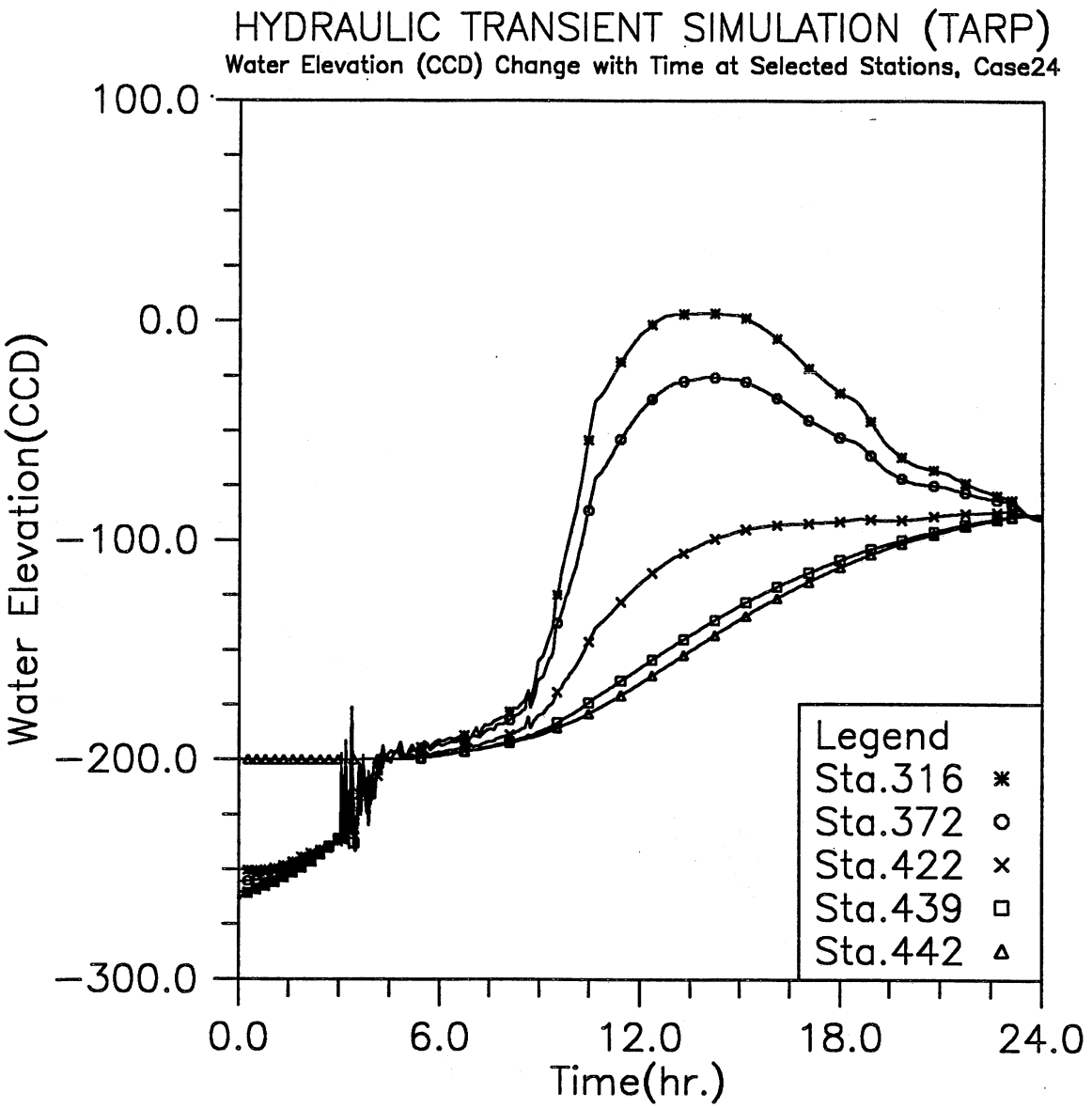

Fig. 3.10(e) Time variation of water elevation at five downstream locations; Modeling case: gate opening in 30 min., initial reservoir level at −198, and 100–year storm event (Case 2–4)

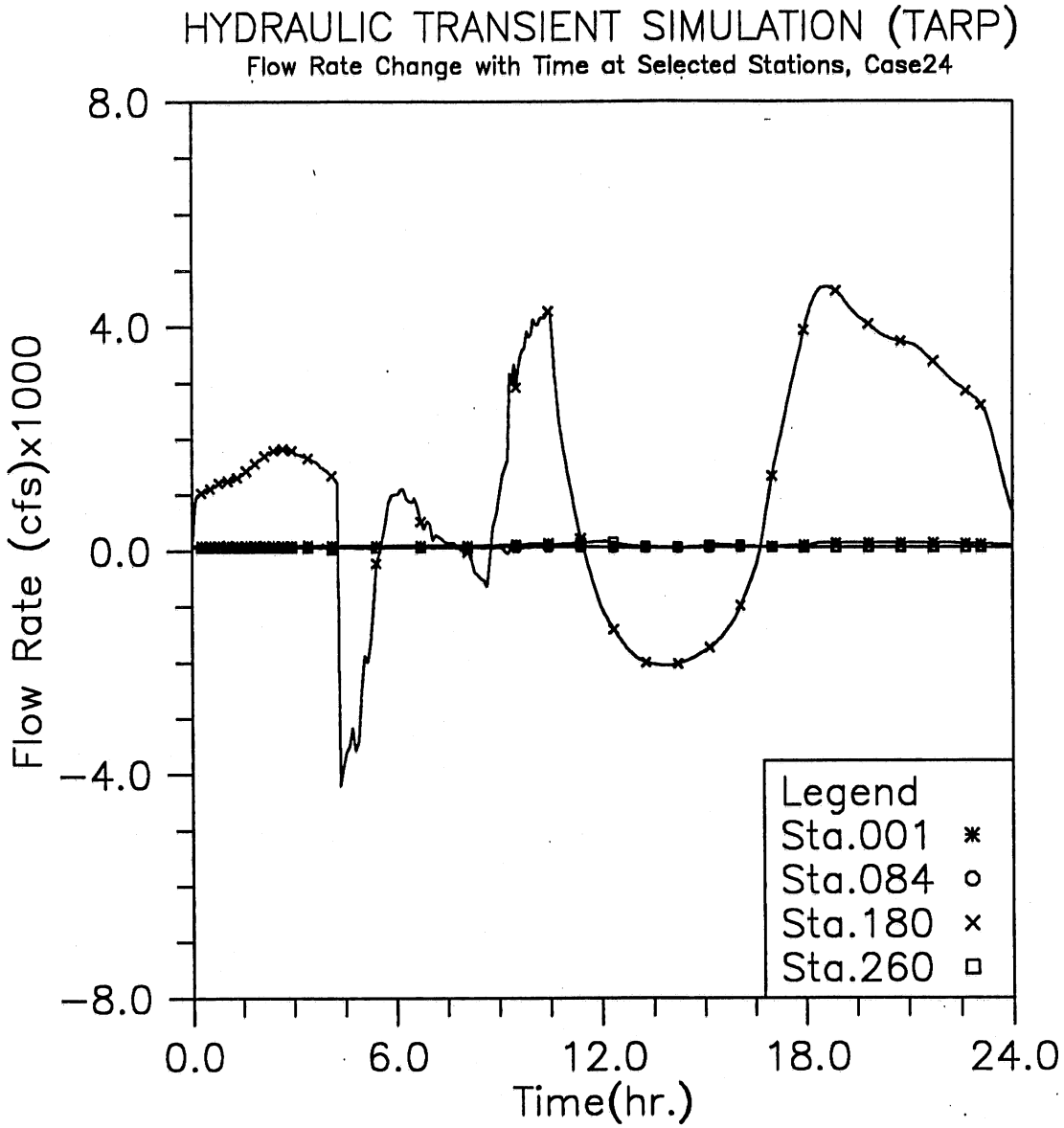

Fig. 3.10(f) Time variation of flow rate at four upstream locations; Modeling case: gate opening in 30 min., initial reservoir level at –198, and 100–year storm event (Case 2–4)

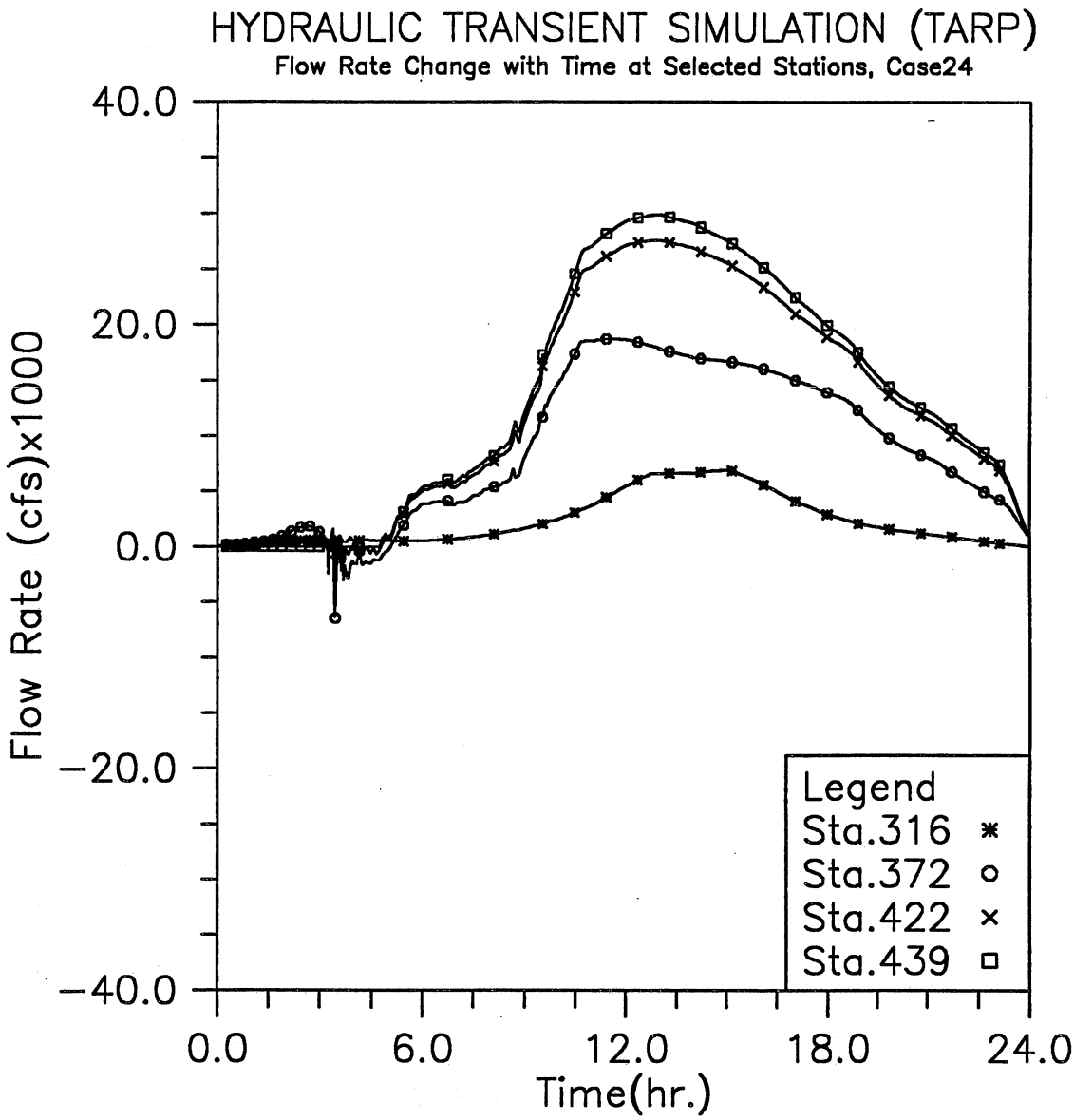

Fig. 3.10(g) Time variation of flow rate at four downstream locations; Modeling case: gate opening in 30 min., initial reservoir level at −198, and 100-year storm event (Case 2-4)

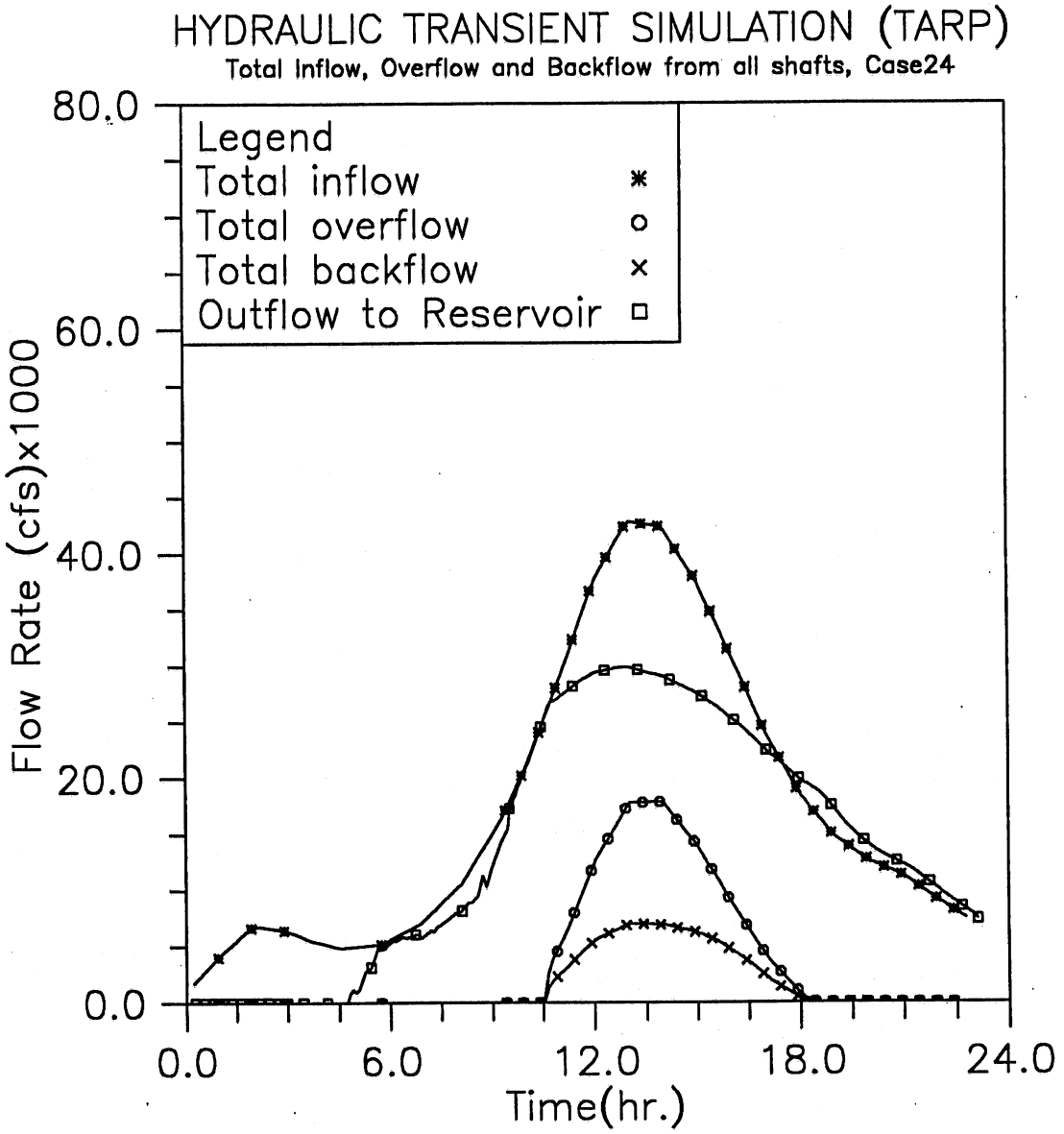

Fig. 3.10(h) Time variation of total inflow, overflow, backflow, and outflow to the reservoir; Modeling case: gate opening in 30 min., initial reservoir level at –198, and 100–year storm event (Case 2–4)

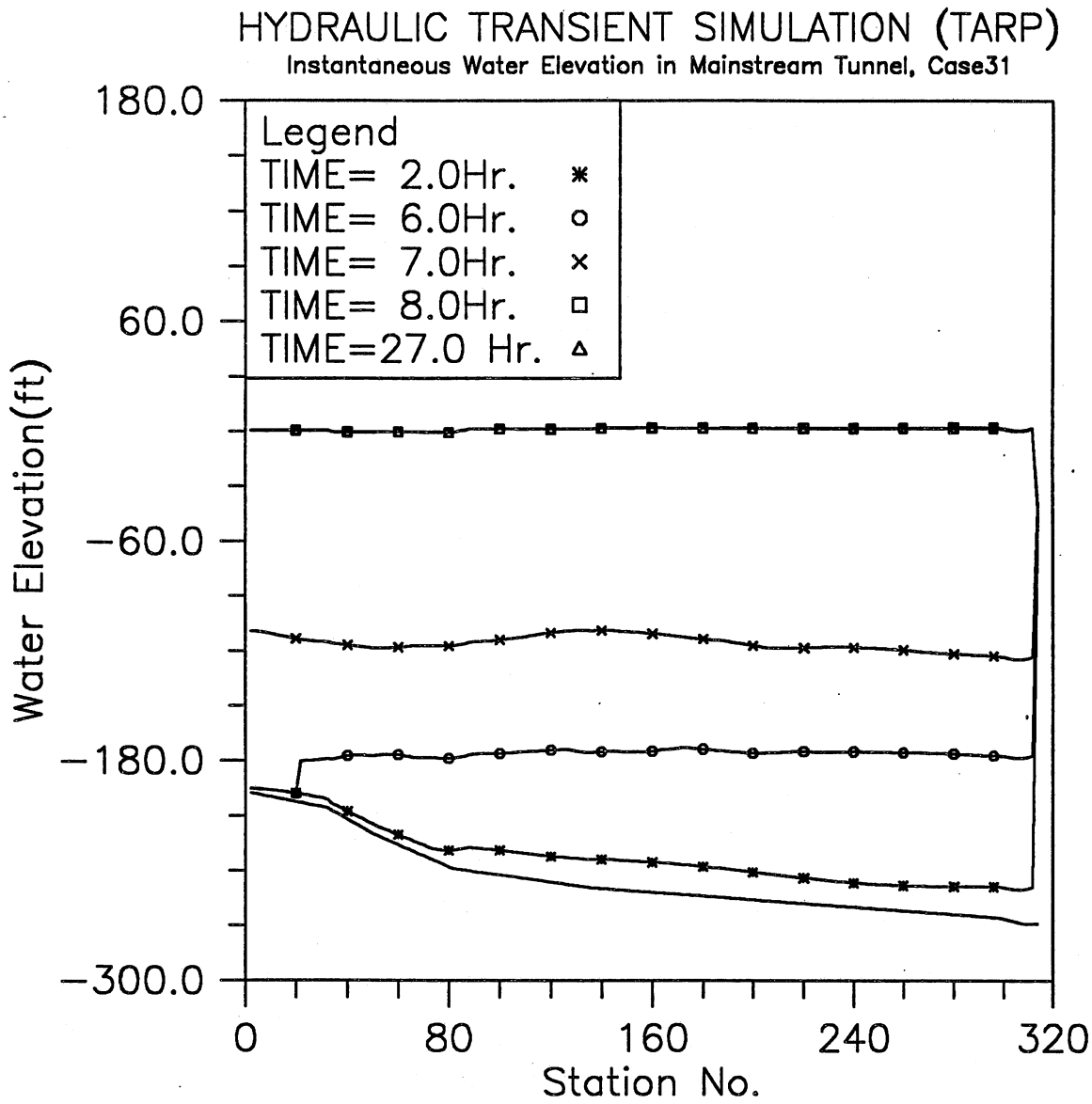

Fig. 3.11(a) Instantaneous hydraulic gradelines along the main tunnel; Modeling case: closed main gate, initial reservoir level at -70, and total of 5,000 cfs storm event (Case 3-1)

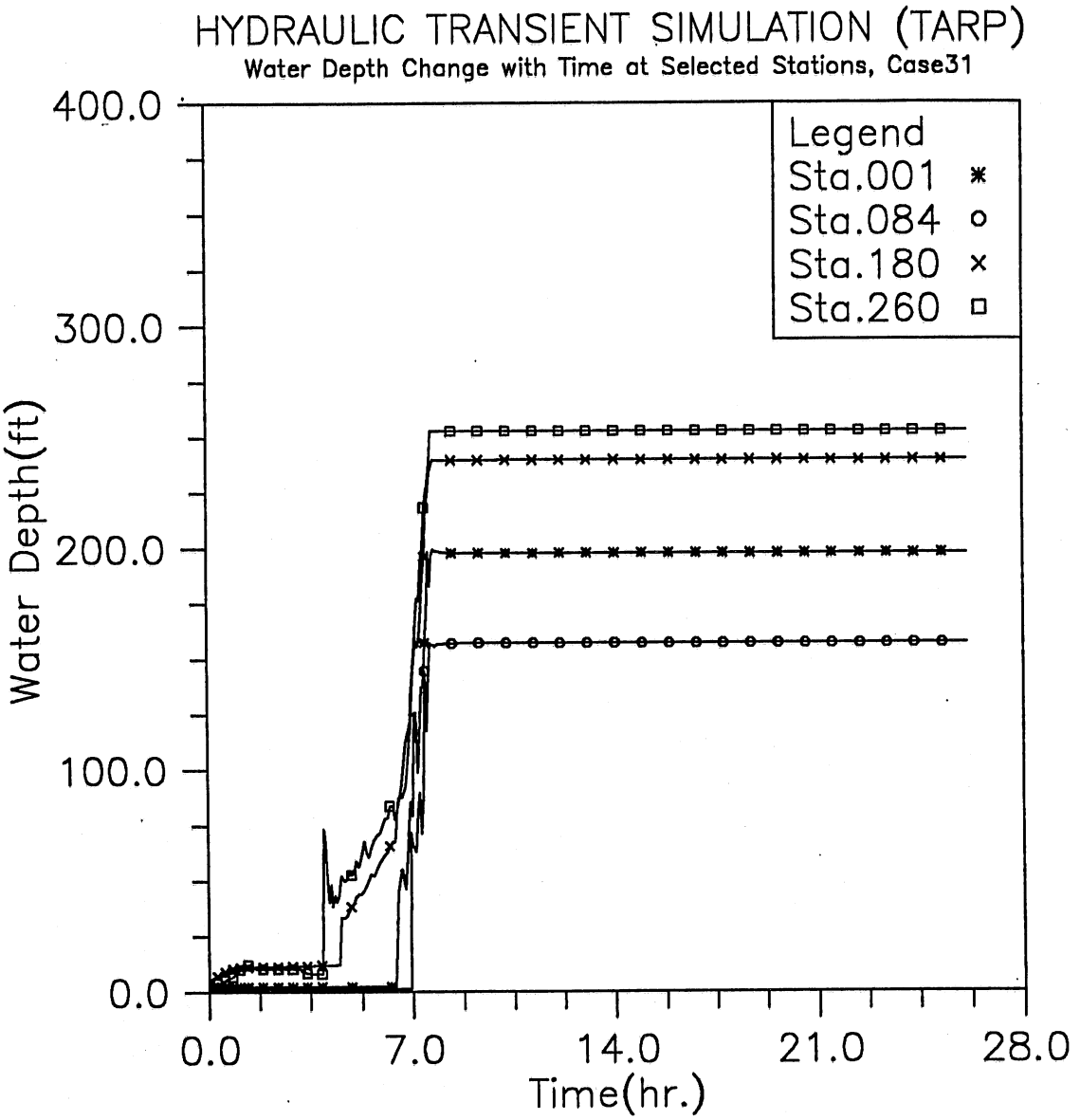

Fig. 3.11(b) Time variation of water depth at four upstream locations; Modeling case: closed main gate, initial reservoir level at –70, and total of 5,000 cfs storm event (Case 3–1)

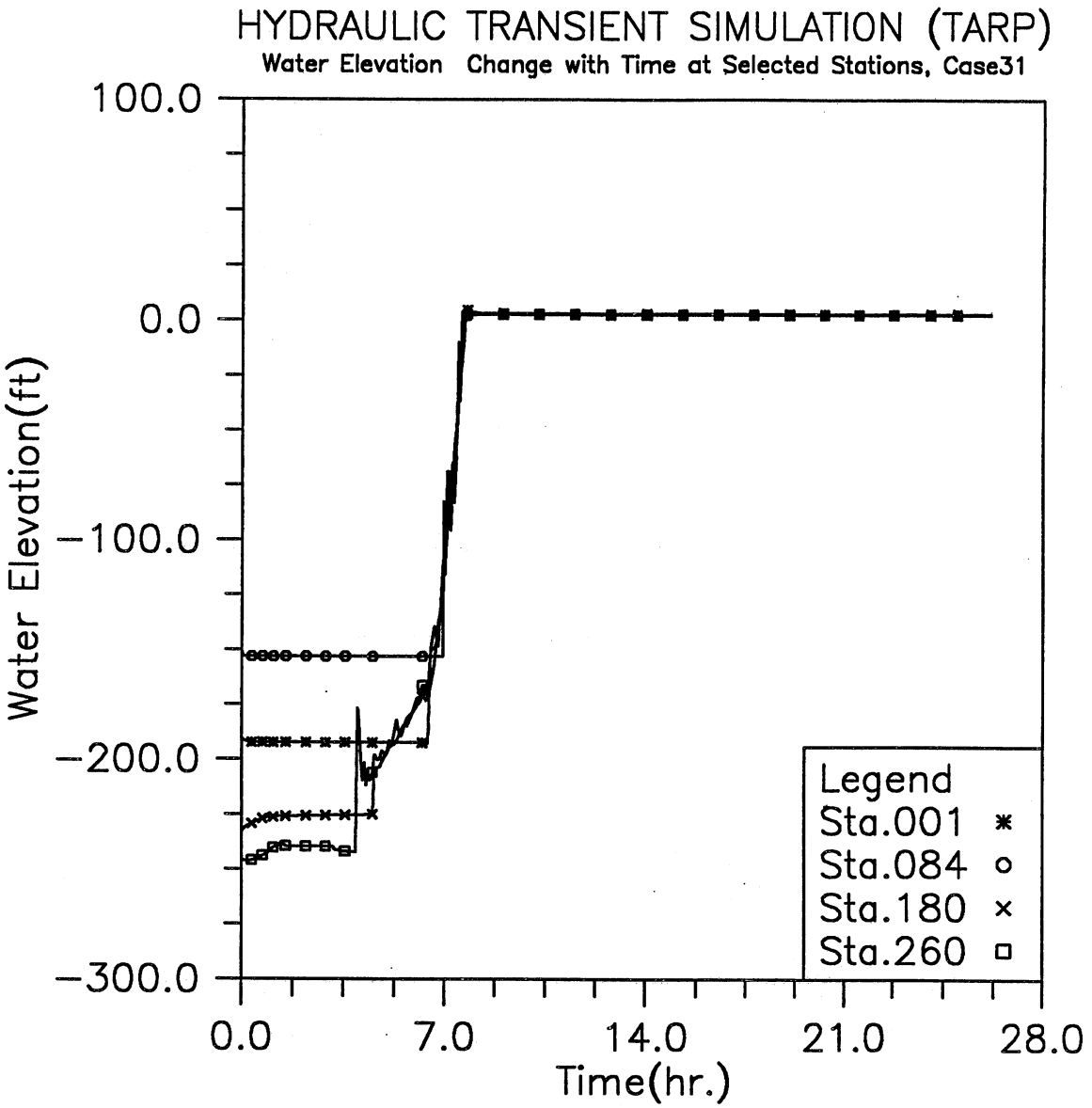

Fig. 3.11(c) Time variation of water elevation at four upstream locations; Modeling case: closed main gate, initial reservoir level at −70, and total of 5,000 cfs storm event (Case 3–1)

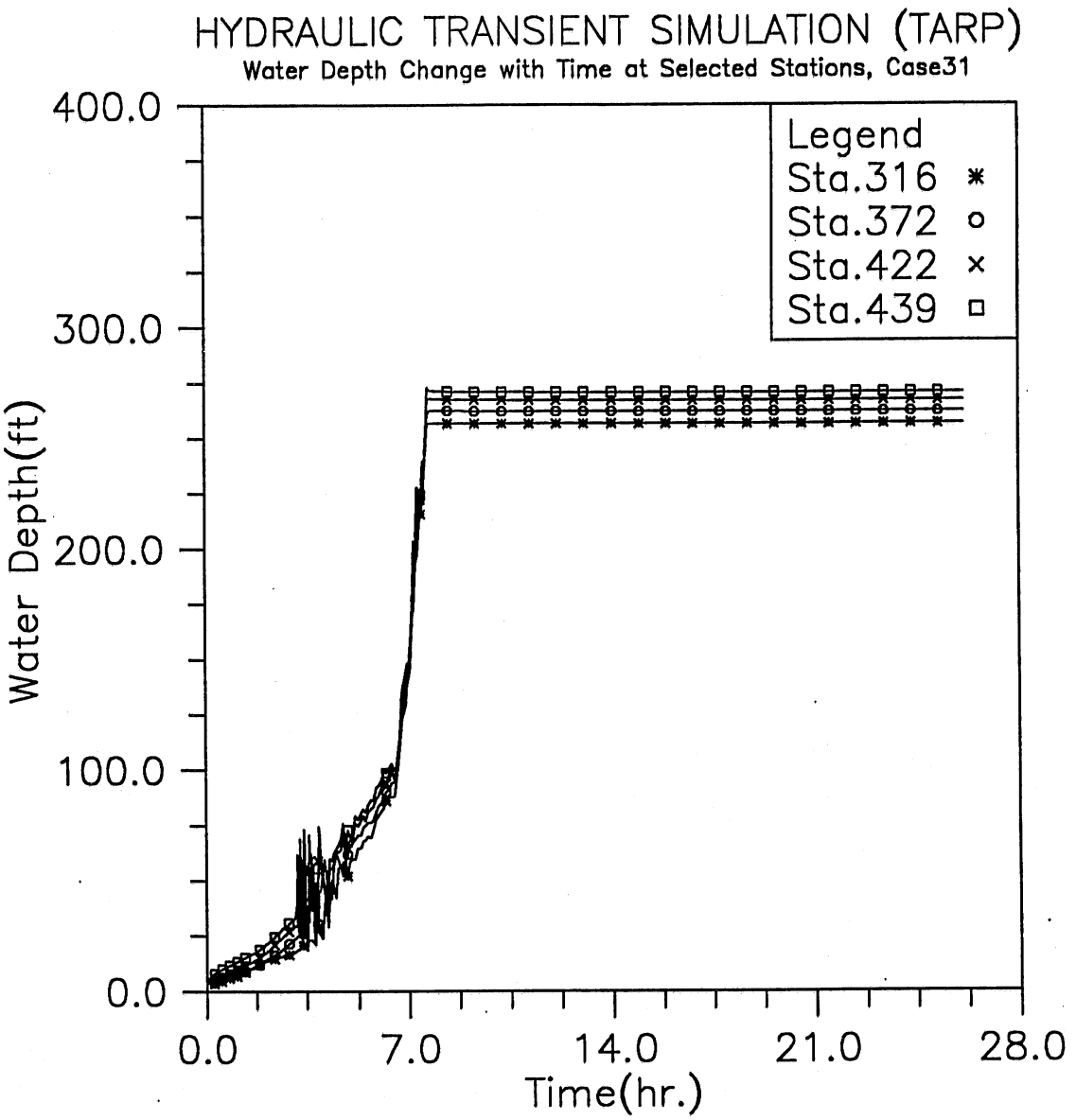

Fig. 3.11(d) Time variation of water depth at four downstream locations; Modeling case: closed main gate, initial reservoir level at –70, and total of 5,000 cfs storm event (Case 3–1)

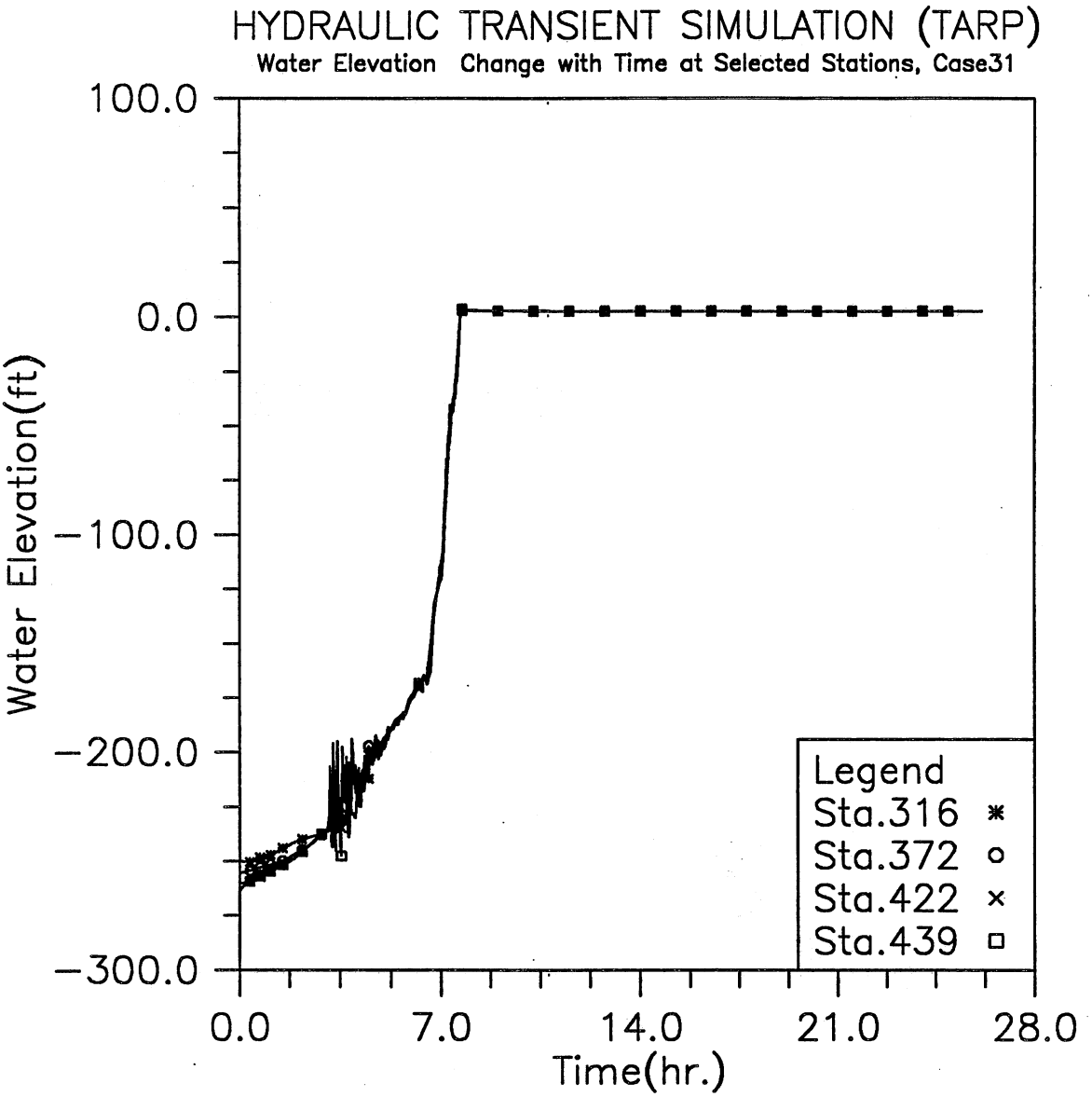

Fig. 3.11(e) Time variation of water elevation at four downstream locations; Modeling case: closed main gate, initial reservoir level at –70, and total of 5,000 cfs storm event (Case 3–1)

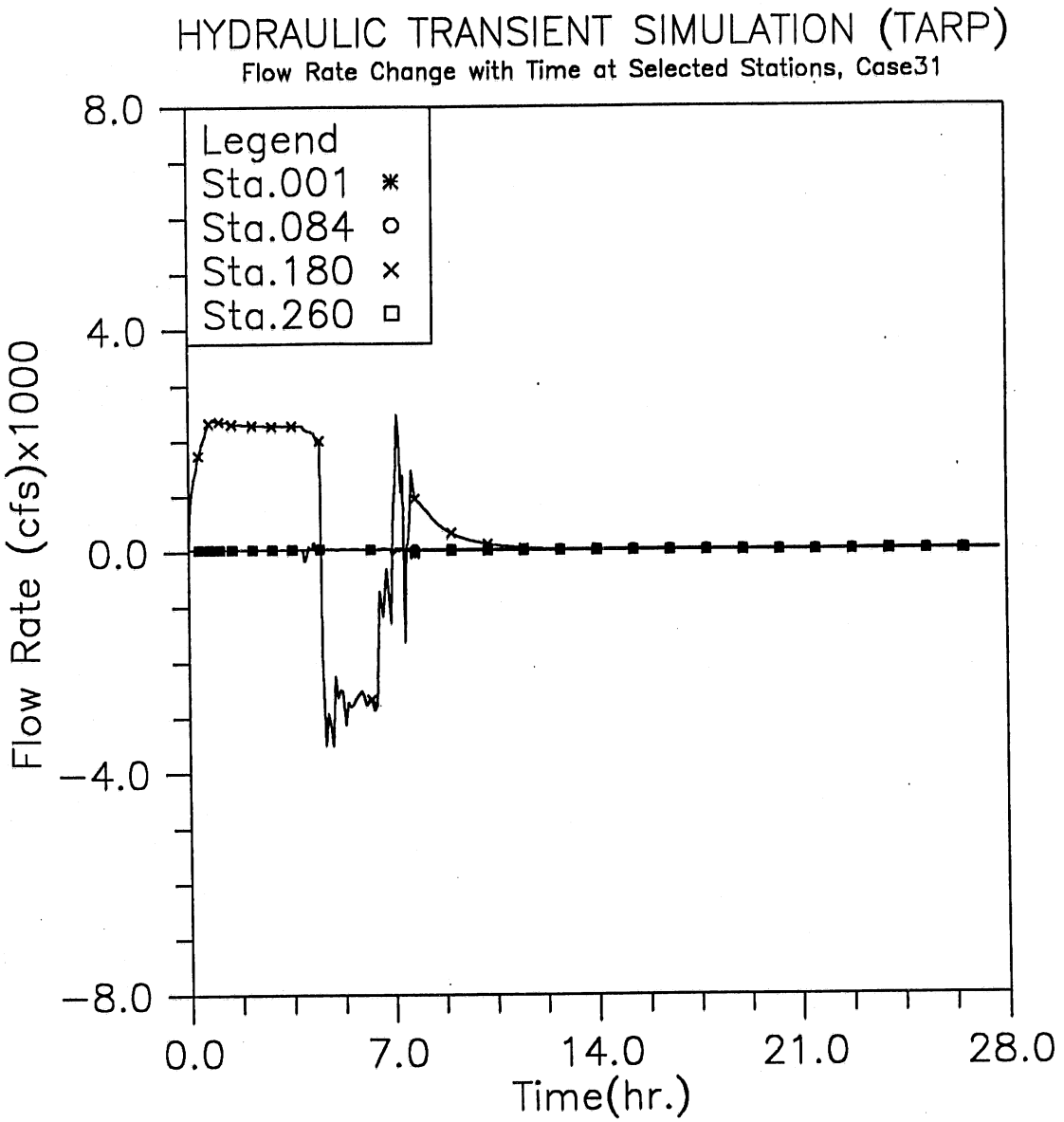

Fig. 3.11(f) Time variation of flow rate at four upstream locations; Modeling case: closed main gate, initial reservoir level at –70, and total of 5,000 cfs storm event (Case 3–1)

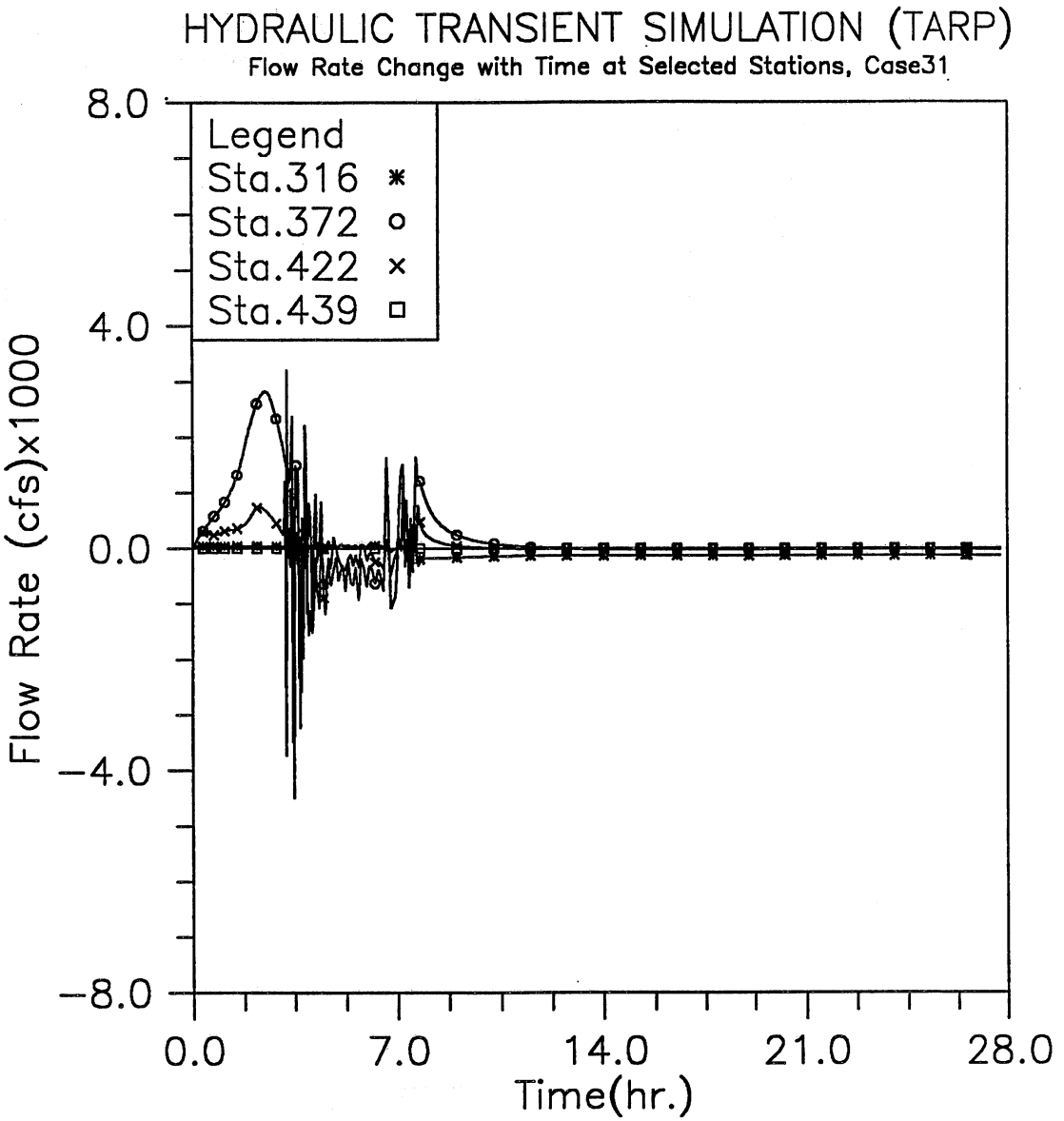

Fig. 3.11(g) Time variation of flow rate at four downstream locations; Modeling case: closed main gate, initial reservoir level at –70, and total of 5,000 cfs storm event (Case 3–1)

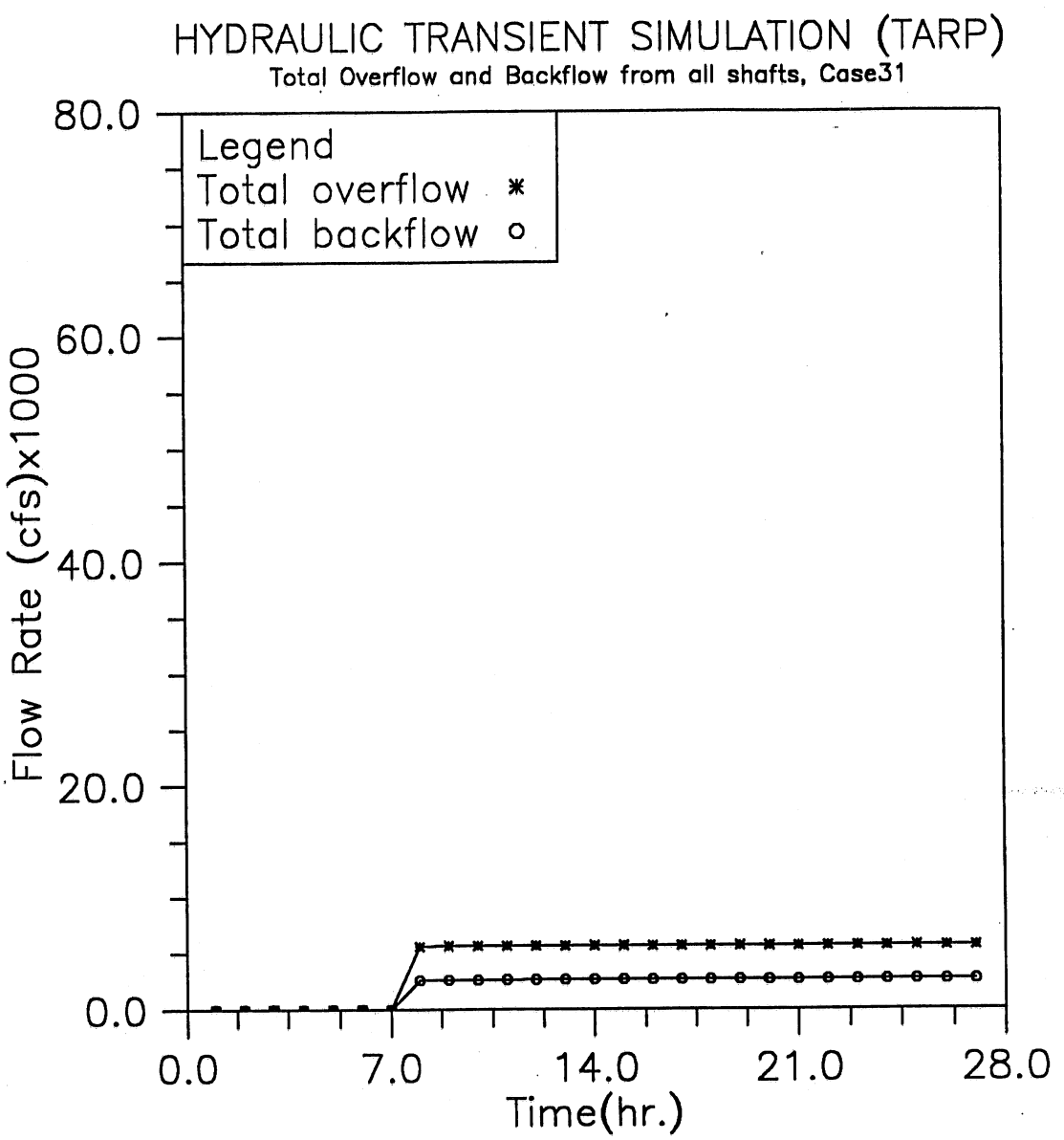

Fig. 3.11(h) Time variation of total overflow and backflow; Modeling case: closed main gate, initial reservoir level at –70, and total of 5,000 cfs storm event (Case 3–1)

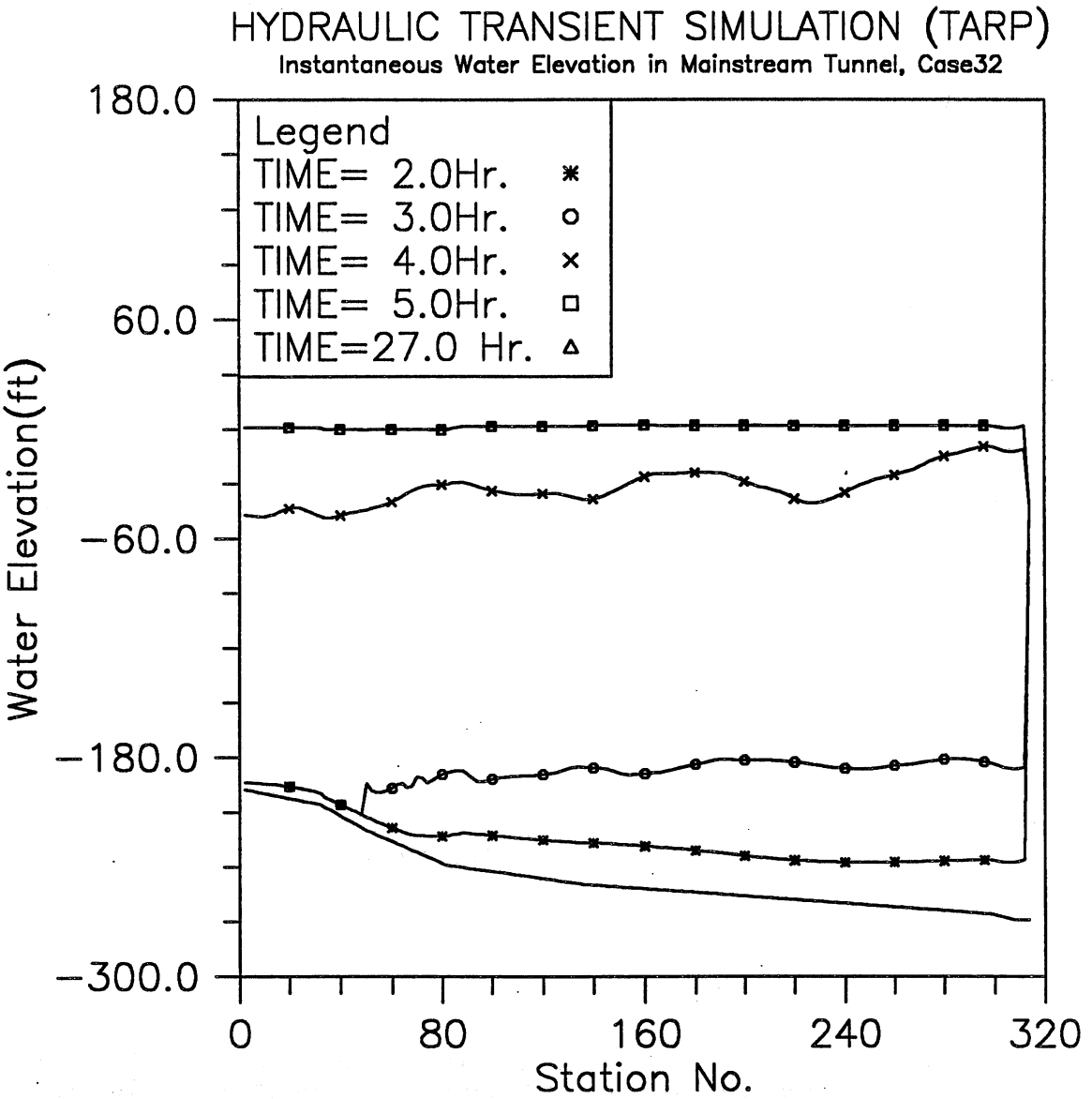

Fig. 3.12(a) Instantaneous hydraulic gradelines along the main tunnel; Modeling case: closed main gate, initial reservoir level at -70, and total of 10,000 cfs storm event (Case 3-2)

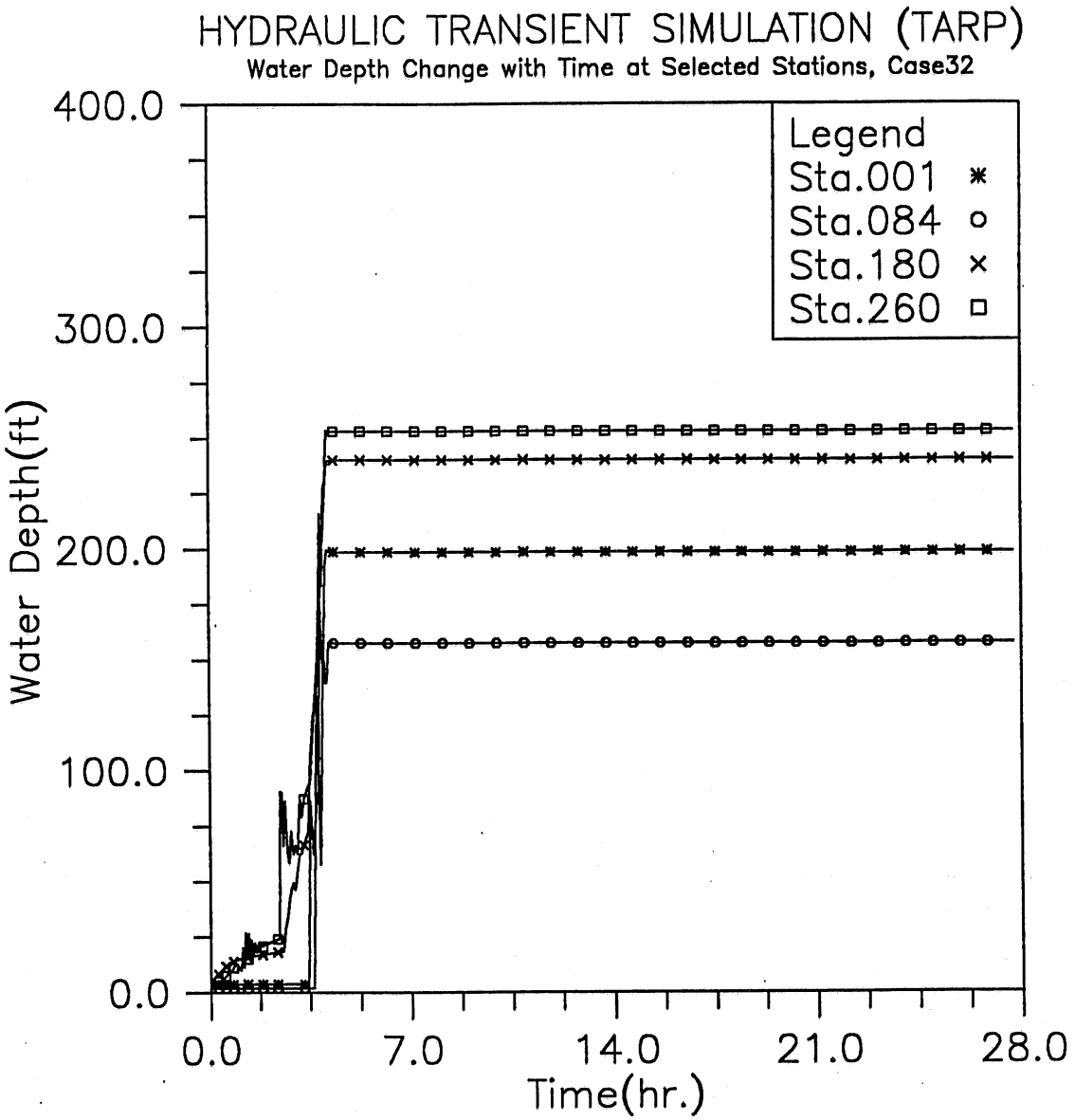

Fig. 3.12(b) Time variation of water depth at four upstream locations; Modeling case: closed main gate, initial reservoir level at –70, and total of 10,000 cfs storm event (Case 3–2)

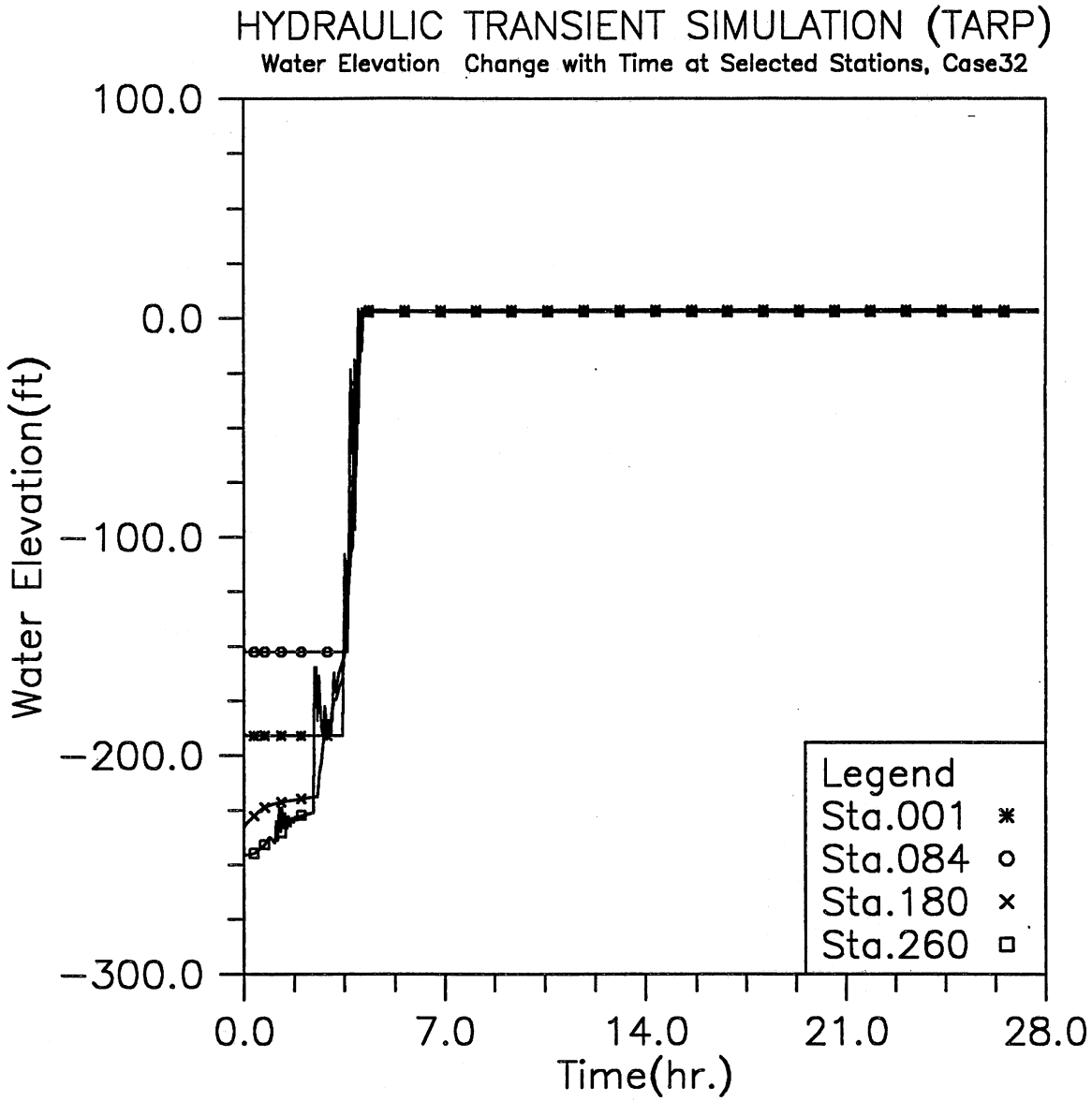

Fig. 3.12(c) Time variation of water elevation at four upstream locations; Modeling case: closed main gate, initial reservoir level at –70, and total of 10,000 cfs storm event (Case 3–2)

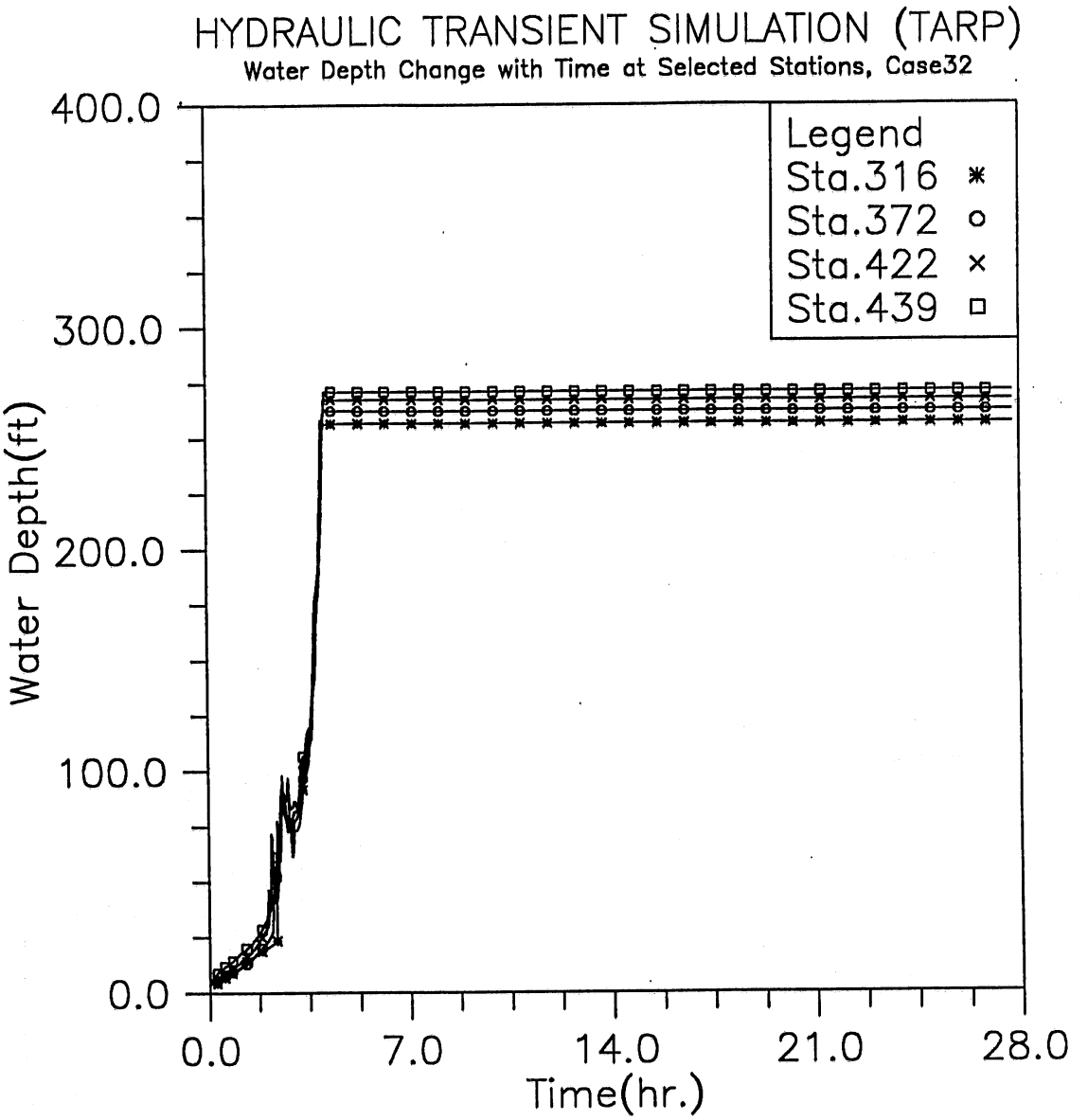

Fig. 3.12(d) Time variation of water depth at four downstream locations; Modeling case: closed main gate, initial reservoir level at –70, and total of 10,000 cfs storm event (Case 3–2)

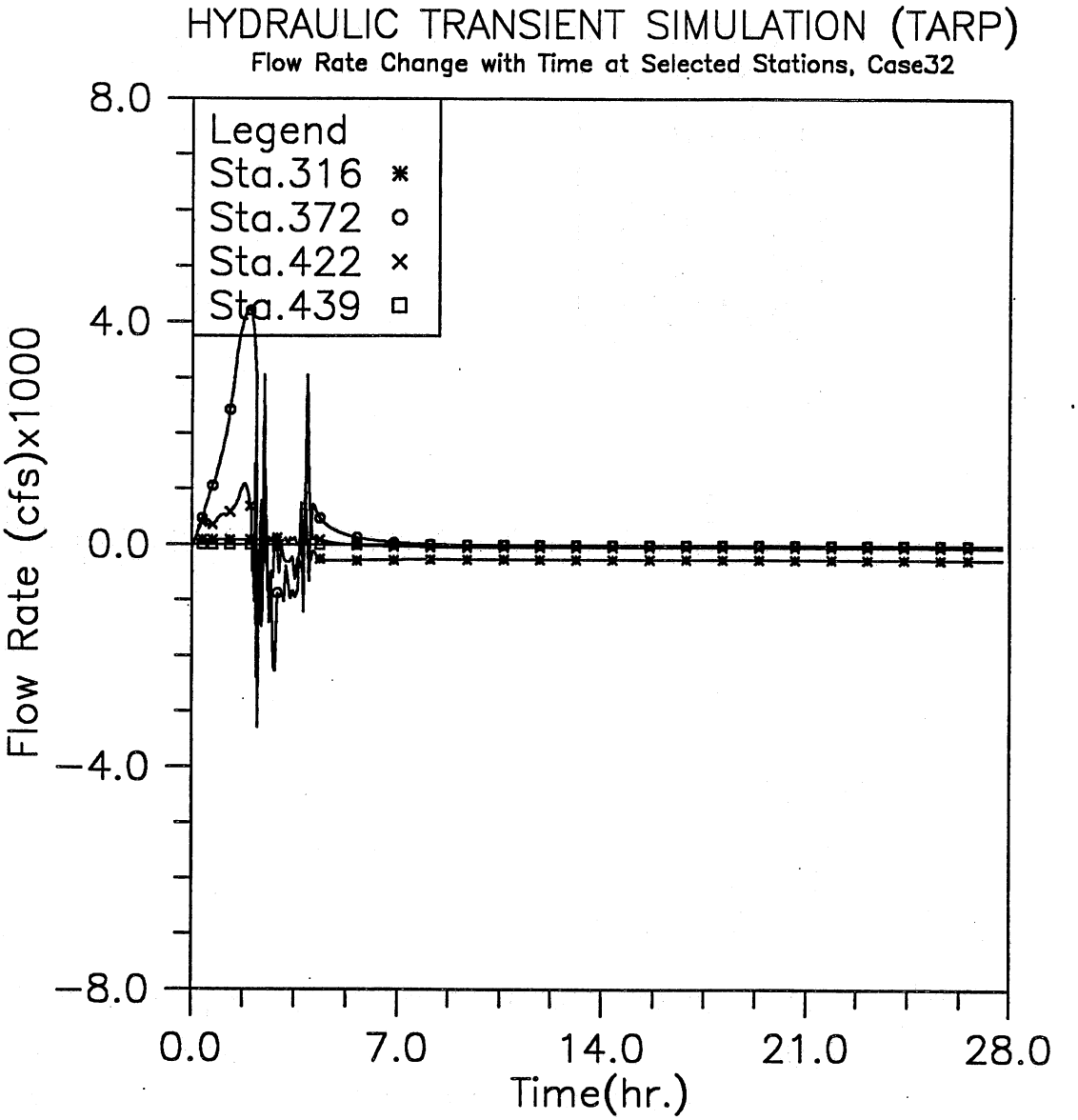

Fig. 3.12(g) Time variation of flow rate at four downstream locations; Modeling case: closed main gate, initial reservoir level at –70, and total of 10,000 cfs storm event (Case 3–2)

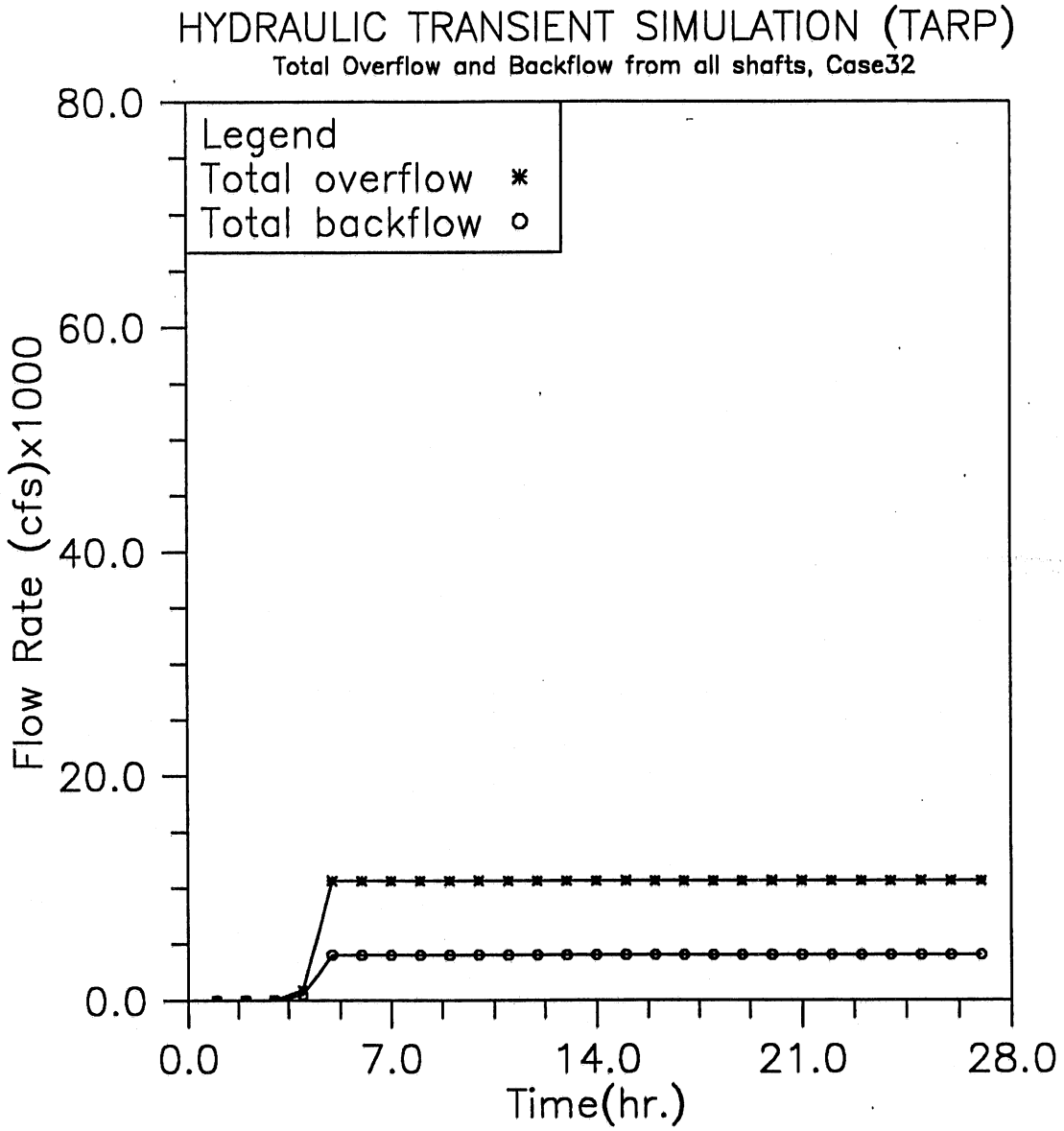

Fig. 3.12(h) Time variation of total overflow and backflow; Modeling case: closed main gate, initial reservoir level at –70, and total of 10,000 cfs storm event (Case 3–2)

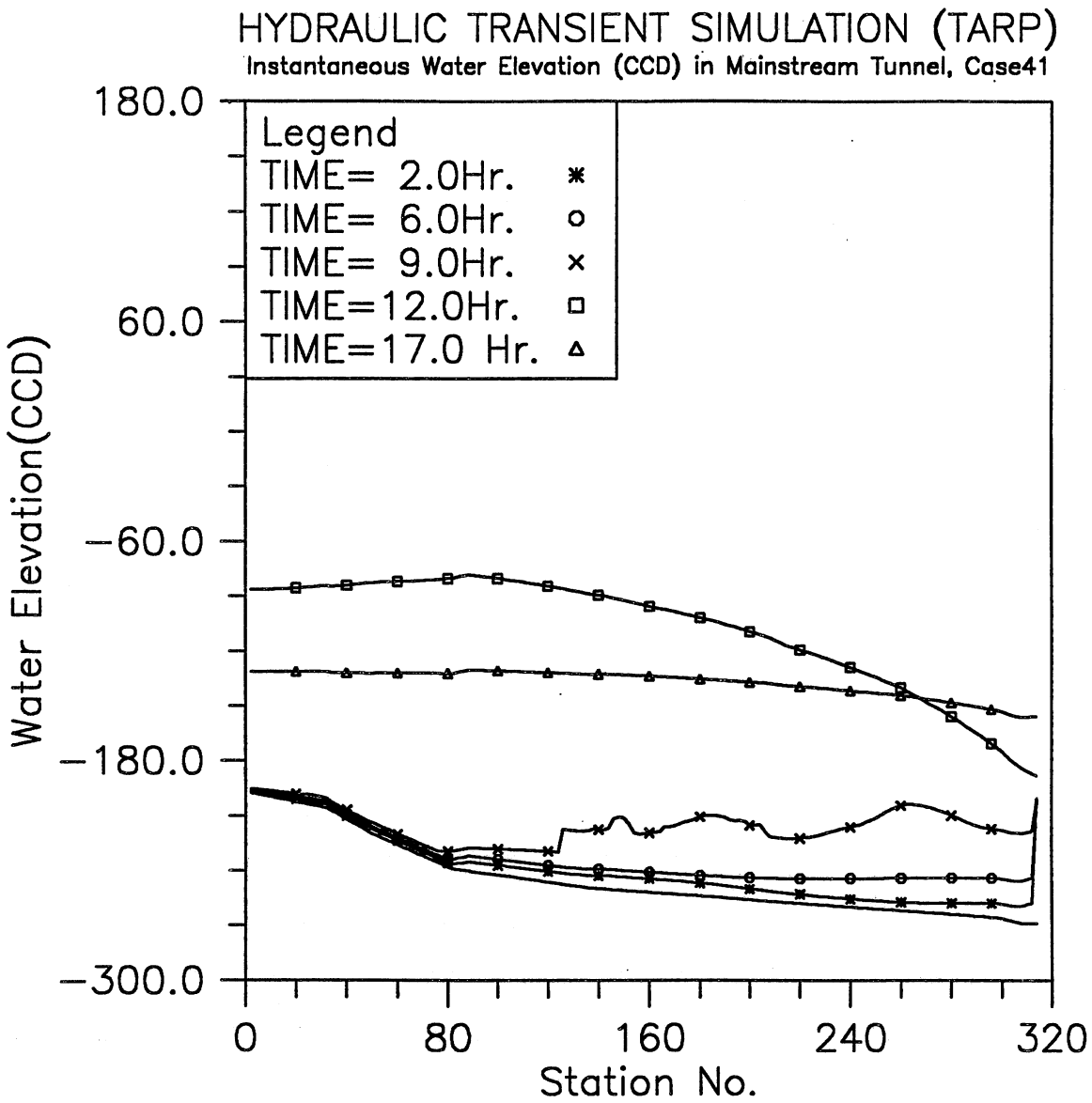

Fig. 3.13(a) Instantaneous hydraulic gradelines along the main tunnel; Modeling case: gate opening in 30 min., initial reservoir level at –198, inflow control Plan 1, and 5–year storm event (Case 4–1)

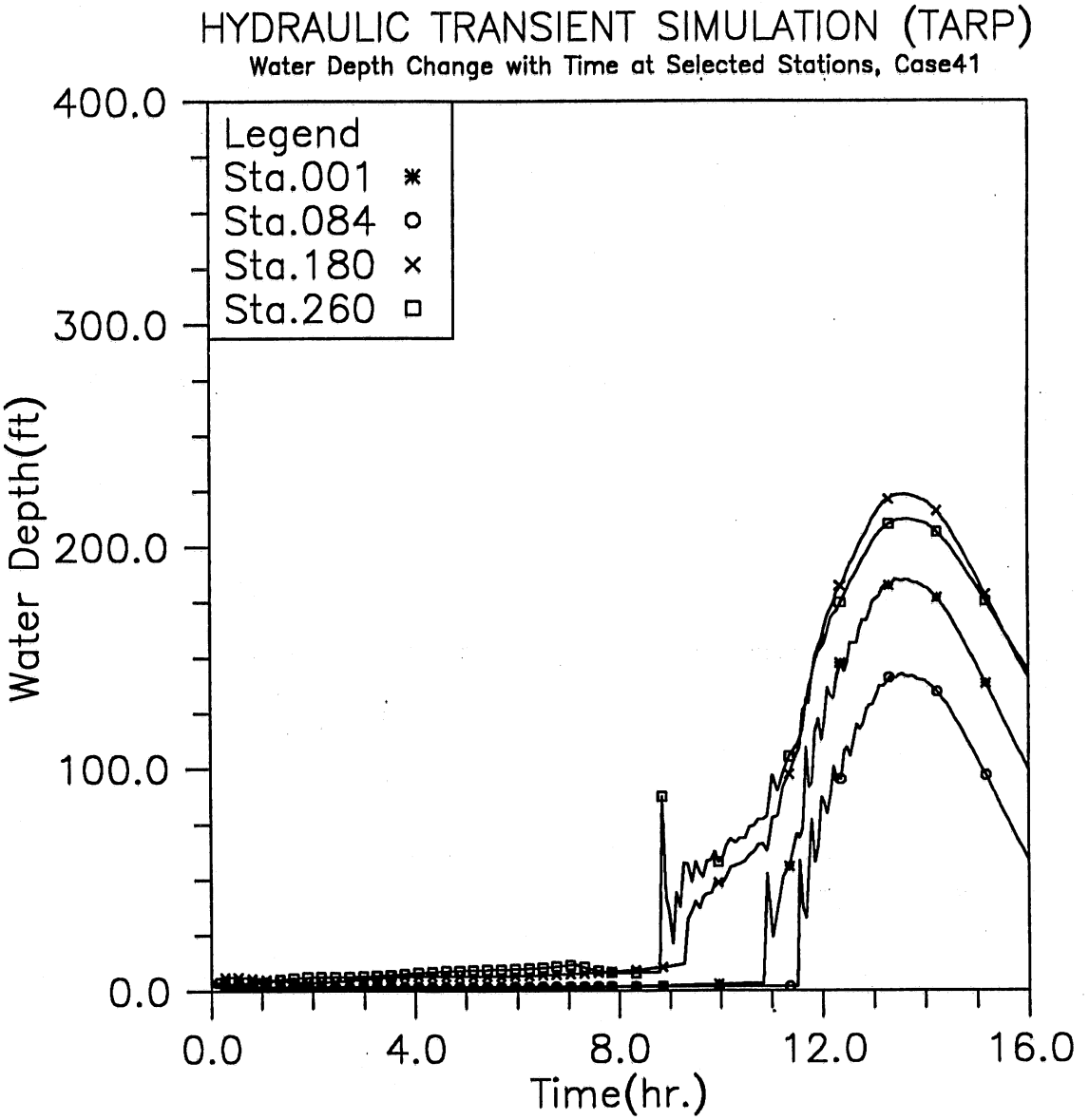

Fig. 3.13(b) Time variation of water depth at four upstream locations; Modeling case: gate opening in 30 min., initial reservoir level at –198, inflow control Plan 1, and 5–year storm event (Case 4–1)

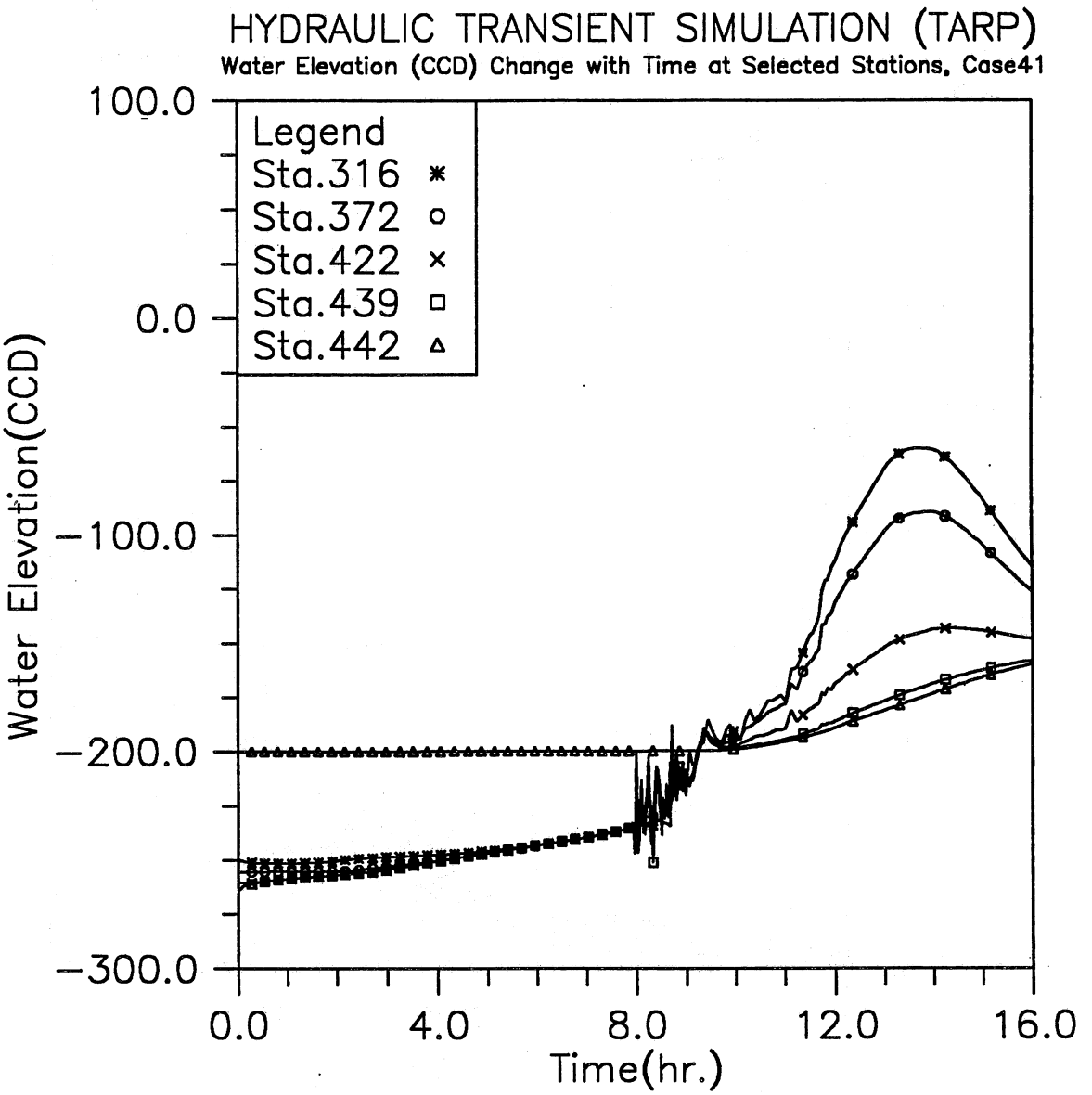

Fig. 3.13(e) Time variation of water elevation at five downstream locations; Modeling case: gate opening in 30 min., initial reservoir level at –198, inflow control Plan 1, and 5–year storm event (Case 4–1)

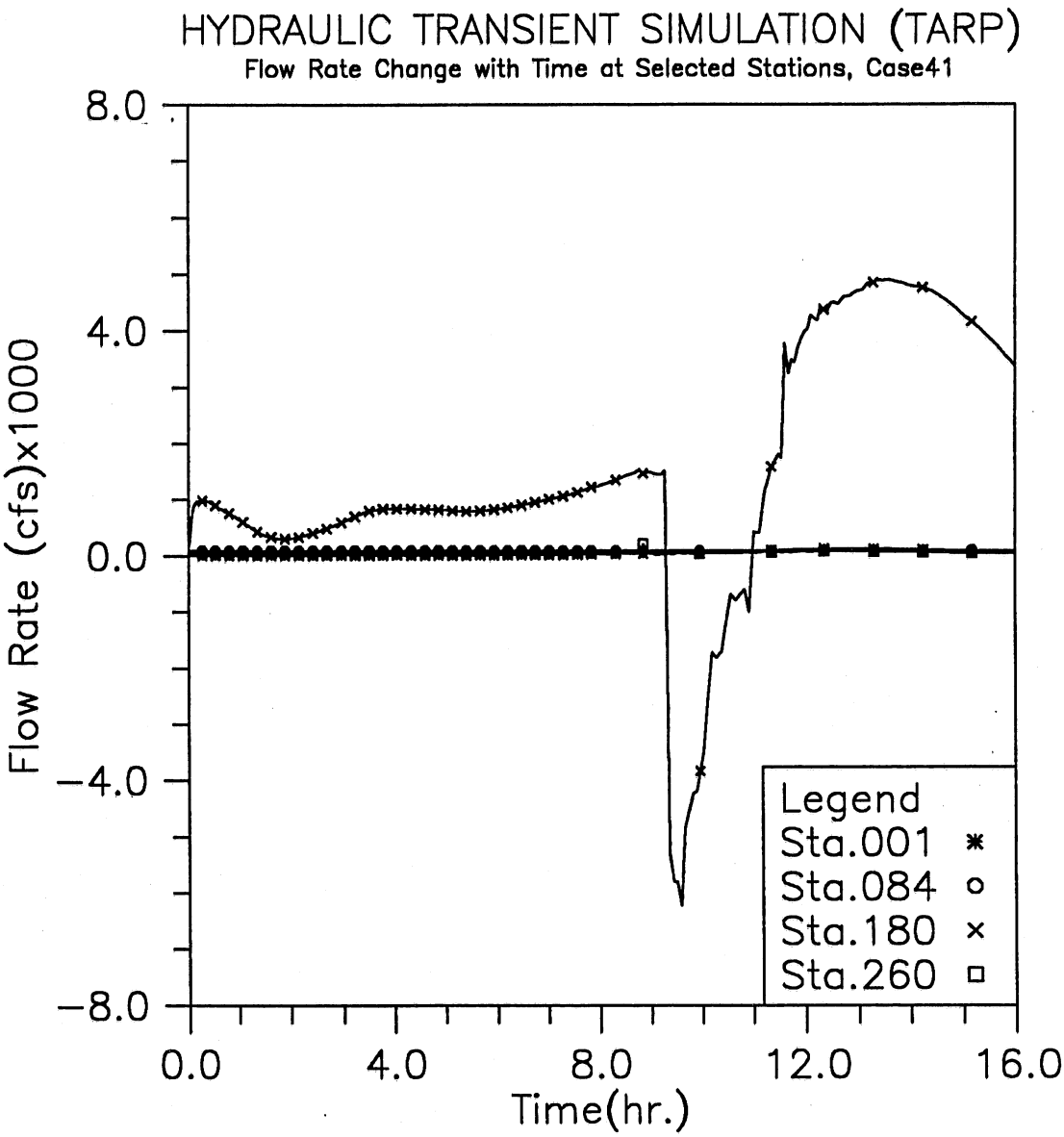

Fig. 3.13(f) Time variation of flow rate at four upstream locations; Modeling case: gate opening in 30 min., initial reservoir level at −198, inflow control Plan 1, and 5–year storm event (Case 4–1)

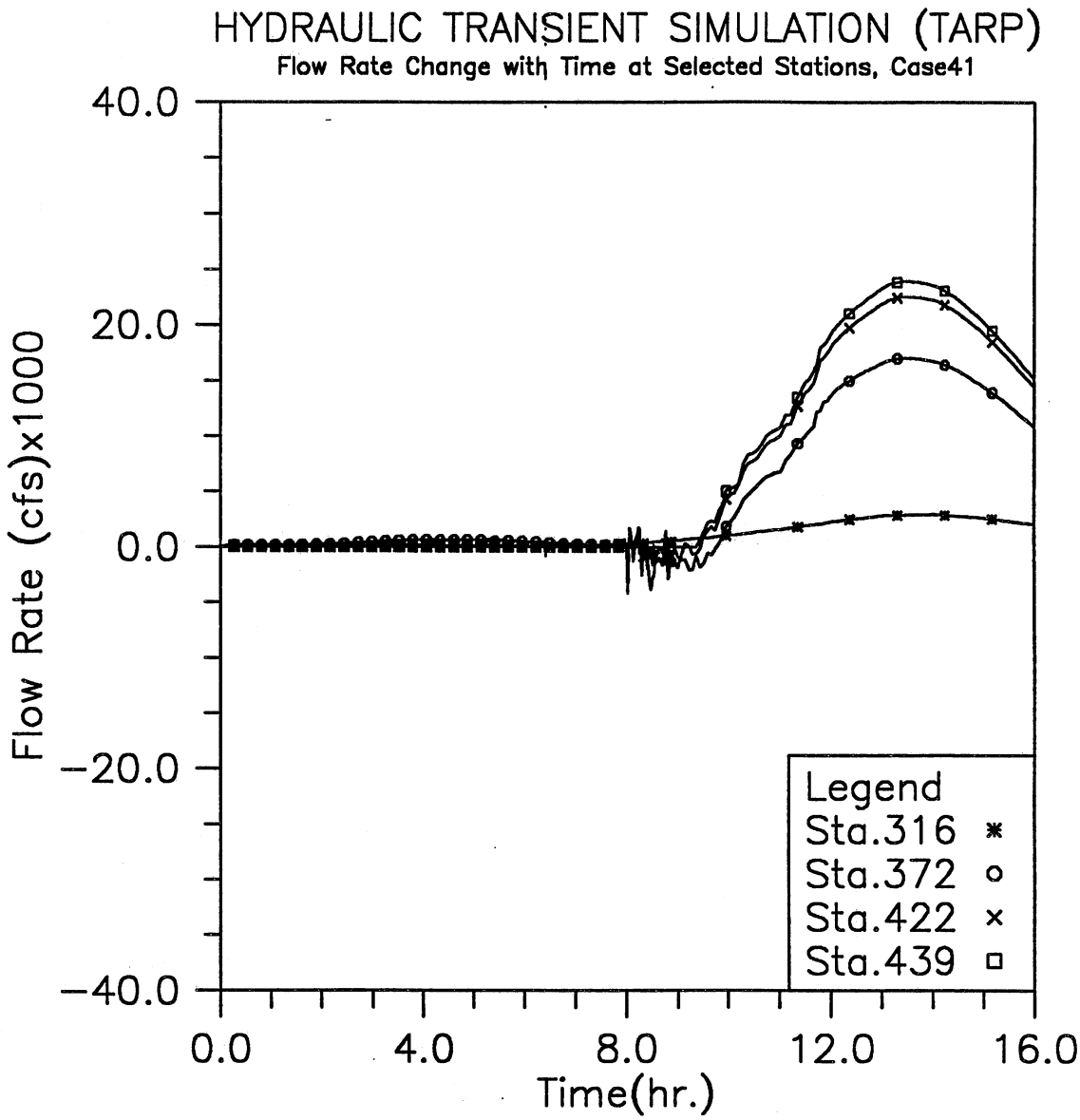

Fig. 3.13(g) Time variation of flow rate at four downstream locations; Modeling case: gate opening in 30 min., initial reservoir level at –198, inflow control Plan 1, and 5–year storm event (Case 4–1)

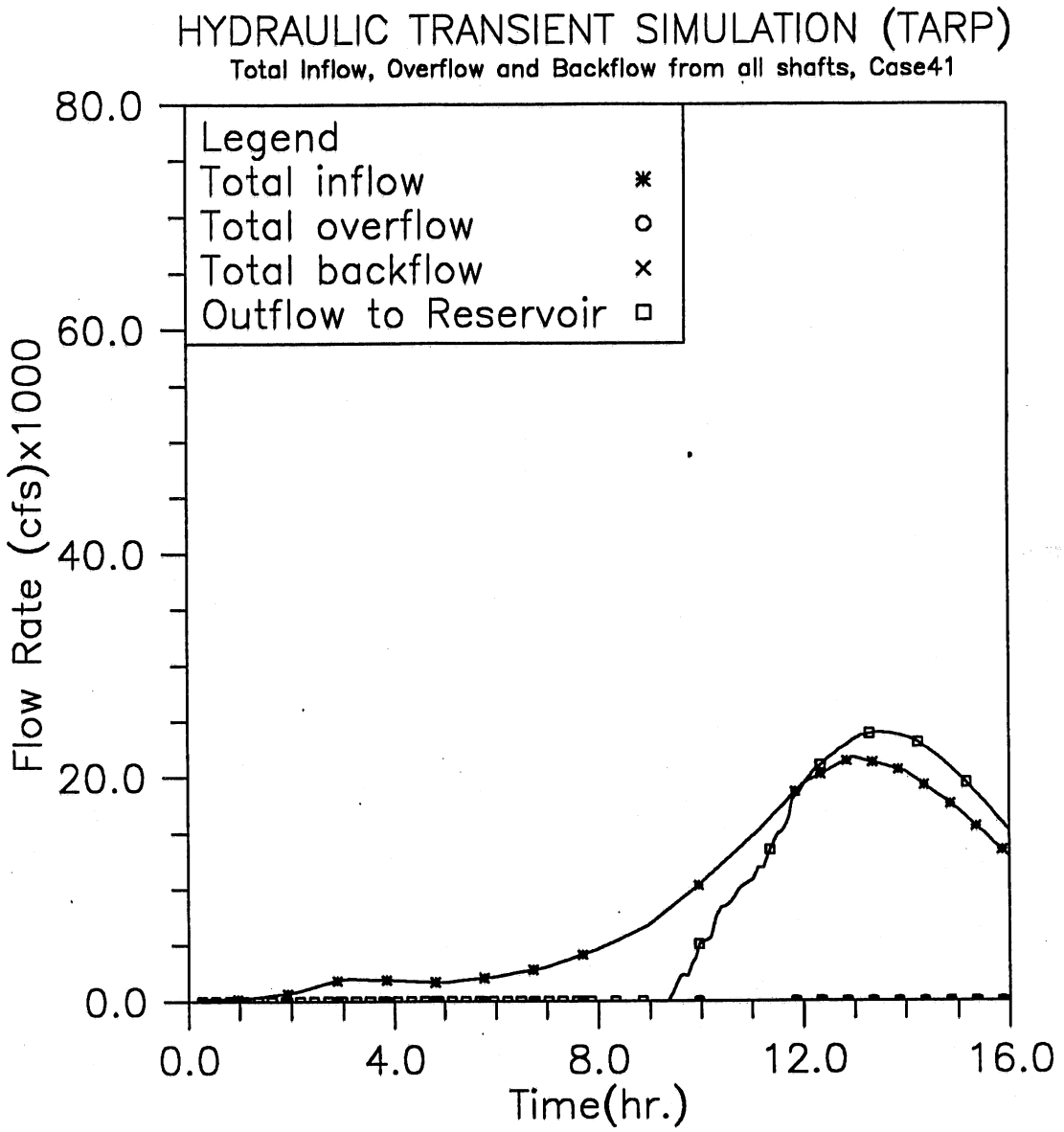

Fig. 3.13(h) Time variation of total inflow, overflow, backflow, and outflow to reservoir; Modeling case: gate opening in 30 min., initial reservoir level at –198, inflow control Plan 1, and 5–year storm event (Case 4–1)

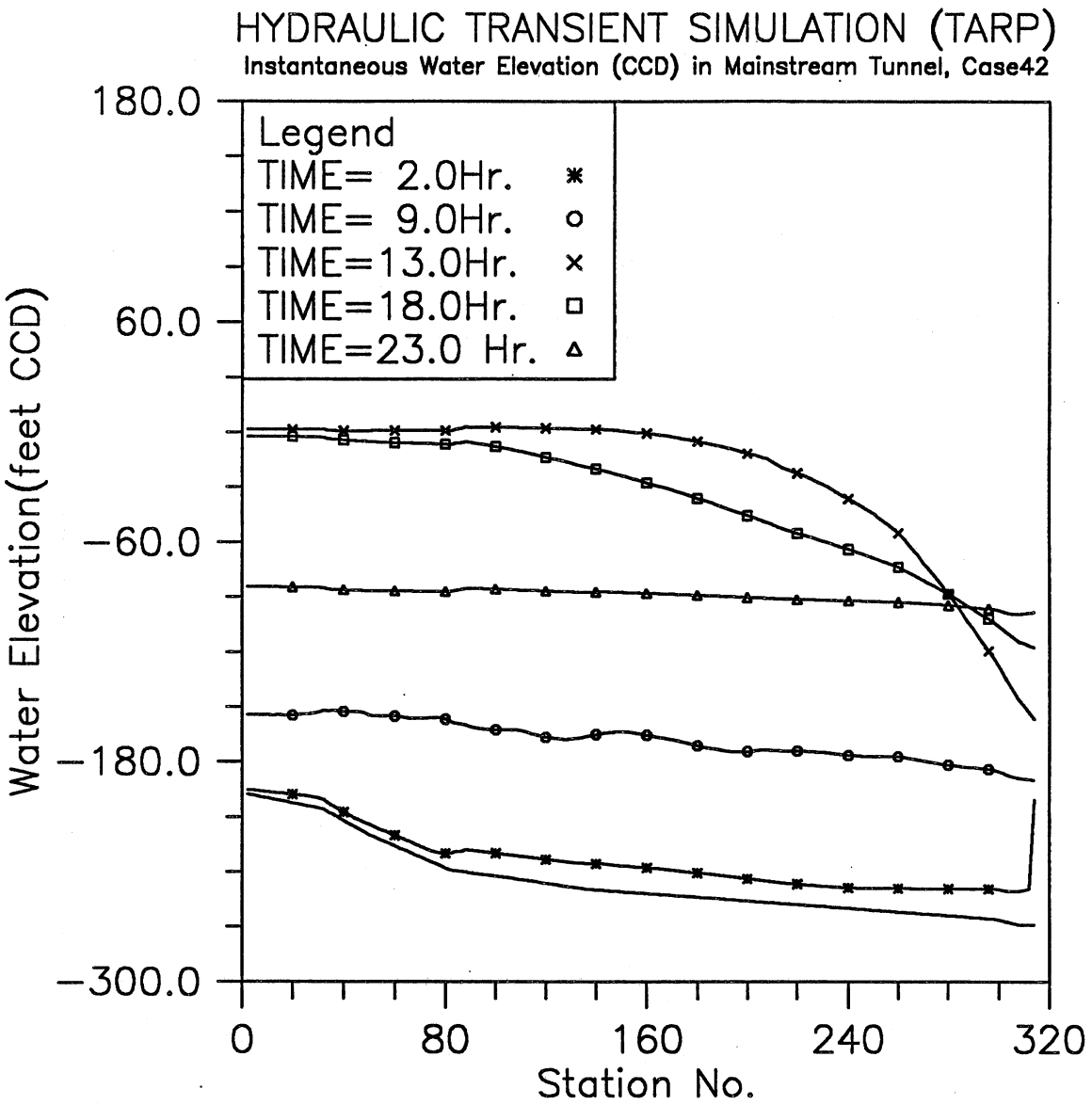

Fig. 3.14(a) Instantaneous hydraulic gradelines along the main tunnel; Modeling case: gate opening in 30 min., initial reservoir level at –198, inflow control Plan 2, and 100–year storm event (Case 4–2)

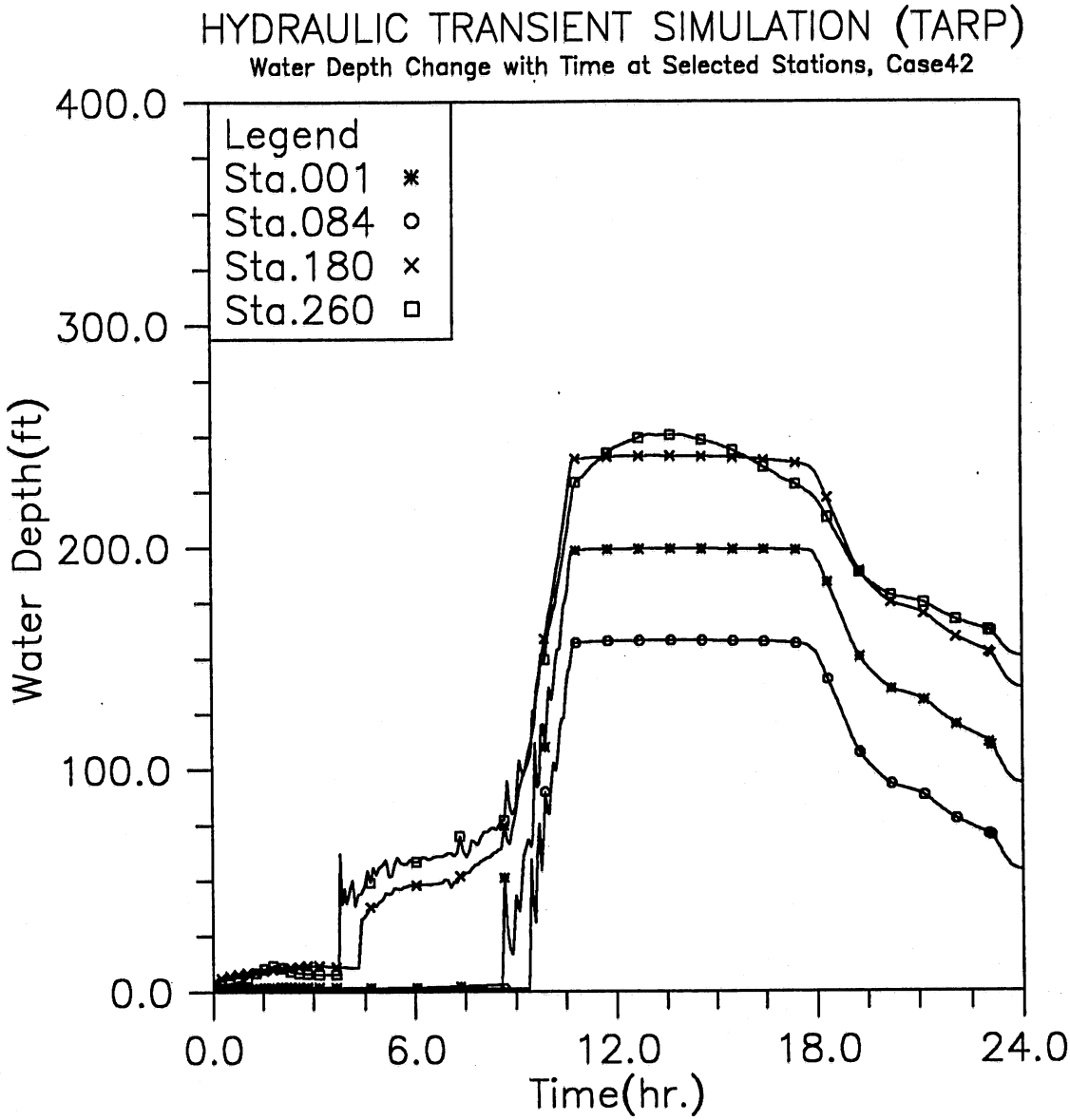

Fig. 3.14(b) Time variation of water depth at four upstream locations; Modeling case: gate opening in 30 min., initial reservoir level at –198, inflow control Plan 2, and 100–year storm event (Case 4–2)

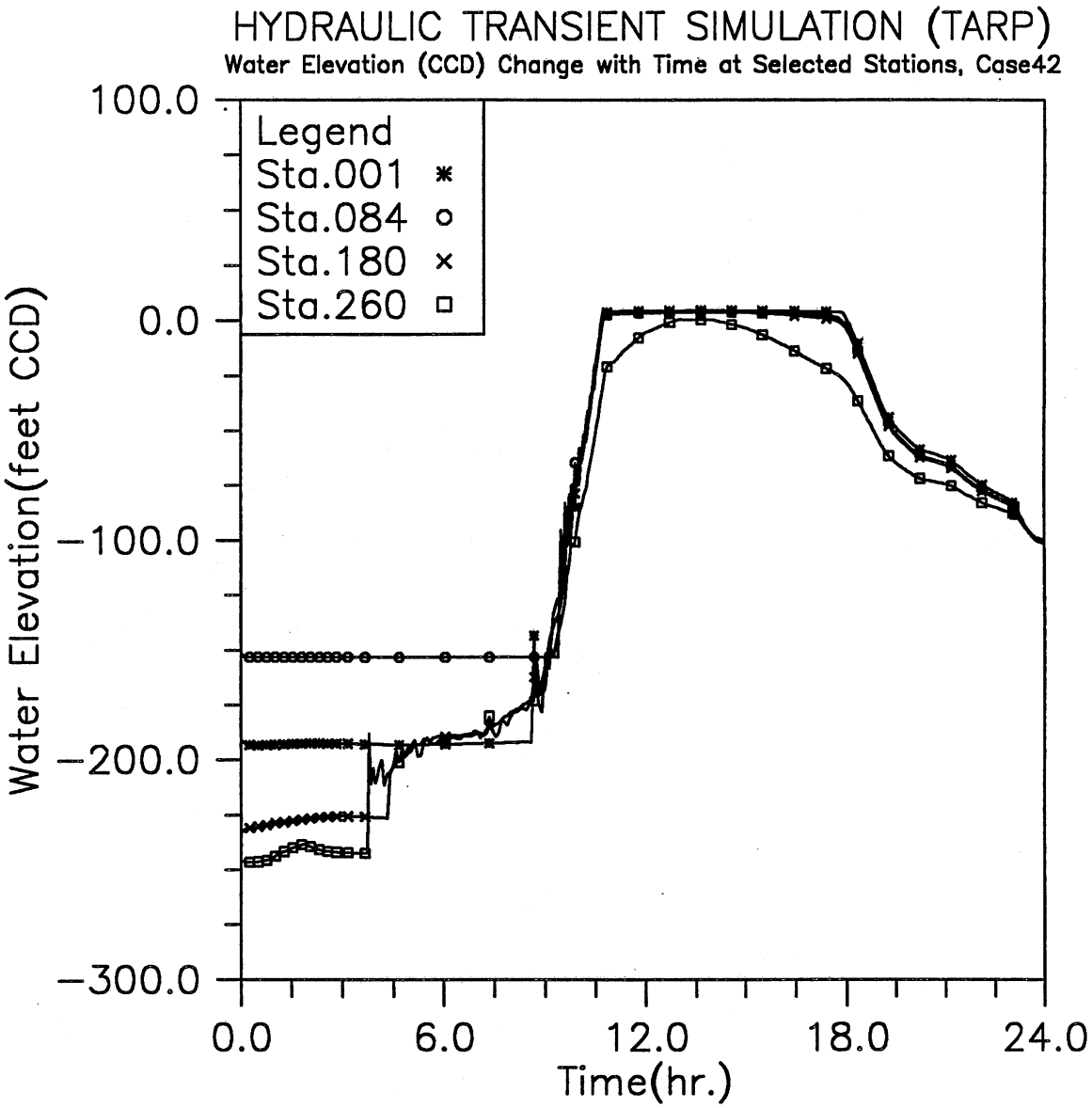

Fig. 3.14(c) Time variation of water elevation at four upstream locations; Modeling case: gate opening in 30 min., initial reservoir level at −198, inflow control Plan 2, and 100–year storm event (Case 4–2)

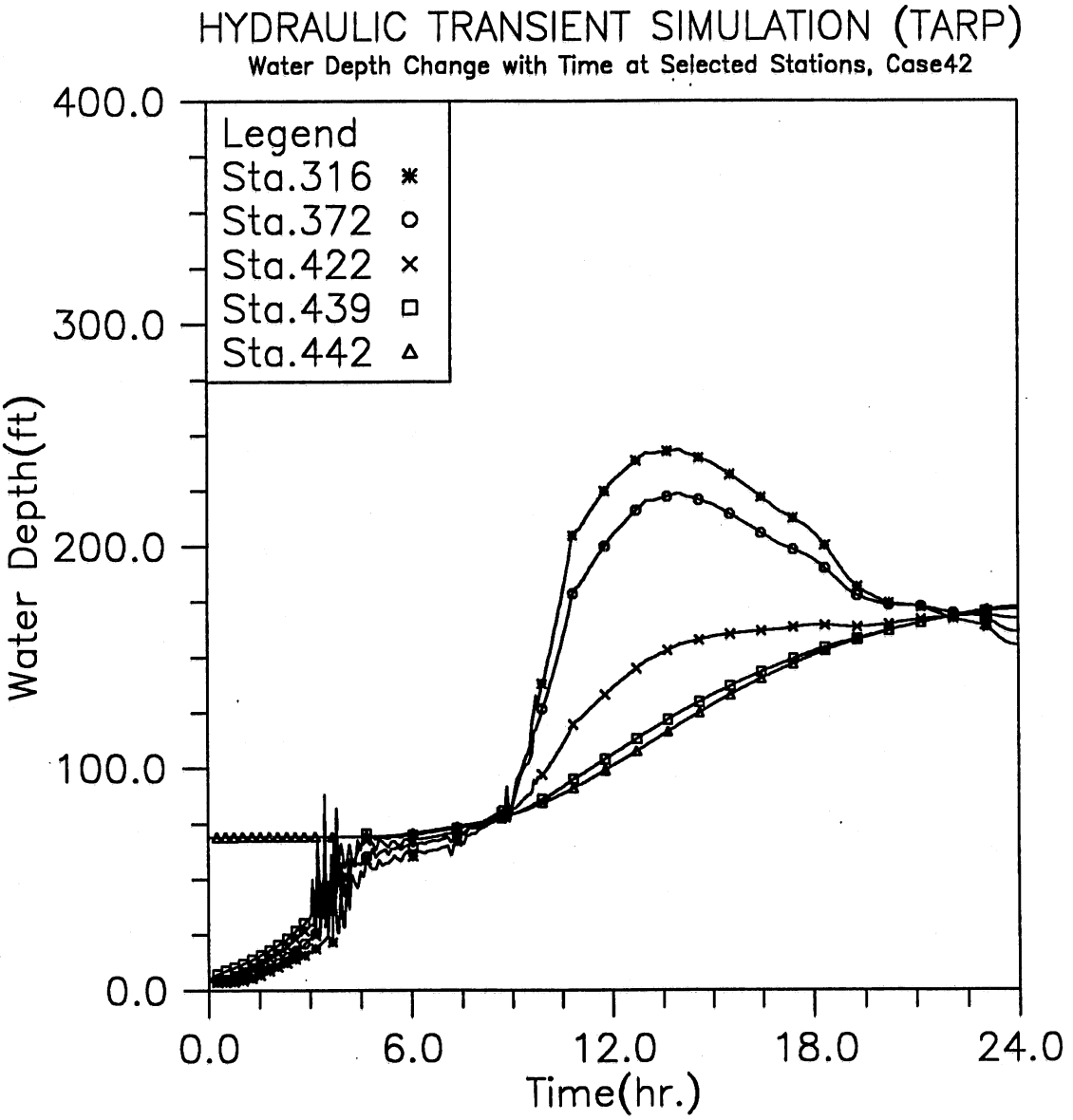

Fig. 3.14(d) Time variation of water depth at five downstream locations; Modeling case: gate opening in 30 min., initial reservoir level at –198, inflow control Plan 2, and 100–year storm event (Case 4–2)

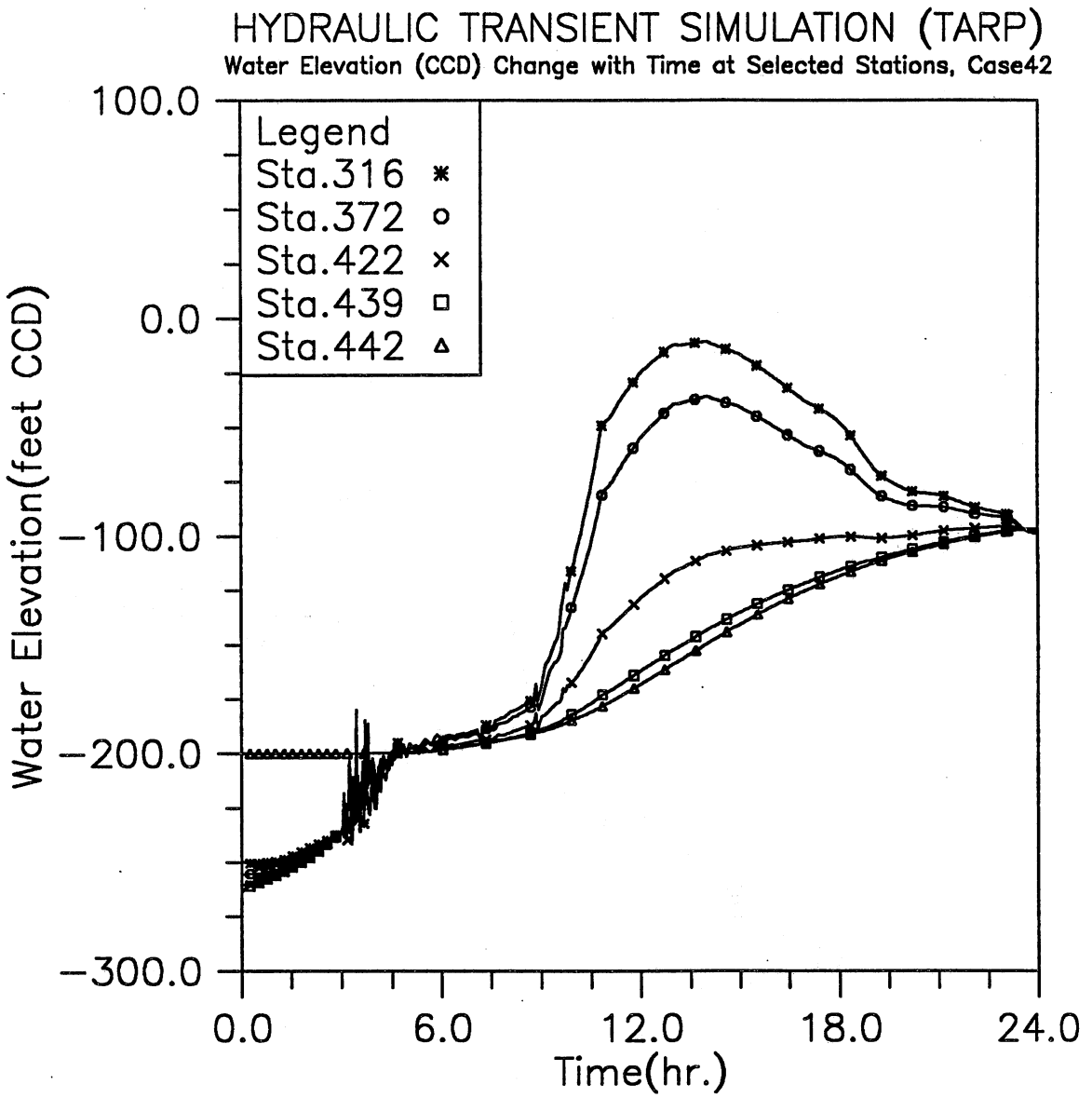

Fig. 3.14(e) Time variation of water elevation at five downstream locations; Modeling case: gate opening in 30 min., initial reservoir level at –198, inflow control Plan 2, and 100–year storm event (Case 4–2)

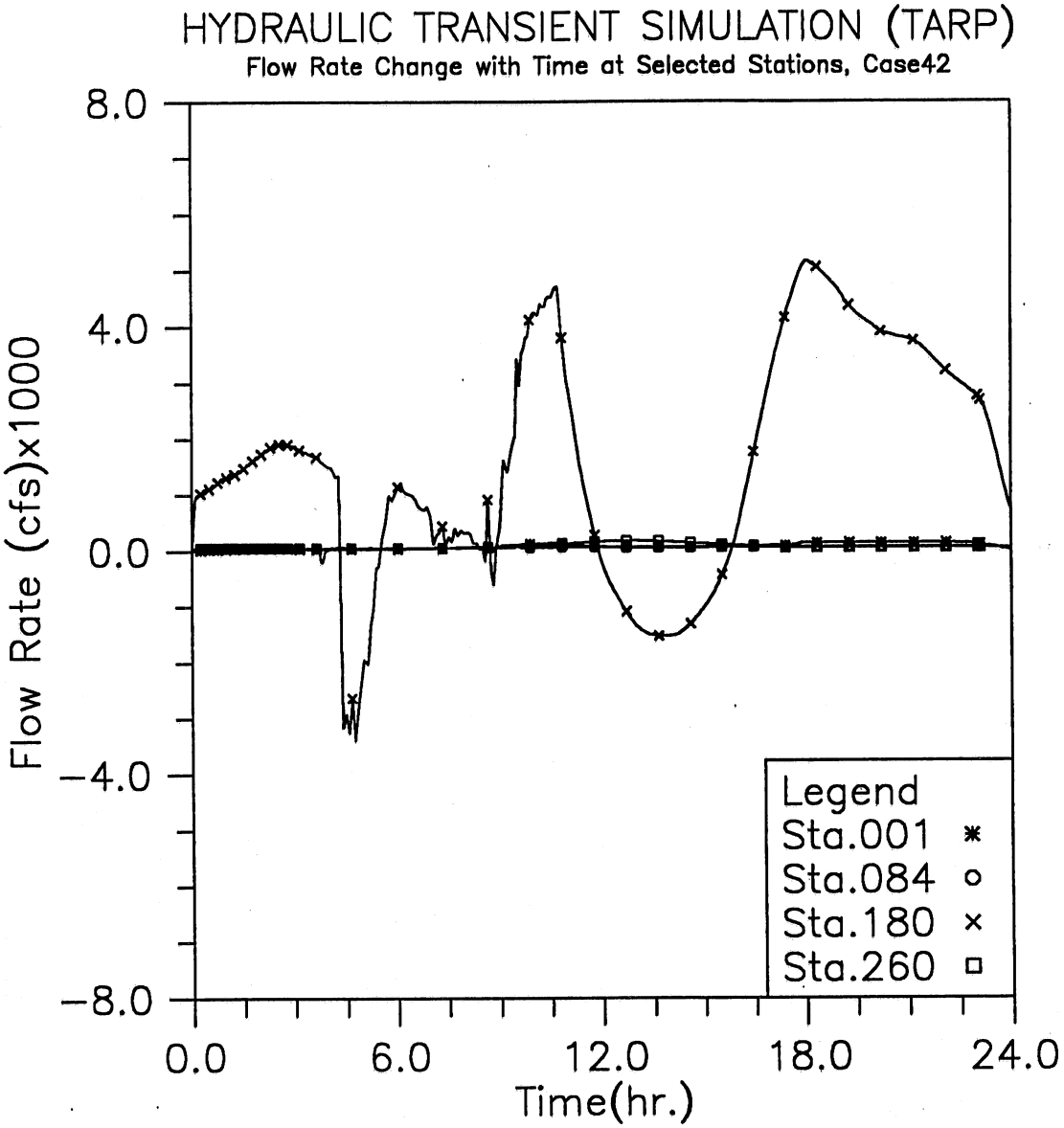

Fig. 3.14(f) Time variation of flow rate at four upstream locations; Modeling case: gate opening in 30 min., initial reservoir level at −198, inflow control Plan 2, and 100–year storm event (Case 4–2)

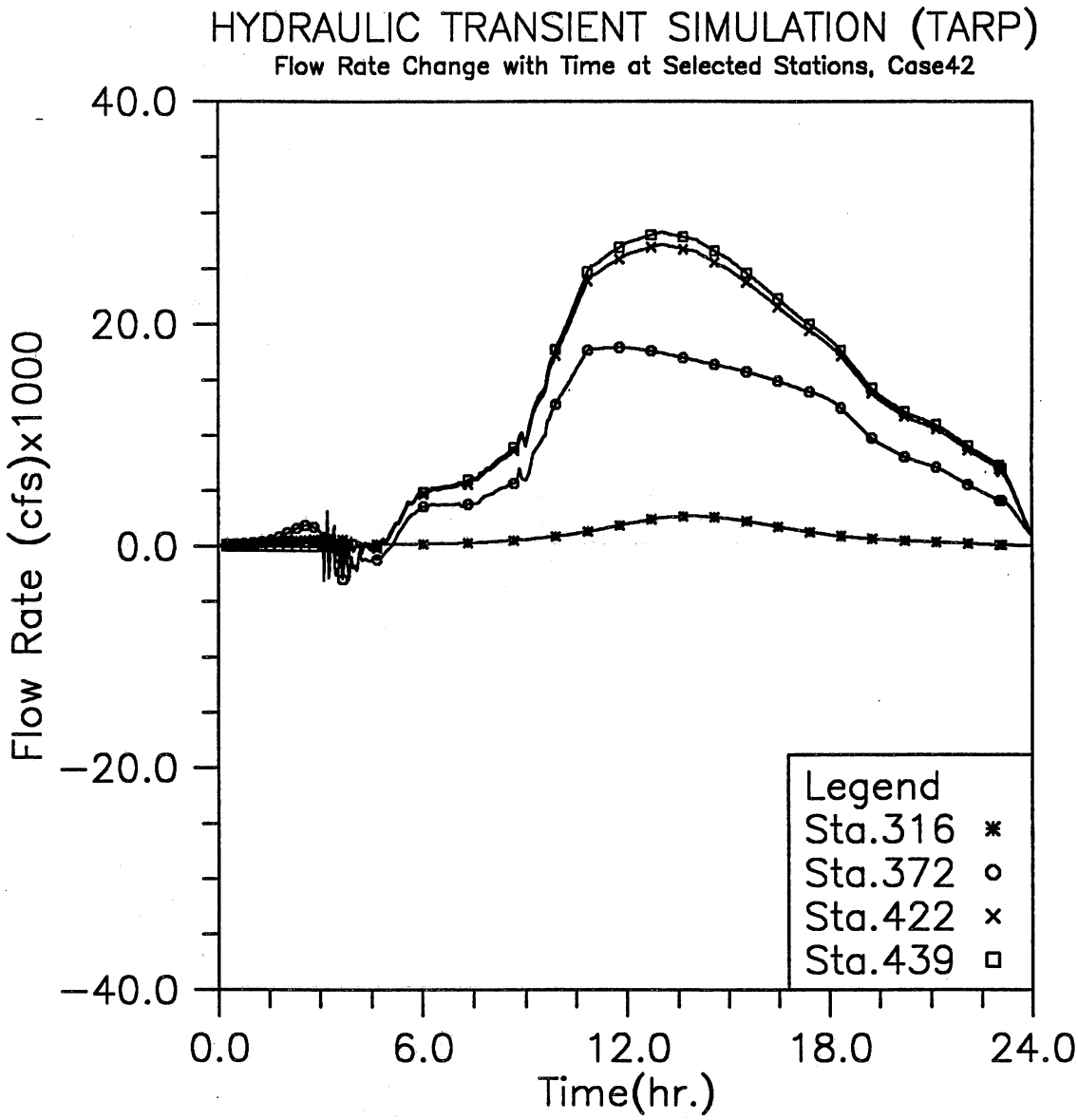

Fig. 3.14(g) Time variation of flow rate at four downstream locations; Modeling case: gate opening in 30 min., initial reservoir level at −198, inflow control Plan 2, and 100–year storm event (Case 4–2)

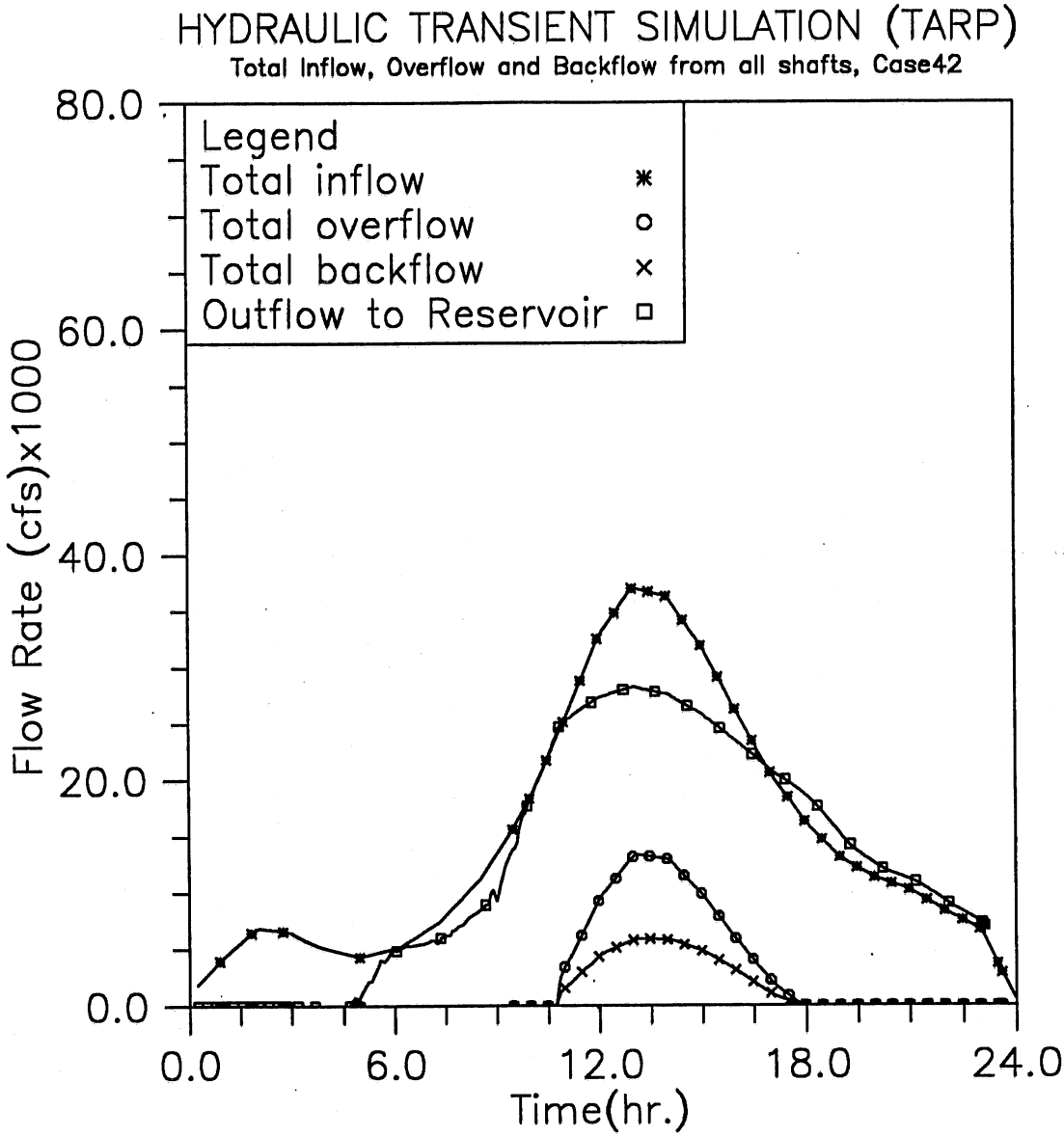

Fig. 3.14(h) Time variation of total inflow, overflow, backflow, and outflow to reservoir; Modeling case: gate opening in 30 min., initial reservoir level at –198, inflow control Plan 2, and 100–year storm event (Case 4–2)

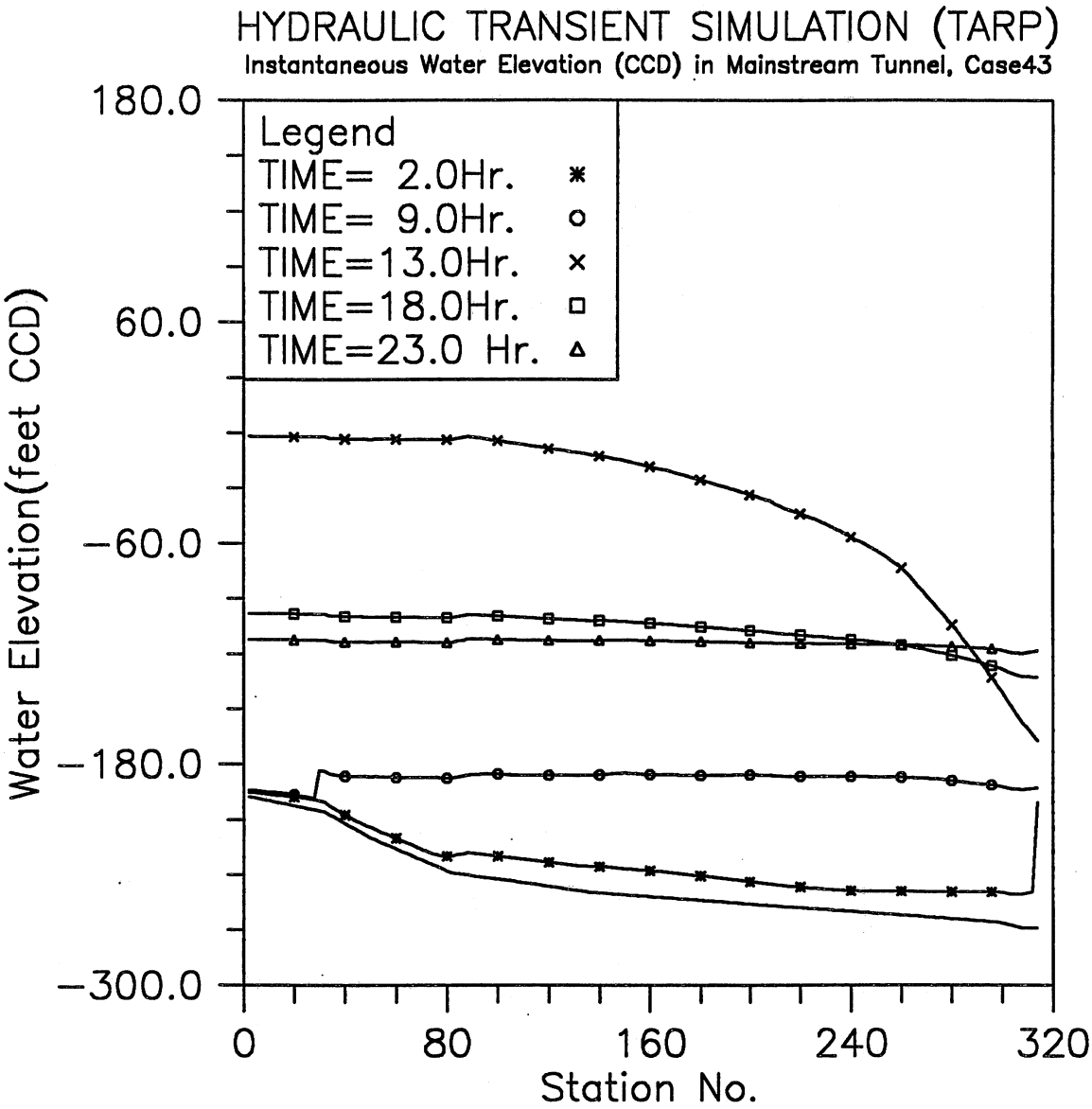

Fig. 3.15(a) Instantaneous hydraulic gradelines along the main tunnel; Modeling case: gate opening in 30 min., initial reservoir level at –198, inflow control Plan 3, and 100–year storm event (Case 4–3)

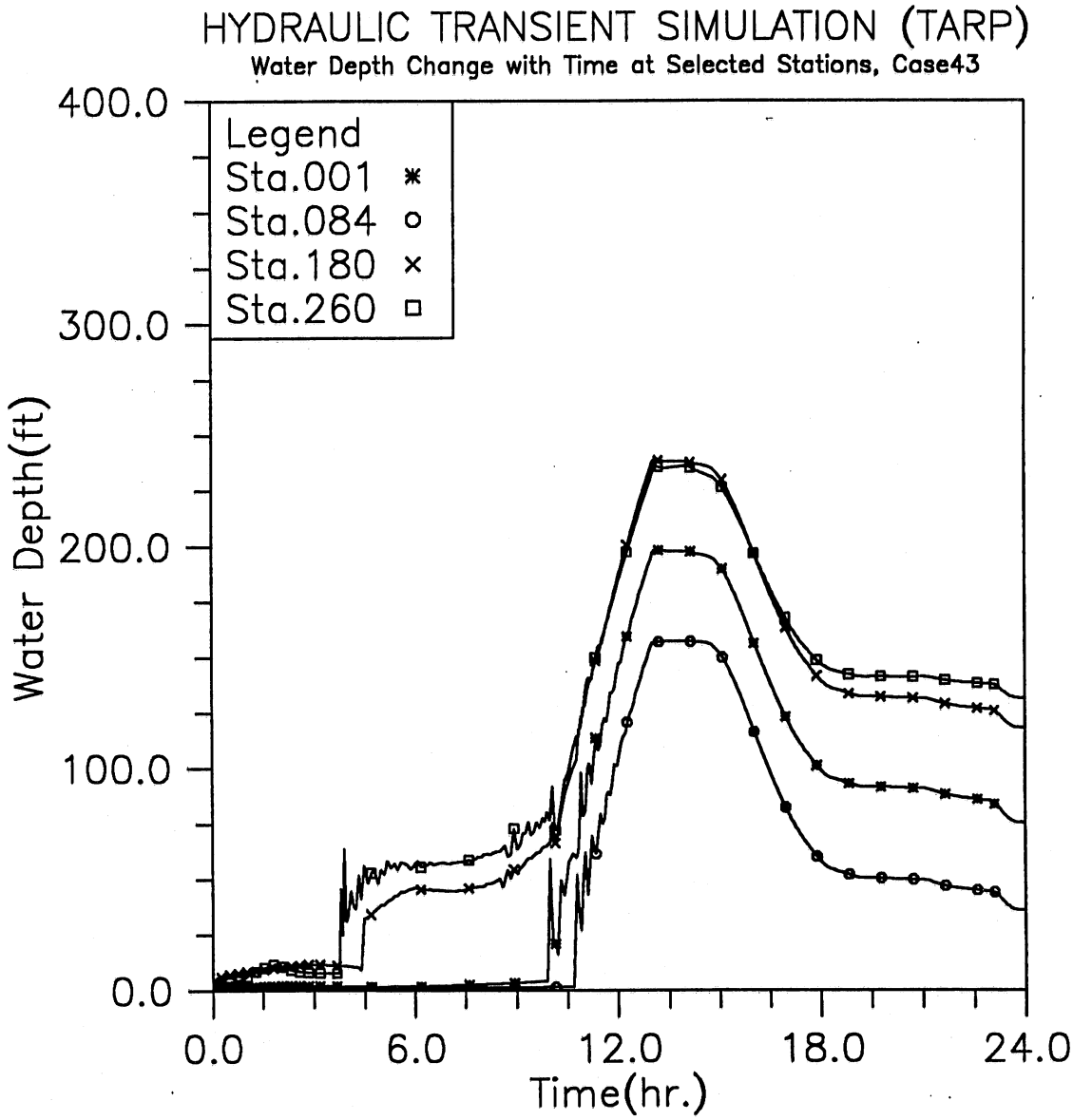

Fig. 3.15(b) Time variation of water depth at four upstream locations; Modeling case: gate opening in 30 min., initial reservoir level at –198, inflow control Plan 3, and 100–year storm event (Case 4–3)

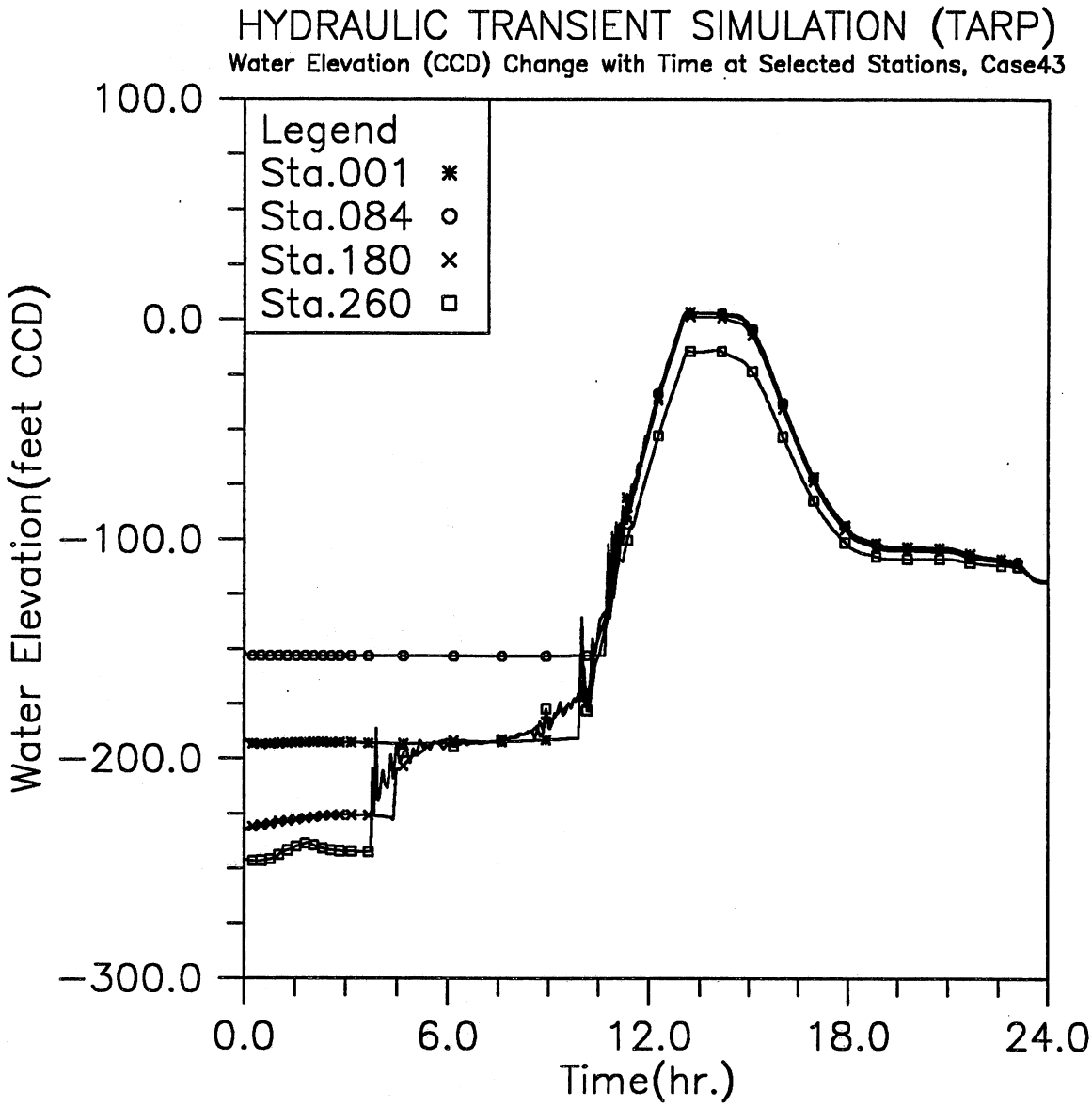

Fig. 3.15(c) Time variation of water elevation at four upstream locations; Modeling case: gate opening in 30 min., initial reservoir level at –198, inflow control Plan 3, and 100–year storm event (Case 4–3)

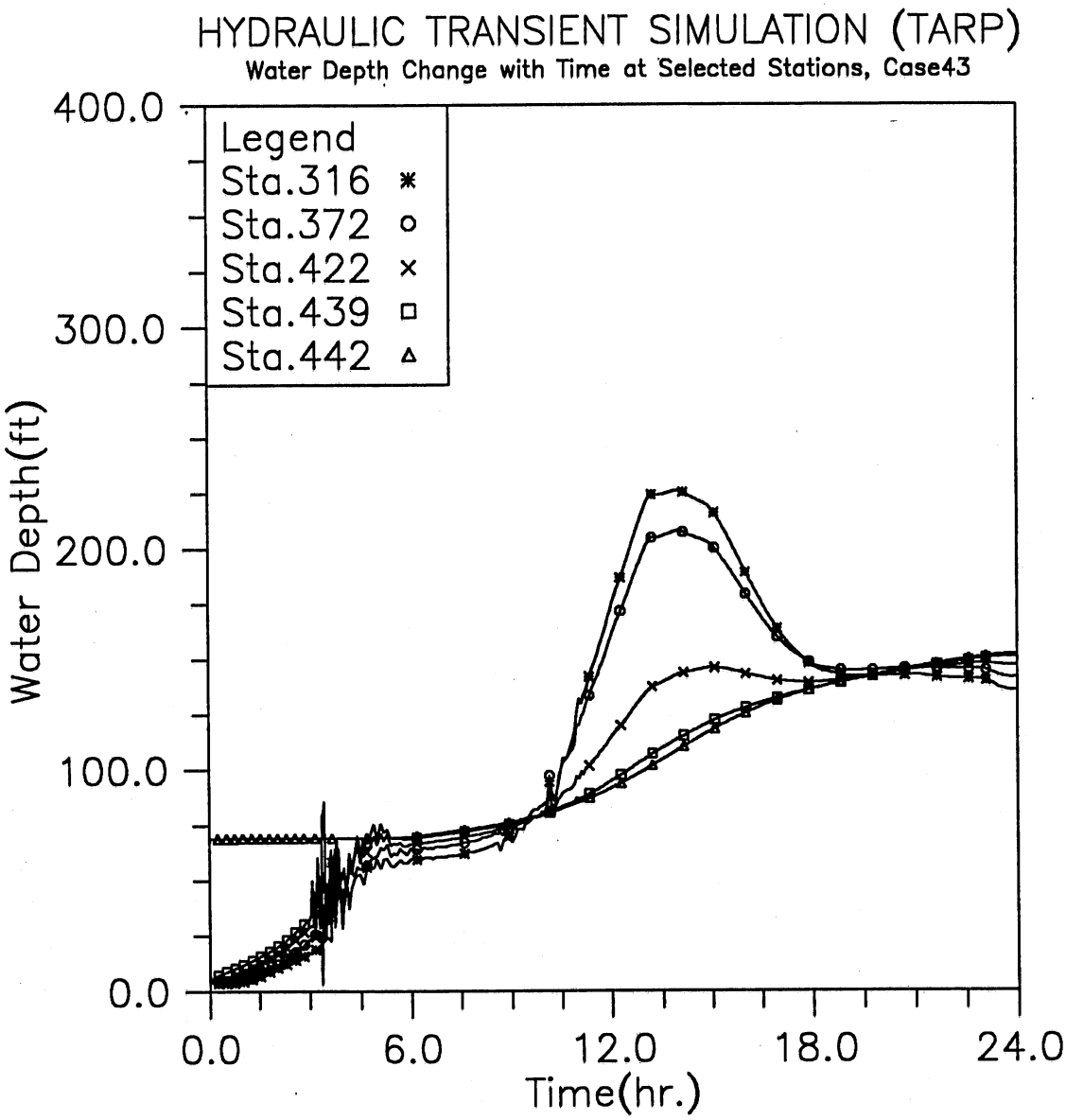

Fig. 3.15(d) Time variation of water depth at five downstream locations; Modeling case: gate opening in 30 min., initial reservoir level at –198, inflow control Plan 3, and 100–year storm event (Case 4–3)

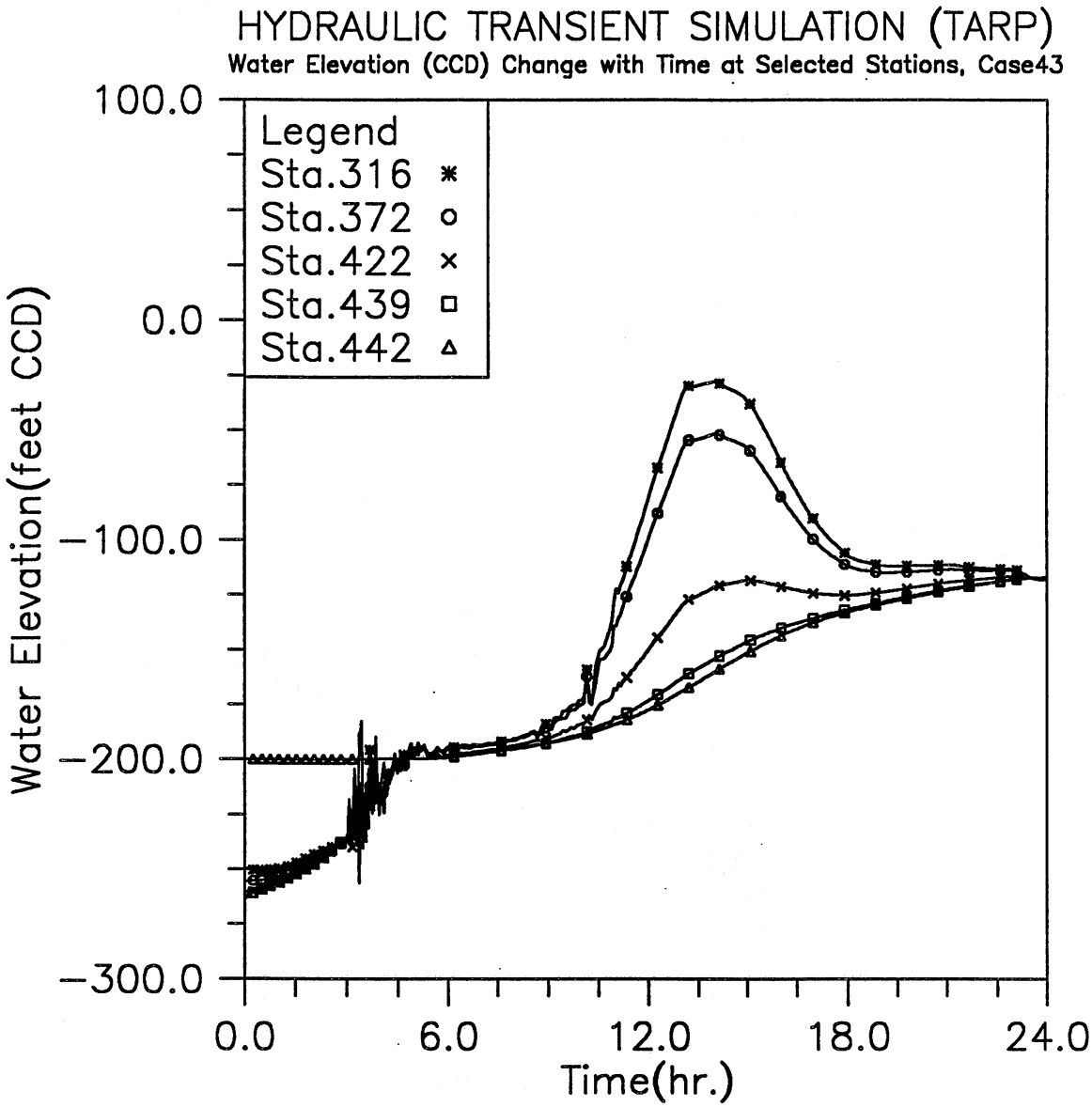

Fig. 3.15(e) Time variation of water elevation at five downstream locations; Modeling case: gate opening in 30 min., initial reservoir level at –198, inflow control Plan 3, and 100–year storm event (Case 4–3)

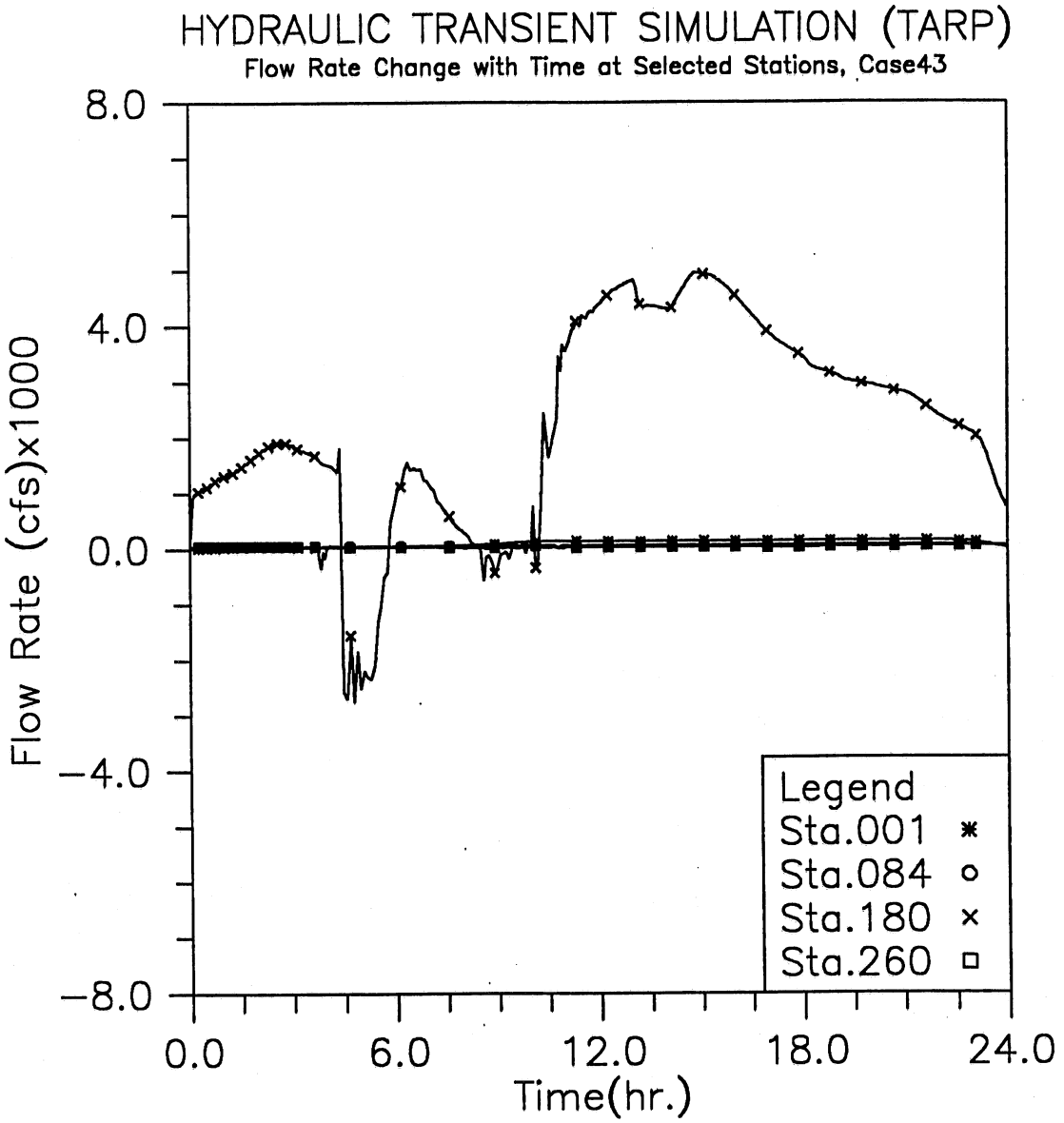

Fig. 3.15(f) Time variation of flow rate at four upstream locations; Modeling case: gate opening in 30 min., initial reservoir level at −198, inflow control Plan 3, and 100-year storm event (Case 4-3)

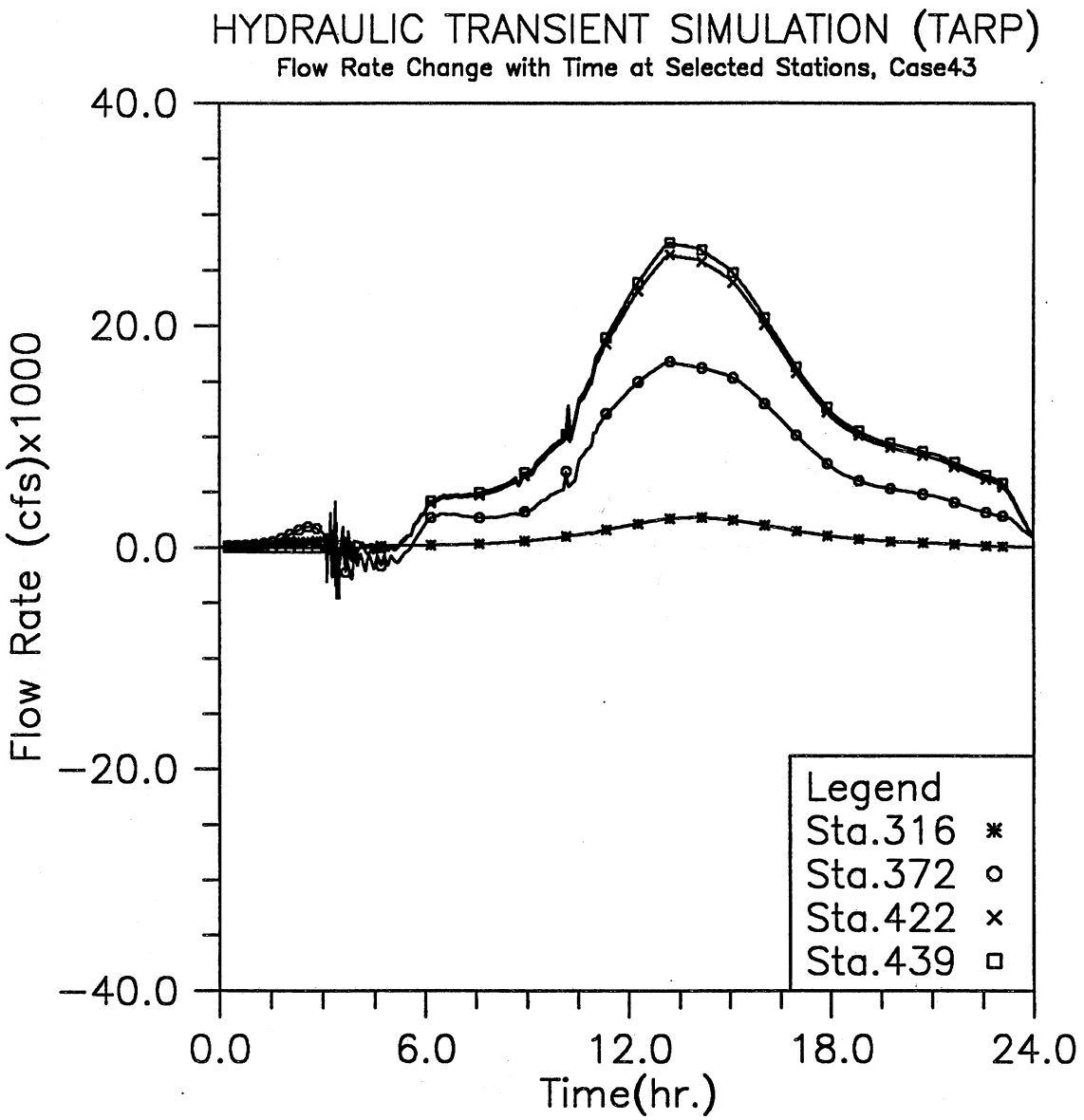

Fig. 3.15(g) Time variation of flow rate at four downstream locations; Modeling case: gate opening in 30 min., initial reservoir level at −198, inflow control Plan 3, and 100-year storm event (Case 4-3)

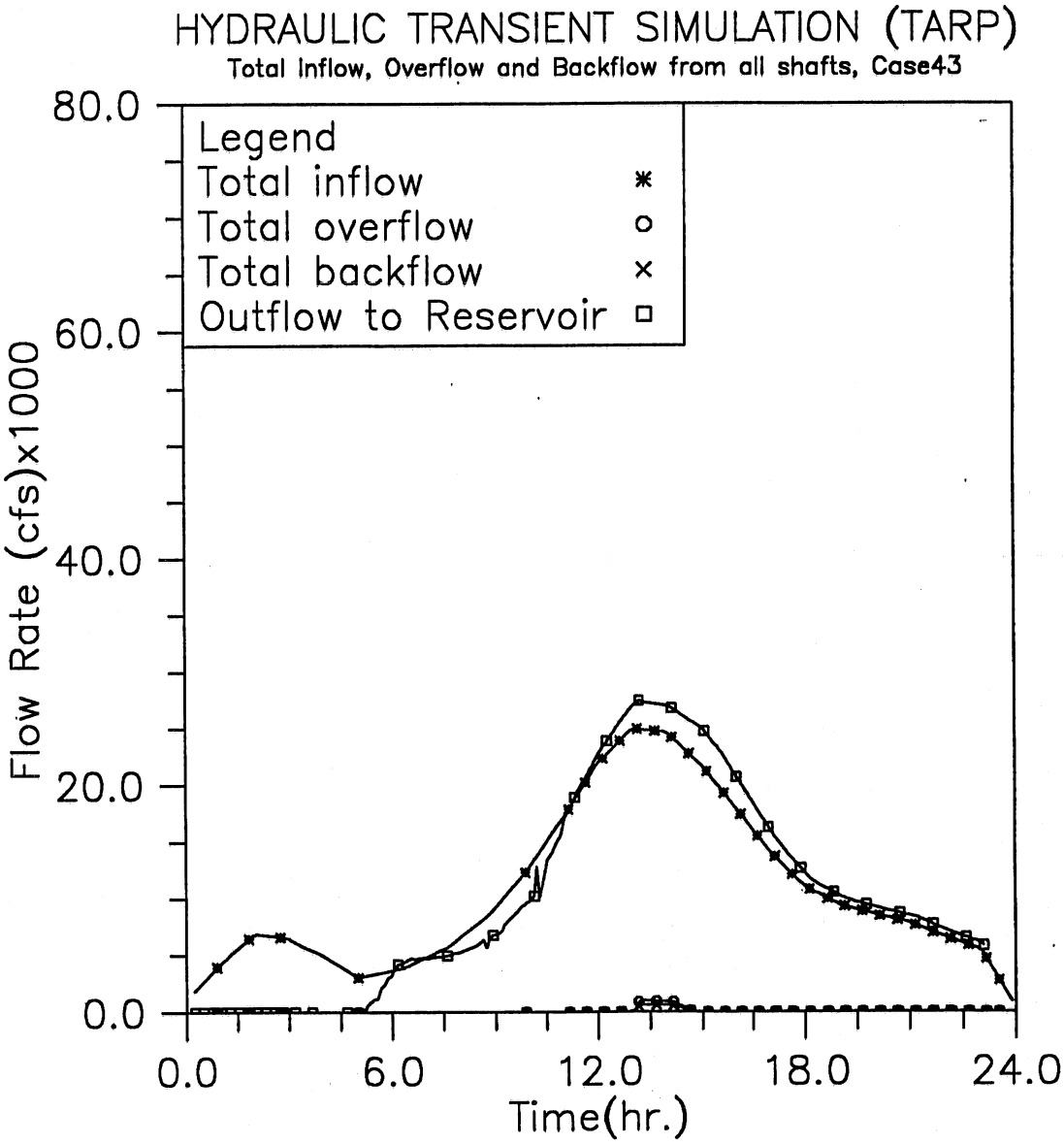

Fig. 3.15(h) Time variation of total inflow, overflow, backflow, and outflow to reservoir; Modeling case: gate opening in 30 min., initial reservoir level at –198, inflow control Plan 3, and 100–year storm event (Case 4–3)

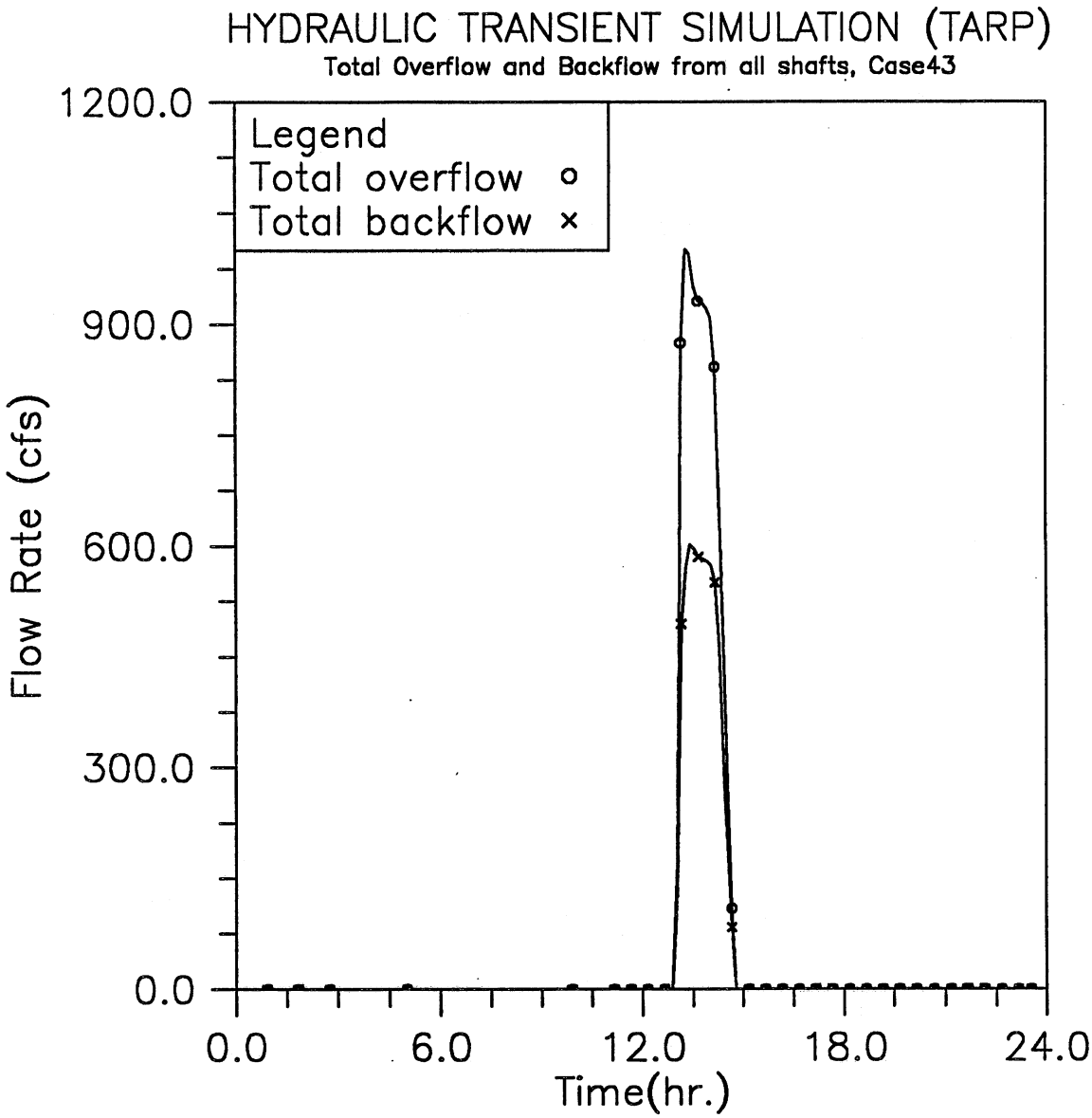

Fig. 3.15(i) Time variation of scaled–up total overflow and backflow; Modeling case: gate opening in 30 min., initial reservoir level at –198, inflow control Plan 3, and 100–year storm event (Case 4–3)

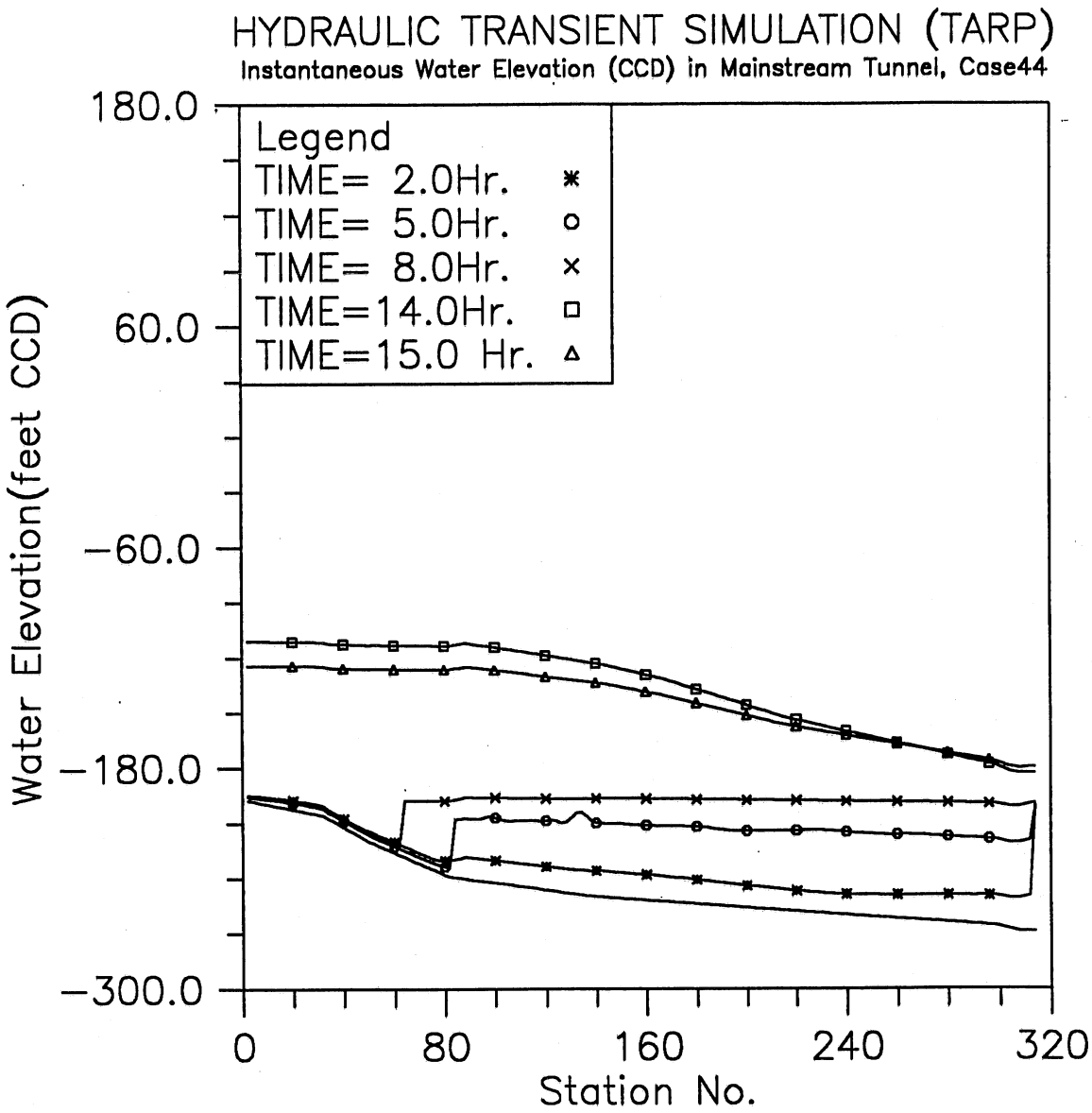

Fig. 3.16(a) Instantaneous hydraulic gradelines along the main tunnel; Modeling case: gate opening in 30 min., initial reservoir level at –198, inflow control Plan 4, and 100–year storm event (Case 4–4)

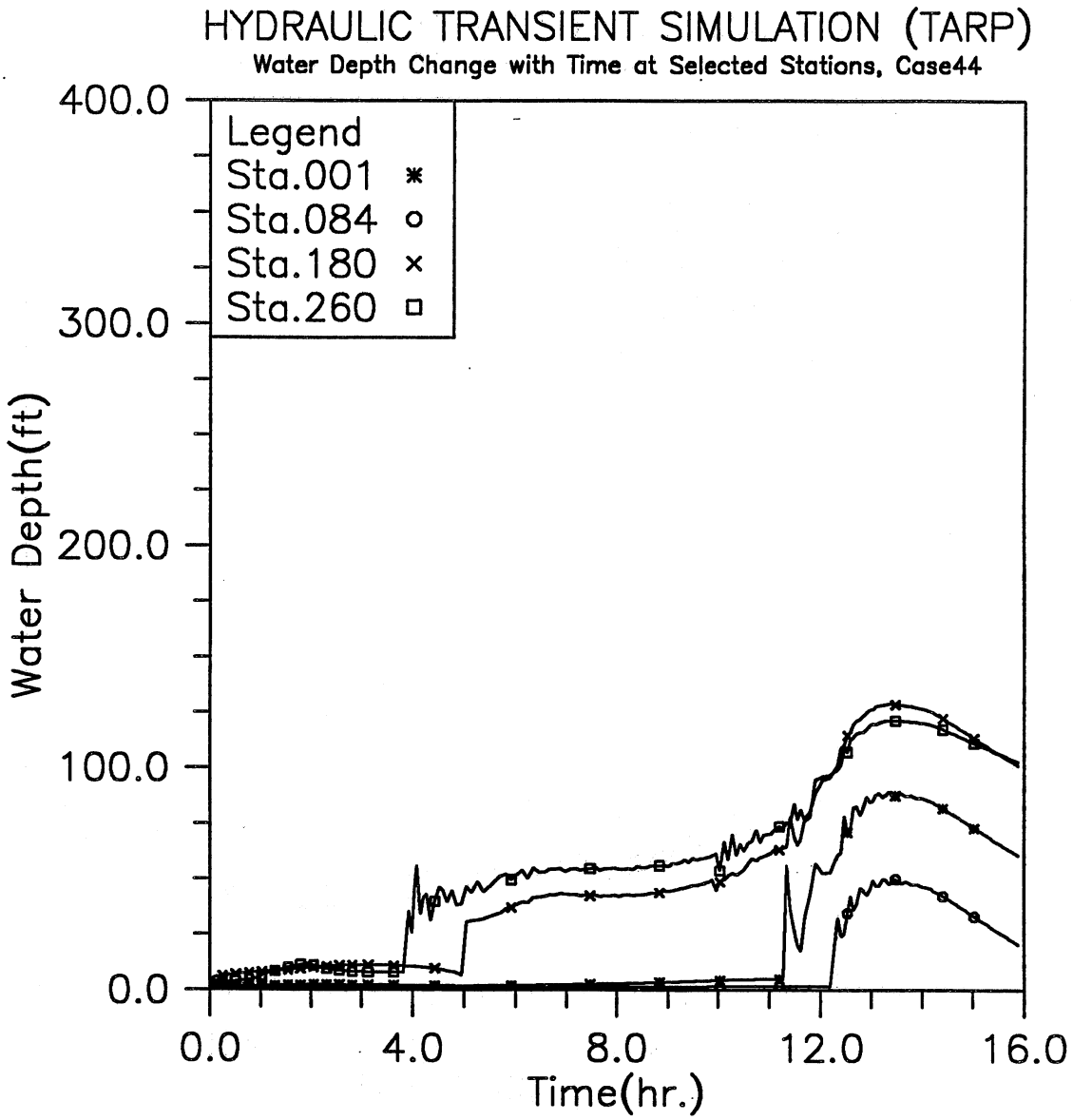

Fig. 3.16(b) Time variation of water depth at four upstream locations; Modeling case: gate opening in 30 min., initial reservoir level at –198, inflow control Plan 4, and 100–year storm event (Case 4–4)

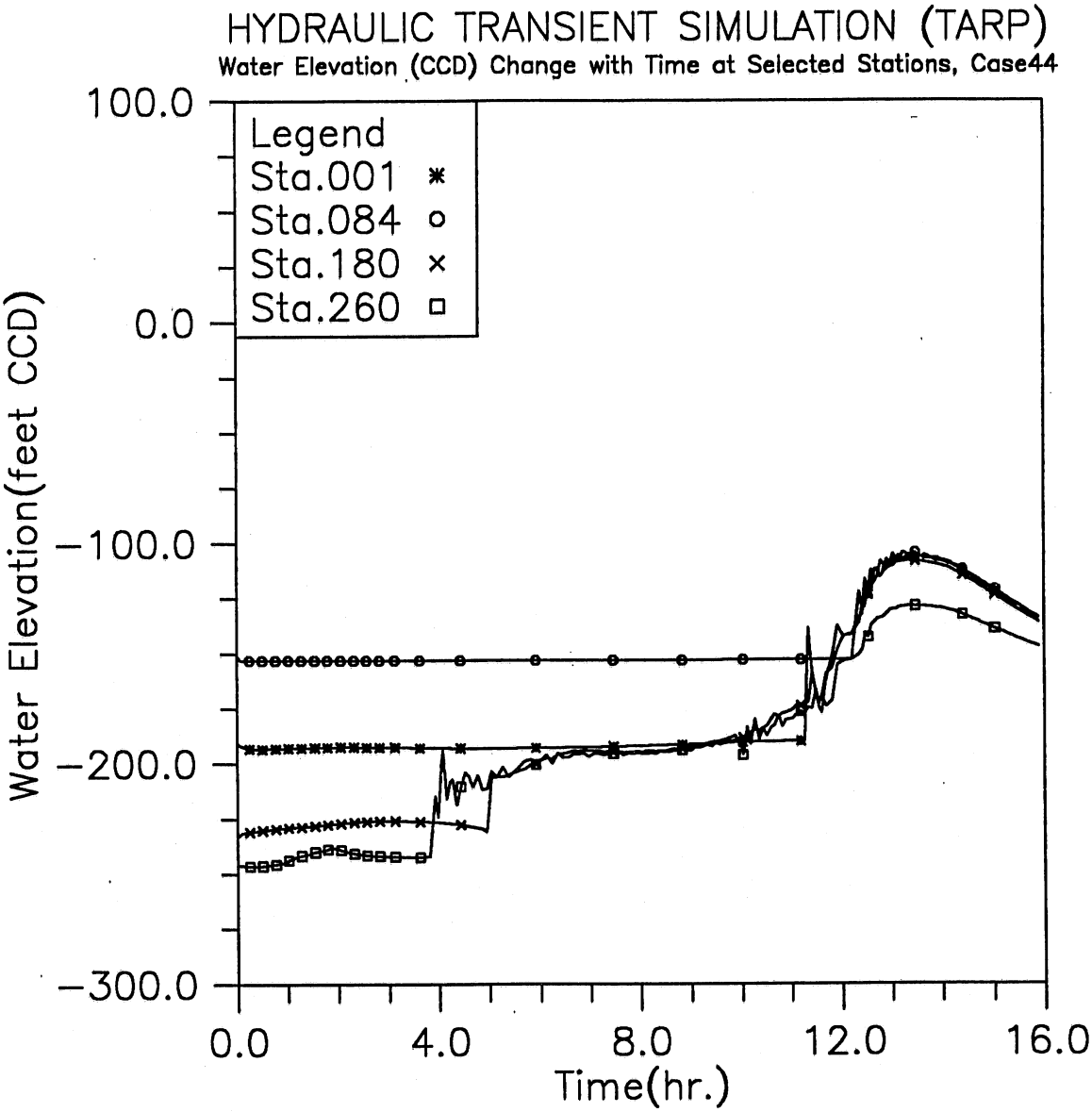

Fig. 3.16(c) Time variation of water elevation at four upstream locations; Modeling case: gate opening in 30 min., initial reservoir level at –198, inflow control Plan 4, and 100–year storm event (Case 4–4)

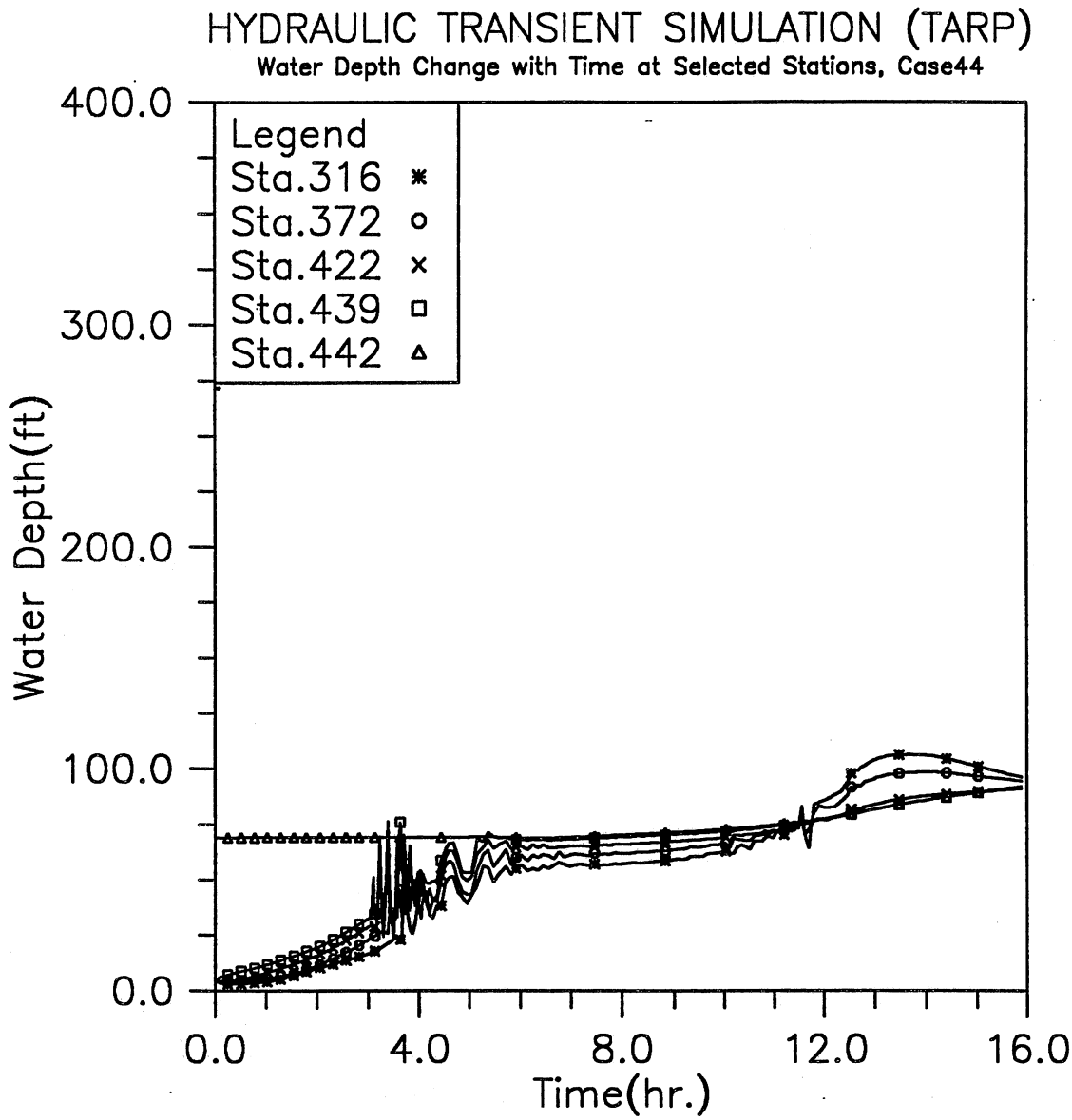

Fig. 3.16(d) Time variation of water depth at five downstream locations; Modeling case: gate opening in 30 min., initial reservoir level at –198, inflow control Plan 4, and 100–year storm event (Case 4–4)

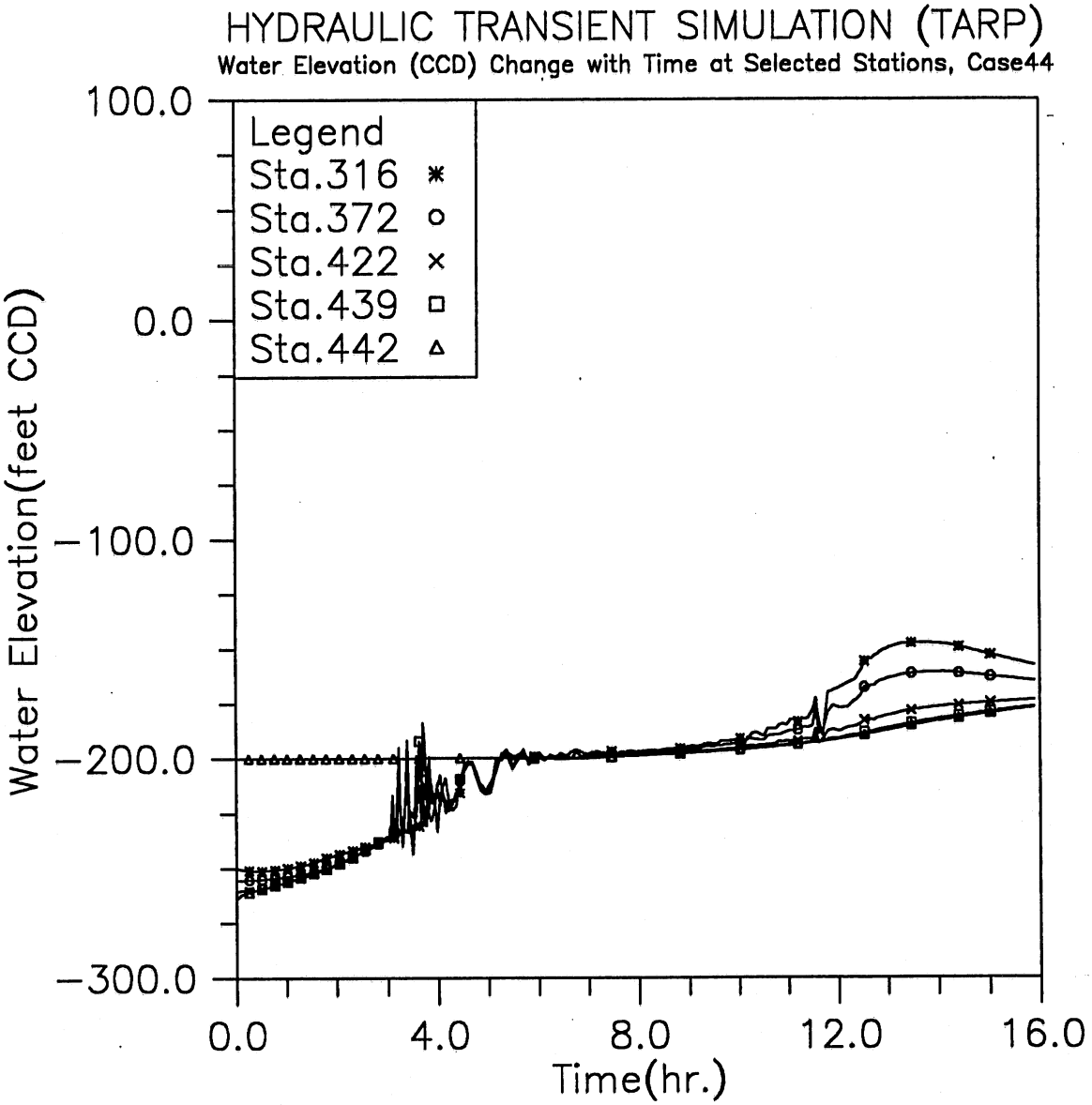

Fig. 3.16(e) Time variation of water elevation at five downstream locations; Modeling case: gate opening in 30 min., initial reservoir level at –198, inflow control Plan 4, and 100–year storm event (Case 4–4)

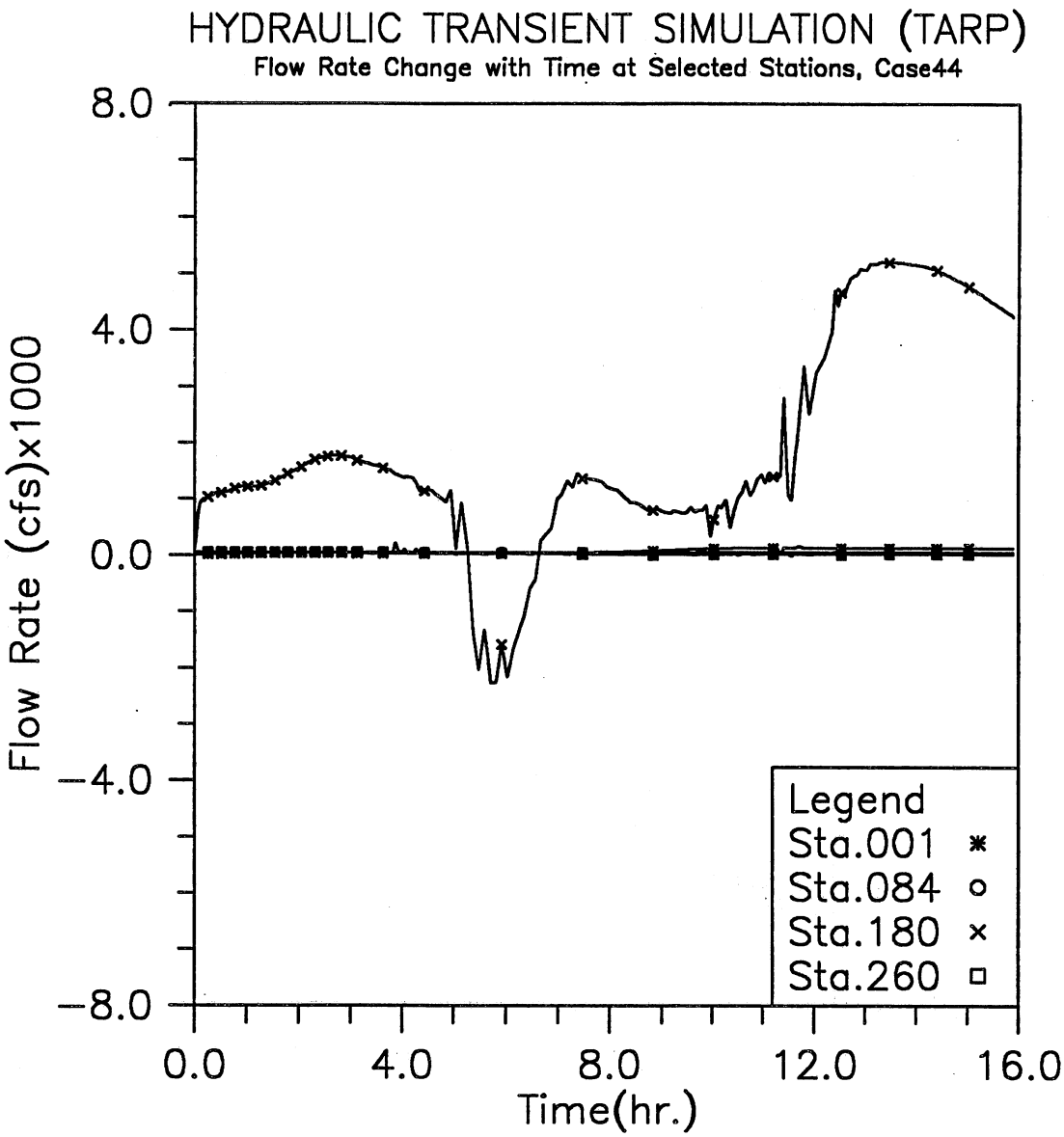

Fig. 3.16(f) Time variation of flow rate at four upstream locations; Modeling case: gate opening in 30 min., initial reservoir level at –198, inflow control Plan 4, and 100–year storm event (Case 4–4)

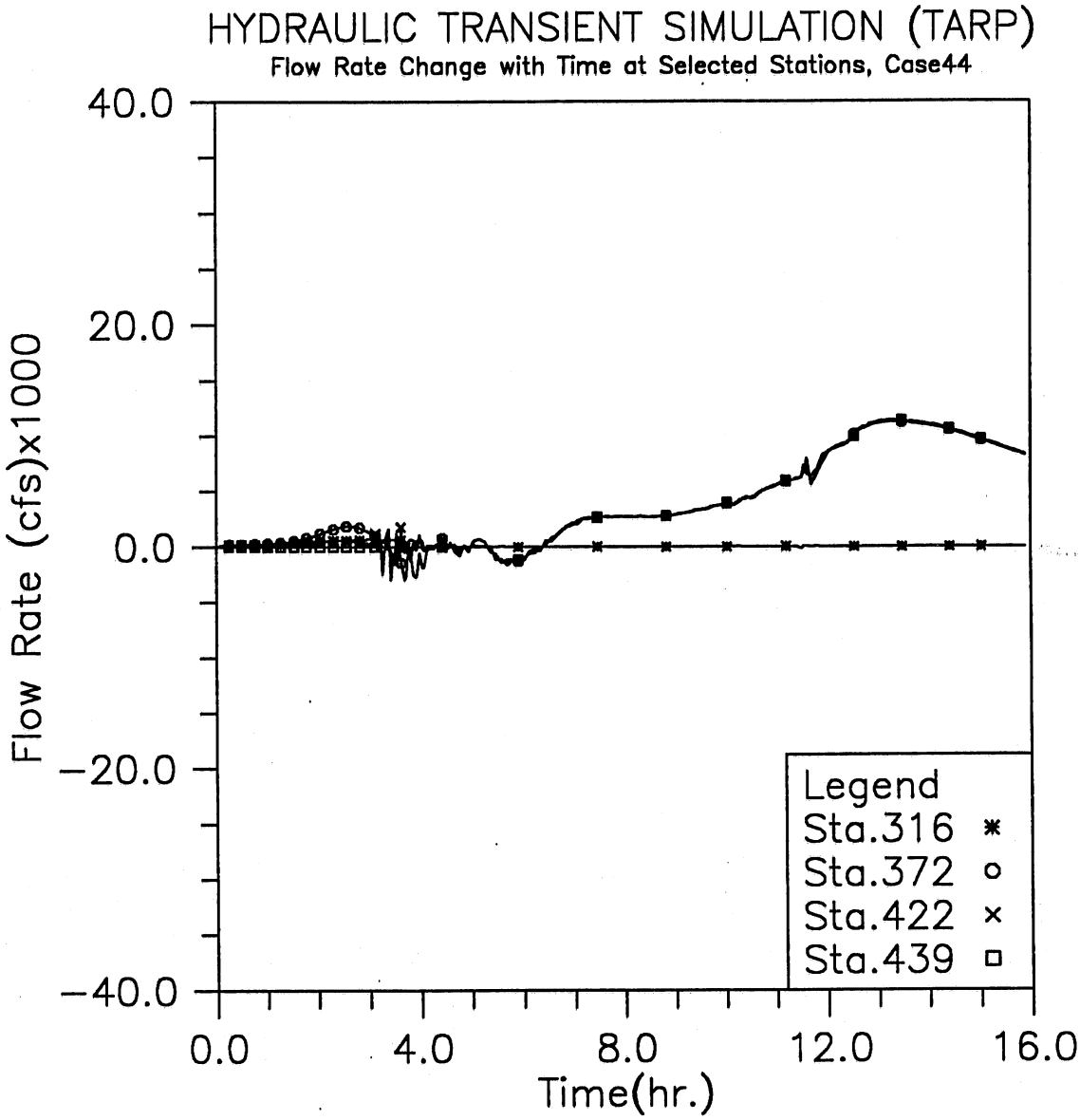

Fig. 3.16(g) Time variation of flow rate at four downstream locations; Modeling case: gate opening in 30 min., initial reservoir level at −198, inflow control Plan 4, and 100-year storm event (Case 4-4)

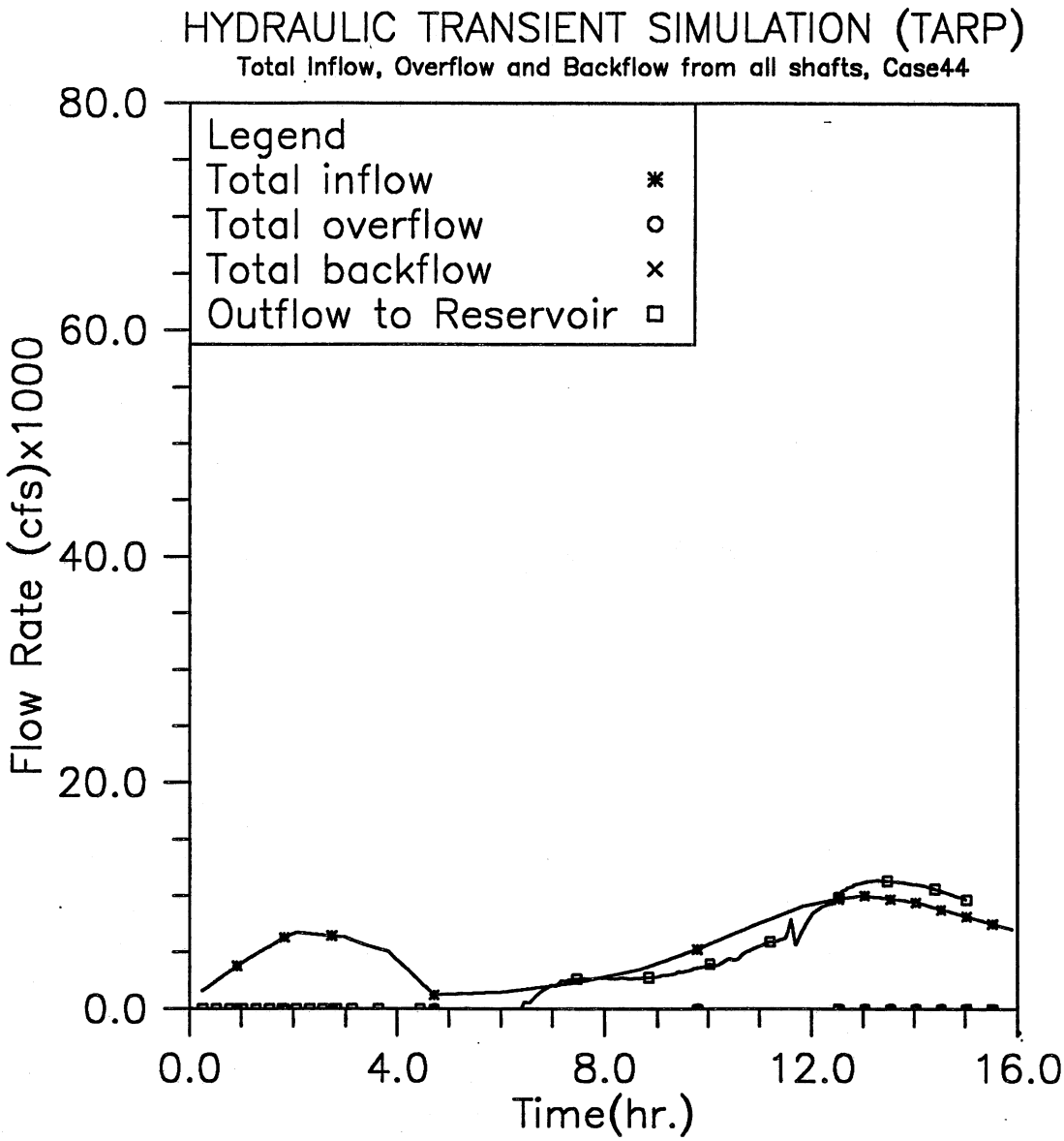

Fig. 3.16(h) Time variation of total inflow, overflow, backflow, and outflow to reservoir; Modeling case: gate opening in 30 min., initial reservoir level at –198, inflow control Plan 4, and 100–year storm event (Case 4–4)

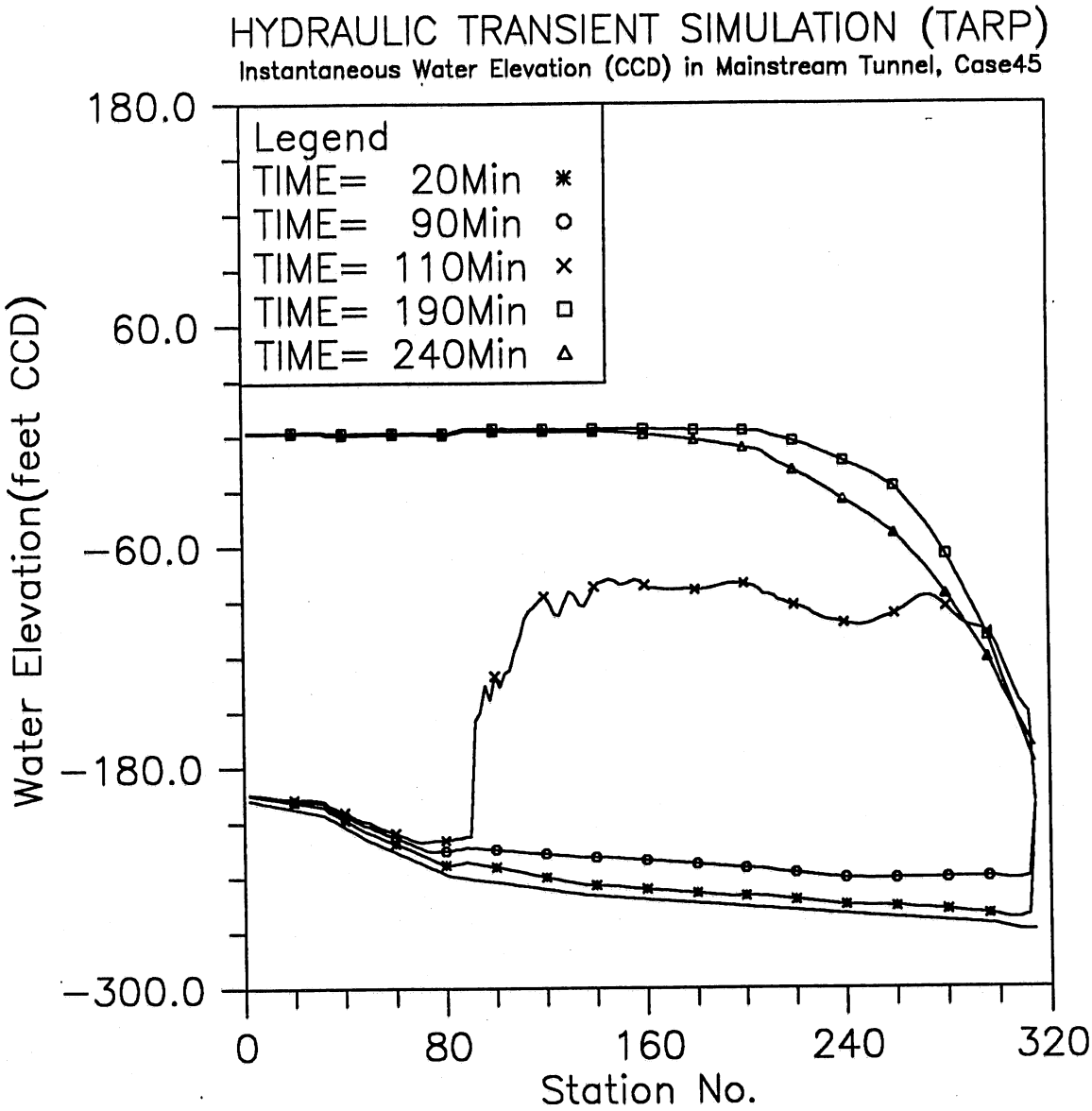

Fig. 3.17(a) Instantaneous hydraulic gradelines along the main tunnel; Modeling case: gate opening in 30 min., initial reservoir level at –198, inflow control Plan 1, and MAX storm event (Case 4–5)

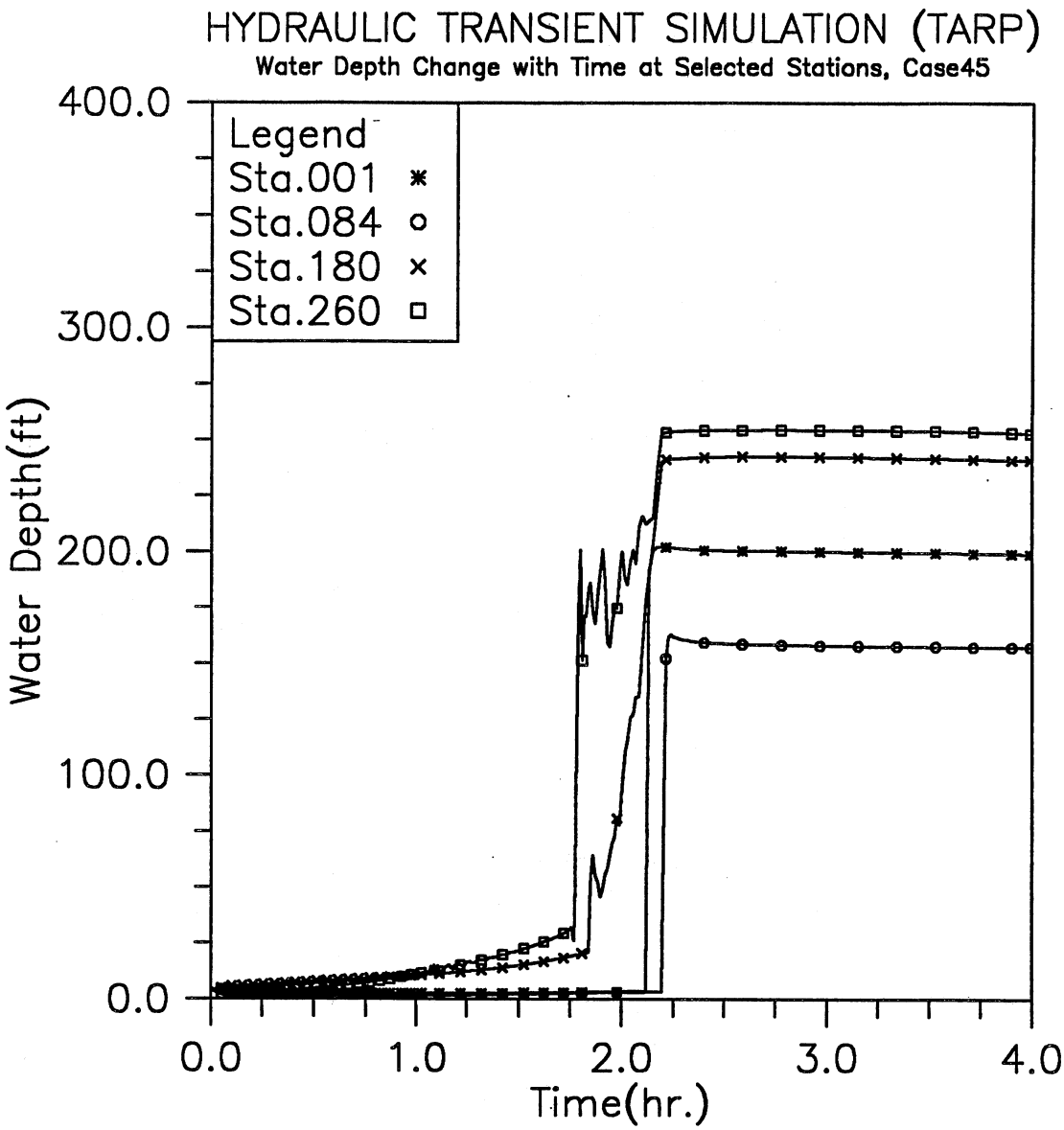

Fig. 3.17(b) Time variation of water depth at four upstream locations; Modeling case: gate opening in 30 min., initial reservoir level at –198, inflow control Plan 1, and MAX storm event (Case 4–5)

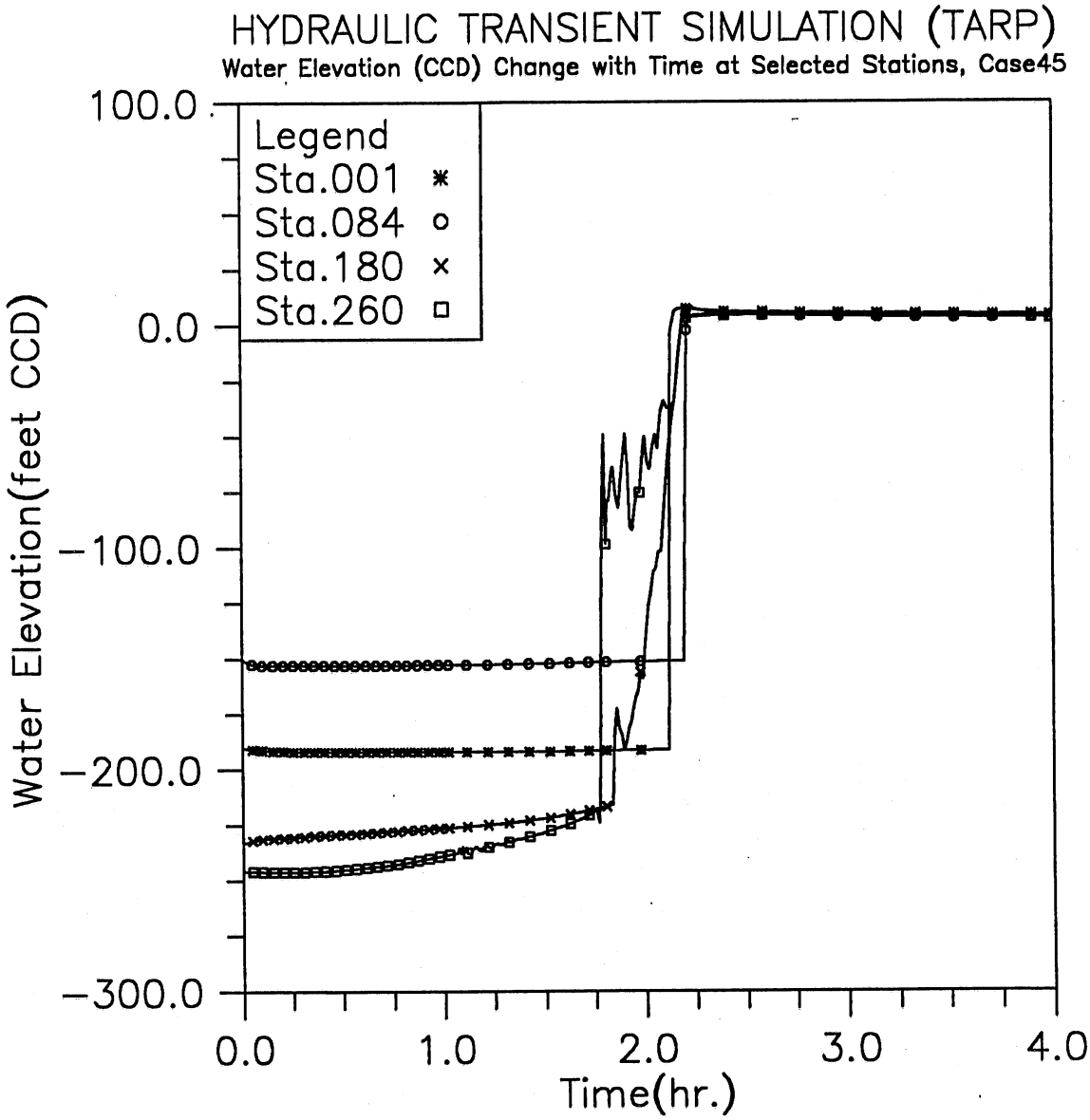

Fig. 3.17(c) Time variation of water elevation at four upstream locations; Modeling case: gate opening in 30 min., initial reservoir level at –198, inflow control Plan 1, and MAX storm event (Case 4–5)

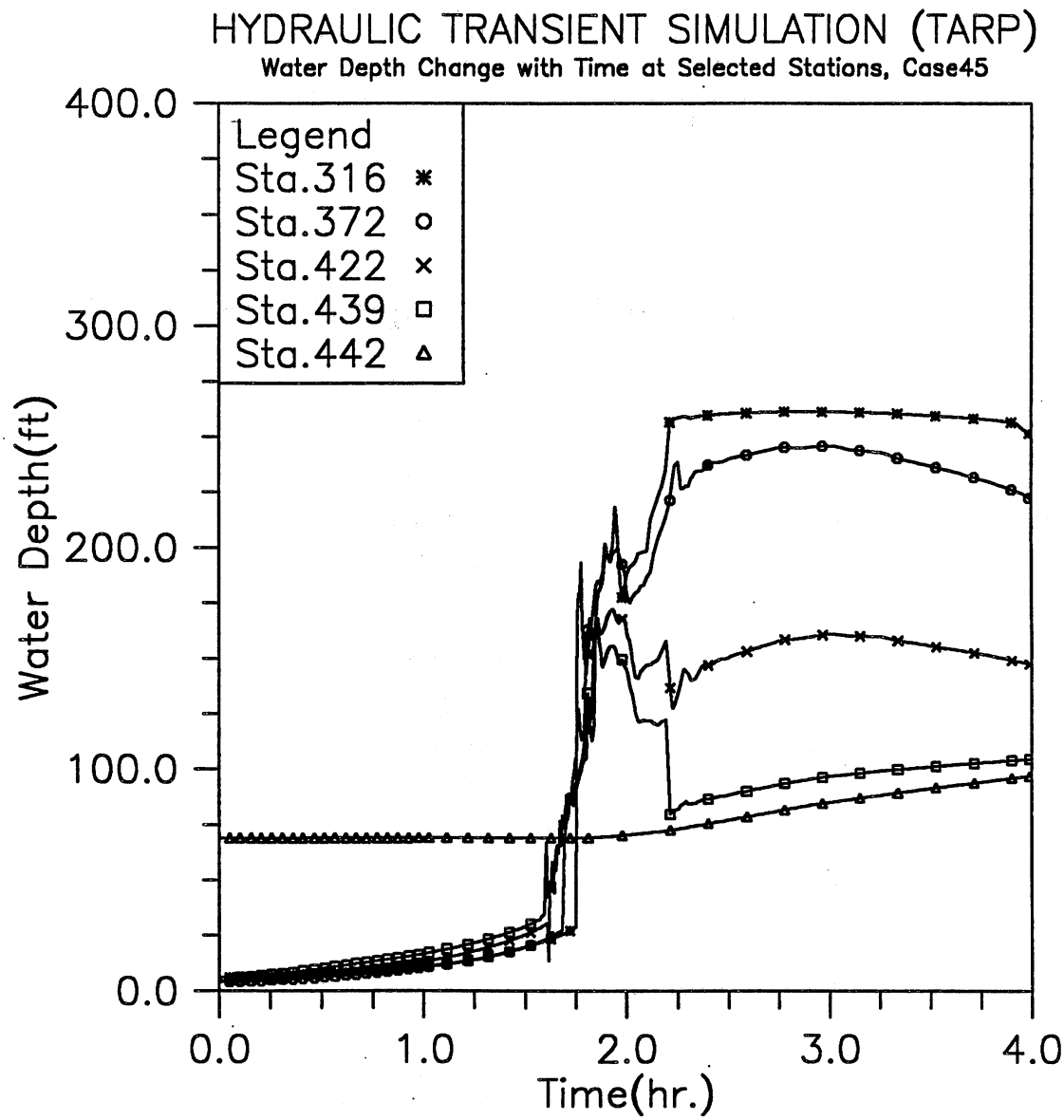

Fig. 3.17(d) Time variation of water depth at five downstream locations; Modeling case: gate opening in 30 min., initial reservoir level at –198, inflow control Plan 1, and MAX storm event (Case 4–5)

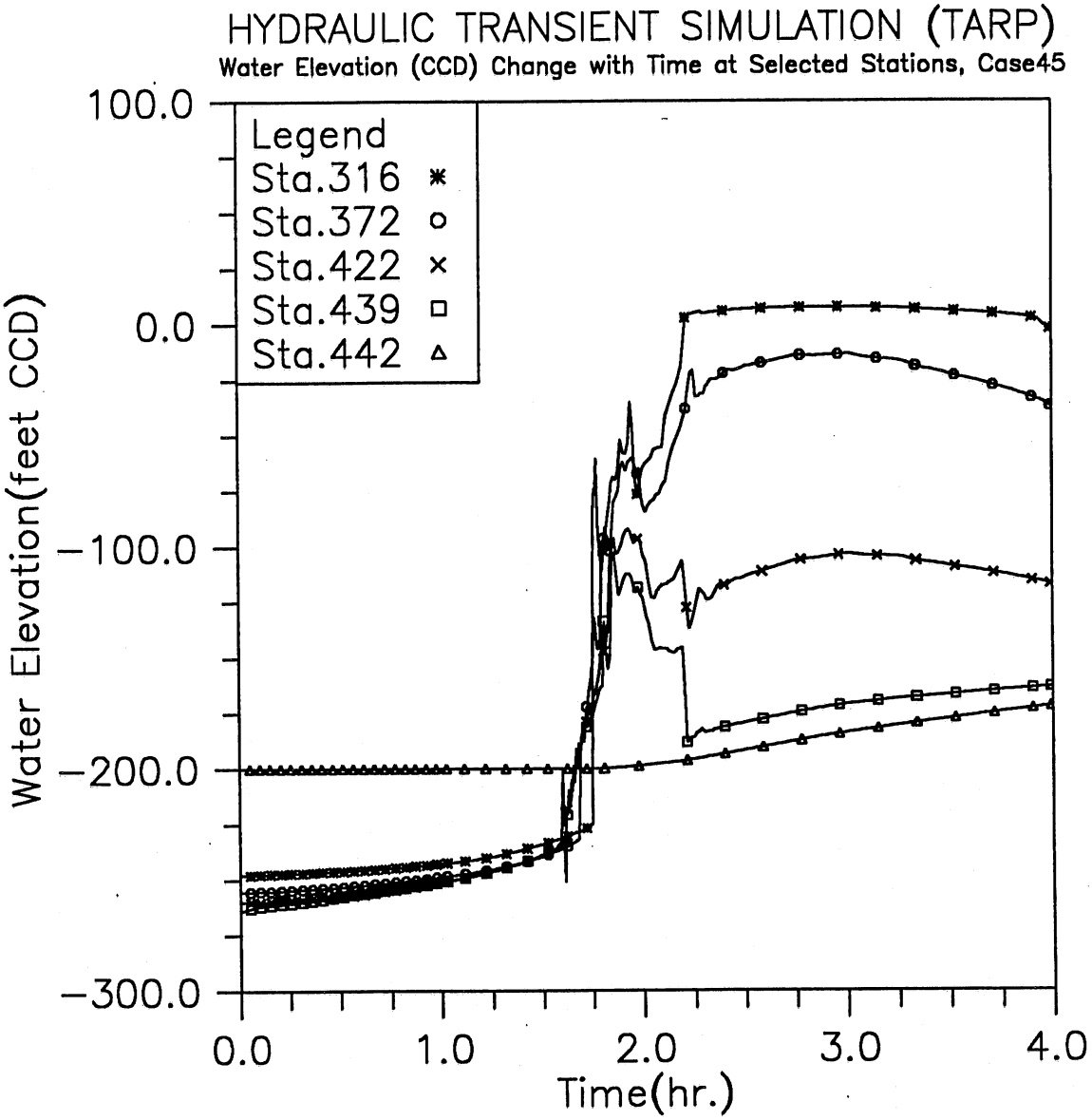

Fig. 3.17(e) Time variation of water elevation at five downstream locations; Modeling case: gate opening in 30 min., initial reservoir level at –198, inflow control Plan 1, and MAX storm event (Case 4–5)

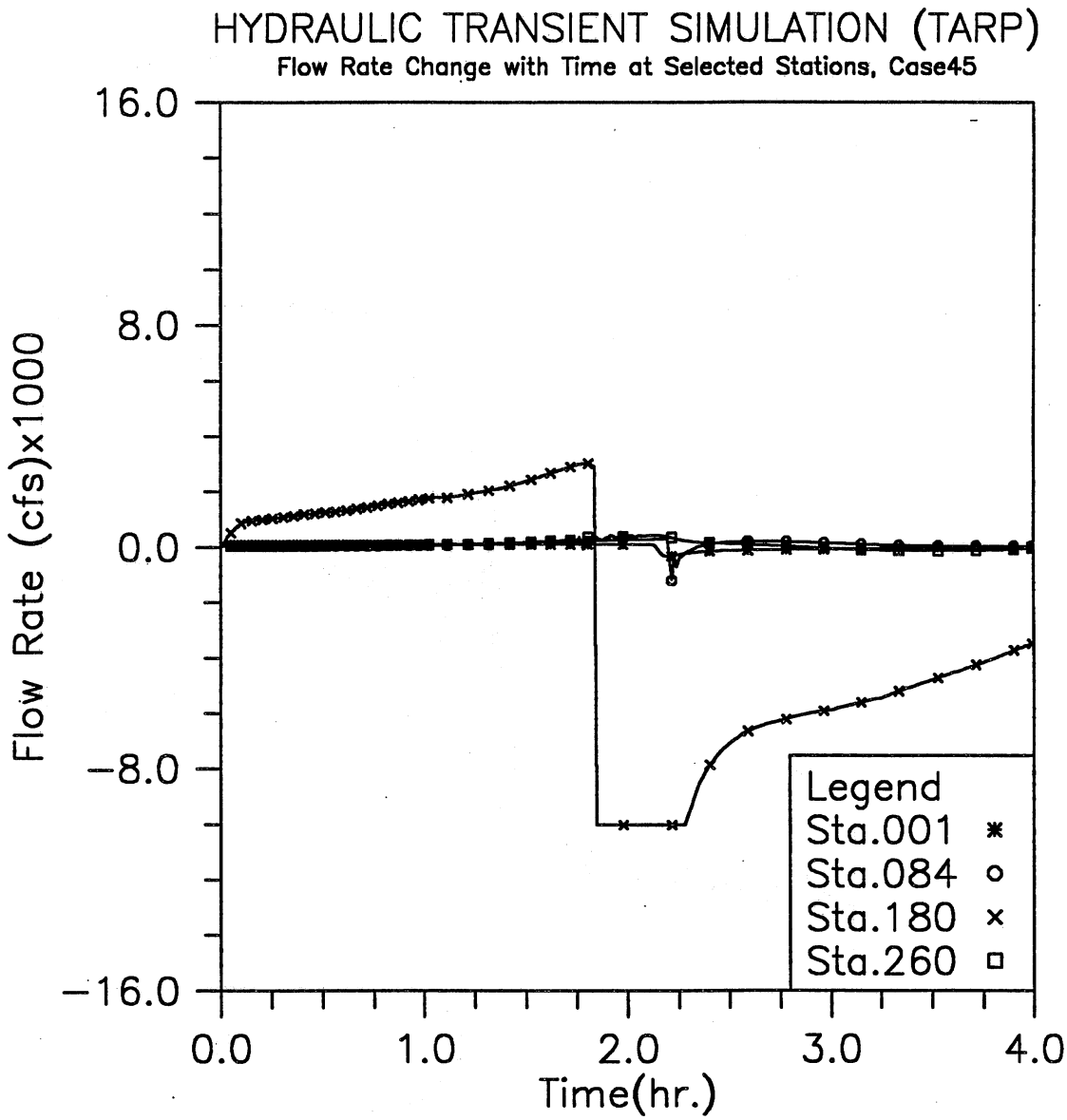

Fig. 3.17(f) Time variation of flow rate at four upstream locations; Modeling case: gate opening in 30 min., initial reservoir level at −198, inflow control Plan 1, and MAX storm event (Case 4–5)

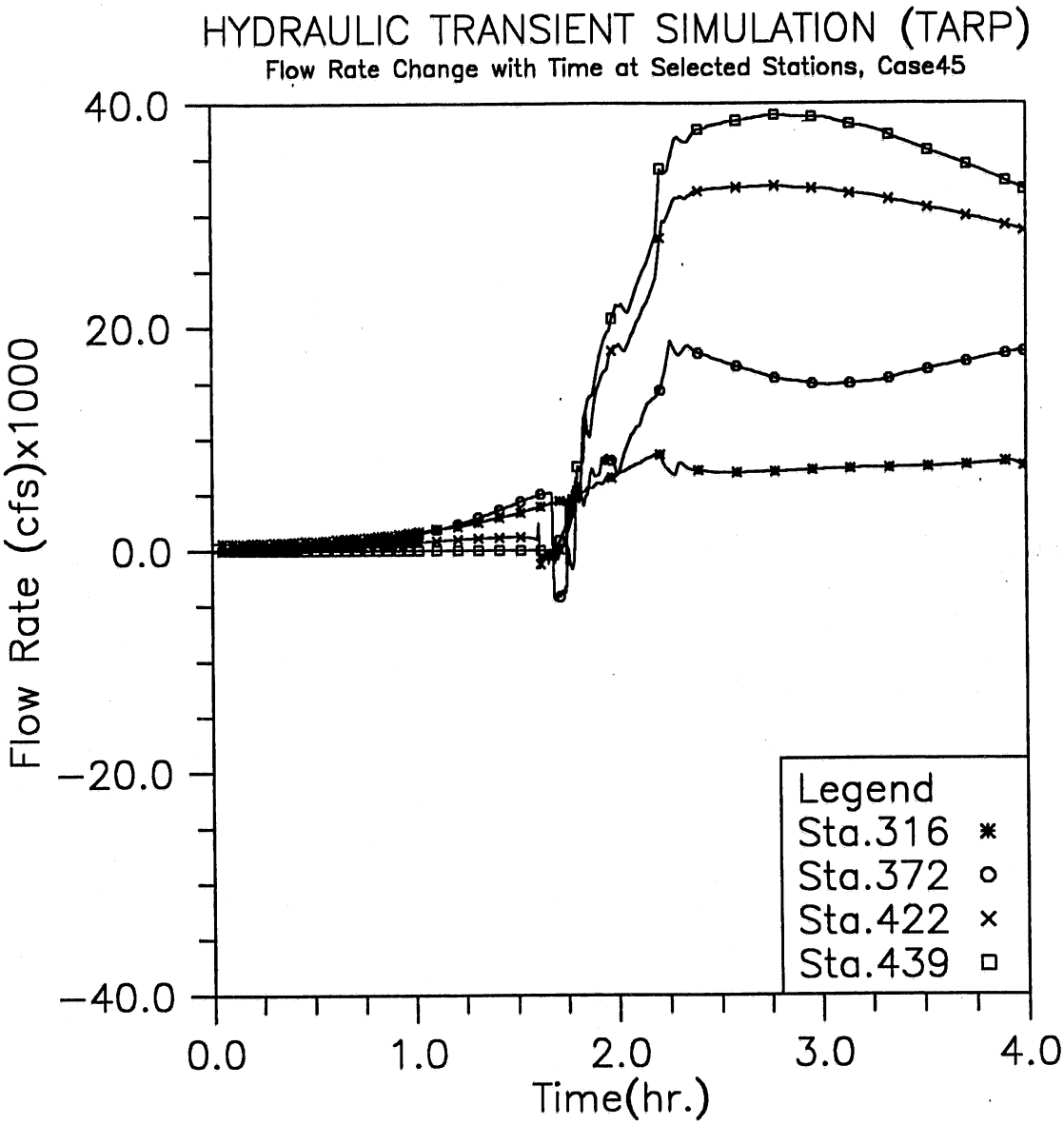

Fig. 3.17(g) Time variation of flow rate at four downstream locations; Modeling case: gate opening in 30 min., initial reservoir level at –198, inflow control Plan 1, and MAX storm event (Case 4–5)

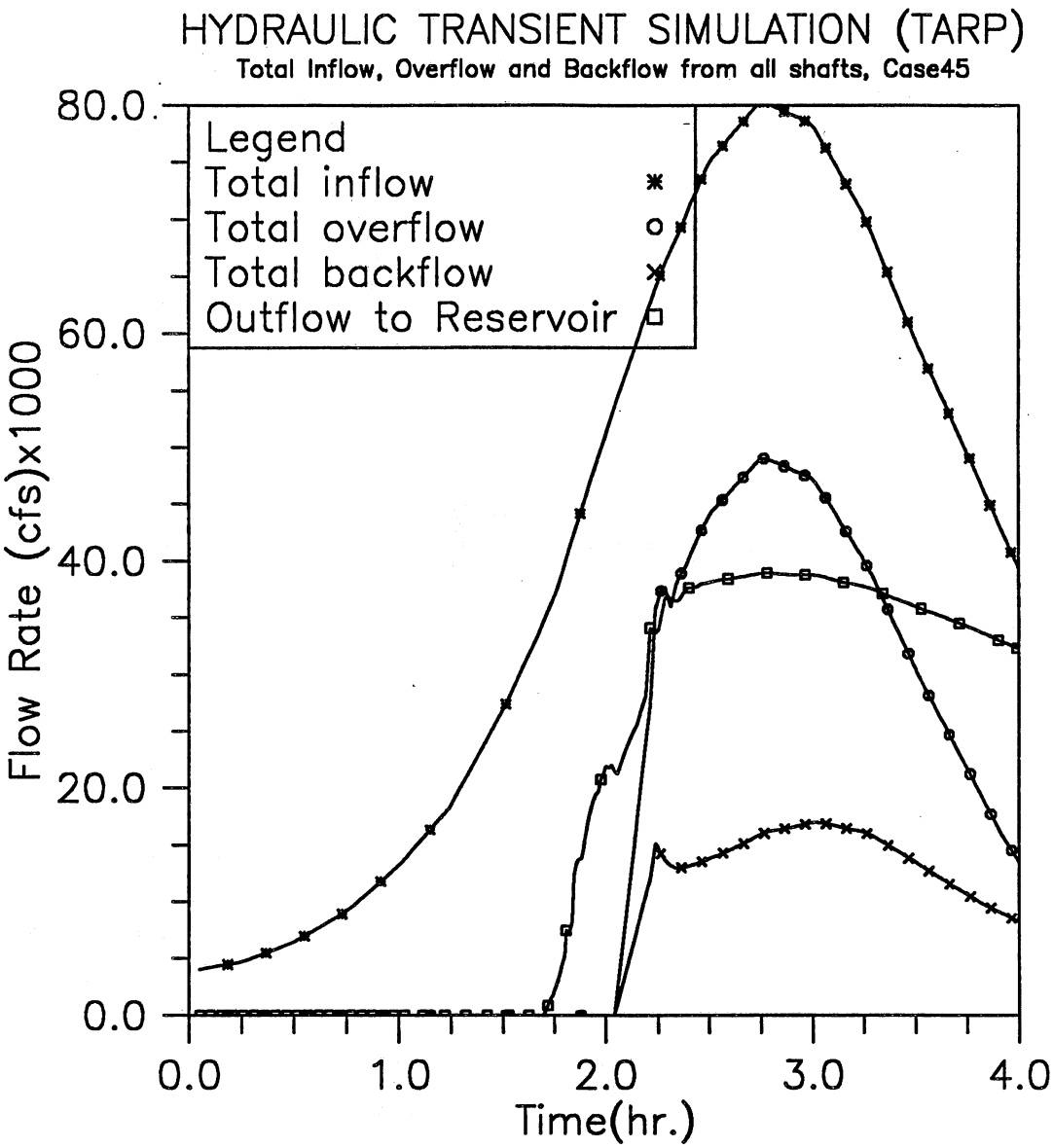

Fig. 3.17(h) Time variation of total inflow, overflow, backflow, and outflow to reservoir; Modeling case: gate opening in 30 min., initial reservoir level at –198, inflow control Plan 1, and MAX storm event (Case 4–5)

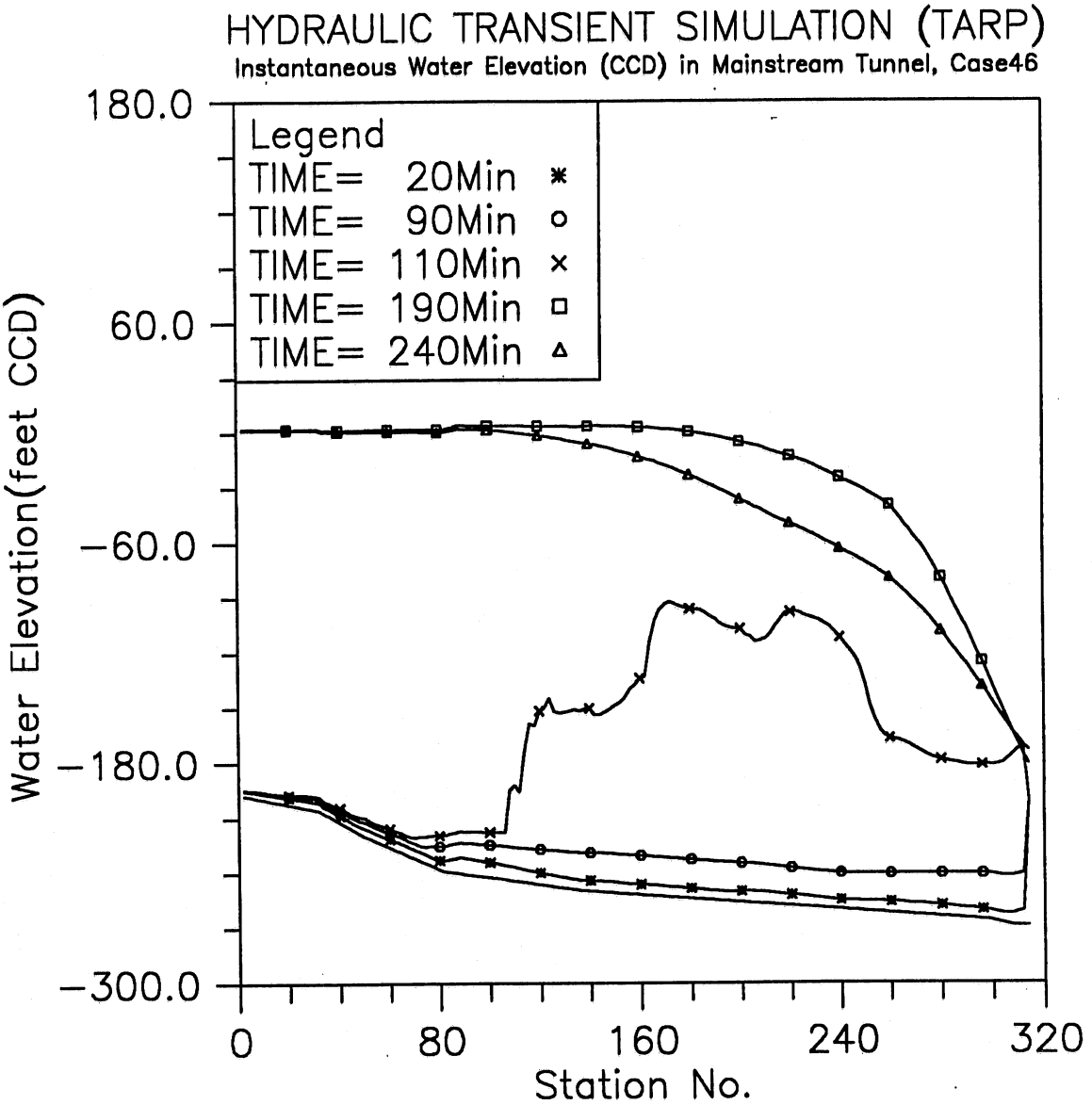

Fig. 3.18(a) Instantaneous hydraulic gradelines along the main tunnel; Modeling case: gate opening in 30 min., initial reservoir level at –198, inflow control Plan 2, and MAX storm event (Case 4–6)

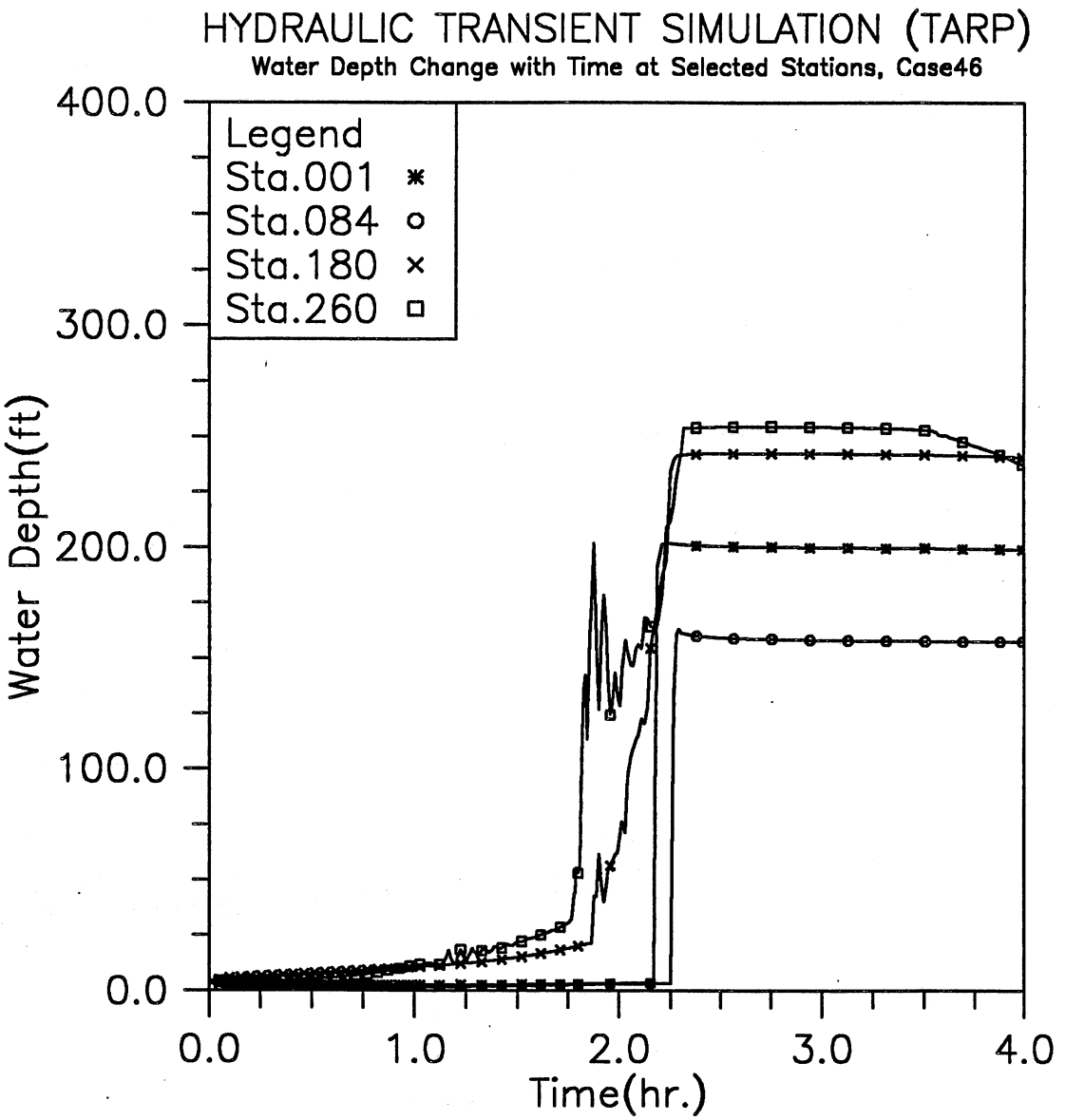

Fig. 3.18(b) Time variation of water depth at four upstream locations; Modeling case: gate opening in 30 min., initial reservoir level at –198, inflow control Plan 2, and MAX storm event (Case 4–6)

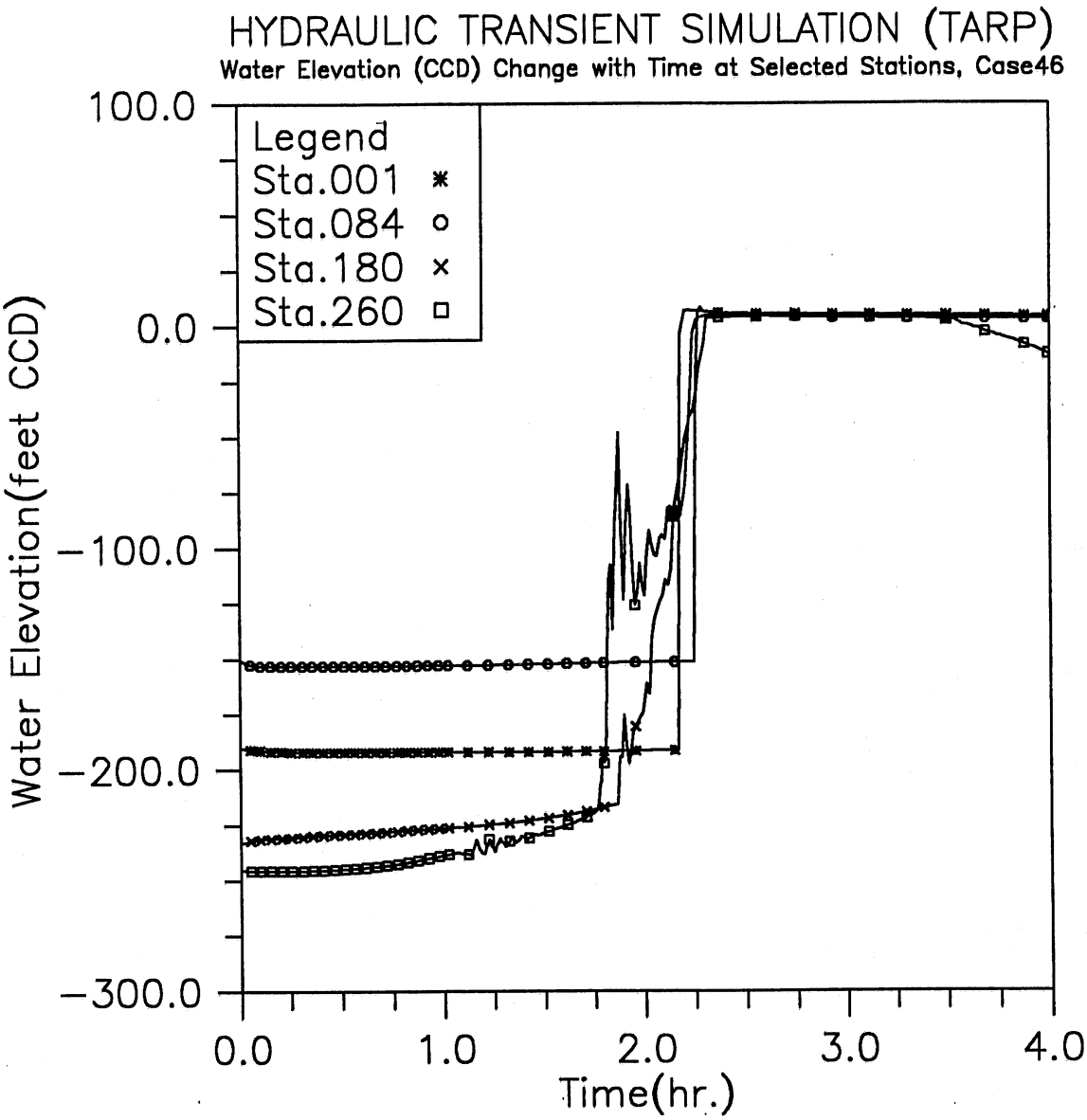

Fig. 3.18(c) Time variation of water elevation at four upstream locations; Modeling case: gate opening in 30 min., initial reservoir level at –198, inflow control Plan 2, and MAX storm event (Case 4–6)

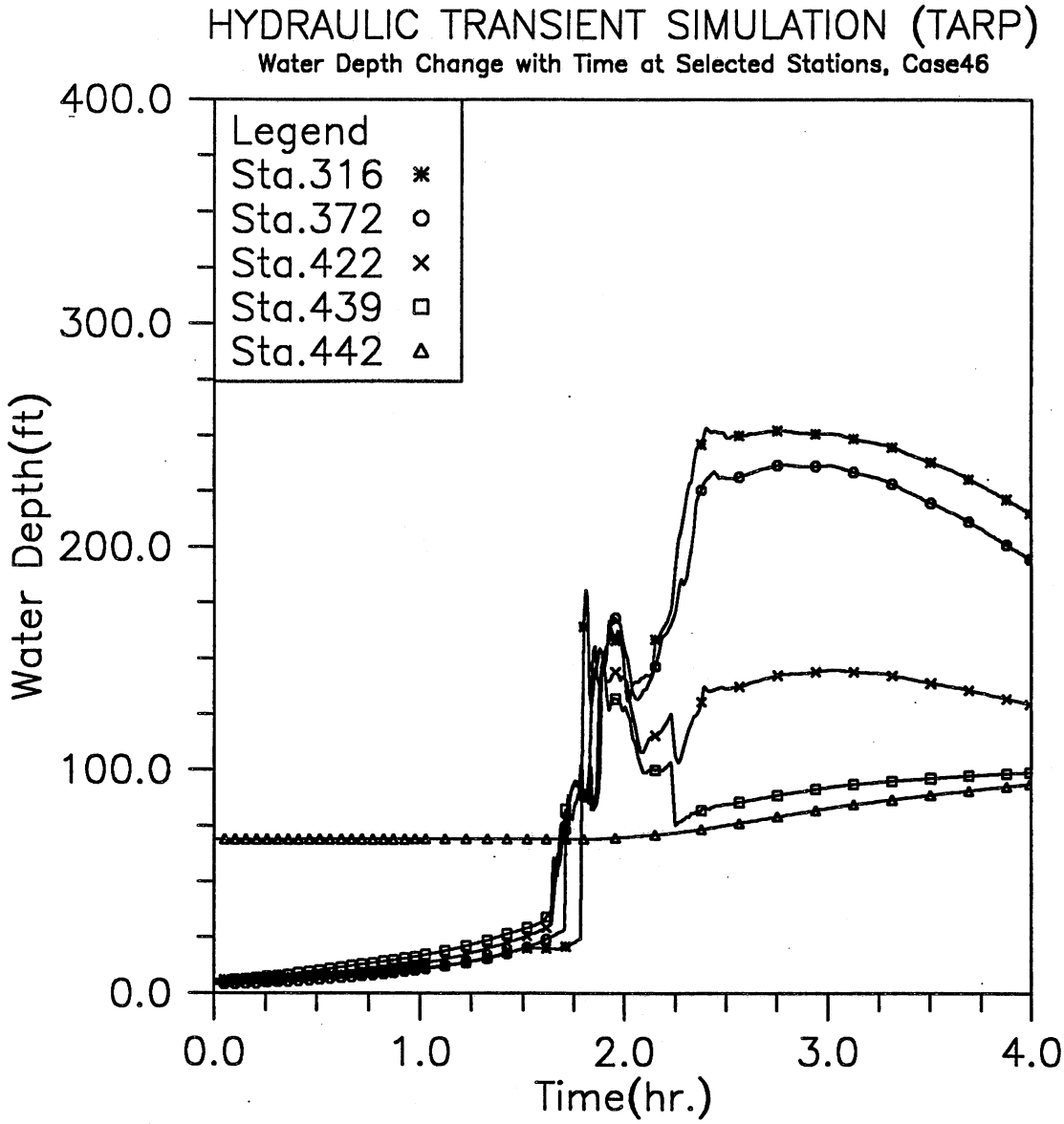

Fig. 3.18(d) Time variation of water depth at five downstream locations; Modeling case: gate opening in 30 min., initial reservoir level at –198, inflow control Plan 2, and MAX storm event (Case 4–6)

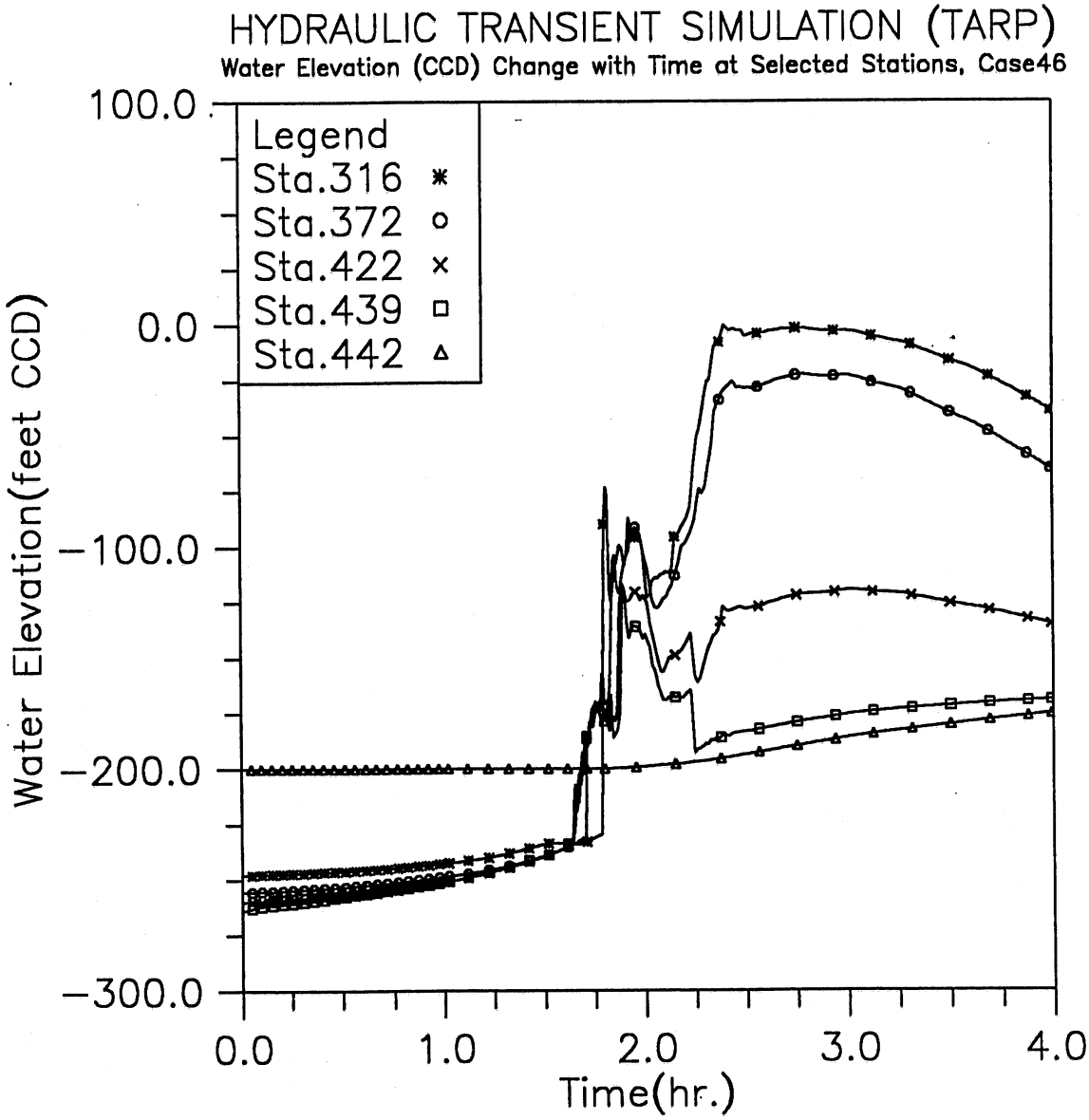

Fig. 3.18(e) Time variation of water elevation at five downstream locations; Modeling case: gate opening in 30 min., initial reservoir level at −198, inflow control Plan 2, and MAX storm event (Case 4–6)

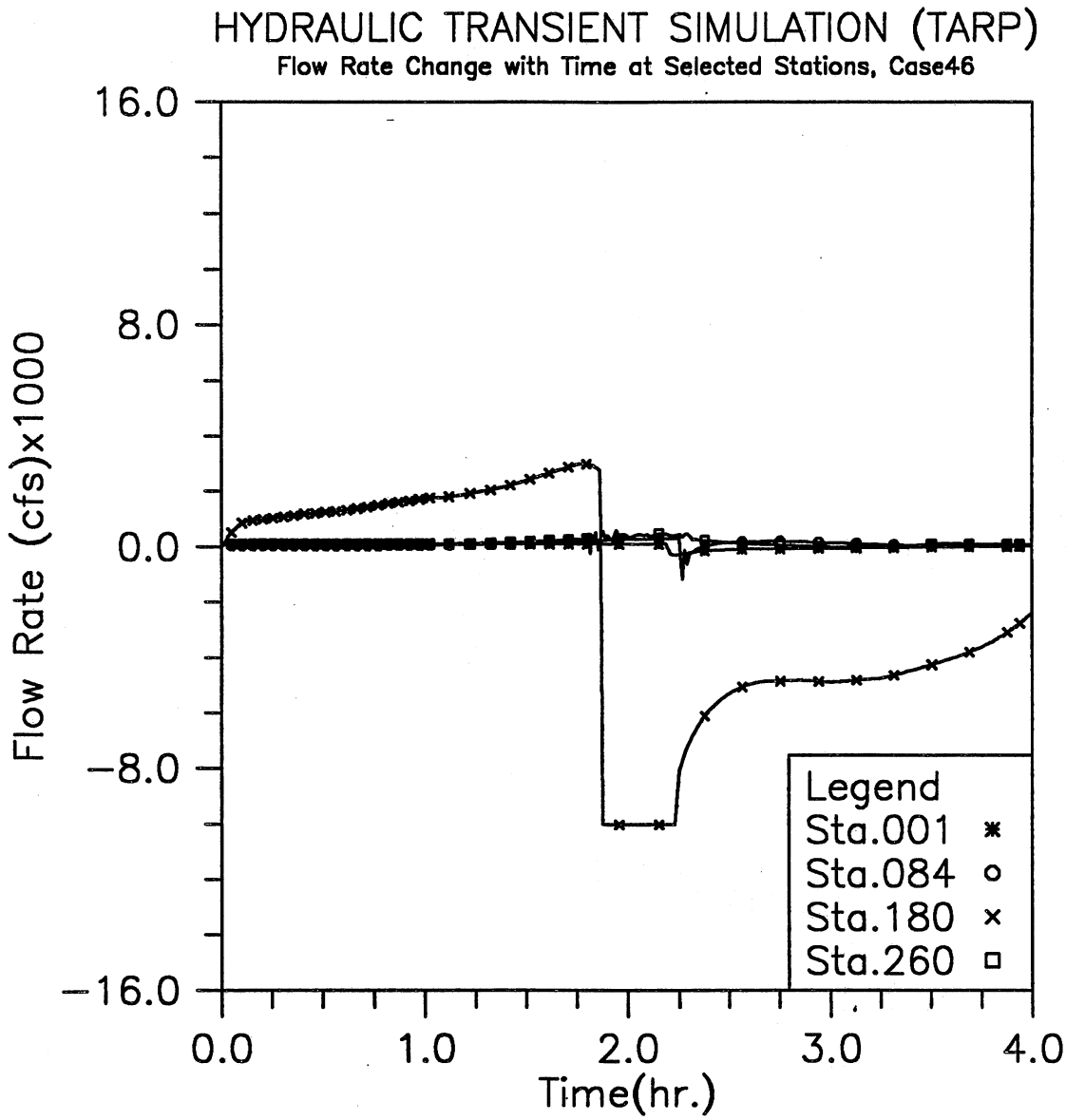

Fig. 3.18(f) Time variation of flow rate at four upstream locations; Modeling case: gate opening in 30 min., initial reservoir level at −198, inflow control Plan 2, and MAX storm event (Case 4–6)

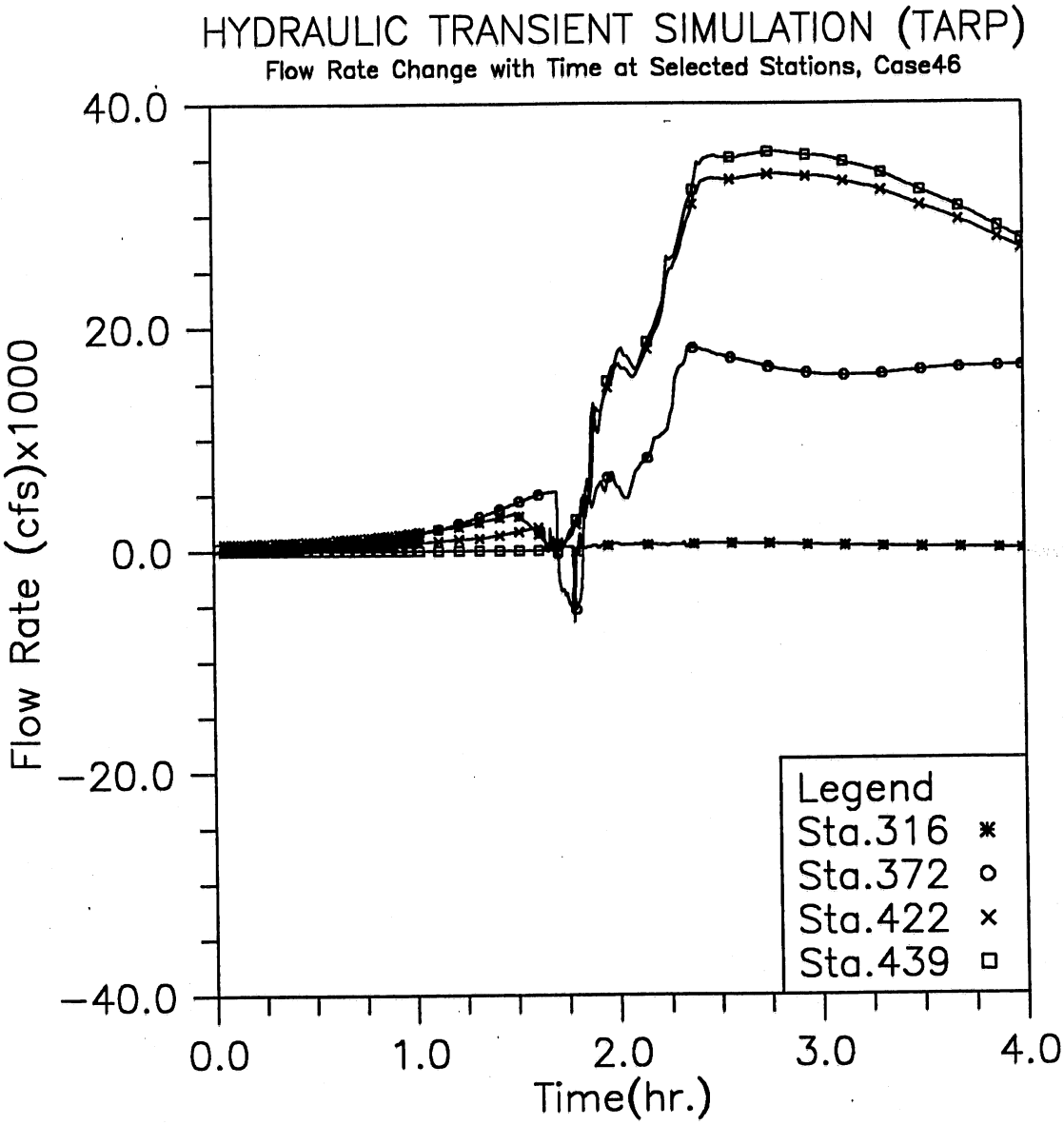

Fig. 3.18(g) Time variation of flow rate at four downstream locations; Modeling case: gate opening in 30 min., initial reservoir level at –198, inflow control Plan 2, and MAX storm event (Case 4–6)

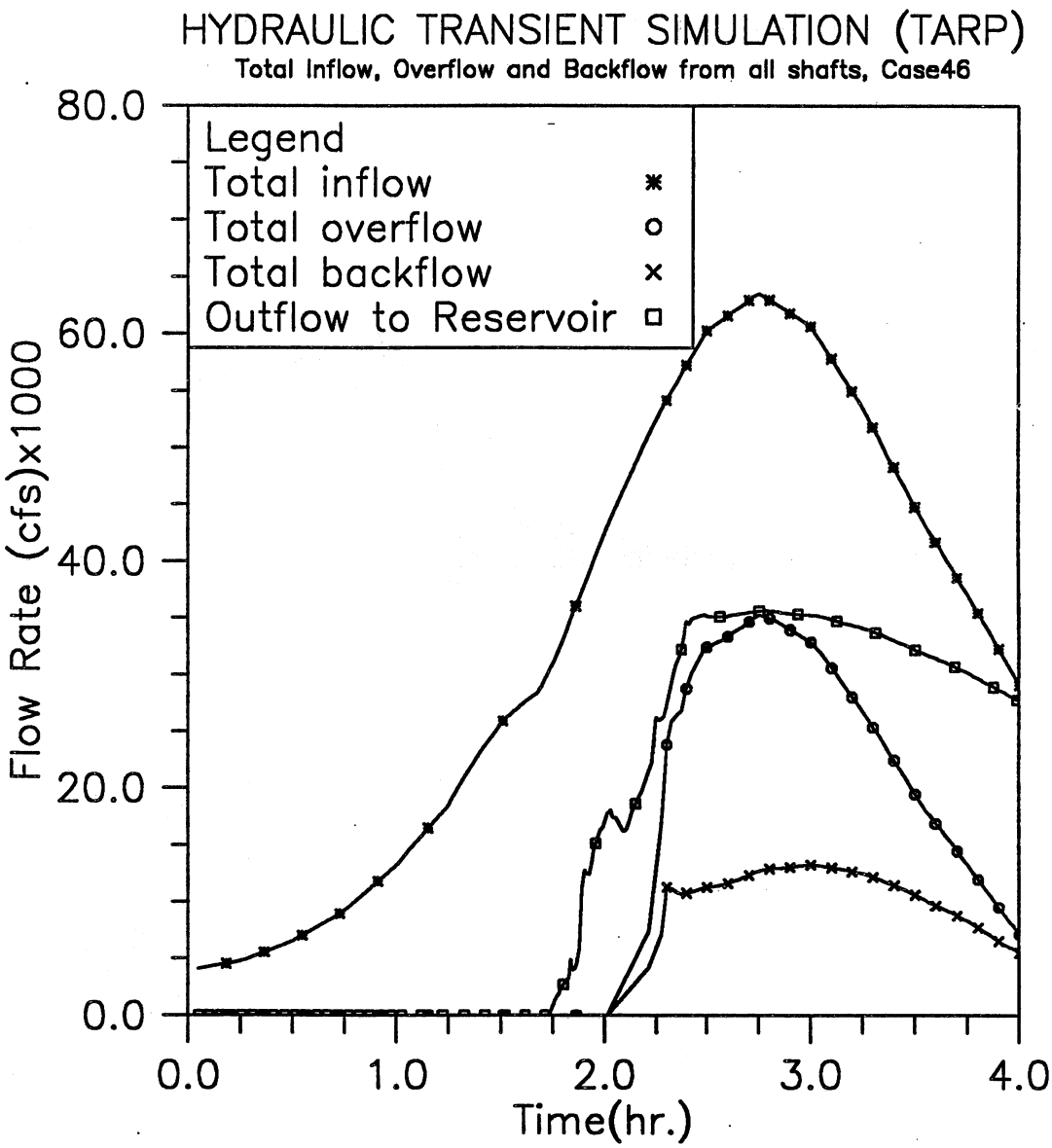

Fig. 3.18(h) Time variation of total inflow, overflow, backflow, and outflow to reservoir; Modeling case: gate opening in 30 min., initial reservoir level at –198, inflow control Plan 2, and MAX storm event (Case 4–6)

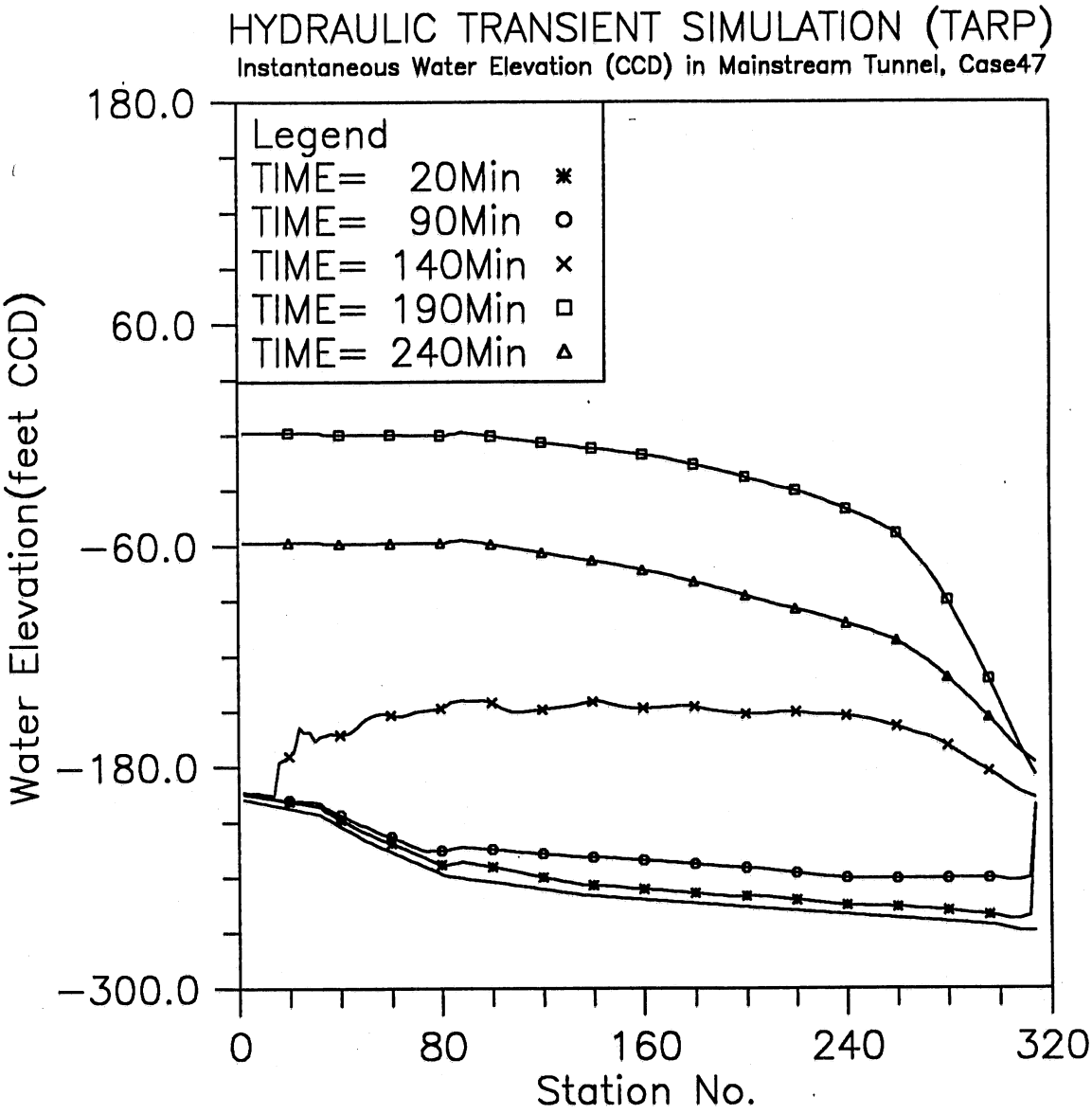

Fig. 3.19(a) Instantaneous hydraulic gradelines along the main tunnel; Modeling case: gate opening in 30 min., initial reservoir level at –198, inflow control Plan 3, and MAX storm event (Case 4–7)

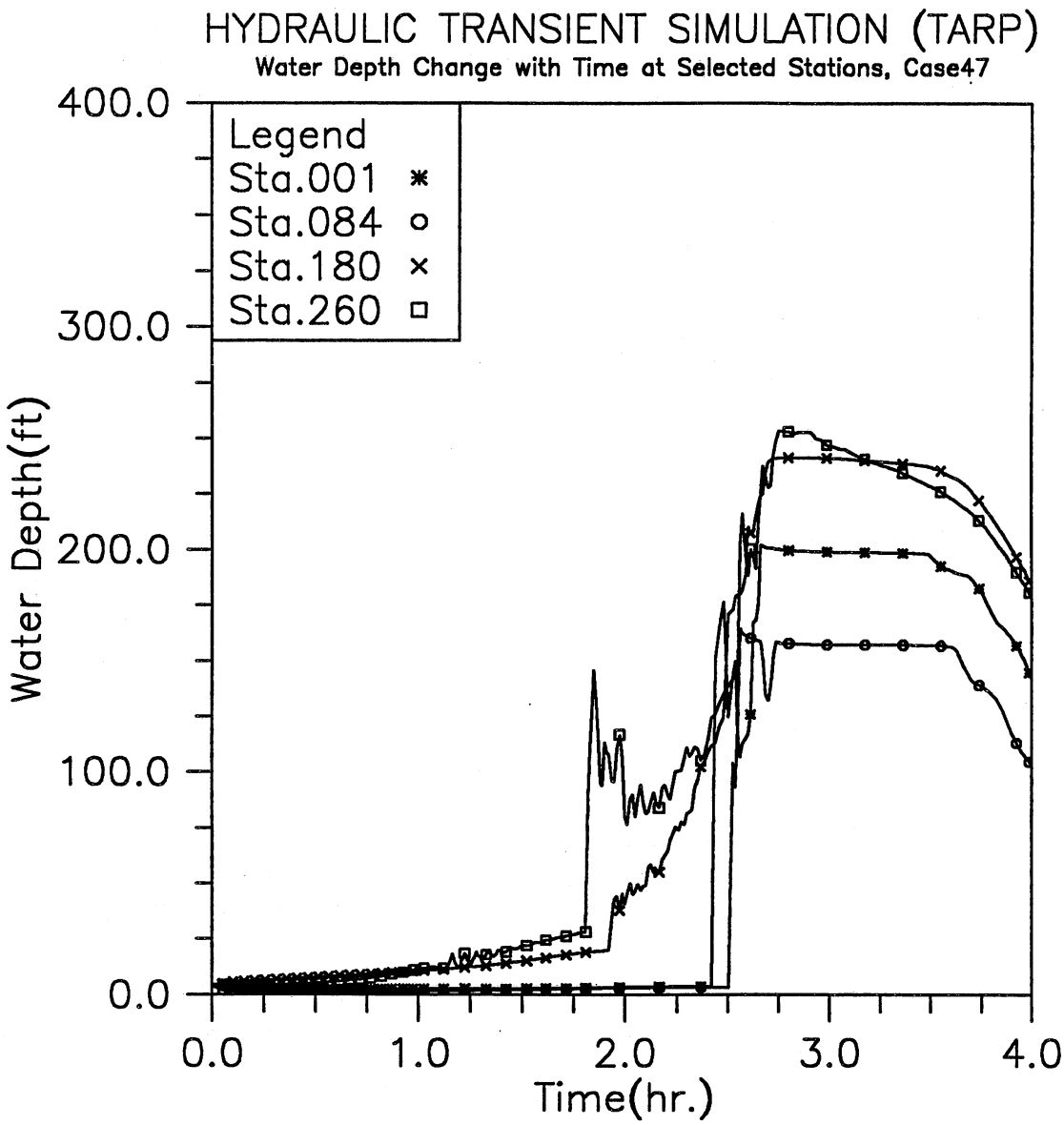

Fig. 3.19(b) Time variation of water depth at four upstream locations; Modeling case: gate opening in 30 min., initial reservoir level at –198, inflow control Plan 3, and MAX storm event (Case 4–7)

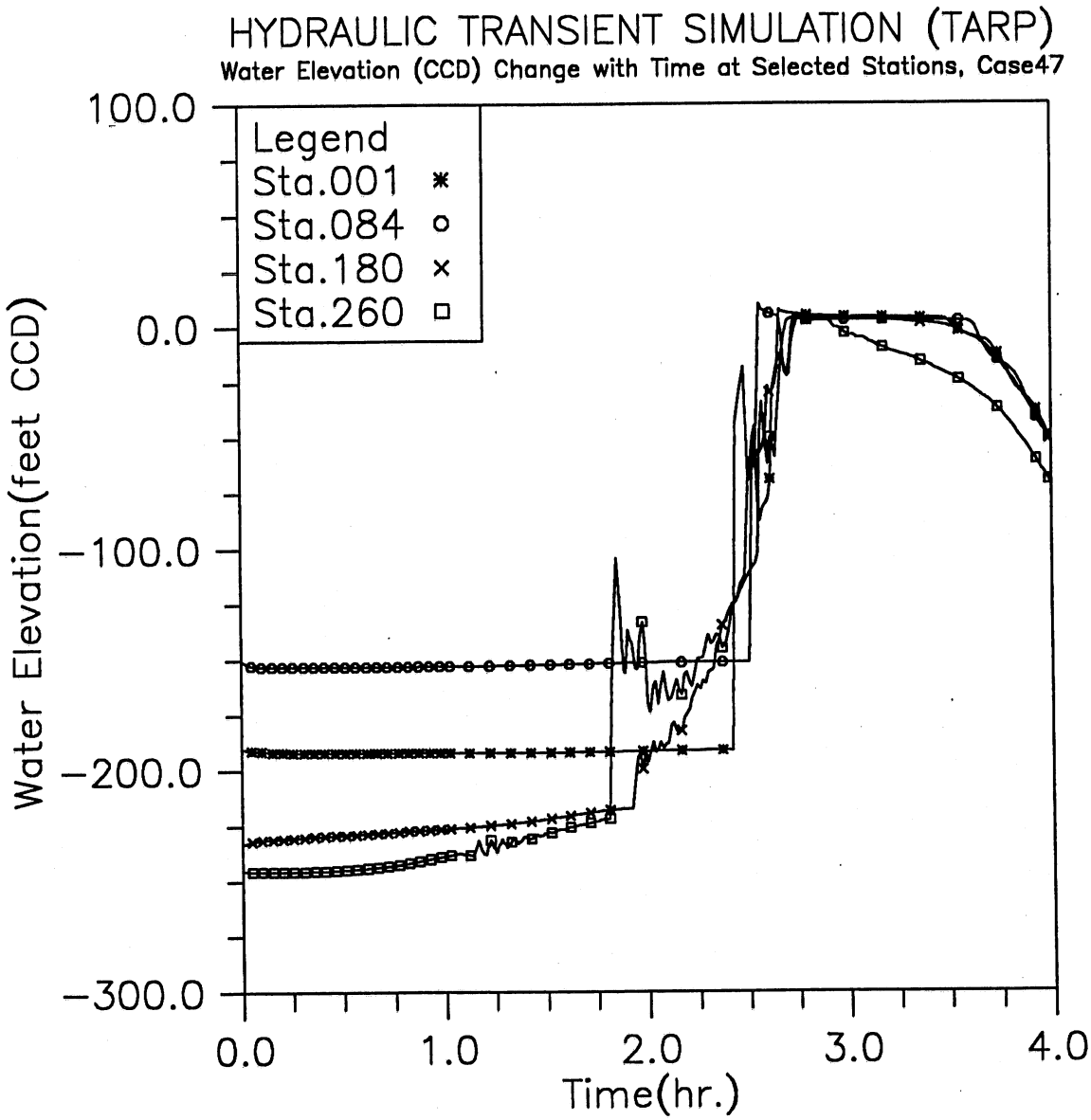

Fig. 3.19(c) Time variation of water elevation at four upstream locations; Modeling case: gate opening in 30 min., initial reservoir level at –198, inflow control Plan 3, and MAX storm event (Case 4–7)

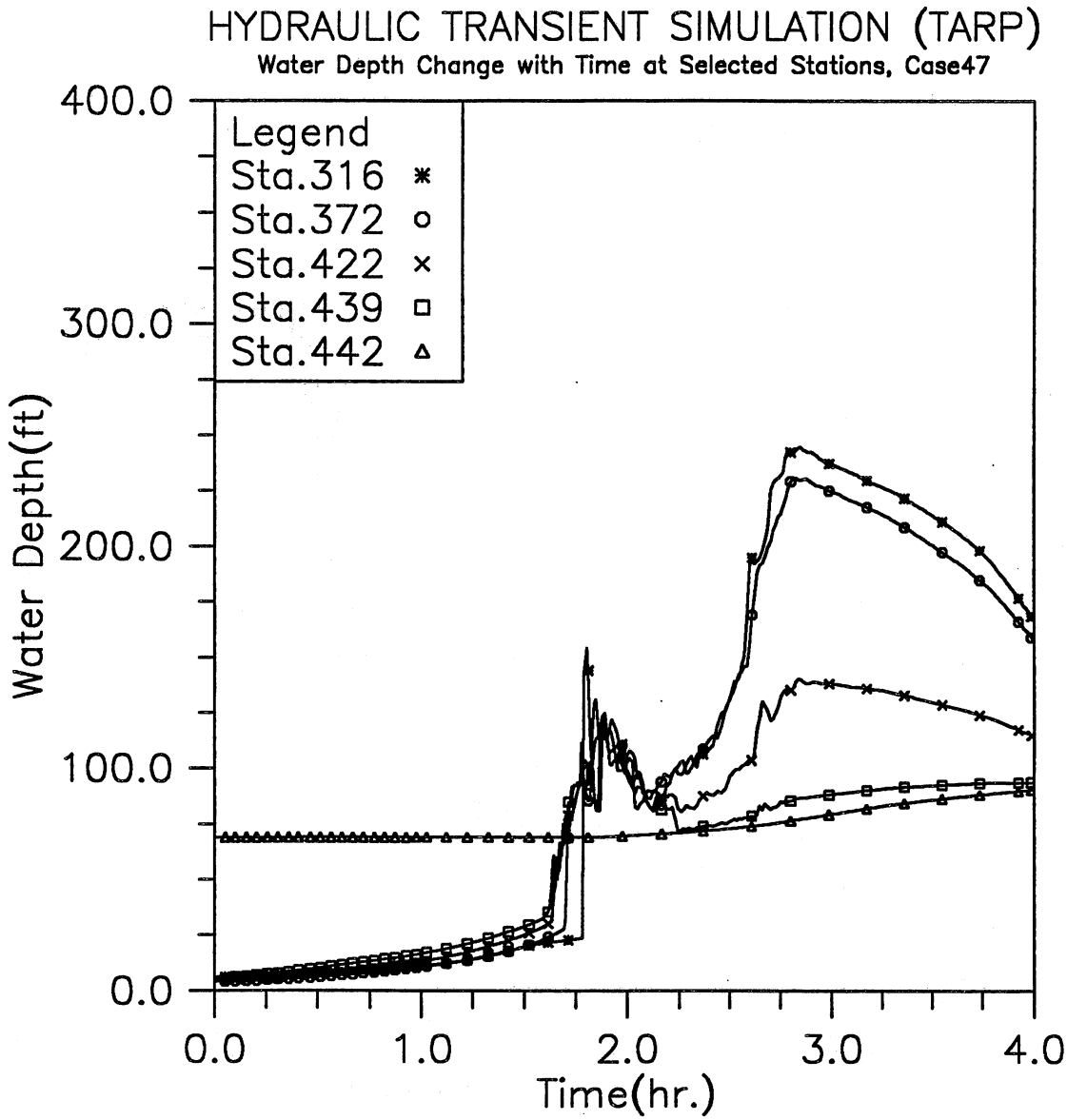

Fig. 3.19(d) Time variation of water depth at five downstream locations; Modeling case: gate opening in 30 min., initial reservoir level at –198, inflow control Plan 3, and MAX storm event (Case 4–7)

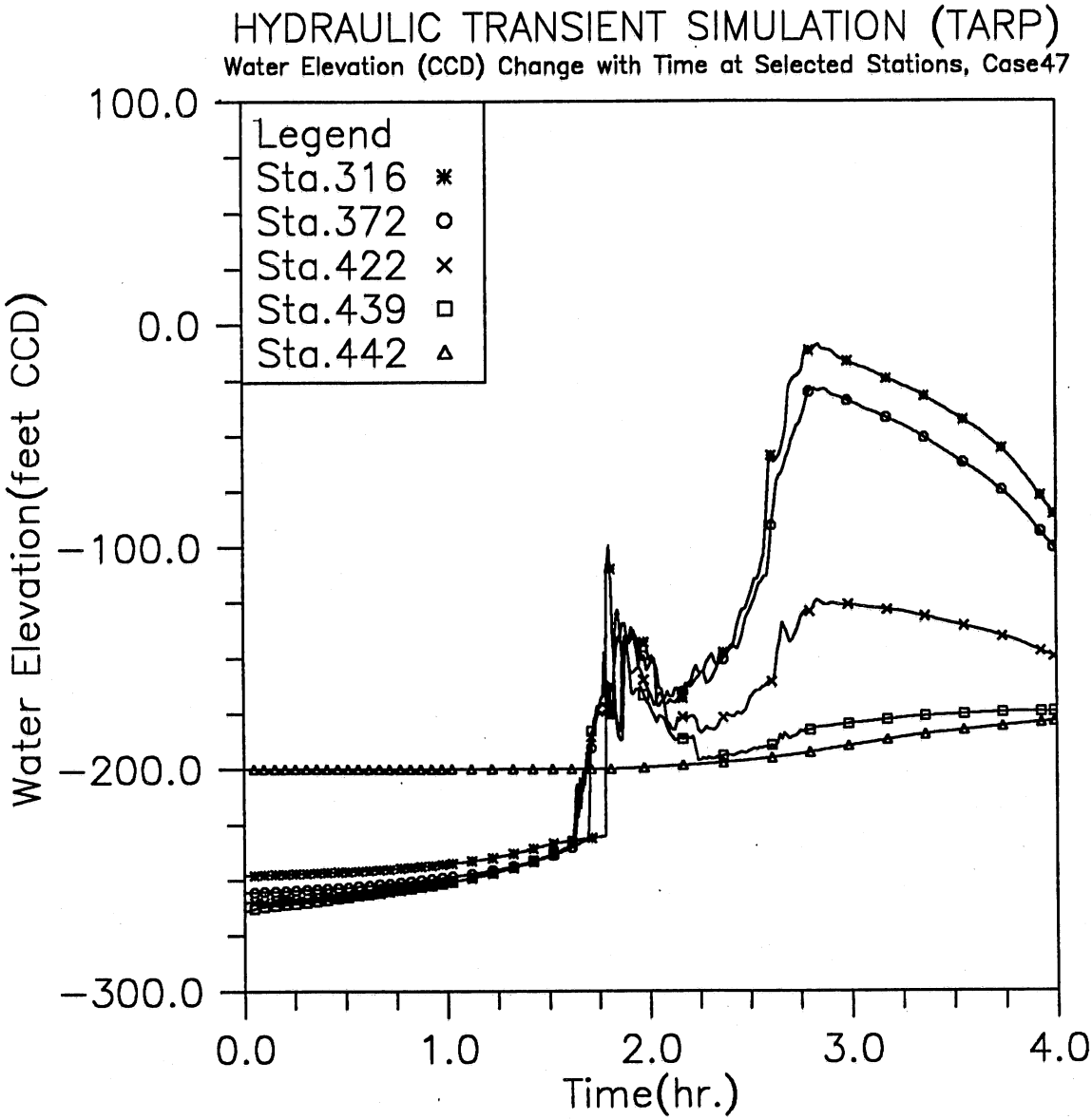

Fig. 3.19(e) Time variation of water elevation at five downstream locations; Modeling case: gate opening in 30 min., initial reservoir level at –198, inflow control Plan 3, and MAX storm event (Case 4–7)

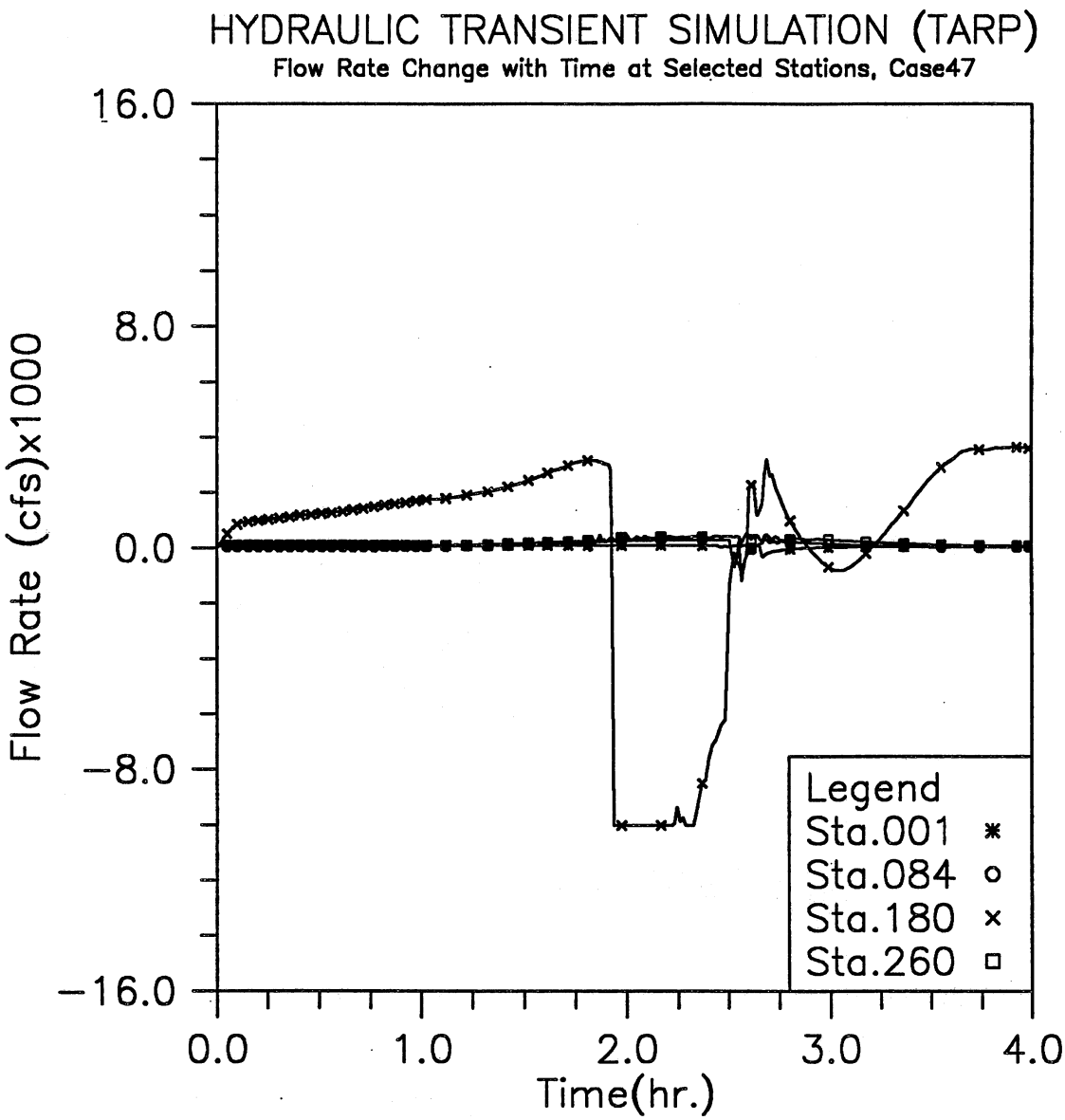

Fig. 3.19(f) Time variation of flow rate at four upstream locations; Modeling case: gate opening in 30 min., initial reservoir level at −198, inflow control Plan 3, and MAX storm event (Case 4–7)

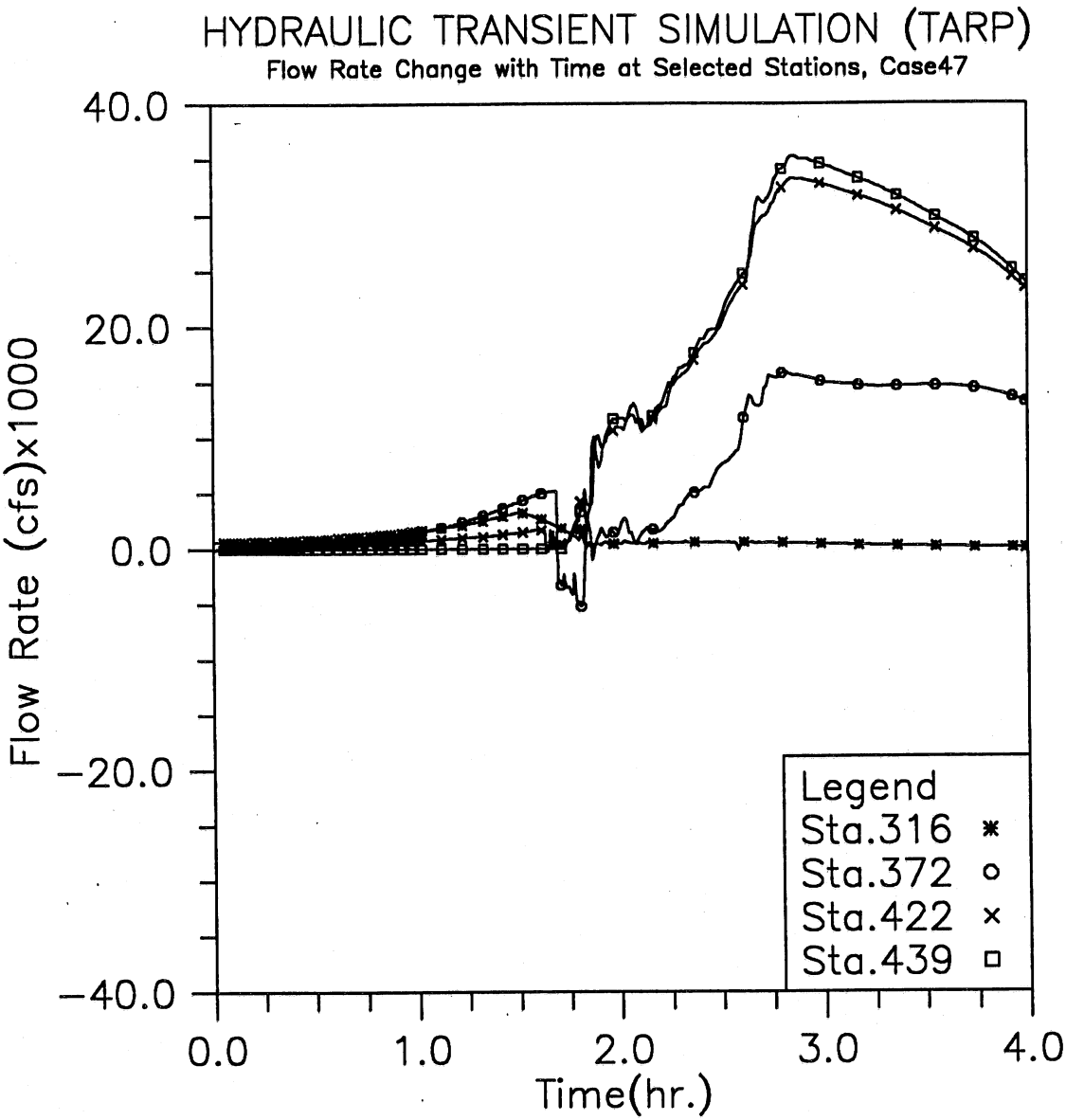

Fig. 3.19(g) Time variation of flow rate at four downstream locations; Modeling case: gate opening in 30 min., initial reservoir level at –198, inflow control Plan 3, and MAX storm event (Case 4–7)

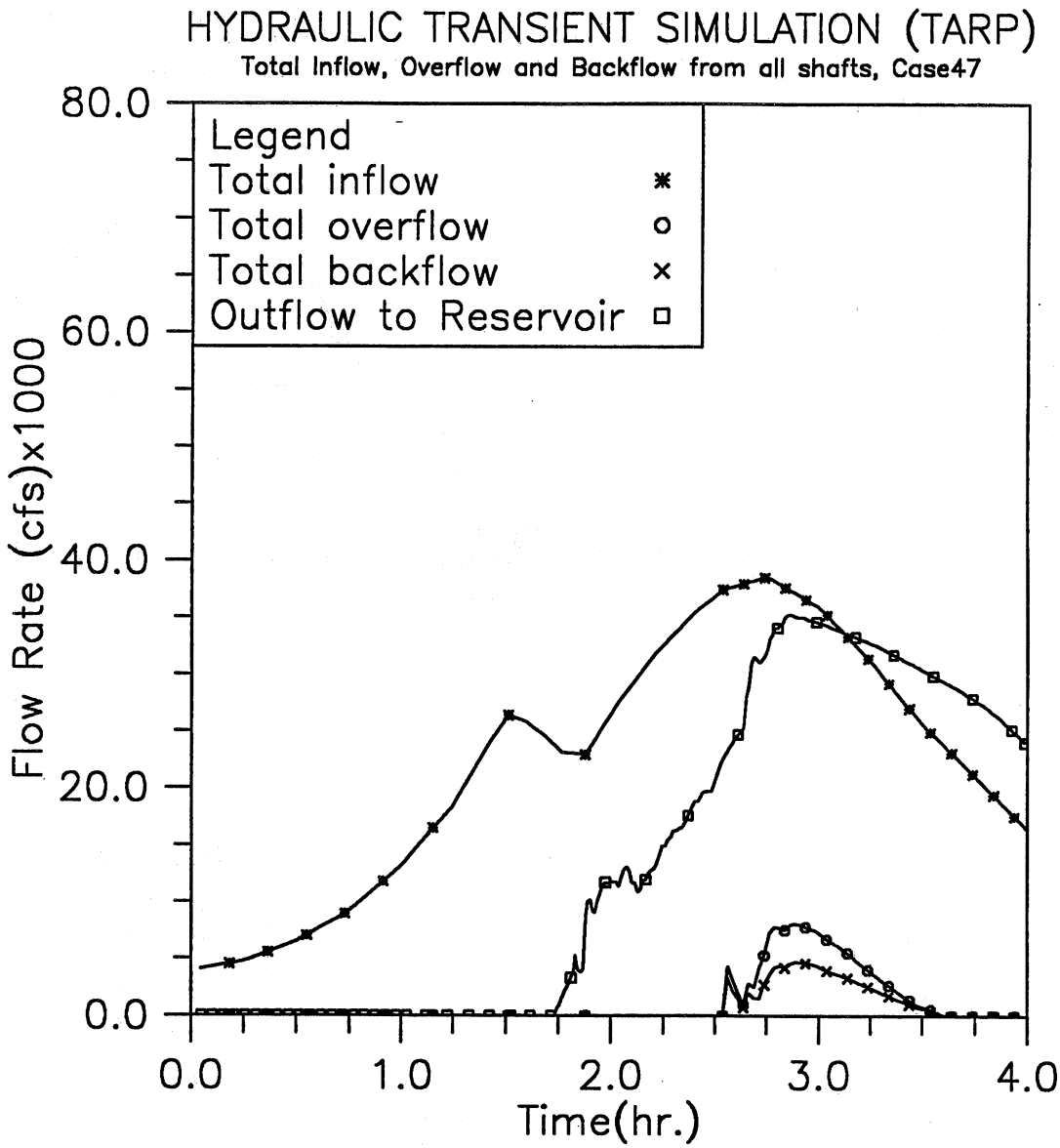

Fig. 3.19(h) Time variation of total inflow, overflow, backflow, and outflow to reservoir; Modeling case: gate opening in 30 min., initial reservoir level at –198, inflow control Plan 3, and MAX storm event (Case 4–7)

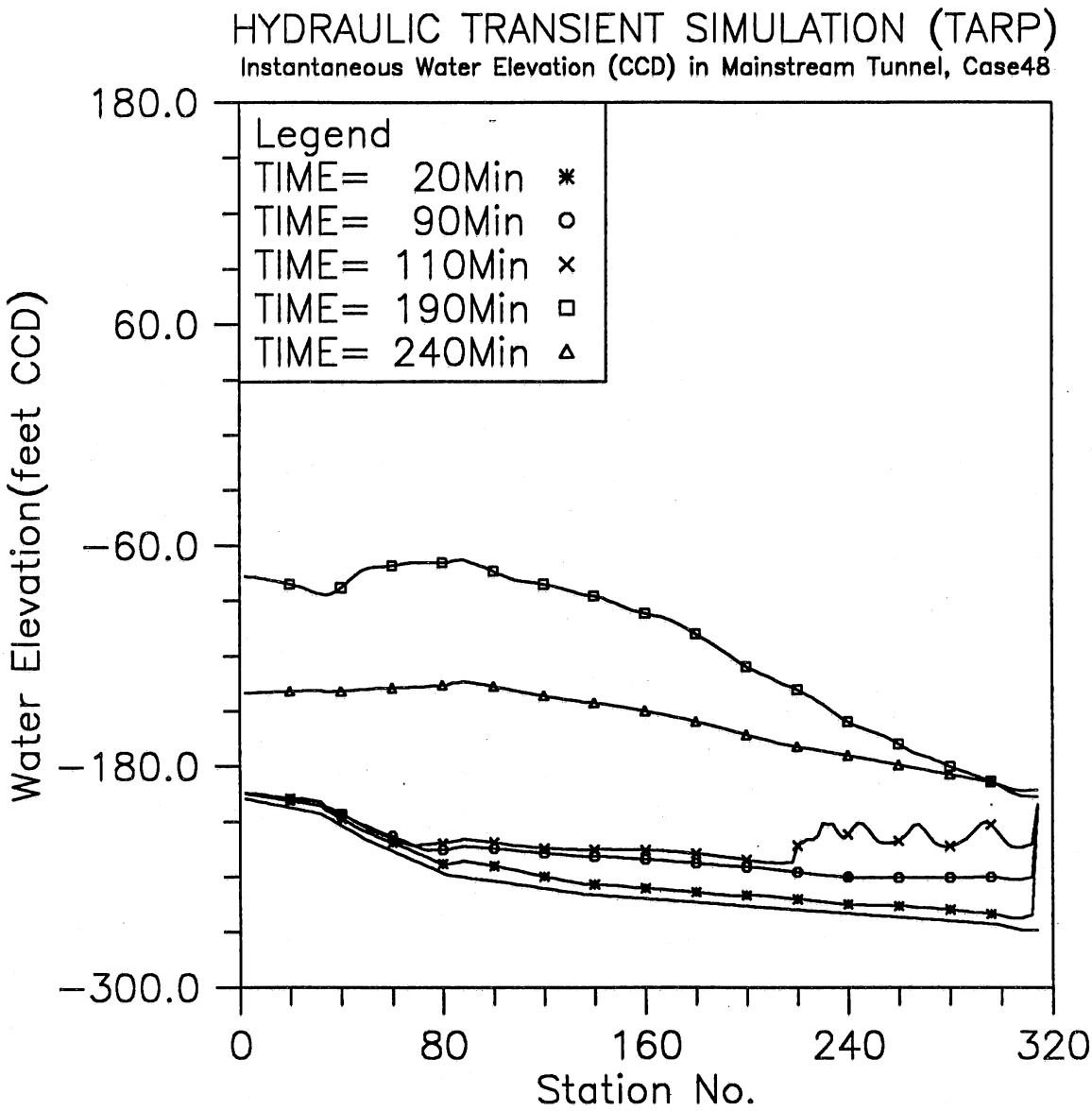

Fig. 3.20(a) Instantaneous hydraulic gradelines along the main tunnel; Modeling case: gate opening in 30 min., initial reservoir level at –198, inflow control Plan 4, and MAX storm event (Case 4–8)

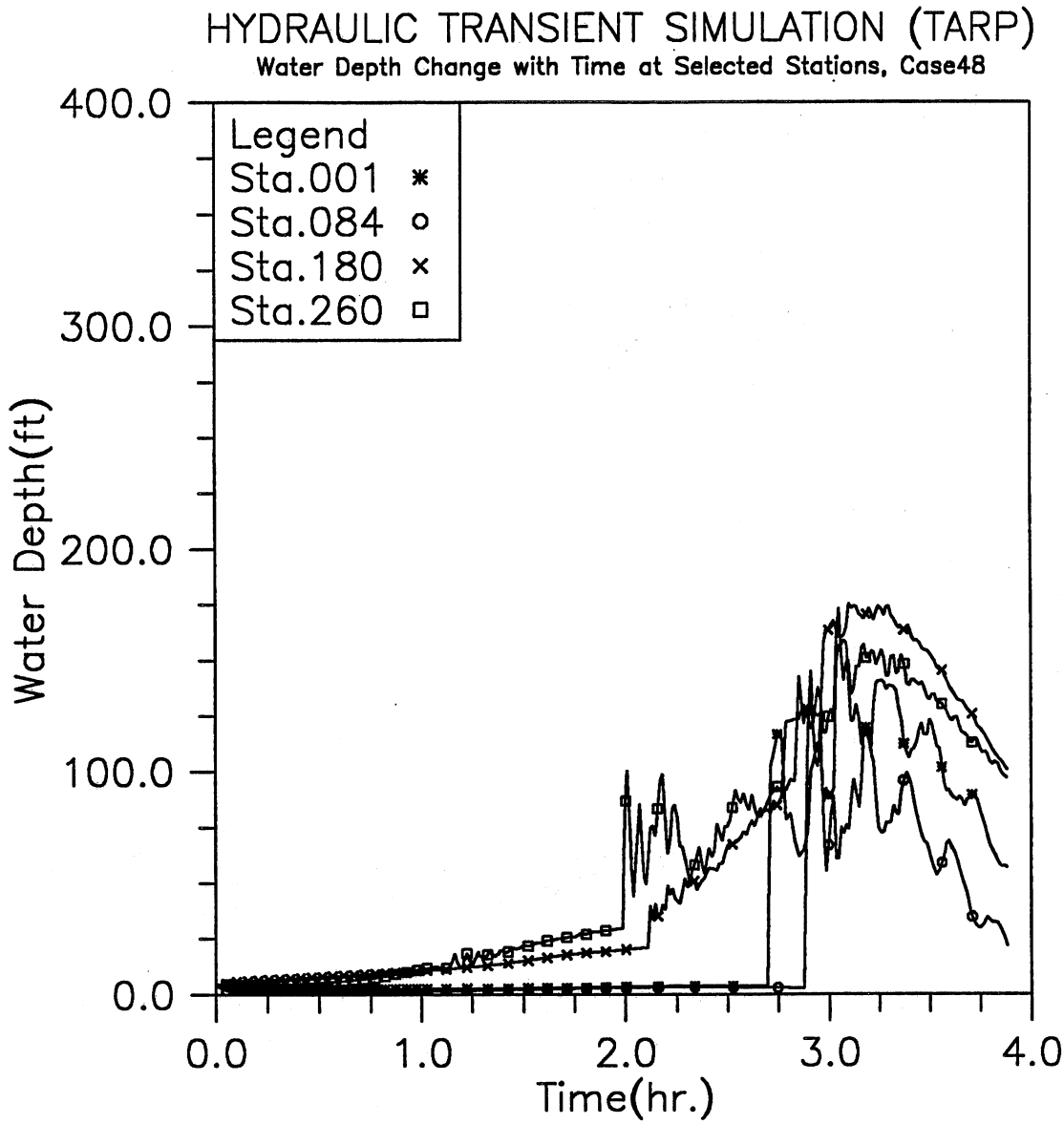

Fig. 3.20(b) Time variation of water depth at four upstream locations; Modeling case: gate opening in 30 min., initial reservoir level at –198, inflow control Plan 4, and MAX storm event (Case 4–8)

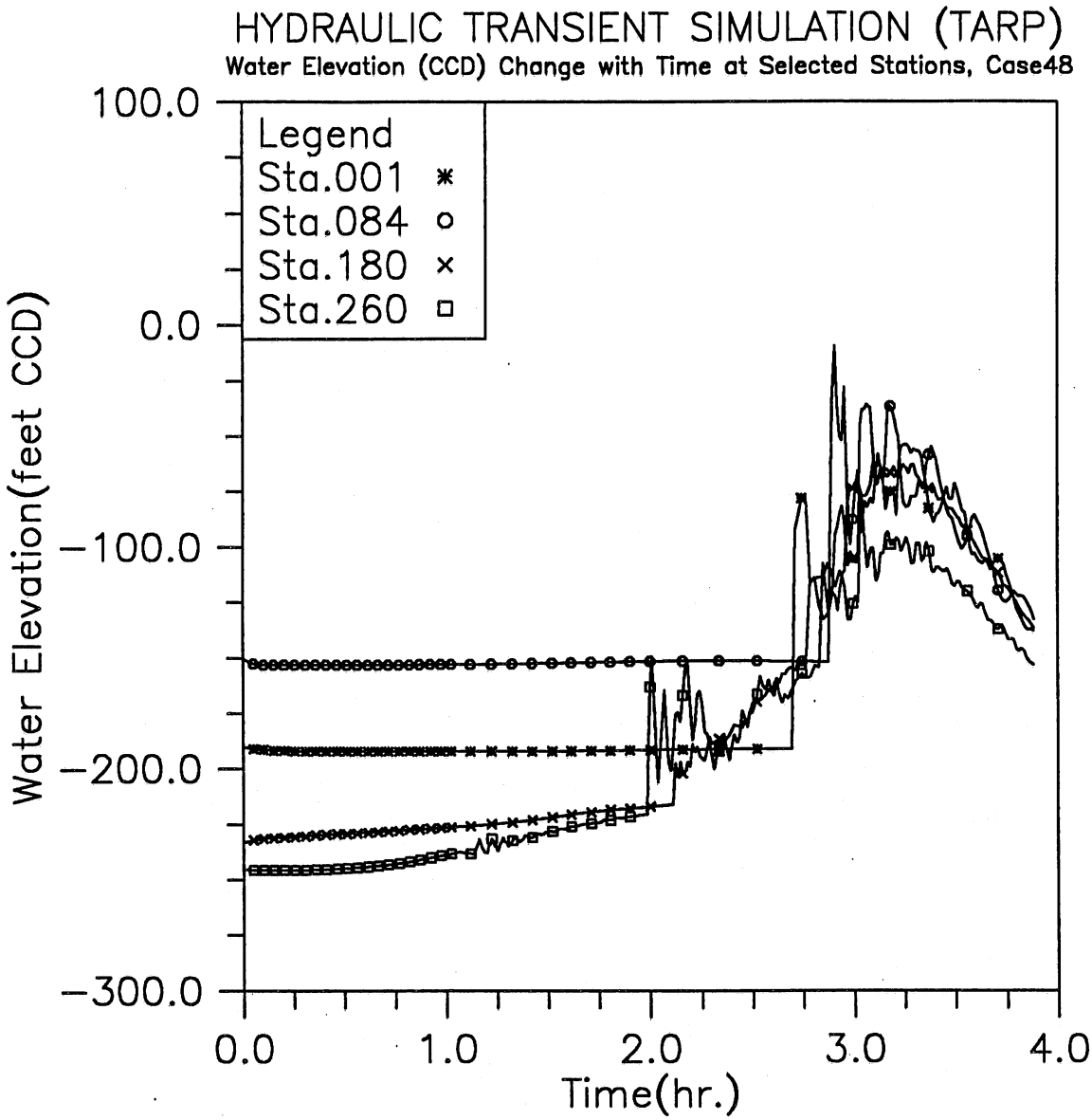

Fig. 3.20(c) Time variation of water elevation at four upstream locations; Modeling case: gate opening in 30 min., initial reservoir level at −198, inflow control Plan 4, and MAX storm event (Case 4–8)

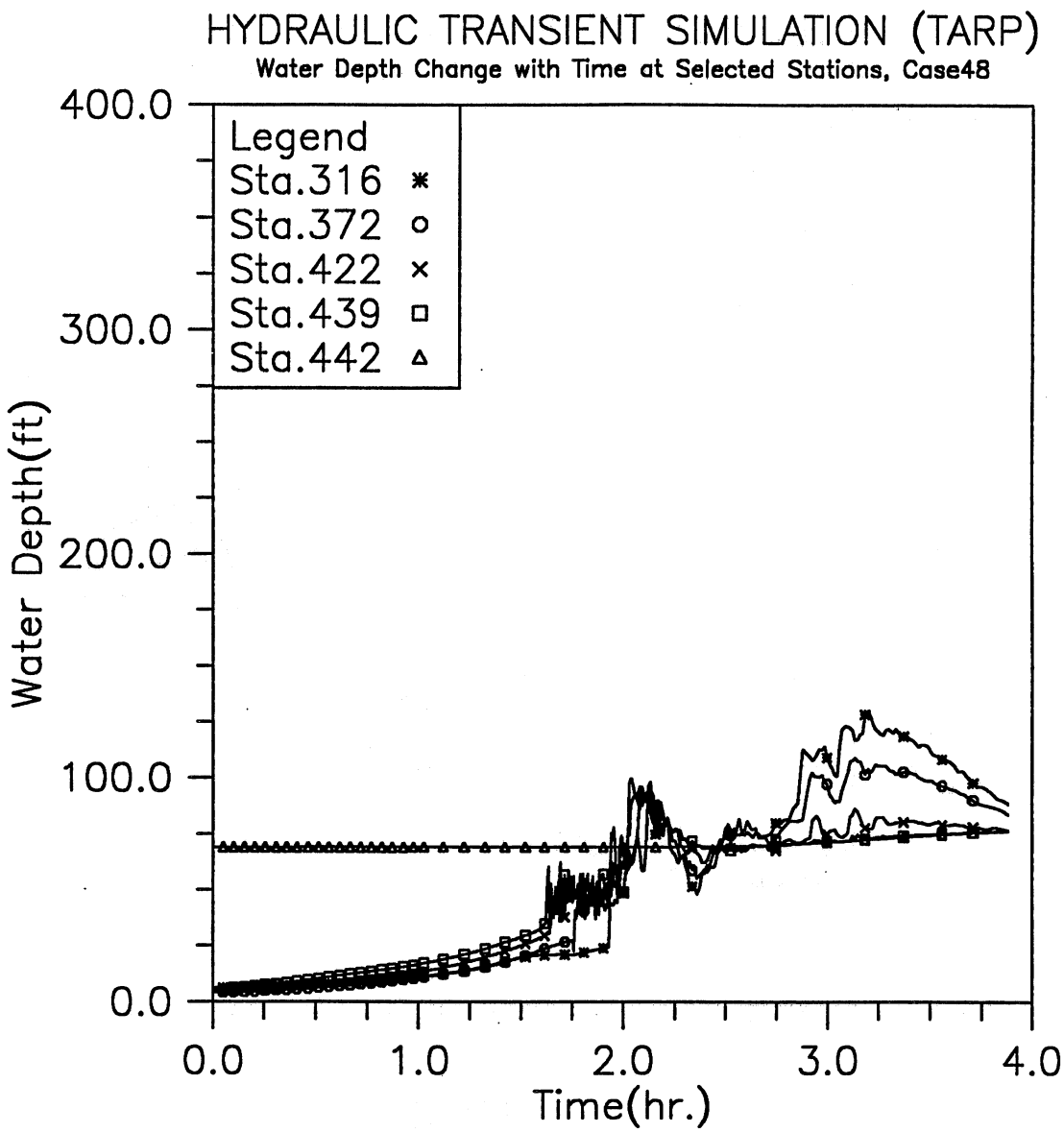

Fig. 3.20(d) Time variation of water depth at five downstream locations; Modeling case: gate opening in 30 min., initial reservoir level at –198, inflow control Plan 4, and MAX storm event (Case 4–8)

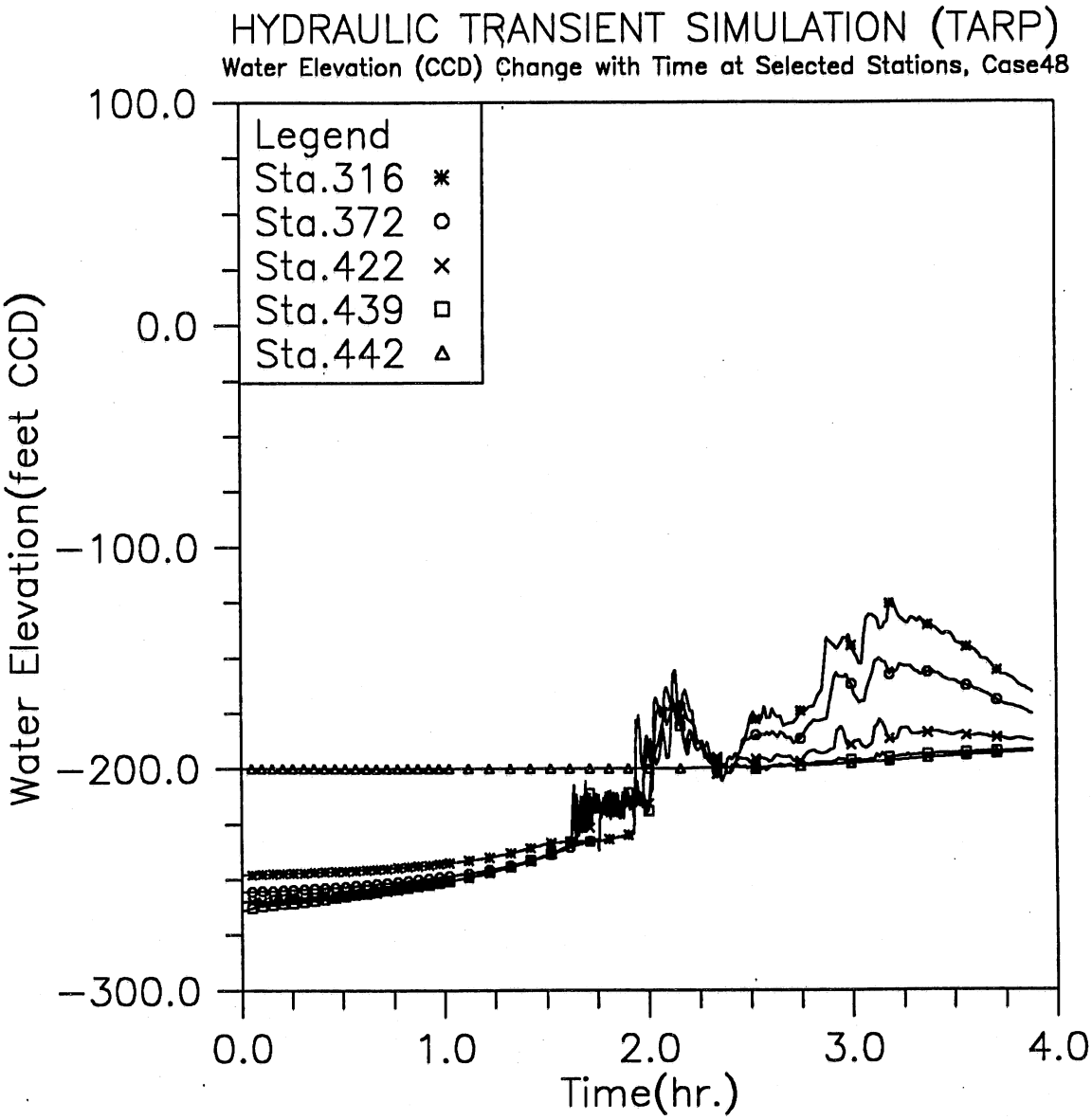

Fig. 3.20(e) Time variation of water elevation at five downstream locations; Modeling case: gate opening in 30 min., initial reservoir level at –198, inflow control Plan 4, and MAX storm event (Case 4–8)

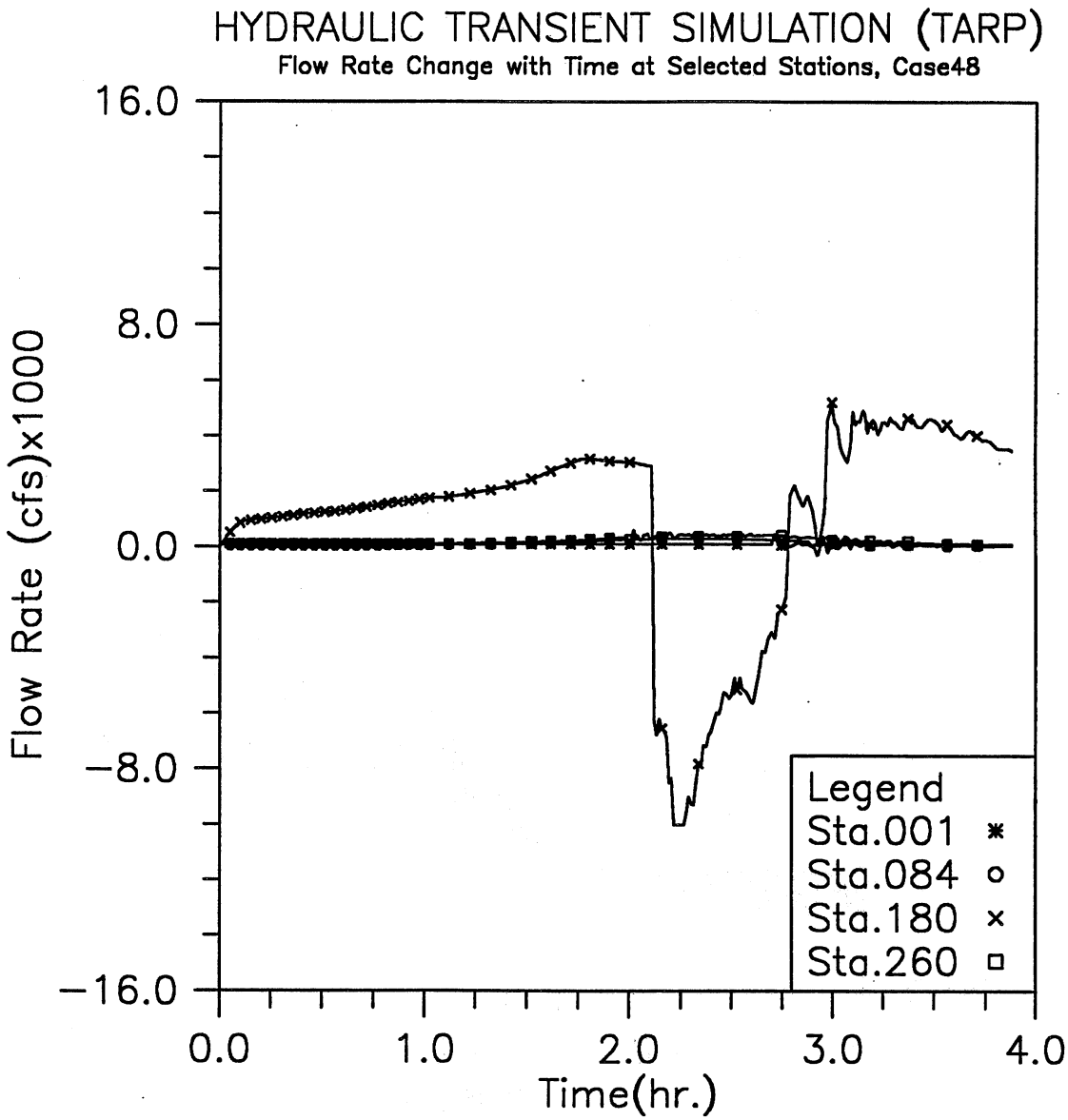

Fig. 3.20(f) Time variation of flow rate at four upstream locations; Modeling case: gate opening in 30 min., initial reservoir level at –198, inflow control Plan 4, and MAX storm event (Case 4–8)

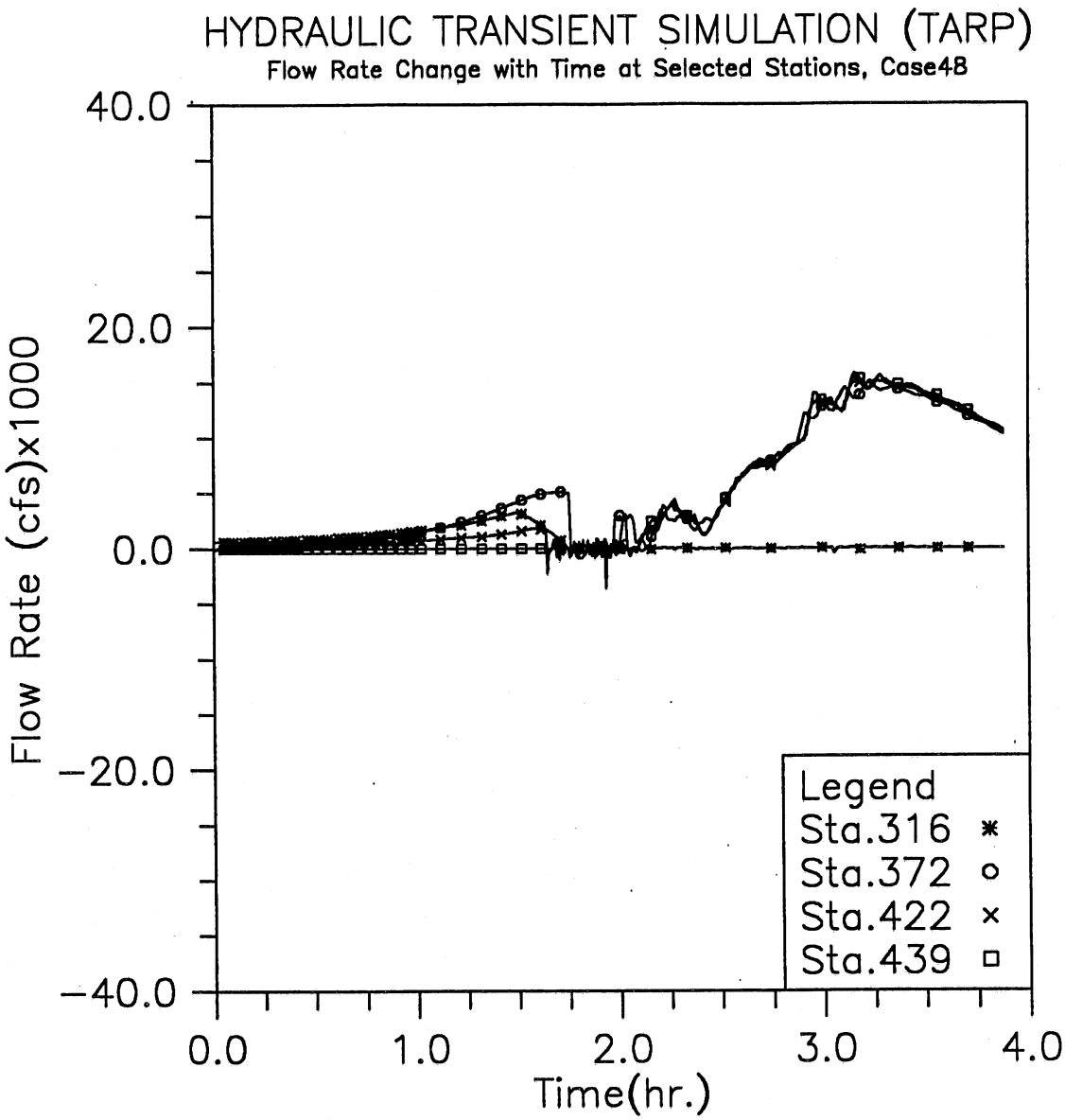

Fig. 3.20(g) Time variation of flow rate at four downstream locations; Modeling case: gate opening in 30 min., initial reservoir level at –198, inflow control Plan 4, and MAX storm event (Case 4–8)

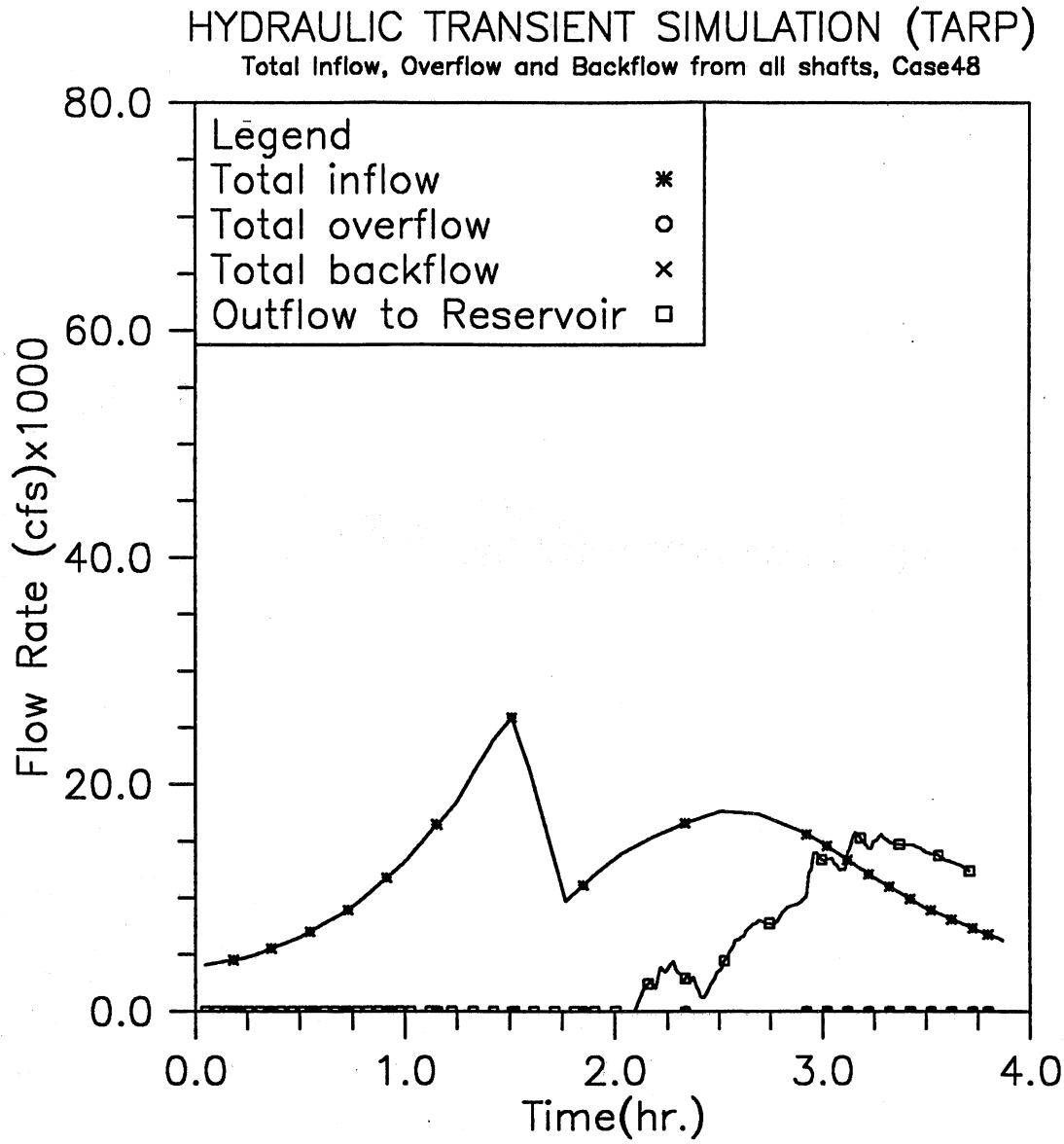

Fig. 3.20(h) Time variation of total inflow, overflow, backflow, and outflow to reservoir; Modeling case: gate opening in 30 min., initial reservoir level at –198, inflow control Plan 4, and MAX storm event (Case 4–8)

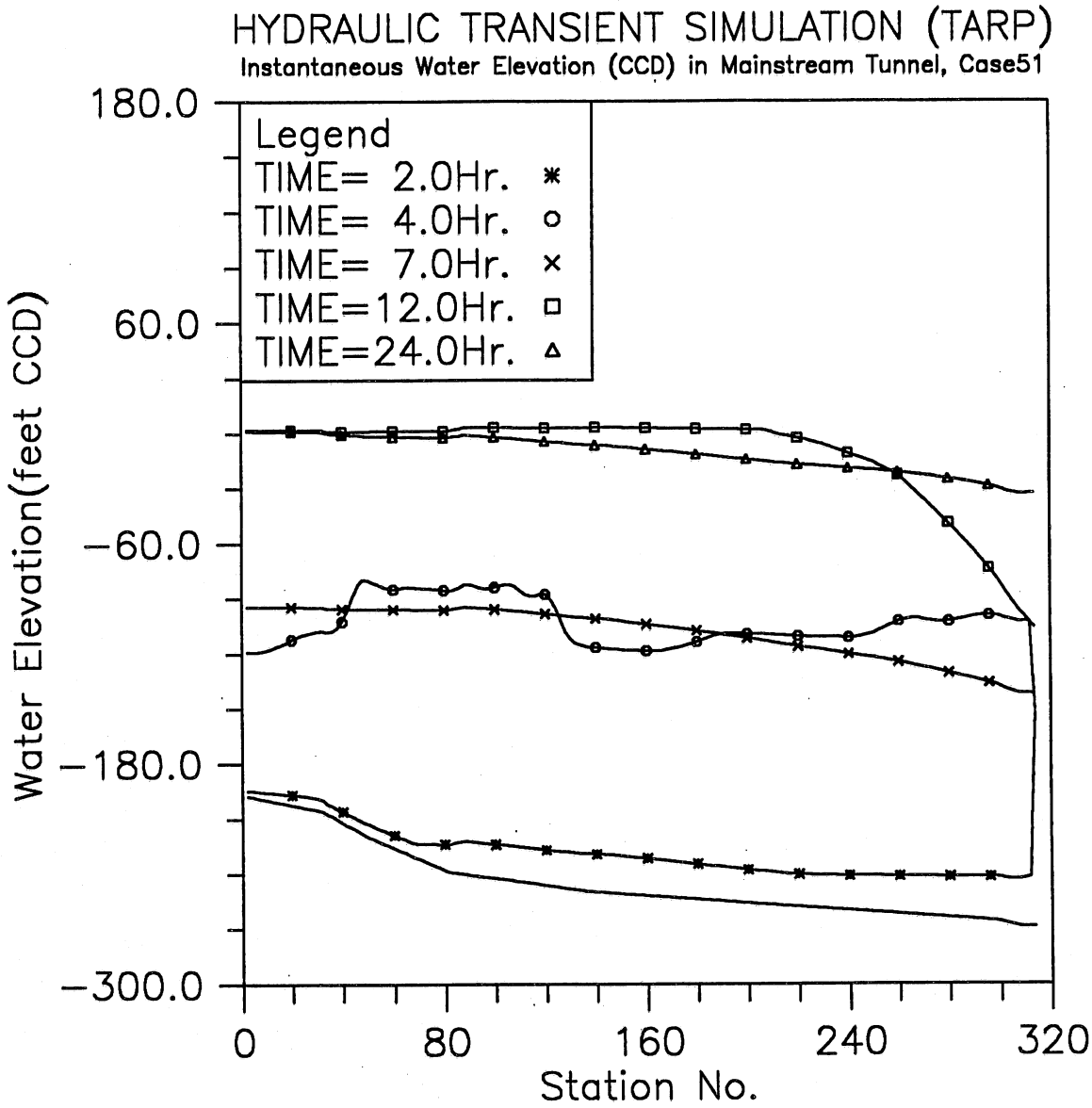

Fig. 3.21(a) Instantaneous hydraulic gradelines along the main tunnel; Modeling case: gate opening in 30 min., initial reservoir level at –150, and 500–year storm event (Case 5–1)

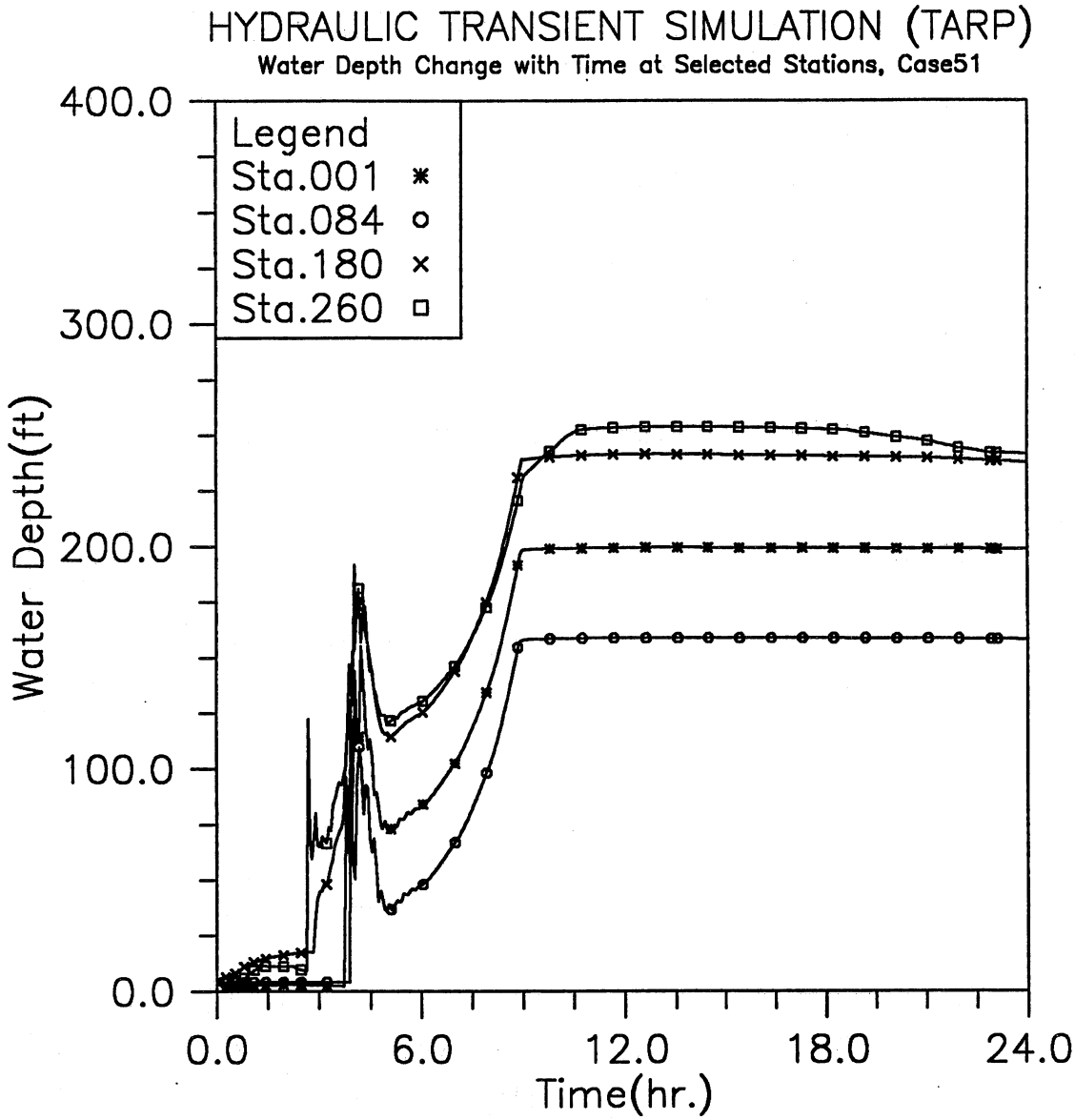

Fig. 3.21(b) Time variation of water depth at four upstream locations; Modeling case: gate opening in 30 min., initial reservoir level at –150, and 500–year storm event (Case 5–1)

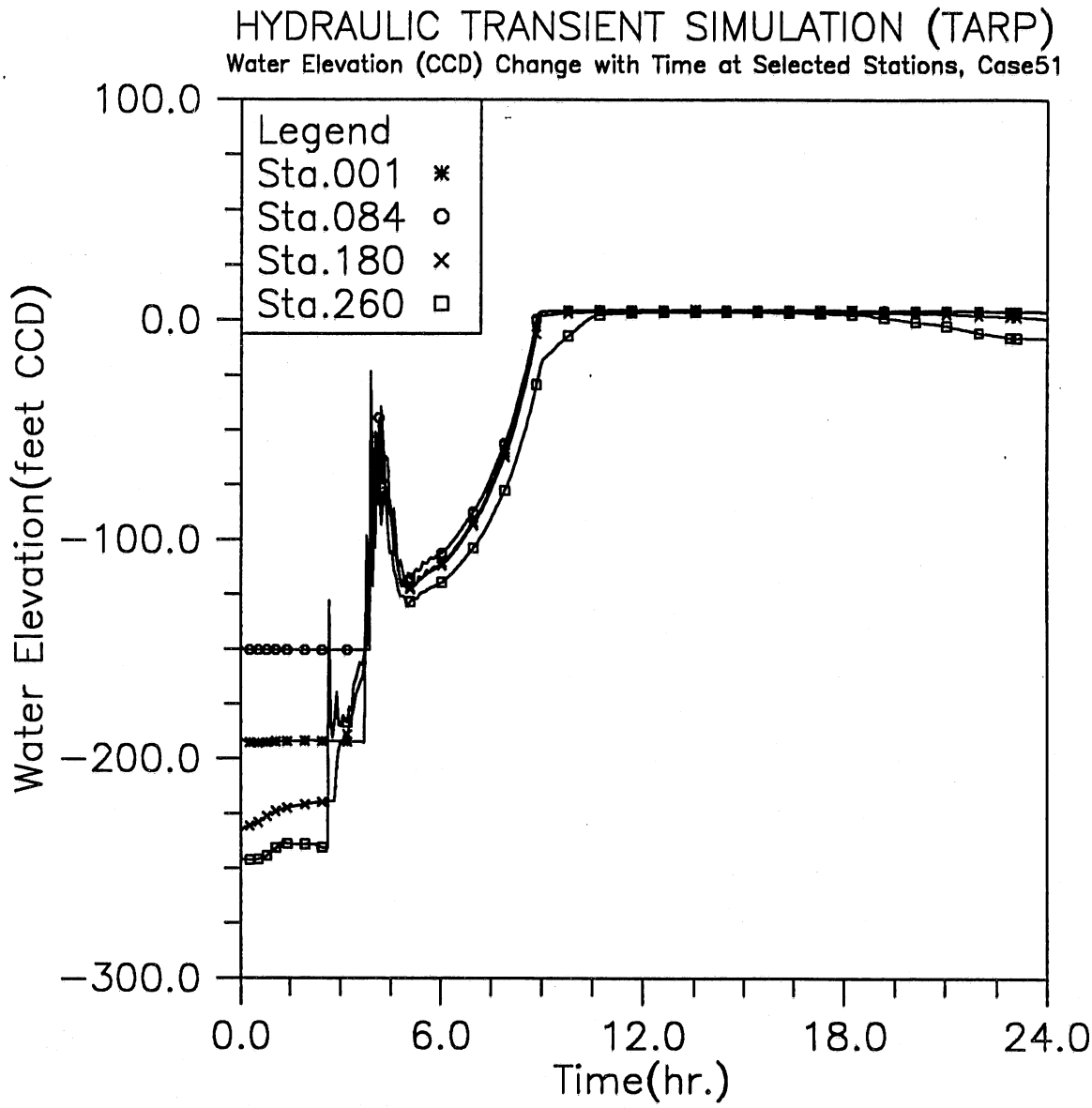

Fig. 3.21(c) Time variation of water elevation at four upstream locations; Modeling case: gate opening in 30 min., initial reservoir level at –150, and 500–year storm event (Case 5–1)

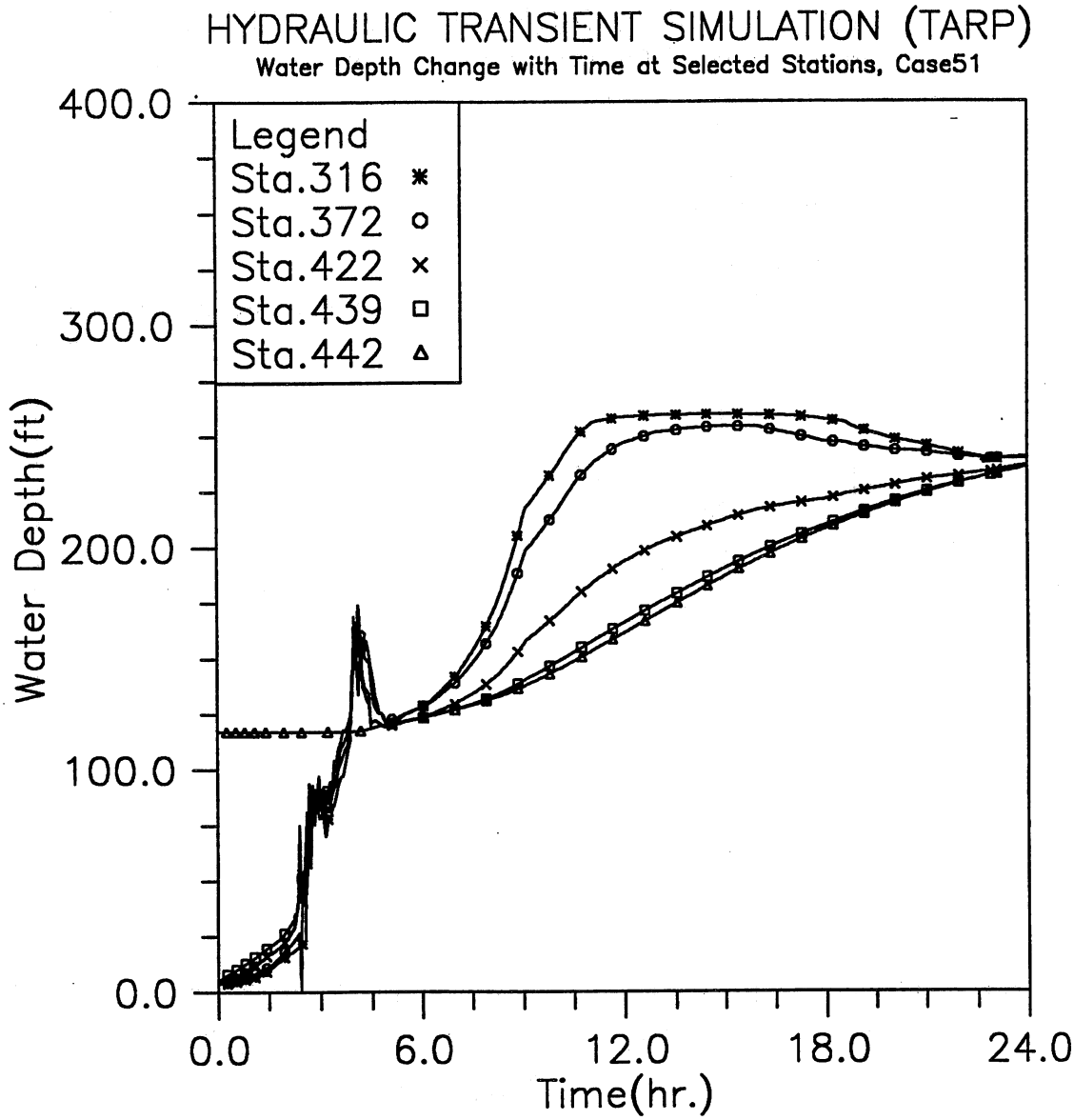

Fig. 3.21(d) Time variation of water depth at five downstream locations; Modeling case: gate opening in 30 min., initial reservoir level at –150, and 500–year storm event (Case 5–1)

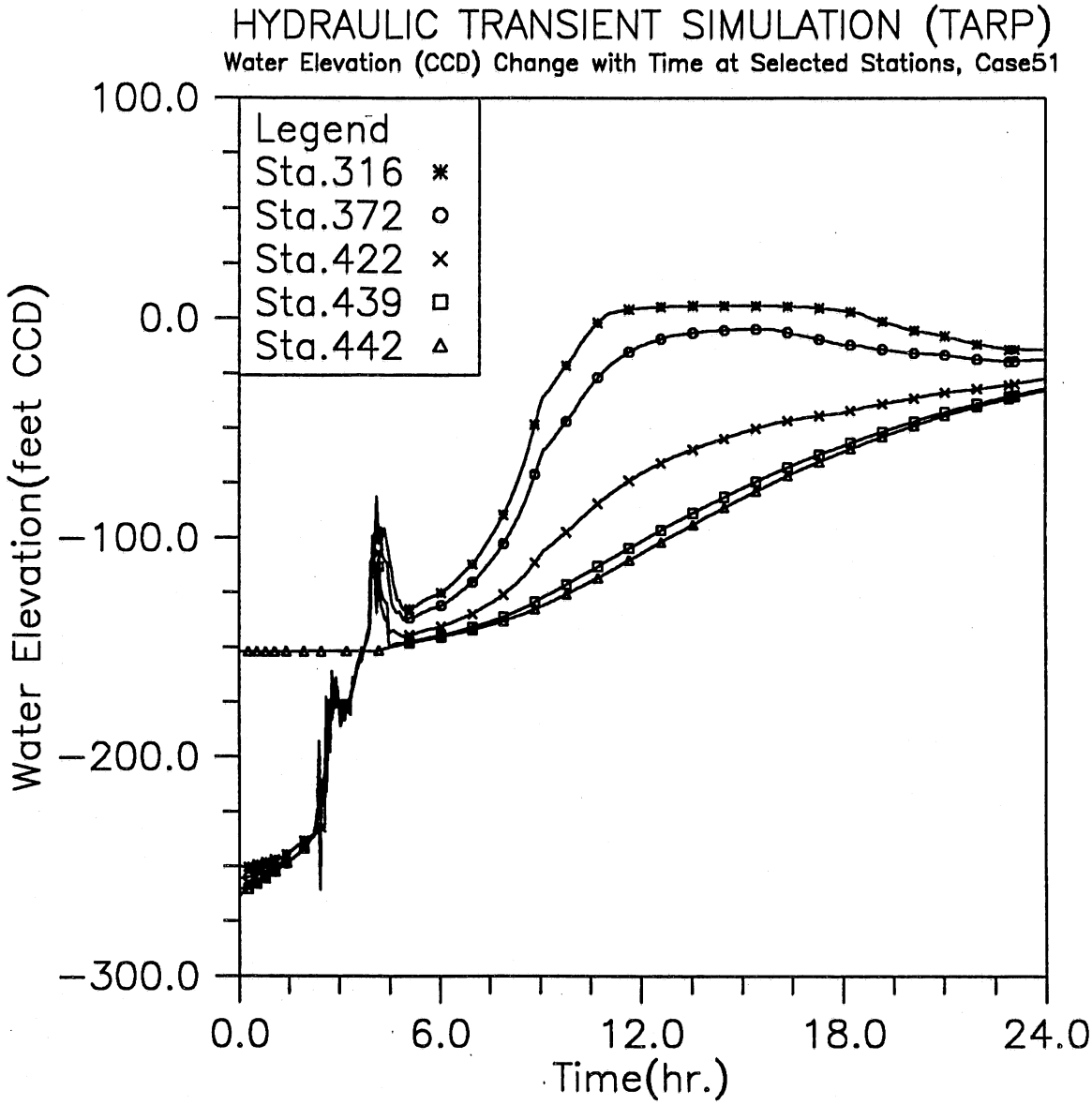

Fig. 3.21(e) Time variation of water elevation at five downstream locations; Modeling case: gate opening in 30 min., initial reservoir level at −150, and 500–year storm event (Case 5–1)

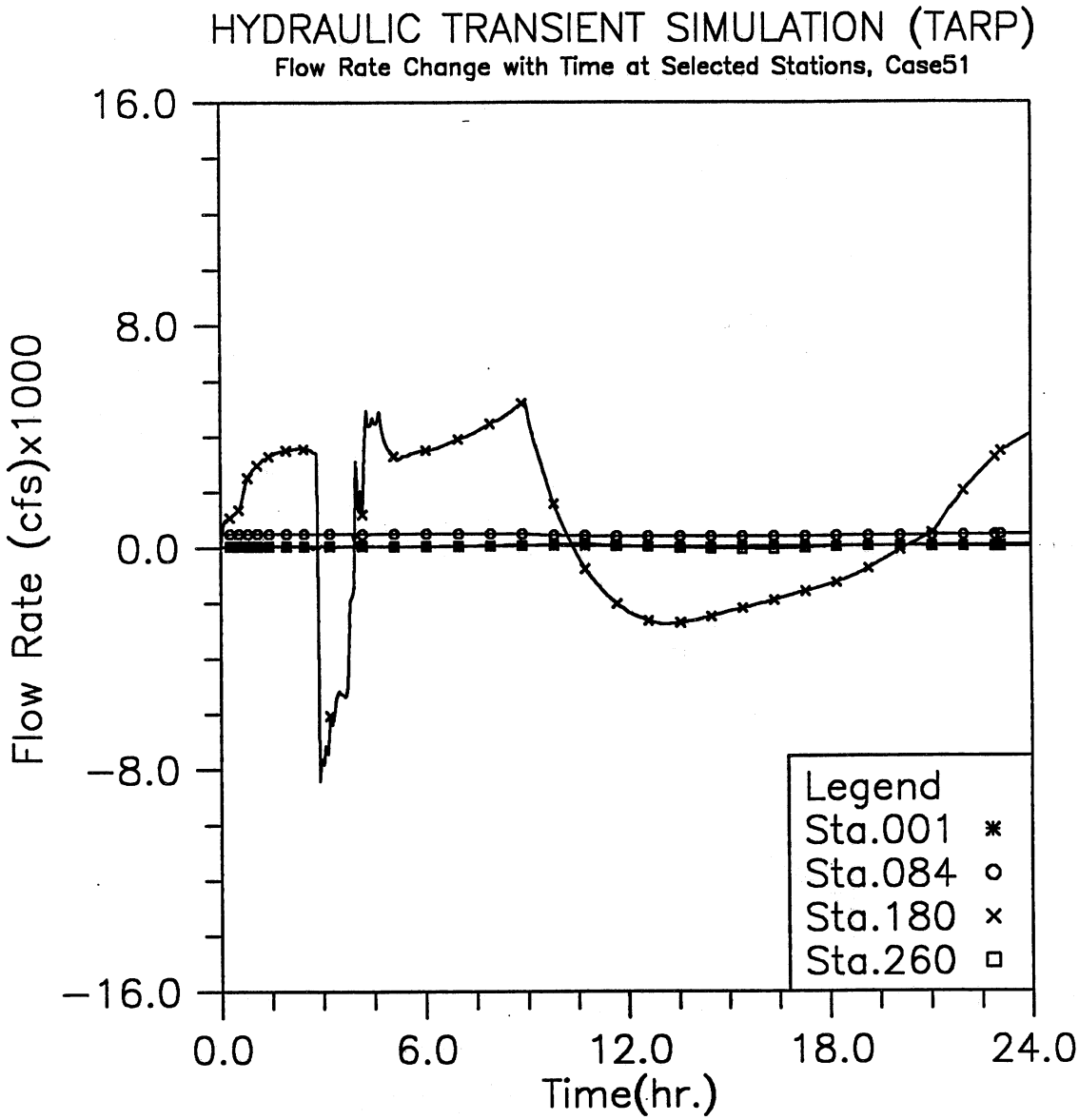

Fig. 3.21(f) Time variation of flow rate at four upstream locations; Modeling case: gate opening in 30 min., initial reservoir level at −150, and 500−year storm event (Case 5−1)

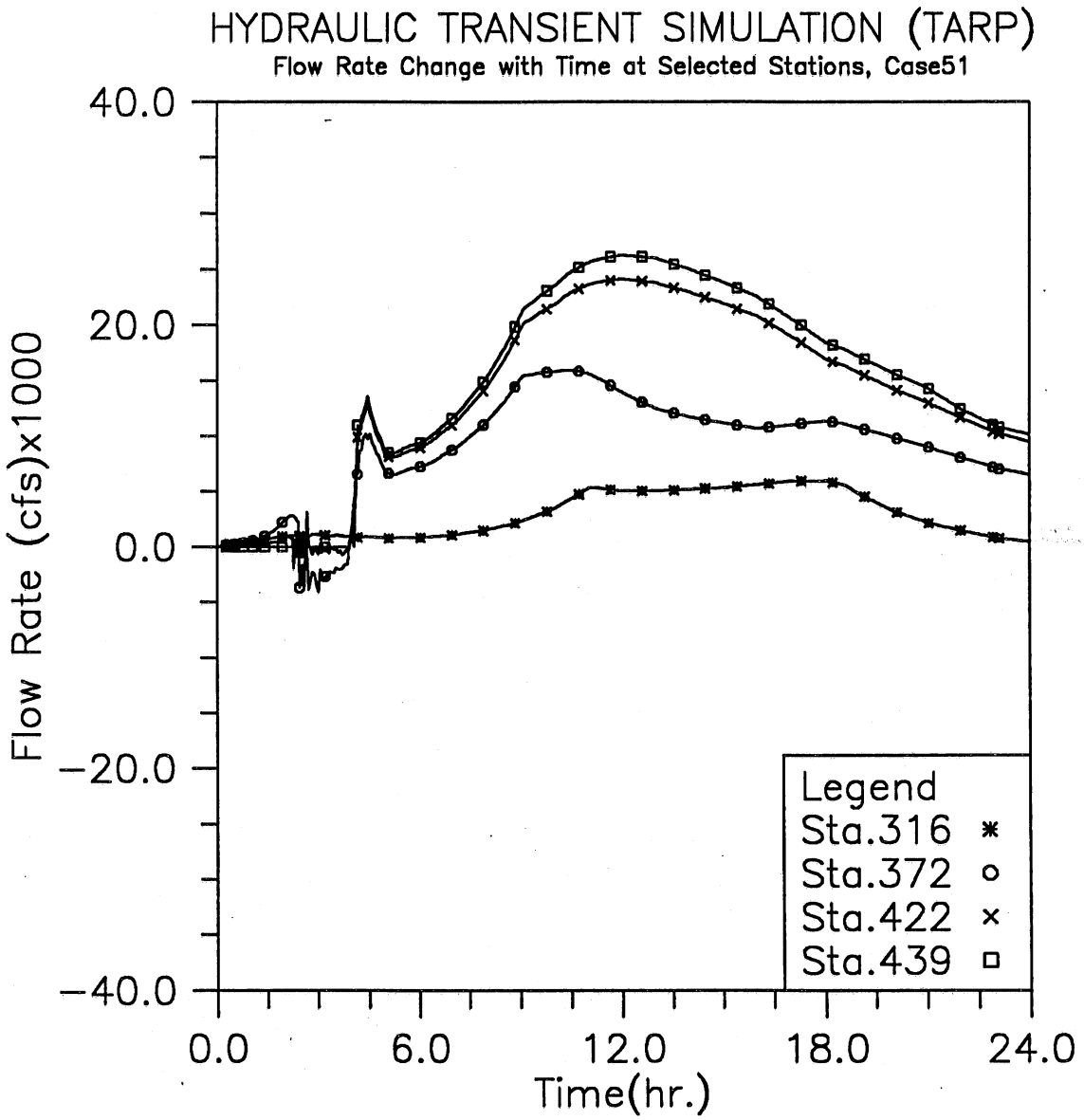

Fig. 3.21(g) Time variation of flow rate at four downstream locations; Modeling case: gate opening in 30 min., initial reservoir level at –150, and 500–year storm event (Case 5–1)

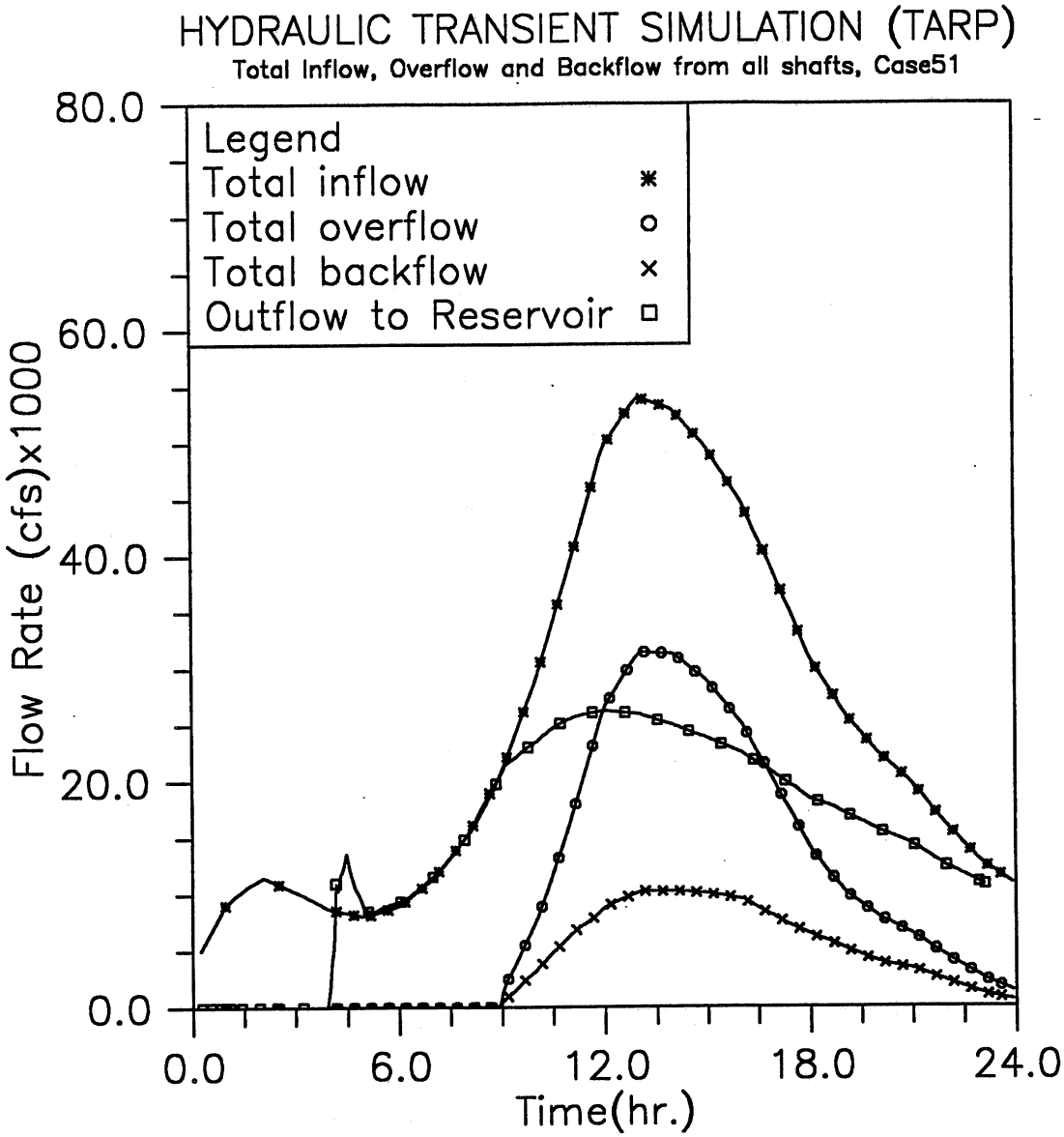

Fig. 3.21(h) Time variation of total inflow, overflow, backflow, and outflow to reservoir; Modeling case: gate opening in 30 min., initial reservoir level at –150, and 500–year storm event (Case 5–1)

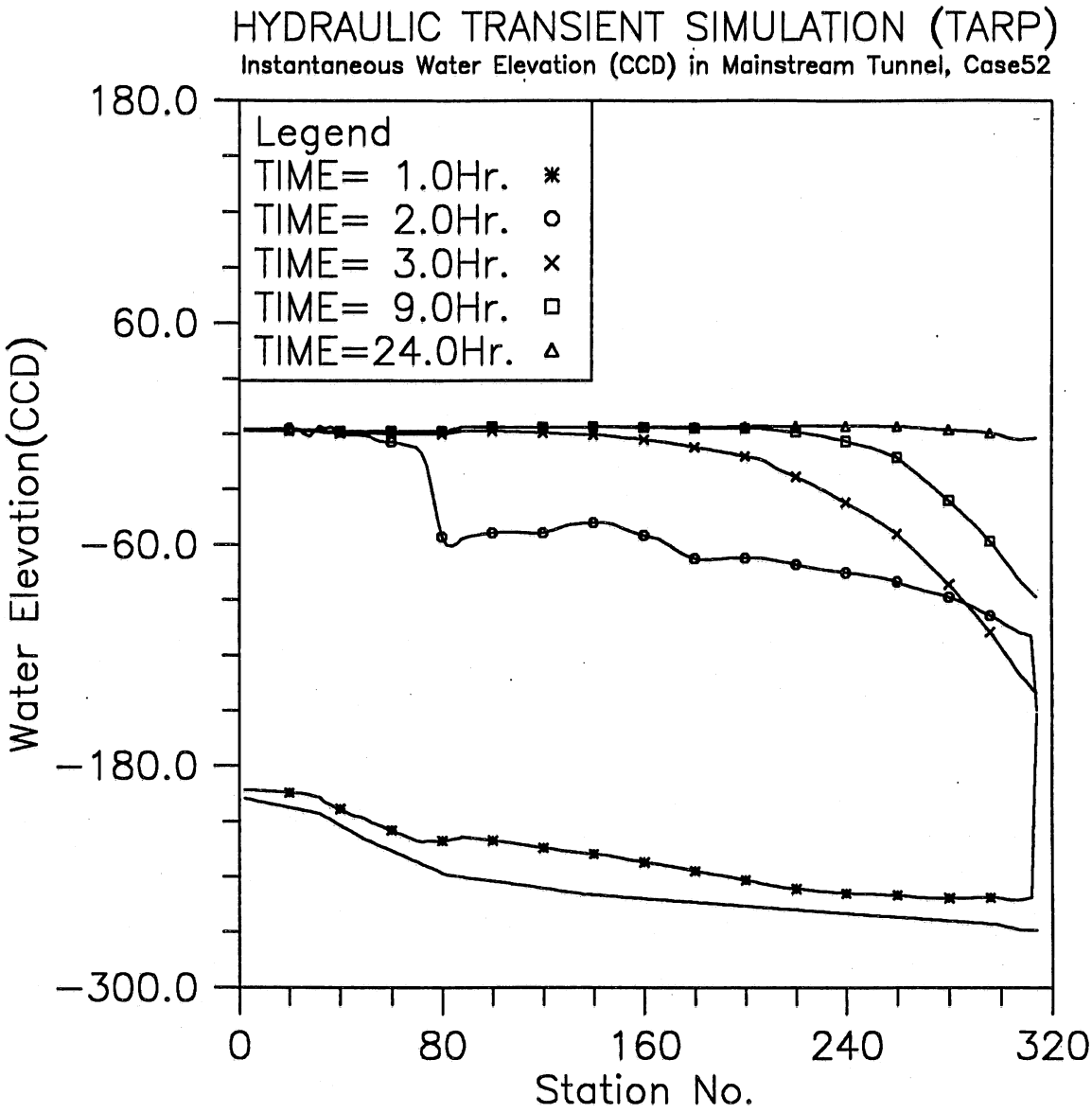

Fig. 3.22(a) Instantaneous hydraulic gradelines along the main tunnel; Modeling case: gate opening in 30 min., initial reservoir level at –150, and PMF event (Case 5–2)

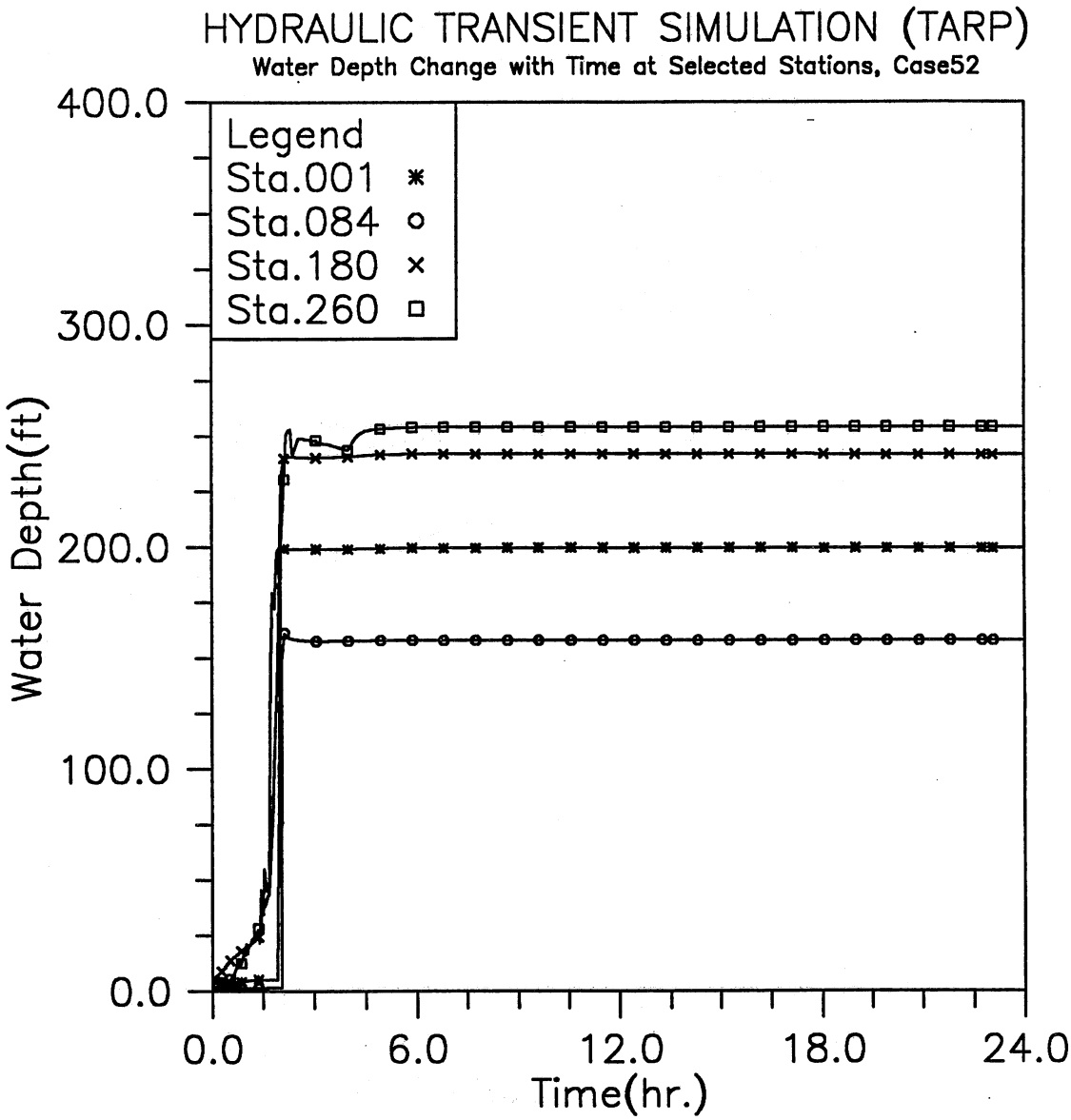

Fig. 3.22(b) Time variation of water depth at four upstream locations; Modeling case: gate opening in 30 min., initial reservoir level at –150, and PMF event (Case 5–2)

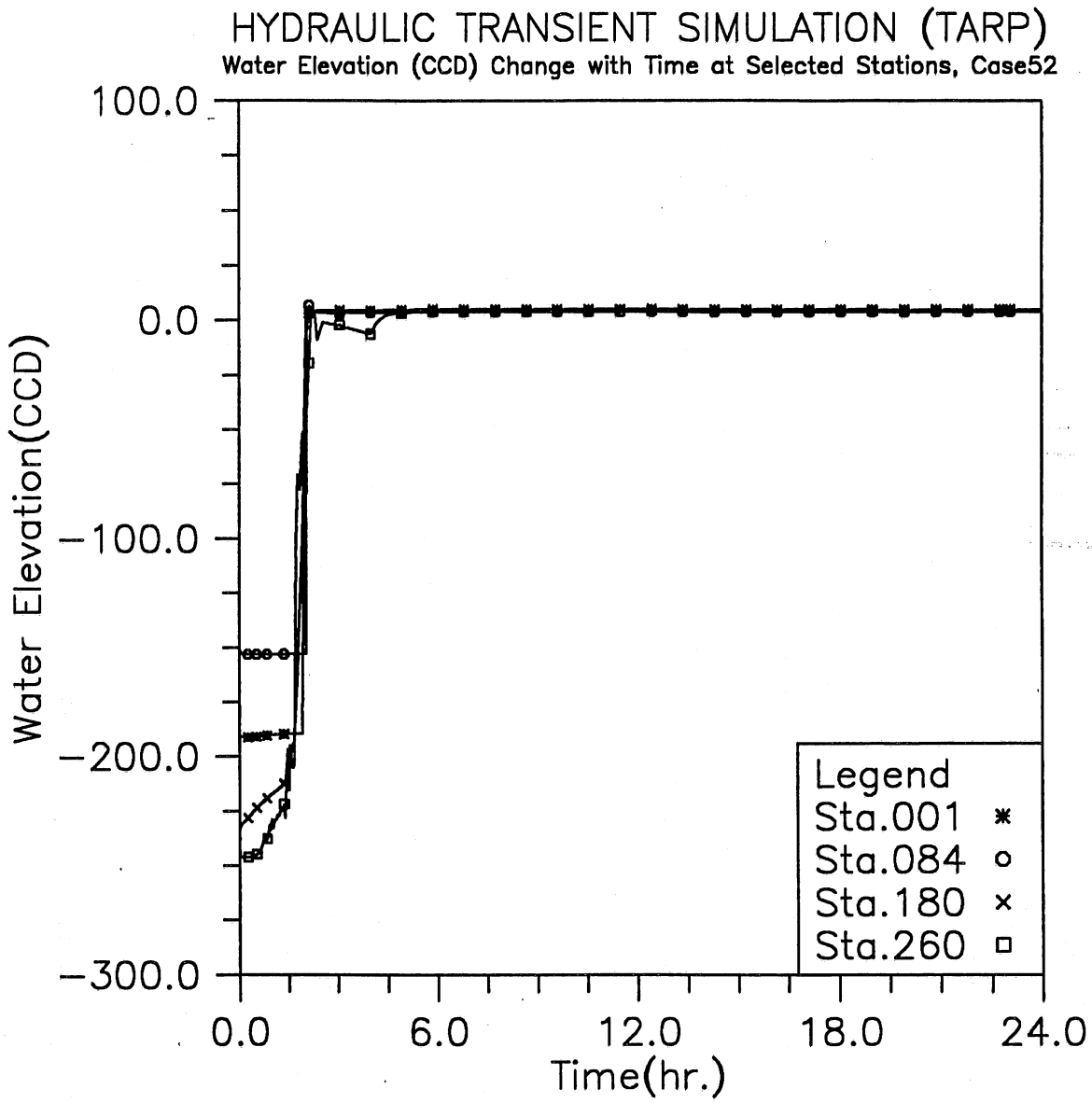

Fig. 3.22(c) Time variation of water elevation at four upstream locations; Modeling case: gate opening in 30 min., initial reservoir level at –150, and PMF event (Case 5–2)

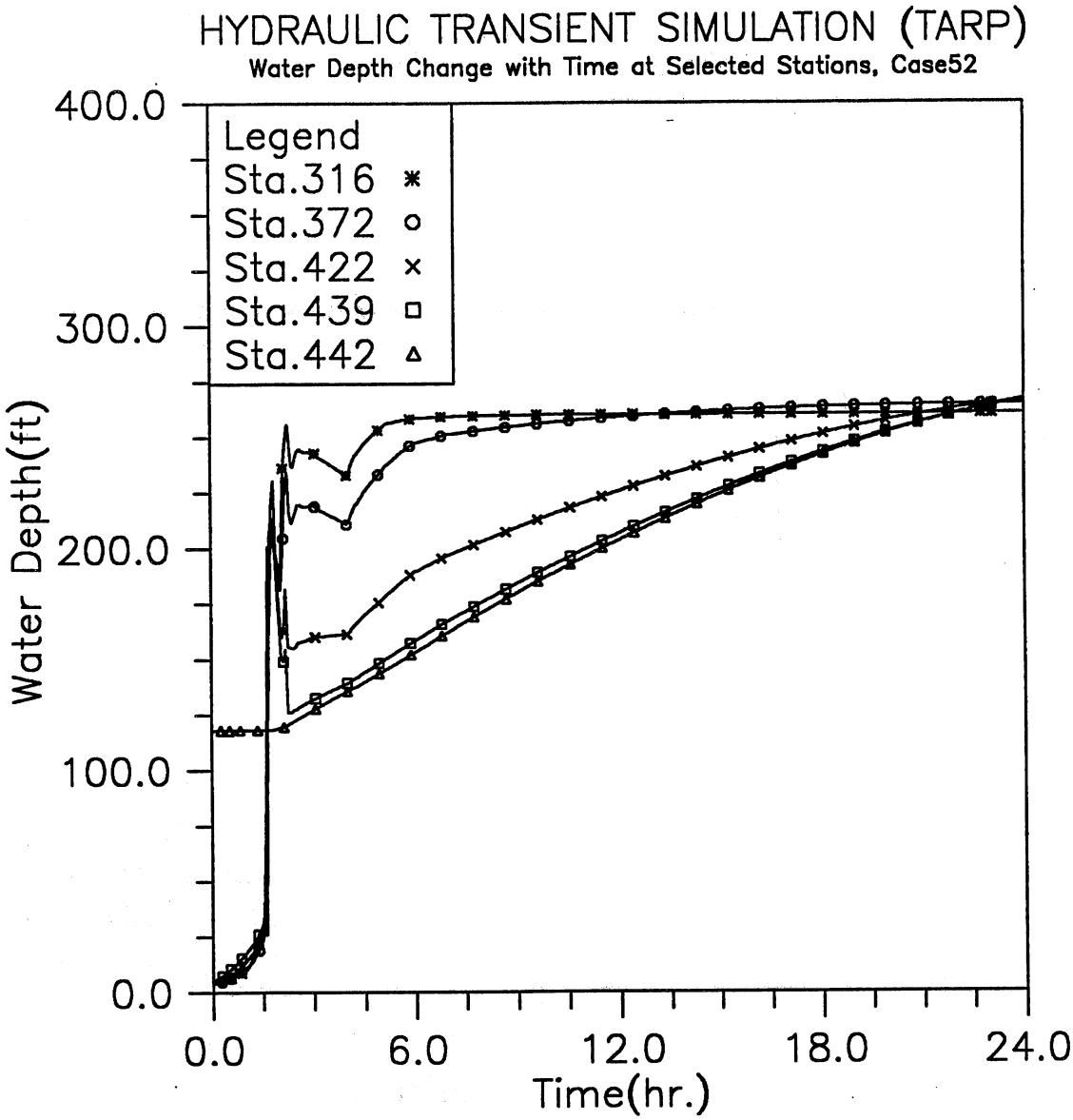

Fig. 3.22(d) Time variation of water depth at five downstream locations; Modeling case: gate opening in 30 min., initial reservoir level at –150, and PMF event (Case 5–2)

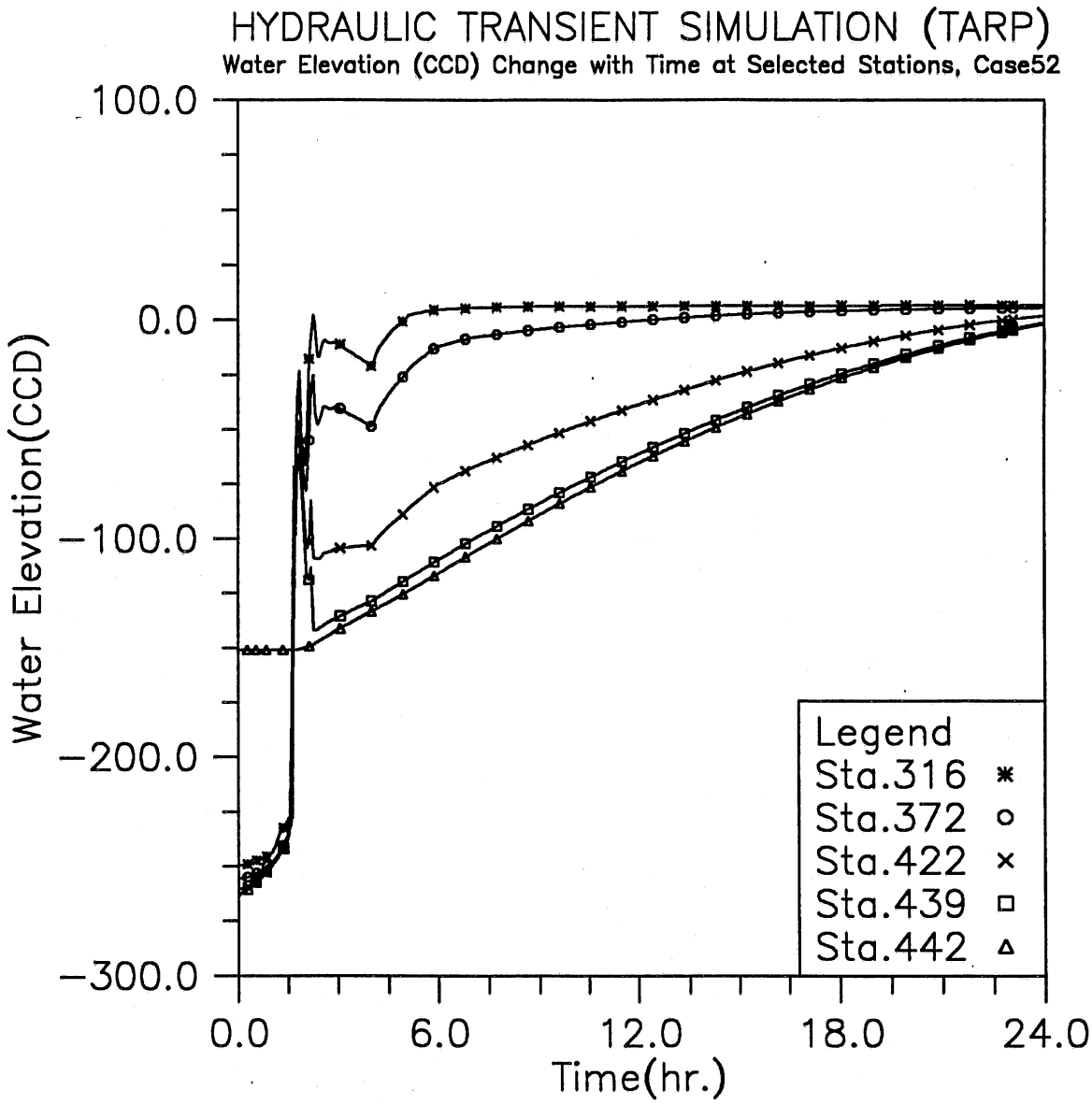

Fig. 3.22(e) Time variation of water elevation at five downstream locations; Modeling case: gate opening in 30 min., initial reservoir level at −150, and PMF event (Case 5–2)

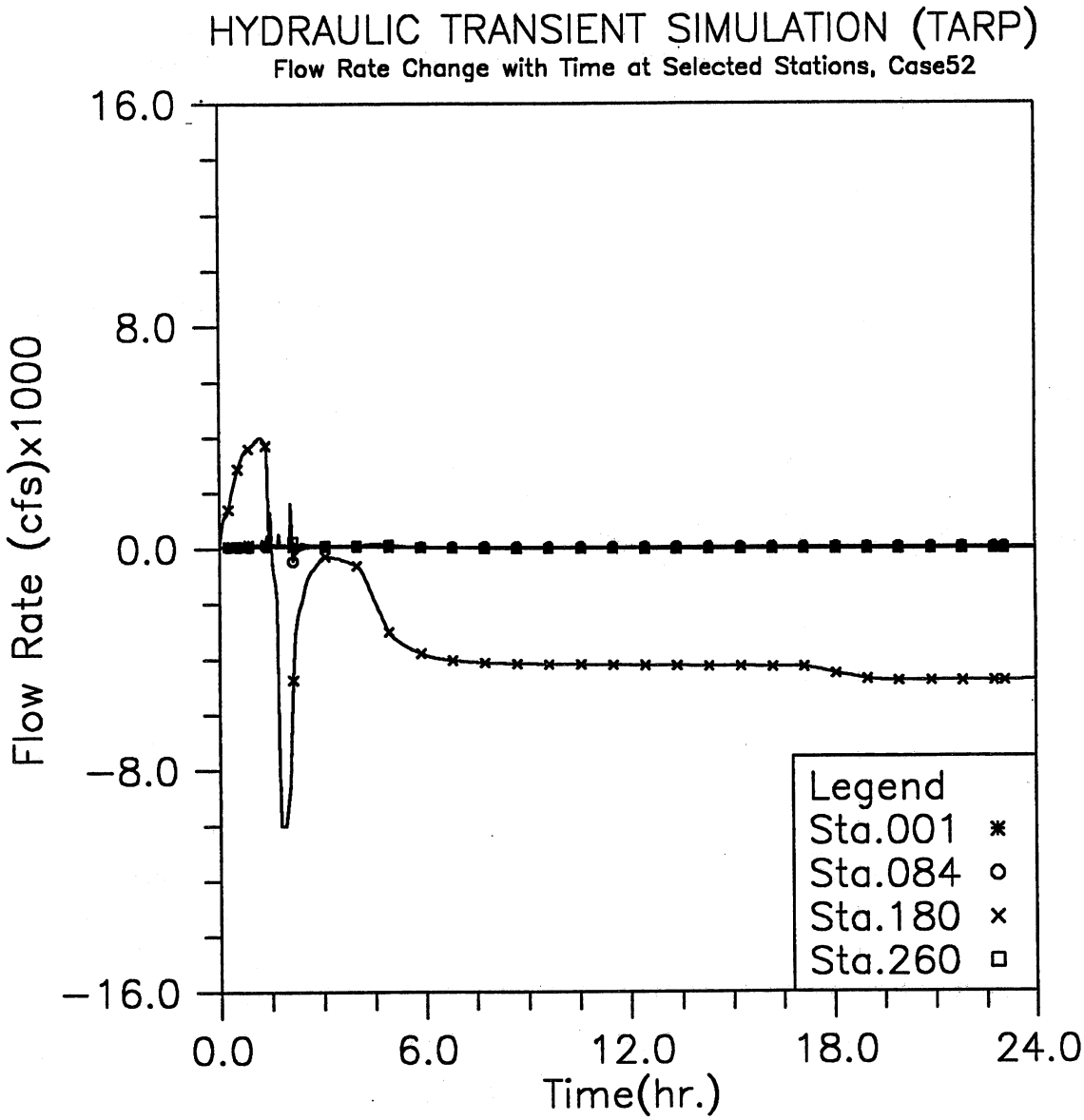

Fig. 3.22(f) Time variation of flow rate at four upstream locations; Modeling case: gate opening in 30 min., initial reservoir level at −150, and PMF event (Case 5–2)

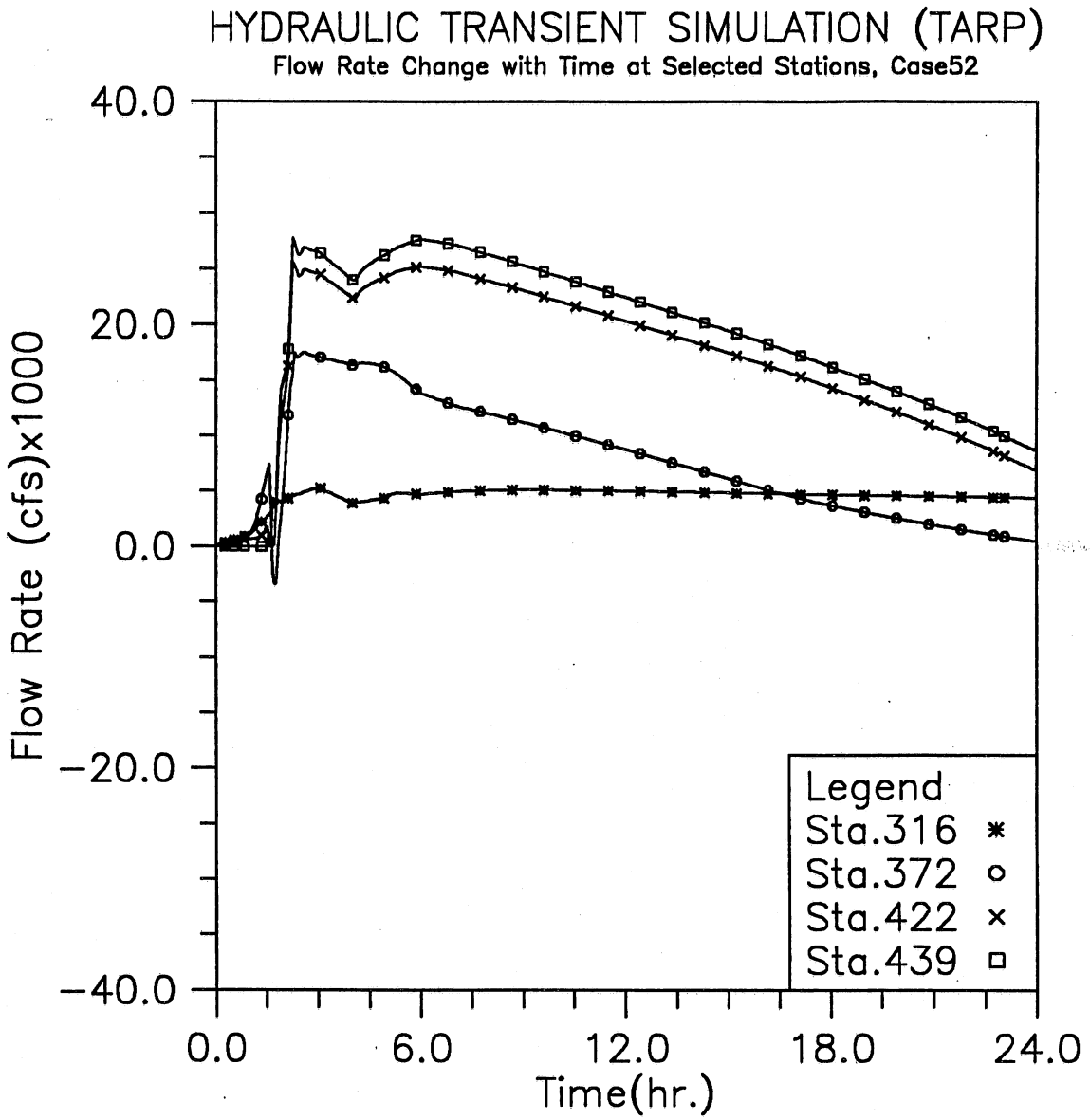

Fig. 3.22(g) Time variation of flow rate at four downstream locations; Modeling case: gate opening in 30 min., initial reservoir level at –150, and PMF event (Case 5–2)

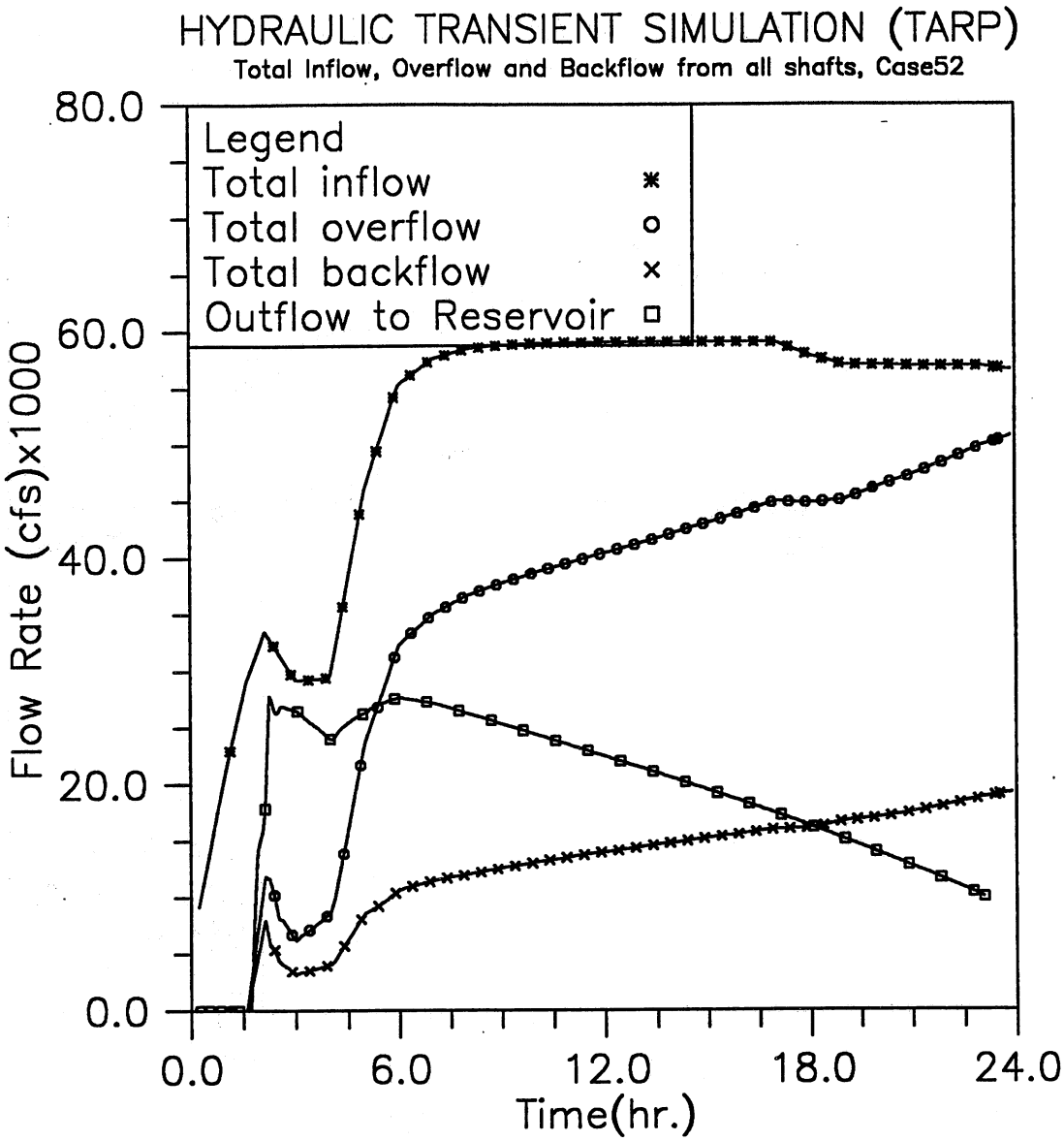

Fig. 3.22(h) Time variation of total inflow, overflow, backflow, and outflow to reservoir; Modeling case: gate opening in 30 min., initial reservoir level at –150, and PMF event (Case 5–2)

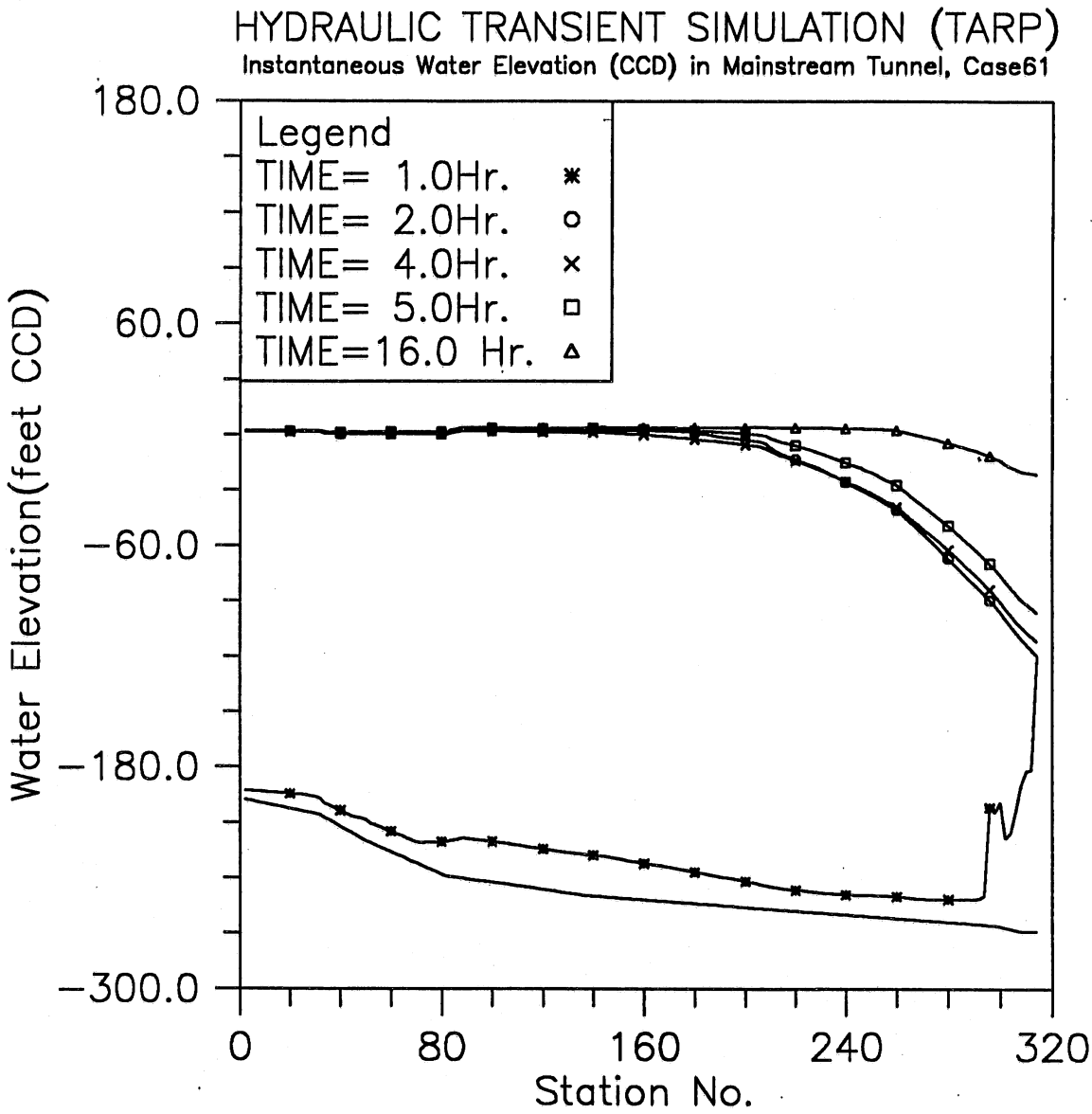

Fig. 3.23(a) Instantaneous hydraulic gradelines along the main tunnel; Modeling case: gate opening at half tunnel height in 10 min., initial reservoir level at –150, and PMF event (Case 6–1)

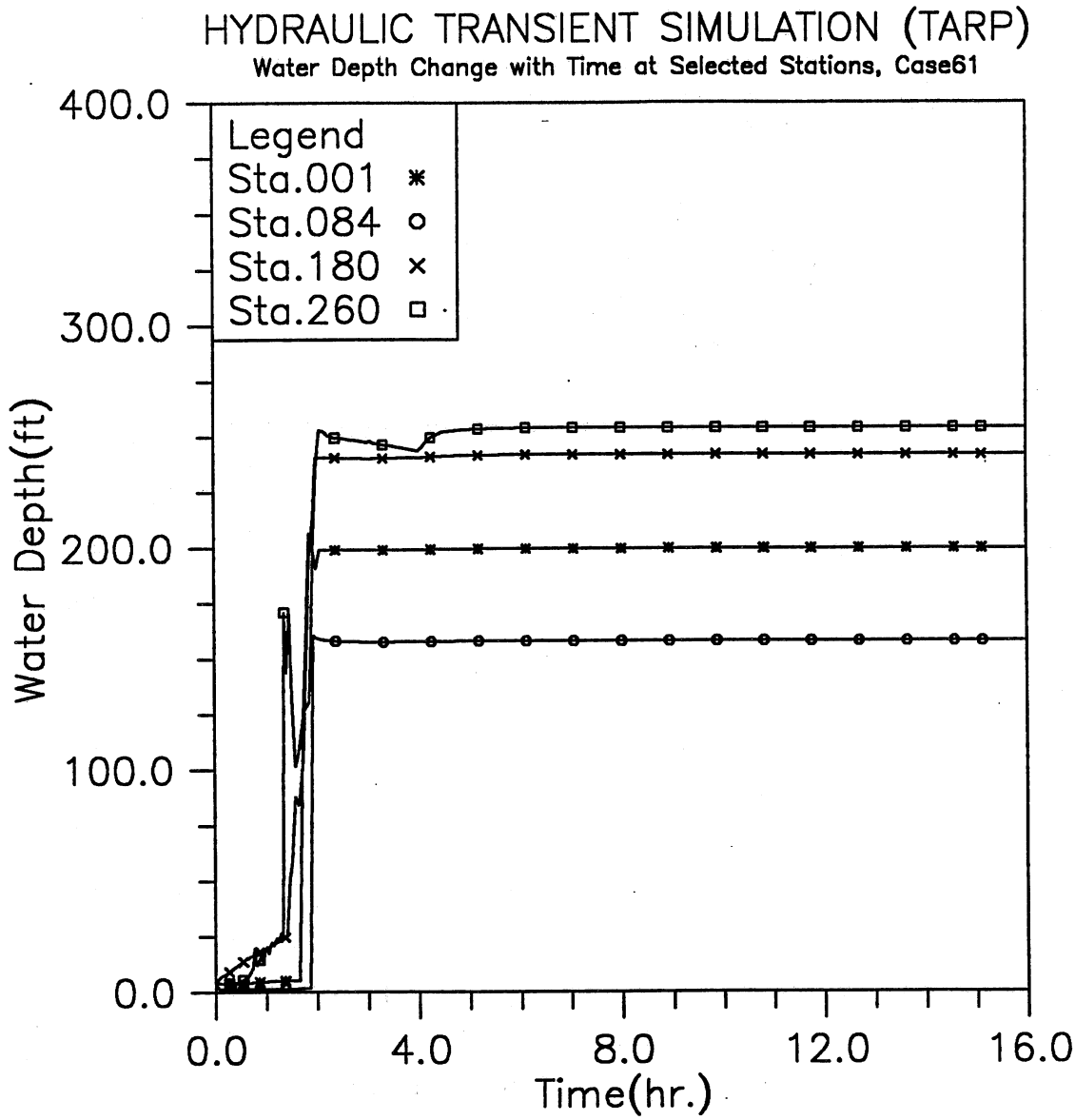

Fig. 3.23(b) Time variation of water depth at four upstream locations; Modeling case: gate opening at half tunnel height in 10 min., initial reservoir level at –150, and PMF event (Case 6–1)

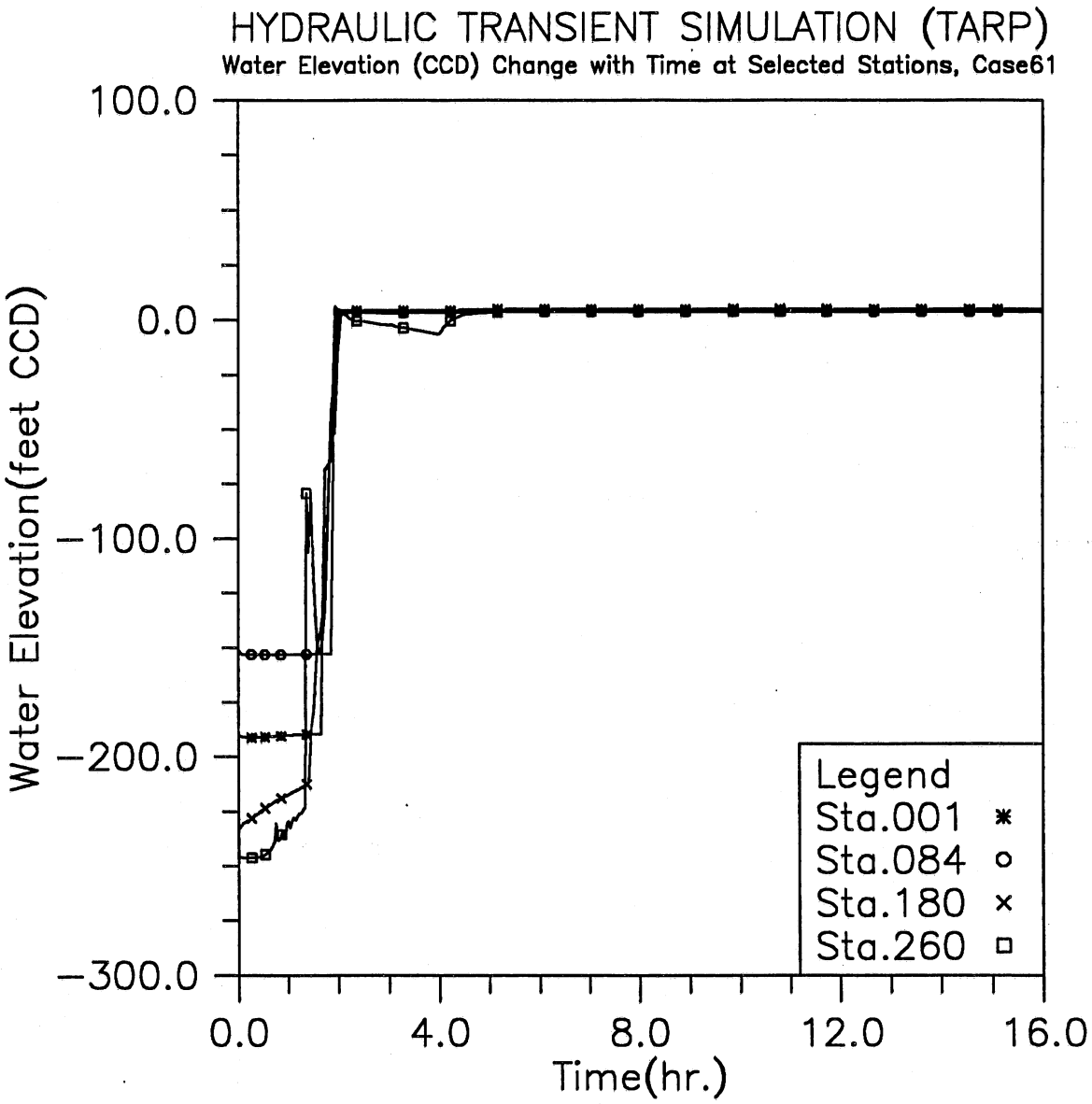

Fig. 3.23(c) Time variation of water elevation at four upstream locations; Modeling case: gate opening at half tunnel height in 10 min., initial reservoir level at −150, and PMF event (Case 6–1)

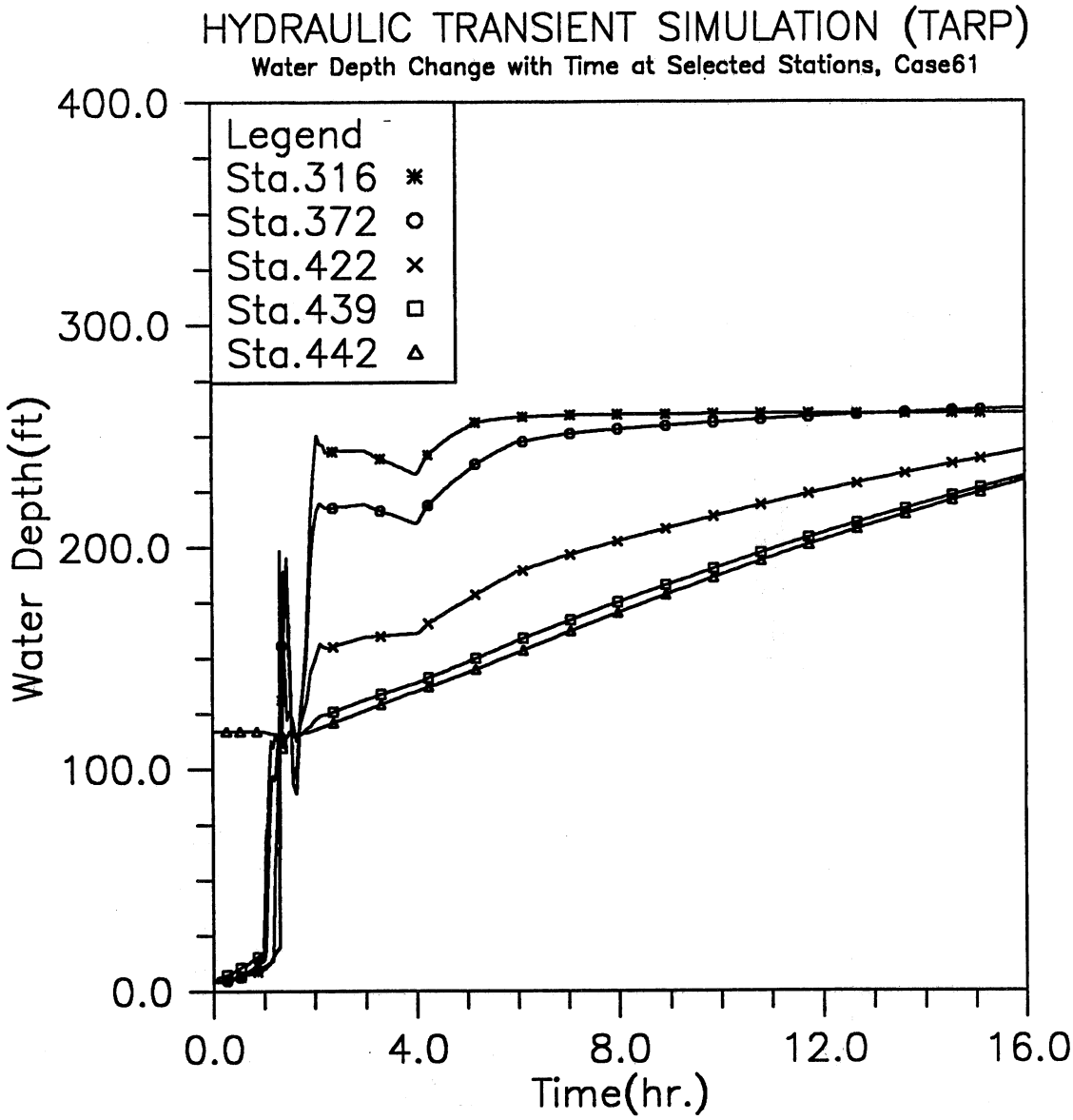

Fig. 3.23(d) Time variation of water depth at five downstream locations; Modeling case: gate opening at half tunnel height in 10 min., initial reservoir level at –150, and PMF event (Case 6–1)

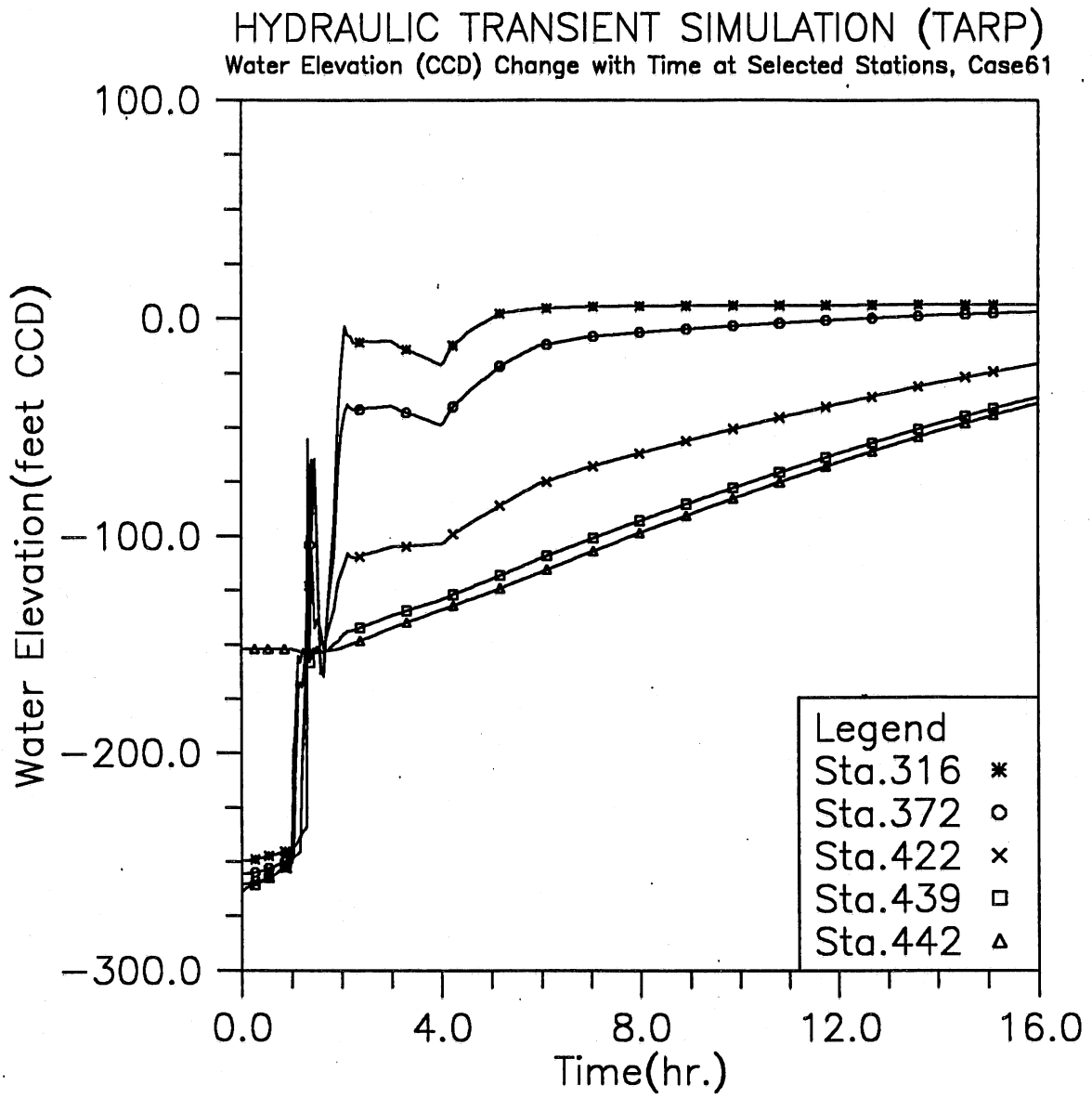

Fig. 3.23(e) Time variation of water elevation at five downstream locations; Modeling case: gate opening at half tunnel height in 10 min., initial reservoir level at −150, and PMF event (Case 6–1)

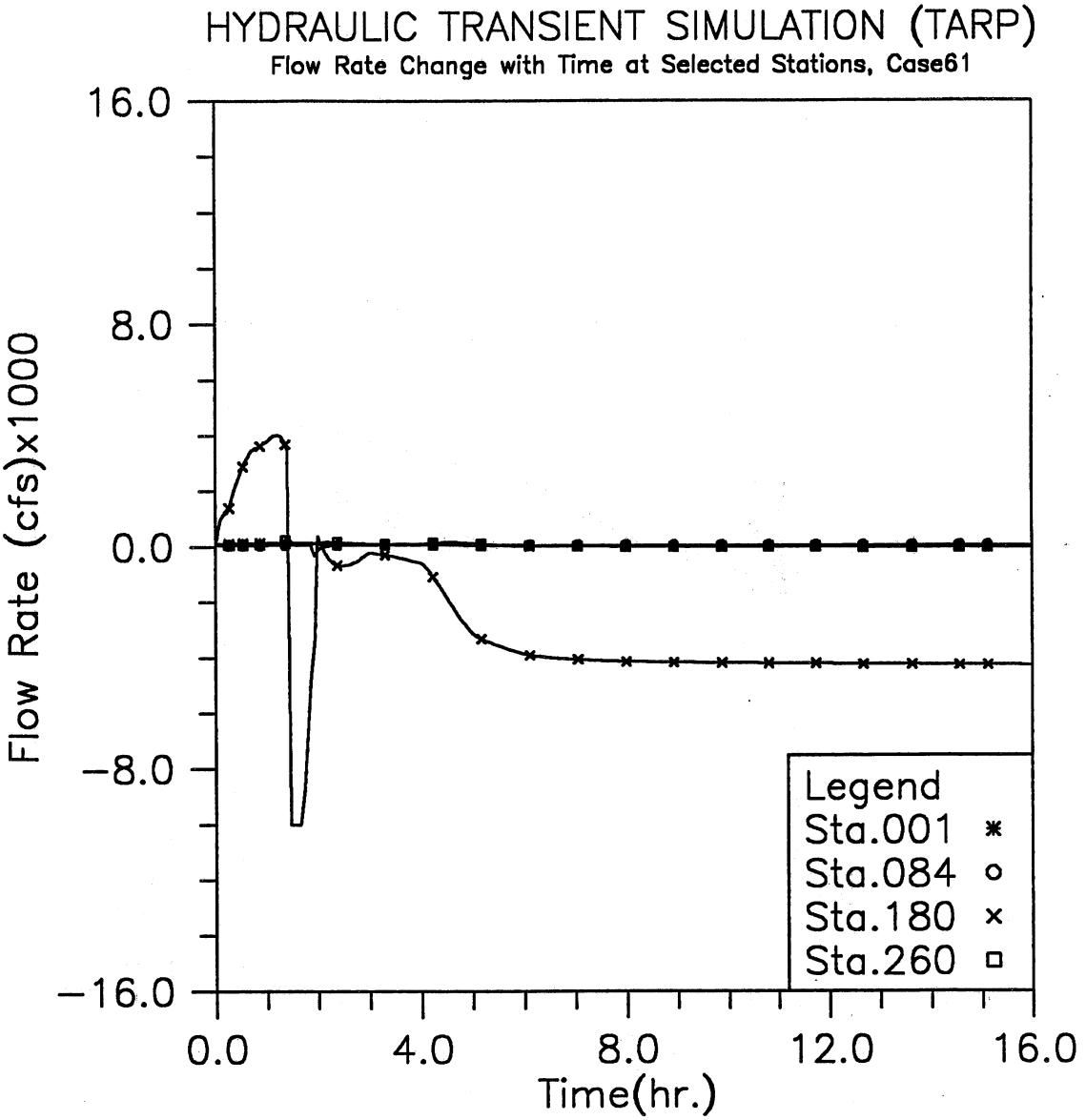

Fig. 3.23(f) Time variation of flow rate at four upstream locations; Modeling case: gate opening at half tunnel height in 10 min., initial reservoir level at −150, and PMF event (Case 6–1)

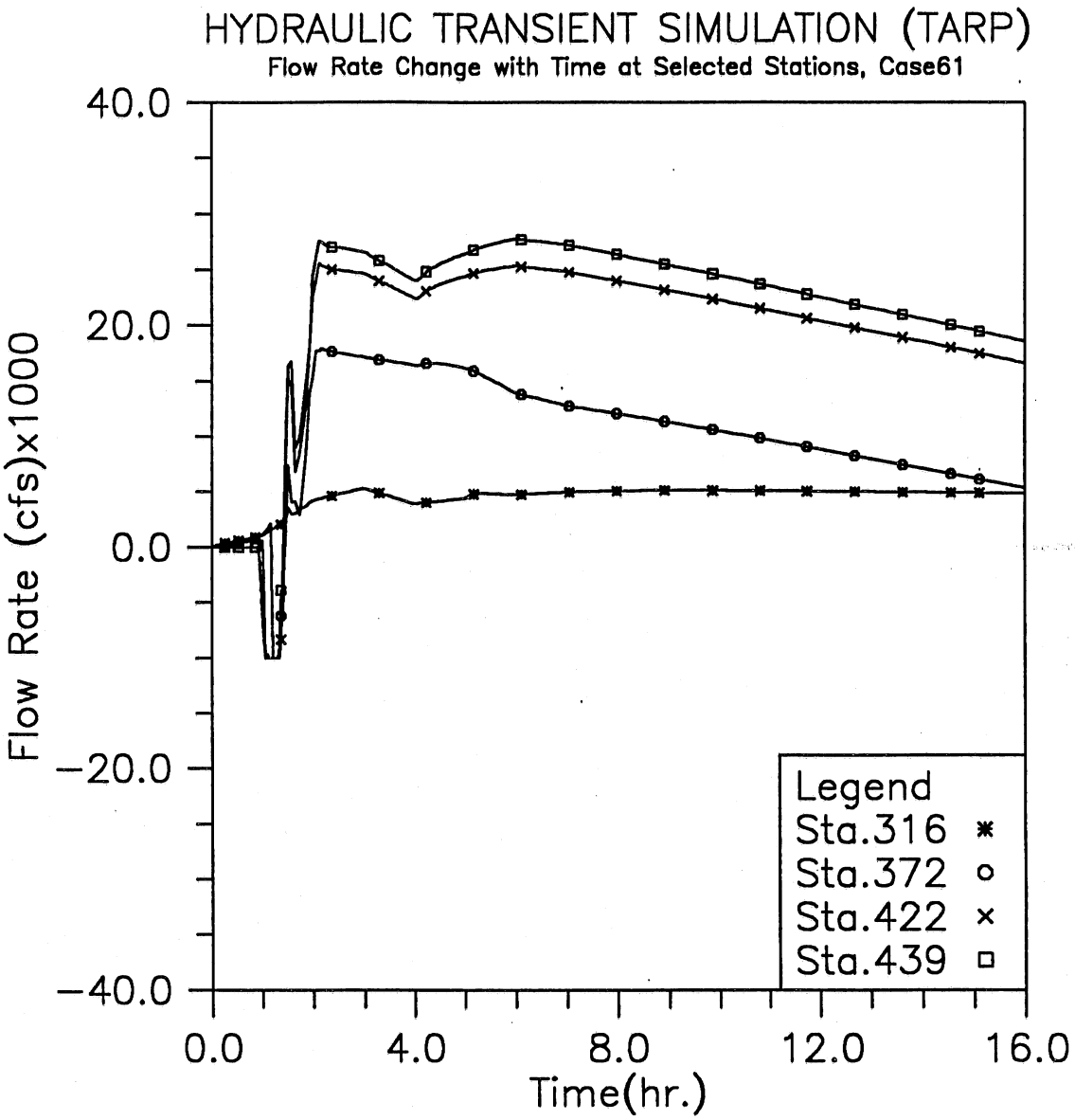

Fig. 3.23(g) Time variation of flow rate at four downstream locations; Modeling case: gate opening at half tunnel height in 10 min., initial reservoir level at –150, and PMF event (Case 6–1)

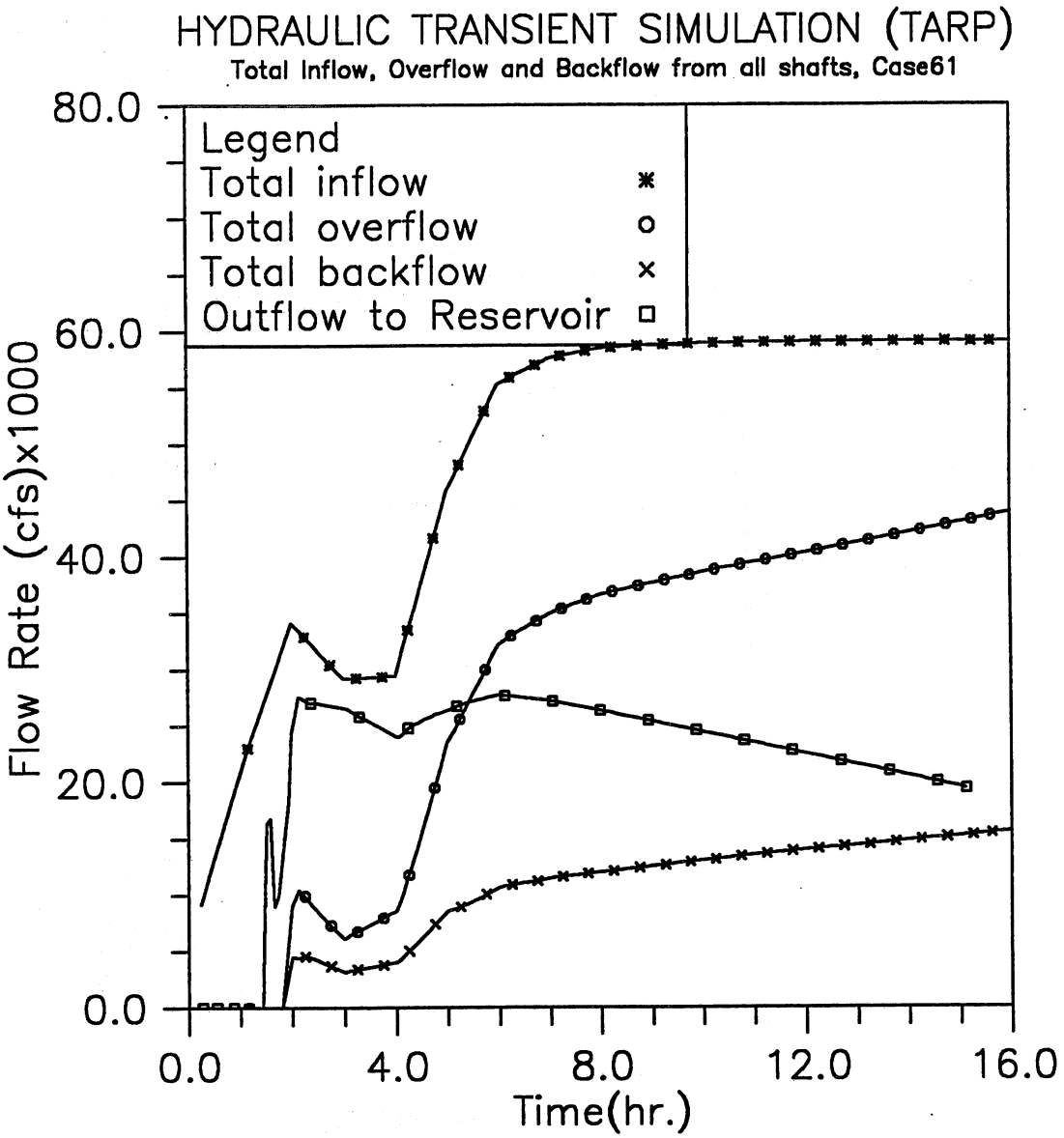

Fig. 3.23(h) Time variation of total inflow, overflow, backflow, and outflow to reservoir; Modeling case: gate opening at half tunnel height in 10 min., initial reservoir level at –150, and PMF event (Case 6–1)

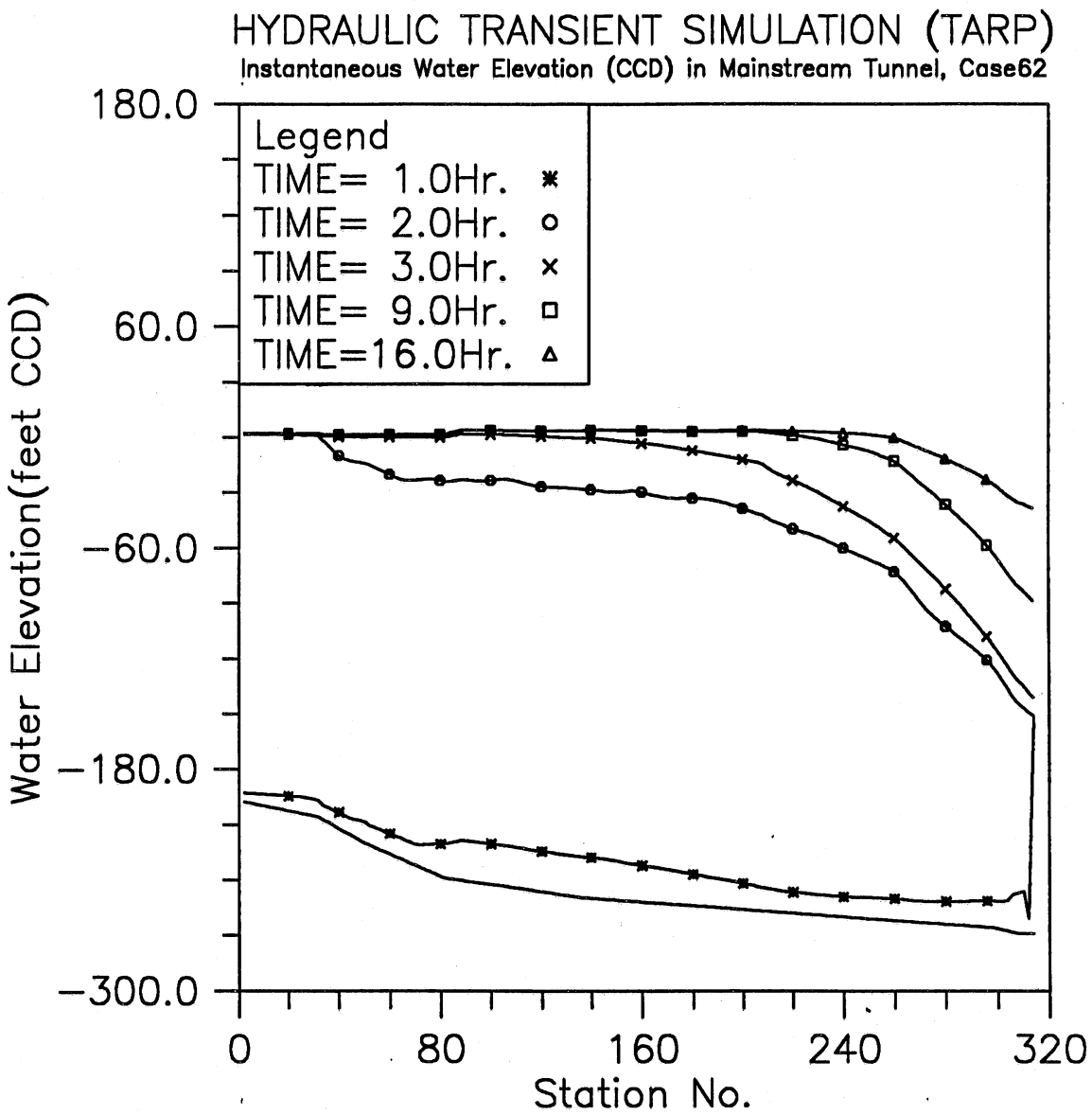

Fig. 3.24(a) Instantaneous hydraulic gradelines along the main tunnel; Modeling case: gate opening at half tunnel height in 30 min., initial reservoir level at –150, and PMF event (Case 6–2)

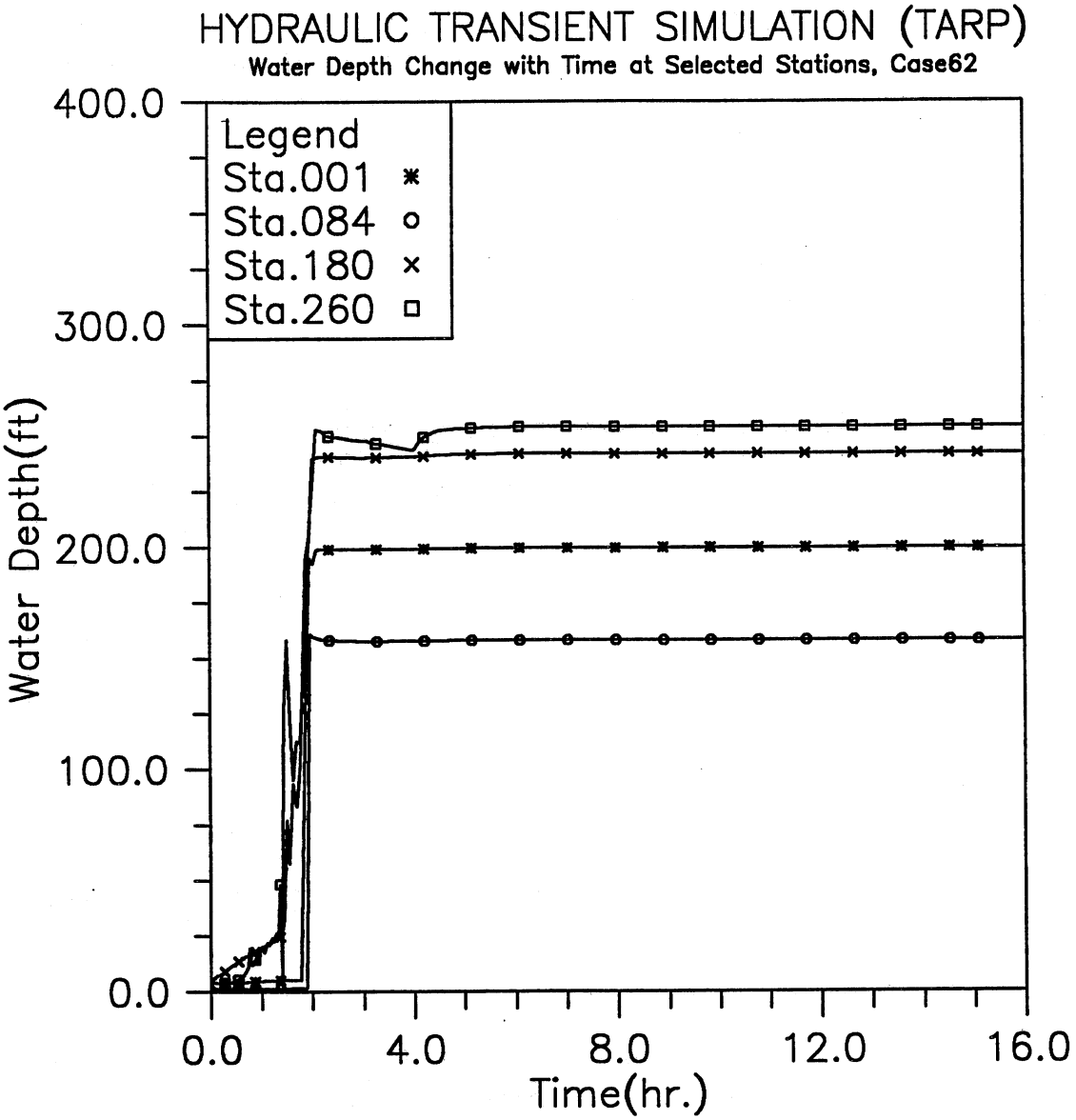

Fig. 3.24(b) Time variation of water depth at four upstream locations; Modeling case: gate opening at half tunnel height in 30 min., initial reservoir level at –150, and PMF event (Case 6–2)

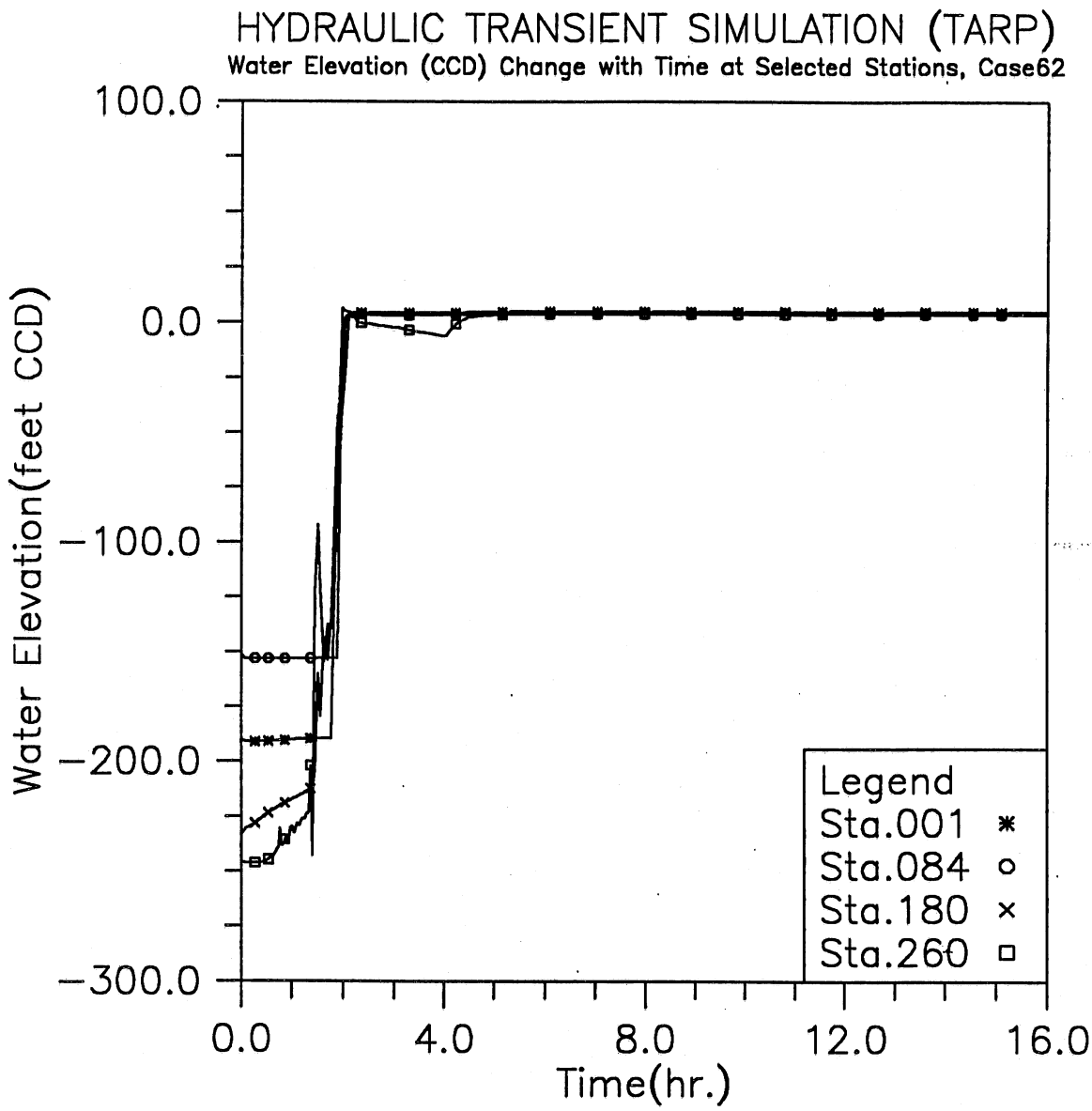

Fig. 3.24(c) Time variation of water elevation at four upstream locations; Modeling case: gate opening at half tunnel height in 30 min., initial reservoir level at −150, and PMF event (Case 6–2)

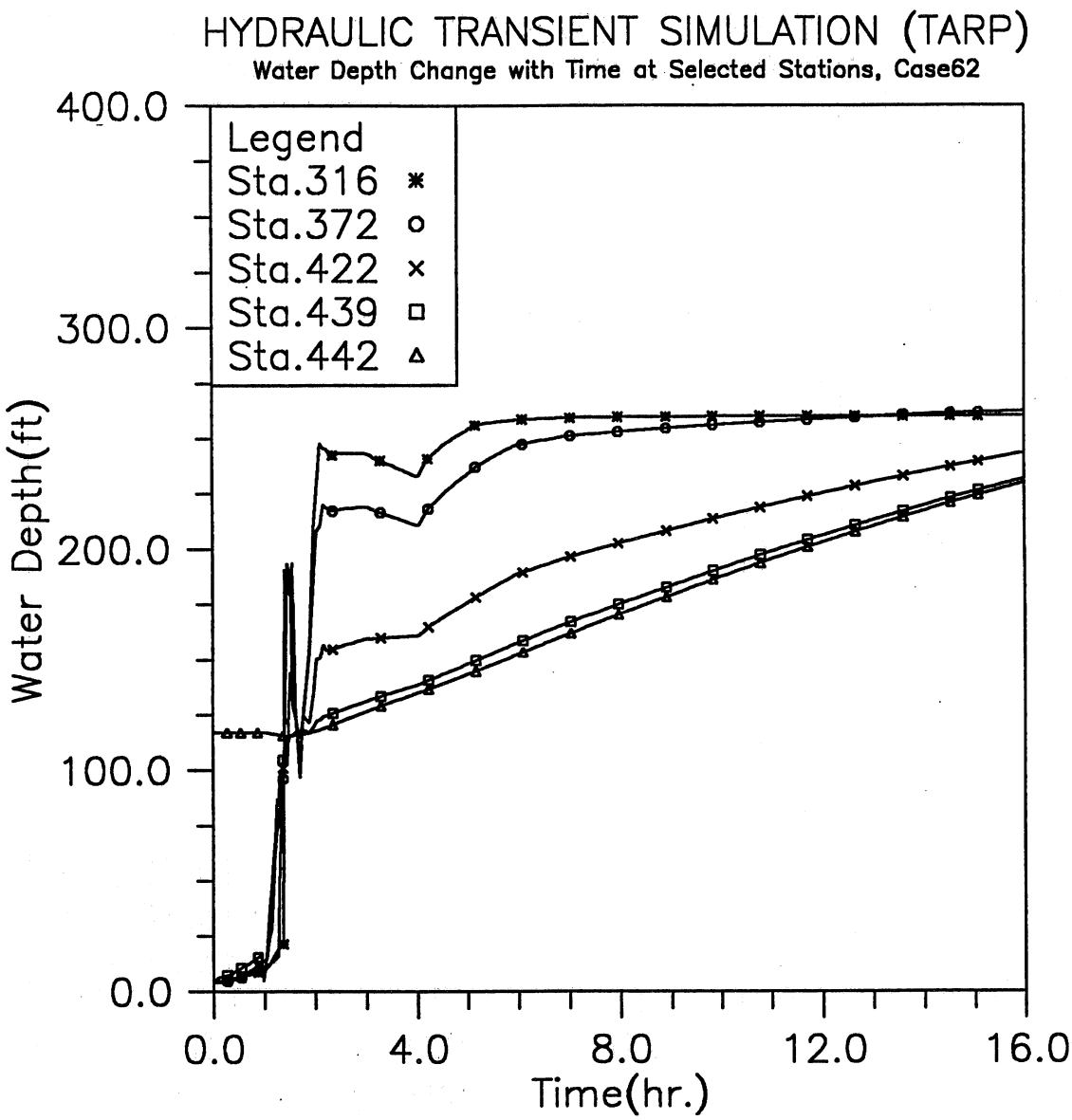

Fig. 3.24(d) Time variation of water depth at five downstream locations; Modeling case: gate opening at half tunnel height in 30 min., initial reservoir level at –150, and PMF event (Case 6–2)

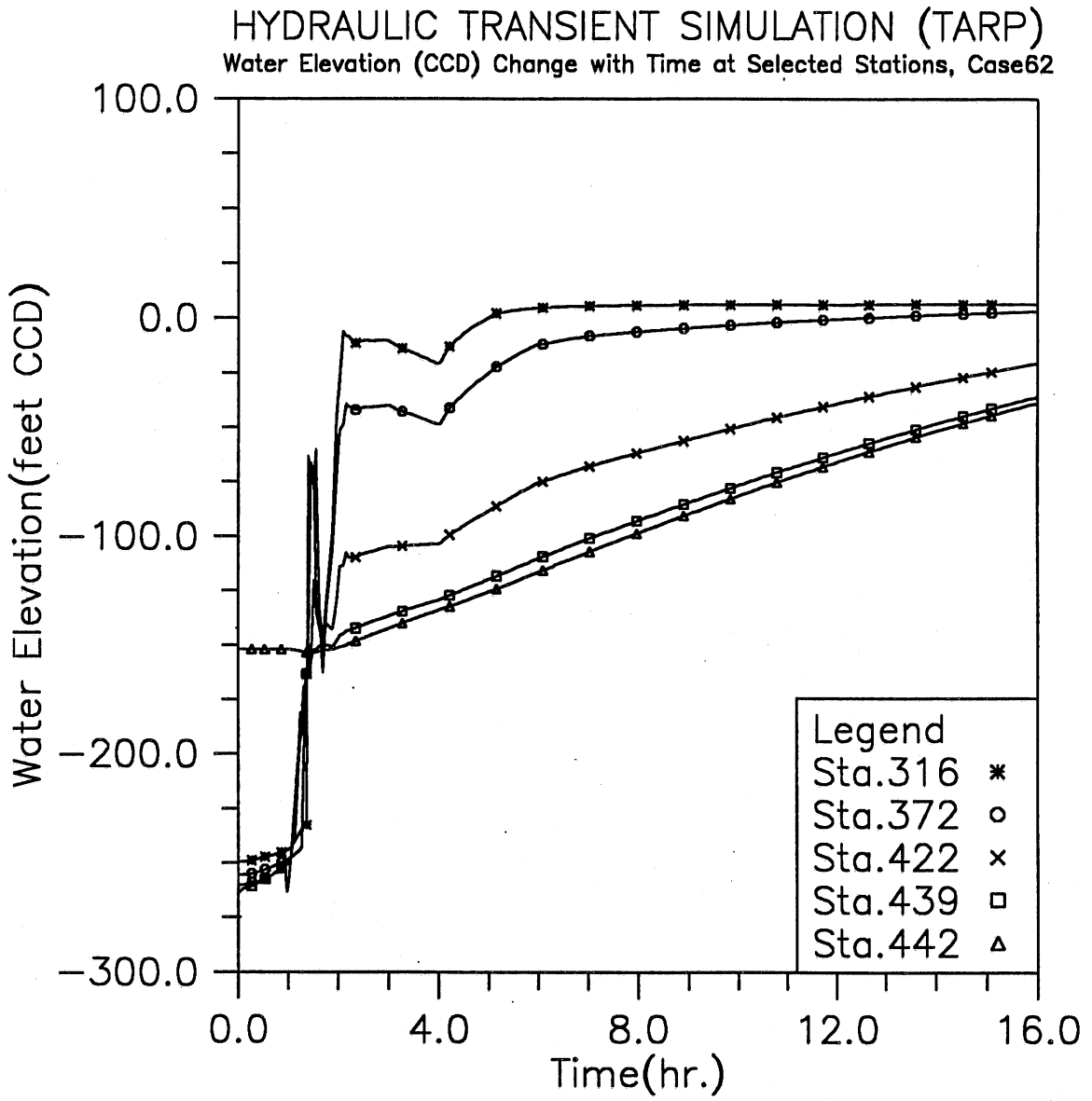

Fig. 3.24(e) Time variation of water elevation at five downstream locations; Modeling case: gate opening at half tunnel height in 30 min., initial reservoir level at −150, and PMF event (Case 6–2)

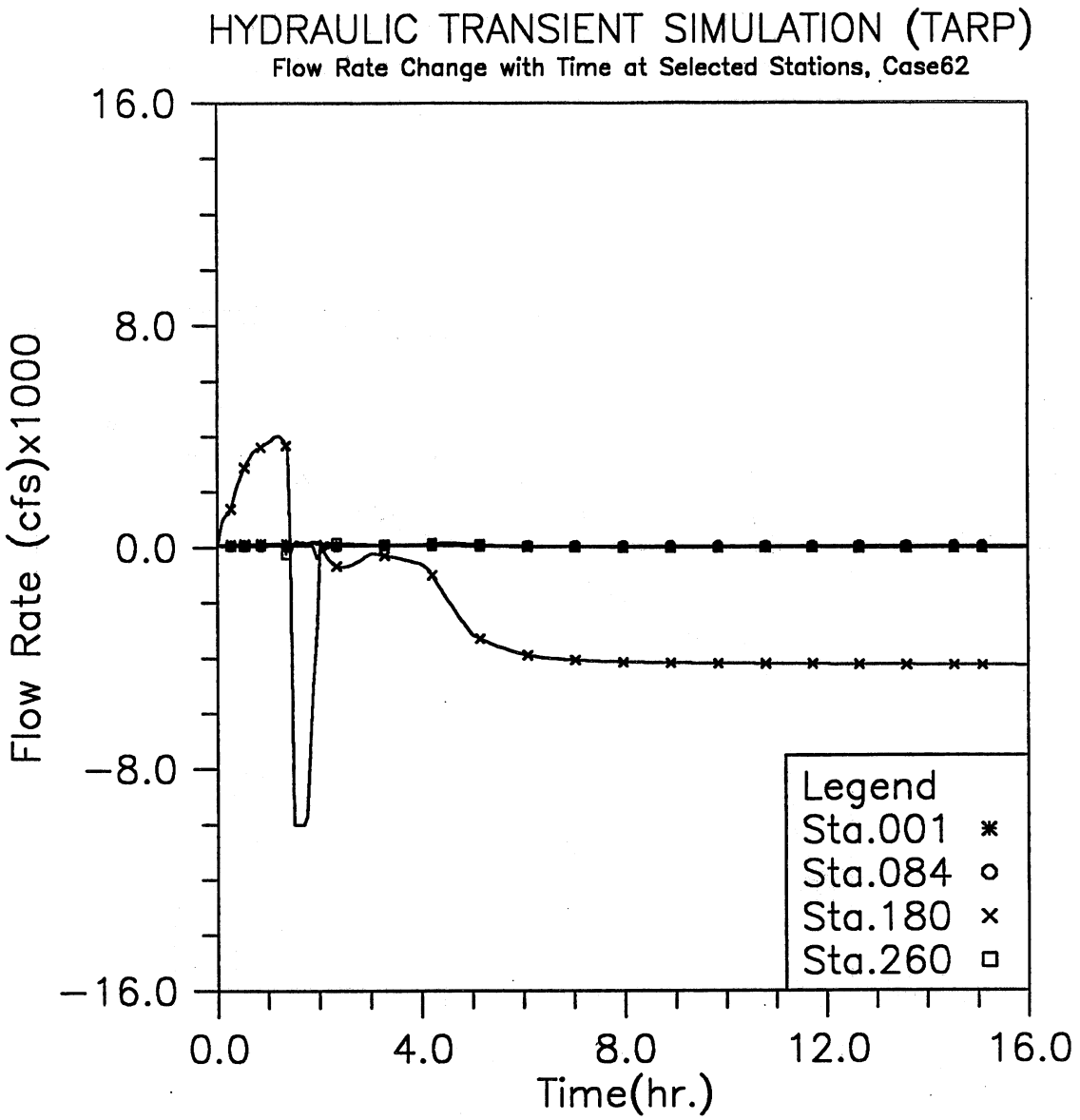

Fig. 3.24(f) Time variation of flow rate at four upstream locations; Modeling case: gate opening at half tunnel height in 30 min., initial reservoir level at −150, and PMF event (Case 6–2)

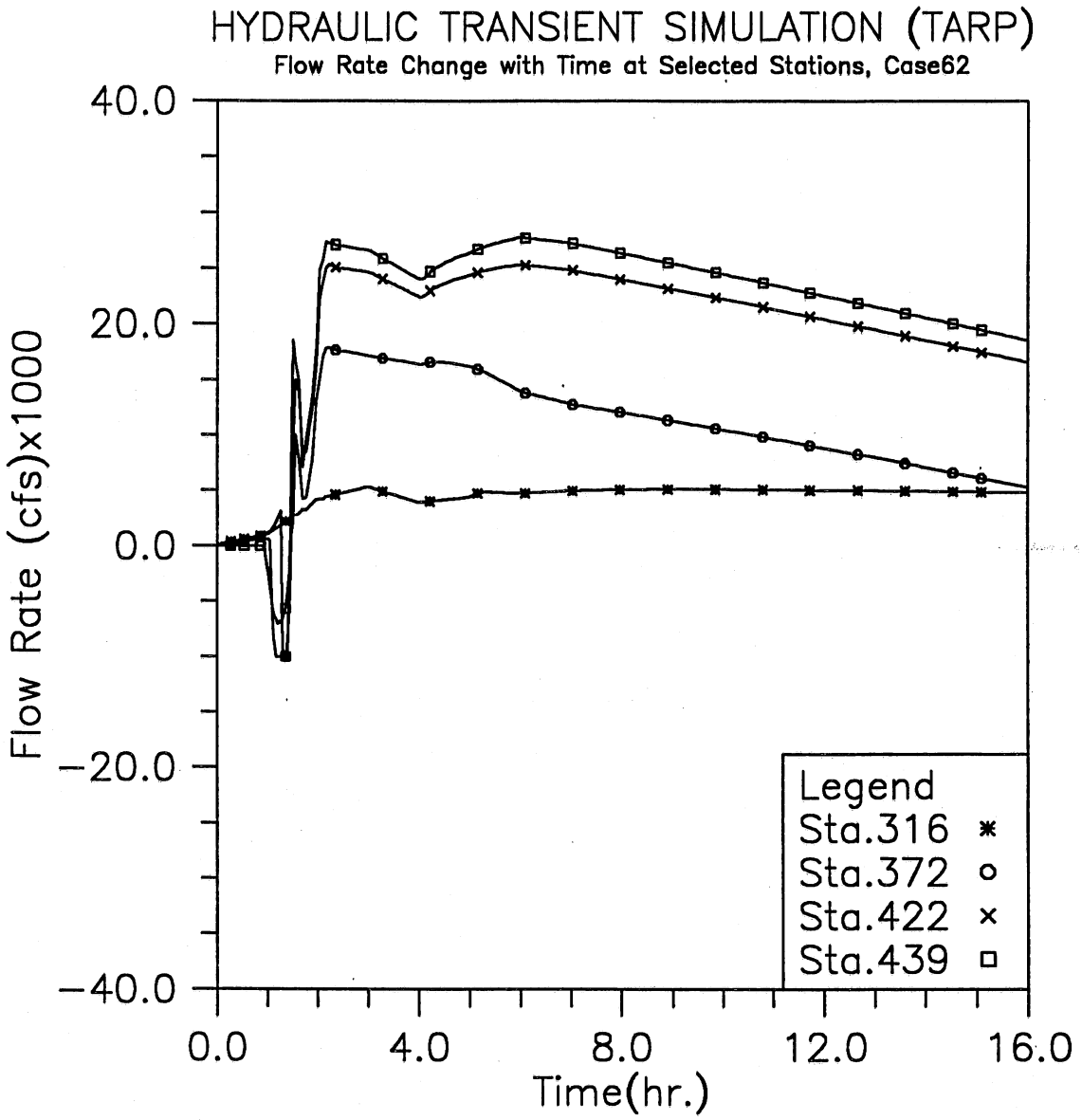

Fig. 3.24(g) Time variation of flow rate at four downstream locations; Modeling case: gate opening at half tunnel height in 30 min., initial reservoir level at –150, and PMF event (Case 6–2)

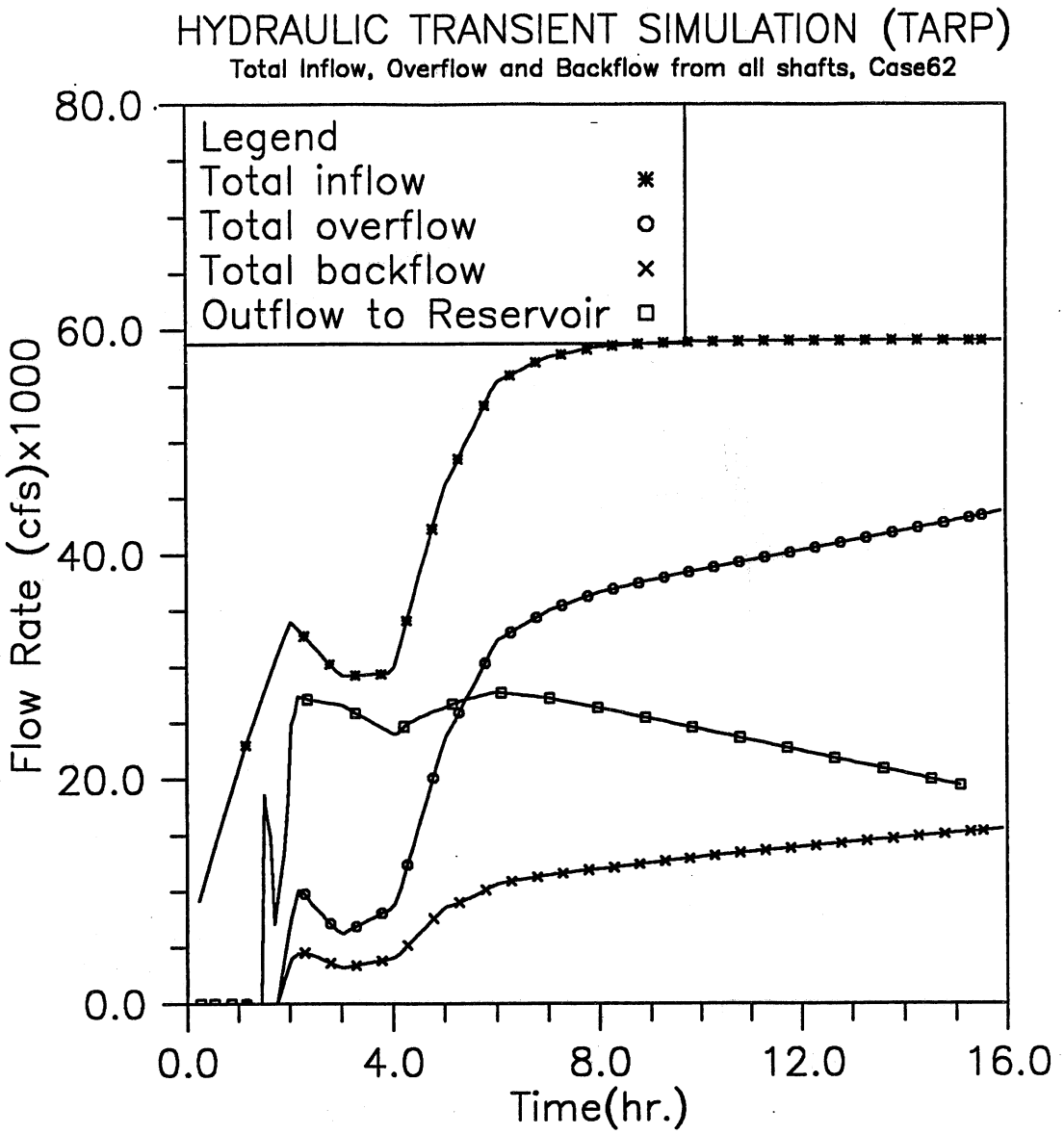

Fig. 3.24(h) Time variation of total inflow, overflow, backflow, and outflow to reservoir; Modeling case: gate opening at half tunnel height in 30 min., initial reservoir level at –150, and PMF event (Case 6–2)

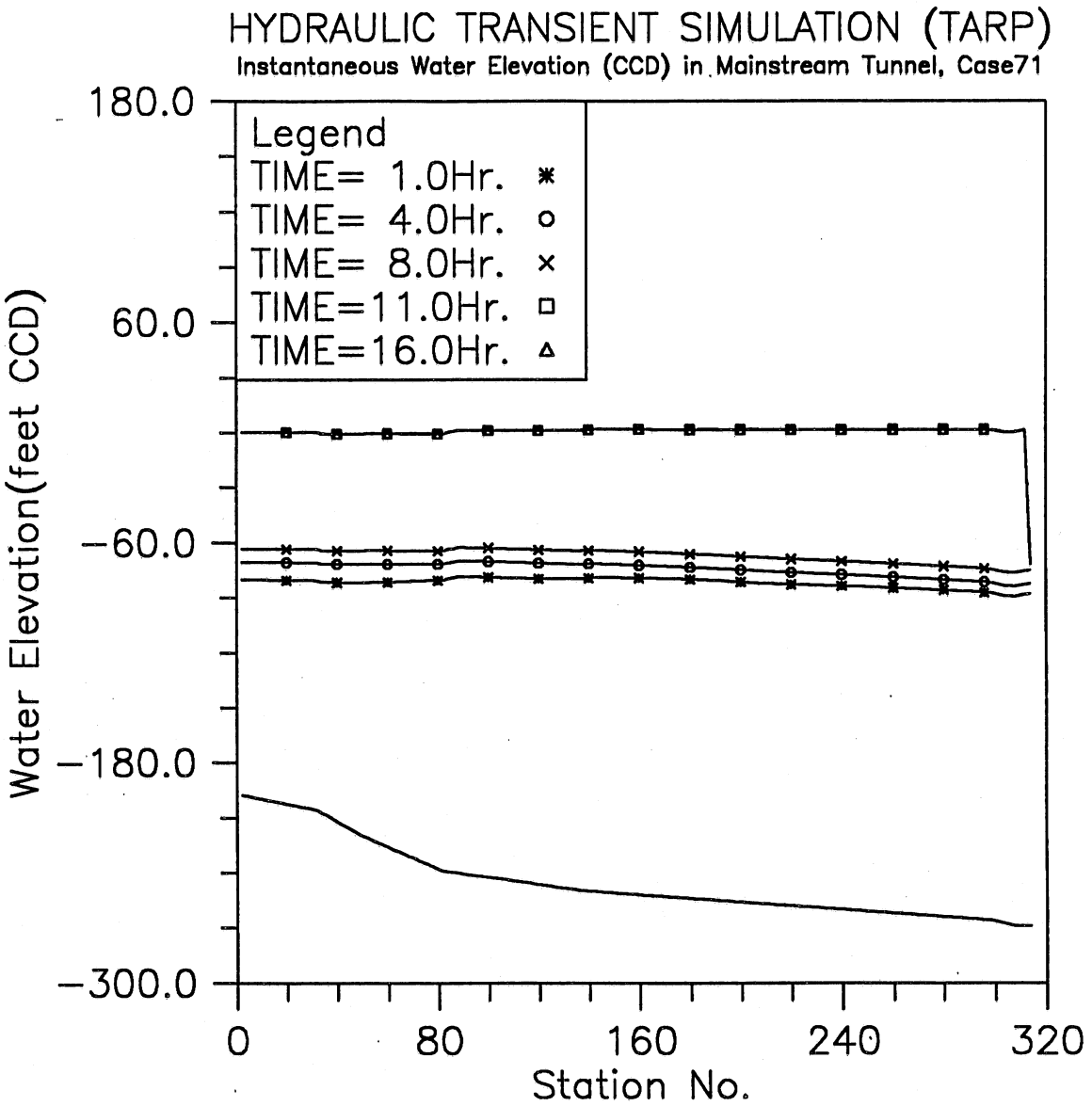

Fig. 3.25(a) Instantaneous hydraulic gradelines along the main tunnel; Modeling case: gate closure in 30 min. after water level in reservoir rises to –70 CCD, initial reservoir level at –88, and steady 5,000 cfs inflow (Case 7–1)

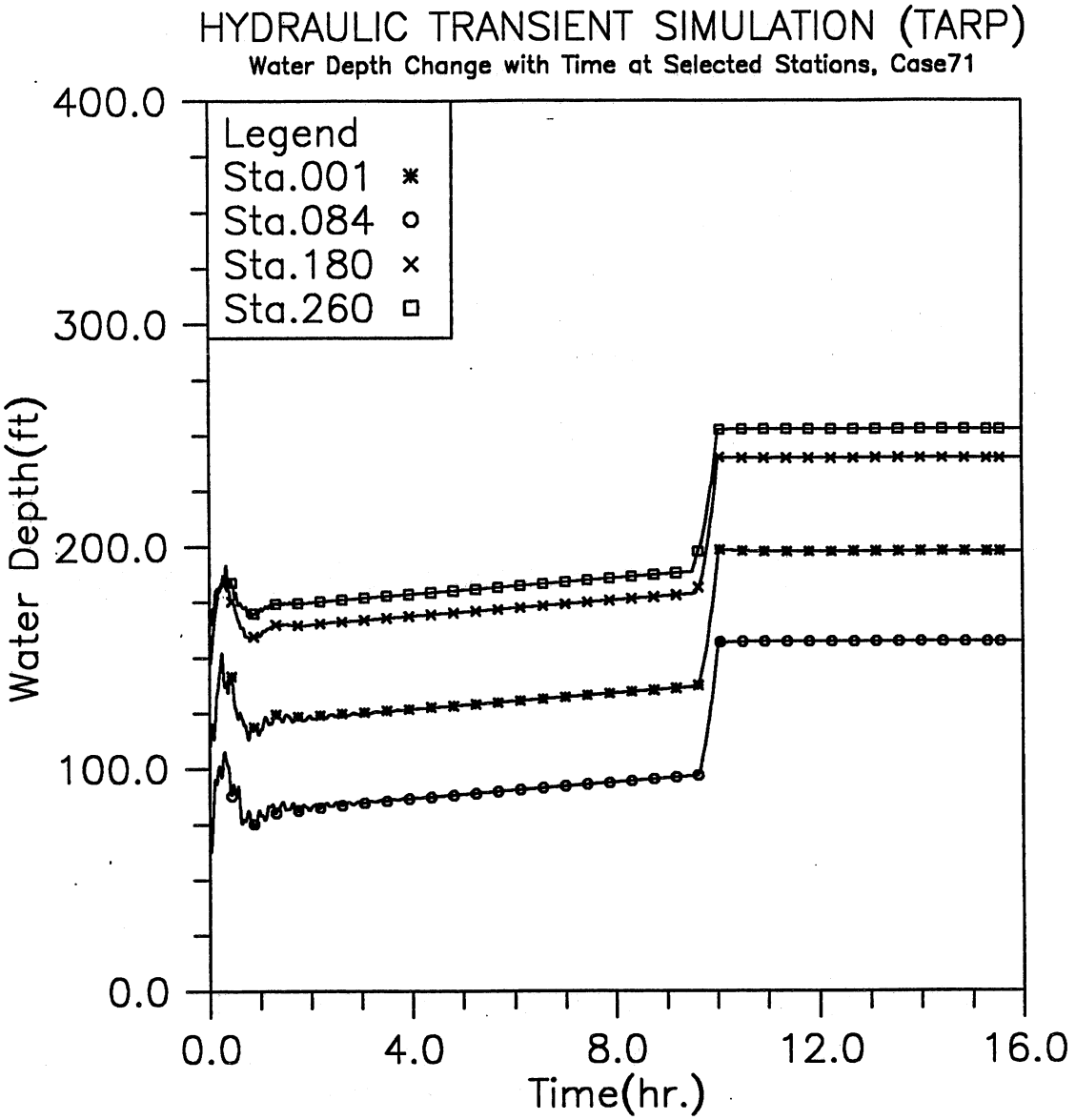

Fig. 3.25(b) Time variation of water depth at four upstream locations; Modeling case: gate closure in 30 min. after water level in reservoir rises to –70 CCD, initial reservoir level at –88, and steady 5,000 cfs inflow (Case 7–1)

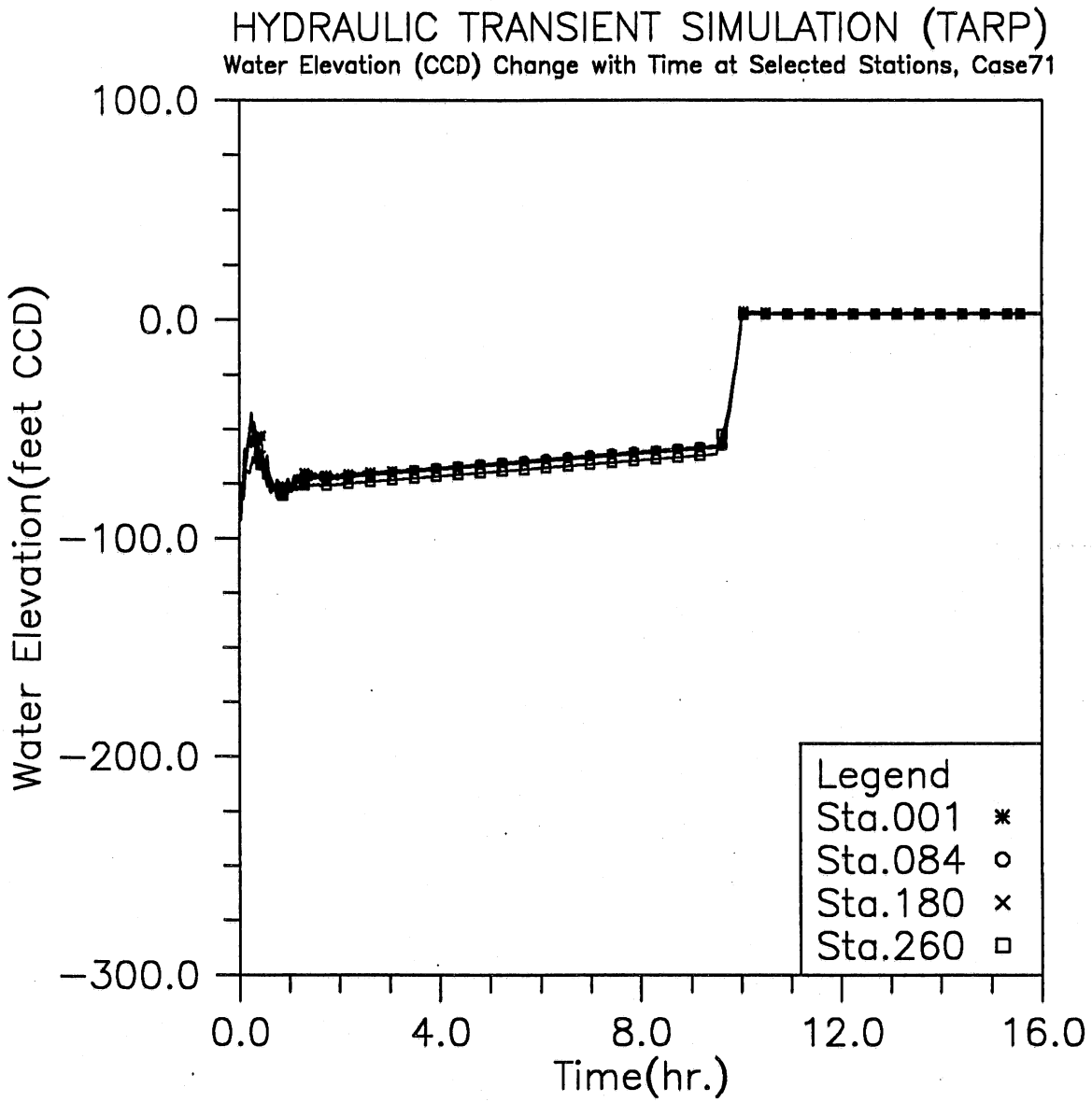

Fig. 3.25(c) Time variation of water elevation at four upstream locations; Modeling case: gate closure in 30 min. after water level in reservoir rises to –70 CCD, initial reservoir level at –88, and steady 5,000 cfs inflow (Case 7–1)

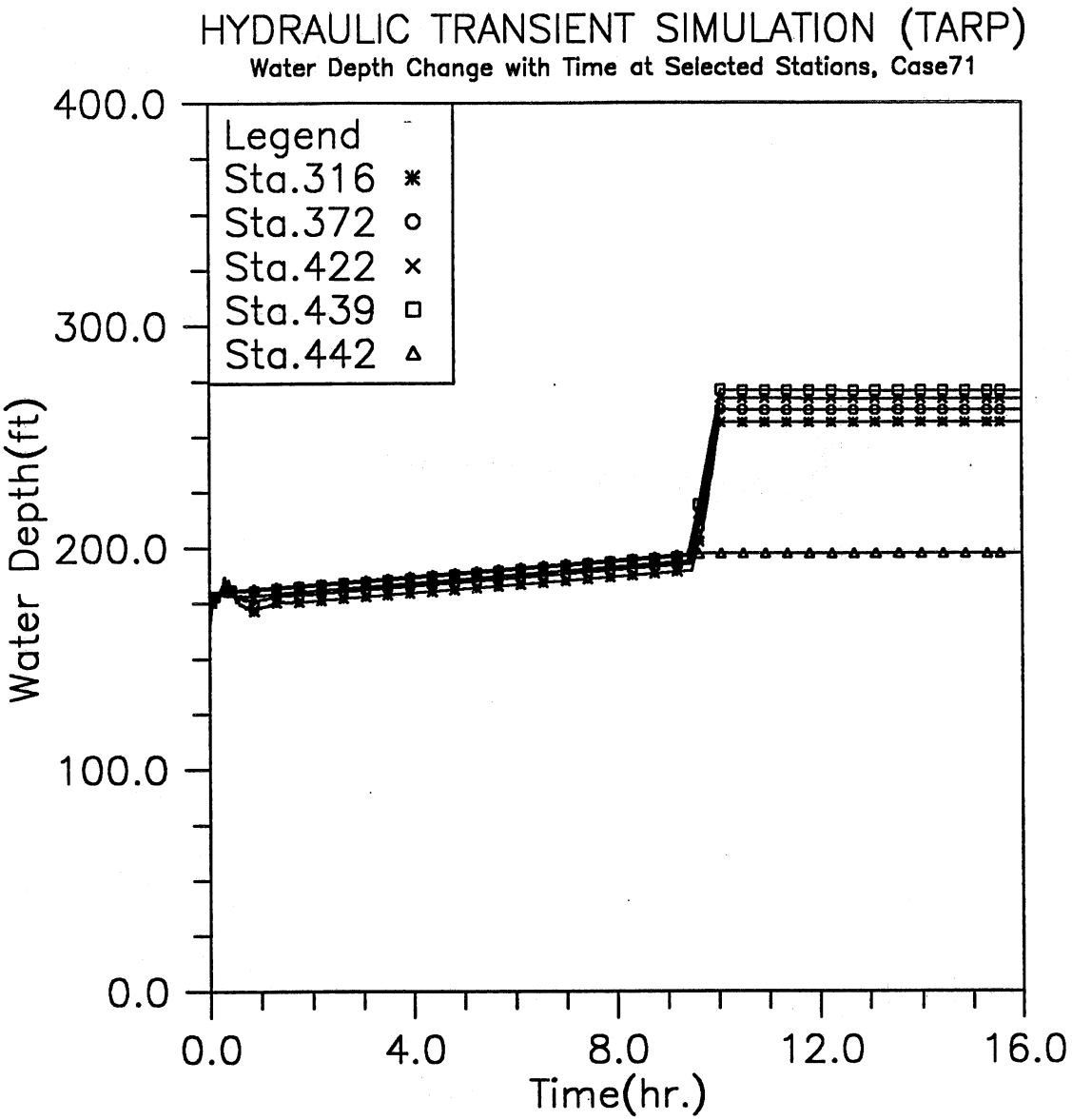

Fig. 3.25(d) Time variation of water depth at five downstream locations; Modeling case: gate closure in 30 min. after water level in reservoir rises to –70 CCD, initial reservoir level at –88, and steady 5,000 cfs inflow (Case 7–1)

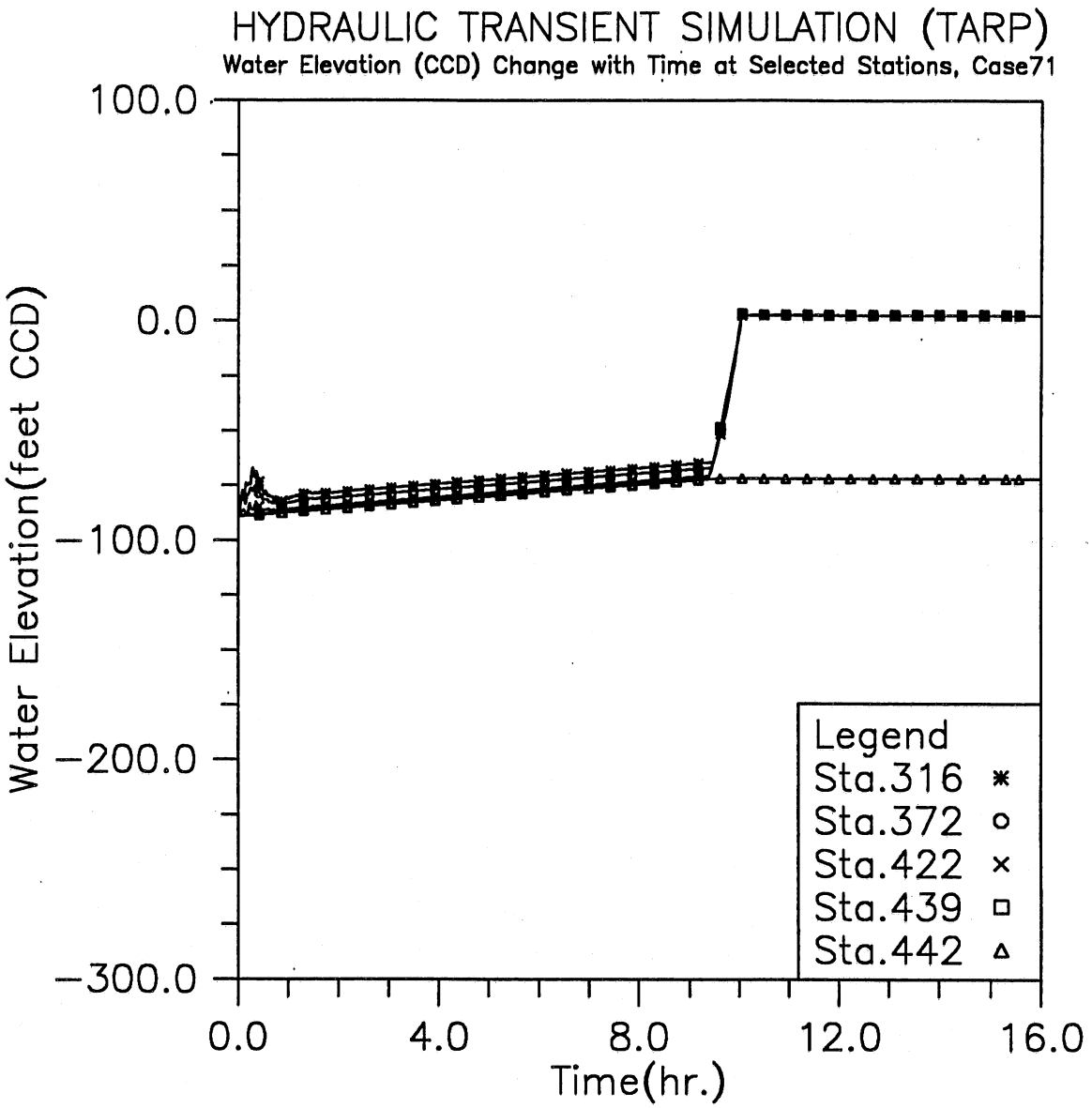

Fig. 3.25(e) Time variation of water elevation at five downstream locations; Modeling case: gate closure in 30 min. after water level in reservoir rises to –70 CCD, initial reservoir level at –88, and steady 5,000 cfs inflow (Case 7–1)

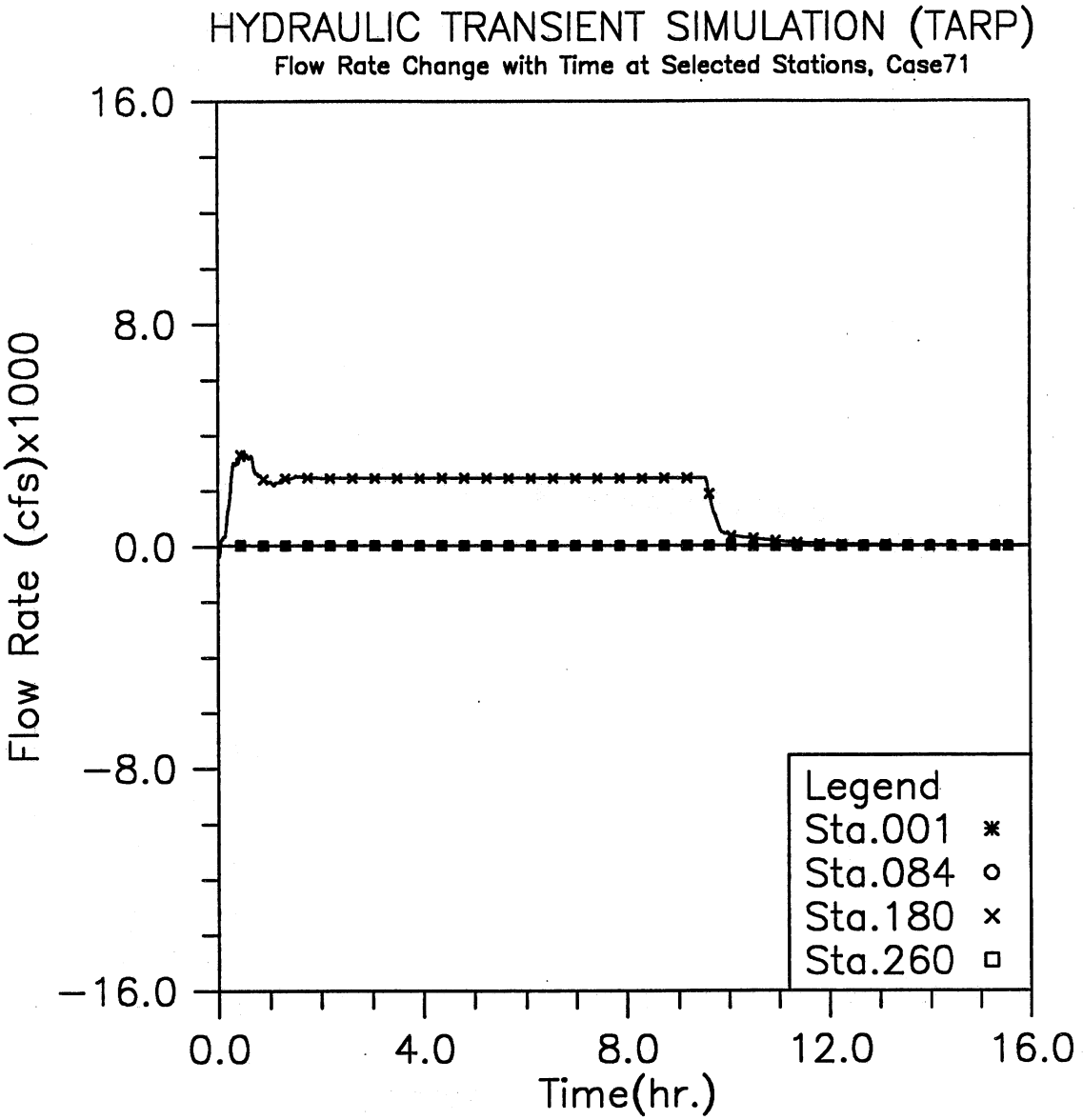

Fig. 3.25(f) Time variation of flow rate at four upstream locations; Modeling case: gate closure in 30 min. after water level in reservoir rises to –70 CCD, initial reservoir level at –88, and steady 5,000 cfs inflow (Case 7–1)

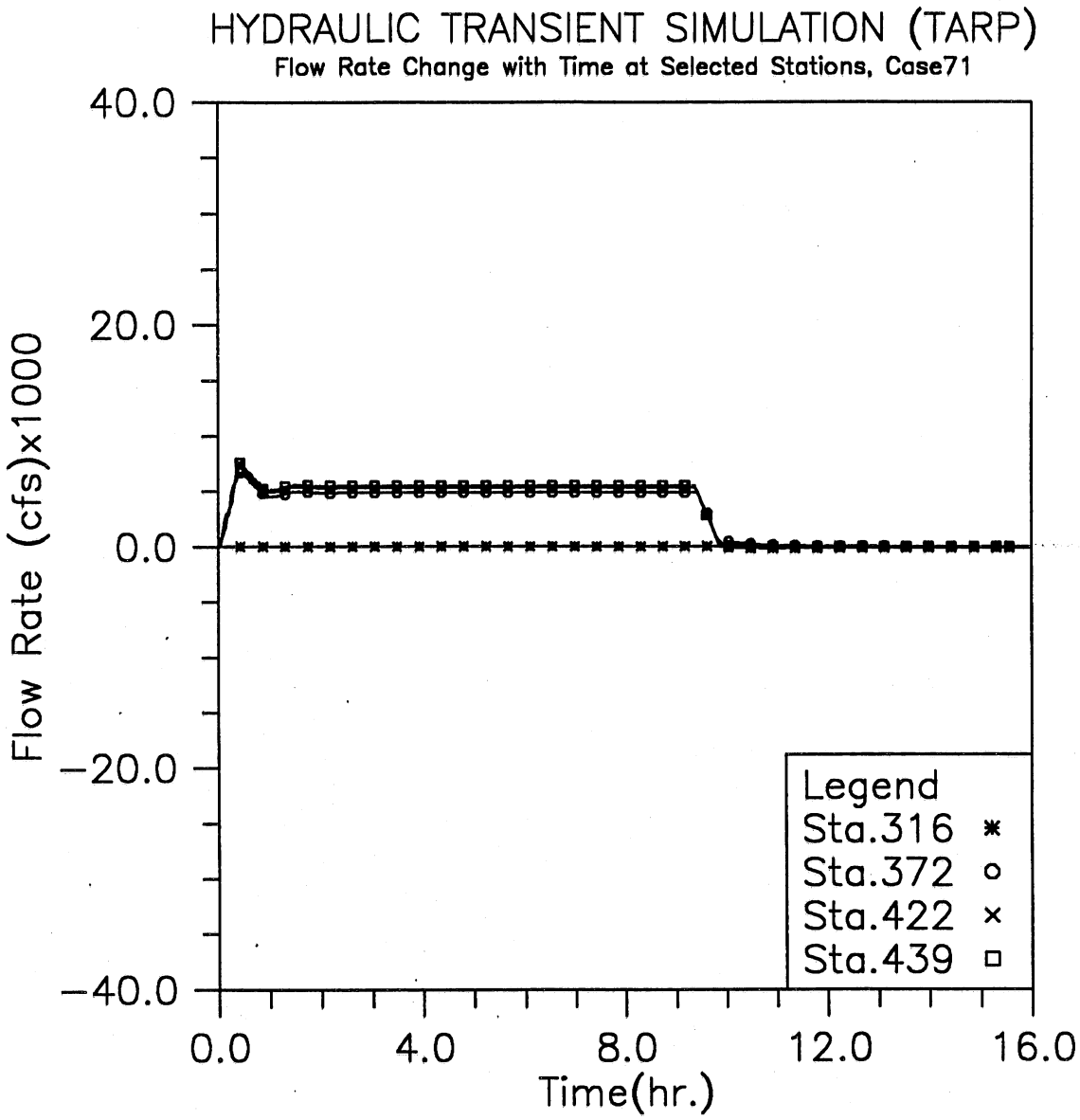

Fig. 3.25(g) Time variation of flow rate at four downstream locations; Modeling case: gate closure in 30 min. after water level in reservoir rises to –70 CCD, initial reservoir level at –88, and steady 5,000 cfs inflow (Case 7–1)

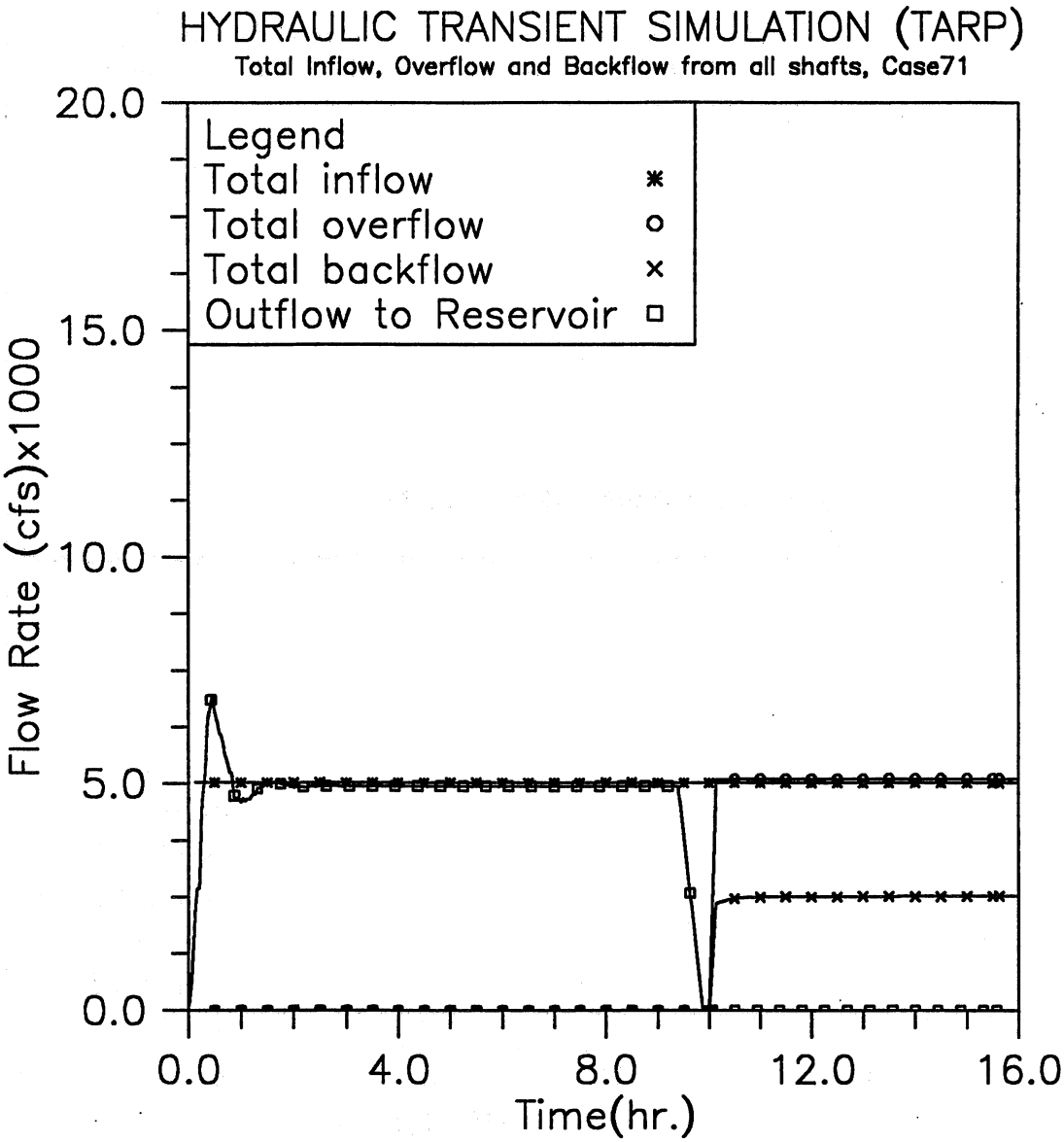

Fig. 3.25(h) Time variation of total inflow, overflow, backflow, and outflow to reservoir; Modeling case: gate closure in 30 min. after water level in reservoir rises to –70 CCD, initial reservoir level at –88, and steady 5,000 cfs inflow (Case 7–1)

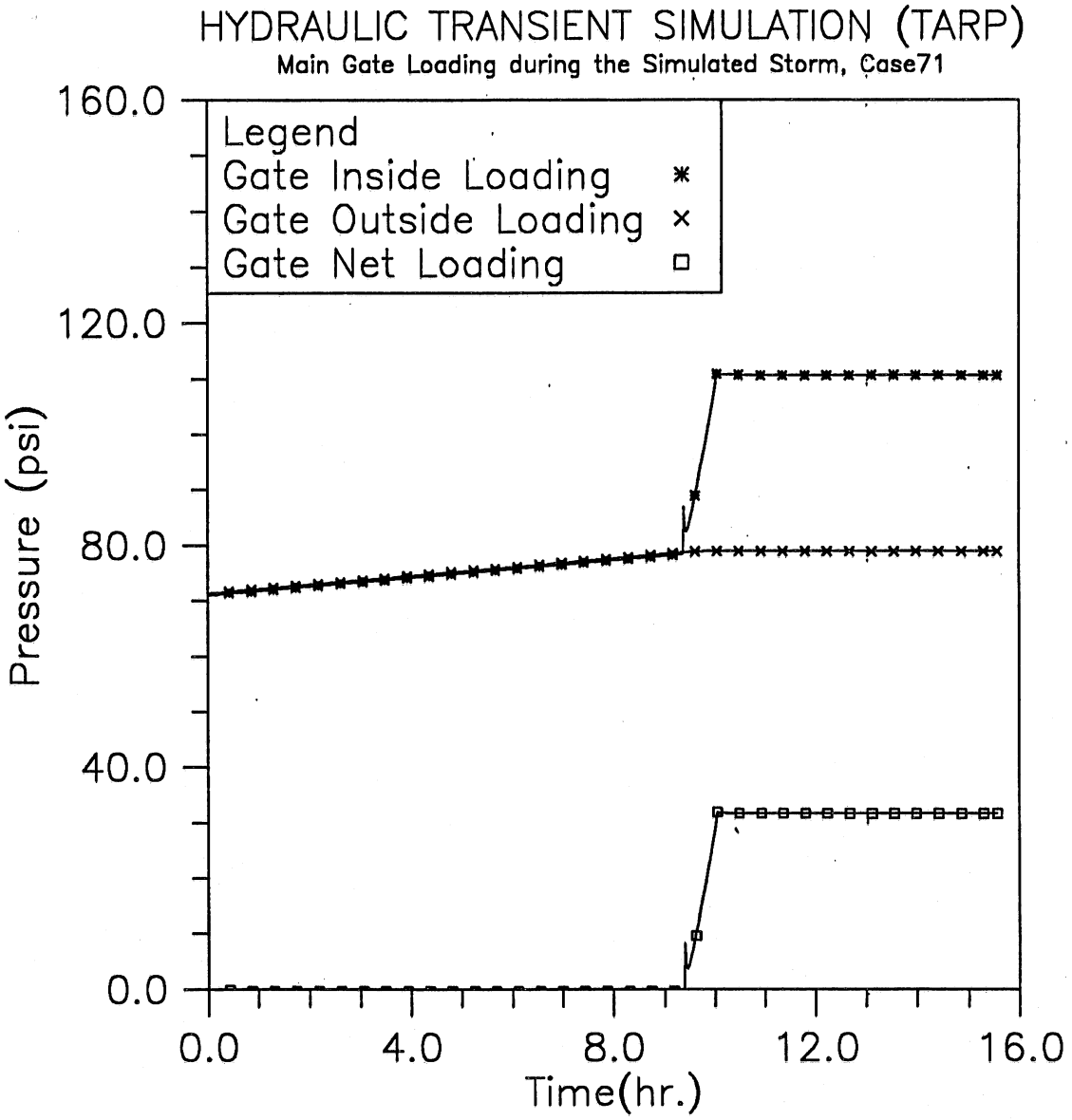

Fig. 3.25(i) Time variation of the averaged loading on the main gate; Modeling case: gate closure in 30 min. after water level in reservoir rises to –70 CCD, initial reservoir level at –88, and steady 5,000 cfs inflow (Case 7–1)

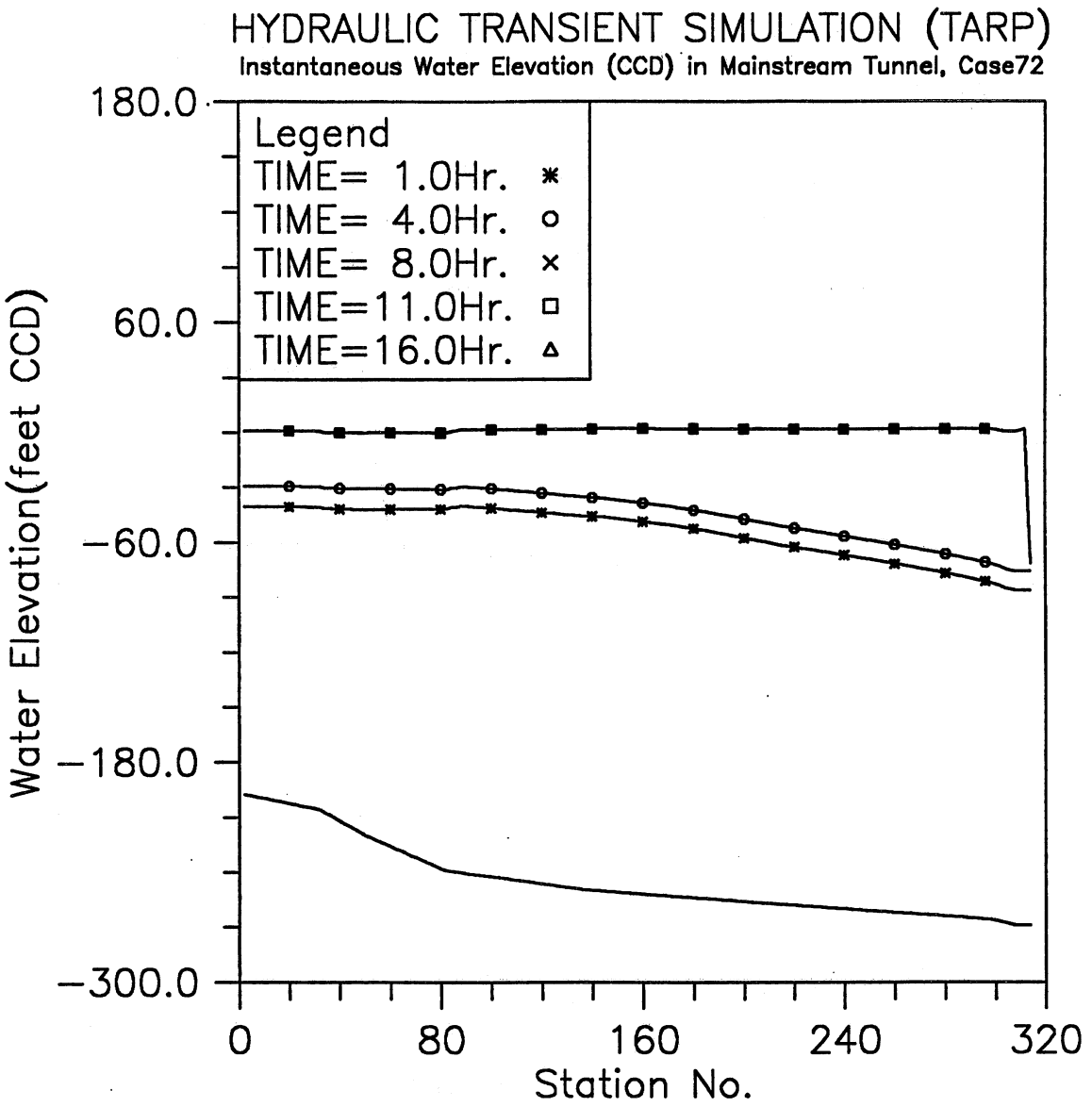

Fig. 3.26(a) Instantaneous hydraulic gradelines along the main tunnel; Modeling case: gate closure in 30 min. after water level in reservoir rises to –70 CCD, initial reservoir level at –88, and steady 10,000 cfs inflow (Case 7–2)

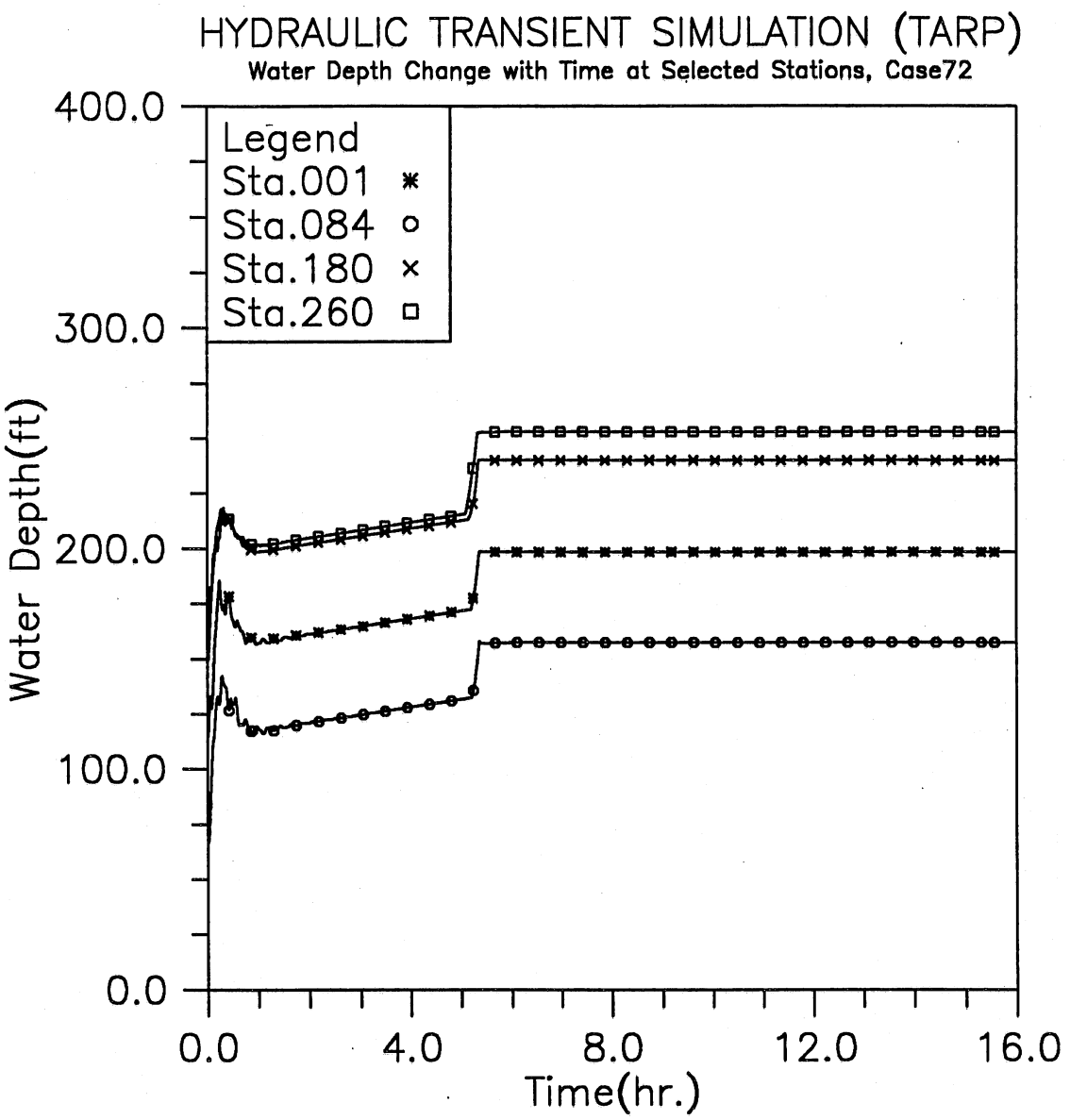

Fig. 3.26(b) Time variation of water depth at four upstream locations; Modeling case: gate closure in 30 min. after water level in reservoir rises to –70 CCD, initial reservoir level at –88, and steady 10,000 cfs inflow (Case 7–2)

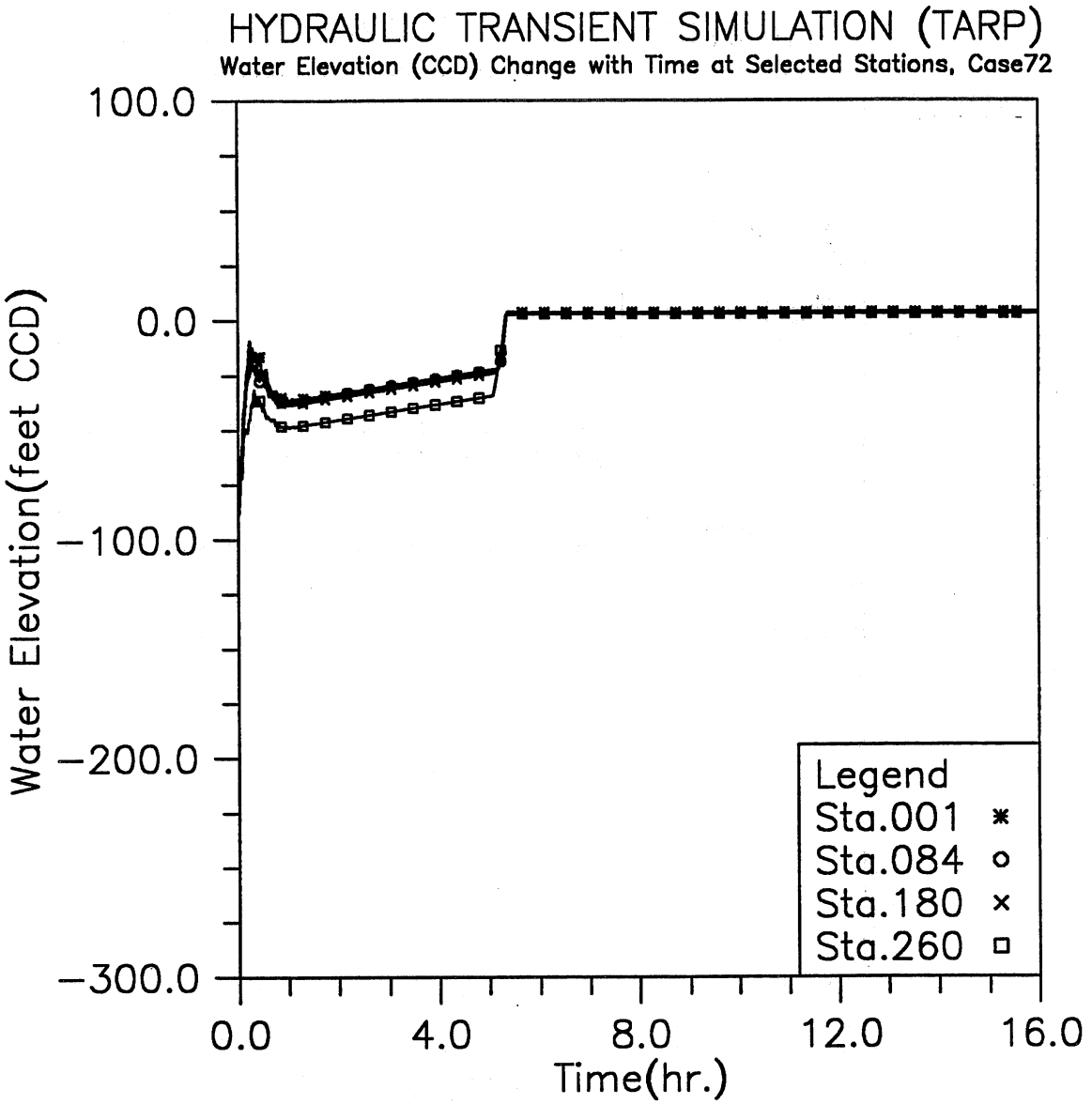

Fig. 3.26(c) Time variation of water elevation at four upstream locations; Modeling case: gate closure in 30 min. after water level in reservoir rises to –70 CCD, initial reservoir level at –88, and steady 10,000 cfs inflow (Case 7–2)

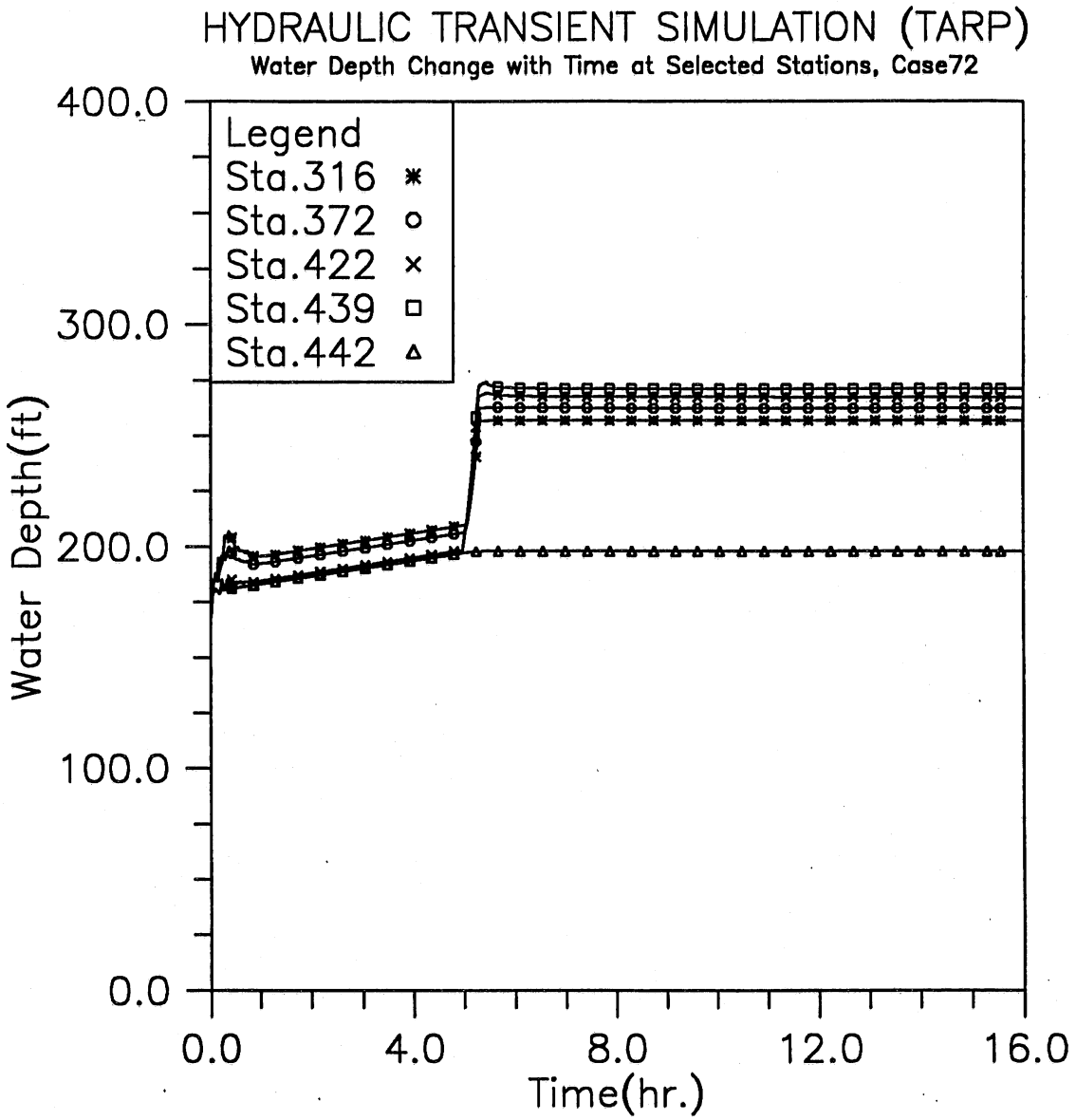

Fig. 3.26(d) Time variation of water depth at five downstream locations; Modeling case: gate closure in 30 min. after water level in reservoir rises to –70 CCD, initial reservoir level at –88, and steady 10,000 cfs inflow (Case 7–2)

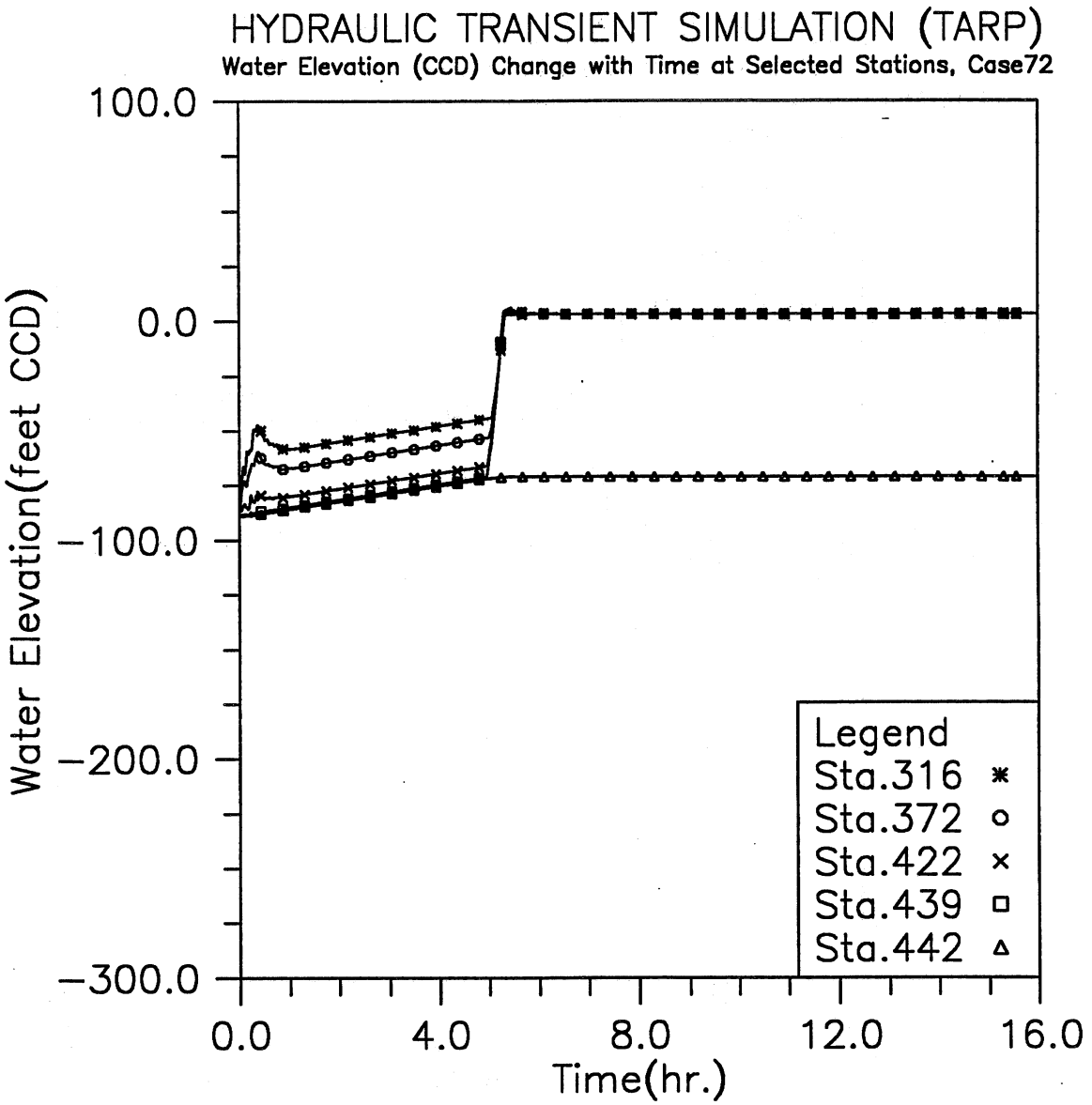

Fig. 3.26(e) Time variation of water elevation at five downstream locations; Modeling case: gate closure in 30 min. after water level in reservoir rises to –70 CCD, initial reservoir level at –88, and steady 10,000 cfs inflow (Case 7–2)

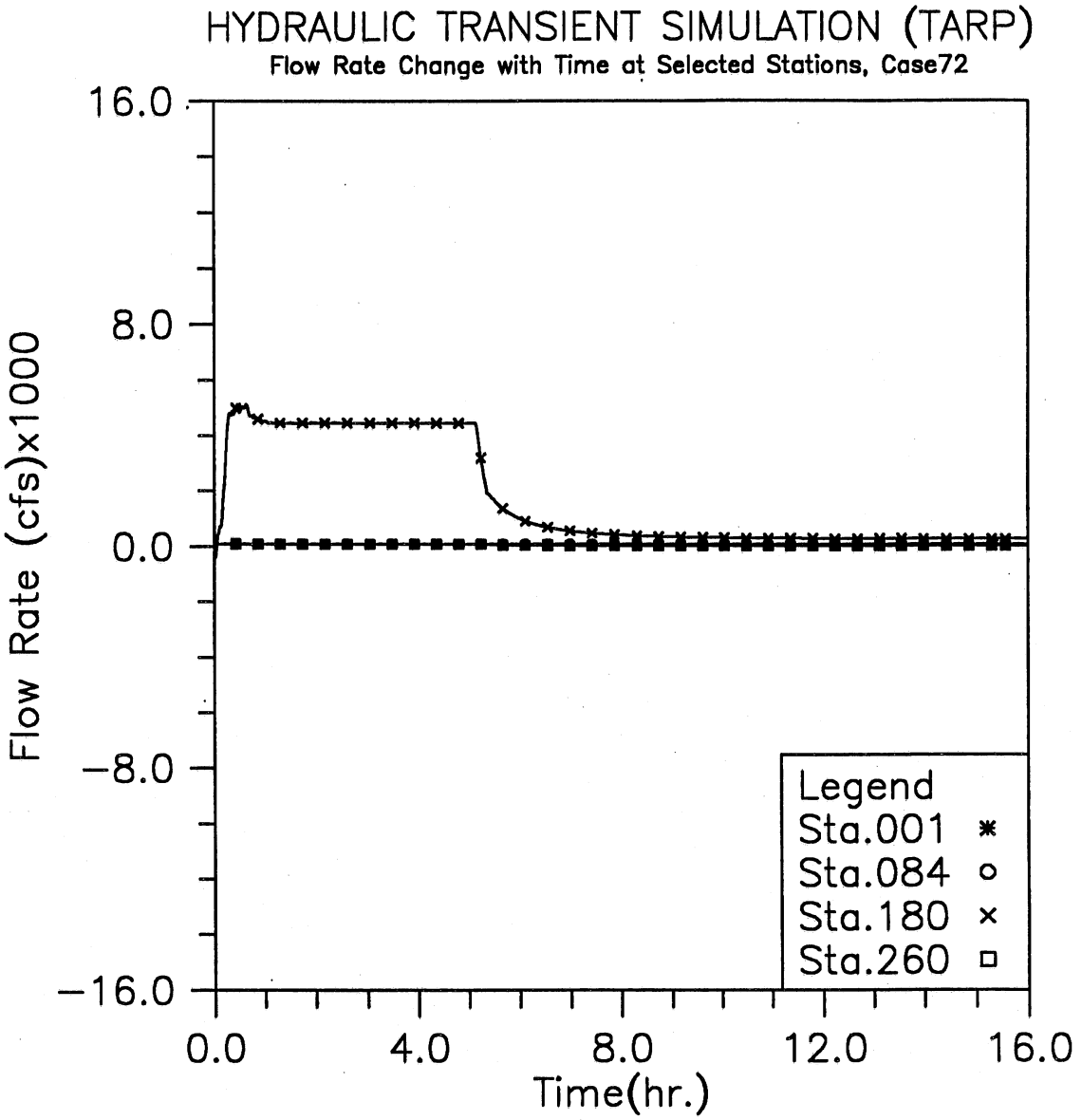

Fig. 3.26(f) Time variation of flow rate at four upstream locations; Modeling case: gate closure in 30 min. after water level in reservoir rises to –70 CCD, initial reservoir level at –88, and steady 10,000 cfs inflow (Case 7–2)

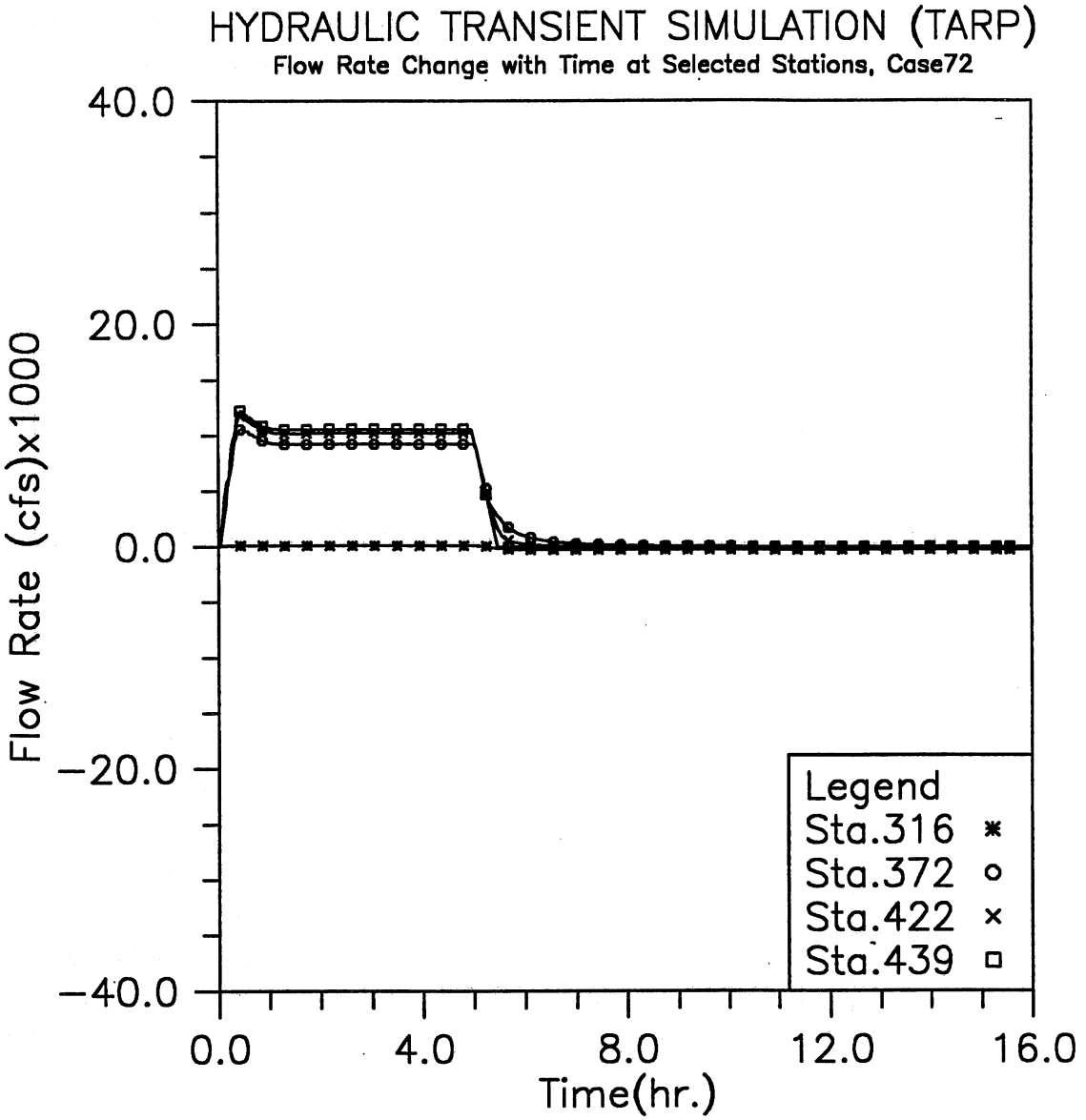

Fig. 3.26(g) Time variation of flow rate at four downstream locations; Modeling case: gate closure in 30 min. after water level in reservoir rises to –70 CCD, initial reservoir level at –88, and steady 10,000 cfs inflow (Case 7–2)

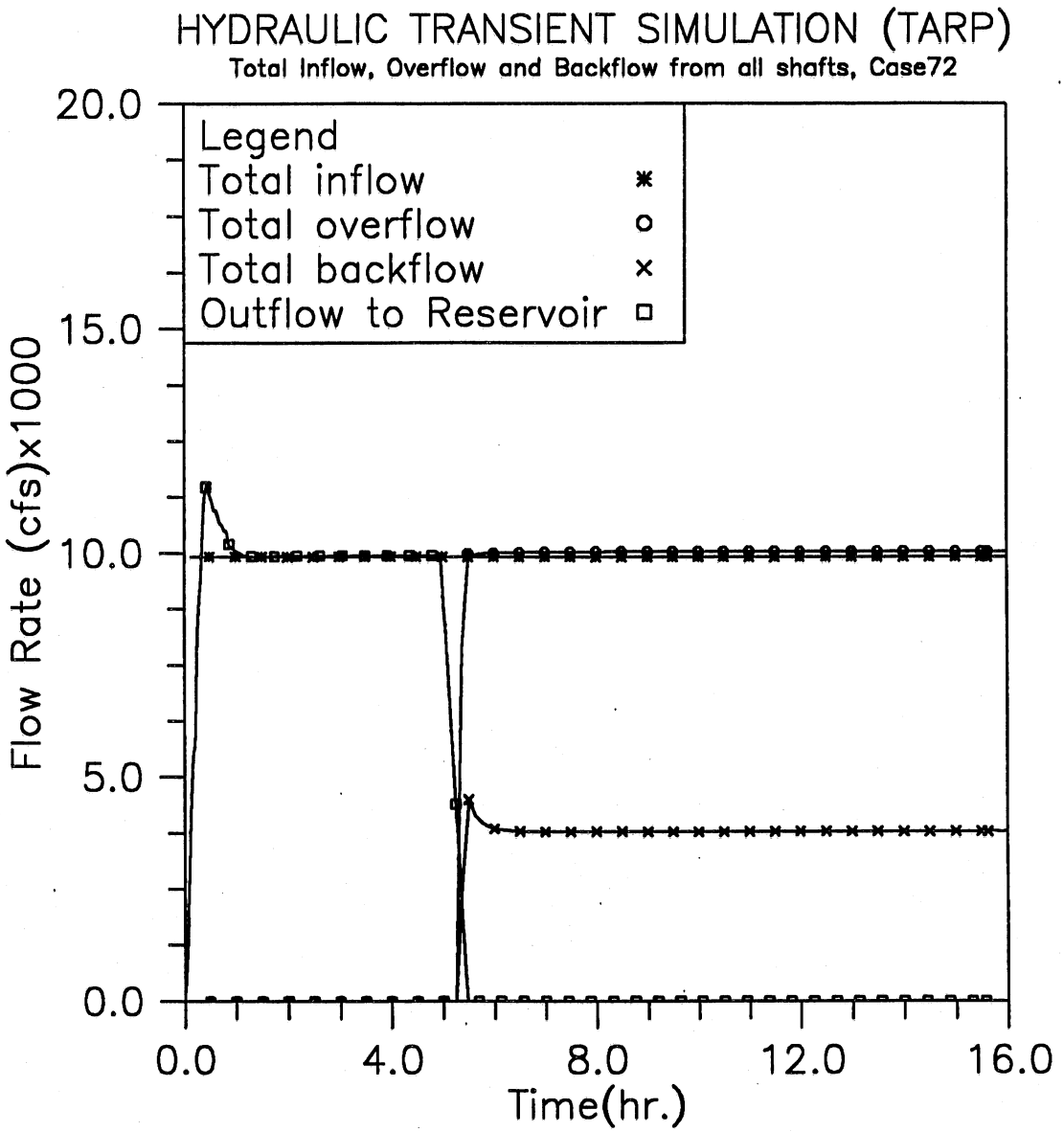

Fig. 3.26(h) Time variation of total inflow, overflow, backflow, and outflow to reservoir; Modeling case: gate closure in 30 min. after water level in reservoir rises to –70 CCD, initial reservoir level at –88, and steady 10,000 cfs inflow (Case 7–2)

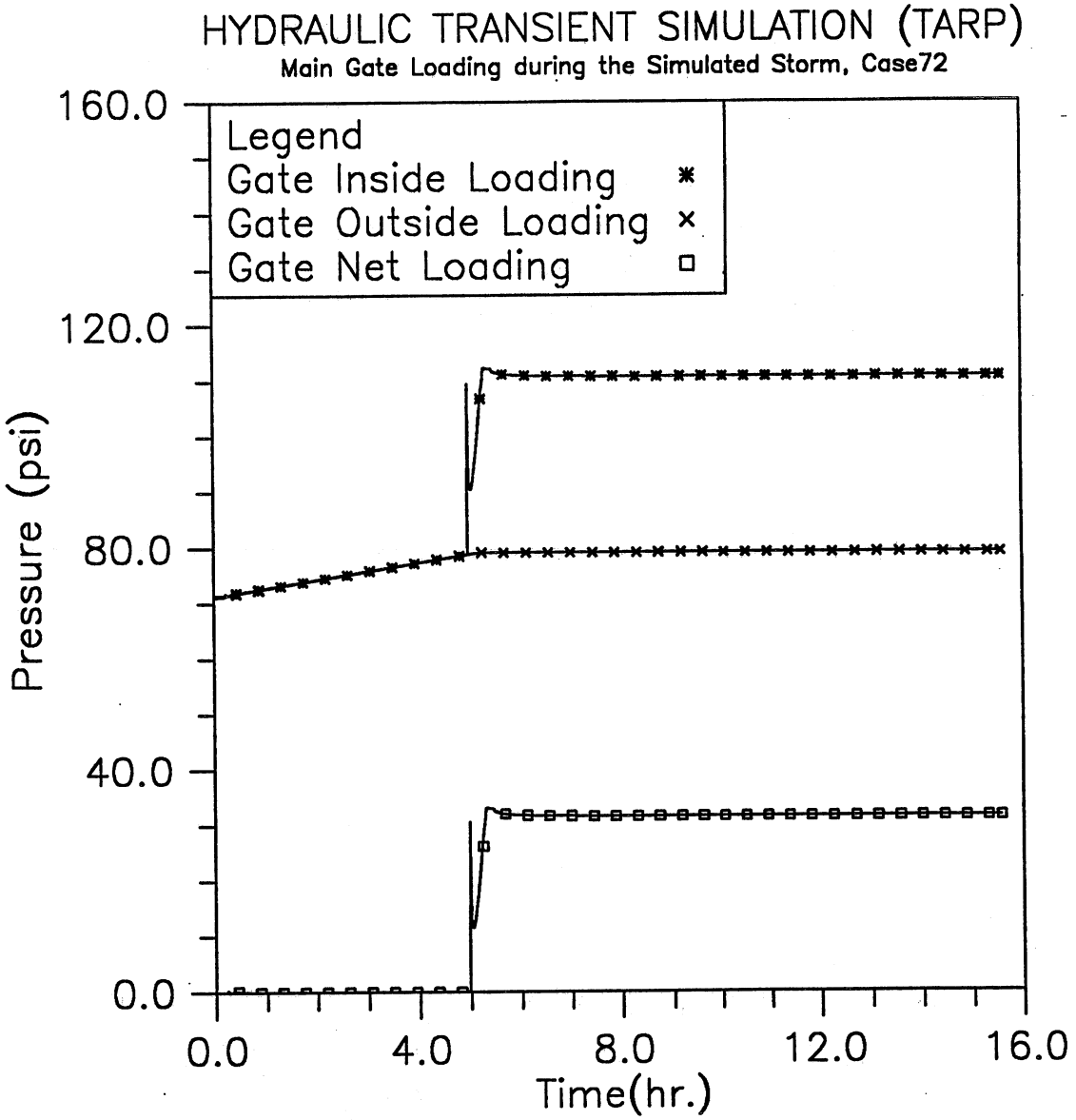

Fig. 3.26(i) Time variation of the averaged loading on the main gate; Modeling case: gate closure in 30 min. after water level in reservoir rises to –70 CCD, initial reservoir level at –88, and steady 10,000 cfs inflow (Case 7–2)

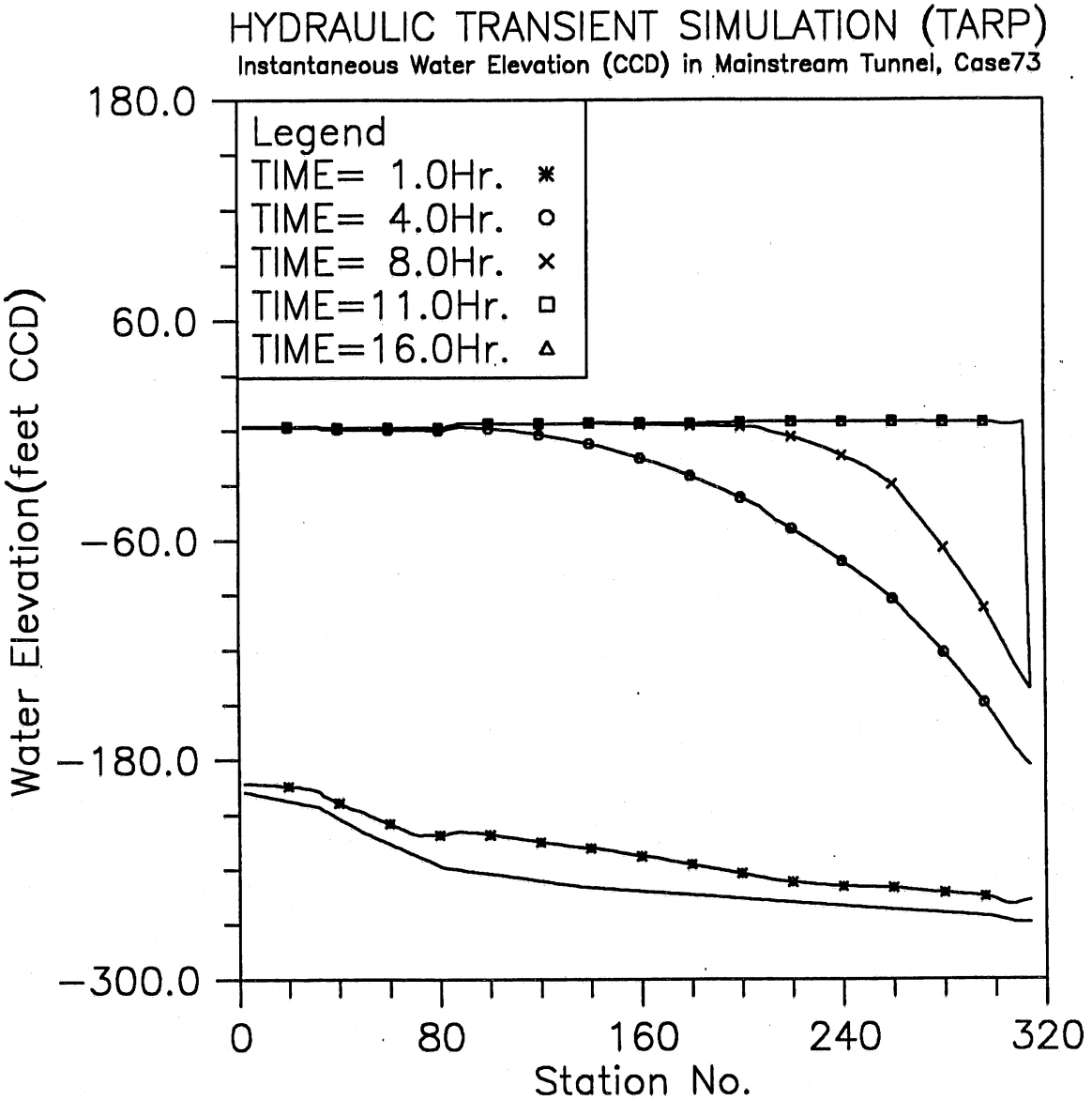

Fig. 3.27(a) Instantaneous hydraulic gradelines along the main tunnel; Modeling case: gate closure in 30 min. after total inflow reaches the maximum value, initially empty reservoir, and PMF storm event (Case 7–3)

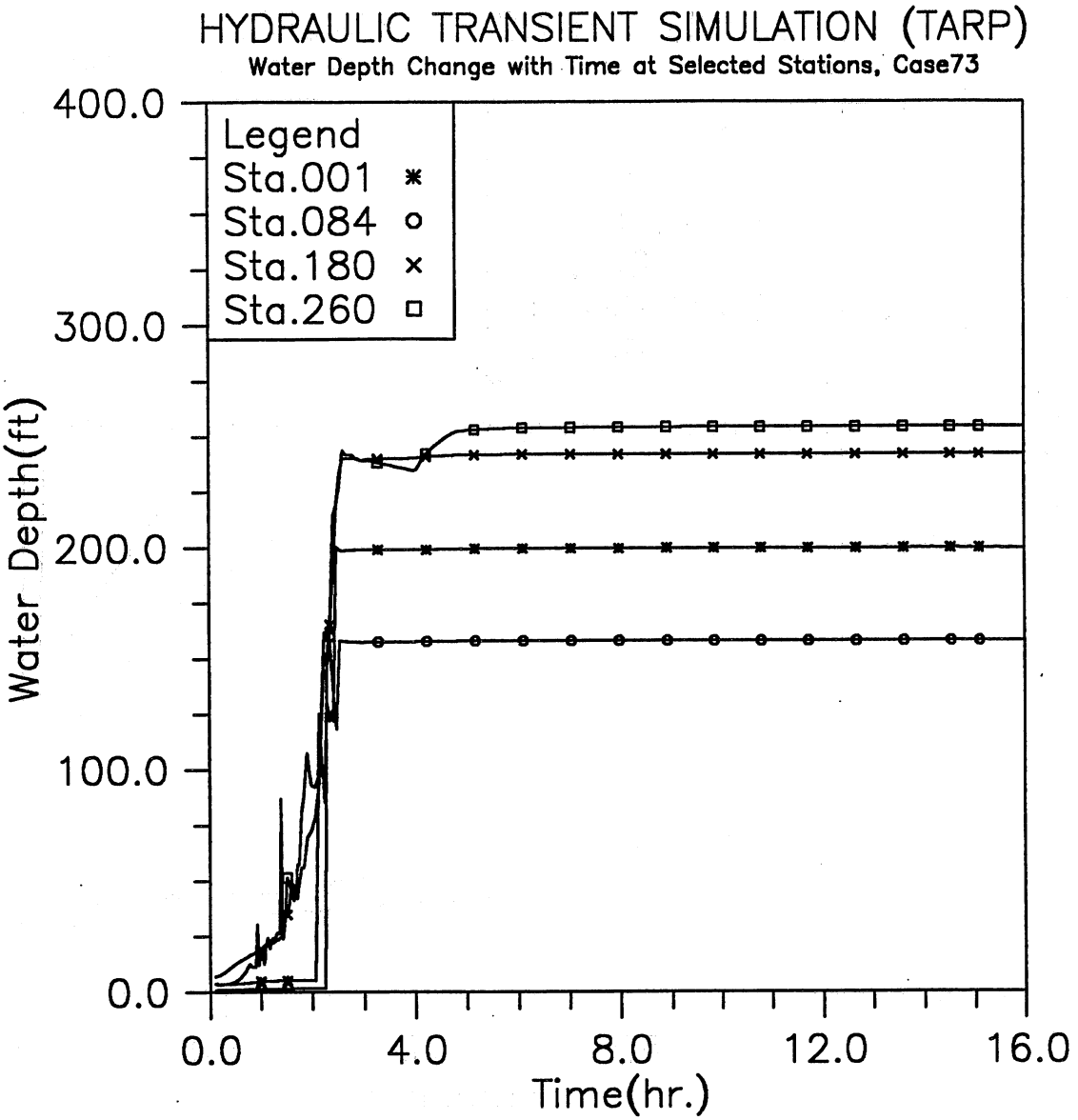

Fig. 3.27(b) Time variation of water depth at four upstream locations; Modeling case: gate closure in 30 min. after total inflow reaches the maximum value, initially empty reservoir, and PMF storm event (Case 7–3)

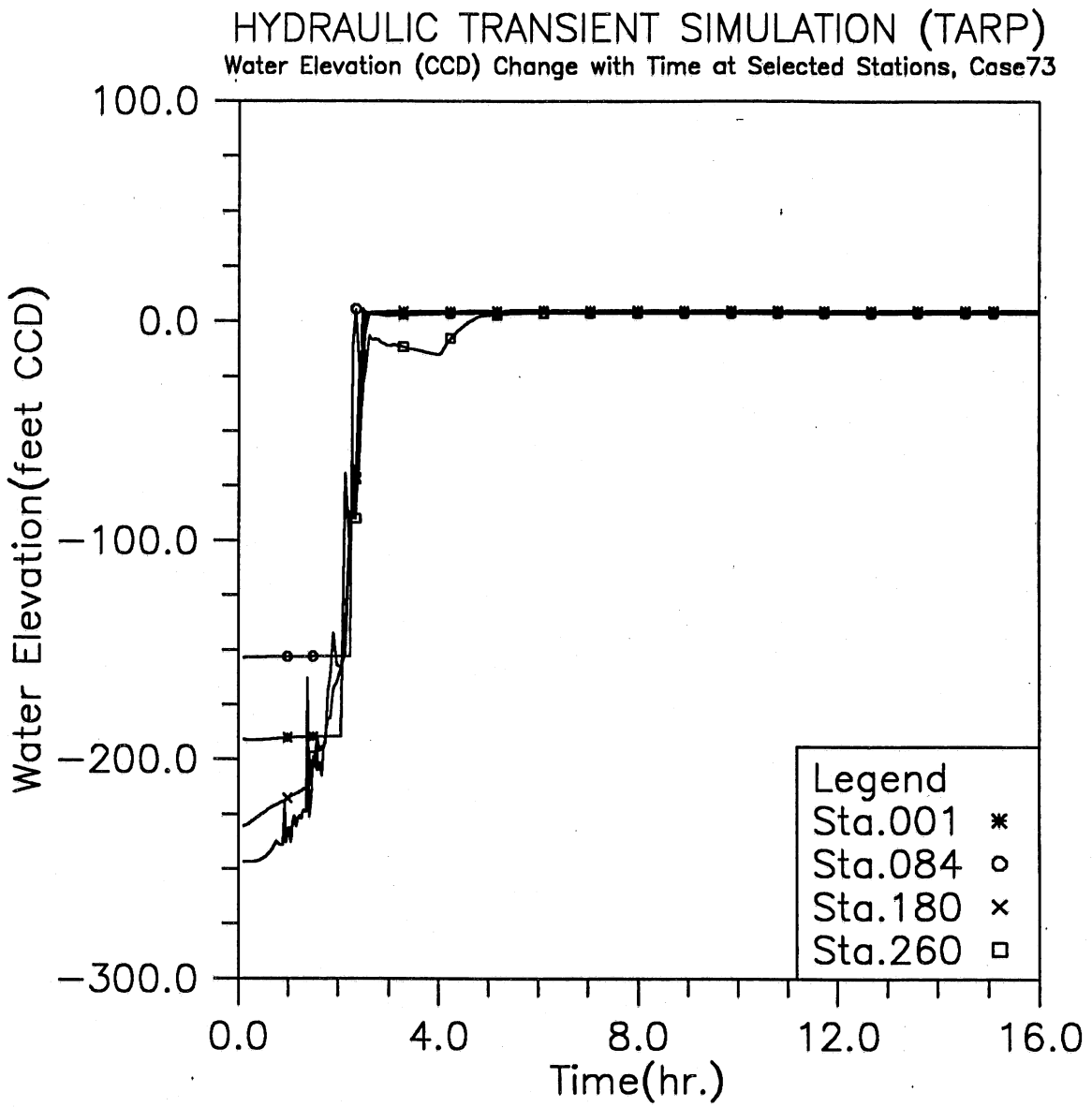

Fig. 3.27(c) Time variation of water elevation at four upstream locations; Modeling case: gate closure in 30 min. after total inflow reaches the maximum value, initially empty reservoir, and PMF storm event (Case 7–3)

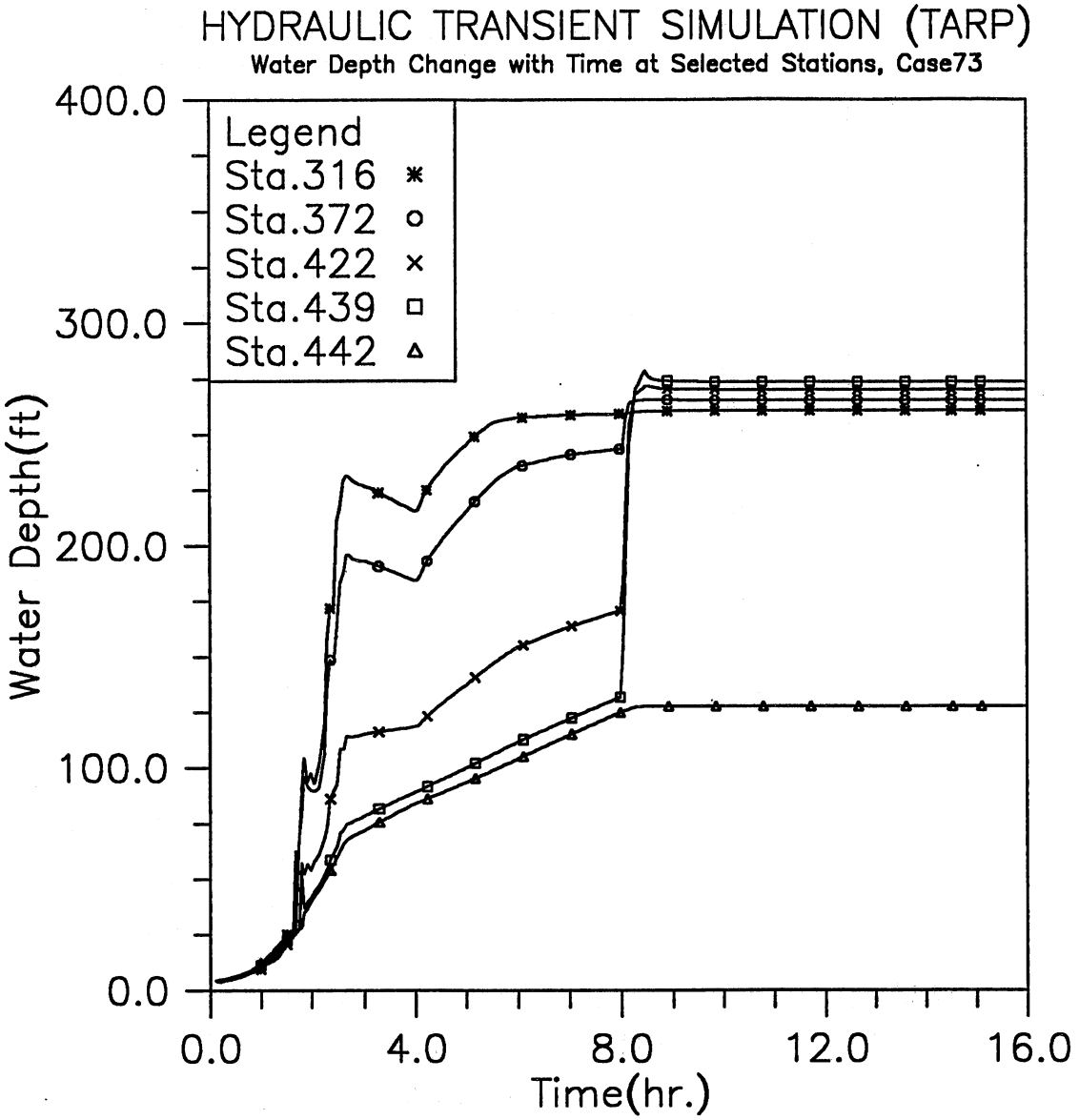

Fig. 3.27(d) Time variation of water depth at five downstream locations; Modeling case: gate closure in 30 min. after total inflow reaches the maximum value, initially empty reservoir, and PMF storm event (Case 7–3)

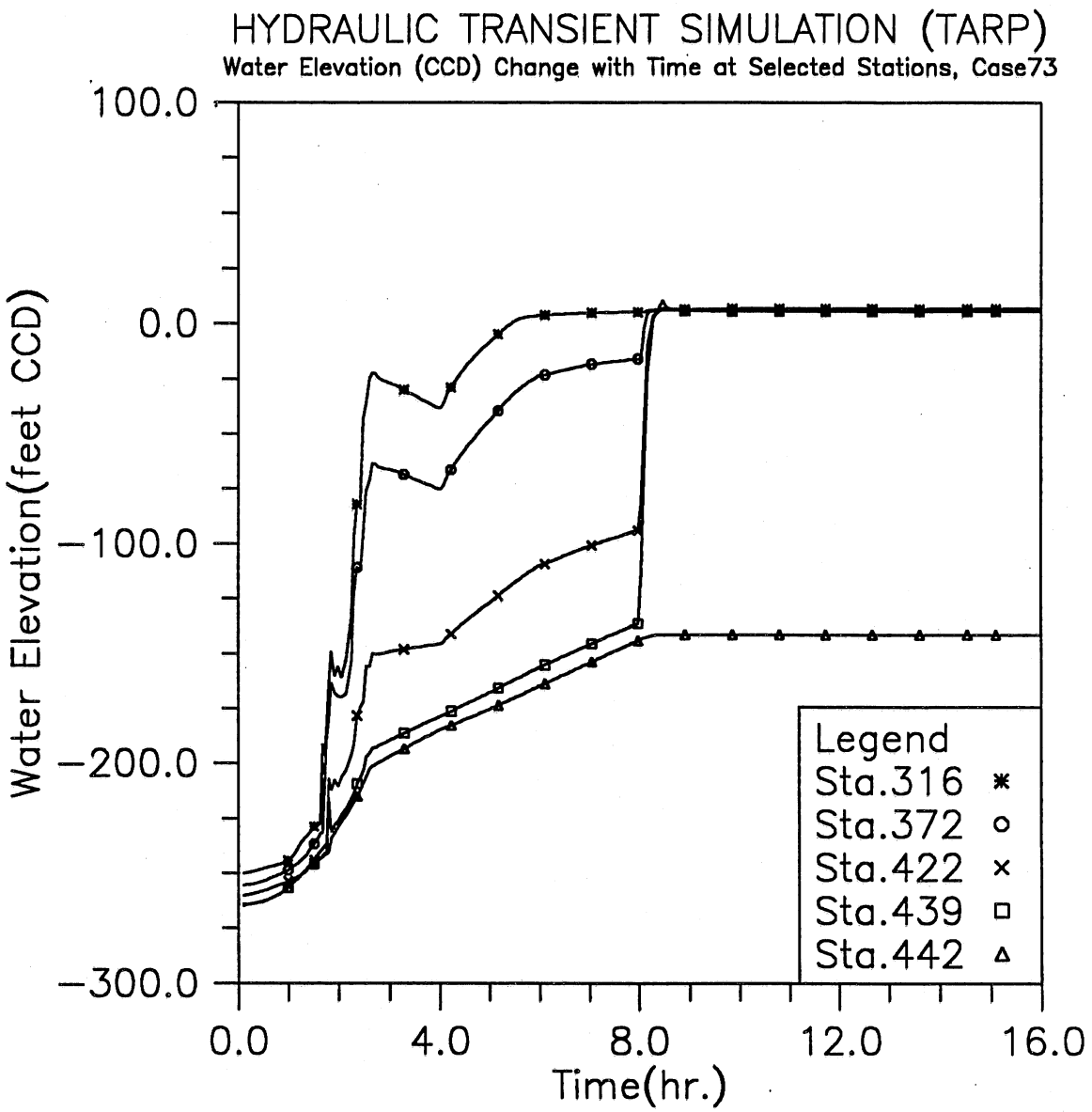

Fig. 3.27(e) Time variation of water elevation at five downstream locations; Modeling case: gate closure in 30 min. after total inflow reaches the maximum value, initially empty reservoir, and PMF storm event (Case 7–3)

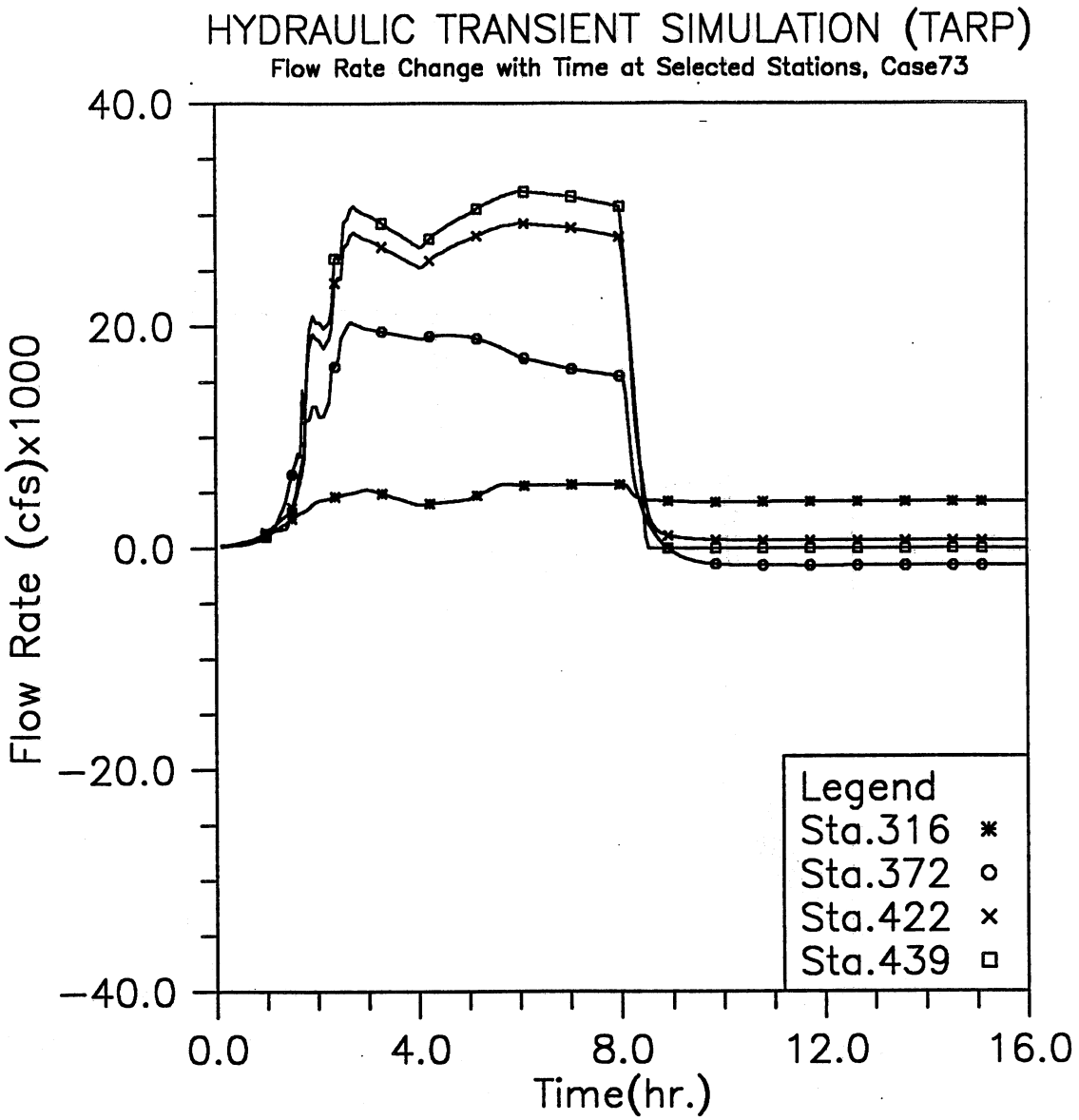

Fig. 3.27(f) Time variation of flow rate at four upstream locations; Modeling case: gate closure in 30 min. after total inflow reaches the maximum value, initially empty reservoir, and PMF storm event (Case 7–3)

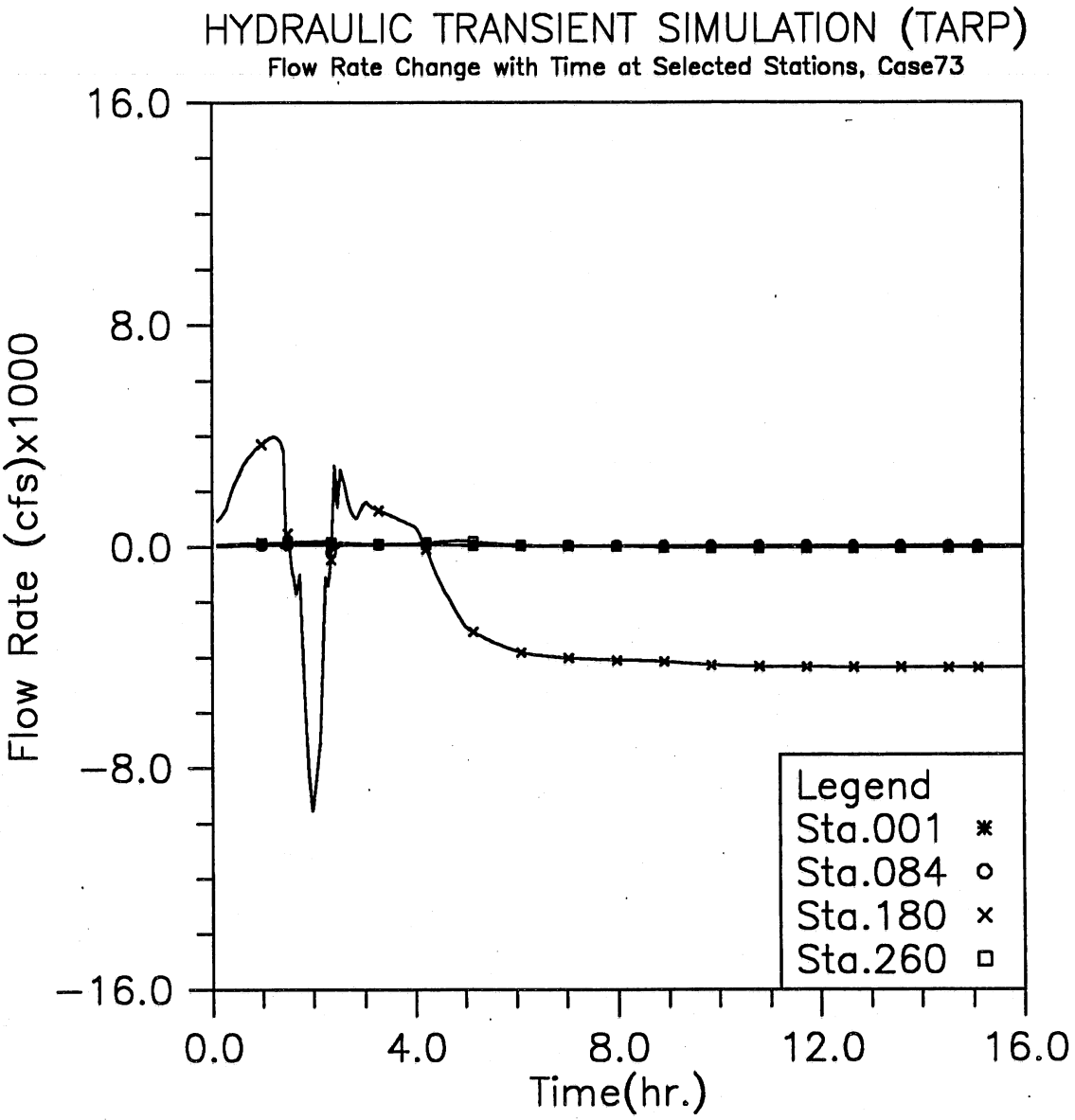

Fig. 3.27(g) Time variation of flow rate at four downstream locations; Modeling case: gate closure in 30 min. after total inflow reaches the maximum value, initially empty reservoir, and PMF storm event (Case 7–3)

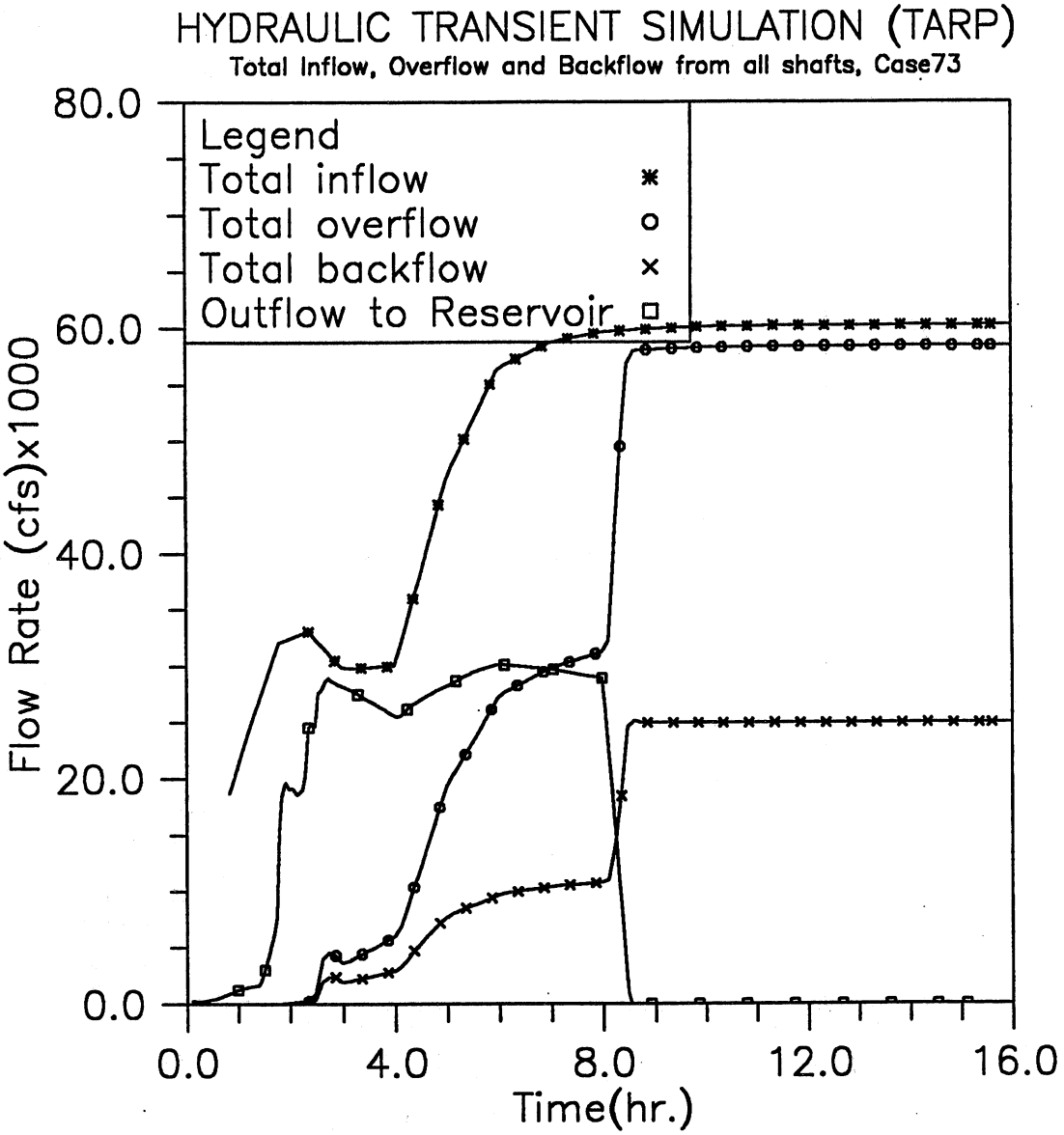

Fig. 3.27(h) Time variation of total inflow, overflow, backflow, and outflow to reservoir; Modeling case: gate closure in 30 min. after total inflow reaches the maximum value, initially empty reservoir, and PMF storm event (Case 7–3)

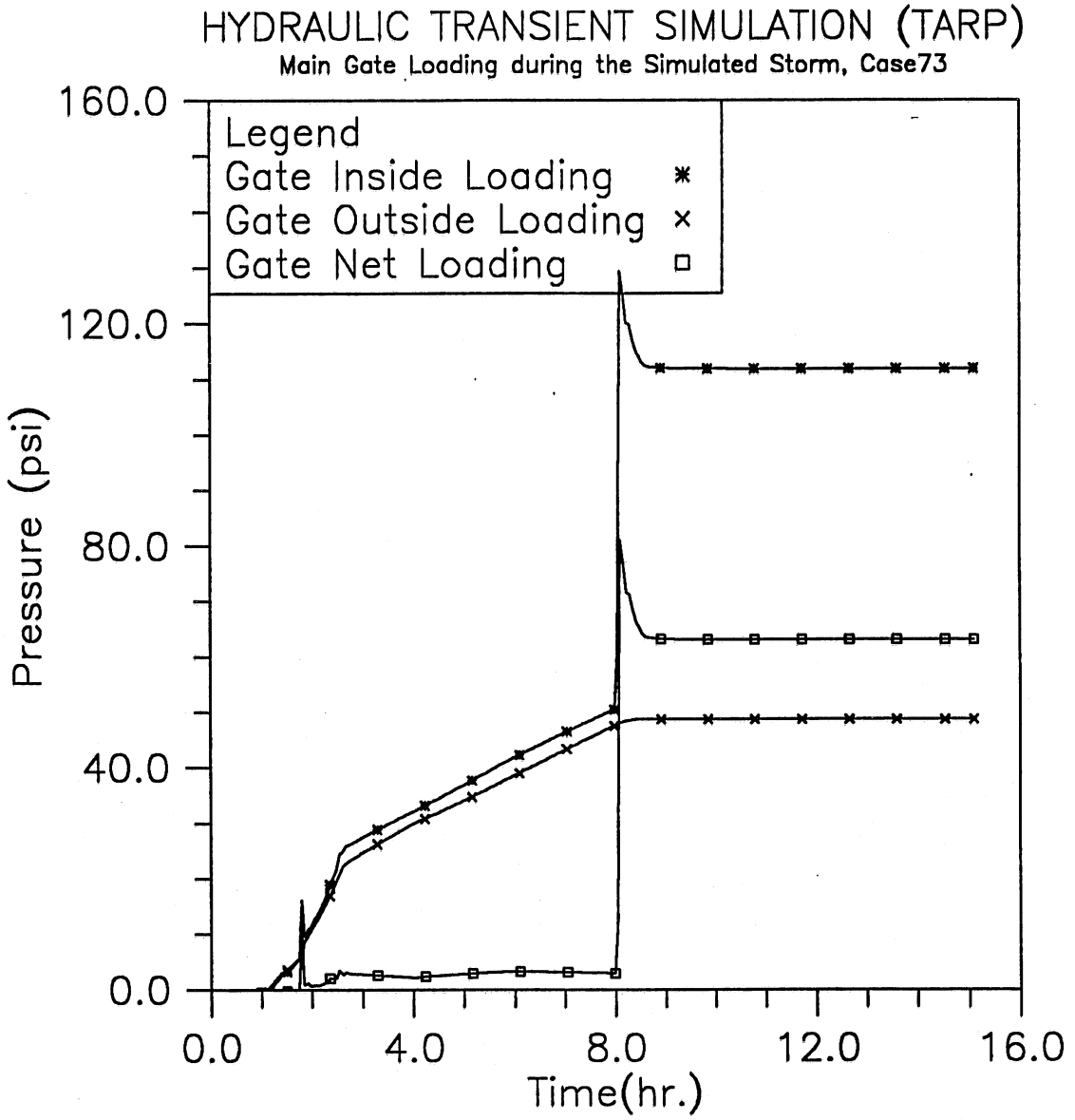

Fig. 3.27(i) Time variation of the averaged loading on the main gate; Modeling case: gate closure in 30 min. after total inflow reaches the maximum value, initially empty reservoir, and PMF storm event (Case 7–3)